NUREG/CP-0119
Vol. 2

Proceedings of the U.S. Nuclear Regulatory Commission

Nineteenth Water Reactor Safety Information Meeting

Volume 2
- Severe Accident Research
- Severe Accident Policy Implementation
- Accident Management

Held at
Bethesda Marriott Hotel
Bethesda, Maryland
October 28–30, 1991

U.S. Nuclear Regulatory Commission

Office of Nuclear Regulatory Research

Proceedings prepared by
Brookhaven National Laboratory

NOTICE

These proceedings have been authored by a contractor of the United States Government. Neither the United States Government nor any agency thereof, or any of their employees, makes any warranty, expressed or implied, or assumes any legal liability or responsibility for any third party's use, or the results of such use, of any information, apparatus, product or process disclosed in these proceedings, or represents that its use by such third party would not infringe privately owned rights. The views expressed in these proceedings are not necessarily those of the U.S. Nuclear Regulatory Commission.

Available from

Superintendent of Documents
U.S. Government Printing Office
P.O. Box 37082
Washington D.C. 20013-7082

and

National Technical Information Service
Springfield , VA 22161

NUREG/CP-0119
Vol. 2
R1,R4,R5,RD

Proceedings of the U.S. Nuclear Regulatory Commission

Nineteenth Water Reactor Safety Information Meeting

Volume 2
- Severe Accident Research
- Severe Accident Policy Implementation
- Accident Management

Held at
Bethesda Marriott Hotel
Bethesda, Maryland
October 28–30, 1991

Manuscript Completed: April 1992

Compiled by: Allen J. Weiss

Office of Nuclear Regulatory Research
U.S. Nuclear Regulatory Commission
Washington, DC 20555

Proceedings prepared by
Brookhaven National Laboratory

ABSTRACT

This three-volume report contains 83 papers out of the 108 that were presented at the Nineteenth Water Reactor Safety Information Meeting held at the Bethesda Marriott Hotel, Bethesda, Maryland, during the week of October 28-30, 1991. The papers are printed in the order of their presentation in each session and describe progress and results of programs in nuclear safety research conducted in this country and abroad. Foreign participation in the meeting included 14 different papers presented by researchers from Canada, Germany, France, Japan, Sweden, Taiwan, and USSR. The titles of the papers and the names of the authors have been updated and may differ from those that appeared in the final program of the meeting.

PROCEEDINGS OF THE
19th WATER REACTOR SAFETY INFORMATION MEETING

October 28-30, 1991

Published in Three Volumes

GENERAL INDEX

VOLUME 1

VOLUME 2

VOLUME 3

REGISTERED ATTENDEES(NON NRC)
19th WATER REACTOR SAFETY INFORMATION MEETING

D. ACKER
CEA FRENCH AT..MIC ENERGY COMMISSION
CEB SACLAY DMT/SEMT
GIF SUR YVETTE, 91191
FRANCE

S. ADDITON
TENERA/ARSAP
7272 WISCONSIN AVE., SUITE 300
BETHESDA, MD 20814
USA

T. AJIMA
NUPEC-NUCLEAR POWER ENG. TEST CENTER
3-17,1-CHOME,TORANOMON,MINATO-KU
TOKYO, 105
JAPAN

R. ALLEN
WESTINGHOUSE SAVANNAH RIVER COMPANY
P.O. BOX 616
AIKEN, SC 29802
USA

R. ALLEN
BATTELLE-PACIFIC NORTHWEST LABS.
P.O. BOX 999
RICHLAND, WA 99352
USA

C. ALLISON
EG&G IDAHO, INC.
P.O. BOX 1625
IDAHO FALLS, ID 83404
USA

A. ALONSO
MADRID POLYTECHNICAL UNIVERSITY
JOSE GUTIERREZ ABASCAL, 2
MADRID, 28006
SPAIN

H. AMARASOORIYA
SCIENTECH, INC.
11821 PARKLAWN DRIVE
ROCKVILLE, MD 20852
USA

T. ANDREYCHEK
WESTINGHOUSE ELECTRIC
PO BOX 355
PITTSBURGH, PA 15230
USA

F. ARAYA
JAPAN ATOMIC ENERGY RES. INST
TOKAI-MURA, NAKA-GUN
IBARAKI-KEN, 319-11
JAPAN

R. ARCHULETA
UNIVERSITY OF CALIFORNIA, SANTA BARBARA
DEPT. OF GEOLOGICAL SCIENCES
SANTA BARBARA, CA 93106
USA

V. ARCIERI
EG&G
11426 ROCKVILLE PIKE, SUITE 300
ROCKVILLE, MD 20852
USA

N. ARNE
KOREA ELECTRIC POWER CORP., NY OFFICE
270 SYLVAN AVENUE
ENGLEWOOD CLIFFS, NJ 07632
USA

V. ASMOLOV
I.V. KURCHATOV INST. OF ATOMIC ENERGY
KURCHATOV SQUARE
MOSCOW, 123182
USSR

M. AZARM
BROOKHAVEN NATIONAL LABORATORY
BUILDING 130
UPTON, NY 11973
USA

S. BALL
OAK RIDGE NATIONAL LABORATORY
P.O. BOX 2008
OAK RIDGE, TN 37831-6010
USA

A. BHATTA
PENN STATE UNIVERSITY
231 SAKETT BLDG.
UNIVERSITY PARK, PA 16802
USA

R. DARI
BROOKHAVEN NATIONAL LABORATORY
BUILDING 197C
UPTON, NY 11973
USA

G. BARDIS
FRAMATOME
TOUR FIAT CEDEX 16
PARIS-LA-DEFENSE, 92084
FRANCE

J. BASSELIER
BELGONUCLEAIRE
AVENUE ARIANE 4,
BRUSSELS, 1200
BELGIUM

J. BAST
STRATEGIC BUSINESS SYSTEMS
6 MOUNTAINVIEW TERRACE
BALLSTON LAKE, NY 12019
USA

J. BASURTO
CNSNS-MEXICO
AV. INSURGENTES SUR 1778
MEXICO CITY, 01030
MEXICO

G. BAUMGARTNER
BASLER & HOFMANN
FORCHSTRASSE 396
ZURICH, 8029
SWITZERLAND

R. BEATY
SCIENCE & ENGINEERING ASSOCIATES, INC.
1421 PRINCE STREET, SUITE 300
ALEXANDRIA, VA 22314
USA

L. BELL
OAK RIDGE NATIONAL LABORATORY
P.O. BOX 2009, MS-8063
OAK RIDGE, TN 37831
USA

R. BELL
NUMARC
1776 EYE STREET NW, SUITE 300
WASHINGTON, DC 20006
USA

G. BERNA
EG&G IDAHO, INC.
P.O. BOX 1625
IDAHO FALLS, ID 83404
USA

R. BEYER
WESTINGHOUSE
206 NAVAJO ROAD
W. PGH, PA 15241
USA

D. BHARGAVA
VIRGINIA POWER
5000 DOMINION BLVD.
GLEN ALLEN, VA 23060
USA

J. BICKEL
EG&G IDAHO, INC.
P.O. BOX 1625, MS 2405
IDAHO FALLS, ID 83415-2406
USA

W. BINNER
RES. CTR. SIEBERSDORF
KRAMERGASSE 1
VIENNA, A-1010
AUSTRIA

D. BLAHNIK
BATTELLE PACIFIC NORTHWEST LABS.
P.O. BOX 999
RICHLAND, WA 99352
USA

M. BOHN
SANDIA NATIONAL LABORATORIES
P.O. BOX 5800, DIVISION 6419
ALBUQUERQUE, NM 87185
USA

R. BOSCH
FOSTER WHEELER ENERGY GROUP
6 PEACH TREE HILL ROAD
LIVINGSTON, NJ 07021
USA

E. BOUCHERON
SANDIA NATIONAL LABORATORIES
P.O. BOX 5800, DIVISION 6418
ALBUQUERQUE, NM 87185-5800
USA

M. BOWMAN
BALTIMORE GAS & ELECTRIC CO.
P.O. BOX 1535
LUSBY, MD 20657
USA

B. BOYACK
LOS ALAMOS NATIONAL LABORATORY
P.O. BOX 1663, MS K551
LOS ALAMOS, NM 87545
USA

R. BOYD
WESTINGHOUSE SAVANNAH RIVER COMPANY
SAVANNAH RIVER SITE
AIKEN, SC 29808
USA

U. BRUDOLT
ABB ATOM
BOX 53
VASTERAS, 72163
SWEDEN

C. BUCHHOLZ
GE NUCLEAR ENERGY
175 CURTNER AVE. M/C 754
SAN JOSE, CA 95125
USA

R. BUDNITZ
FUTURE RESOURCES ASSOCIATES INC
2000 CENTER STREET, SUITE 418
BERKELEY, CA 94704
USA

J. BUTLER
NUMARC
1776 EYE STREET NW, SUITE 300
WASHINGTON, DC 20006
USA

N. BUTTERY
NUCLEAR ELECTRIC PIC
PWR PROJECT GROUP, BOOTHS HALL
KNUTSFORD, CHESHIRE WA168QP
UK

A. CAMP
SANDIA NATIONAL LABORATORIES
P.O. BOX 5800, DIVISION 6412
ALBUQUERQUE, NM 87185
USA

J. CAREW
BROOKHAVEN NATIONAL LABORATORY
BUILDING 475B
UPTON, NY 11973
USA

D. CASADA
OAK RIDGE NATIONAL LABORATORY
P.O. BOX 2009
OAK RIDGE, TN 37831-8063
USA

R. CHAMBERS
EG&G IDAHO, INC.
P.O. BOX 1625
IDAHO FALLS, ID 83415-1560
USA

F. CHANG
ARGONNE NATIONAL LABORATORY
9700 S. CASS AVENUE
ARGONNE, IL 60439
USA

S. CHAVEZ
EG&G IDAHO, INC.
P.O. BOX 1625, MS-2508
IDAHO FALLS, ID 83404
USA

C. CHEN
GILBERET/COMMONWEALTH
P.O. BOX 1498
READING, PA 19603
USA

S. CHENG
INSTITUTE OF ENERGY RESEARCH, AEC
P.O. BOX 3-3
LUNG-TAN, 32500
TAIWAN

R. CHEVERTON
OAK RIDGE NATIONAL LABORATORY
P.O. BOX 2009, BLDG 9204-1
OAK RIDGE, TN 37831-8047
USA

O. CHOPRA
ARGONNE NATIONAL LABORATORY
9700 S. CASS AVENUE
ARGONNE, IL 60439
USA

S. CHOW
STONE & WEBSTER ENG. CORP.
#3 EXECUTIVE CAMPUS, ROUTE 70
CHERRY HILL, NJ 08003
USA

L. CHU
BROOKHAVEN NATIONAL LABORATORY
BUILDING 130
UPTON, NY 11973
USA

R. COLE, JR.
SANDIA NATIONAL LABORATORIES
P.O. BOX 5800, DIVISION 6418
ALBUQUERQUE, NM 87185-5800
USA

M. CONFLANT
DIRECTORATE SAFETY INSTALLATION NUCLEAR
CEN/FAR DRSN BP NO. 6
FONTENAY-AUX-ROSES, 92265
FRANCE

C. COOPER
AEA TECHNOLOGY, WINFRITH
WINFRITH TECHNOLOGY CENTRE
DORCHESTER, DORSET DT2 8DH
UK

J. COOPER
MPR ASSOCIATES, INC.
1050 CONNECTICUT AVE, NW
WASHINGTON, DC 20036
USA

W. COPELAND
WESTINGHOUSE SAVANNAH RIVER COMPANY
SAVANNAH RIVER SITE
AIKEN, SC 29808
USA

E. CORUS
SANDIA NATIONAL LABORATORIES
41 EAGLE TR
TIJERAS, NM 87059
USA

P. CORTICELLI
ENEA
VIO MARTIRI DI MONTESOLE
BOLOGNA, 40100
ITALY

W. CORWIN
OAK RIDGE NATIONAL LABORATORY
P.O. BOX 2008, BLDG 4500S
OAK RIDGE, TN 37831-6151
USA

D. COX
OAK RIDGE NATIONAL LABORATORY
P.O. BOX 2009
OAK RIDGE, TN 37831-8038
USA

K. COZENS
NUMARC
1776 EYE STREET NW, SUITE 300
WASHINGTON, DC 20006
USA

D. CRAMER
WESTINGHOUSE SAVANNAH RIVER COMPANY
SAVANNAH RIVER SITE
AIKEN, SC 29808
USA

R. CURTIS
JUPITER CORPORATION
15909 WHITE ROCK RD.
GAITHERSBURG, MD 20878
USA

D. DAHLGREN
SANDIA NATIONAL LABORATORIES
P.O. BOX 5800, DIVISION 6410
ALBUQUERQUE, NM 87185
USA

R. DAIL
APTECH ENGINEERING SERVICES, INC
9672 PENNSYLVANIA AVE
UPPER MARLBORO, MD 20772
USA

R. DALLMAN
UNC ANALYTICAL SERVICES
P.O. BOX 5400
ALBUQUERQUE, NM 87185
USA

P. DAMERELL
MPR ASSOCIATES, INC
1050 CONNECTICUT AVE, NW
WASHINGTON, DC 20036
USA

DANKO
UNIV OF TENNESSEE
COLLEGE OF ENGINEERING, PERKINS HALL
KNOXVILLE, TN 37996-2000
USA

N. DAVIES
AEA [illegible]OLOGY
R [illegible]
W[illegible]ON, CHESHIRE WA3 6AT
UK

M. DAVISTER
U.S. DEPARTMENT OF ENERGY, DP-621
19901 GERMANTOWN ROAD
GERMANTOWN, MD 20874
USA

B. DE L'EPINOIS
DIRECTORATE SAFETY INSTALLATION NUCLEAR
CEN/FAR DRSN BP NO. 6
FONTENAY-AUX-ROSES, 92265
FRANCE

R. DE WIT
NATL INST. OF STANDARDS & TECHNOLOGY
ROOM B144, MATERIALS BLDG.
GAITHERSBURG, MD 20899
USA

J. DEBOR
SCIENCE APPLICATIONS INTL. CORP.
1710 GOODRIDGE DRIVE
MCLEAN, VA 22102
USA

R. DENNING
BATTELLE COLUMBUS
505 KING AVE.
COLUMBUS, OHIO 43201
USA

J. DEVOS
CEA FRENCH ATOMIC ENERGY COMMISSION
CEB SACLAY DMT/SEMT
GIF SUR YVETTE, 91190
FRANCE

K. DEWALL
EG&G IDAHO, INC.
P.O. BOX 1625
IDAHO FALLS, ID 83404
USA

H. DIETERSHAGEN
KNOLLS ATOMIC POWER LAB, GENERAL ELEC.
P.O. BOX 1072
SCHENECTADY, NY 12301-1072
USA

M. DIMARZO
UNIVERSITY OF MARYLAND
M.E. DEPT.
COLLEGE PARK, MD 20742
USA

C. DIPALO
SCIENCE APPLICATIONS INTL. CORP.
1710 GOODRIDGE DRIVE
MCLEAN, VA 22102
USA

S. DOCTOR
BATTELLE PACIFIC NORTHWEST LABS.
P.O. BOX 999
RICHLAND, WA 99352
USA

M. DROUIN
SCIENCE APPLICATIONS INTL. CORP.
2109 AIR PARK RD., S. E.
ALBUQUERQUE, NM 87106
USA

R. DUFFEY
BROOKHAVEN NATIONAL LABORATORY
BUILDING 197C
UPTON, NY 11973
USA

R. DURANTE
ASCI TECHNOLOGIES
15400 CALHOUN DRIVE, SUITE 100
ROCKVILLE, MD 20855
USA

K. DWIVEDY
VIRGINIA POWER
5000 DOMINION BLVD.
GLEN ALLEN, VA 23060
USA

J. EAST
WESTINGHOUSE SAVANNAH RIVER COMPANY
SAVANNAH RIVER SITE
AIKEN, SC 29808
USA

K. EBISAWA
JAPAN ATOMIC ENERGY RES. INST.
TOKAI-MURA, NAKA-GUN
IBARAKI-KEN, 319-11
JAPAN

J. EDSON
EG&G IDAHO, INC.
P.O. BOX 1625
IDAHO FALLS, ID 83415-2406
USA

Z. ELAWAR
ARIZONA PUBLIC SERVICE
P.O. BOX 52034
PHOENIX, AZ 85029
USA

P. EMAIN
ELECTICITÉ DE FRANCE
12-14, AVENUE DUTRIEVOZ
VILLEURBANNE, 69628
FRANCE

G. EMBLEY
GENERAL ELECTRIC
P.O. BOX 1072
SCHENCTADY, NY 12301
USA

B. ETTINGER
MPR ASSOCIATES, INC.
1050 CONNECTICUT AVE. NW
WASHINGTON, DC 20036
USA

B. EVANS
NUMARC
1776 EYE STREET NW, SUITE 300
WASHINGTON, DC 20006
USA

R. FAKORY
S3 TECHNOLOGIES
8930 STANFORD BLVD.
COLUMBIA, MD 21045
USA

M. FELTUS
PENN STATE UNIVERSITY
231 SAKETT BLDG.
UNIVERSITY PARK, PA 16802
USA

R. FERCH
ATOMIC ENERGY CONTROL BOARD
P.O.BOX 1046, STATION B
OTTAWA, ONTARIO K1P 5S9
CANADA

M. FISCHER
SIEMENS-KWU
LAMPERICHUHL 45
ERLANGEN, W8520
GERMANY

S. FLEGER
SCIENCE APPLICATIONS INTL. CORP.
1710 GOODRIDGE DRIVE
MCLEAN, VA 22102
USA

M. FONTANA
OAK RIDGE NATIONAL LABORATORY
P.O. BOX 2009
OAK RIDGE, TN 37831-8063
USA

T. FORTUNATO
BETTIS ATOMIC POWER LABORATORY
P.O. BOX 79
WEST MIFLIN, PA 15122
USA

E. FOX
OAK RIDGE NATIONAL LABORATORY
P.O. BOX 2009
OAK RIDGE, TN 37831-8063
USA

W. FRID
SWEDISH NUCLEAR POWER INSPECTORATE
P.O. BOX 27106
STOCKHOLM, S-102 52
SWEDEN

T. FUNAHASHI
TOSHIBA CORPORATION
8, SHINSUGITA-CHO, ISOGO-KU
YOKOHAMA, 235
JAPAN

H. FURUKAWA
HITACHI WORKS, HITACHI LTD.
1-1, 3-CHOME, SAIWAI-CHO
HITACHI-SHI, IBARAKI-KEN 317
JAPAN

R. GAMBLE
SARTREX CORP.
1700 ROCKVILLE PIKE, STE. 400
ROCKVILLE, MD 20852
USA

D. GERTMAN
EG&G IDAHO, INC.
P.O. BOX 1625 MS 2405
IDAHO FALLS, ID 83404
USA

B. GILBERT
EG&G IDAHO, INC.
P.O. BOX 1625 MS-2405
IDAHO FALLS, ID 83404
USA

J. GLEASON
WYLE LABORATORIES
P.O. BOX 07-7717
HUNTSVILLE, AL 35807-7777
USA

M. GOMOLINSKI
CEA FRENCH ATOMIC ENERGY COMMISSION
31 RUE DE CHAVEVTON
PARIS, 75012
FRANCE

W. GRANT
MPR ASSOCIATES, INC.
1050 CONNECTICUT AVE. NW
WASHINGTON, DC 20036
USA

R. GREENE
OAK RIDGE NATIONAL LABORATORY
P.O. BOX 2009
OAK RIDGE, TN 37831-8038
USA

E. GROUNDWATER
SCIENCE APPLICATIONS INTL. CORP.
1710 GOODRIDGE DRIVE
MCLEAN, VA 22102
USA

E. GROVE
BROOKHAVEN NATIONAL LABORATORY
BUILDING 130
UPTON, NY 11973
USA

T. HAKE
SANDIA NATIONAL LABORATORIES
P.O. BOX 5800, DIVISION 6412
ALBUQUERQUE, N.M. 87185
USA

R. HALL
BROOKHAVEN NATIONAL LABORATORY
BUILDING 130
UPTON, NY 11973
USA

R. HAMMERSLEY
FAUSKE & ASSOCIATES
16W070 W. 83RD. ST.
BURR RIDGE, IL 60521
USA

S. HAO
BECHTEL
9801 WASHINGTON BLVD.
GAITHERSBURG, MD 20878-5350
USA

F. HARPER
SANDIA NATIONAL LABORATORIES
P.O. BOX 5800, DIVISION 6413
ALBUQUERQUE, NM 87185-5800
USA

C. HARRISON
ATOMIC ENERGY CONTROL BOARD
270 ALBERT ST.
OTTAWA, ONTARIO K1P 5S9
CANADA

L. HARROP
HM NUCLEAR INSTALLATIONS INSPECTORATE
ST. PETERS HOUSE, BALLIOL ROAD
BOOTLE, MERSEYSIDE L20 3LZ
UK

E. HARVEGO
EG&G IDAHO, INC.
P.O. BOX 1625
IDAHO FALLS, ID 83415-2406
USA

R. HARVEY
YANKEE ATOMIC ELECTRIC CO.
580 MAIN ST.
BOLTON, MA 01740
USA

H. HASHEMIAN
ANS CORPORATION
9111 CROSS PARK DRIVE
KNOXVILLE, TN 37923
USA

M. HASSAN
BROOKHAVEN NATIONAL LABORATORY
BUILDING 130
UPTON, NY 11973
USA

J. HAWTHORNE
MATERIALS ENGINEERING ASSOCIATES
9700-B MARTIN L. KING, JR. HWY
LANHAM, MD 20706
USA

N. HAYASHI
NUPEC-NUCLEAR POWER ENG. TEST CENTER
3-17,1-CHOME,TORANOMON,MINATO-KU
TOKYO, 105
JAPAN

G. HEDRICK
DUKE ENGINEERING & SERVICES, INC
P.O. BOX 1004, M/S ST02A
CHARLOTTE, NC 28201-1004
USA

S. HENRY
BALTIMORE GAS & ELECTRIC CO.
P.O. BOX 1535
LUSBY, MD 20657
USA

H. HEPER
UNIVERSITY OF MARYLAND
9314 CHERRY HILL ROAD #217
COLLEGE PARK, MD 20740
USA

D. HIDINGER
GENERAL ELECTRIC
P.O. BOX 1072
SCHENCTADY, NY 12301
USA

J. HIGGINS
BROOKHAVEN NATIONAL LABORATORY
BUILDING 130
UPTON, NY 11973
USA

P. HILL
PENNSYLVANIA POWER & LIGHT
TWO NORTH NINTH STREET
ALLENTOWN, PA 18101
USA

R. HOBBINS
EG&G IDAHO, INC.
P.O. BOX 1625
IDAHO FALLS, ID 83415-1560
USA

N. HOBSON
HM NUCLEAR INSTALLATIONS INSPECTORATE
ST. PETERS HOUSE, BALLIOL ROAD
BOOTLE, MERSEYSIDE L20 3LZ
UK

L. HOCHREITER
WESTINGHOUSE ELECTRIC
PO BOX 355
PITTSBURGH, PA 15230
USA

S. HODGE
OAK RIDGE NATIONAL LABORATORY
P.O. BOX 2009
OAK RIDGE, TN 37831-8057
USA

P. HOFMANN
KERNFORSCHUNGSZENTRUM KARLSRUHE
P.O. BOX 3640
KARLSRUHE, W-7500
GERMANY

C. HOFMAYER
BROOKHAVEN NATIONAL LABORATORY
BUILDING 475C
UPTON, NY 11973
USA

P. HOLDEN
AEA TECHNOLOGY
RISLEY
WARRINGTON, CHESHIRE WA3 6QRO
UK

H. HOLMSTRÖM
OECD NUCLEAR ENERGY AGENCY
38, BOULEVARD SUCHET
PARIS, F-75016
FRANCE

R. HOPPE
BETTIS ATOMIC POWER LABORATORY
P.O. BOX 79
WEST MIFLIN, PA 15122
USA

Y. HORIKAWA
THE KANSAI ELECTRIC POWER CO., INC.
1100 17TH STREET, N.W., SUITE 500
WASHINGTON, DC 20036
USA

D. HORSCHEL
SANDIA NATIONAL LABORATORIES
P.O. BOX 5800, DIVISION 6473
ALBUQUERQUE, NM 87185-5800
USA

T. HSU
VIRGINIA POWER
5000 DOMINION BLVD.
GLEN ALLEN, VA 23060
USA

F. HSU
BROOKHAVEN NATIONAL LABORATORY
BUILDING 130
UPTON, NY 11973
USA

Y. HUANG
INSTITUTE OF ENERGY RESEARCH AEC
P.O. BOX 3-3
LUNG-TAN, 32500
TAIWAN

T. HUNT
GULF STATES UTILITIES
P.O. BOX 220
ST. FRANCISVILLE, LA 70775
USA

T. HUNT
EG&G IDAHO, INC.
P.O. BOX 1625
IDAHO FALLS, ID 83415-2406
USA

S. HYTEN
WYLE LABORATORIES
P.O. BOX 07-7777
HUNTSVILLE, AL 35807-7777
USA

S. INAMDAR
ONTARIO HYDRO
700 UNIVERSITY AVE.
TORONTO, ONTARIO M5G 1X6
CANADA

L. INNES
ATOMIC ENERGY CONTROL BOARD
270 ALBERT ST.
OTTAWA, ONTARIO K1P 5S9
CANADA

J. IRELAND
LOS ALAMOS NATIONAL LABORATORY
P.O. BOX 1663, MS K551
LOS ALAMOS, NM 87545
USA

H. ISBIN
NRC-NSRRC
2815 MONTEREY PKWY
ST. LOUIS PARK, MN 55416
USA

J. ISHIGURO
JAPAN NUS
910 CLOPPER ROAD
GAITHERSBURG, MD 20877
USA

R. JACOBS
PENN STATE UNIVERSITY
DEPARTMENT OF PSYCHOLOGY
UNIVERSITY PARK, PA 16802
USA

M. JACOBUS
SANDIA NATIONAL LABORATORIES
P.O. BOX 5800, DIVISION 6419
ALBUQUERQUE, NM 87185
USA

J. JANSKY
BTB-JANSKY
GERLINGER STRASSE 151
LEONBERG, 7250
GERMANY

D. JARRELL
BATTELLE-PACIFIC NORTHWEST LABS.
P.O. BOX 999
RICHLAND, WA 99352
USA

J. JARVIS
BECHTEL
9801 WASHINGTON BLVD.
GAITHERSBURG, MD 20878-5356
USA

A. JIMENEZ
CSN
JUSTO DORADO 11
MADRID, 28040
SPAIN

G. JOHNSON
EG&G IDAHO, INC.
P.O. BOX 1625
IDAHO FALLS, ID 83404
USA

B. JOHNSON
BATTELLE-PACIFIC NORTHWEST LABS.
P.O. BOX 999
RICHLAND, WA 99352
USA

J. JONES
OAK RIDGE NATIONAL LABORATORY
P.O. BOX 2009
OAK RIDGE, TN 37831-8063
USA

K. JONES
EG&G IDAHO, INC.
P.O. BOX 1625 MS-2508
IDAHO FALLS, ID 83404
USA

C. JUPITER
JUPITER CORPORATION
SUITE 503 WHEATON PLAZA N, 2730 UNIVERSITY BLVD. WEST
WHEATON, MD 20902
USA

H. KARWAT
TECHN. UNIV. MUNICH
FORSCHUNG AREA
GARCHING, BAVARIA W-8046
GERMANY

W. KASTENBERG
UCLA
48-121 ENGINEER IV
LOS ANGELES, CA 90024
USA

S. KATANISHI
JAPAN ATOMIC ENERGY RES. INST
TOKAI-MURA, NAKA-GUN
IBARAKI-KEN, 319-11
JAPAN

W. KATO
BROOKHAVEN NATIONAL LABORATORY
BUILDING 197C
UPTON, NY 11973
USA

S. KAWAKAMI
NUPEC-NUCLEAR POWER ENG. TEST CENTER
3-13,4-CHOME,TORANOMON,MINATO-KU
TOKYO, 105
JAPAN

K. KAWANISHI
MITSUBISHI HEAVY INDUSTRIES, LTD.
2-1-1, SHINHAMA, ARAI-CHO
TAKASAGO-SHI, HYOGO-KEN 676
JAPAN

D. KELLY
EG&G IDAHO, INC.
P.O. BOX 1625 MS-2405
IDAHO FALLS, ID 83404
USA

J. KELLY
SANDIA NATIONAL LABORATORIES
P.O. BOX 5800, DIVISION 6401
ALBUQUERQUE, NM 87185-5800
USA

M. KHATIB-RAHBAR
ENERGY RESEARCH, INC.
PO BOX 2034
ROCKVILLE, MD 20847
USA

HHO KIM
KOREA INSTITUTE OF NUCLEAR SAFETY
P.O. BOX 16 DAEDUK-DANJI
DAEJON, 305353
KOREA

H. KIM
KAERI
P.O. BOX 7 DAEDUK-DANJI
DAEJON,
KOREA

I. KIM
BROOKHAVEN NATIONAL LABORATORY
BUILDING 130
UPTON, NY 11973
USA

S. KINNERSLY
AEA TECHNOLOGY, WINFRITH
WINFRITH TECHNOLOGY CENTRE
DORCHESTER, DORSET DT2 8DH
UK

E. KINTNER
NRC/RAC
P.O. BOX 682
NORWICH, VT 05055
USA

P. KLOEG
KEMA
UTRECHTSEWEG 310
ARNHEM, 6812 AR
THE NETHERLANDS

G. KLOPP
COMMONWEALTH EDISON
1400 OPUS PLACE, SUITE 400
DOWNERS GROVE, IL 60515
USA

L. KMETYK
SANDIA NATIONAL LABORATORIES
P.O. BOX 5800, DIVISION 6418
ALBUQUERQUE, NM 87185-5800
USA

S. KOBAYASHI
ISHIKAWAJIMA-HARIMA HEAVY INDUSTRIES
1,SHIN-NAKAHARA-CHO, ISOGO-KU
YOKOHAMA, 235
JAPAN

T. KODAMA
MITSUBISHI HEAVY INDUSTRIES, LTD.
2-1-1, SHINHAMA, ARAI-CHO
TAKASAGO-SHI, HYOGO-KEN 676
JAPAN

E. KOHN
ONTARIO HYDRO
700 UNIVERSITY AVE.
TORONTO, ONTARIO M5A
CANADA

C. KOT
ARGONNE NATIONAL LABORATORY
9700 S. CASS AVENUE
ARGONNE, IL 60439
USA

P. KRISHNASWAMY
BATTELLE COLUMBUS
505 KING AVE.
COLUMBUS, OHIO 43201
USA

P. KUAN
EG&G IDAHO, INC.
P.O. BOX 1625 MS-1560
IDAHO FALLS, ID 83404
USA

T. KUBOKOYA
TOSHIBA CORPORATION
8, SHINSUGITA-CHO, ISOGO-KU
YOKOHAMA, 235
JAPAN

Y. KUKITA
JAPAN ATOMIC ENERGY RES. INST
TOKAI-MURA, NAKA-GUN
IBARAKI-KEN, 319-11
JAPAN

M. KURIHARA
MITSUBISHI HEAVY INDUSTRIES, LTD.
4-1, 2-CHOME, SHIBAKOUEN , MINATO-KU
TOKYO, 105
JAPAN

Y. KUSAMA
JAERI, TAKASAKI RAD. CHEM. RES. INST.
1233 WATANUKI-MACHI
TAKASAKI, GUNMA, 370-12
JAPAN

K. KUSSMAUL
MPA STUTTGART
P.O. BOX 2009
STUTTGART 60, D-7000
GERMANY

J. LAKE
EG&G IDAHO, INC.
P.O. BOX 1625 MS-2507
IDAHO FALLS, ID 83415-1560
USA

M. LAMBERT
ÉLECTICITÉ DE FRANCE
12-14, AVENUE D'ITRIEVOZ
VILLEURBANNE, 69628
FRANCE

F. LANDY
PENN STATE UNIVERSITY
RESEARCH BLDG. D
UNIVERSITY PARK, PA 16802
USA

D. LEAVER
TENERA
1340 SARATOGA-SUNNYVALE ROAD
SAN JOSE, CA 95129
USA

C. LECOMTE
CEA FRENCH ATOMIC ENERGY COMMISSION
CEN/FAR DRSN BP NO. 6
FONTENAY-AUX-ROSES, 92265
FRANCE

J. LEE
KOREA INSTITUTE OF NUCLEAR SAFETY
P.O. BOX 16 DAEDUK-DANJI
DAEJON, 305353
KOREA

S. LEE
FAUSKE & ASSOCIATES
16W070 W. 83RD ST
BURR RIDGE, IL 60521
USA

J. LEHNER
BROOKHAVEN NATIONAL LABORATORY
BUILDING 130
UPTON, NY 11973
USA

R. LIN
LOS ALAMOS NATIONAL LABORATORY
P.O. BOX 1663, MS K557
LOS ALAMOS, NM 87545
USA

M. LINDQUIST
WESTINGHOUSE HANFORD CO.
BOX 1970,
RICHLAND, WA 99352
USA

M. LIVOLANT
CEA FRENCH ATOMIC ENERGY COMMISSION
CEN/FAR DRSN BP NO. 6
FONTENAY-AUX-ROSES, 92265
FRANCE

R. LOFARO
BROOKHAVEN NATIONAL LABORATORY
BUILDING 130
UPTON, NY 11973
USA

J. LOPEZ-MONTERO
MADRID POLYTECHNICAL UNIVERSITY
JOSE GUTIERREZ ABASCAL, 2
MADRID, 28006
SPAIN

F. LOSS
MATERIALS ENGINEERING ASSOCIATES
9700-B MARTIN L. KING, JR. HWY
LANHAM, MD 20706
USA

K. LYNCH
GROVE ENGINEERING
15215 SHADY GROVE RD., STE. 202
ROCKVILLE, MD 20850
USA

P. MacDONALD
EG&G IDAHO, INC.
P.O. BOX 1625
IDAHO FALLS, ID 83415-2406
USA

A. MacKINNEY
NUMARC
1776 EYE STREET NW, SUITE 300
WASHINGTON, DC 20006
USA

L. MADONI
BROOKHAVEN NATIONAL LABORATORY
BUILDING 130
UPTON, NY 11973
USA

D. MAGALLON
CEC-JRC ISPRA
JRC EURATUM ISPRA
ISPRA, VARESE 21020
ITALY

H. MAGLEBY
EG&G IDAHO, INC.
P.O. BOX 1625
IDAHO FALLS, ID 83415-2406
USA

M. MANAHAN
PENN STATE UNIVERSITY
231 SACKETT
UNIVERSITY PARK, PA 16802
USA

P. MANBECK
BALTIMORE GAS & ELECTRIC CO.
P.O. BOX 632
LUSBY, MD 20657
USA

R. MANOL
SIEMENS/KWU
HAMMERBACHENSTR 12
ERLANGEN,
GERMANY

J. MARRINUCCI
GILBERET/COMMONWEALTH
P.O. BOX 1498
READING, PA 19603
USA

P. MARSILI
ENEA-DISP
VIA V. BRANCATI, 48
ROME, 00144
ITALY

I. MASAOKA
HITACHI RESEARCH LABORATORY
3-1, SAIWAI-CHO
HITACHI-SHI, IBARAKI-KEN 317
JAPAN

H. MASSIE
DNF SAFETY BOARD
625 INDIANA AVENUE, SUITE 700
WASHINGTON, DC 20004
USA

A. MATSUMOTO
JAPAN ATOMIC ENERGY RES. INST
TOKAI-MURA, NAKA-GUN
IBARAKI-KEN, 319-11
JAPAN

B. MAVKO
J. STEFAN INSTITUTE
JAMOVA 39
LJUBLJANA, 61000
SLOVENIA

B. MAVKO
J. STEFAN INSTITUTE
JAMOVA 39
LJUBLJANA, 61000
SLOVENIA

E. McCRAW
DUKE ENGINEERING & SERVICES, INC
P.O. BOX 1004, M/S ST02A
CHARLOTTE, NC 28201-1004
USA

W. McCURDY
MPR ASSOCIATES, INC
1050 CONNECTICUT AVE, NW
WASHINGTON, DC 20036
USA

D. McMULLAN
KNOLLS ATOMIC POWER LAB, GENERAL ELEC
P.O. BOX 1072
SCHENECTADY, NY 12301-1072
USA

C. MEDICH
SIET
VIA NINO BIXIO N. 27
PIACENZA, 29100
ITALY

J. MEINCKE
CONSUMERS POWER COMPANY
27780 BLUE STAR HIGHWAY
COVERT, MI 49043
USA

B. MENKE
MATERIALS ENGINEERING ASSOCIATES
9700-B MARTIN L. KING, JR. HWY
LANHAM, MD 20706
USA

J. METCALF
STONE & WEBSTER ENG. CORP.
245 SUMMER STREET
BOSTON, MA 02107
USA

Y. MEYZAUD
FRAMATOME
TOUR FIAT CEDEX 16
PARIS LA-DEFENSE, 92084
FRANCE

L. MILLER
SCIENCE APPLICATIONS INTL. CORP.
1710 GOODRIDGE DR.
MC LEAN, VA 22102
USA

S. MIRSKY
SCIENCE APPLICATIONS INTL. CORP.
1710 GOODRIDGE DRIVE
MCLEAN, VA 22102
USA

D. MODEEN
NUMARC
1776 EYE STREET N.W. SUITE 300
WASHINGTON, DC 20006
USA

S. MODRO
EG&G IDAHO, INC.
4417 S. HOLMES AVE.
IDAHO FALLS, ID 83404
USA

K. MOKHTARIAN
CBI TECHNICAL SERVICES
800 JORIE BLVD.
OAK BROOK, IL 60521
USA

F. MOODY
GE NUCLEAR ENERGY
175 CURTNER AVENUE
SAN JOSE, CA 95125
USA

N. MORAY
UNIVERSITY OF ILLINOIS
DEPT. OF MECH. & IE
URBANA, IL 61801
USA

D. MORRISON
MITRE CORPORATION
7525 COLSHIRE DRIVE
MCLEAN, VA 22102
USA

V. MUBAYI
BROOKHAVEN NATIONAL LABORATORY
BUILDING 130
UPTON, NY 11973
USA

M. MUHLHEIM
OAK RIDGE NATIONAL LABORATORY
P.O. BOX 2009, MS-8065
OAK RIDGE, TN 37831-8065
USA

M. MURASE
HITACHI LTD.
1168 MORIYAMA-CHO
HITACHI-SHI, IBARAKI 316
JAPAN

K. MURATA
SANDIA NATIONAL LABORATORIES
P.O. BOX 5800
ALBUQUERQUE, NM 87185-5800
USA

S. NAFF
EG&G IDAHO, INC.
P.O. BOX 1625
IDAHO FALLS, ID 83415
USA

H. NAGASAKI
NUPEC-NUCLEAR POWER ENG. TEST CENTER
3-17,1-CHOME,TORANOMON,MINATO-KU
TOKYO, 105
JAPAN

T. NAKAYAMA
HITACHI WORKS, HITACHI LTD.
1-1, 3-CHOME, SAIWAI-CHO
HITACHI-SHI, IBARAKI-KEN 317
JAPAN

K. NAMATAME
JAPAN ATOMIC ENERGY RES. INST
TOKAI-MURA, NAKA-GUN
IBARAKI-KEN, 319-11
JAPAN

H. NARIAI
UNIVERSITY OF TSUKUBA
1-CHOME, TENNODAI
TSUKUBA-SHI, IBARAKI-KEN 305
JAPAN

D. NAUS
OAK RIDGE NATIONAL LABORATORY
P.O. BOX 2009
OAK RIDGE, TN 37831-8063
USA

C. NEGIN
GROVE ENGINEERING
15215 SHADY GROVE RD., STE. 202
ROCKVILLE, MD 20850
USA

A. NELSON
US GEOLOGICAL SURVEY
P.O. BOX 25046
DENVER, CO 80225
USA

W. NELSON
EG&G IDAHO, INC.
PO BOX 1625
IDAHO FALLS, ID 83415
USA

S. NESBIT
DUKE ENGINEERING & SERVICES, INC
800 MARYLAND AVE., SW, . JITE 890
WASHINGTON, DC 20024
USA

J. NESTELL
MPR ASSOCIATES, INC
1050 CONNECTICUT AVE, NW
WASHINGTON, DC 20036
USA

MAW NI
ATOMIC ENERG. / COUNCIL
67 LANE 144 KEELUNG RD, SECT 4
TAIPEI, TAIWAN
ROC

M. NICHOLS
UNIVERSITY OF MINNESOTA
271 19TH AVE SOUTH
MINNEAPOLIS, MN 55455
USA

T. NISHIMOTO
JAPAN ELEC. POWER INFORMATION CENTER
1726 M ST., NW, STE. 403
WASHINGTON, DC 20036
USA

H. NIU
ATOMIC ENERGY COUNCIL
67 LANE 144 KEELUNG RD, SECT 4
TAIPEI, TAIWAN 10772
ROC

A. NONAKA
NUPEC-NUCLEAR POWER ENG. TEST CENTER
3-13,4-CHOME,TORANOMON,MINATO-KU
TOKYO, 105
JAPAN

H. NOURBAKHSH
BROOKHAVEN NATIONAL LABORATORY
BUILDING 130
UPTON, NY 11973
USA

J. O'BRIEN
EG&G IDAHO, INC.
301 RANCH DR.
IDAHO FALLS, ID 83404
USA

D. O'MALLEY
TITAN CORP.
4201 CATHEDRAL AVE, NW APT 1410W
WASHINGTON, DC 20016
USA

S. OBERMEIRER
US GEOLOGICAL SURVEY
922 NATIONAL CENTER
RESTON, VA 22092
USA

Y. OCHI
COMPUTER SOFTWARE DEVELOPMENT
2-4-1,SHIBA KOEN
TOKYO, MINATO-KU 105
JAPAN

R. ODETTE
UNIVERSITY OF CALIFORNIA, SANTA BARBARA
DEPT. OF CHEM. & NUCLEAR ENGINEER
SANTA BARBARA, CA 93106
USA

B. OLAND
OAK RIDGE NATIONAL LABORATORY
P.O. BOX 2009
OAK RIDGE, TN 37831-8063
USA

R. OLMSTEAD
AECL RESEARCH
CHALK RIVER LABORATORY
CHALK RIVER, ONTARIO K0J1J0
CANADA

R. OLSON
BALTIMORE GAS & ELECTRIC CO.
P.O. BOX 1535
LUSBY, MD 20657
USA

A. ONYEMAECHI
S3 TECHNOLOGIES
8930 STANFORD BLVD.
COLUMBIA, MD 21045
USA

M. ORTIZ
EG&G IDAHO, INC.
P.O. BOX 1625 M/S 2404
IDAHO FALLS, ID 83415-2402
USA

L. OTT
OAK RIDGE NATIONAL LABORATORY
P.O. BOX 2009
OAK RIDGE, TN 37831-8057
USA

N. PAL
PAL CONSULTANTS INC
1885 THE ALAMED STREET 100H
SAN JOSE, CA 951.
USA

D. PALMROSE
EG&G IDAHO, INC.
P.O. BOX 1625 M/S 2404
IDAHO FALLS, ID 83415-2412
USA

F. PANISKO
BATTELLE-PACIFIC NORTHWEST LABS.
P.O. BOX 999
RICHLAND, WA 99352
USA

M. PARADIES
SYSTEM IMPROVEMENTS, INC.
238 PETERS ROAD,SUITE 301
KNOXVILLE, TN 37923
USA

S. PARISH
COUNCIL FOR NUCLEAR SAFETY
P.O. BOX 7106
HENNOPSMEER 0046
SOUTH AFRICA

M. PARKS
SANDIA NATIONAL LABORATORIES
P.O. BOX 5800, DIVISION 6473
ALBUQUERQUE, NM 87185-5800
USA

W. PASEDAG
U.S. DEPARTMENT OF ENERGY
NE-42
WASHINGTON, DC 20585
USA

M. PATTERSON
SCIENTECH, INC
11821 PARKLAWN DRIVE
ROCKVILLE, MD 20852
USA

P. PAUL
DUKE POWER CO
P.O. BOX1006
CHARLOTTE, NC 28201
USA

A. PAYNE, JR.
SANDIA NATIONAL LABORATORIES
P.O. BOX 5800, DIVISION 6412
ALBUQUERQUE, NM 87185-5800
USA

W. PENNELL
OAK RIDGE NATIONAL LABORATORY
P.O. BOX 2009
OAK RIDGE, TN 37831-8056
USA

K. PEREIRA
ATOMIC ENERGY CONTROL BOARD
P.O.BOX 1046, STATION B
OTTAWA, ONTARIO K1P 5S9
CANADA

G. PEREZ
CNSNS-MEXICO
AV. INSURGENTES SUR, 1776
MEXICO CITY, 01030
MEXICO

G. PETRANGELI
ENEA-DISP
VIA V. BRANCATI, 48
ROME, 00144
ITALY

J. PHILLIPS
EG&G IDAHO, INC.
P.O. BOX 1625 MS-2406
IDAHO FALLS, ID 83415-1560
USA

L. PHILPOT
GILBERET/COMMONWEALTH
P.O. BOX 1498
READING, PA 19603
USA

B. PIKUL
MITRE CORPORATION
7525 COLSHIRE DRIVE
MCLEAN, VA 22102
USA

G. PINO
ENEA-DISP
VIA V. BRANCATI, 48
ROME, 00144
ITALY

M. PODOWSKI
RPI, TROY NEW YORK
DEPT. OF NUCLEAR ENGINEERING
TROY, NY 12180-3592
USA

S. POPE
HALLIBURTON NUS
18804 LINDENHOUSE RD.
GAITHERSBURG, MD 20879
USA

L. PRICE
EG&G IDAHO, INC.
P.O. BOX 1625
IDAHO FALLS, ID 83415-2406
USA

J. PUGA
UNESA
P.O. GERVAS 3
MADRID, 28020
SPAIN

C. PUGH
OAK RIDGE NATIONAL LABORATORY
P.O. BOX 2009, MS 8063
OAK RIDGE, TN 37922
USA

D. RAKOVICH
ONTARIO HYDRO
700 UNIVERSITY AVE
TORONTO, ONTARIO M5G 1X6
CANADA

J. RANTAKIVI
FINNISH CENTRE FOR RAD. & NUCL. SAFETY
P.O. BOX 268
HELSINKI, SF-00101
FINLAND

W. REECE
EG&G IDAHO, INC.
P.O. BOX 1625 MS-2405
IDAHO FALLS, ID 83404
USA

J. REMPE
EG&G IDAHO, INC.
P.O. BOX 1625 MS-2508
IDAHO FALLS, ID 83404
USA

M. REOCREUX
CEA FRENCH ATOMIC ENERGY COMMISSION
CEN CADARACHE DRS/SEMAR
ST PAUL LEZ DURANCE, 13108
FRANCE

W. RETTIG
U.S. DEPARTMENT OF ENERGY
785 DOE PLACE
IDAHO FALLS, ID 83402
USA

L. RIB
ABCL TECHNOLOGIES
15400 CALHOUN DRIVE, SUITE 100
ROCKVILLE, MD 20855
USA

M. RIGHTLEY
SANDIA NATIONAL LABORATORIES
P.O. BOX 5800, DIVISION 6483
ALBUQUERQUE, NM 87185-5800
USA

G. ROBINSON
PENN STATE UNIVERSITY
231 SAKETT BLDG.
UNIVERSITY PARK, PA 16802
USA

U. ROHATGI
BROOKHAVEN NATIONAL LABORATORY
BUILDING 475B
UPTON, NY 11973
USA

G. ROMBOLD
NUMARC
1776 EYE STREET NW, SUITE 300
WASHINGTON, DC 20006
USA

A. ROOSEBOOM
SZW/NUCLEAR SAFETY DEPARTMENT
KERSENGAARDE 215
vOORBURG, 2272NO
THE NETHERLANDS

E. ROTH
WESTINGHOUSE
1310 BEULAH ROAD
PITTSBURGH, PA 15217
USA

H. RYALS
BETTIS ATOMIC POWER LABORATORY
P.O. BOX 79
WEST MIFLIN, PA 15122
USA

B. SAFFELL
BATTELLE COLUMBUS
505 KING AVE
COLUMBUS, OH 43201
USA

R. SALIZZONI
WESTINGHOUSE SAVANNAH RIVER COMPANY
-SAVANNAH RIVER SITE
AIKEN, SC 29802
USA

P. SAMANTA
BROOKHAVEN NATIONAL LABORATORY
BUILDING 130
UPTON, NY 11973
USA

R. SAMMATARO
GENERAL DYNAMICS
75 EASTERN POINT ROAD
GROTON, CT 06340
USA

J. SANCHEZ
CSN
JUSTO DORADO 11
MADRID, 28040
SPAIN

O. SANDERVAG
SWEDISH NUCLEAR POWER INSPECTORATE
P.O. BOX 27106
STOCKHOLM, S-102 52
SWEDEN

L. SANTOMA'
CSN
JUSTO DORADO 11
MADRID, 28040
SPAIN

M. SARRAM
UNITED ENGINEERS
30 S. 17TH ST.
PHILADELPHIA, PA 19101
USA

K. SATO
HITACHI,LTD
3-1-1 SAIWAI-CHO
HITACHI-SHI, IBARAKI-KEN 317
JAPAN

R. SCHMIDT
BATTELLE COLUMBUS
505 KING AVE.
COLUMBUS, OHIO 43201
USA

R. SCHNEIDER
ABB/C-E
1000 PROSPECT HILL ROAD
WINDSOR, CT 06095
USA

G. SCHUECKTANZ
UNIVERSAL TESTING LABORATORIES
5959 SHALLOWFORD RD., SUITE 531
CHATANOOGA, TN 37421
USA

E. SCHULTZ
INDUSTRIAL POWEP CO. LTD -TVO
27160 OLKILUOTO
SUOMI, SF-27160
FINLAND

G. SCHWARZ
ATOMIC ENERGY CONTROL BOARD
270 ALBERT ST.
OTTAWA, ONTARIO K1P 5S9
CANADA

W. SEDDON
HM NUCLEAR INSTALLATIONS INSPECTORATE
ST. PETERS HOUSE, BALLIOL ROAD
BOOTLE, MERSEYSIDE L20 3LZ
UK

B. SEHGAL
ELECTRIC POWER RESEARCH INSTITUTE
3412 HILLVIEW AVE, P.O. BOX 10412
PALO ALTO, CA 94303
USA

S. SERHAN
GILBERT/COMMONWEALTH
P.O. BOX 1498
READING, PA 19603
USA

S. SETH
MITRE CORPORATION
7525 COLSHIRE DRIVE
MCLEAN, VA 22102
USA

W. SHA
ARGONNE NATIONAL LABORATORY
9700 S. CASS AVENUE
ARGONNE, IL 60439
USA

W. SHACK
ARGONNE NATIONAL LABORATORY
9700 S. CASS AVENUE, BLDG 212
ARGONNE, IL 60439
USA

R. SHARMA
AMERICAN ELECTRIC POWER
ONE RIVERSIDE PLAZA
COLUMBUS, OHIO 43215
USA

I. SHARON
QUANTUM TECHNOLOGIES
2626 BUTTERFIELD RD.
OAKBROOK, IL 60521
USA

K. SHIBA
JAPAN ATOMIC ENERGY RES. INST
TOKAI-MURA, NAKA-GUN
IBARAKI-KEN, 319-11
JAPAN

J. SHIN
ELASCO SERVICES, INC.
TWO WORLD TRADE CENTER
NEW YORK, NY 10048
USA

J. SIENICKI
ARGONNE NATIONAL LABORATORY
9700 S. CASS AVENUE, BLDG 206
ARGONNE, IL 60439
USA

F. SIMONOM
BATTELLE-PACIFIC NORTHWEST LABS.
P.O. BOX 999
RICHLAND, WA 99352
USA

A. SIMPKINS
WESTINGHOUSE SAVANNAH RIVER COMPANY
SAVANNAH RIVER SITE
AIKEN, SC 29808
USA

C. SLATER
EG&G IDAHO, INC.
P.O. BOX 1625
IDAHO FALLS, ID 83404
USA

G. SLAUGHTER
OAK RIDGE NATIONAL LABORATORY
P.O. BOX 2008, BLDG 4500S
OAK RIDGE, TN 37831-6152
USA

S. SLOAN
EG&G IDAHO, INC.
PO BOX 1625
IDAHO FALLS, ID 83415
USA

G. SLOVIK
BROOKHAVEN NATIONAL LABORATORY
BUILDING 475B
UPTON, NY 11973
USA

L. SMITH
LOS ALAMOS NATIONAL LABORATORY
P.O. BOX 1663, MS E561
LOS ALAMOS, NM 87544
USA

K. SODA
JAPAN ATOMIC ENERGY RES. INST
TOKAI-MURA, NAKA-GUN
IBARAKIKEN, 319-11
JAPAN

M. SOEJIMA
MITSUBISHI HEAVY INDUSTRIES, LTD.
1-1,1-CHOME,WADASAKI-CHO,HYOGO-KU
KOBE-SHI, 652
JAPAN

C. SORRELL
VIRGINIA POWER
5000 DOMINION BLVD.
GLEN ALLEN, VA 23060
USA

W. SPEZIALETTI
WESTINGHOUSE SAVANNAH RIVER COMPANY
37 VARDEN DRIVE
AIKEN, SC 29803
USA

K. STAHLKOPF
ELECTRIC POWER RESEARCH INSTITUTE
3412 HILLVIEW AVE., P.O. BOX 10412
PALO ALTO, CA 94303
USA

R. STAROK
MPR ASSOCIATES, INC
1050 CONNECTICUT AVE. NW
WASHINGTON, DC 20036
USA

M. STRAND
JUPITER CORPORATION
2730 UNIVERSITY BLVD. WEST, #403
WHEATON, MD 20902
USA

D. STRAWSON
MPR ASSOCIATES, INC
1050 CONNECTICUT AVE, NW
WASHINGTON, DC 20036
USA

E. STURBE
TRACTEBEL
AV. ARIANE 7
BRUSSELS, B-1200
BELGIUM

M. SUBUDHI
BROOKHAVEN NATIONAL LABORATORY
BUILDING 130
UPTON, NY 11973
USA

K. SUH
FAUSKE & ASSOCIATES
16W070 W. 83RD ST
BURR RIDGE, IL 60521
USA

R. SUMMERS
SANDIA NATIONAL LABORATORIES
P.O. BOX 5800, DIVISION 6418
ALBUQUERQUE, NM 87185-5800
USA

J. SUN
ARGONNE NATIONAL LABORATORY
9700 S. CASS AVENUE
ARGONNE, IL 60439
USA

M. TAEB
S3 TECHNOLOGIES
8930 STANFORD BLVD.
COLUMBIA, MD 21045
USA

H. TAKEDA
NUPEC-NUCLEAR POWER ENG. TEST CENTER
3-13,4-CHOME,TORANOMON,MINATO-KU
TOKYO, 105
JAPAN

K. TAKUMI
NUPEC-NUCLEAR POWER ENG. TEST CENTER
3-13,4-CHOME,TORANOMON,MINATO KU
TOKYO, 105
JAPAN

J. TAYLOR
BROOKHAVEN NATIONAL LABORATORY
BUILDING 130
UPTON, NY 11973
USA

T. THEOFANOUS
UNIVERSITY OF CALIFORNIA, SANTA BARBARA
6740 CORTONE DR.
SAN GOLETA, CA 93117
USA

W. THOMAS
QUANTUM TECHNOLOGY, INC.
2625 BUTTERFIELD RD.
OAK BROOK, IL 60521
USA

S. THOMPSON
SANDIA NATIONAL LABORATORIES
P.O. BOX 5800, DIVISION 6418
ALBUQUERQUE, NM 87185-5800
USA

H. THORNBURG
ABB ATOM, INC.
901 S. WARFIELD DRIVE
MT. AIRY, MD 21771
USA

J. TILLS
JACK TILLS & ASSOCIATES, INC.
PO BOX 549
SANDIA PARK, NM 87047
USA

D. TONG
AEA TECHNOLOGY, SRD
WIGSHAW LANE
CULCHETH, CHESHIRE WA3 4NE
UK

T. TRAN
WESTINGHOUSE SAVANNAH RIVER COMPANY
SAVANNAH RIVER SITE
AIKEN, SC 29808
USA

P. TROY
NEWMAN & HOLTZINGER
1615 L STREET, N.W.
WASHINGTON, DC 20036
USA

J. TUCCIARONE
WESTINGHOUSE SAVANNAH RIVER COMPANY
SAVANNAH RIVER SITE
AIKEN, SC 29808
USA

M. TUTTLE
LAMONT-DOHERTY GEOLOGICAL OBS
COLUMBIA UNIVERSITY
PALISADES, NY 10964
USA

K. UMEKI
NUPEC-NUCLEAR POWER ENG. TEST CENTER
3-13,4-CHOME,TORANOMON,MINATO-KU
TOKYO, 105
JAPAN

L. UNGER
SYSTEM IMPROVEMENTS
238 PETERS BLVD., SUITE 301
KNOXVILLE, TN 37923
USA

R. VALENTIN
ARGONNE NATIONAL LABORATORY
9700 S. CASS AVENUE, BLDG 308
ARGONNE, IL 60439
USA

S. VAN HEMEL
STAR MOUNTAIN, INC.
113 CLERMONT AVENUE
ALEXANDRIA, VA 22304
USA

J. VEEDER
AECL RESEARCH
CHALK RIVER LABORATORY
CHALK RIVER, ONTARIO K0J1J0
CANADA

R. VOGEL
CONSULTANT
2081 ROBIN HOOD LANE
LOS ALTOS, CA 94024
USA

W. VON RIESEMANN
SANDIA NATIONAL LABORATORIES
P.O. BOX 5800, DIVISION 6473
ALBUQUERQUE, NM 87185-5800
USA

R. VOSS
WESTINGHOUSE SAVANNAH RIVER COMPANY
SAVANNAH RIVER SITE
AIKEN, SC 29808
USA

B. WALSH
SCIENCE & ENGINEERING ASSOCIATES, INC.
6100 UPTOWN BLBD., NE
ALBUQUERQUE, NM 87110
USA

D. WALTERS
NUMARC
1776 EYE STREET NW, SUITE 300
WASHINGTON, DC 20006
USA

S. WANG
INSTITUTE OF ENERGY RESEARCH, AEC
P.O. BOX 3-3
LUNG-TAN, 32500
TAIWAN

L. WARD
EG&G
11426 ROCKVILLE PIKE, SUITE 300
ROCKVILLE, MD 20852
USA

K. WASHINGTON
SANDIA NATIONAL LABORATORIES
P.O. BOX 5800, DIVISION 6429
ALBUQUERQUE, NM 87185-5800
USA

R. WATSON
SANDIA NATIONAL LABORATORIES
P.O. BOX 5800, DIVISION 6473
ALBUQUERQUE, NM 87185-5800
USA

J. WERNER
U.S. DEPARTMENT OF ENERGY
785 DOE PLACE
IDAHO FALLS , ID 83402
USA

P. WHEATLEY
EG&G IDAHO, INC.
P.O. BOX 1625 M/S 2412
IDAHO FALLS, ID 83415-2412
USA

D. WHITEHEAD
SANDIA NATIONAL LABORATORIES
P.O. BOX 5800, DIVISION 6412
ALBUQUERQUE, NM 87185
USA

B. WHITESEL
NUMARC
1776 EYE STREET NW, SUITE 300
WASHINGTON, DC 20006
USA

K. WHITT
SOUTHERN NUCLEAR
40 INVERNESS CENTER PARKWAY
BIRMINGHAM, AL 35201
USA

G. WILKOWSKI
BATTELLE COLUMBUS
505 KING AVE.
COLUMBUS, OHIO 43201
USA

K. WILLIAMS
SCIENCE APPLICATIONS INTL. CORP.
2109 AIR PARK RD., S. E.
ALBUQUERQUE, NM 87106
USA

J. WILSON
AEA TECHNOLOGY
HARWELL LABORATORY
DIDLOT, OXFORDSHIRE OX11 ORA
UK

H. WINGO
WESTINGHOUSE SAVANNAH RIVER COMPANY
SAVANNAH RIVER SITE
AIKEN, SC 29808
USA

G. WIRE
WESTINGHOUSE
5893 KEYSTONE DR.
BETHEL PARK, PA 15102
USA

F. WITT
WESTINGHOUSE
P.O. BOX 2728
PITTSBURGH, PA 15230-2728
USA

M. WITTE
LAWRENCE LIVERMORE NATIONAL LAB
P.O. BOX 808, L-196
LIVERMORE, CA 94550
USA

L. WOLF
KFK/PMDR, BATTELLE-EUROPE
POSTFACH 900160,AM ROMESHOF 35
FRANKFURT AM MAIN 90, 6000
GERMANY

L. WOLF
NATIONAL ACADEMY OF SCIENCE
2101 CONSTITUTION AVENUE NW
WASHINGTON, DC 20418
USA

N. WOODY
WESTINGHOUSE SAVANNAH RIVER COMPANY
SAVANNAH RIVER SITE
AIKEN, SC 29808
USA

W. WULFF
BROOKHAVEN NATIONAL LABORATORY
BUILDING 475B
UPTON, NY 11973
USA

M. YOKOTA
TOKYO ELECTRIC POWER
1901 L ST N.W. SUITE 720
WASHINGTON, DC 20036
USA

K. YOON
B&W NUCLEAR SERVICE
PO BOX 10935
LYNCHBURG, VA 24503
USA

R. YOUNGBLOOD
BROOKHAVEN NATIONAL LABORATORY
BUILDING 130
UPTON, NY 11973
USA

G. ZIGLER
SCIENCE & ENGINEERING ASSOCIATES, INC.
6100 UPTOWN BLBD., NE
ALBUQUERQUE, NM 87110
USA

F. ZIKRIA
HALLIBURTON NUS CORP.
910 KLOPPER ROAD
GAITHERSBURG, MD 20878
USA

P. ZMOLA
C & P ENGINEERING
5408 NEWINGTON ROAD
BETHESDA, MD 20816
USA

R. ZOGRAN
MPR ASSOCIATES, INC.
1050 CONNECTICUT AVE. NW
WASHINGTON, DC 20036
USA

F. ZWICKY
BASLER & HOFMANN
FORCHSTRASSE 395
ZURICH, 8029
SWITZERLAND

PROCEEDINGS OF THE
NINETEENTH WATER REACTOR SAFETY INFORMATION MEETING
October 28-30, 1991

CONTENTS - VOLUME 2

BWR LOWER PLENUM DEBRIS BED MODELS FOR MELCOR

S. A. Hodge, L. J. Ott

Oak Ridge National Laboratory
Oak Ridge, Tennessee 37831

ABSTRACT

Work is underway at Oak Ridge National Laboratory (ORNL) to incorporate certain models of the Boiling Water Reactor Severe Accident Response (BWRSAR) code into a local version of MELCOR. Specifically, the BWR lower plenum debris bed and bottom head response models taken from BWRSAR are being tested within the local MELCOR code structure. Upon successful completion of testing, recommendations for formal adoption of these models will be made to the Nuclear Regulatory Commission (NRC) and to the MELCOR code development staff at Sandia National Laboratories (SNL). The SNL code development staff retain exclusive responsibility for maintaining the configuration control for the official version of MELCOR.

The BWR lower plenum debris bed and bottom head response models permit the calculation of heatup, melting, and relocation of the debris after dryout. They predict the response of the lower plenum internal structures and the bottom head as well as the composition and timing of material release from the vessel. They have been previously applied in severe accident analyses for the Containment Performance Improvement (CPI) Program and the Mark I shell survivability study (NUREG/CR-5423), and in recent assessments of candidate accident management strategies.

This paper provides a brief description of the purpose and operation of these models.

1. INTRODUCTION

Boiling Water Reactors (BWRs) have unique features (Figures 1-4) for which special models must be provided if best-estimate severe accident calculations are to be performed. The Boiling Water Reactor Severe Accident Technology (BWRSAT) Program at ORNL has developed and incorporated into its BWRSAR code several advanced models for application to BWR severe accident analyses[1,2,3]. All of these models have been made publicly available as they were developed, tested, and used in ongoing BWR severe accident studies at Oak Ridge. Many, particularly the earlier models applicable to the period of the accident sequence before relocation of core material into the lower plenum, have been incorporated into other codes such as MELCOR[4,5]. The lower plenum debris bed formation and behavior models, however, remained unique to the BWRSAR code until recently.

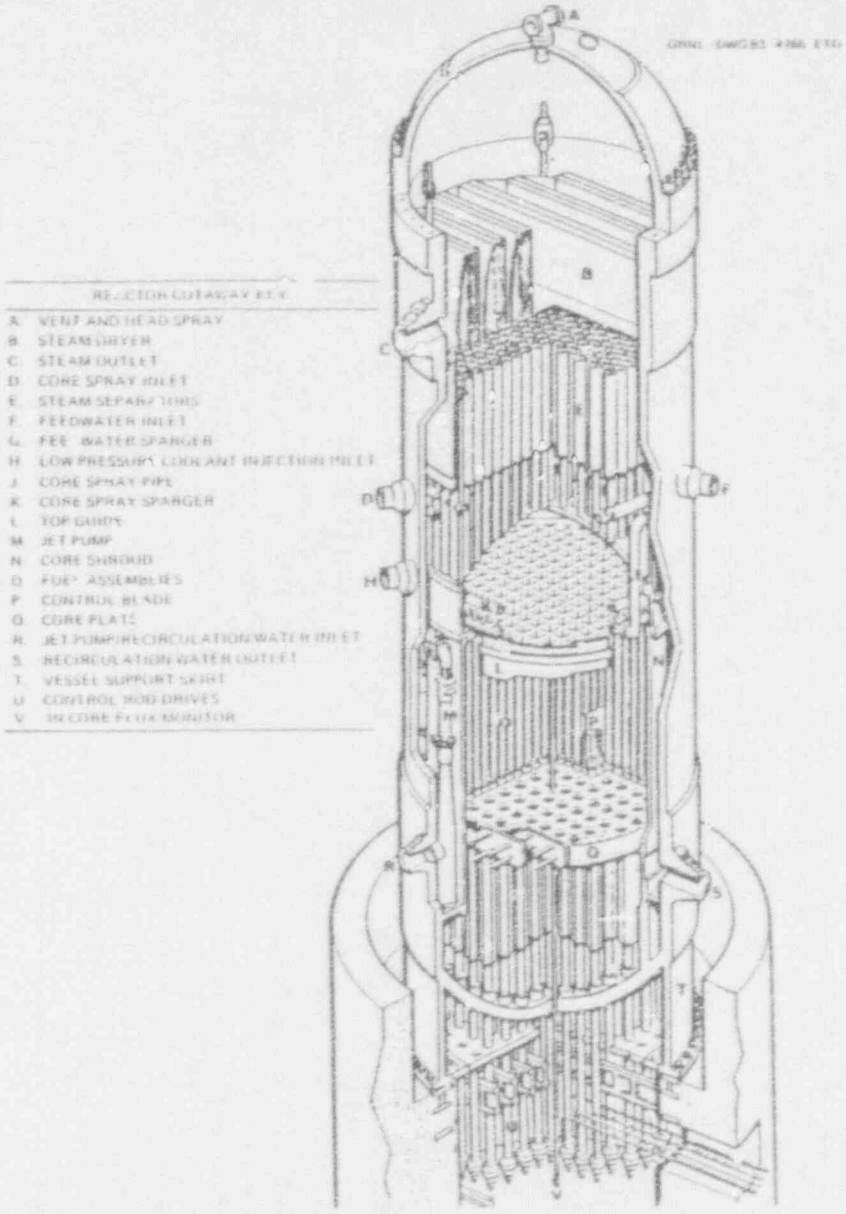

Fig. 1. Identification of BWR reactor vessel internal components. The core plate (Q) separates the core region from the lower plenum.

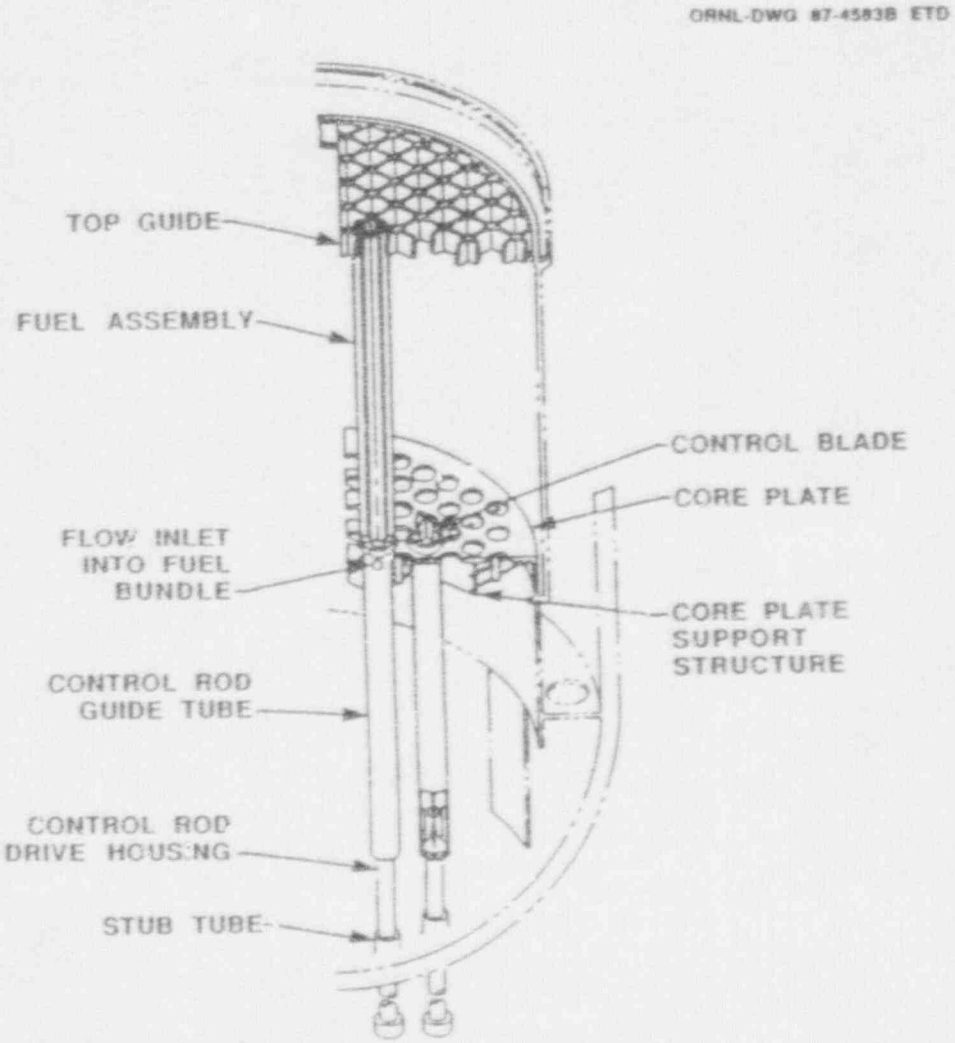

Fig. 2. Arrangement of BWR core, core plate, control rod guide tubes, and supporting components.

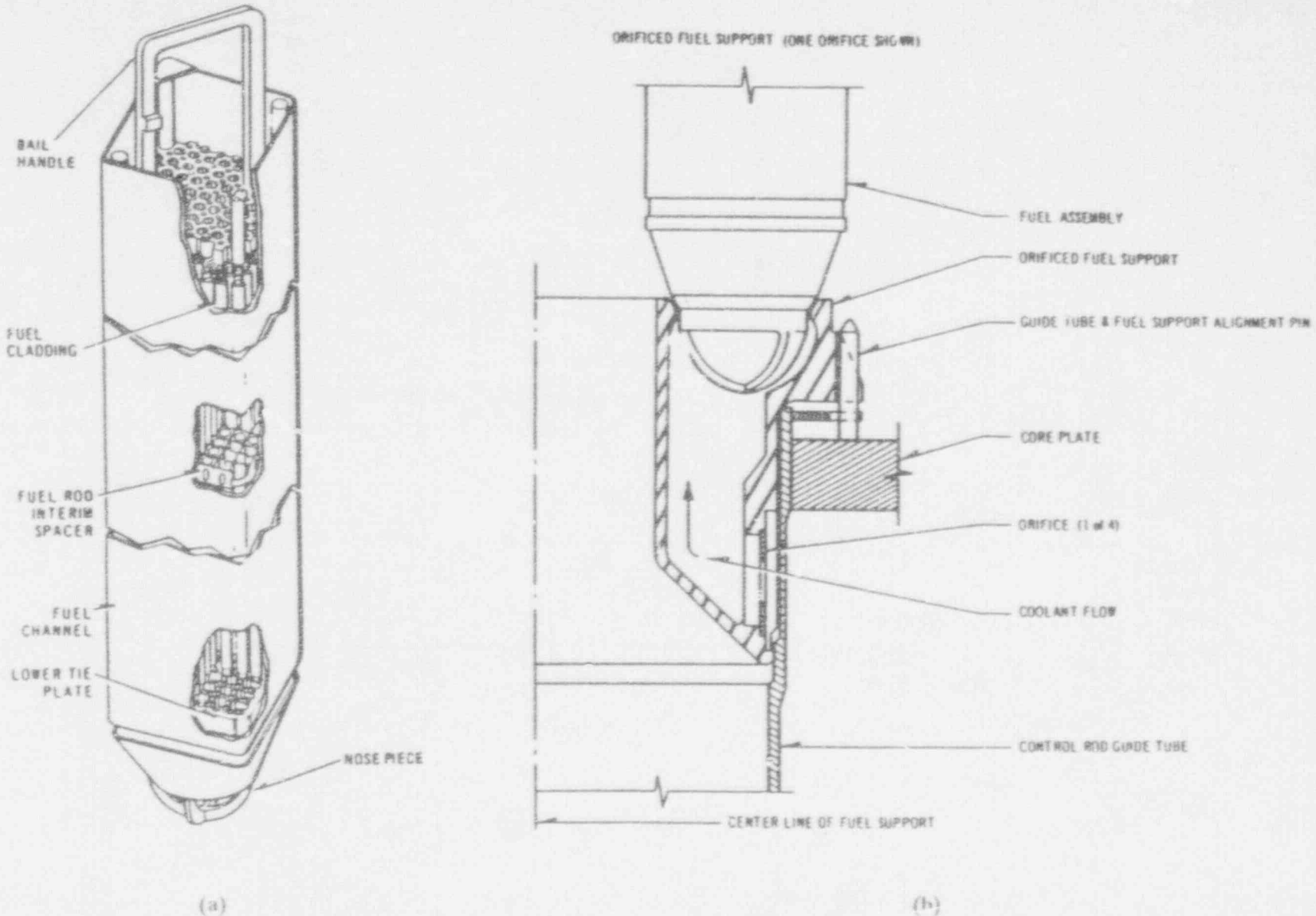

Fig. 3. BWR fuel assembly (a) and method of support (b) by orificed fuel support piece and control rod guide tube.

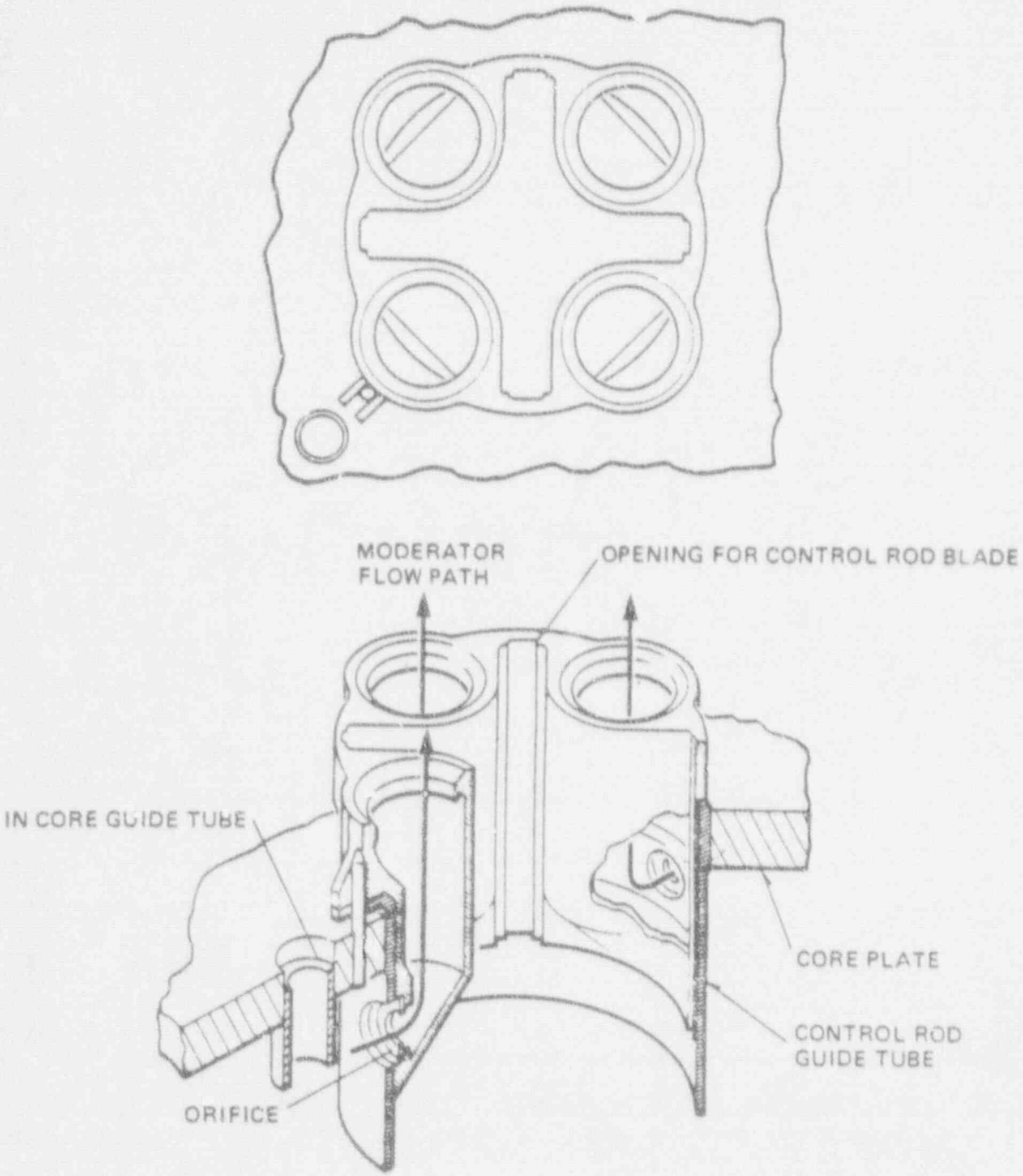

Fig. 4. Arrangement of a fuel support piece and coolant flow paths from the vessel lower plenum into the four fuel assemblies that it supports.

It is the purpose of this paper to explain the operation of the lower plenum debris bed and bottom head response models including the practical improvements made prior to transposition of this modeling approach into the more general MELCOR code, which will be employed in future BWR severe accident studies at ORNL. The discussion begins with a brief description of the events leading to movement of relocating core structural material beyond the core plate and the corresponding accumulation of debris in the reactor vessel lower plenum. The representation of the structure of the bottom head debris beds and the calculational nodalization of the adjacent reactor vessel wall are then described in detail.

Finally, the modifications and improvements accomplished during the period of transposition of these models into MELCOR are discussed. The desirability of these practical modifications of and improvements to the lower plenum debris bed models was demonstrated during previous severe accident analysis applications.

2. DEBRIS BED FORMATION IN THE LOWER PLENUM

The following discussion provides a brief synopsis of the events leading to movement of relocating core structural material and fuel beyond the core plate and the accumulation of debris within the reactor vessel lower plenum. The illustrative dimensions given in this description are those applicable to the 638 cm (251 in.) ID BWR-4 reactor vessel installed at 1067 MWe plants such as Peach Bottom and Browns Ferry. Any discussion of the behavior of core debris relocated into the bottom head must begin with consideration of the role of the core plate, which serves as a boundary between the core region and the reactor vessel lower plenum.

2.1 MATERIAL RELOCATION AND CORE PLATE FAILURE

The primary function of the BWR core plate is to provide lateral alignment for the upper portion of the control rod guide tubes, as shown in Figures 1 and 2. Each of the 185 control rod guide tubes supports four fuel assemblies via an orificed fuel support piece as shown in Figure 3. It should be noted [Figure 3(b)] that the support piece rests within the upper portion of the control rod guide tube and that the core plate provides an alignment pin for proper location of both the guide tube and the support piece. An isometric drawing of the placement of the fuel support piece is provided in Figure 4, together with a plan view showing the cruciform opening for the control blade.

The core plate, which is 5.1 cm (2 in.) thick and weighs 9300 kg (20,500 lbs.), provides vertical support to only the 24 outermost fuel assemblies (of the 764 assemblies that make up the core). The support arrangement for these 24 peripheral assemblies is shown in Figure 5.

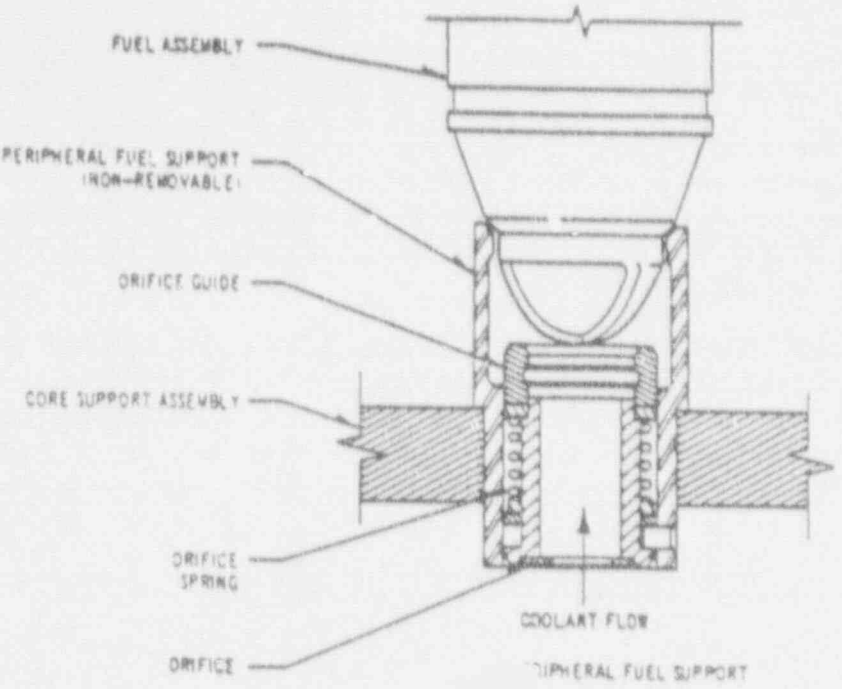

Fig. 5. Orifice arrangement for the outer fuel assemblies, the only assemblies supported by the core plate.

The stainless steel core plate is characterized by large holes [28 cm (11 in.) ID] to accommodate the passage of the control rod guide tubes and smaller holes [5.1 cm (2 in.) ID] for the in-core instrument guide tubes as shown in the plan view of Figure 6. The core plate is supported around the outer periphery and, thus, resembles a perforated drum membrane. There is, however, significant central support provided by the stiffener plates and stiffener rods indicated in Sections A-A and B-B of Figure 6.

Clearly the events to occur within the BWR reactor vessel lower plenum under severe accident conditions would depend upon the manner in which relocating materials from the core region were to pass the core plate boundary. Both MELCOR and BWRSAR have models to predict the downward relocation of core debris onto the core plate and the core plate response. These core degradation models are beyond the scope of this paper, but are discussed elsewhere[3,5].

Boiling water reactors are fitted with an Automatic Depressurization System (ADS) that, upon actuation, causes rapid opening of several (five at Peach Bottom) of the reactor vessel safety/relief valves (SRVs). The BWR Emergency Procedures Guidelines[6] direct the operators, under severe accident conditions, to manually actuate the ADS when the core has become partially uncovered (but before any significant core damage has occurred). The flashing attendant to the resulting rapid depressurization of the reactor vessel causes the loss of all water from the core region and core plate dryout. Without restoration of coolant injection to the reactor vessel (and termination of the accident sequence), the subsequent core heatup and degradation causes the downward movement of molten material onto the dry core plate.

At this point, a systematic discussion of the progression of severe accident events should include a detailed consideration of the expected response of the core plate to the accumulation of debris over its upper surface. This subject, however, is addressed in a separate report[7] prepared under the auspices of the BWR Core Melt Progression Phenomena Program. It will suffice here to

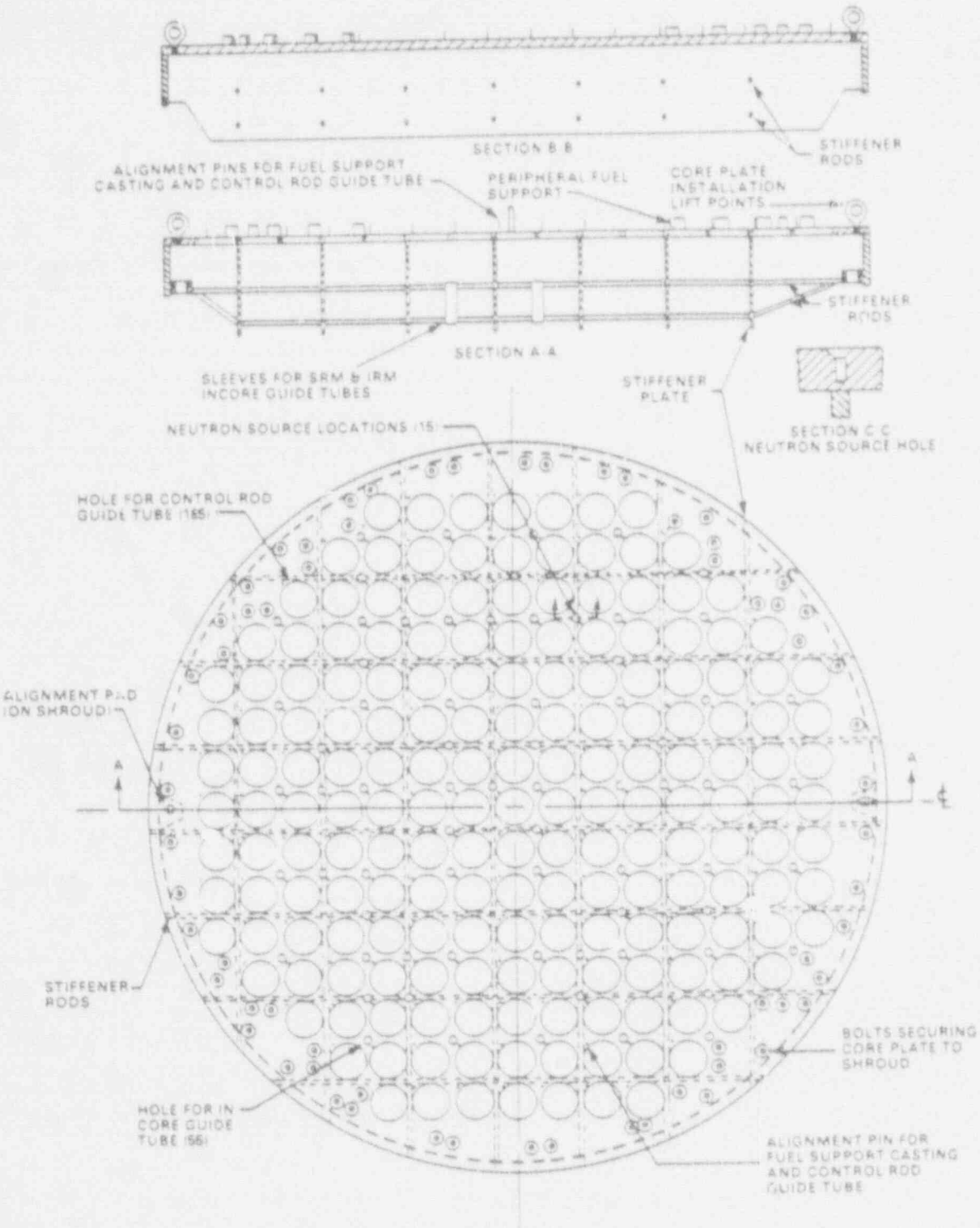

Fig. 6. Elevation and plan views of the BWR core plate.

point out that the available codes (APRIL, BWRSAR, MELCOR and SCDAP/RELAP) employ different approaches, all of which are addressed in Reference 7. Therefore, the following is limited to a brief review of the BWRSAR approach.

After core plate dryout, mass builds up over the core plate in a regular but somewhat discontinuous manner by the candling process over fuel rod cladding and by rapid relocation of molten control blade and channel box structural material (stainless steel and zirconium, respectively). The molten material freezes upon coming in contact with the core plate, and leakage through the intact core plate is not represented. Heat transfer from the relocated material increases the temperature of the core plate. Each radial region of the core plate is considered to fail due to the accumulated load and loss of strength when the regionally calculated mass-averaged temperature of the combined debris and core plate exceeds a user-specified temperature, usually 1420 K (2100°F). In practice, the mass-averaged temperature increases so rapidly after core plate dryout that adjusting the assumed failure temperature has little effect on the calculated time of failure.

Each failed core plate region and its accumulated debris fall into the lower plenum producing a burst of steam as the fallen materials is quenched. However, it is expected that the fuel pellet columns, encased in ZrO_2 sheaths, would remain standing since the weight of the fuel is supported by the control rod guide tubes, not by the core plate. After failure of a core plate region, additional relocating material in that radial region falls directly into the lower plenum. During the relocation process, material balances are performed to keep track of the individual material species (such as Fe, Zr, UO_2) as they accumulate on the core plate and in the lower plenum.

2.2 ACCUMULATION OF DEBRIS IN THE BOTTOM HEAD

Fortunately, the development of BWR reactor vessel lower plenum debris bed models can proceed without the necessity for prior resolution of the numerous uncertainties regarding the means by which relocating core and structural material might pass through the core plate boundary. This is true because the lower plenum models can be established in such a manner that they can be driven by information provided by a separate and independent core plate calculation. This is the approach that has been taken with the BWRSAR lower plenum debris bed and bottom head response models, which in effect are driven by the masses and associated energies entering from the core plate region. The operation of these models is described in Section 3.

Before leaving this discussion of the downward relocation of debris within the core region, however, it is important to recognize that the movement of debris might occur in a much more sudden and massive manner than that described previously. If much of the relocating molten core debris were to not reach the core plate, but instead were to form a frozen crust above the plate, subsequent debris bed formation and melting above the core plate would lead to an accident event sequence more like the Three Mile Island experience (PWR) than the sequence predicted by BWRSAR. Thus, the question of core plate survival in the BWR severe accident sequence is pivotal.

It should be noted that the BWRSAR models do predict retention and buildup of a debris bed above the core plate for cases in which the core plate is sufficiently cooled by reactor vessel water injection to forestall dryout, heatup, and structural failure. The required water injection rate is small if continuous, larger if the flow is intermittent and in both cases the integrated effect must be sufficient to prevent core plate failure but insufficient to terminate the accident. This scenario seems most unlikely for prolonged BWR severe accident sequences since any injection system, if available, is capable of injection rates ample to recover the core and terminate the accident although

operator action (specified in existing written procedures) would be necessary to enhance the flow in some cases. For this reason, the BWRSAR models for the progression of an unmitigated severe accident are based upon the assumption of a total loss of injection such as would occur in Station Blackout.

3. LOWER PLENUM DEBRIS BED AND BOTTOM HEAD RESPONSE MODELS

It is the purpose of this Section to explain the operation of the models that establish the lower plenum debris beds from the materials and associated energies passed from the core region through the core plate. The discussion begins with a brief description of the structures within the BWR lower plenum and the numerous penetrations of the bottom head itself. As before, the illustrative dimensions are those applicable to the 1067 MWe plants such as Peach Bottom and Browns Ferry.

3.1 DESCRIPTION OF THE BWR LOWER PLENUM

The portion of the BWR reactor vessel below the elevation of the core plate is formed by a cylindrical section of 638 cm (251 in.) ID joined with a hemispherical section of radius 319 cm (125-1/2 in.). As shown in Figures 1 and 2, much of the volume immediately beneath the core plate is occupied by the control rod guide tubes. Also passing through this volume are source range, intermediate range, and power range detector assemblies as indicated on Figures 7 and 8.

There are more than 200 bottom head penetrations as necessary to accommodate the 185 control rod drive mechanism assembly penetrations, 55 instrument tube penetrations, and a 5.1 cm (2 in.) drain line penetration near the low point of the head. The general arrangement of the in-core instrument housings and the stub tubes for the control rod drive mechanism assemblies is indicated in Figure 9.

The BWR bottom head is clad with Inconel [thickness 0.32 cm (0.125 in.)] while the control rod drive mechanism assembly and instrument guide tube penetrations are stainless steel. Cross-sections of the control rod drive mechanism assembly and instrument tube penetrations and their weldments are illustrated in Figure 10. Each in-core instrument tube is held in place by an Inconel-to-stainless steel weld located at the inner surface of the bottom head wall, whereas the control rod drive mechanism assemblies are held in place by similar welds at the upper ends of the Inconel stub tubes. These latter welds would be located about 10 cm (4 in.) within the lower plenum debris bed expected to be formed during an unmitigated BWR severe accident.

Given the perforated status of the BWR bottom head, it is reasonable to expect that the initial pressure boundary failure after lower plenum debris bed dryout would occur through the vessel penetrations and not by meltthrough of the 21 cm (8-7/16 in.) thick bottom head itself. The question of the mode of bottom head penetration failure has been the subject of separate analyses[8,9] and will not be addressed here.

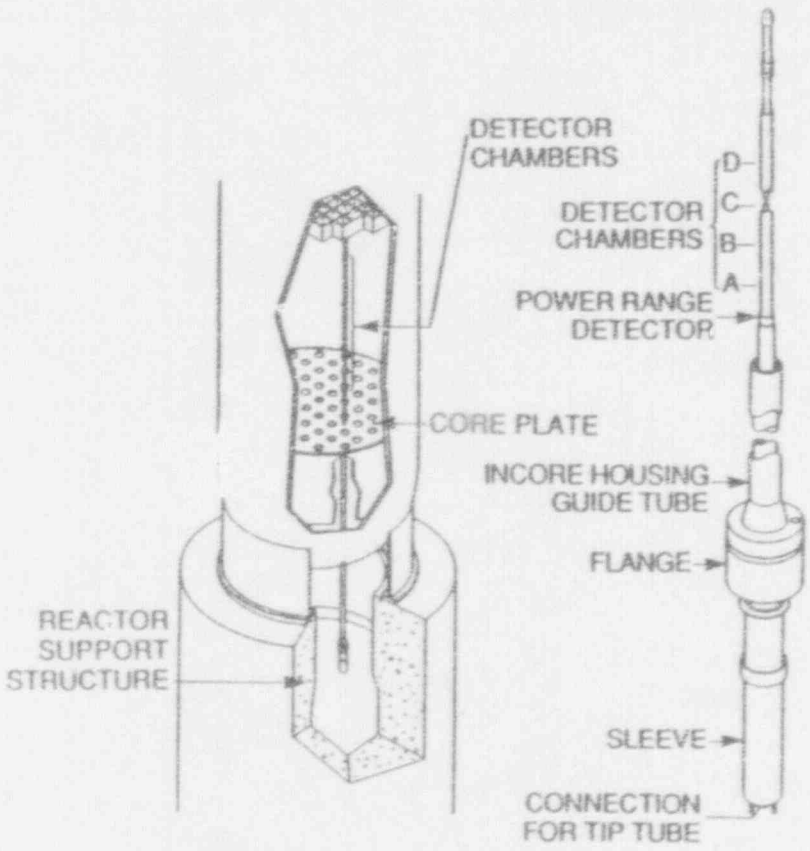

Fig. 7. Mechanical arrangement of one of the 43 local power range detector assemblies. The annular gap clearance between the in-core housing guide tube and the instrument tube is specified as 0.40 inches.

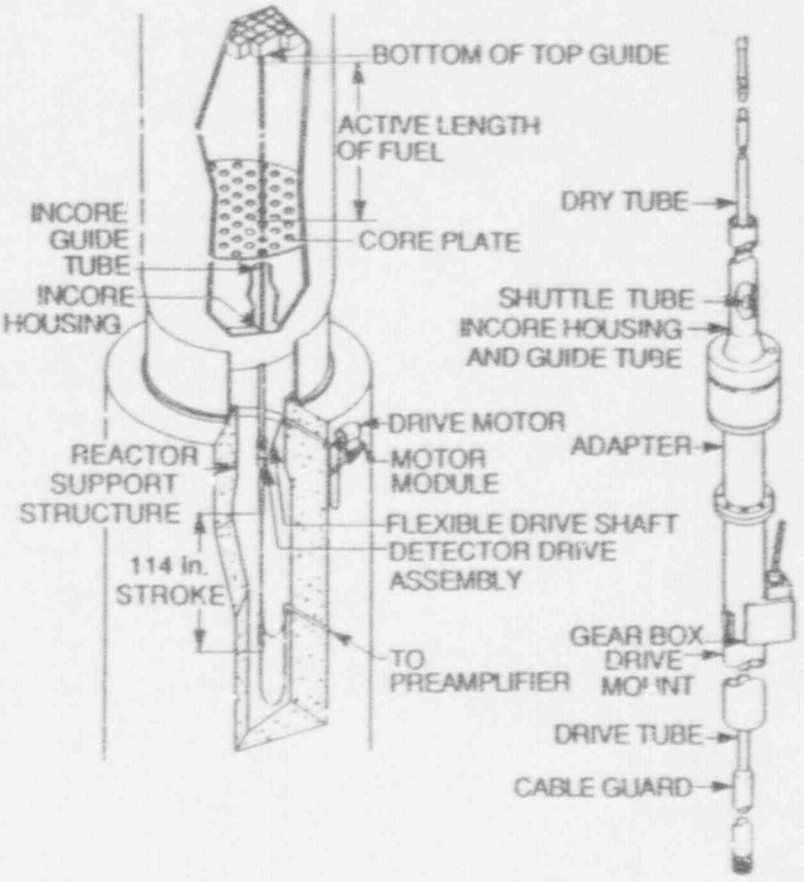

Fig. 8. Mechanical arrangement of the four source range and eight intermediate range detector in-core instrument assemblies.

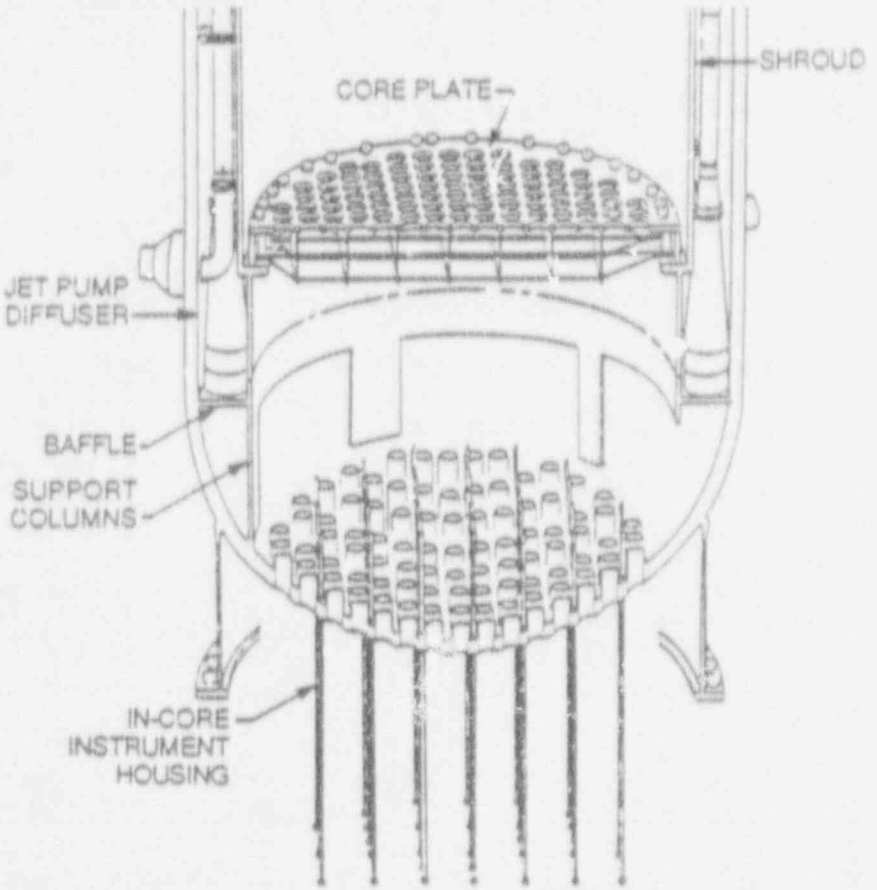

Fig. 9. The BWR reactor vessel bottom head accomodates 241 penetrations and therefore is thicker than the remainder of the reactor vessel pressure boundary.

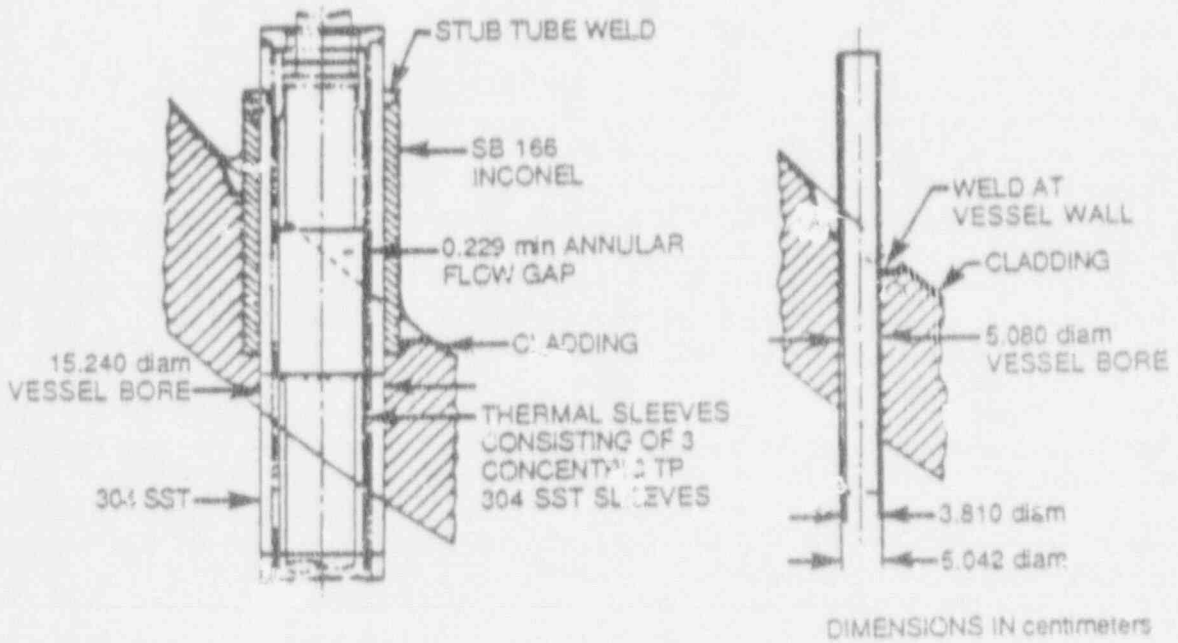

Fig. 10. The BWR control rod drive mechanism assemblies are held in place by stainless steel-to-Inconel welds at the upper ends of the stub tubes, whereas the in-core instrument tubes are supported by stainless steel-to-Inconel welds at the vessel wall.

3.2 QUENCHING OF THE RELOCATING DEBRIS

As discussed in Section 2, structural deformation and downward relocation of molten control blade, channel box, and candling clad material onto the dry core plate is expected to cause local creep rupture failures of the core plate and the introduction of relocating material into the lower plenum water. The models for dealing with this relocating material within the lower plenum debris bed are based upon the assumption that the water, while it lasts, would quench the debris.

The argument that the falling heated masses of core debris would be quenched in the reactor vessel lower plenum is buttressed by the geometry of the structures and the large water mass present in the BWR lower head. For the Peach Bottom example, there are 185 control rod guide tubes of 28 cm (11 in.) outer diameter on a 30.5 cm (12 in.) pitch in the vessel lower plenum; thus, within a unit cell, the debris must pass through a 0.032 m^2 (0.340 ft^2) opening (see Figure 11) that is 366 cm (12 ft) in length. This, plus the fact that there is sufficient water in the lower plenum [73000–95000 kg (160,000–210,000 lbs), depending on the temperature] to completely quench more than one molten core, leads to the assumption that the relocating debris is quenched as it falls through the water. It should be noted, given the progressive relocation from the core region, that the majority of the debris entering the lower plenum would be solid when it enters the water. The rate of quench of the relocated debris is determined by algorithms within the MELCOR COR package.

As the relocated core material accumulates in the BWR reactor vessel lower plenum, it is expected that the composition of the quenched debris bed would vary with height. Lowermost in the bed would be the mostly metallic debris (control blades, canisters, candled clad and dissolved fuel) that had either accumulated on the core plate before local plate failure or had subsequently relocated downward within the same local region before fuel pellet stack collapse. Higher, within the middle region of the bed, would be the collapsed fuel and ZrO_2 from the central region of the core. The initial local core plate structural failures would cause temporary bursts of steaming as the relocated metallic debris was quenched; however, with the collapse of the central core fuel pellet stacks, a constant heat source (the decay heat associated with the pellets would be introduced to the lower plenum reservoir, initiating a rapid continuous boiloff of the remaining water.

After lower plenum dryout, the debris bed temperature would increase, causing thermal attack and failure of the control rod guide tube structure in the lower plenum, which the debris would completely surround to a depth of about 3 m (10 ft). Since the control rod drive mechanism assemblies and the control rod guide tubes support the core, the remaining standing outer regions of the core would be expected to collapse into the vessel lower plenum when these support columns fail. Thus, the uppermost portion of the completed lower plenum debris bed should be composed of the collapsed metallic and fuel material from the relatively undamaged outer regions of the core. The stainless steel of the control rod guide tubes and mechanism assemblies would be subsumed into the surrounding debris as it becomes molten.

The lower plenum debris bed nodalization is illustrated in Figure 12 together with a brief description of the models employed for the calculation of the bed response. The vessel bottom head is represented at each debris bed node in contact with the wall, while the wall itself is sectioned into three radial segments with the outer segment capable of transferring heat to the containment (drywell) atmosphere. The debris bed and bottom head representations are described in greater detail in the following Sections.

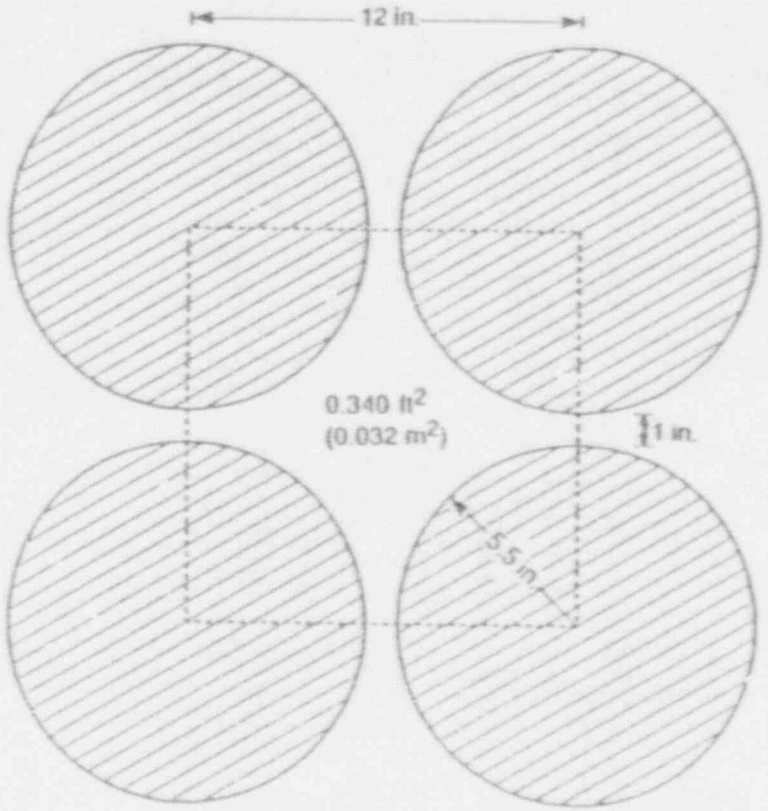

Fig. 11. Control rod guide tube spacing and available open flow area in the BWR reactor vessel bottom head.

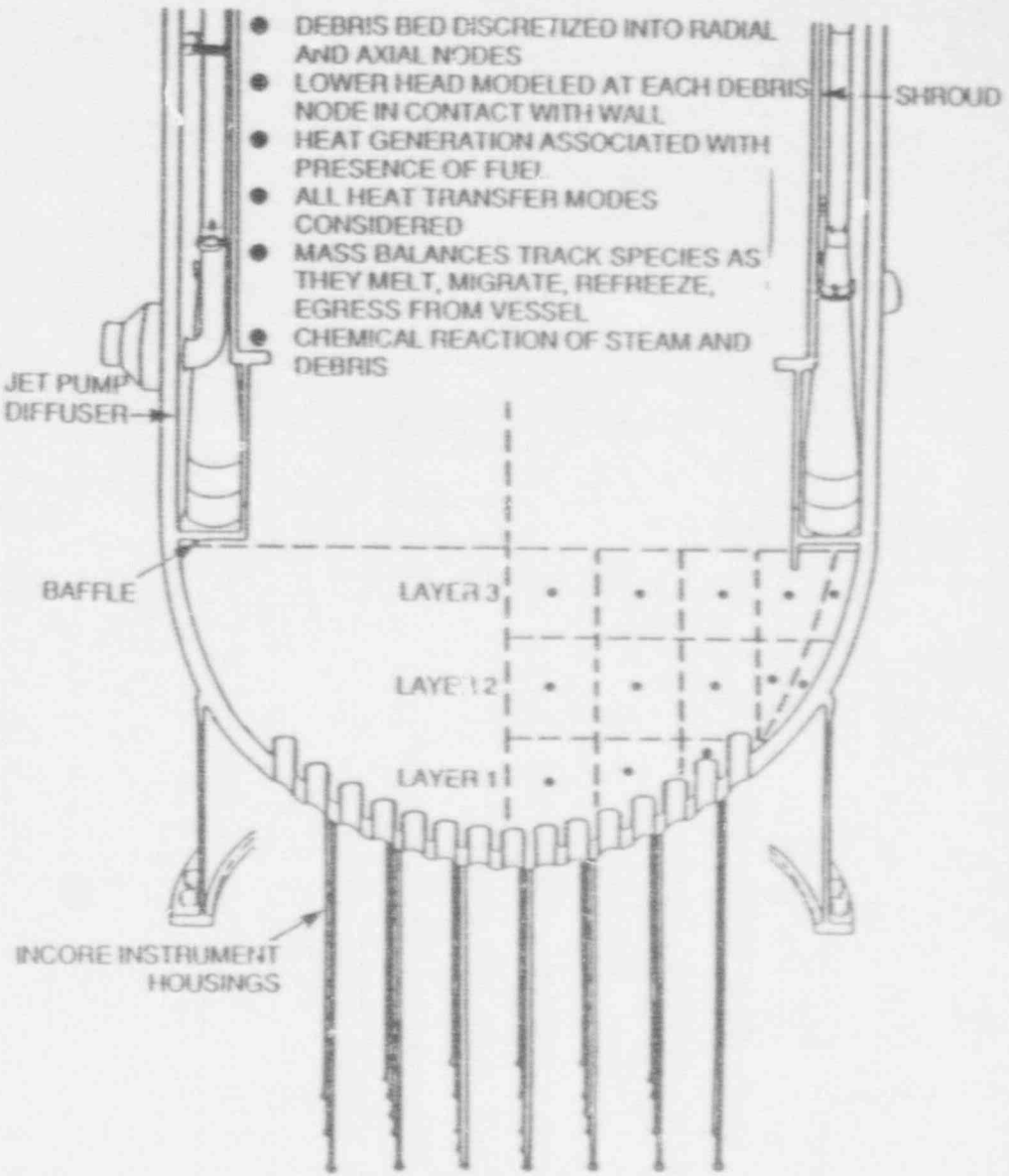

Fig. 12. Description of models and illustration of noding employed for the BWR reactor vessel bottom head debris bed.

3.3 STRUCTURE OF THE DEBRIS BED

A drawing of the debris bed nodalization initially employed for a recent calculation of the late phase of a short-term blackout severe accident sequence is provided in Figure 13. The drawing is to-scale, correctly indicating the relative sizes of the calculational control volumes as initially established. These volumes (surfaces of revolution) are listed in the following Table.

Table 1. Reactor vessel control volumes considered in the lower plenum debris bed calculation

Nodal Designation	Volume m^3	Volume ft^3
(1,1)	1.784	63.0
(1,2)	.784	63.0
(1,3)	1.784	63.0
(2,1)	4.117	145.4
(2,2)	5.273	186.2
(2,3)	10.109	357.0
(2,4)	15.889	561.1
(2,5)	1.625	57.4
(3,1)	1.515	53.5
(3,3)	1.937	68.4
(3,2)	3.715	131.2
(3,4)	10.568	373.2
(3,5)	0.597	21.1
TOTAL	60.697	2143.5

It should be noted that the entire debris bed is contained below the center of curvature of the bottom head hemisphere. The volume occupied by the debris is of course dependent upon the assumed bed porosity, which is user-input. Normally, a porosity of 0.40 is employed for the solid oxides and a porosity of 0.20 is employed for the metals; these are considered to be reasonable values based upon the available data[10].

The lower plenum debris bed model constructs the bed control volumes in the following manner. Record is kept of the accumulation of the different material species as they relocate into the lower plenum, and of their associated internal energies. As many as 20 different material species can be considered.

The first debris layer is comprised of the control blade, channel box, and candling clad material that relocates prior to any fuel pellet relocation. While the composition of the first debris layer is primarily metallic, it does include the small amount of ZrO_2 and UO_2 that is predicted to be carried downward with the candling clad as a eutectic mixture. The layer is established at the time

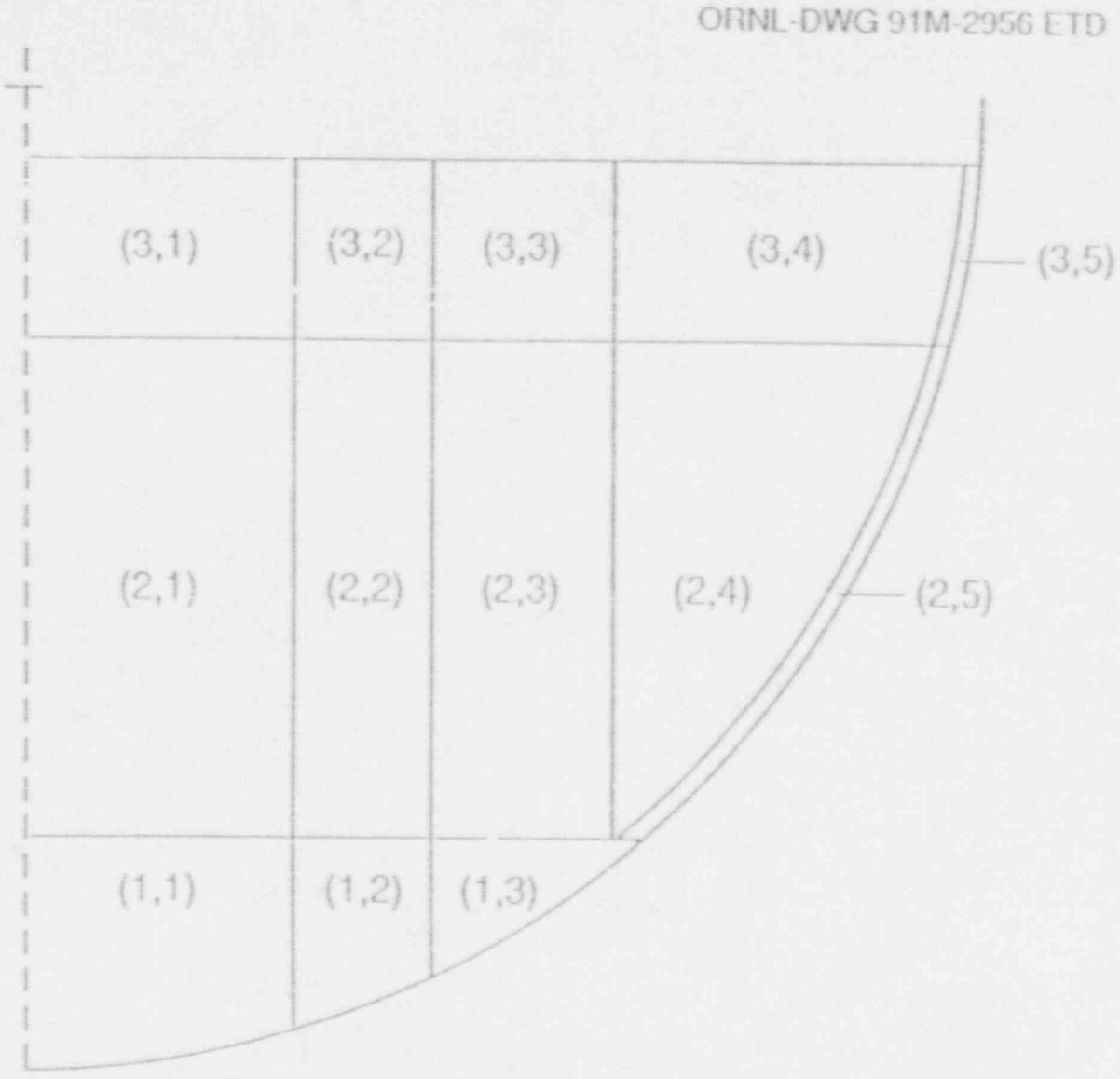

Fig. 13. A to-scale representation of the nodalization of the lower plenum debris bed as established for the late phase of a short-term station blackout calculation based upon the Peach Bottom plant.

of initial fuel pellet movement into the lower plenum and normally contains all of the material relocated below the core plate prior to that time. However, a maximum (lower) height for the first layer may be set by the user.

Figure 13 shows that the first layer is divided into three control volumes. The vertical interfaces are established so that these three volumes are equal, as indicated on Table 1.

The second debris layer begins to be formed at the time of initial fuel pellet movement and normally consists of the material relocated into the lower plenum from that time forward. If, however, the user has chosen to limit the height of the first layer, the excess material above that height that normally would have been included with the first layer is instead added to the second layer inventory.

The second layer consists of five control volumes, as shown on Figure 13. The vertical interfaces between nodes (2,1), (2,2), and (2,3) are simple extensions of the interfaces between nodes (1,1), (1,2), and (1,3). Therefore, as indicated in Table 1, the volumes associated with nodes (2,1) and (2,2) are not equal.

The control volume associated with node (2,5) is intended to represent the cooler mass of oxidic debris expected to exist close to the heat sink of the bottom head wall. (Such a provision is not considered necessary for the bottom debris layer, since it is normally comprised almost entirely of metallic debris.) User input determines the width of node (2,5) perpendicular to the wall.

Finally, the vertical interface between nodes (2,3) and (2,4) is established so that the volumes associated with these nodes are equal. [There is, however, a restriction that the radial distance between this vertical interface and the point of intersection of the inner boundary of node (2,5) with the upper surface of layer one must be at least 2.5 cm (1 in.). This is to provide a minimum floor area for node (2,4); this restriction is invoked whenever the user chooses to limit the height of layer one, as in this example.] As indicated in Table 1, the control volumes associated with nodes (2,3) and (2,4) are the largest within the debris bed.

The five control volumes associated with debris layer two continue to grow as additional debris moves downward past the core plate. Heat generation within the control volumes of the debris bed is associated with the decay heat of the fuel and, after penetration failures have occurred, with the chemical reaction of steam, passing from the vessel atmosphere through the bed, with the zirconium metal of the debris.

The heat balances for each debris node are initiated at the time of lower plenum dryout. Heat transfer by conduction is calculated for node-to-node and node-to-wall energy transfer. Additionally, radiation and convection from the surface nodes to the vessel gaseous contents and to intact structures above the debris bed are considered. Radiation to the shroud and axial conduction along the vessel wall causes boiloff of water remaining in the downcomer jet pump region. Also included in the nodal heat balances are the change-of-phase heat of fusion of species (or eutectic mixtures) as they melt or refreeze within the bed.

Within the debris bed, molten material moves downward from one control volume to another as long as void space (free volume) remains within the lower control volume. Once the interstitial spaces in the lower control volumes are filled, the molten liquid can move horizontally within the bed as necessary to keep the liquid level approximately constant within a layer. An exception occurs in the case of the two outermost control volumes in layer two after penetration weld failure occurs at the wall. For these two volumes, simultaneous movement downward to the void space

in the (single) underlying control volume and horizontally to exit the vessel through the failed penetration weld can occur. In all cases, the rate of movement of molten material through the debris bed is controlled by a user-input time constant, usually set at one minute. Thus, for example, if the calculational timestep is 0.2 minute (and with the one-minute timestep), 20% of the molten material within a control volume can move horizontally or vertically (or both, for the outermost middle layer nodes) each timestep.

All aspects of the lower plenum debris bed calculation can proceed indefinitely (including penetration failure and the escape of molten material from the vessel) without formation of the third debris layer shown on Figure 13. The purpose of this third layer is to accommodate the relocation of the outer, undamaged regions of the core that might occur gradually due to melting or suddenly, upon failure of the supporting control rod guide tube structure in the lower plenum. After bottom head dryout, the debris in the bottom and middle debris layers begins to heat up, and it is assumed that the debris thermally attacks and fails (at a user input debris temperature) the control rod guide tubes, which the debris completely surrounds to a depth of 2.4 to 3.0 m (8 to 10 ft). The material (stainless steel) of the control rod drive mechanism assembly housings and guide tubes is subsumed into the surrounding debris of the bottom, middle, and upper layers, as appropriate.

The vertical interfaces between the layer three control volumes are extensions of the interfaces between the layer two control volumes, as shown on Figure 13. The vessel structural masses as they exist at the initiation of the lower plenum debris bed for the recent calculation of Peach Bottom short-term station blackout are outlined in Table 2. (Layer three was established immediately after lower plenum dryout in this calculation.)

Table 2. Material masses (kg) included in the initial setup of the debris bed layers for Peach Bottom short-term station blackout

Material	Layer 1	Layer 2	Layer 3	Total
Zr	12147.	32349.	5398.	49894.
Fe	12724.	38412.	41797.	92933.
Cr	3095.	9344.	10167.	22605.
Ni	1378.	4164.	4519.	10061.
B_4C	269.	753.	84.	1106.
ZrO_2	837.	11850.	4337.	17024.
FeO	24.	84.	0.	108.
Fe_3O_4	41.	197.	23.	261.
Cr_2O_3	17.	74.	6.	97.
NiO	3.	14.	2.	19.
B_2O_3	6.	15.	0.	20.
UO_2	892.	120757.	40298.	161947.
Totals	31432.	218013.	106631.	356076.

As the temperature of the debris bed increases, the lower plenum model calculates the melting, migration, freezing, and remelting of the materials composing the bed. The eutectic mixtures formed and the associated melting temperatures assigned for the recent Peach Bottom calculation are listed in Table 3. (Other combinations of materials to form eutectic mixtures can be specified by user input.) Eventually, temperatures near the wall are such that penetrations fail and a path is opened for gas blowdown and passage of molten material from the vessel. In general, most of the debris bed is still solid when penetration failure and vessel blowdown are predicted to occur, so that relatively little of the debris is expelled during blowdown.

Table 3. Eutectic mixture compositions considered for the lower plenum debris bed

Eutectic Mixture	Mole Fractions	Melting Temperature K	°F
Zr - SS[a]	0.193 - 0.807	1723	2642.
Fe - Cr - Ni[b]	0.731 - 0.190 - 0.079	1733	2660.
Zr - SS - UO_2	0.300 - 0.600 - 0.100	1873	2912.
ZrO_2 - UO_2	0.750 - 0.250	2573	4172.

[a] SS represents stainless steel.
[b] This is the stainless steel eutectic mixture.

3.4 THE VESSEL BOTTOM HEAD WALL

The nodalization employed for the reactor vessel bottom head wall is shown in Figure 14. Eight wall nodes are always placed adjacent to debris bed layer one whereas the number of wall nodes adjacent to debris layer two depends upon the particular calculation. The five wall nodes shown adjacent to debris control volume (2,5) in Figure 14 are appropriate to the Peach Bottom short-term station blackout calculation. For other calculations, the code can assign one or two additional wall nodes adjacent to debris layer two as required by the thickness of the layer; thus, the total number of nodes adjacent to control volume (2,5) can vary between five and seven.

The bottom head wall adjacent to control volume (3,5) is divided into two nodes, numbers 14 and 15 on Figure 14. Wall node 16 represents the portion of the wall between the top of debris layer three and the bottom of the shroud baffle. One wall node (node 17 in Figure 14) represents the wall adjacent to the water trapped above the shroud baffle in the downcomer region; the upper surface of this last node is at the elevation of the center of curvature of the hemispherical bottom head.

Should the user choose not to form a third debris layer in the calculation (by setting an unattainably high control rod guide tube failure temperature), then the code simply divides the

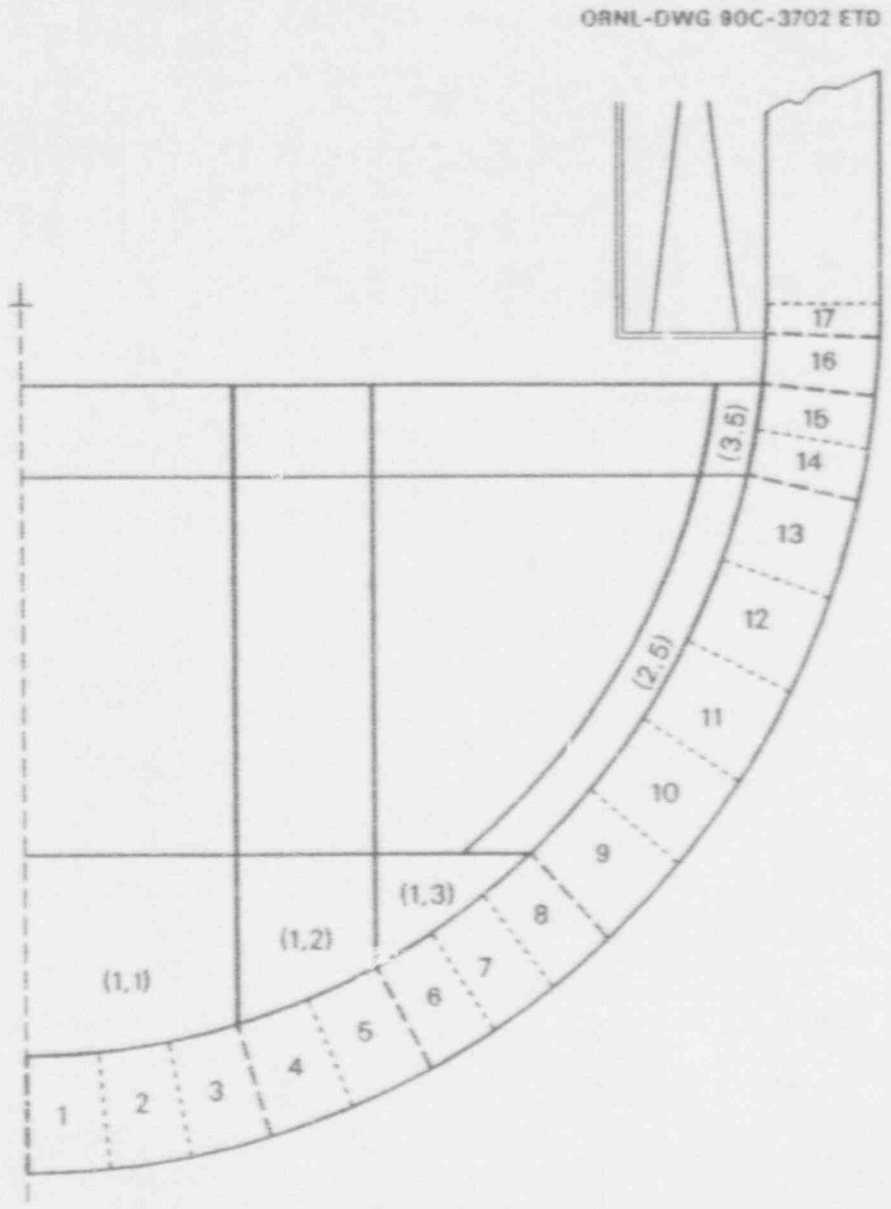

Fig. 14. BWRSAR nodalization of the reactor vessel bottom head wall.

portion of bottom head wall between the (moving) upper surface of debris layer two and the bottom of the shroud baffle into three equal nodes. The total number of nodes and the placement of the uppermost wall node adjacent to the downcomer region above the shroud baffle remain the same.

For the purpose of calculating the bottom head wall temperatures, each wall node is divided into three equal-volume segments as shown in Figure 15. Heat is transferred from the adjacent debris bed control volumes into the wall nodes by conduction. Heat transport along and across the wall by conduction from segment-to-segment is also calculated. Wall nodes above the elevation of the upper debris bed surface receive heat transfer by radiation from the bed.

Although not indicated in Figure 15, the thickness of the BWR reactor vessel wall increases at some point (plant-specific) between the cylindrical section of the vessel and the lower portion of the bottom head where the penetrations are located. The vessel wall nodalization established by the bottom head wall model recognizes the user-input location of this transition point and adjusts the thickness of the wall nodes above and below this location accordingly. Furthermore, the lengths of the two adjacent wall nodes are adjusted (one shortened, one lengthened) so that the transition point falls exactly on their nodal boundary.

The rate of heat transfer from the inner segment of the uppermost wall node (number 17 in Figures 14 and 15) to the water in the downcomer region is governed by nucleate boiling and conduction through the wall.

Heat transfer from the outer segment of each wall node to the drywell atmosphere is calculated using a user-input convection heat transfer coefficient. Different drywell atmosphere temperatures are used for the portions of the vessel wall above and below the attachment point of the vessel support skirt (item T in Figure 1). This is because the temperature of the atmosphere within the pedestal region of the drywell would be much higher than the temperature in the remainder of the drywell, especially after molten debris had begun to leave the vessel.

3.5 METAL-STEAM REACTION IN THE DEBRIS BED

As mentioned previously, BWR bottom head penetration failure mechanisms have been described elsewhere[8,9]. In brief, for the case of heatup of a quenched debris bed, failure is expected to occur by overflow of molten materials into the instrument housing guide tubes. Since the bottom layer of debris is composed almost entirely of metals while UO_2 constitutes more than half of the middle layer, the temperature of the middle layer increases much more rapidly after bottom head dryout than does that of the bottom layer. For this reason, melting of the in-core housing guide tubes would occur first in the middle layer. The criteria employed for initiation of reactor vessel blowdown through the in-core instrument housing guide tubes are first, that the middle layer debris bed temperature be above the melting point of stainless steel and second, that the level of liquid components of the debris within the reactor vessel lower plenum has risen into the middle debris layer so that molten material is available to pour into the failed portion of the tubes.

After failure of the reactor vessel pressure boundary, a leak path from the vessel to the drywell atmosphere is created. Subsequently, the vessel gaseous content blows down if the reactor vessel is at pressure or, if the vessel is depressurized, slowly leaks out as the gas temperature increases and the water in the reactor vessel downcomer region surrounding the jet pumps is boiled away. The leak path for the steam generated from the water surrounding the jet

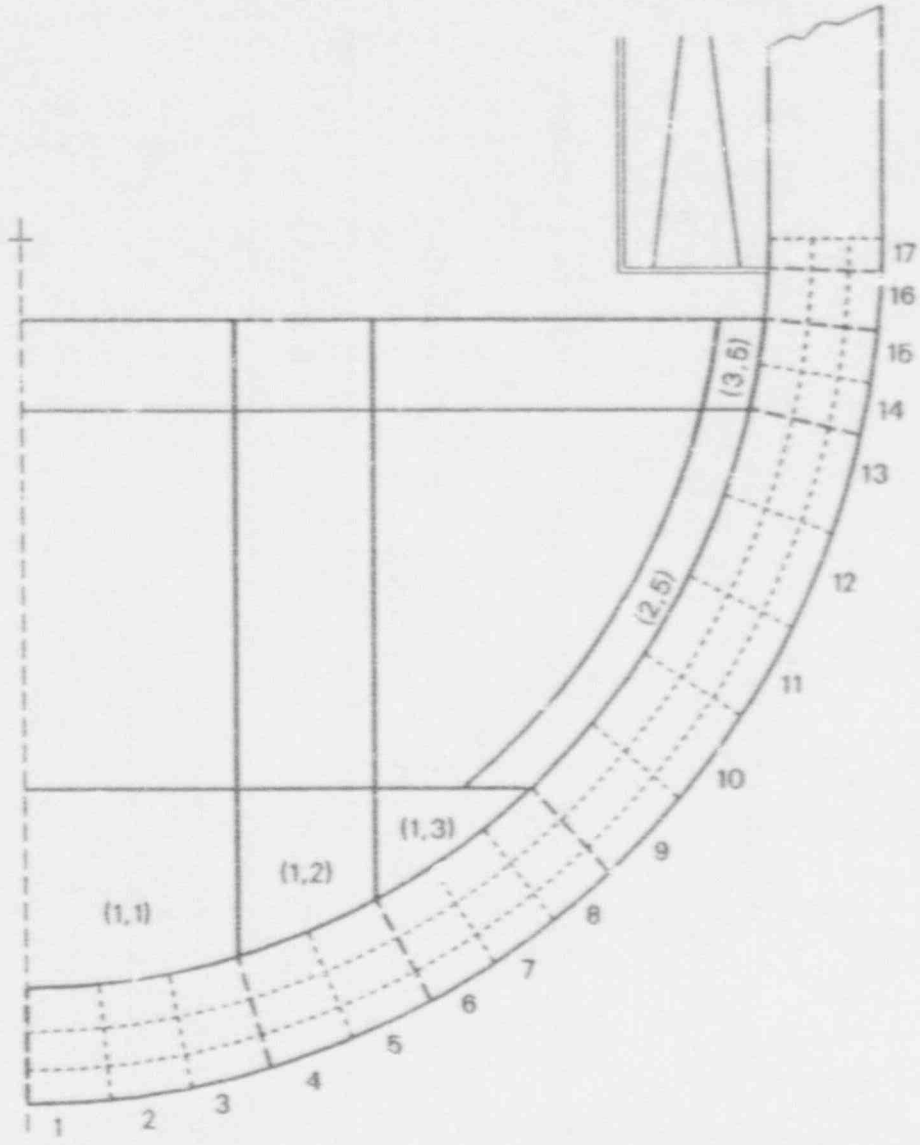

Fig. 15. Each reactor vessel bottom head wall node is divided into three radial segments for the wall temperature calculation.

pumps is up through the downcomer region, down through the core region, and out through the debris bed. Thus, the steam available in the vessel after the time of pressure boundary failure would pass through the debris and would react with the zirconium metal during its passage.

Only the steam/zirconium reaction is represented in the lower plenum debris bed model , but this is a major heat source in the control volume energy balances, particularly for cases in which the reactor vessel is pressurized at the time of penetration failure. Stainless steel oxidation in the bottom head debris is not represented since this is expected to be a secondary effect and because the temperatures at which rapid stainless steel oxidation occurs are close to the melting point; thus, stainless steel tends to relocate rather than to undergo excessive oxidation. The upshot of this is that much of this metal is expected to leave the vessel in a molten state without oxidizing.

3.6 ABLATION INDUCED BY FLOW OF MOLTEN MATERIAL

As discussed in Section 3.5, failure of the instrument housing guide tubes within the middle debris layer provides a path for molten materials in the vicinity to pour through the bottom debris layer and the reactor vessel bottom head wall. The Lower plenum debris bed and bottom head response model considers the potential for this flowing liquid to ablate the material surrounding the original instrument housing guide tube locations in both the bottom debris layer and in the vessel wall.

The user-input parameters employed by the model that are most important in determining the calculated reactor vessel wall temperatures are listed in Table 4.

Table 4. User-input parameters affecting the vessel wall temperature calculation

Parameter		Representative Value	
DTHEAD	Time constant for relocation of molten material (vertically or horizontally) within the debris bed	1.00 min	
HPIPES	Coefficient for heat transfer between molten material flowing through the instrument tube locations in the bottom debris layer and the surrounding metallic debris and bottom head wall	1022.1 $\frac{W}{m^2 K}$	$\left(180.0 \frac{Btu}{h\ ft^2\ ^\circ F}\right)$
TABLAT	Ablation temperature of material in bottom debris layer and vessel wall	1756 K	(2700 °F)
THKCRS	Thickness of the debris node adjacent to the vessel wall	5.08 cm	(0.167 ft)

Movement of the molten material through the bed to the instrument housing guide tubes is controlled by input time constant DTHEAD. The augmentation of this flow by ablation of the surrounding metallic material of the bottom layer and the vessel bottom head is controlled by input parameters HPIPES and TABLAT. Heat transfer from the melting (ablating) surfaces surrounding the flowing debris to the interior of the remaining solid portions of the bottom layer or wall nodes is calculated by the model.

Ablation of the material in the bottom debris layer shrinks the size of the control volume(s) through which the molten material is flowing. Whenever the total mass within a control volume has been reduced to less than 20% of its initial mass, or the ablated volume exceeds 80% of the current volume occupied by solid debris, the shrunken control volume is merged with the overlying control volume and the nodalization of the debris bed is adjusted accordingly.

4. RECENT DEBRIS BED MODEL IMPROVEMENTS

Two sets of model improvements have been implemented into the BWR-specific lower plenum debris bed models previously developed at ORNL for use in severe accident calculations with the BWRSAR code. These improvements were recently recommended (Reference 11) as a result of a review carried out in preparation for the transposition of these debris bed models into the MELCOR code. The recommended improvements, while straightforward, involved extensive changes over several subroutines and, therefore, could be implemented and tested much more easily and quickly within the BWRSAR code framework than within the sophisticated MELCOR architecture. Thus, it was more practical to carry out these modifications before installation of the lower plenum debris bed model within MELCOR.

The first model improvement provides for updating each timestep the representative density, porosity, specific heat, and thermal conductivity used for the debris mixture within each debris bed control volume. Previously, the model logic applied a single user-input value of bed porosity and continued use of the initially established overall bed values of density and specific heat throughout the calculation. While the thermal conductivity was previously calculated each timestep, the value for each control volume was based simply upon the relative amounts of metals and oxides within the volume. With the current improvements, the local porosity is now based upon the relative mass fractions of metals and oxides while the control volume representative density, specific heat, and thermal conductivity are mass-averaged values based upon the relative local amounts of each debris constituent.

The second model improvement extends the applicability of the lower plenum debris bed model to the smaller BWR reactor vessels such as those at Hatch or Duane Arnold. The following Table provides information concerning the relative sizes of three U.S. boiling water reactor facilities (all of the BWR-4 design):

Table 5. Size parameters for three representative US BWRs

Parameter	Browns Ferry	Hatch	Duane Arnold
Rated Power, MWt	3293	2436	1593
Net Power, MWe	1065	768	515
Core Equivalent Diameter, m	4.752	4.069	3.299
Reactor Vessel Internal Diameter, m	6.375	5.537	4.648
Radius of Vessel Bottom Head, m	3.188	2.769	2.324

As indicated, the reactor vessel internal diameter is reduced from 6.375 m (251 in.) at Browns Ferry to 4.648 m (183 in.) at Duane Arnold to accommodate the smaller core at the latter plant. This reduces the cross-sectional area of the vessel by a factor of 0.53. Since the core height is not changed, the reduction in core volume is of the same proportion. However, the corresponding reduction in the volume of the hemispherical portion of the vessel lower plenum is a factor of 0.38.

There is certainly nothing magical about the relative magnitudes of these reductions in reactor vessel cross-sectional area and volume; they arise simply because the area varies as the vessel diameter squared while the bottom head volume varies as the diameter cubed. However, the effect upon the required nodalization of the lower plenum debris bed is significant: *The entire volume of relocated core and structural debris will fit within the hemispherical portion of the vessel lower plenum at Browns Ferry; it will not at Duane Arnold.*

To accommodate application to the smaller reactor vessels, the lower plenum debris bed model has been modified to accept the gradual relocation of the outer regions of the core into the lower plenum, which is the method usually predicted by MELCOR, in lieu of the sudden relocation employed by BWRSAR. Normal settling of the bed due to debris melting and relocation during the period that the additional material from the outer region is being added will preclude any overflow from the hemispherical region in most applications.

Should future testing reveal a need for additional modifications in the event of overflow of debris from the bottom head hemisphere, they will be developed at that time. This is not expected to be the case. In the meantime, logic modifications have been implemented to preclude code interrupt if temporary conditions for overflow do occur, by the simple expedient of delaying the addition of debris until bed settling makes room for it within the hemispherical region.

5. SUMMARY

The coding developed within the Boiling Water Reactor Severe Accident Response (BWRSAR) code framework for calculating the behavior of a BWR lower plenum debris bed after

dryout and the associated bottom head response is currently being made operational within the MELCOR code at Oak Ridge National Laboratory (ORNL). This NRC-sponsored effort [Boiling Water Reactor Severe Accident Technology (BWRSAT) Program] is to test the Oak Ridge lower plenum debris bed and bottom head models within the structure of a local version of MELCOR and, when successful, to make recommendations for formal adoption of these models to the NRC and to the MELCOR code development staff at Sandia National Laboratories (SNL).

The purpose of these models within MELCOR is to permit the calculation of material releases from the reactor vessel as controlled by the melting rate of the internal debris. The models represent the heatup and melting of the lower plenum debris bed after dryout, and include its effect upon the lower plenum structures and the vessel bottom head.

The installation of the lower plenum debris bed and bottom head response models at ORNL is expected to be completed by December 31. At that time, these models will be passed to the MELCOR development staff at SNL for independent review and, upon their approval, for ultimate formal release to outside users.

6. REFERENCES

1. L. J. Ott, "Advanced Severe Accident Response Models for BWR Application," *Nuclear Engineering and Design*, 115, 289-303, 1989.
2. L. J. Ott, "Advanced Severe Accident Response Models for BWR Application," Fifteenth Water Reactor Safety Information Meeting, National Bureau of Standards, Gaithersburg, MD, October 29, 1987.
3. S. A. Hodge and L. J. Ott, *Boiling Water Reactor Severe Accident Response (BWRSAR) Code Description and Assessment*, letter report to Dr. Thomas J. Walker, Division of Systems Research, RES, USNRC, February 1, 1989.
4. R. M. Summers et al., *MELCOR 1.8.0: A Computer Code for Nuclear Reactor Severe Accident Source Term and Risk Assessment Analyses*, NUREG/CR-5531 (SAND90-0364), Sandia National Laboratories, January 1991.
5. R. M. Summers et al., "MELCOR Primer, Version 1.8.0," Sandia National Laboratories, May 1989.
6. *The BWR Owner's Group Emergency Procedure Guidelines*, Revision 4, March 1987.
7. W. I. van Rij and L. J. Ott, *A Survey of Current Models of BWR Core Plate Failure Used in the Severe Accident Codes APRIL, BWRSAR, MELCOR, MELPROG, and SCDAP/RELAP*, letter report ORNL/NRC/LTR-90/14 to Dr. Robert W. Wright, Division of Systems Research, RES, USNRC, July 31, 1990.
8. S. A. Hodge and L. J. Ott, *Failure Modes of the BWR Reactor Vessel Bottom Head*, letter report to Dr. Thomas J. Walker, Division of Systems Research, RES, USNRC, May 10, 1989.
9. J. L. Rempe et al., *Light Water Reactor Lower Head Failure Analysis*, NUREG/CR-5642 (EGG-2618), Idaho National Engineering Laboratory, December 1991.
10. G. E. Mueller and A. Sozer, *Thermal-Hydraulic and Characteristic Models for Packed Debris Beds*, NUREG/CR-4689 (ORNL/TM-10117), Oak Ridge National Laboratory, December 1986.
11. S. A. Hodge, *Lower Plenum Debris Bed Model Improvements for MELCOR*, letter report to Mr. Yi-Shung Chen, Division of Systems Research, RES, USNRC, February 25, 1991.

MELCOR PEER REVIEW

by

B. E. Boyack, V. K. Dhir, J. A. Gieseke, T. J. Haste, M. A. Kenton, M. Khatib-Rahbar, M. T. Leonard, and R. Viskanta

ABSTRACT

MELCOR is a fully integrated, engineering-level computer code that models the progression of severe accidents in light water reactor nuclear power plants. The newest version of MELCOR is Version 1.8.1, July 1991. MELCOR development has reached the point that the United States Nuclear Regulatory Commission sponsored a broad technical review by recognized experts to determine or confirm the technical adequacy of the code for the serious and complex analyses it is expected to perform. For this purpose, an eight-member MELCOR Peer Review Committee was organized. The Committee has completed its review of the MELCOR code; the review process and findings of the MELCOR Peer Review Committee are documented in a summary report to be issued soon. The Committee has determined that recommendations in five areas are appropriate: (1) MELCOR numerics, (2) models missing from MELCOR Version 1.8.1, (3) existing MELCOR models needing revision, (4) the need for expanded MELCOR assessment, and (5) documentation.

Introduction

MELCOR is a fully integrated, engineering-level computer code that models the progression of severe accidents in light water reactor nuclear power plants. MELCOR is being developed at Sandia National Laboratories (SNL) for the United States Nuclear Regulatory Commission (USNRC) as a second-generation plant risk assessment tool and as the successor to the Source Term Code Package.

MELCOR has been under development since 1982. The newest version of MELCOR is Version 1.8.1, July 1991. The code has now reached sufficient maturity that a number of organizations inside and outside the NRC are using or are planning to use the code. Although quality control and validation efforts are in progress, there is a need to have a broad technical review by recognized experts to determine or confirm the technical adequacy of the code for the serious and complex analyses it is expected to perform. A peer review committee has been organized using recognized experts from the national laboratories, universities, MELCOR user community, and independent contractors to perform this assessment.

The objective of this paper is to summarize the findings of the MELCOR Peer Review Committee that was formed to fulfill the charter described in the following section.

Committee Charter

The charter of the MELCOR Peer Review Committee was to (1) provide an independent assessment of the MELCOR code through a peer review process, (2) determine the technical adequacy of MELCOR for the complex analyses it is expected to perform, and (3) issue a final report describing the technical findings of the Committee.

Peer Review Process

The Committee developed and followed a multistep process for the MELCOR Peer Review. The steps in the process are as follows:

1. Identify design objectives for the MELCOR code.
2. Identify targeted applications for the MELCOR code.
3. Identify the MELCOR code version to be reviewed.
4. Identify and distribute the MELCOR Document Data Base to Committee members.
5. Select plants and severe accident scenarios.
6. Develop a common Committee perspective regarding technical adequacy
7. Identify dominant phenomena for the plants and scenarios.
8. Define a "Standard of Technical Adequacy" to be used in developing findings.
9. Define a process for reviewing for technical adequacy.
10. Assess technical adequacy of individual models and/or correlations within the MELCOR phenomenological packages (bottom-up review).
11. Assess technical adequacy of the integral code against the MELCOR design objective and the MELCOR-targeted applications (top-down review).
12. Document findings in a summary report.

Major Findings

Perspectives

The NRC identified both the design objectives and targeted applications for the MELCOR code for the MELCOR Peer Review Committee. After defining a standard of technical adequacy and a process for evaluating technical adequacy, the Committee conducted a thorough review from two perspectives. The Committee first reviewed the individual models and correlations in each MELCOR phenomenological package or major code subdivision (bottom-up review); this resulted in the development of numerous findings. The Committee next reviewed the integral performance of the total code, leading to additional findings (top-down review). The MELCOR Peer Review Committee recognizes that resources for MELCOR development, revision, and enhancement are, and will continue to be, limited. Therefore, the Committee made a concerted effort to prioritize its findings. Those findings presented by way of the Committee recommendations are believed to be the minimum set of efforts that will permit MELCOR to fulfill its design objectives and effectively function for its targeted applications.

In developing its recommendations, the Committee, at the direction of the NRC, assigned primary importance to the adequacy of MELCOR for use in probabilistic risk assessment (PRA)-targeted applications and considered mechanistic accident management (AM) studies to be of secondary importance for MELCOR application. The Committee screened each identified code deficiency by considering the importance of the deficiency relative to the potential impact on (1) the time of containment failure and (2) the magnitude of fission product release to the environment.

Finally, the Committee concluded that the technical requirements, when satisfied, will result in a technically adequate MELCOR for PRA applications, although the requirements may not always be sufficient for some parametric AM studies. If at a future time the role of the MELCOR code is expanded to include detailed AM studies focusing on timing and the magnitudes of key phenomena, Committee recommendations for needed improvements have been provided in the summary report.

Degree of Completion

The Committee determined that MELCOR is not a completed code and that additional development, as discussed below, is needed before MELCOR can reasonably satisfy its design objectives and be applied with confidence to its targeted applications. Completion of MELCOR can be measured in several ways. First, code completion can be measured relative to the existence of the needed models for all dominant phenomena that are to be predicted. Second, code completion can be measured relative to existence of the documentation needed to understand, appropriately apply, and interpret the code. Third, code completion can be measured relative to its demonstrated technical adequacy. The Committee determined that by each of these measures, further effort will be required before MELCOR can be considered to be complete.

Having made this point, the Committee also finds that considerable progress has been made in developing the MELCOR code. The component parts of MELCOR have been developed and assembled such that integrated calculations of some severe accident sequences in both boiling and pressurized water reactors (BWRs and PWRs) can be completed. Limited benchmarks have been prepared for some of the individual models and correlations and a limited set of benchmarks have been completed for the integrated code. An extensive set of documentation has been prepared, including a code manual, reference manuals for the phenomenological packages, and users' guides.

Recommendations

The Committee has determined that recommendations in five areas are appropriate: (1) MELCOR numerics, (2) models missing from MELCOR Version 1.8.1, (3) existing MELCOR models needing revision, (4) need for expanded MELCOR assessment, and (5) documentation.

MELCOR Numerics. The Committee concluded that code numerics are the source of a primary concern regarding the technical adequacy of the code. During the course of the MELCOR Peer Review, the results of several time-step sensitivity studies were made available to the Committee. These studies indicated that convergence to limiting values is not currently guaranteed as the time step decreases. In fact, key quantities vary erratically as the time step is changed. The Committee has concluded that an improved understanding of the time-step sensitivities is important, that other input parameter and modeling sensitivities can be expected, and that correction of the MELCOR numerics problems should be considered to be a high-priority activity.

Models Missing From MELCOR Version 1.8.1. The Committee concludes that models for the following phenomena, not currently modeled, should be given the highest priority for incorporation in MELCOR:

- PWR primary system natural circulation in components with countercurrent flows,
- high-pressure melt ejection and direct containment heating,
- ice condenser,
- nonexplosive interactions between debris and water,
- fission product vapor scrubbing,
- additional reactor coolant system fission product deposition processes, and
- fission product reactions with surfaces.

The Committee notes that funded model development activities are currently either planned or under way for either part or all of the PWR primary system natural circulation model, the high-pressure melt ejection and direct containment heating model, and the ice condenser model.

Existing MELCOR Models Needing Revision. The Committee's bottom-up review of the MELCOR phenomenological packages identified individual models that were of concern. The Committee completed a screening activity to determine which models should receive priority attention using as screening criteria (1) the time of containment failure and (2) the magnitude of the source term. The Committee recommends that the following issues, ranked by the Committee as "very important," be given the highest priority.

- An evaluation should be made to determine whether the water condensation/evaporation model used in the Hydrodynamic Behavior (CVH) Package is implemented adequately as it supplies model information to the Radionuclide (RN) package. Currently, condensation is treated independently in the CVH package from the calculations of aerosol particle growth and deposition in the RN package. The Committee feels that separating condensation growth from other growth calculations is a questionable procedure and the validity of this approach should be demonstrated by comparison with more exact models or data.
- Inconsistencies in treatment of chemical reactions between CORCON and VANESA should be resolved, and improvements should be made to the CORCON/MOD2 phase diagrams. Consolidation of CORCON and VANESA into a unified code as currently planned for CORCON/MOD3 is desirable. The Committee did not review CORCON/MOD3 models; however, based on a brief presentation to the Committee by SNL, it appears this code has the potential for remedying most of these concerns. A peer review of CORCON/MOD3 models would be desirable before its implementation into MELCOR.
- The model for condensation in containment (mass transfer) should be revised. With the existing model, steam condensation rates, predicted for conditions when the thermal resistance of the structure on which condensation occurs does not dominate, will be in serious error. The model used for condensation in the presence of noncondensables is seriously flawed.
- The pool scrubbing model is largely derived from previously available models but assumes spherical bubble shapes while correcting for bubble flattening by using coefficients derived from comparisons to other models. Impaction of particles from steam/air jets entering the pool would be expected to provide significant deposition for larger particles, but the effect is ignored in the current model. Decontamination factors computed with the current model are quite low in comparison with other models and the existing data base.

Need for Expanded MELCOR Assessment. The Committee concluded that the ability of MELCOR to calculate severe accident phenomena is not sufficiently demonstrated. Such a demonstration would be based on a documented collection of (1) sensitivity studies, (2) benchmarking activities using experimental data, and (3) code-to-code assessments.

The Committee has concluded that review of a comprehensive set of well-defined and executed sensitivity analyses is an important and necessary component of the effort to determine technical adequacy. Unfortunately, this comprehensive set of MELCOR sensitivity analyses does not presently exist. Rather, a sparse set of sensitivity studies exists.

By any measure, the MELCOR integral benchmarking effort is very small. The Committee has concluded that a more comprehensive and ongoing integral assessment program is needed. While encouraging an increasing pace for the integral assessment effort, the Committee emphasizes the importance of maintaining an overall perspective about the need to benchmark the individual models by using test data. A complete assessment of the technical adequacy of an integral code considers both the component parts and the adequacy of the integrated coded package. The review of the component parts focuses on the pedigree, applicability, and fidelity of the individual models and correlations. The Committee emphasizes the importance of having technically adequate detailed models and correlations which are, in reality, the building blocks of the integral code.

Although code-to-code comparisons cannot and should not displace or replace code benchmarking efforts against test data, the Committee concludes that code-to-code comparisons can provide useful supplementary insights. For severe accident phenomena, their value lies not in the absolute, i.e., what is right and what is wrong, but in focusing attention on what is different. The Committee recommends that comparison activities continue in the future.

Documentation. The availability, content, completeness, and quality of documentation is an important factor influencing the outcome of a code peer review activity. The NRC has recently prepared and issued documentation guidance to organizations involved in the development of software for the NRC's Office of Nuclear Regulatory Research. Each of the documentation elements identified by the NRC exist in one form of MELCOR documentation or another. The body of existing documentation represents a significant and positive accomplishment. The Committee was able, for example, to accomplish a significant portion of its review using the documentation that has already been prepared. The Committee does, however, have concerns about particular aspects of the documentation and these are detailed in the following paragraphs.

The MELCOR summary report and phenomenological package reference manual cover the elements of the code or theory manual. The Committee determined, however, that the level of detail was less than that needed by the user community. After extensive interactions with the SNL staff, the Committee felt that the detailed descriptions of the models and correlations were lacking in some cases. That is, what was modeled was described but the descriptions of pedigree, applicability, and benchmarking were either inadequate or missing. The Committee recommends that careful consideration be given to producing a "Models and Correlations" document for MELCOR equivalent the similar documents prepared for the NRC's thermal-hydraulic systems codes. At a minimum, the Committee recommends that all new model development be accompanied by detailed documentation of model pedigree, applicability, and fidelity (benchmarking).

A particular area of concern to the Committee is the dispersed nature of model documentation when other computer codes, or parts of other computer codes, have been imported into MELCOR. In several areas, MELCOR documentation simply references the manuals for the parent code without sufficient supporting discussion of which portion(s) of the parent code models have been incorporated unchanged into MELCOR, which have been modified, and how the imported models have been incorporated into the MELCOR framework. The ideal solution would be to incorporate into the MELCOR documentation a complete description of each imported physical model. At a minimum, the Committee recommends that references to parent code documentation in the MELCOR documentation be accompanied by a clear and specific discussions of how and why the imported models have been selected for MELCOR implementation.

The MELCOR developmental assessment documentation is sparse. The Committee recommends that the MELCOR developmental assessment be expanded and that the results of the assessment effort be thoroughly documented. The Committee recommends that as future assessments are completed, careful consideration be given to documentation of the assessments, individually and collectively, so that the lessons learned in the assessment process are incorporated into the MELCOR development effort and and immediately helpful to the user community.

The design of the MELCOR code, with its strong emphasis on user input for modeling both the facility and parametric studies of the many and complex physical processes being examined, places a uniquely difficult burden on the MELCOR user. Effective use of MELCOR demands a knowledgeable and well-informed user. Documentation of practical modeling guidelines is needed. The ongoing collection of user lessons learned or practical guidelines does not seem to be occurring. The Committee recommends that a structured and ongoing process of collecting, documenting, and distributing practical user guidelines to the MELCOR user community be developed and executed.

Planned MELCOR Improvements and Assessment*

Randall M. Summers
Lubomyra N. Kmetyk

Sandia National Laboratories

Abstract

Although MELCOR is now being successfully applied in severe accident analyses, it is not yet complete and additional development and assessment is needed before MELCOR can fully satisfy its design objectives and be applied with confidence to its targeted applications. A number of current and planned improvements and assessment activities necessary to reach that stage are described in this paper. Modifications that have been implemented in the latest release of the code, version 1.8.1, are summarized, the status of work in progress on new models such as direct containment heating, in-vessel natural circulation, and materials interactions is given, and several additional models and other enhancements planned for the near future are described. The results of recent assessment calculations performed at Sandia are summarized, and assessment efforts that have just begun or are planned for the near future are briefly mentioned.

1. INTRODUCTION

MELCOR [1] is a fully integrated, engineering-level computer code that models the progression of severe accidents in light water reactor (LWR) nuclear power plants. MELCOR is being developed at Sandia National Laboratories for the U.S. Nuclear Regulatory Commission (USNRC) as a second-generation plant risk assessment tool and the successor to the Source Term Code Package (STCP) [2]. The entire spectrum of severe accident phenomena, including reactor coolant system and containment thermal-hydraulic response, core heatup, degradation and relocation, and fission product release and transport, is treated in MELCOR in a unified framework for both boiling water reactors and pressurized water reactors. MELCOR has been especially designed to facilitate sensitivity and uncertainty analyses. Its current uses include estimation of severe accident source terms and their sensitivities and uncertainties in a variety of applications.

Version 1.8.1 of MELCOR was frozen in March of 1991 and distributed in July. This version included several significant improvements, summarized in the following paragraphs. (The discussion in this paper assumes some knowledge of the capabilities of previous versions of MELCOR.)

* This work was supported by the U.S. Nuclear Regulatory Commission and was performed at Sandia National Laboratories, which is operated for the U.S. Department of Energy under Contract Number DE-AC04-76DP00789.

1. Error Correction: The bulk of the changes involved corrections of errors of varying degrees of severity. Many of them incorporated improved numerics to increase computational efficiency. The result has been a faster running, more robust code with fewer instances of demonstrably wrong calculated behavior. Improvements in input and output processing were also implemented in several places.

2. Time-Specified Control Volumes: The capability to define control volumes with conditions (temperature, pressure, composition, etc.) specified as constants or by user-defined control functions was added. These control volumes provide a much more convenient means to specify known boundary conditions, a particularly useful feature in simulating experiments.

3. Radionuclide Modeling: Several problem areas in the modeling of radionuclide behavior were addressed. Implementation of the model for fission product removal by sprays was completed. The interface with the Control Volume Hydrodynamics (CVH) package was upgraded to allow transport of fission products with bulk fluids as the CVH package subcycles, thus eliminating potentially serious discrepancies. Substantial modifications were made to the MELCOR implementation of MAEROS [3] to resolve mass conservation and computational cost concerns. The filter model was enhanced to treat demisters, HEPA filters, and charcoal bed filters. Finally, the model for absorption of beta decay energy in control volumes was modified to consider the actual thickness of the volume atmosphere.

4. Heat Structure Modeling: Two fundamental problems with the Heat Structure package were addressed. The thermal coupling of heat structures to the hydrodynamics was modified to attempt to damp oscillations that may occur when structures with high surface area communicate with control volumes with low total heat capacity. The water condensation/evaporation model was altered to eliminate discontinuous behavior with the introduction of noncondensibles to a pure steam environment.

5. Core Modeling: Three model upgrades in the Core package were implemented. More flexibility and user control were provided for the failure of structures such as the core plate. Modeling of the effects of conglomerate debris (introduced by melt relocation onto lower portions of core structures) on convective and radiative heat transfer rates was added. Limits were placed on heat transfer rates from particulate debris beds by applying a dryout heat flux correlation. This latter change can drastically alter the course of the calculation at the point of massive debris relocation into the lower plenum.

6. Transport Properties Modeling: In the Material Properties package, the modeling of transport properties (i.e., viscosity and thermal conductivity) for pure fluids and fluid mixtures was substantially enhanced to include Chapman-Enskog and Eucken relationships based on Lennard-Jones potentials for individual gases and semi-theoretical weighting formulas for combinations of gases.

7. Core-Concrete Interactions Modeling: New correlations to treat debris-concrete and inter-layer heat transfer, taken from the developmental version of CORCON-MOD3, were incorporated into the MELCOR implementation of CORCON-MOD2 [4]. Also, through work sponsored by the DOE for metallic fuel reactors, the Cavity package was modified to treat metallic uranium and aluminum during molten core-concrete interactions.

2. CURRENT DEVELOPMENT

MELCOR 1.8.1 has recently undergone a comprehensive technical review by recognized experts to determine the technical adequacy of the code for the serious and complex analyses it is expected to perform. The review process and findings are documented in a previous paper for this session and in a report soon to be issued [5]. These findings corroborated those of a prior review conducted internally at Sandia [6], and work had already begun in several areas recognized as deficient. The status of improvements in these areas is described in the following sections.

2.1 Ice Condenser Model

Modeling of ice condensers has recently been incorporated by modifying the degassing model in the Heat Structure package. In principle, the phase change associated with melting ice is not unlike the phase change simulated by the degassing model. In both cases, an endothermic process occurring over a known temperature range consumes a characteristic amount of energy during the liberation of a reaction product. Therefore, it is logical to model an ice condenser as a number of vertical heat structures composed of a special ice-bearing material defined by user input. The user activates the ice condenser logic by including a prescribed keyword in the input for the heat structures. The properties for the base material should be specified to simulate the transient thermal response of the composite metal/ice matrix, and the properties of the internal "gas" source should be chosen to simulate the phase change associated with melting ice.

A number of adjustable parameters have been included in the MELCOR ice condenser model to account for details lacking in the modeling. A special ice condenser Nusselt number multiplier may be defined by the user to account for effects not explicitly modeled that may affect the rate of heat transfer to the ice. Similarly, an ice condenser radionuclide deposition surface area enhancement factor may also be defined by the user to account for unmodeled effects that will enhance the rate of fission product deposition in the ice condenser. Finally, a parameter may be adjusted by user input to control the rate of decrease of the ice surface area as the ice melts. The code automatically accounts for the volume change associated with the reduction in ice mass as melting proceeds and deposits the water in the pool of the ice condenser control volume. The dynamic response of the inlet and outlet doors to the ice condenser compartment is readily simulated with the Control Function package in MELCOR.

A simple ice condenser test problem was constructed to compare the response of the MELCOR model with a CONTAIN [7] calculation of the same problem. This test problem simulated a simple LWR steam blowdown into containment, discharging 200,000 kg of superheated water (540 K) and 1 kg of fission product aerosol into a 500 m^3 reactor cavity volume over a period of 20 seconds. The resulting steam entered an ice condenser compartment containing 1000 m^3 of ice, and the gaseous effluent from the ice condenser entered an upper containment volume of 59,500 m^3. The MELCOR model predictions were in good agreement with CONTAIN results for pressure response, steam condensation, and fission product deposition, as shown in Figures 1 and 2.

2.2 Fine-Scale Natural Circulation Model

Natural circulation within the reactor pressure vessel has been shown in several PWR analyses to have a major impact on core and vessel heating rates and the timing and location of vessel failure. In comparing cases with and without natural circulation modeling it has been found that natural circulation delays vessel failure by over an hour, leads to 25% greater oxidation of the Zircaloy, and results in nearly 2000 kg of additional steel (from the melting of control rod drives) in the melt ejected from the vessel [8]. In addition, the mode of RCS failure (i.e., hot leg versus lower head) can only be ascertained if natural circulation is modeled.

No model currently exists in MELCOR to treat natural circulation flows on the scale required for credible and inexpensive core heatup calculations. The MELCOR hydrodynamics models were not designed to model flow processes on a fine scale such as in TRAC [9], and the code's capability to model natural circulation effects is limited to flows through well-defined loops of several typically quite large control volumes. Thus, although MELCOR can currently model natural circulation coarsely with the hydrodynamics (CVH) package (but neglecting the momentum flux terms, which may be important for multidimensional flows), the calculation cost would be prohibitive for intended MELCOR applications if the system were nodalized on a fine scale with control volumes small enough to resolve the re-entrant core flows that may be of interest in, for example, a PWR TMLB' sequence.

Improvement in the treatment of natural circulation in MELCOR is underway to model fine-scale circulation patterns within the core and between the core and upper plenum. In addition, single-phase counter-current flow between the reactor vessel and hot leg piping or steam generator will be treated. Implementation of a natural circulation model in the Core package is greatly complicated, however, by the overlapping jurisdiction with the CVH package. Model development efforts have so far focused on defining this interface between the two packages. The principal difficulties are ensuring that the Core package natural circulation model does not lead to gross inconsistencies in quantities (e.g., temperature, flow rates) predicted by the CVH package and that numerical instabilities in calculating flows are not introduced.

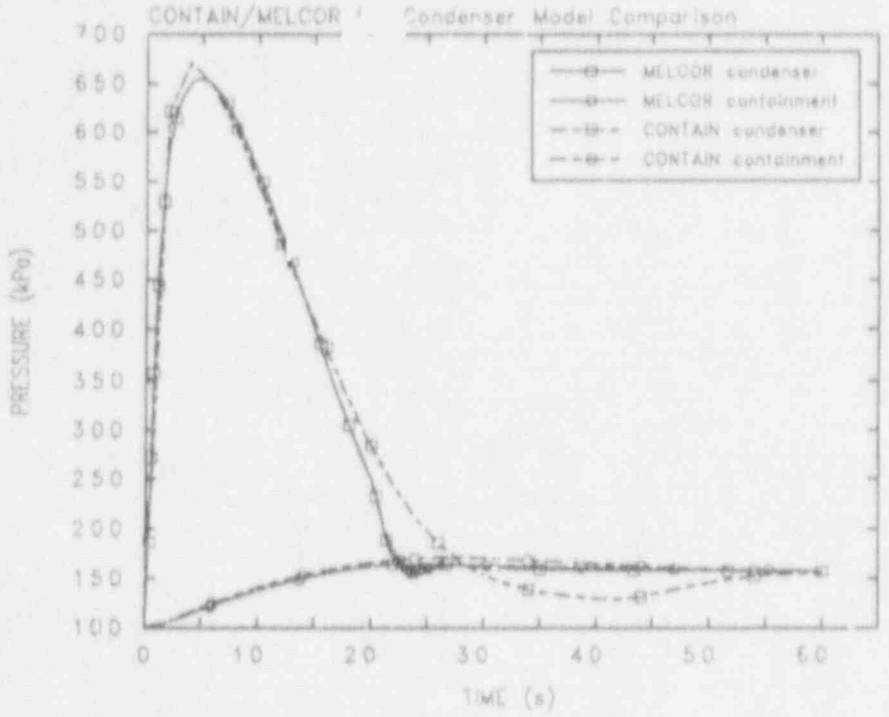

Figure 1. Pressure Response

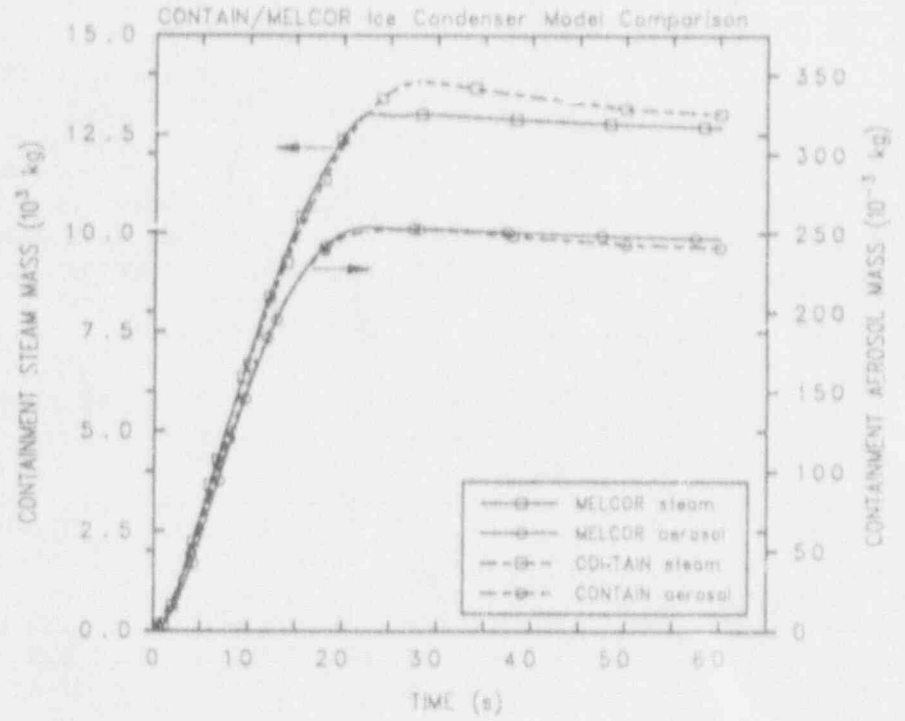

Figure 2. Steam and Aerosol Masses in Containment

The Core package, of course, can calculate any internal flows within a particular core control volume without conflict with the CVH package, which currently does not track detailed conditions within a control volume that are determined by other packages. The internal flow model is now planned to be a simplified version of the CVH approach based on known flows at the doma boundary. The interfacing problem occurs at the boundary between two control volumes (e.g., between the upper plenum and the core). To eliminate inconsistencies between the two packages, one or the other must be solely responsible for determining flows at this boundary, or competing solutions must somehow be reconciled.

Two basic strategies to resolving this problem have been identified. The first is to require the CVH package to calculate the flow distribution across the boundary using donor quantities based on local fluid conditions calculated by the COR package (i.e., local pressures, temperatures, and mass compositions). This flow distribution would then be used by the COR package on the next cycle as new boundary conditions to recalculate and update the internal flow distribution and local fluid conditions. The alternative strategy is to allow the COR package to calculate the flow distribution at the boundary between control volumes and directly transfer these flows to CVH, either as explicit mass and energy sources and sinks for the associated volumes or as imposed mass and energy flows through the connecting flow paths. Work on evaluating both strategies, especially to resolve concerns regarding numerical stability, is now in progress.

2.3 Direct Containment Heating Model

Direct containment heating phenomena have been shown to pose a potential threat to reactor containments. The rapid dispersal of core materials and resultant heating and chemical reactions can lead to rapid pressure increases in the containment. MELCOR currently has very limited capability to model debris ejection and dispersal phenomena, and the MELCOR peer review concluded that the lack of modeling compromises the code's use for some important PRA sequences as well as for audit calculations of the results of other codes.

A model has been developed within the context of the CONTAIN project that represents the global response of the containment to such events [10]. CONTAIN treats only ex-vessel phenomena, so the amount of melt ejected is a parameterized boundary condition. Adaptation of direct containment heating models from CONTAIN has begun, but MELCOR improvements to model DCH phenomena are planned to include additional parametric capabilities and user flexibility, as well as a more generalized interface to debris ejection from the reactor vessel. The planned model will allow MELCOR to calculate the integrated response of the containment to a DCH event without the use of fully mechanistic modeling. The planned model will be sufficiently flexible to encompass parametrically the uncertainties currently being addressed by ongoing experimental research and CONTAIN analyses.

2.4 CORCON-MOD3 Implementation

Core-concrete interaction phenomena are currently modeled in MELCOR by CORCON-MOD2, which was incorporated into MELCOR in 1986 without significant modification, with fission product release during these interactions treated by the MELCOR implementation of VANESA [11]. The CORCON development staff is planning release of a new version, CORCON-MOD3, which will integrate VANESA with CORCON and will include new or improved models for condensed phase chemistry, bubble behavior, interlayer mixing, oxidic and metallic phase diagrams, and nonideal solution chemistry, as well as the addition of a time-dependent melt radius option.

We have begun the process of implementing CORCON-MOD3 into MELCOR. Updates to CORCON to create an interim version of MOD3 have been received from the CORCON code development staff and are now being reviewed for formal incorporation into MELCOR. We hope to receive the final updates to create the released stand-alone version of CORCON-MOD3 later this fall, after which we will finalize the MELCOR implementation of MOD3.

2.5 Core Materials Interactions Model

Severe LWR accidents often generate conditions under which core materials begin to rapidly melt, oxidize, or otherwise interact with one another. When the molten materials mix or contact certain other solids, reactions can occur that produce new mixtures with properties which may differ from those of the reactants. For example, melting points (or liquidus and solidus temperatures) may change significantly as materials interact with one another or as the composition of mixtures changes.

The exact analysis of all the reactions and products that could conceivably occur is virtually impossible at this time. However, to accurately describe the course of an accident it is necessary to consider and effectively treat the materials interactions that will significantly affect melt progression. In the past, the MELCOR Core package included only a crude model for treating materials interactions. User input allowed certain solid materials to be transported by molten Zircaloy or molten steel. This model was intended to simulate parametrically the movement of fission-product-bearing materials (i.e., fuel) with molten Zircaloy. Each molten material was treated separately in a sequential fashion; there was no consideration of independent, multicomponent phases.

We are presently working to improve the MELCOR Core package treatment of materials interactions. Because the basic data for such an improvement is sparse and still uncertain, and because in a large system code like MELCOR, flexibility rather than detailed modeling is the more important objective, the approach being adopted will emphasize modularity and adaptability. The proposed new materials interactions model will replace the current treatment of melting, candling, and freezing of individual core materials by similar treatment for a mixture of materials. Additionally, the mixture will have the potential to dissolve solid materials at temperatures below their solidus if

phase interactions permit. The details of each physical process will be contained in one or more subroutines that can be easily replaced or modified as warranted by new phenomenological research. Certain parametric features of the model will be adapted from BWRSAR [12], but the general approach will also have much in common with that used in MELPROG [13] and SCDAP [14].

2.6 Lower Plenum Modeling Studies

The Boiling Water Reactor Severe Accident Technology program at Oak Ridge National Laboratory (ORNL) is conducting studies to investigate the effects of more sophisticated modeling on lower plenum debris behavior and reactor vessel failure and assess the need for improvement. In particular, their objectives are to incorporate specific locally-developed BWR accident response models for lower plenum debris beds into MELCOR and examine their behavior in an integrated MELCOR environment. To that end, the relevant subroutines have been extracted from BWRSAR and are being incorporated into MELCOR, bypassing the current Core package models for cells in the lower plenum.

These studies are scheduled for completion at the end of 1991 and will likely result in specific recommendations for additional MELCOR modeling changes or enhancements. Together with the NRC, Sandia will evaluate the ORNL recommendations and assess the proposed modeling changes and enhancements. This assessment will determine the amount of additional work required to integrate the changes in accordance with MELCOR design philosophy and coding conventions, a step essential to long-term maintenance of the new models.

3. FUTURE DEVELOPMENT

Additional improvements are planned for MELCOR in the near future, as described in the following sections. Most of these improvements address specific deficiencies identified during the MELCOR peer review and assessment programs.

3.1 Numerical Sensitivities

Concerns have been raised recently regarding the sensitivities of certain results calculated by MELCOR to machine type, time step size, and small changes in modeling parameters. These sensitivities severely impact the overall credibility of the code and its capability to perform meaningful sensitivity and uncertainty studies, one of its principal design objectives. The MELCOR peer review recommended that resolution of these sensitivities be given the highest priority.

These problems have long been recognized by the code development staff but have only recently been brought to user attention by the availability of computing environments in which several systems are available to a single user. These sensitivities are not unique to MELCOR, but are typical of large complicated, integrated systems codes. One major cause is "event" driven

models that change the course of a calculation at a discrete set of times (from finite time steps) when some condition is satisfied. MELCOR models are highly event laden, and subtle interactions between different events or changes in their order can greatly magnify small differences in calculations. Of course, some of these sensitivities may in fact be physically real, reflecting chaotic processes caused by the complex interplay of real phenomenological events.

To address these concerns, the level of effort for code maintenance is being significantly increased. These types of difficulties are usually extremely difficult and time-consuming to diagnose, often involving very subtle numerical and phenomenological model interactions. Special emphasis is now being placed on investigating such numerical sensitivities to identify their underlying causes and to develop strategies to eliminate or mitigate them. Calculations that have demonstrated serious sensitivities are being thoroughly examined by MELCOR code development staff diagnose the causes. Also, small test calculations are being developed to further diagnose the problems and to develop and test various fixes.

3.2 Momentum Exchange

Momentum exchange between liquid and vapor phases sharing a flow path (the so-called "inter-phase force") is responsible for both entrainment and flooding phenomena in MELCOR. The present model is very simple, based on experimentally determined parameters for the flooding curve, but it lacks adequate capability to differentiate between various types of flow paths. In particular, the MELCOR peer review committee has concluded that the current model is inadequate for prediction of pressurizer drainage under PWR severe accident conditions. Other difficulties, such as the persistence of suspended liquid pools in stacked control volumes and inadequate consideration of the effects of variations in the flow path geometry (e.g., circular tubes vs. narrow slits), have also been encountered. The current model can underpredict coupling of the phases in some cases, but may seriously overpredict it in others. This can result in inaccurate evaluation of entrainment effects, such as liquid carryover from the reactor cavity during high pressure blowdown, and of phenomena such as flooding of rooms through narrow apertures.

We are currently assessing the adequacy of the current modeling approach in light of the observed deficiencies to determine how best to modify it to apply to these other geometries and flow conditions. We then plan to incorporate enhancements to address the observed difficulties and to provide additional flexibility for the user to properly deal with complex flow path geometries. We believe that a relatively simple extension of the present model to other flow regimes and geometries will be adequate for MELCOR (we do not anticipate the need for a full flow regime map as in TRAC). Implementation of these enhancements will be assessed against the more detailed treatments of interphase flow processes in codes such as TRAC or RELAP5, which have been extensively validated for these processes.

3.3 Two-Phase Natural Circulation

A major difficulty in the CVH package was recently discovered when trying to run the FLECHT-SEASET natural circulation test for the assessment program. Severe problems in code performance were experienced at the beginning of circulation of two-phase mixtures across the top of the steam generator tubes. The models in the CVH package for the treatment of two-phase pools and the logic for depletion of control volume atmospheres are suspected as likely causes. We plan to conduct a more thorough diagnosis of the source(s) of the problems observed and to investigate and possibly implement simple fixes. Major modifications to these two models may be required, however.

3.4 Fission Product Release

An updated version of the CORSOR model [15] for fission product release, suitable for implementation in MELCOR, has been developed at Battelle Columbus, as documented in an October 1990 draft report for the NRC. This version has incorporated improvements in the release formulation and the release coefficients, including consideration of mass transport limitations and the use of the Booth model for diffusion of fission product species. We plan to review the new models, implement them in the code, and test them in the MELCOR environment.

3.5 Water Condensation

Deficiencies were identified by the MELCOR peer review in the treatment of condensation of water at the pool/atmosphere interface in a control volume and on structures in the Heat Structure package. In particular, for subcooled quiescent pools the calculation of natural convection from a stably stratified warm saturated liquid layer (at the interface) to the subcooled bulk is physically incorrect and can lead to substantial over-predictions in steam condensation rates. We plan to eliminate the first-order error of such an unphysical modeling approach and evaluate ways to account for the transient nature of conduction in quiescent, stable pools.

The heat structure condensation model does not account for the resistance of the condensate film in the presence of noncondensibles, and the use of correlations based on a low mass transfer limit will result in incorrect mass transfer coefficients under high mass transfer conditions. Results from CONTAIN calculations have confirmed the need for modeling these effects in some shorter term transients. We plan to revise the model to include both effects, similar to the current CONTAIN model, with extensive testing of the revised model on a variety of calculations to determine the impact of the new model and to ensure its robustness.

3.6 Debris Heat Transfer

Heat transfer from debris to water as it relocates from the core region to form a debris bed or pool in the lower plenum, with full or partial quenching, was identified by the MELCOR peer review as a very important missing model. Adaptation of the coarse mixing model in the Fuel Dispersal Interactions (FDI) package, used for ex-vessel debris heat transfer calculations during low pressure debris ejection, is planned to treat in-vessel debris streams as well.

The formation of fully or partially coolable debris beds in the reactor cavity with associated heat transfer (prior to the initiation of core-concrete interactions) was also identified by the MELCOR peer review as a very important missing model. Following a review and careful determination of the requirements of such a model and its interfaces to the CORCON core-concrete interactions models, we plan to implement a debris bed model that takes into account appropriate dryout heat flux limitations.

3.7 Fission Product Deposition and Chemistry

Several fission product transport phenomena not currently treated by MELCOR were identified by the MELCOR peer review as very important missing models. The existing MELCOR deposition models are most suitable for analysis of containment volumes, and the use of an input value for the diffusional boundary layer thickness, valid for containment, is questionable in primary system flows where flow and geometry effects dominate. The peer review committee has suggested that specific models now available for deposition from flowing gas streams onto surfaces, including inertial deposition from turbulent flow, diffusional deposition from turbulent flow, impaction from flow direction changes, and impaction on obstacles, be examined for implementation into MELCOR.

Other significant omissions are the effect on vapor pressure of dilution in mixed deposits, and the interaction of these deposits with surfaces (chemisorption). There is also now a considerable amount of information available on aqueous chemistry that could form the basis for a first order model (at least for iodine chemistry). The scrubbing of fission product vapors, now neglected, should be added. We plan to reassess all the phenomena described above in light of research over the past ten years and examine existing approximate or simple models for these effects for implementation into MELCOR.

4. ASSESSMENT

One of the key findings of the peer review was the need for expanded MELCOR assessment. A comprehensive, multi-year, assessment plan has been developed and activities are underway to begin addressing this need. Only a very small portion of the plan has been accomplished to date, but it is a high priority to obtain assessment results for each of the major phenomena treated by the

code as soon as possible, in particular to provide input for developing user guidelines. The plan anticipates the participation of a number of organizations, including universities and foreign institutions.

A draft assessment plan was submitted to the NRC in March 1991. That draft summarized previous and current NRC MELCOR assessment activities, reviewed and prioritized assessment needs for the different phenomenological areas modeled by the MELCOR code, proposed some general procedural and documentation requirements for a useful, efficient assessment program, and identified a number of specific MELCOR assessment tasks to be done by various participants in the next few years, sorted into an assessment program time line. This first draft has been reviewed within the NRC and sent to a few other national laboratories for further comment, and an updated draft is due in March 1992.

Assessment calculations have been completed recently and documented for the LACE LA4 aerosol transport experiment, the FLECHT SEASET natural circulation tests, the HDR V44 steam blowdown experiment and T31.5 hydrogen mixing international standard problem (ISP23), and the PHEBUS B9+ core damage international standard problem (ISP28).

In the LACE aerosol experiment LA4, the behavior of double-component, hygroscopic and nonhygroscopic, aerosols in a condensing environment was monitored. Results using MELCOR 1.8.1 gave good agreement with experimental data for most aspects of both the thermal/hydraulic and the aerosol behavior. Comparisons were also made to CONTAIN calculations. Sensitivity studies were done on time step effects and machine dependencies; thermal/hydraulic parameters such as condensation on heat structures and on pool surface, and radiation heat transfer; and aerosol parameters such as number of MAEROS components and sections assumed, the degree to which plated aerosols are washed off heat structures by condensate film draining, and the effect of non-default values for shape factors and diameter limits. A letter report on this assessment analysis was sent to the NRC in June 1991, and a formal report [16] was published in October 1991.

We have also completed MELCOR 1.8.1 calculations for the FLECHT SEASET natural circulation experiments done in a scale-model Westinghouse-PWR test facility, with code results compared to experimental data. Single-phase liquid and two-phase natural circulation cooling modes were studied, as well as reflux condensation. Sensitivity studies were done, for both single-phase and two-phase natural circulation conditions, on time step effects and machine dependencies; nodalization studies and studies on several code modeling options were also done. Good agreement was found between prediction and observation for steady-state, single-phase liquid natural circulation. The code could reproduce the major thermal/hydraulic response characteristics in two-phase natural circulation, but only through a number of nonstandard input modeling modifications; MELCOR could not reproduce the requisite physical phenomena with "normal" input models. Because the same response is observed in similar tests at other facilities over a range of scales and is expected to occur in full-scale plants as well, the ability of the user to "match" the observed behavior through a small set of nonstandard input modeling changes allows MELCOR to be used in PRA studies in which such physics are expected to

be encountered, while awaiting corrections to the code models involved. The inability of MELCOR to correctly represent two-phase natural circulation more severely impacts its potential use in those accident management applications where a greater degree of accuracy would be required. The time step control algorithm in MELCOR did not run this problem efficiently; a substantial reduction in time step resulted in significantly less oscillation predicted at the cost of only a small increase in run time. A letter report on this assessment analysis was sent to the NRC in October 1991, and a formal report [17] is now being reviewed for publication.

Earlier, MELCOR was used to simulate the HDR experiment V44, a reactor-scale steam blowdown experiment conducted by Kernforschungszentrum Karlsruhe (KfK) at the decommissioned HDR reactor facility near Frankfurt, West Germany. Those analyses were run with a version of MELCOR containing most, but not all, of the code changes incorporated in MELCOR 1.8.1. Results were compared to experimental data, to results obtained using an older MELCOR version (1.6.0) and to a CONTAIN calculation, with good agreement demonstrated. Sensitivity studies were done on the time step control used, on the degree of noding detail included, and on heat transfer coefficients and the user-specified characteristic lengths used in calculating energy transfer between control volumes and heat structures. A letter report on this assessment analysis [18] was sent to the NRC in March 1991, but no formal report is currently planned.

The analyses described above were done as part of a technical assessment program. In addition, Sandia has submitted MELCOR analyses for several recent international standard problems, as part of a separate program. In general, MELCOR has done a very credible job in reproducing the essential features of these standard problems.

MELCOR has been used to simulate PHEBUS test B9+, an in-pile severe fuel damage experiment done at the Cadarache Nuclear Center in France to investigate cladding oxidation, the mechanical behavior of a zirconia layer containing molten zircaloy, dissolution and relocation of the melt, as part of International Standard Problem (ISP) 28. Those analyses were run at the start of FY91 with MELCOR 1.8.0, and are now being repeated with MELCOR 1.8.1. Comparisons of the thermal behavior of the bundle during high fission power heating and oxidation phases show good agreement with the test data. Sensitivity studies were done on core nodalization detail, insulation thermal conductivity used, inlet mass flow and core power (within experimental uncertainties), radiation view factors, and convective heat transfer coefficients. A letter report on the MELCOR results [19] was submitted to the standard problem group in December 1990, and a letter report on the posttest recalculations with the 1.8.1 code is planned.

HDR test T31.5 was analyzed with MELCOR 1.8.0 for the ISP23 exercise. In this experiment, a steam source was injected into one of the containment compartments to simulate a pipe rupture or loss-of-coolant accident. As with the HDR V44 test and analysis, both short-term containment pressurization and temperature buildup, and long-term cooling and natural convection, were examined. In a follow-on phase in this experiment, a mixture of hydrogen and helium gases was injected to investigate hydrogen transport and mixing in a

large multi-volume containment. Letter reports were written on both the blind pretest analyses [20] and the posttest analyses and sensitivity studies [21].

MELCOR 1.8.0 was also used to analyze the TMI-2 standard problem. This allowed for comparisons of the model predictions in MELCOR to both full-scale, plant data and to the results of more mechanistic analyses. The calculations were capable of simulating the course of events in the accident and predicting the major trends, although improvements needed in various models were identified. The most recent results were presented at last year's Water Reactor Safety Information Meeting [22].

While MELCOR has been used extensively to analyze BWR accident scenarios, the TMI-2 analysis was the first use in a PWR configuration. Recently, a pair of demonstration calculations were done for the MELCOR Peer Review, in which a station blackout scenario was analyzed from full-power steady state operation, through core damage and relocation to reactor cavities, including containment pressurization, hydrogen burns, etc., for both a typical PWR and a typical BWR.

Work is currently in progress on calculations for the LOFT LP-FP-2 integral test and the ACRR ST-1/ST-2 in-pile fission product release and collection tests. The LOFT LP-FP-2 assessment analysis will examine primary system thermal/hydraulics, in-vessel core damage, and fission product and aerosol release, transport, and collection, individually and in interaction, in a "top-down" configuration, while most of the other assessment analyses completed or upcoming examine such phenomena in a more isolated, "bottom-up" situation. Additional calculations planned for the near future include the CORA 13 core damage international standard problem (ISP31); the ACRR DF-4 in-pile BWR fuel damage and relocation experiment; the Semiscale S-SG-7 integral PWR steam generator tube rupture test; the Marviken-V ATT-2b and ATT-4 aerosol transport and deposition experiments (in a primary system piping geometry, in contrast to the open containment geometry studied in the LACE LA4 assessment analysis); the SURC-2 large-scale urania-concrete interaction test; PNL ice condenser tests 11-6 and 16-11 (which also were used recently to validate the CONTAIN ice condenser model); and the ACRR MP-1 in-pile late-phase melt progression experiment.

5. CONCLUSION

MELCOR computer code development has reached the point where it is now being successfully applied in severe accident analyses. However, as stated in the MELCOR Peer Review report, MELCOR is not a completed code and additional development and assessment is needed before MELCOR can reasonably satisfy its design objectives and be applied with confidence to its targeted applications. Plans are now in place to address the most important findings of the peer review. Numerics issues are being aggressively pursued, the remaining few missing models are being developed and implemented, deficiencies in existing models are being addressed, and a comprehensive assessment program has been initiated.

We envision that MELCOR 2.0.0, with a targeted release in late 1993, will include all capabilities originally envisioned for the code plus additional capabilities that were not originally mandated (for example, limited applications in accident management). We believe that the bulk of the serious deficiencies will have been eliminated by this time. Furthermore, although it will by no means be complete, a substantial assessment base will have been established to guide analysts in using the code and giving credibility to its calculated results.

6. REFERENCES

1. R.M. Summers, R.K. Cole, Jr., E.A. Boucheron, M.K. Carmel, S.E. Dingman, J.E. Kelly, MELCOR 1.8.0: A Computer Code for Severe Nuclear Reactor Accident Source Term and Risk Assessment Analyses, NUREG/CR-5531, SAND90-0364, Sandia National Laboratories (January 1991).

2. J.A. Gieseke, et al., Source Term Code Package--A User's Guide (Mod 1), NUREG/CR-4587, BMI-2138, Battelle Columbus Division, Columbus, OH (July 1986).

3. F. Gelbard, MAEROS User Manual, NUREG/CR-1391, SAND80-0822, Sandia National Laboratories (December 1982).

4. R.K. Cole, Jr., D.P. Kelly, and M.A. Ellis, CORCON-Mod2: A Computer Program for Analysis of Molten-Core Concrete Interactions, NUREG/CR-3920, SAND84-1246, Sandia National Laboratories (August, 1984).

5. B.E. Boyack, et al., MELCOR Peer Review, Final Report (to be published).

6. R.M. Summers, "MELCOR Improvement Needs Assessment," letter report to R.B. Foulds, NRC, (September 28, 1990).

7. K.K. Murata, et al., User's Manual for CONTAIN 1.1, a Computer Code for Severe Nuclear Reactor Accident Containment Analysis, NUREG/CR-5026, SAND87-2309, Sandia National Laboratories (November 1989).

8. J.E. Kelly, R.J. Henninger, and J.F. Dearing, MELPROG-PWR/MOD1 Analysis of a TMLB' Accident Sequence, NUREG/CR-4742, SAND86-0217, Sandia National Laboratories (1987).

9. D.R. Liles, et al., TRAC-PF1/MOD1 Correlations and Models, NUREG/CR-5069, LA-11208-MS, Los Alamos National Laboratory (December 1988).

10. D.C. Williams, et al., Containment Loads Due to Direct Containment Heating and Associated Hydrogen Behavior: Analysis and Calculations With the CONTAIN Code, NUREG/CR-4896, SAND87-0633, Sandia National Laboratories (May 1987).

11. D.A. Powers, J.E. Brockmann, and A.W. Shiver, VANESA: A Mechanistic Model of Radionuclide Release and Aerosol Generation During Core Debris Interactions with Concrete, NUREG/CR-4308, SAND85-1370, Sandia National Laboratories (September 1985).

12. L.J. Ott, "Advanced Severe Accident Response Models for BWR Application," Proceedings of the USNRC 15th Water Reactor Safety Research Information Meeting, NUREG/CR-0090 (October 1987).

13. S.S. Dosanj, editor, MELPROG-PWR/MOD1: A Two-Dimensional, Mechanistic Code for Analysis of Reactor Core Melt Progression and Vessel Attack Under Severe Accident Conditions, SAND88-1824, NUREG/CR-5193, Sandia National Laboratories (May 1989).

14. C.M. Allison and E.C. Johnson, ed., SCDAP/RELAP5/MOD2 Code Manual, NUREG/CR-5273, EGG-2555, EG&G Idaho, Inc. (September 1989).

15. M.R. Kuhlman, D.J. Lehmicke, and R.O. Meyer, CORSOR User's Manual, NUREG/CR-4173, BMI-2122 (March 1985).

16. L.N. Kmetyk, MELCOR 1.8.1 Assessment: LACE Aerosol Experiment LA4, SAND91-1532, Sandia National Laboratories (September 1991).

17. L.N. Kmetyk, MELCOR 1.8.1 Assessment: FLECHT SEASET Natural Circulation Experiments, SAND91-2218, Sandia National Laboratories (to be published).

18. L.N. Kmetyk, "MELCOR 1.8.0 Assessment: HDR Containment Experiment V44," letter report to R.B. Foulds, NRC (March 20, 1991).

19. G.M. Martinez, "MELCOR Calculations of ISP28 SFD PHEBUS Test: B9+", letter report to B. Adroguer, CEN/Cadarache (December 14, 1990).

20. S.E. Dingman, "MELCOR Blind Calculations for HDR Tests 31.4 and 31.5", short report submitted for the ISP-23 calculations (August 18, 1988).

21. G.M. Martinez, "MELCOR Post-Test Calculations of the HDR Experiment", letter report to R.B. Foulds, NRC (September 29, 1989).

22. E.A. Boucheron, "MELCOR Analysis of the TMI-2 Accident", NUREG/CP-0114, Proceedings of the Eighteenth Water Reactor Safety Information Meeting, Rockville, MD, October 22-24, 1990 (published April 1991).

NEW CONTAINMENT MODELING FEATURES OF THE CONTAIN CODE*

K. K. Murata, D. C. Williams, R. G. Gido, R. O. Griffith,
K. E. Washington, and D. Y. L. Louie**
Sandia National Laboratories
Albuquerque, NM 87185

ABSTRACT

Two revisions of the CONTAIN code, CONTAIN 1.11 and 1.12, have recently been released. The purpose of this paper is to highlight the new features of these revisions and to discuss other new code features currently under development. The features of CONTAIN 1.11 discussed here include a quasi-mechanistic concrete outgassing model, the connected structure option for heat conduction between compartments, and a new approach for modeling forced convective heat transfer. The direct containment heating (DCH) models released as part of CONTAIN 1.12 are also discussed. New code features currently under development include a revised gas combustion model and a new multifield DCH model. New features of the revised combustion model include the treatment of spontaneous recombination and diffusion flames. CONTAIN plant calculations comparing the old and the revised combustion models are presented. The new features of the multifield DCH model are discussed, and demonstration calculations using this model to analyze a small scale experiment are presented.

INTRODUCTION

The CONTAIN code is the United States Nuclear Regulatory Commission's (USNRC) best-estimate code for the integrated analysis of phenomena in reactor containments during severe accidents. While the most recent complete set of documentation applies to the CONTAIN 1.10 code version,[1,2] two major revisions beyond CONTAIN 1.10 have recently been released. The purpose of this paper is to highlight the new features of the recent revisions and to discuss the new code features currently under development. Discussions will be limited to those features that address containment issues either through new or significantly improved modeling or by providing the user with a means of conveniently assessing uncertainties for those modeling areas in which the phenomena are poorly understood. The variants of CONTAIN that model reactors with heavy water or liquid metal coolant are not discussed here but are documented elsewhere.[3,4]

---

* This work supported by the United States Nuclear Regulatory Commission and performed at Sandia National Laboratories, which is operated for the U. S. Department of Energy Under Contract Number DE-AC04-76DP00789.

** Los Alamos Technical Associates, Albuquerque, NM.

The CONTAIN 1.11 code revision was not widely distributed. However, it contains a number of new features including (1) a quasi-mechanistic concrete outgassing model, (2) the connected structure option for heat conduction between compartments, or cells, and (3) a new approach for calculating forced convective heat transfer. The concrete outgassing model addresses a potentially important source of steam that could significantly affect pressures, the distribution of heat loads, and the steam inerting of hydrogen burns. The connected structure option allows heat conduction between cells through a common wall to be modeled, while allowing a full range of processes to be modeled at the wall-atmosphere interfaces. The new approach for forced convective heat transfer calculates forced convective velocities from flow path velocities for use in heat transfer correlations and in the direct containment heating (DCH) models. The CONTAIN 1.11 features are discussed in the first major section below.

The principal new feature of CONTAIN 1.12 is the DCH modeling. The DCH models, which had previously been used in unofficial versions of CONTAIN, represent a major extension of code capabilities. The basic single field debris model (SDM) treats the interactions of suspended core debris droplets with the atmosphere and with structures. It is similar to the interim model used in earlier analyses.[5] However, the modeling of debris trapping has been made more mechanistic. Cavity dispersal models, which were not part of the interim model, have also been incorporated into CONTAIN 1.12. The DCH models are discussed in the second major section below.

New code features currently under development include a revised gas combustion model and improved models for DCH. The revised combustion model incorporates updated flame speed and burn completeness correlations and introduces two new types of continuous burn models. The need for continuous burn modeling was clearly indicated in earlier DCH analyses.[5] Continuous burns are also recognized as a potentially important mode for burning hydrogen in containments when igniters are operating. To demonstrate the revised model, CONTAIN plant calculations comparing the old and the revised models are presented. The effects of the burn modeling on the predicted pressures and thermal loads within a containment are discussed. New DCH modeling is also under development to remove modeling limitations identified in earlier analyses. In particular, a multifield debris model (MDM) for suspended debris droplets has been developed to replace the SDM used in CONTAIN 1.12, and the debris chemistry model has been extended to treat chromium and aluminum. The multifield formulation is designed to track debris droplets with different debris composition, temperature, and size, whereas only average debris properties can be tracked in the SDM. Thus, the effects of distributions in droplet composition, temperature, and size and the correlations between these quantities cannot be readily evaluated in the SDM. Demonstration calculations of a small scale DCH experiment are presented to illustrate the importance of the multifield approach.

NEW MODELS IN CONTAIN 1.11

This section discusses the CONTAIN concrete outgassing model, the connected structure option, and the new approach for forced convection modeling in CONTAIN 1.11.

Improvements in the CONTAIN Concrete Outgassing Model

A quasi-mechanistic model for concrete outgassing[6] was installed in CONTAIN 1.11. The objective of this model was to have a simple, computationally efficient model that could be used, if necessary, for all of the concrete structures within a typical containment nodalization for scenarios that could last many days. This model assumes that concrete outgassing is controlled primarily by the penetration of the temperature field into the concrete and neglects the time required for the volatilized gases to migrate to the heated concrete face. The original CONTAIN 1.11 model was benchmarked against the more mechanistic SLAM and USINT codes and gave good agreement in the test cases.[6] Application of the original model to concrete nodalizations and timesteps typical of CONTAIN input decks for plant analysis, however, revealed problems with numerical robustness. Significant improvements have subsequently been made in the numerics. The principal changes involve the correction of bugs that could lead to large energy conservation errors and the implementation of a revised algorithm that tracks the position of the outgassing interface in a continuous manner.

In the quasi-mechanistic model, the evaporable water is assumed to gas within a user-specified band $[T_{lo}, T_{hi}]$ of temperatures. The fraction of evaporable water released from a given location in the concrete is assumed to be given by $(T - T_{lo})/(T_{hi} - T_{lo})$, where T is the concrete temperature. The lower bound T_{lo} of this band is by default the saturation temperature; $T_{hi} - T_{lo}$ is by default 10 K.

Figure 1 illustrates the method used in CONTAIN 1.12 to calculate the outgassing of evaporable water. One problem with the original algorithm is its assumption of uniform temperatures within each node. In general, a spatially continuous temperature profile is required to ensure that the outgassing is continuous. The revised algorithm provides this continuity through an assumed quadratic temperature dependence within a node. This dependence is determined from the node temperature and the two adjacent node interface temperatures. (These are given as T_1, T_1, and T_2, respectively, in the figure.) The node interface temperatures are determined as usual from the conduction solution without outgassing; however, the node temperature for an outgassing node is iterated until it is consistent with the heat conducted into the node and the latent heat required to vaporize the incremental change in the released water. As one can infer from the above discussion, the cross-hatched area in Figure 1 is proportional to the amount of evaporable water that has been released.

Figure 2 compares the performance of the revised algorithm with the original algorithm. This figure gives the amount of water outgassed per square meter from a 2 m thick concrete slab, as a result of a 1000 K surface temperature

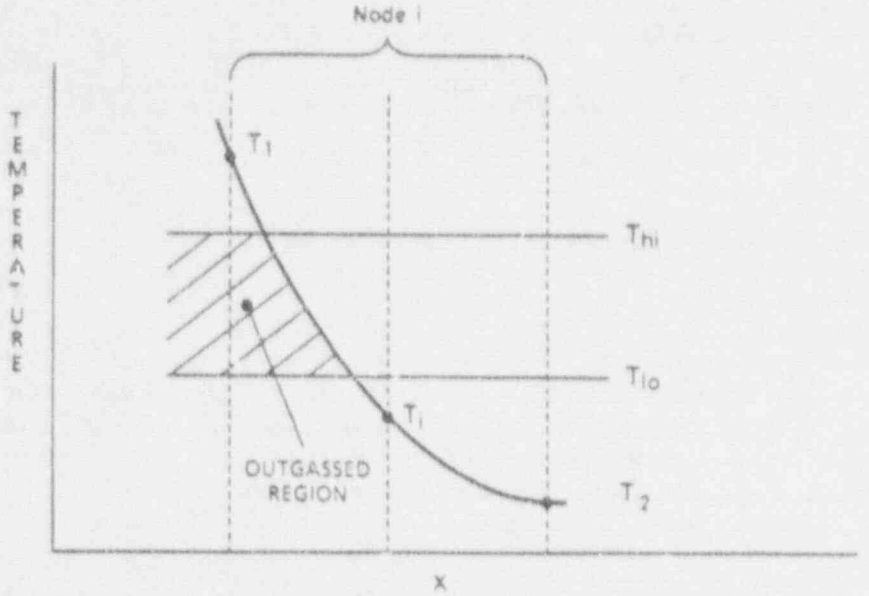

Figure 1. The temperature profile constructed as a function of the distance x within the ith structure node for outgassing purposes. According to the text, the shaded area is proportional to the amount of evaporable water that has been released from the concrete.

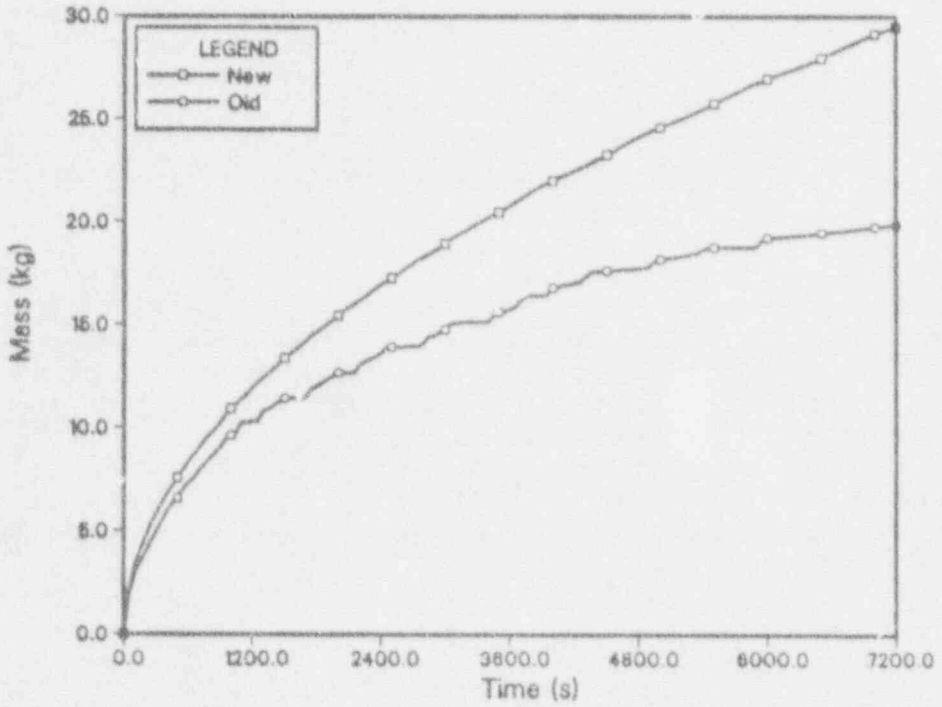

Figure 2. The amount of water outgassed per square meter of concrete as a function of time with the old and revised outgassing algorithms. The outgassing corresponds to a 1000 K surface temperature suddenly applied to concrete initially at 300 K.

boundary condition applied to one surface. On the order of 80 nodes are used to model the slab, with fine nodes adjacent to the heated surface. It is apparent that the outgassing with the original algorithm is subject to bursts as soon as the temperature field penetrates into the coarsely nodalized region of the concrete. The revised algorithm gives considerably smoother behavior.

In a recent study, the quasi-mechanistic model was used to show that outgassing is important in determining the late time containment pressure in a TMLB' scenario for the Surry plant configuration.[7] Two bounding cases in this study consider outgassing from only the concrete in the reactor cavity and from all of the concrete in the containment. The late time containment pressure was predicted to be 7.6×10^5 Pa and 17.2×10^5 Pa, respectively, in these two cases after 6 days. This variation shows that outgassing is important in determining the late time containment pressure.

The Connected Structure Option

New designs for passively cooled containments often require that decay heat be removed from containment by conduction through an inner containment shell. This shell is typically cooled externally by water sprays and by natural convection of outside air. Because of architectural limitations arising from the use of control-volume-oriented model processing, CONTAIN has difficulty in modeling the processes associated with heat transfer structures when a single heat transfer structure connects two different control volumes, or cells. Conduction between cells through such a structure can be modeled only if dry convective heat transfer is assumed to be the only important process occurring at one of the exposed structure faces. This approach to modeling conduction between cells therefore precludes the modeling of forced convection, condensation and evaporation heat transfer, surface films, radiative heat transfer, aerosol deposition, and fission product heating at one of the structure faces. This is a serious limitation for passively cooled containments.

The new connected structure option models conduction between two cells by using two heat transfer structures, one in each cell. The "outer" surfaces of these structures are assumed to be in contact, and thus the two structures actually form a composite structure. The full suite of processes described above may be modeled on the faces of the connected structures that are exposed to the cell atmospheres. However, architectural constraints still pose problems, since the conduction solution cannot be obtained at one time for all nodes in the composite structure and the proper boundary condition at the common surface is not in general known when the first of the two structures is processed. The boundary condition at the common surface is therefore determined by successive approximation. When the first structure is processed, a guess is made for the updated flux boundary condition at the common surface that would be consistent with the updated conditions for both structures after they are processed. These successive guesses converge to a self-consistent solution of the composite structure over several timesteps, provided the thermal diffusion length over a timestep does not exceed the thickness of either structure.

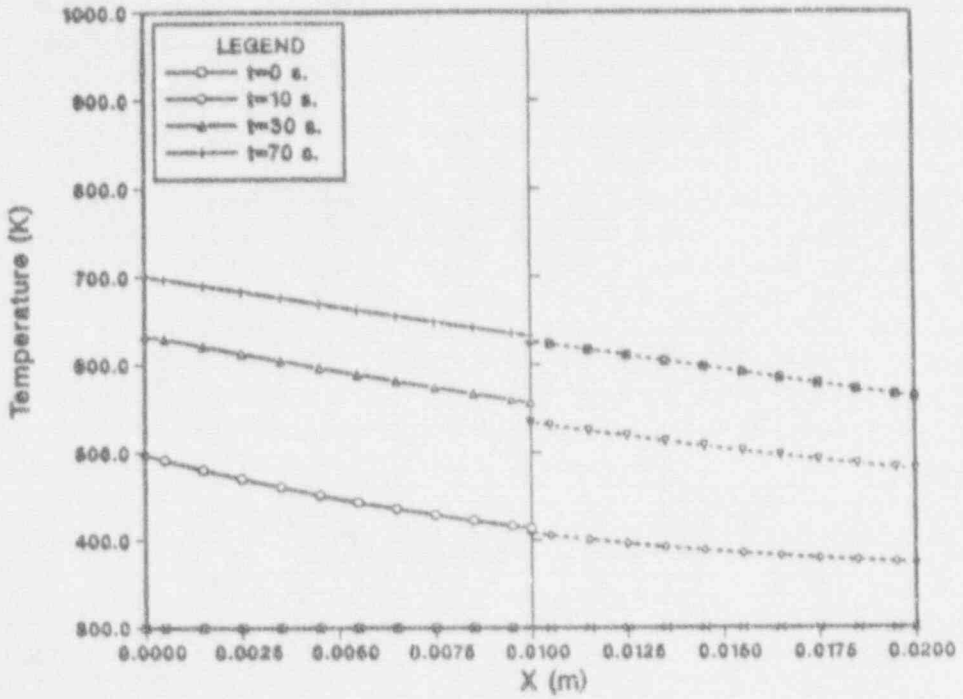

Figure 3. The transient response of two connected structures, initially at 300 K, that are suddenly subjected to a 1000 K gas temperature on the x = 0 face and a 300 K gas temperature on the face at x = 0.02 m. The structures are each 0.01 m thick. The timestep is 10 s.

Figure 3 illustrates an extreme case for the transient response of a 2.0 cm thick iron plate represented by two connected structures. (Note that an accurate calculation of this transient response requires a post-CONTAIN-2.12 bugfix.) The plate is initially at 300 K. The left face at x = 0 is suddenly exposed to a gas at 1000 K at t = 0 s, whereas the right face is exposed to a gas at 300 K. The convective heat transfer coefficient at each face is taken to be 2000 W/m^2-K, a value that is typical of condensation heat transfer. The calculational timesteps are taken to be 10 s, which is a factor of two larger than that given by the diffusion length criterion. The iteration of the temperature profiles to a self-consistent solution is illustrated by the calculated results for the first, third, and seventh timesteps. The calculated temperature discontinuities shown in Figure 3 at the midplane are reasonable even though this example represents an extreme case. Because the exposed face boundary conditions are also calculated explicitly, in actual applications it is desirable that the variations in the surface temperatures at the exposed faces vary much more slowly per timestep than shown here. In such a situation, the temperature discontinuities shown in Figure 3 would be considerably smaller.

A New Approach for Forced Convective Heat Transfer Modeling

CONTAIN is a control-volume code in which gas velocities and momentum are neglected within cells for the purpose of calculating atmosphere thermodynamic states and intercell flow. This stagnant cell approximation is, however, supplemented by natural convective heat transfer correlations for use in calculating heat transfer to structures. In addition, the user may specify forced convective heat transfer coefficients in tabular form for situations in which natural convection is not appropriate. Such forced convective heat transfer may be appropriate during a blowdown or for heat transfer structures of relatively small characteristic length that are sitting in the natural convection field of larger structures. It has been argued, for example, that such coupling between structures is important in the analysis of the LA-4 experiment.[8] The difficulty with the tabular method of specifying forced convective heat transfer is that the user often does not know a priori which velocities to use. A new approach in CONTAIN 1.11 allows forced convective velocities to be calculated from flow path velocities, provided the containment nodalization is sufficiently detailed to capture the flow pattern in question. This approach allows the user to specify the general linear combination of velocities in the flow paths attached to a cell that define the forced convective velocity for a particular structure. By default, the forced convective velocity is defined as the average of cell inlet and outlet velocities. The inlet velocity is calculated by assuming that the incoming flows mix together and channel into a user-specified hydraulic area. By default, the hydraulic area used for the inlet and outlet velocities is the cell volume to the two-thirds power. This option should make it considerably easier for the user to model forced convective heat transfer.

DIRECT CONTAINMENT HEATING MODELS IN CONTAIN 1.12

The DCH models are the principal new models in CONTAIN 1.12. They are a refinement of unreleased interim models that were exercised extensively to analyze experiments and to investigate the important physical processes that determine DCH loads in nuclear power plants.[5] The single field debris model (SDM) is the basic debris droplet interaction model. Debris chemical reactions involving Zr and Fe in the debris with oxygen and steam in the atmosphere are modeled, using transport rates determined by both gas- and drop-side diffusion. Debris-structure and debris-gas heat transfer are modeled, as well as other debris-structure interactions, such as debris trapping. The intercell transport of the droplet field is calculated directly by the implicit flow solver, where it is treated as a separate field from the gas field but presently assumed to flow without slip with respect to the gas.

A number of refinements and additions to the original interim model[5] are reflected in the SDM. One refinement is in the Fe chemistry, which now uses an equilibrium model, as opposed to one in which the Fe reactions go to completion. The trapping model has also been expanded to offer the user a wider variety of methods for calculating trapping rates. The original approach of a user-specified trapping rate has been retained, but since the user often specified a rate corresponding to settling, an option for

gravitational-fall-time (GFT) modeling of the rate may now be specified directly. In addition, a new time-to-first-impact (TFI) model uses a jet expansion law and the distance to the first surface encountered by the jet to calculate trapping rates. Finally, the TFI approach is coupled to a Kutateladze criterion to determine trapping rates in the time-of-flight (TOF/KU) option. In the latter option, if the debris is re-entrained after the first impact according to a Kutadelaze criterion, it is assumed to strike a second surface. The debris is assumed to be trapped on that surface if the re-entrainment criterion for that surface is not satisfied. For re-entrained debris, either the mean cell convective velocity or GFT criterion may be used to determine the final trapping rate.

Two models are present in CONTAIN 1.12 to describe the details of the debris-steam interactions in the cavity: CORDE[9] and GASBLOW[10]. CORDE models a number of processes in the cavity, beginning with the debris/steam blowdown from the vessel, which is assumed to start from an instrument tube failure. The ablation of the hole in the vessel is modeled concurrently with the jet of molten debris and steam from the vessel. The jet initially is composed of molten debris until steam blowthrough, after which the jet becomes a two-phase mixture of steam and debris.

CORDE assumes that the debris will accumulate largely as a liquid pool on the cavity floor prior to steam blowthrough from the vessel. After steam blowthrough, the molten debris is assumed to be pushed away from the region beneath the vessel and to form a hydraulic step. CORDE models entrainment as occurring from this step. As in the SDM, heat transfer and chemical reactions of the entrained debris are modeled. The amount of debris dispersed from the cavity will depend on a number of processes, including impaction on surfaces, re-entrainment, crusting of debris on surfaces, and levitation by gas flow in the vertical direction.

Because of the similarities between CORDE and GASBLOW, only the GASBLOW models that are substantially different from those in CORDE have been implemented. A significant difference in the GASBLOW modeling is that debris entrainment is assumed to occur from the entire cavity floor, not just the hydraulic step. Seven different GASBLOW models for the entrainment process and three different GASBLOW models for heat transfer to the ablating vessel wall are available as options within the CORDE implementation.

It should be noted that although the CORDE module in CONTAIN 1.12 was tested on several full scale containment problems, numerical difficulties have been encountered in applications to small scale systems. Although these problems have reportedly been addressed in the latest version of CORDE[9], this version has yet to be evaluated and officially incorporated into CONTAIN.

RECENT CODE DEVELOPMENT

This section discusses recent code development that extends the models present in CONTAIN 1.12. These extensions are presently being incorporated into a new code version, CONTAIN 1.2. The first subsection below discusses the revised

gas combustion model and presents the results of sample plant calculations exercising the revised model. The second subsection discusses recent DCH modeling features, including the ability to treat chromium and aluminum chemistry and an extension of the SDM to multiple fields.

The Revised Gas Combustion Model

The hydrogen deflagration modeling in CONTAIN 1.12 is based on the HECTR 1.5 code.[11] With the advent of the HECTR 1.8 code,[12] the correlations used for flame speed and burn completeness in CONTAIN 1.12 appeared to be out of date. Also, the deflagration model applies only to one of the several types of burns of interest in containment analysis. Thus, the gas combustion model has been revised to include the HECTR 1.8 correlations for flame speed and burn completeness. Also, two additional types of burns are modeled: diffusion flames, which can occur when a combustible gas enters a compartment containing oxygen, and bulk spontaneous recombination, which is expected to occur at sufficiently high temperature. One further change is to use a new diluent inerting criterion that takes into account the inerting effect of excess nitrogen, which is the amount present in excess of the ratio with oxygen found in air. The diluting effect of excess nitrogen is important to consider if previous burns have occurred. It should be noted that nitrogen is not considered to contribute to diluent inerting in either CONTAIN 1.12 or the HECTR 1.8 code.

The purpose of the diffusion flame model is to allow the user to explore the effects of burning hydrogen in a jet rather than in a deflagration involving premixed gases. The burning of premixed gases could be physically reasonable when igniters are first turned on, or when igniters are on and the atmosphere subsequently deinerts. However, in cases in which hydrogen is being introduced to containment with igniters on and the atmosphere is not inerted, quasi-continuous burning such as calculated in the diffusion flame model may be physically more reasonable. The effect of such quasi-continuous burning is illustrated in the sample plant calculations discussed below.

The diffusion flame model is a relatively simple one that is not intended to be fully mechanistic. The parametric nature of the model stems principally from the fact that the dynamics of the diffusion flame are not modeled. While the user may specify the inerting concentrations above which the diffusion flame cannot initiate, there is no modeling of the dynamics of the flame front that determine whether the diffusion flame is stable. For example, the tendency of the flame to blow out at high jet velocities is not modeled. There is also no explicit modeling of entrainment processes that would cause some of the bulk hydrogen (if any) in the cell with the diffusion flame to be carried into the flame and recombined. The diffusion flame model, given non-inerted conditions and the presence of an ignition source in the downstream cell, simply burns the combustible gas flowing into a cell through a flowpath or from an external source, utilizing the oxygen in the cell. Note that there is presently no provision for jet self-ignition, which can happen, for example, when the incoming gas is sufficiently hot. The diffusion flame and spontaneous recombination models are solved implicitly with the intercell flow and atmosphere thermodynamic models to prevent numerical stability problems.

The bulk spontaneous recombination model is also a simple parametric model. The model uses a recombination threshold temperature and a recombination rate const[illegible] are specified by the user. This model provides a physically reasonab[illegible] description of spontaneous recombination for DCH parametric studies.[5] The unconditional hydrogen burn (UCHB) approach used in previous DCH studies to simulate spontaneous recom[illegible]nation utilizes the CONTAIN deflagration model with a user-specified flame speed and with ignition thresholds set to zero. The UCHB method requires determining a suitable "ignition time" in each cell in advance, and code restarts with input changes are in addition required if conventional deflagrations prior to the start of spontaneous recombination are also modeled. The UCHB approach also introduces numerical artifacts such as "dead-time," during which no burning is allowed. Calculations comparing the new spontaneous recombination model with the UCHB approach are discussed in the next section.

Sample Plant Calculations With the Revised Gas Combustion Model. The sample plant calculations discussed here are intended to illustrate the effects of the changes in the gas combustion model. Although a DCH event is involved, the principal focus of these calculations is the hydrogen behavior, not the DCH behavior. Thus, the effect of different models or assumptions regarding hydrogen behavior is investigated but only a base case is considered with respect to the DCH parameters. In addition only the single-field DCH model in CONTAIN 1.12 is used in the plant calculations.

These calculations are based on a Surry TMLB' scenario. The scenario selected corresponds to one that was previously used to study the mitigation effects of intentional early depressurization (ED) of the pressure vessel on the DCH event.[7] In early depressurization, the pressure vessel is postulated to be depressurized, to the extent possible, through opening of the pressurizer relief valves and head valves at the point of steam generator dryout. Although the calculated vessel pressure at vessel failure, 1.5 MPa, is much lower than the set-point pressure of the pressurizer relief valves, it is assumed to be sufficient to cause a DCH event. Significant mitigation of the DCH loads, however, is found because of the reduction in the inventory of steam and hydrogen in the vessel, which reduces the driving force for the DCH event.

The plant configuration is shown in Figure 4. As indicated in this figure, Cell 1 corresponds to the reactor cavity; Cell 2, the basement and lower annulus; Cell 3, the upper and middle crane wall annulus; Cell 4, the dome and steam generator cubicles; and Cell 5, the pressurizer compartment.

As discussed in the earlier study,[7] the pressure vessel conditions and the steam and hydrogen sources to containment for the ED scenario prior to vessel breach were calculated at INEL using the SCDAP/RELAP codes. These sources are directed into the pressurizer compartment (Cell 5). The steam and hydrogen blowdown rates from the vessel and the core debris entrainment rates during the DCH event were calculated separately, as described in the earlier study. Fifty percent of the core is assumed to participate in the DCH event.

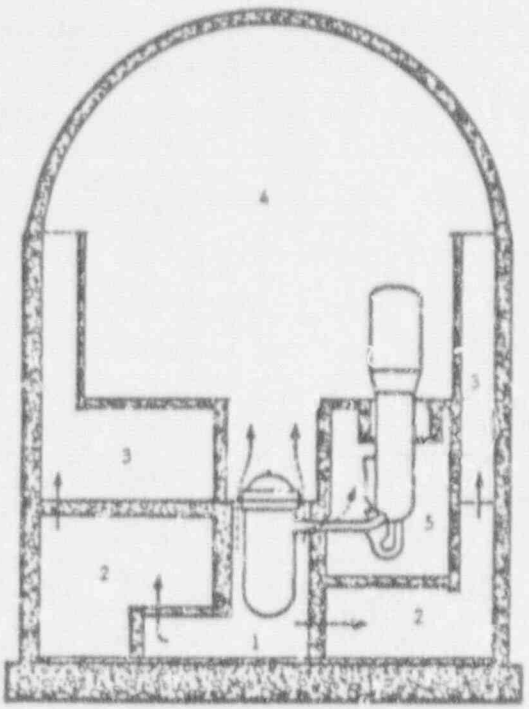

Figure 4. The 5-cell model of the Surry containment.

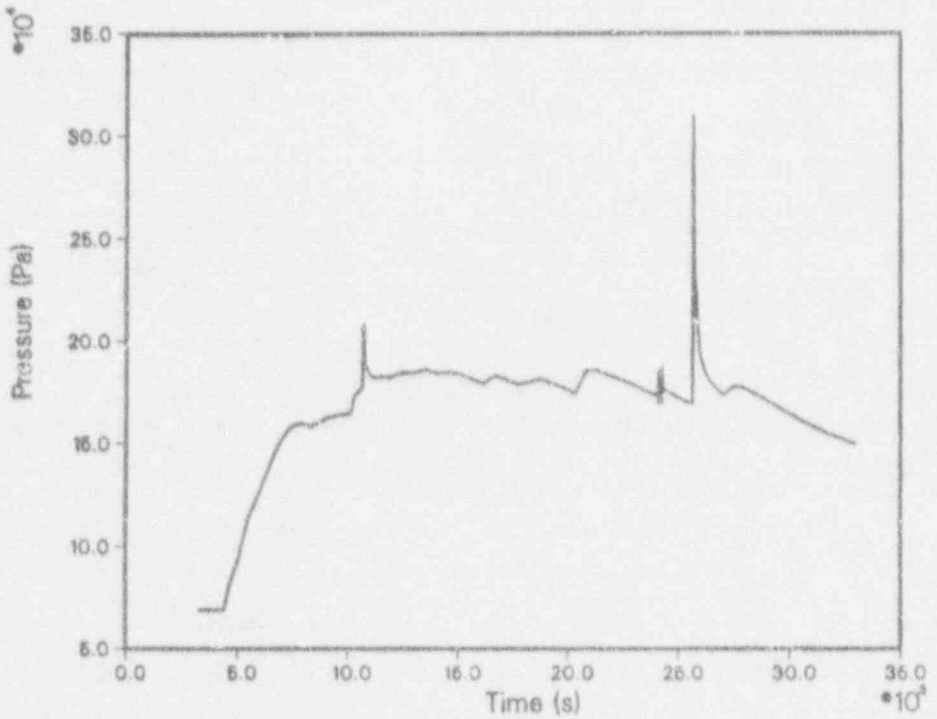

Figure 5. The calculated dome pressure in Case 1.

Table I.
Hydrogen Burn Modeling Features Used
in the Surry Plant Calculations

	Deflagrations	Diffusion Flames	Spontaneous Recombination
Case 1	x		
Case 2	x		x
Case 3	x	x	x
Case 4			x
Case 5			x*

* Uses the UCHB approach

The sample calculations performed here address the effect of hydrogen burns prior to vessel breach and during the DCH event. A series of five sample calculations were run, as summarized in Table I. The hydrogen burning modeling in the runs was varied as follows: In Cases 1-3, independently powered ignitors are assumed to be turned on at all times, and in Cases 4-5, ignition sources (except for bulk spontaneous recombination induced by the hot debris) are assumed not to be available. Furthermore, in Case 1, the hydrogen in the problem is assumed to burn only according to the new deflagration model, even during the DCH event after vessel breach. In Case 2, the hydrogen is also assumed to burn only according to the deflagration model prior to vessel breach. During the DCH event, however, both deflagrations and bulk spontaneous recombination are modeled. In Case 3, both diffusion flames and deflagrations are modeled. In addition, during the DCH event, spontaneous recombination is modeled. In Cases 4 and 5, it is assumed that because of the absence of ignition sources, no hydrogen is burned prior to the DCH event. However, bulk spontaneous recombination is assumed to occur during DCH. In Case 4, the spontaneous recombination is modeled using the new approach, whereas in Case 5 the unconditional hydrogen burn (UCHB) approach discussed above is used.

The calculated results will be discussed in the following order: First, the deflagration behavior calculated in Case 1 with the revised modeling will be compared with that obtained with the old modeling. Second, the effect of diffusion flames on the hydrogen burn history prior to vessel breach (Case 3) will be discussed. Finally, the effect of the revised modeling on the DCH event will be discussed.

Figure 5 gives the dome pressures calculated in Case 1 with the new modeling. Only the period prior to vessel breach, which occurs at 33000 seconds, is shown. Three groups of deflagrations occur, at approximately 11000, 24000, and 26000 seconds. The first group corresponds to a propagating burn involving the basement and annulus (Cells 1, 2, and 3); the second, a set of

Table II.
Comparison of Deflagration Burns
Obtained With the Old and New Burn Correlations
in the Surry ED Scenario

	Burn Group 1: Propagating Burn		Burn Group 2: Multiple Burns in One Cell		Burn Group 3: Propagating Burn	
	New	Old	New	Old	New	Old
Initiating Cell	1	1	5	5	5	5
Peak Pressure (10^5 Pa)	2.07	1.99	1.78*	1.80*	3.09	2.39
Peak Temperature (K)	638	633	954*	825*	843	762
Cumulative H_2 Burned (kg)	79.3	73.7	93.9	121.9	383.0	303.9
Initiating Time (s)	10680	10680	24080	24040	25619	25728
Group Burn Time (s)	77.8	127.1	9.2	36.8*	52.0	137.1

*Refers to initial burn only

multiple burns in the pressurizer compartment (Cell 5); and the third corresponds to a propagating burn in all five containment cells. The characteristics of these burns are also given in Table II, under the column labeled "New."

The observed burns either shortly follow or coincide with the three periods in which the steam/hydrogen mixtures vented to containment are particularly rich in hydrogen. The fact that the burns do not always involve the pressurizer compartment (Cell 5) is due to steam inerting. The burns that do occur in the pressurizer compartment are in fact deinerting burns; i.e., ones whose timing is dictated by the point at which the diluent mole fraction drops below the inerting limit (by default, 55%). The deinerting of the pressurizer compartment coincides with the venting of hydrogen-rich steam/hydrogen mixtures into the pressurizer compartment, which tends to decrease the steam mole fraction.

For comparison, the burn characteristics obtained in the old deflagration modeling are also presented in Table II. One can see that the burns with the new modeling have a significantly shorter burn time than with the old modeling. This is consistent with the expected differences between the old and new flame velocity correlations at high concentrations of diluent, which in the present calculations is primarily steam. For atmospheres with steam concentrations close to the inerting limit of 55%, one would expect the new correlation to give higher flame velocities than the old correlation, for a given hydrogen concentration. Conversely, for relatively dry atmospheres, the

new correlation gives lower flame velocities. The faster burns are consistent with the calculated steam concentration of approximately 50% during the burns.

As shown in Table II, the amounts burned in the propagating burns (Burn Groups 1 and 3) with the new correlations are substantially larger than with the old. This fact is believed to be primarily the result of the change in the burn completeness correlation, although the amounts of hydrogen burned for a given burn completeness may also be indirectly affected by the changes in the flame velocity correlation. For example, in cells with highly restrictive flow paths, a faster burn will not allow as much gas to be expelled from the cell during the burn, which will allow more to burn in the cell. Conversely, in cells with large heat transfer areas and nonrestrictive flow paths, a slower burn will allow more heat to be transferred from the gas during the burn, which will reduce the gas expansion rate and allow more hydrogen to burn.

The relationship between the old and new burn completeness correlations depends on both the hydrogen mole fraction at ignition and the diluent mole fraction. At 50% diluent mole fraction, the new completeness correlation gives a higher completeness up to 8% hydrogen, at which the completeness becomes unity. For somewhat lower diluent mole fractions, burns are more complete at lower hydrogen concentrations with the new correlation (at 40% diluent, the point at which higher completeness is obtained with the new correlation is 6.6% hydrogen). For relatively low diluent concentrations, the new correlation gives a lower completeness than the old.

It should be noted that the number of burns occurring in the second burn group in Table II differs substantially between the new and old correlations. Two burns occur in succession in the pressurizer compartment (Cell 5) in this group with the new correlations, whereas six burns occur in succession with the old correlations. This difference is believed to be due to the inclusion of the effects of excess nitrogen in the new diluent inerting criterion, which tends to inhibit burns within a cell as oxygen is depleted. The large number of multiple burns in Cell 5 with the old correlations tends to decrease the hydrogen reaching the surrounding cells. This decrease contributes to the relative weakness of the third burn when the old correlations are used.

The diffusion flame modeling in Case 3 apparently changes the character of the hydrogen burns appreciably. (The burns in Case 2 prior to vessel breach are identical to those in Case 1.) This change is most clearly seen in the total hydrogen burned, since the diffusion flames do not increase the pressure appreciably above the background value calculated in the absence of burns. Figure 6 compares the cumulative total hydrogen burned, prior to vessel breach, for Cases 1 and 3. The continuous initial rise in the hydrogen burned in Case 3 indicates that the hydrogen burns initially in the form of diffusion flames in these cells and not as a deflagration. The sporadic nature of the diffusion flame burning shown in Figure 6 is due to the fact that the compartment atmospheres typically have steam molar fractions close to the bulk inerting limit of 0.55 (the default value for diffusion flames) and in addition the intercell flows typically have steam/hydrogen molar ratios close to the flow inerting ratio of 9 (the default value). While local deflagrations still occur in the pressurizer compartment (Cell 5) around 24000

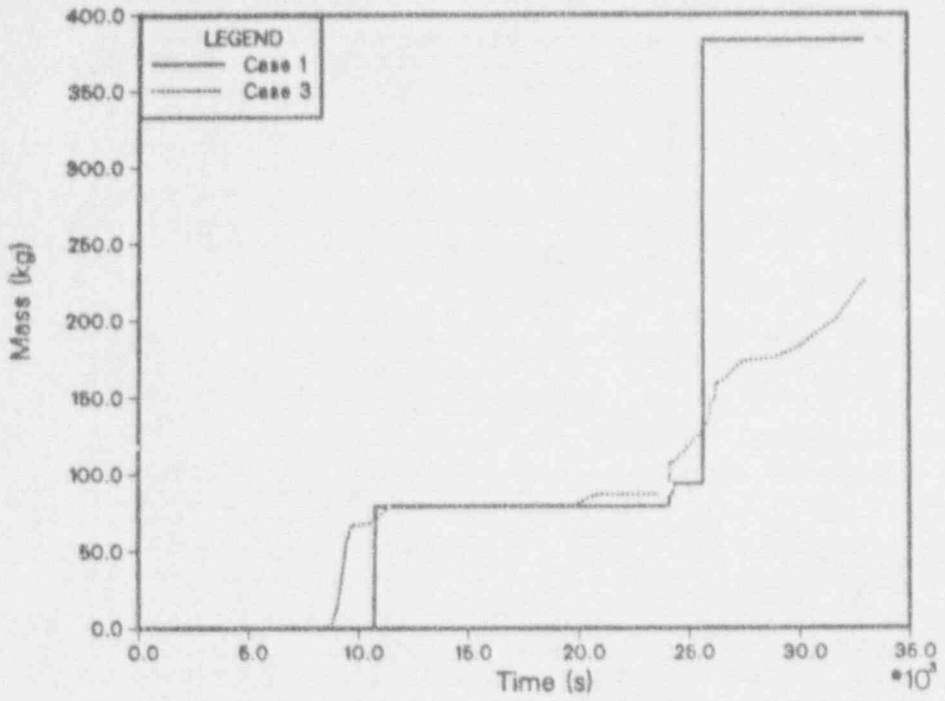

Figure 6. A comparison of the cumulative hydrogen burned in Case 1 and Case 3 versus time.

and 26000 seconds in Case 3, the diffusion flame modeling alters the hydrogen distributions sufficiently to eliminate the propagating burns that occur in Case 1 at 11000 and 26000 seconds.

As indicated by Figure 6, the total hydrogen burned prior to vessel breach is considerably less with the diffusion flames modeled in Case 3 than without. As discussed below, the additional hydrogen present in Case 3 increases the severity of the containment loads from the DCH event at vessel breach when spontaneous recombination is modeled. However, whether more or less hydrogen is burned with diffusion flames is clearly scenario dependent. If the diffusion flames had burned more efficiently (i.e., if inerted conditions were not present part of the time) or if a major deflagration had not occurred in the absence of diffusion flames, then the relationship between the amounts burned in the two cases could be inverted.

The diffusion flame model controls not only the burning of intercell gas flows but also the burning of external sources such as the steam/hydrogen mixture vented into the pressurizer compartment (Cell 5) from the primary system. However, the user-specified bulk steam inerting mole fraction for diffusion flames in the present calculations is set to the default value of 0.55 (the same value used for deflagrations), and thus, when inerted, the pressurizer compartment is inerted against both deflagrations and diffusion flames. When this compartment deinerts through the influx of a hydrogen-rich steam/hydrogen mixture, the resulting deflagration typically dominates the hydrogen burning, although some diffusion flame burning of the mixture could also occur.

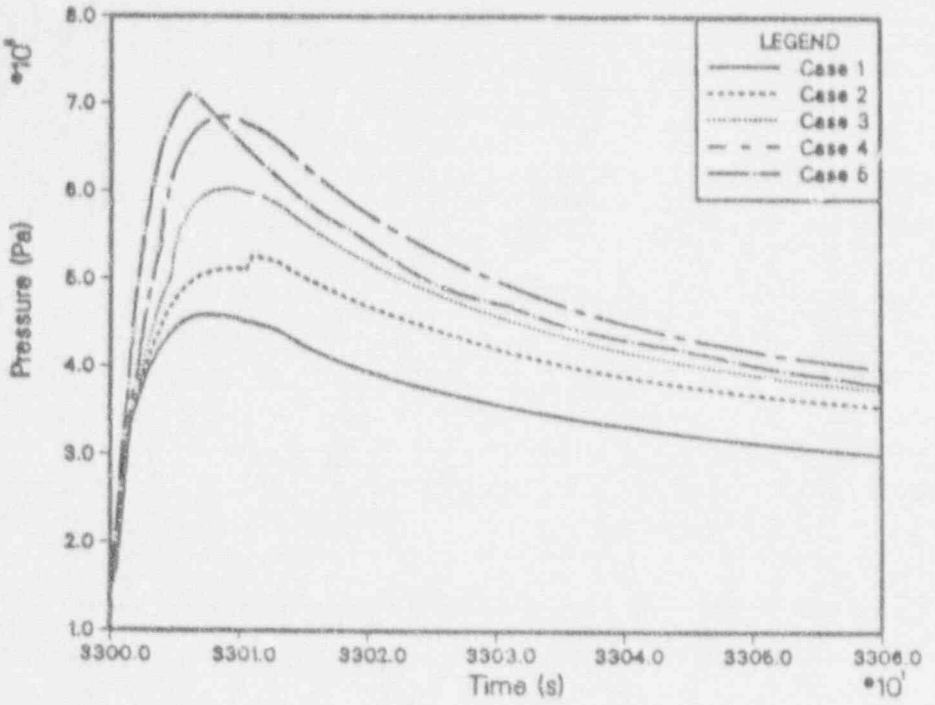

Figure 7. The dome gas pressure calculated in various cases during the DCH event.

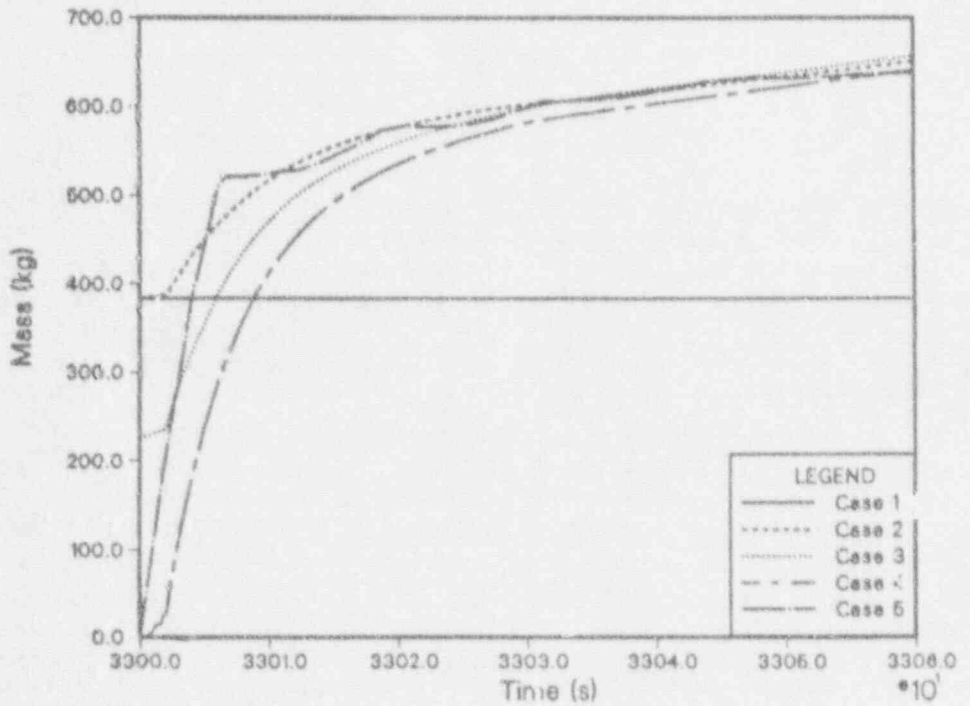

Figure 8. The cumulative hydrogen burned in various cases. The time period shown corresponds to the DCH event.

Cases 4 and 5, which do not have burns prior to vessel breach, are of interest primarily with respect to the burns occurring during the DCH event following vessel breach at 33000 seconds.

The discussion of the burns during DCH is simplified considerably by the fact that at the time of vessel failure, the upper containment is inert in Cases 1-3 so that diffusion flames and deflagrations cannot initiate. In Case 3, a small amount of hydrogen (a few kilograms) is burned in a diffusion flame in the lower containment (Cell 2) during the DCH event, but this amount is negligible. In addition, in Cases 4 and 5 diffusion flames and deflagrations are assumed to be absent. Thus, all five cases can essentially be discussed in the context of the high temperature bulk spontaneous recombination process.

In previous calculations of the present scenario,[7] the containment was not calculated to be inert during the DCH event when deflagrations occurred prior to vessel breach. Thus, deflagrations could also occur during the DCH event. The change from noninert to inert conditions with prior deflagrations reflects the fact that the new inerting criterion takes excess nitrogen into account.

Figure 7 gives the dome pressure calculated in each of the five cases during the DCH event. Case 1 (which models only deflagrations according to the default criteria before and during DCH) gives the lowest pressure, since no hydrogen is in fact burned during DCH. Cases 2-5 assume that spontaneous recombination occurs during debris dispersal. Except for Case 5, these latter cases differ primarily in the amounts of hydrogen burned prior to vessel breach. As discussed above, in Case 2, deflagrations are modeled before vessel breach. In Case 3 both deflagrations and diffusion flames are modeled before vessel breach, while in Case 4 and Case 5 no burns are modeled prior to vessel breach. Cases 2-4 use the new spontaneous recombination model after vessel breach, with a threshold temperature of 773 K, while Case 5 uses the UCHB approach, with a flame speed of 5 m/s and an ignition time corresponding to the time of vessel breach. This value of the flame speed was chosen to be conservative in the sense that hydrogen burning at this rate significantly reenforces the pressures that would otherwise be generated during DCH. For comparison purposes, the recombination rate in the spontaneous recombination model was taken to be the inverse of the burn time in the UCHB approach.

Figure 8 gives the total amounts of hydrogen burned in the five cases as a function of time, including the hydrogen burned prior to vessel breach. One can deduce from this figure that the change in peak pressure from the baseline provided by Case 1 is approximately proportional to the amount of hydrogen burned during DCH up to the point of peak pressure, which is not too surprising.

What is surprising is the sensitivity of the peak pressure to the existing hydrogen present in containment at vessel breach. A mass balance shows that approximately 440 kg of hydrogen is generated from the metal-steam reactions during DCH, with another 5 kg present in the vessel at vessel breach. This is to be compared to the 515 kg vented into containment prior to vessel breach. The change in peak pressure from Case 2 to Case 3 (more than a factor of two relative to that between Case 2 and Case 1) corresponds to a change in

existing hydrogen of 150 kg, which is only one third of the amount generated during DCH. This sensitivity could be explained if much of the hydrogen generated during DCH were confined to the oxygen-poor lower regions of containment, or if the generation of the hydrogen occurred relatively late. Examination of the hydrogen distributions at the end of the calculations at 33060 s shows that an amount corresponding to about two-thirds of the generated hydrogen is retained in the basement and lower annulus. This observation explains the sensitivity of the peak pressure to the existing hydrogen in the present scenario. Note that this sensitivity may not be present to the same degree in fully pressurized scenarios because more vessel steam would probably improve the transport of hydrogen from DCH to the upper containment.

The distinct difference in the timing of the hydrogen burning between Case 5 and the other cases is due to the fact that a constant burning rate is assumed in the UCHB approach and an exponential burning rate is assumed in the spontaneous recombination model. The pressure trace and amount burned for Case 5 also reflect an artifact introduced by the use of the deflagration model for "continuous burning"; namely, the oscillations in the burning rate after the point of peak pressure. These are due to the "dead time" in the deflagration modeling, which is the period after the end of one deflagration during which a second deflagration cannot start. Also, the sudden jump observed in the pressure in Case 2 near the peak pressure is a numerical artifact related to flow oscillations caused by the explicit nature of the debris chemistry model, and thus the jump should be ignored as a contribution to the pressure.

Recent DCH Modeling Improvements

Improvements to the DCH modeling in CONTAIN 1.12 are presently under development for inclusion in the future CONTAIN 1.2 code version. The first is an extension of the debris chemistry model to include reactions involving Cr and Al in addition to Zr and Fe. While Cr chemistry is of interest in plant analysis, the principal motivation for this extension lies in being able to analyze DCH experiments that use Fe-Al thermite to simulate core debris. The previous approach for modeling Cr and Al reactions treated Cr and Al as an equivalent amount of Zr. Since one can define the equivalent amount in terms of either the hydrogen or energy produced and since it is important to produce the correct amounts of both, the equivalent amount of Zr was computed on the basis of hydrogen generated, and the Zr enthalpy functions were modified to give the appropriate heat of reaction and specific heat. Needless to say, such an approach is cumbersome and requires significant alterations in input whenever the debris simulant composition is changed.

A second improvement is an extension of the droplet interaction model to include multiple fields. The SDM can, of course, track only a single droplet size and only the average debris temperature and composition in a cell. The pitfalls of such a representation are related to the fact that distributions of composition, temperature, and size may exist among the debris droplets. For example, newly entrained debris, with a relatively high metal content, may constitute only a small fraction of the airborne debris. In this case

averaging the new debris in with the old burned-out but still airborne debris could introduce serious distortions in the metal burnup and heat transfer rates. Because of metal burning, new drops are likely to be much hotter than the average, yet could represent much less than the total heat and mass transfer area available for airborne debris. The limitations of the SDM and the approaches previously taken to compensate for these limitations are discussed in detail in Reference 5. However, without a multifield model there is no good way to assess quantitatively the distortions introduced by the single field approach. Recent DCH experiments, furthermore, indicate that the debris size distribution is very broad. As indicated by the MDM demonstration calculations discussed below, use of a single droplet size is not adequate for these very broad distributions, at least for small scale experiments in which the efficiency of debris interactions is not very high.

The MDM presently has a number of ways to characterize the multiple fields. Different sizes may be assigned to the various fields. Debris droplets entrained at different times may be assigned to different debris fields, or "generations." Also, debris droplets may be assigned to different fields according to composition. The MDM is still under development. Its final form will be dictated by the needs of ongoing experiment analyses and by the modeling details required to extrapolate the results of experiment analyses to full scale.

MDM Demonstration Calculations. This section discusses a series of demonstration calculations that have been completed with the MDM. These calculations investigate the sensitivities present with respect to debris droplet composition, history, and size distributions in the analysis of a small scale experiment. The importance of the MDM in predicting scale dependencies for small scale experiments is also discussed.

These calculations are based on the Integral Effects Test (IET) series being conducted at Sandia National Laboratories. For these experiments the Surtsey facility has been modified to represent the lower compartments and structures of the Zion plant in a 1:10 linear scale. The calculations use a 14-cell CONTAIN model that was developed to perform pre- and post-test analyses of the IET experiments. The initial conditions and sources used were derived from the IET-1 experiment.[13] Calculations using a rescaled 14-cell model were also performed at 1:39 scale, which corresponds to that of experiments to be performed at the CWTI facility[14] at Argonne National Laboratory and the results are compared to those at 1:10 scale.

It should be emphasized that the present calculations were undertaken to investigate the modeling sensitivities that can be examined specifically with the MDM and to investigate the effects of these sensitivities in predicting scale dependencies. For these purposes it is not necessary to do a best-estimate calculation for IET-1, as long as the results agree reasonably well with the experiment. Thus, features such as the quasi-mechanistic trapping models available in CONTAIN 1.12 and the recent Cr/Al chemistry models were not used in the present calculations. Consequently, they should not be construed as representing a best-estimate analysis for IET-1.

Table III gives the results from the various calculations for the pressure rise, the amount of steam reacted, and the heat transfer from the debris during debris dispersal. The sensitivity being examined in each case are discussed in conjunction with each individual calculation below. The "IE" series of calculations used the normal 1:10 experimental scale, and the "CW" calculations used 1:39. The airborne debris droplet size distribution in each case was chosen to be consistent with the recent experiments in the Surtsey facility. Unless otherwise indicated in the table, only a single size was used, with a drop diameter of 1 mm. In the case of multiple sizes, a lognormal distribution was used, with a mass median diameter of 1 mm and a geometric standard deviation of 4. Unlike the mass and energy in the problem, which were assumed to scale like the volume, the droplet sizes were assumed not to change with scale. An invariant size distribution is consistent with the assumption that intensive parameters, such as gas kinetic energy densities, determine the size distribution. It should be noted that in CONTAIN only the airborne debris is allowed to react with and transfer heat to the atmosphere. The area for heat and mass transfer with respect to the debris therefore scales like the volume.

The calculations in Table III labeled IE-B0, IE-B1, and CW-B0 are bounding cases given for comparison purposes. In IE-B0 and CW-B0 the debris is excluded, and the pressure rise is due only to the steam blowdown from the

Table III.
The Pressure Rise, Percentage of Steam Reacted, and Energy Transferred from the Debris, Calculated With Various Particle Distribution Assumptions

Run	Description	ΔP (MPa)	Reacted Steam	Energy Transfer
IE-B0	Blowdown Only	0.024	-	-
IE-B1	Adiabatic Equilibration	0.535	74%	79%
IE-1	SDM	0.076	26%	17%
IE-2	MDM, 2 bins	0.075	21%	16%
IE-3	MDM, 1 Bin	0.080	34%	17%
IE-4	MDM, 2 Bins, 10 Generations	0.075	21%	16%
IE-7	MDM, 20 Bins, 10 Sizes	0.088	31%	22%
CW-B0	Blowdown Only	0.022	-	-
CW-1	SDM	0.036	10%	5%
CW-2	MDM, 2 Bins	0.034	6%	5%
CW-7	MDM, 20 Bins, 10 Sizes	0.058	18%	13%

pressure vessel. In IE-B1 the debris is assumed to react and come to thermodynamic equilibrium with the gas in an adiabatic, well-mixed volume. Thus, IE-B1 gives the maximum possible pressure rise, reacted steam, and heat transfer.

In the IE-1 calculation, the SDM was used, with relative debris-gas velocities selected to correspond to gravitational terminal velocities. (The latter velocities were used to provide a basis for comparison with the MDM calculations, for which the new quasi-mechanistic trapping and convective velocity models were not invoked.) The results from Table III for IE-1 show a pressure rise of only 0.076 MPa. Only 26% of the available steam reacts and 17% of the debris energy is transferred to the gas. By comparing these numbers with those for the adiabatic bounding calculation, IE-B1, one can see that the debris interactions are relatively incomplete. This is apparently due to the fact that the airborne debris does not have sufficient time to interact with the gas before being trapped and effectively removed from the problem.

A number of calculations were run to check on the sensitivity to droplet composition. The variation of composition between different droplets could be important if the metals are assumed to be initially segregated from the oxides in the fresh debris droplets. Thus, to the extent possible, the metals were assumed in the present calculations to be completely segregated initially. (The distribution of compositions that arises when fresh debris is mixed with older, burned-out debris in the same cell is handled through the use of different droplet generations, as discussed below.) In IE-2, the MDM was used with two compositional bins, one for metals and their reaction products and one for Al_2O_3. As shown in Table III, somewhat less steam is reacted than in IE-1. In IE-3, only one bin was used, and considerably more steam was reacted than in IE-1. This difference between IE-2 and IE-3 is due to the fact that the total reactive droplet surface area increases when the metals are assumed mixed with the Al_2O_3 in one bin and the droplet size is kept fixed. Although the SDM is a single field model, the IE-1 and IE-3 calculations do not give the same results, primarily because the approximate "mrat" and "zrrat" formalism was invoked in the SDM to keep track of the assumed segregation of metals. This formalism calculates the reactive droplet surface area by assuming that the metal burnup has reached steady state within a cell, a condition that was not achieved in the present calculations. Consequently, while this formalism prevented the steam from reacting to the extent found in IE-3, it predicted somewhat more reacted steam than is correct for the segregated case.

In IE-4, the sensitivity to droplet history was checked by splitting the entrained debris into ten generations with respect to the time of entrainment and into two compositional bins. As indicated above, the use of a number of generations could be important if fresh droplets in a cell are mixed with older, burned-out droplets, or if droplets of the same composition in the same cell for some reason have signficantly different thermal histories. Essentially the same results were obtained in IE-4 as in IE-2, as could be expected because the debris does not have much time to react or transfer heat

to the atmosphere before being trapped or transported to the next cell downstream.

Because of the relatively inefficient debris-gas interactions in the present calculations, the use of an appropriate droplet size distribution could be important. For inefficient interactions, the smaller droplets in a distribution should react more completely and thus contribute proportionately more to the pressure rise than the larger droplets. To check on the sensitivity to size distributions, calculations were run with 5 and 10 different droplet sizes, with separate bins for metals and oxides. The droplet sizes were selected as discussed above. Since the calculated results for 5 and 10 sizes were found similar, only the results for 10 sizes (IE-7) are given. As shown in Table III, the pressure rise, reacted steam, and heat transfer all increased significantly in IE-7 relative to IE-2.

The sensitivities present in extrapolating from 1:10 scale to 1:39 scale can be inferred from the "CW" cases shown in Table III. These calculations were done with a rescaled Surtsey 14-cell deck, as discussed above. Each "CW" calculation corresponds to the "IE" calculation with the same number. Although the steam-only case, CW-B0, gives comparable results, in the other "CW" cases the pressure rise, reacted steam, and heat transfer are significantly smaller than in the corresponding "IE" calculation. The decreased effect of the debris is due to the fact that both the debris trapping time and the duration of the DCH event are approximately proportional to the linear scale. Thus, the time available in the "CW" calculations for the debris to react and transfer heat to the atmosphere is reduced considerably compared to the "IE" calculations.

The ratios by which the pressure rise attributable to the debris, the percentage of steam reacted, and heat transferred are reduced in going from 1:10 to 1:39 scale can be derived from Table III. These ratios are summarized in Table IV. Quite clearly, these ratios are sensitive to the assumed droplet size distribution and, to a lesser extent, the treatment of droplet

Table IV.
Ratios by Which the Pressure Rise Attributable to the Debris, the Amount of Reacted Steam, and the Energy Transfer From the Debris Are Reduced in Going From 1:10 (IET) Scale to 1:39 (CWTI) Scale

Case	Ratio		
	Pressure Rise	Reacted Steam	Energy Transfer
SDM	3.7	2.6	3.4
MDM, 2 Bins	4.2	3.5	3.2
MDM, 20 Bins, 10 Sizes	1.8	1.7	1.7

composition. Furthermore, the use of a distribution of sizes appears to reduce the dependence on scale considerably. It should be noted that these conclusions depend strongly on the CONTAIN assumption that only suspended debris droplets interact with the atmosphere. Alternative modes of interaction, such as between the gas and debris films on surfaces, have been proposed for which the expected dependence of the pressure rise on scale is relatively weak. Also, if the droplet diameters had been taken to be much smaller than assumed here, there would in general be much less sensitivity to size distribution and composition and much less dependence on scale than calculated here. However, much smaller diameters would also lead to more efficient debris interactions, which may not be consistent with the experimental results.[13]

SUMMARY AND CONCLUSIONS

The new features of the CONTAIN 1.11 and CONTAIN 1.12 code revisions have been reviewed. The numerical robustness of the CONTAIN concrete outgassing algorithm in CONTAIN 1.11 has been significantly improved through a continuous tracking method for the outgassing interface. Also, the connected structure option has been shown to be a viable way to overcome architectural limitations in CONTAIN in the modeling of heat conduction between cells. This option allows heat conduction between cells to be modeled, while allowing the full CONTAIN suite of models to be used for the atmosphere-structure interfaces. This flexibility could be important in modeling the inner containment shell in passively cooled containment designs. Finally, a new approach for calculating forced convective heat transfer has been discussed.

The DCH models present in CONTAIN 1.12 have been reviewed. Improvements in the SDM over the original interim model include equilibrium Fe chemistry and improved modeling of debris trapping. The features of the CORDE and GASFLOW cavity dispersal models, which only recently have been incorporated into CONTAIN, have also been discussed.

A revised gas combustion model is currently under development. This model includes updated flame velocity and burn completeness correlations for deflagrations as well as new modeling for spontaneous recombination and diffusion flames. The revised model has been exercised in a set of plant calculations based on a Surry early depressurization scenario. In these plant calculations, the revised model was found to give considerably stronger deflagration burns than the old model. These stronger burns were found consistent with the behavior of the new correlations at high steam concentrations. When invoked, diffusion flame modeling was found to have a large effect in suppressing deflagrations. The peak pressures generated during the DCH event following vessel breach were found to be surprisingly sensitive to the existing hydrogen at vessel breach and thus to the prior hydrogen burn history. This sensitivity is apparently due to the low efficiency in the early depressurization scenario for transporting hydrogen generated during DCH to the upper containment. This efficiency may not be as low in fully pressurized scenarios because more steam would be available to transport the hydrogen generated during DCH.

DCH modeling improvements under development include the MDM and an extension of the debris chemistry modeling to include Cr and Al. The results of demonstration calculations for the MDM have been presented. These explore the sensitivities present with respect to debris droplet composition, history, and size distributions in the analysis of the IET-1 experiment. The implications of these sensitivities for extrapolating the results of such an analysis to a smaller scale were discussed. An accurate representation of the debris droplet size distributions, as afforded by the MDM, was found to be important in extrapolating the results of the analysis to a smaller scale. Also, if the metals are assumed to be initially segregated from the oxides in fresh debris droplets, the improvement afforded by the MDM in representing debris composition was also found to be significant, although not as striking as in the case of droplet sizes.

REFERENCES

1. K. K. Murata et al., "User's Manual for CONTAIN 1.1: A Computer Code for Severe Nuclear Reactor Accident Containment Analysis," NUREG/CR-5026, SAND87-2309, Sandia National Laboratories, Albuquerque, NM, 1989.

2. K. E. Washington et al., "Reference Manual for the CONTAIN 1.1 Code for Containment Severe Accident Analysis," NUREG/CR-5715, SAND91-0835, Sandia National Laboratories, Albuquerque, NM, 1991

3. S. C. Billups et al., "User's Manual for CONTAIN-HWR/0, Rev.1, A Computer Code for Severe Accident Containment Analysis for Heavy Water Nuclear Reactors," SAND91-1482, Sandia National Laboratories, Albuquerque, NM, to be published.

4. K. K. Murata et al., "CONTAIN LMR/1B-Mod.1: A Computer Code for Containment Analysis of Accidents in Liquid-Metal-Cooled Nuclear Reactors," SAND91-1490, Sandia National Laboratories, Albuquerque, NM, to be published.

5. D. C. Williams et al., "Containment Loads Due to Direct Containment Heating and Associated Hydrogen Behavior: Analysis and Calculations With the CONTAIN Code," NUREG/CR-4896, SAND87-0633, Sandia National Laboratories, Albuquerque, NM, 1987.

6. K. E. Washington and D. E. Carroll, "Assessment of Models for Steam Release from Concrete and Implications for Modeling Corium Behavior in Reactor Cavities," presented at the Sixteenth Water Reactor Safety Information Meeting, Gaithersburg, MD, October 24-2., 1988.

7. R. G. Gido et al., "PWR Dry Containment Parametric Studies," NUREG/CR-5630, SAND90-2339, Sandia National Laboratories, Albuquerque, NM, April 1990.

8. F. Gelbard et al., "CONTAIN Code Calculations for the LA-4 Experiment," presented at the Second International Conference on Containment Design and Operation, Toronto, Canada, October 14-17, 1990.

9. B. W. Morris and G. J. Roberts, "User's Manual for CORDE and the CONTAIN/CORDE Interface," AEA TRS 5033, AEA Winfrith, November, 1990.

10. M. Pilch, Sandia National Laboratories, private communication, 1991.

11. S. E. Dingman et al., "HECTR Version 1.5 User's Manual," NUREG/CR-4507, SAND86-0101, Sandia National Laboratories, Albuquerque, NM, April 1986.

12. C. C. Wong, "HECTR Analysis of the Nevada Premixed Combustion Experiments," NUREG/CR-4916, SAND87-0956, Sandia National Laboratories, Albuquerque, NM, November 1988.

13. M. D. Allen, "Quick-Look Report on the Integral Effects Test (IET-1) in the Surtsey Test Facility," Letter Report to the NRC, Sandia National Laboratories, 1991.

14. A. Sharon et al., "DCH Experiments in the CWTI Facility at Argonne National Laboratory," Nineteenth Water Reactor Safety Information Meeting, Bethesda, MD, October 28-30, 1991.

CORA Experiments on the Materials Behavior of LWR Fuel Rod Bundles at High Temperatures

P. Hofmann, S. Hagen*, G. Schanz, G. Schumacher**, L. Sepold*

Kernforschungszentrum Karlsruhe
Institut für Materialforschung
*Hauptabteilung Ingenieurtechnik
** Institut für Neutronenphysik und Reaktortechnik
Postfach 3640, 7500 Karlsruhe 1
Federal Republic of Germany

Abstract

The chemical interactions that may occur in a fuel rod bundle with increasing temperature up to the complete melting of the components are described. The materials behavior of BWR and PWR fuel rod bundles has been studied in integral experiments (CORA program) and extensive separate-effects tests. The kinetic results of the most important chemical interactions are represented. In most cases, the reaction products have lower melting points or ranges than the original components. This results in a relocation of liquefied components, at temperatures often far below their melting points. In addition, the influence of thin oxide layers, which form on Zircaloy surfaces during normal reactor operation, on the chemical interactions is indicated. As a result of the various studies three distinct temperature regimes can be defined in which liquid phases form in the fuel rod bundles in different, but large quantities. Their influence on damage progression and on possible accident management measures to avoid an uncontrolled core melt-down accident are described.

1. Introduction

The accident at the TMI-2 reactor, Harrisburg, has shown that even if the design basis accident temperature limit of 1200 °C is clearly exceeded due to a small leak in the cooling system of a light water reactor (LWR), along with a temporary failure of the emergency cooling system, this does not necessarily lead to an uncontrolled core meltdown accident. Despite severe damage to the fuel elements and other reactor components as a result of melting of wide core regions, it was possible to transfer the TMI-2 core into a coolable configuration [1]. Comprehensive research programs have been initiated to provide the data base and subsequent understanding of those physical and chemical processes which dominate the initiation, progression, termination and environmental consequences of severe accidents [2].

One of the ongoing research programs on core-melt progression phenomena is the CORA program which will be described in detail in this paper [3]. To study severe accident sequences, which imply severe fuel damage (SFD), fuel rod bundles are heated electrically in the CORA experiments at an initial heatup rate of about 1K/s in the presence of steam. The maximum temperatures attained are around 2400 °C. The hot fuel rod bundle is either cooled slowly or by means of a quenching device which simulates cold emergency cooling water entering the reactor core from the bottom simulating flooding conditions. Thus, the conditions prevailing in the CORA facility simulate partial sequences of still controllable accidents or even severe accidents involving core meltdown. As soon as the major underlying damage mechanisms are known, information can be provided inter alia on how long the core still possesses a geometry capable of being cooled during high temperature transients.

Regarding the chemical behavior of reactor core materials it can be stated that most components enter into reactions with each other or with the environment (steam) when the temperature is sufficiently high because the multicomponent system is not stable thermodynamically [4].

2. CORA Experimental Facility

The CORA experimental facility with the fuel rod test bundle in its center has been represented schematically in Figure 1. The superheated steam from the steam generator and superheater enters the test bundle at the bottom end. The

steam that is not consumed and the hydrogen produced in the zirconium-steam and stainless steel-steam reactions flow from the upper bundle outlet through two parallel condensers into a mixing chamber where the hydrogen is sufficiently diluted with air to avoid the risk of an oxyhydrogen explosion. Beneath the test bundle a cylinder filled with cold water is positioned which can be raised for quenching the heated test bundle. Above the high temperature shield there is a surge condenser which serves as an additional safety measure for CORA plant operation [3].

The test train consists mainly of the test bundle accommodating 2 m long fuel rod simulators which are held in their positions by three grid spacers (two Zircaloy spacers and one Inconel spacer) and are surrounded by a shroud. A maximum of 59 rods can be introduced into each bundle. In the 25-rod bundle 16 rods are heated over 1 m length (Figure 1). Heating is carried out electrically using tungsten heating elements, which are installed in the center of the heated rods and surrounded by annular UO_2 pellets. The total heating power available is 96 kW which can be distributed among the three groups of heated rods. The unheated rods are filled with solid UO_2 pellets and hence correspond in their construction exactly to LWR rods [3].

The most important materials used for the fuel rod simulators are original PWR cladding tubes made from Zircaloy-4 and UO_2 pellets. Both types of fuel rod simulator, heated and unheated, can be exposed to an internal pressure of up to 10 MPa so that the influence of ballooned and burst cladding tubes on the material behavior at high temperatures can be studied. Moreover, the test bundles can contain absorber materials, an (Ag,In,Cd) alloy for PWR tests, and B_4C for the BWR tests.

The advantages of the CORA out-of-pile experimental facility include, above all, the accessibility of the test bundle after testing. The high temperature shield can be lowered down and the bundle can be viewed in the "frozen" condition without requiring any manipulation whatsoever. In this way, the danger of the mechanical impact on heavily embrittled components and their post-test fragmentation can be avoided. Another advantage offered by the CORA facility is the possibility of quenching heated fuel elements with cold water. This allows the extent of damage to the core during reflooding to be determined [3].

Manifold and comprehensive test instrumentation makes it possible to study the progressionof the bundle damage thoroughly as a function of temperature. For instance, the temperature in the test bundle is measured by means of high tem-

perature thermocouples and two-colour pyrometers. The composition of the gas, especially the hydrogen content in the test atmosphere, is determined using two quadrupole mass spectrometers. Employment of so-called videoscopes (video cameras with an optical system for observation through the pressure vessel and the insulation material of the fuel rod bundle itself) allows the development of damage of the bundle to be continuously recorded on video and on photographic films.

3. Test Program and Objectives

The CORA program currently provides a total of 21 internationally coordinated tests with UO_2 bundles. To be able to investigate the differences in damage sequences in the cores of pressurized water reactors and boiling water reactors, the test bundles have been designed appropriately. This applies also to the configuration of the rods with the different absorber materials (Ag,In,Cd) and B_4C. The arrangement of the fuel and absorber rods in the PWR can be seen from Figure 1 for a small and for a large fuel rod bundle. The BWR core cell design of the CORA bundle is illustrated in Figure 1 for the large bundle only.

The objectives of the CORA program are to investigate out-of-pile the integral material behavior of PWR and BWR fuel rod bundles up to about 2400 °C.

Of special interest are the

a) oxidation behavior and the critical temperature at which the temperature escalation starts as a result of the exothermal Zircaloy/steam interaction,

b) fragmentation of embrittled fuel rods, particularly during cooldown and water quenching; characterization of the resulting debris,

c) onset of liquid phase formation due to chemical interactions of bundle components such as fuel rods, absorber materials, spacer grids, and stainless steel structural materials with each other,

d) influence of liquid phases and molten components on bundle damage progression,

e) extent of UO_2 and ZrO_2 dissolution by molten Zircaloy or α-Zr(O),

f) relocation and solidification behavior of liquid materials,

g) extent of bundle blockage formation,

h) coolability of the damaged fuel elements by simulating a rising water level; quench behavior,

i) timing and magnitude of H_2 generation,

j) development of material behavior models in combination with CORA and supporting separate-effects tests,

k) quantification of safety margins presently existing in the safety systems of operating reactors, and to explore possibilities of ending a high temperature transient before it can lead to an uncontroiled core meltdown,

l) performance of out-of-pile reference tests with the possibility to study many parameters for comparison with the limited number of in-pile experiments in the ACRR, LOFT, NRU, PBF, PHEBUS reactors and the TMI-2 accident [2].

The CORA experiments have been performed under various boundary conditions. The parameters which have been varied are: maximum temperature, system pressure, initial heatup rate, rod internal pressure, steam supply, termination of the test (slow cooldown or water quenching), bundle size, chemical conditions of the bundle components (as-received, pre-oxidized).

The completed and planned CORA experiments are listed in Table 1. The table shows that by November 1991 a total of 14 experiments have been performed successfully with different boundary conditions. The CORA-2 and CORA-3 tests had been planned as reference tests using no absorber material to observe the fuel rod/cladding interactions as well as the interactions of the Inconel spacer grid with the Zircaloy-4 cladding material. The CORA-3 test was carried out as a high-temperature experiment (max. temperature about 2400 °C). Typical PWR absorber materials (Ag,In,Cd) were inserted in the CORA-5 and CORA-12 test bundles to evaluate the effects of absorber material on core damage. Moreover, CORA-12 was the first PWR test in which the hot bundle was quenched by cold water, simulating flooding conditions. CORA-16 was the first test involving BWR materials, without quenching, to study the interactions that occur between the B_4C absorber material and the stainless steel of the control blade and then the stainless steel from the blade with Zircaloy from the channel box walls and the fuel rod cladding. CORA-17 was the first BWR test with quenching. In the CORA-15 bundle all rods, except the two absorber rods, were exposed to a high internal pressure in order to study the influence of ballooning and bursting of the fuel element cladding tubes on the material behavior of the bundle. In CORA-9 a higher system pressure (rod external pressure) of 10 bar was simulated to cause the cladding

tubes to collapse onto the fuel. The CORA-7 and CORA-18 tests were the first PWR and BWR experiments, respectively, involving a larger number of fuel rods (57 and 59, respectively compared to 25 for the smaller bundles). They served to study the axial and especially the radial melt distribution and the formation of crusts (blockages). The tests CORA-7 and -18 were terminated below 2000 °C to obtain more information on the chemical composition of the intermediate interaction products and relocated molten materials. CORA-13 was a PWR test which was quenched from a higher temperature than that in the test CORA-12. CORA-13 was selected as an International Standard Problem (ISP-31) by the OECD/CSNI. CORA-29 was the first PWR test with pre-oxidized bundle components. The max. ZrO_2 layer thickness on the cladding outer surface was about 12 µm. CORA-31 was the first BWR test with a much lower initial heatup rate of about 0.3 K/s, compared to about 1 K/s for all the other previous tests, to study the fuel rod bundle (core) behavior for a severe accident initiated from a shutdown power plant. CORA-30 was an analogous PWR test with an even lower inital heatup rate of 0.2 K/s.

4. Test Sequence and Post-test Examination of the Bundle

The test sequence can be broken down into three phases. During the initial 3000 s the bundle is heated with argon, which has been preheated to approx. 600 °C in the steam superheater. Within the time interval of 3000 s to approx. 5000 s electric power is supplied which increases linearly with time from 6 kW to a predetermined maximum value. Beginning at 3300 s superheated steam (2 g/s to 6 g/s) is fed into the test bundle in addition to argon (8 g/s). The test is terminated by reduction of the electric power and simultaneous interruption of the steam supply. Cooling of the test bundle proceeds either slowly in flowing Argon or quickly by quenching with cold water [3].

After the test the degraded bundle is carefully photographed, cast into epoxy resin for preservation of geometry of the damage and, after disassembly from the test facility, it is cut to prepare transverse and longitudinal sections. The subsequent preparation of metallographic micrographs is the prerequisite of investigating the manifold material interactions between the components of an LWR fuel element. Besides the examination of the microstructures, analysis of the chemical compositions of the reaction products formed and of the solidified melts is of particular importance. Using a scanning electron microscope, energy dispersive X-ray (EDX) and wavelength dispersive X-ray (WDX) analyses are made [5]. With the re-

sults in hand, information can be provided on the type of chemical interactions and their extent by a comparison with results obtained in parallel studies on single effects. The additional assessment of the structures formed on the basis of information available from phase diagrams, moreover, furnishes indications of maximum temperatures which have been reached locally, the formation of molten phases and their resolidification temperatures.

5. Test Results

It is not proposed here to present and discuss the results of the individual CORA tests; the intention is rather to present in a more comprehensive framework the general fuel rod bundle and material behavior [4,5,6,7,8,9,10].

5.1 Separate-Effects Tests

To be able to describe in detail the integral material behavior of the test bundle subjected to a temperature transient the results of separate-effects studies must also be discussed. These results regarding the temperature dependence of the reactions and the chemical composition and microstructure of the reaction products formed in that process are important to explain the observed final condition of the bundles and the approach adopted in post-test examinations [6,7,8,9].

The kinetic results of the separate-effects tests performed are summarized in Figure 2. The reaction zone growth rates for important LWR core material couples are plotted versus the reciprocal temperature. The chemical interaction rates vary over several orders of magnitude. The fastest interactions occur between Zircaloy and stainless steel, (Ag,In,Cd) alloy and Zircaloy, and Zircaloy and Inconel 718. For each material couple a critical temperature exists above which rapid and complete liquefaction of the specimens occurs. In all cases these critical temperatures are well below the melting points of the individual materials. As one can recognize, liquefaction of the materials, including UO_2 fuel, can occur well below 2000 °C. Oxide layers on the surface delay the chemical interactions, but cannot prevent them [4,5,6,7,8,9].

5.2 General Bundle Behaviour

All CORA experiments exhibit similar macroscopic post-test appearance in the upper part of the test bundles. Partial to complete oxidation and embrittlement of the cladding and fragmentation of cladding as well as of fuel takes place. This al-

so holds for the kind of cladding deformation known as "flowering" which is mainly to be found in the upper regions of the bundles and is caused by differences in the zirconium oxide growth around the cladding circumference on the outer and inner surface. The resulting hoop stresses are eventually relieved by axial splitting and flattening of the cladding tubes.

In contrast to the upper regions, the appearance of the lower zones in the bundle is more dependent on the presence of absorber material with respect to the amount and distribution of accumulated fragments and relocated solidified melts (blockage zones).

5.3 Macroscopic Appearance of the Bundle after the Test

The macroscopic post-test appearance of the CORA-5 test bundle is represented in Figure 3 as an example. This is a PWR test bundle with a central (Ag,In,Cd) absorber rod, two Zircaloy-4 grid spacers and one Inconel grid spacer. The maximum measured cladding temperature was about 2000 °C. Wide spread destruction of the test bundle, along with severe oxidation of the Zircaloy cladding tubes, the formation of metallic and ceramic melts, which solidify at different axial elevations and give rise to bundle blockages of different sizes, can be recognized. The micrographs of cross-sections prepared at different axial elevations of the bundle (Figure 3) make the extent of damage clearly visible. The lower cross-section (208 mm) shows clearly the original fuel rod and absorber configuration consisting of 16 heated and 8 unheated fuel rods as well as one absorber rod with a Zircaloy guide tube. At the same time, relocated metallic melts, some of them attacking the Zircaloy cladding material chemically, can be recognized. The upper cross-section (853 mm) shows a cut through the Zircaloy grid spacer plane. The cladding material has almost completely melted down, while dissolving some of the solid UO_2 fuel. Some of the solidified melt can be found again in the central bundle zone (408 mm) where strong oxidation of the cladding material can be observed. The still metallic portion between the ZrO_2 layer and UO_2 had melted and relocated; the annular cavities formed are clearly visible (Figure 3) [10].

Reaching higher temperatures, as in test CORA-3 (about 2400 °C), resulted in very severe damage of the fuel rod bundle with extended UO_2 fuel and ZrO_2 dissolution by molten oxygen-poor Zircaloy beyond about 1760 °C, the melting point of Zircaloy-4 (Figure 4). The liquefied and molten materials (including UO_2) relocated and formed a complete blockage of the bundle cross-section in the lower part of the bundle on solidification (Figure 4, longitudinal section 70 - 170 mm). Both metallic and ceramic molten materials were detected. The microstructures of the

solidified melts indicated UO_2 fuel dissolution by molten Zircaloy to various extents. Part of the metallic melt relocated within the bundle, even down to the bottom of the bundle (Figure 4, cross-section elevation 20 mm) and had melted the cladding and dissolved some of the UO_2 fuel [5]. The metallographic structures seen in the destructive post-test examination of the CORA tests correspond very closely to those obtained in TMI-2 core fragment and core bore examinations [4,13] and by in-pile experiments [2].

5.4 Temperature Escalation

The critical temperature above which uncontrolled temperature escalation takes place due to the exothermal zirconium/steam reaction crucially depends on the heat loss from the bundle, i.e. on bundle insulation. With the good bundle insulation in the CORA test facility, temperature escalation starts between 1100 and 1200 °C giving rise to a maximum heating rate of 15 K/s. The maximum temperatures attained are about 2000 °C; the oxide layers formed and the consumption of the available steam set limits on the temperature escalation due to rate-controlled diffusion processes. The temperature escalation starts in the hotter upper half of the bundle and the oxidation front subsequently migrates from there both upwards and downwards [5].

5.5 Melting of the Cladding Material

After attainment of the melting point of the Zircaloy cladding material at about 1760 °C and/or of oxygen-stabilized α-Zr(O) at approx. 2050 °C the Zircaloy melt flows over large distances, starting from locations where the oxide layer on the cladding tubes might be penetrated due to chemical and/or mechanical effects. However, the longer simultaneous contact of Zircaloy with the fuel and ZrO_2 on the cladding tube surface exists, the more UO_2 dissolution predominates because it proceeds faster than the dissolution of ZrO_2 [4]. The cladding integrity can be destroyed far below the melting point of Zircaloy by eutectic interactions with Inconel grid spacer or absorber materials (stainless steel or absorber alloy) resulting in liquid phases at temperatures as low as 1250 °C.

5.6 UO_2 Fuel Dissolution

Vigorous chemical interactions take place between the metallic melts from the cladding material and the solid UO_2 pellets. In this way, the UO_2 is liquefied at about 1000 K below its melting point (2850 °C) while forming a (Zr,U,O) melt [4]. UO_2 liquefaction results in an increased release of fission products and initiates a

mechanism of "low temperature" relocation of the fuel in the reactor core. The (Zr,U,O) melts formed solidify in cooler zones forming metallic cooling channel blockages (crust formation) or, due to interactions with steam, forming ceramic $(Zr,U)O_2$ masses. All CORA tests have made the considerable dissolution of the UO_2 pellets in the upper bundle zones evident [5,10]. Whereas at the maximum temperatures achievable purely ceramic melts cannot yet be formed, the relocation of the melt with high uranium and oxygen contents can be observed; in the process of solidification the melts decompose forming ceramic phases with metallic phases as secondary constituents (Figures 3, 4).

5.7 Grid Spacers

5.7.1 Inconel Spacers

The Ni base alloy Inconel 718 reacts with the Zircaloy cladding material forming a eutectic. According to separate-effects tests, the first liquid phases occur from 1000 °C onward, and above 1250 °C they cause rapid liquefaction of the Inconel spacer and part of the Zircaloy cladding. Only small quantities of Inconel (or stainless steel) are necessary to dissolve large quantities of Zircaloy. ZrO_2 layers present on the Zircaloy surface delay the eutectic interactions with Inconel and shift melting down of the grid spacer and the Zircaloy cladding towards higher temperatures but are unable to prevent it. However, in all cases Inconel liquefaction due to the reaction with Zircaloy takes place below its melting point (1450 °C) [7]. It was possible to observe this liquefaction directly in the CORA experiments; melting down was completed within a few seconds. The zirconium-rich melt generated severely damaged the fuel rods around the spacer grid. The melt produced in this interaction was found to have been distributed over the whole lower half of the bundle and some of it was collected in the zone of the lowest grid spacer.

5.7.2 Zircaloy Spacers

The chemical behavior of the Zircaloy spacers differs clearly from that of the Inconel spacers. The upper grid spacers positioned in the hot bundle zone undergo partial melting and contribute to the liquefaction of solid UO_2. The lower, colder grid spacers act as "material catcher" for solid and liquid bundle components and thus exert a major influence on the development of cooling channel blockages (crusts).

5.8 Behavior of (Ag,In,Cd) Absorber Material

The influence exerted by the temperature on absorber rod failure is of considerable interest. For PWR absorber rods consisting of (Ag,In,Cd) absorber material, stainless steel cladding and Zircaloy guide tube, premature failure was clearly observed [9,10].

The (Ag,In,Cd) absorber material melts at approx. 800 °C and initially remains within the stainless steel cladding tube without chemical reaction with steel because the system is thermodynamically stable. Due to the eccentric location of the absorber rod within its Zircaloy guide tube or due to ballooning of the stainless steel cladding by Cd vapour pressure, a contact is established between Zircaloy and the steel components and different eutectic melts are formed between 1200 and 1400 °C, i.e. below the melting point of the stainless steel cladding (1450 °C). This is the moment when the (Ag,In,Cd) absorber melt starts to relocate. On the one hand, the gap between the cladding and the guide tube becomes filled; on the other hand, the material flows out into the cooling channels and downwards and there it reacts with the cladding tubes of the fuel rods. The absorber melt is distributed over large zones; it contains Zircaloy and steel components. The melt is formed similarly to the Zircaloy cladding Inconel grid spacer melts (eutectic reactions), and is observed in the same range of temperature. This melt also contributes considerably to premature damage of the fuel rods at "low" temperatures. In the presence of (Ag,In,Cd) absorber material two blockage zones develop in the test bundle as a result of solidified melts. The main constituents of the metallic melt that relocates first are (Ag,In,Zr,Fe,Cr,Ni) with the cadmium portion in the melt heavily reduced due to evaporation. The other zone is a ceramic melt consisting mainly of (U,Zr,O) in the form of $(Zr,U)O_2$ [10]. Due to the differences in solidification temperature, the two melts are stratified with the ceramic material overlying the metallic material (Figure 3).

5.9 Behavior of B_4C Absorber Material

Boron carbide (B_4C) is used as absorber material in BWRs. In experiments with B_4C, absorber material damage propagation starts upon melting of the two-layered stainless steel cladding at approx. 1250 °C. Melting of the steel is prompted by the eutectic interaction with the B_4C absorber material. The failure temperature of 1250 °C, which is clearly below the melting temperature of steel (approx. 1450 °C), results from the formation of eutectic melts originating between the steel constituents (Fe,Cr,Ni) and boron on the one hand, as well as carbon on the other hand. Single-effects investigations have shown that first liquid phases

develop from approx. 1000 °C upwards; rapid liquefaction occurs above 1250 °C [8].

Both, the boron carbide/steel melt formed and the melt constituents react eutectically with the coolant channel wall made of Zircaloy, giving rise to Zircaloy liquefaction around 1250 °C. In this way, the Zircaloy cladding material is already liquefied well below its melting point of 1760 °C. The result of this lowering of the melting point is the beginning of UO_2 dissolution at "low" temperatures. In the upper bundle zone the Zircaloy cooling channel wall is destroyed so that the melt can spread radially and relocate downward. As a result, coolant channel blockages develop in the bottom part of the bundle.

5.10 Influence of Quenching

Quenching of the hot bundles by water caused further fragmentation and an enhanced Zr/H_2O reaction resulting in a temperature rise at the top of the bundle, although the electric power supply was shut off, and in additional hydrogen generation. Some further meltdown of material in the upper bundle regions was observed due to the additional exothermic Zr/steam interactions and the resulting high temperatures.

The water entering the bundle and the developing steam cause a thermal shock on the embrittled materials, generating new surfaces. The steam reacts with the metallic components of the newly formed surfaces, and, as a result of the exothermal Zr/H_2O reaction, local temperature escalations take place again. The additional hydrogen formed at this point in time is quite considerable, i.e. up to about 80 % of the total hydrogen [11]. In the LOFT experiment FP-2 the percentage of hydrogen generated during the reflood was approx.80 % [12].

5.11 Hydrogen Generation

The results from the CORA tests support the conclusion that hydrogen generation during severe accidents will continue, assuming a sufficient steam supply, up to complete consumption of the available Zircaloy and stainless steel. One of the mechanisms for reducing hydrogen generation is the removal of hot materials from the high temperature oxidation zone into a cooler zone. During the tests, because little material relocated from the high temperature region to the steam-cooled region, hydrogen generation continued until either termination of the test or complete consumption of the available Zircaloy and stainless steel. Re-

flood of the hot bundle (quenching) resulted in an additional strong hydrogen generation as described in section 5.10.

5.12 Influence of Bundle Size

The larger fuel rod bundles (CORA-7 and CORA-18) with 57 and 59 fuel rods, respectively, compared with 25 fuel rods in the smaller bundles, did not show any different material behavior. In general, similar physical and chemical phenomena were observed as in the smaller bundles. Temperature escalation started at about 1200 °C and continued even after shut-off of the electric power, as long as steam was available. The (Ag,In,Cd) absorber rods or B_4C absorber blades failed at around 1250 °C and initiated the damage progression within the bundles. After the tests, the upper parts of the bundles were free of any absorber material. This material has relocated to the lower, i.e. cooler, part of the bundle.

5.13 Influence of Heat-up Rate

The only CORA experiments performed so far with lower heat-up rates of 0.2 K/s and 0.3 K/s, respectively, (CORA-30 and -31) compared to 1 K/s demonstrated clearly that no temperature escalation due to the exothermal Zircaloy/steam interactions takes place. The chemical interaction energy formed caused only an increased heatup rate between 1200 and 1800 °C of about 1 K/s. The oxide layer which has formed on the cladding outer surface during heatup delays the chemical interactions between Zircaloy and steam since the diffusion of oxygen through the ZrO_2 layer is the rate-determining step. The Zircaloy will be almost completely oxidized, or at least converted into α-Zr(O), before reaching the melting point of oxygen-poor (as-received) Zircaloy at about 1760 °C. As a result, large UO_2 fuel liquefaction by molten Zircaloy will not take place; this means smaller fission product release rates and it requires much higher temperatures (≈ 2850 °C) before UO_2 melting and relocation occurs.

6. Summary of the Major Results

This is a summary of major results from the CORA experiments and separate-effects investigations performed so far:

- Temperature escalation due to the zirconium-steam reaction starts in the upper, i.e. hotter bundle half at about 1100 °C and propagates from there

downwards and upwards. The maximum temperatures measured are approx. 2000 °C.

- Fuel rod failure in the test bundles without absorber material starts at the level of the Inconel grid spacer. Inconel reacts eutectically with Zircaloy as early as 1000 °C while forming liquid phases. ZrO_2 layers on the external side of the cladding tube delay melting and shift its onset towards higher temperatures, although they cannot prevent melting. Above 1250 °C the spacer is completely liquefied within a short period of time.

- The behavior of the Zircaloy grid spacers depends on the temperature attained locally. The upper spacer (hot zone) partly melts and contributes to the chemical dissolution of UO_2. The lower spacer is located in a relatively cold zone where it acts as a material catcher where melt rivulets and melt droplets as well as solid embrittled cladding tube and fuel fragments are caught.

- The unoxidized part of the Zircaloy cladding first melts in the upper bundle zone because of the higher temperatures prevailing there. Due to the progressing chemical dissolution of UO_2, melts consisting of (Zr,U,O) develop with different contents of uranium and oxygen which relocate into the bottom part of the bundle after the ZrO_2 layer has failed. The melt solidifies in the colder zone, causing coolant channel blockages of different sizes.

- Thick ZrO_2 layers on the external cladding tube surfaces prevent substantial amounts of metallic Zircaloy melt from relocating, so that the Zircaloy remains in contact with the UO_2 fuel. Thin ZrO_2 layers are dissolved chemically by metallic Zircaloy. This causes the oxide layer to rupture locally and the (Zr,O,U) metallic melt to escape.

- Most of the melt relocates along the surface as rivulets (candling) and, to a minor extent, in the free fall as droplets, i.e. without contact with other surfaces (slumping). Film flow type of melt relocation down the rods was not observed.

- At the higher test temperatures of 2400 °C, compared to 2000 °C, larger amounts of molten material are produced so that the blockage zone in the lower bundle region is clearly larger. The formation of a distinct crust consisting of metallic material was observed, on which the metallic and ceramic melts formed later accumulated.

- Cladding tube and fuel fragments of various sizes accumulate on the solidified lumps of melt which develop and are relocated while the bundle continues to cool down. The smallest particles are as UO_2 powder and are of the order of micrometers in size.

- In the presence of PWR absorber material (Ag,In,Cd) the sequence of failure starts with the release, relocation and resolidification of the (Ag,In,Cd) melt. However, most of the melt reacts with the Zircaloy cladding material forming a metallic melt of the type (Ag,In,Zr). Due to its zirconium content this melt is capable of dissolving UO_2 even below the melting point of Zircaloy. On account of the different solidification temperatures of the melts a stratification develops such that the metallic lumps of melt rich in absorber material are superimposed by metallic and/or ceramic (Zr,U,O) blockages formed later.

- In the experiments involving BWR absorber material (B_4C) the first molten phases occurred from approx. 1250 °C upwards after failure of the absorber rod cladding made of stainless steel. After failure of the steel cladding the B_4C/steel melt produced reacted with the Zircaloy of the coolant channel walls forming melts of eutectic compositions. The reaction caused the channel wall to be destroyed and hence the melt to propagate towards the outside and mainly downwards. As a consequence of this, partial coolant channel blockages develop in the lower bundle section.

- Water quenching (flooding) of the hot degraded fuel rod bundle caused additional fragmentation and an enhanced Zircaloy/stem interaction resulting in a renewed temperature rise, a meltdown of material, and in an additional strong hydrogen generation.

7. Conclusions

- Core melt progression is a noncoherent stage-by-stage process that results in melting and liquefaction of materials mainly due to eutectic interactions at different temperatures.

- Control rod materials can separate by liquid relocation processes from fuel rod materials at temperatures as low as 1250 °C. Therefore, reflood water must be sufficiently borated to avoid recriticality and power generation du-

ring early phase core degradation, that means, prior to the disintegration of the core into a rubble bed.

- Significant molten UO_2 relocation can begin at the Zircaloy melting temperature of about 1760 °C, that means about 1000 K below the melting point of UO_2. The low-temperature early fuel relocation is important for the release of fission products and the redistribution of decay heat sources in a damaged core.

- Reflood of a damaged core can fragment oxidation-embrittled Zircaloy cladding, fracture solidified once-molten materials (blockages), induce locally a renewed temperature rise and strong additional hydrogen generation. Accident management strategies must consider the consequences of reflood phenomena.

- The results of the integral CORA tests and of separate-effects tests allow thedefinition of three temperature regimes in which large quantities of liquid phases form which cause fuel rod bundle (core) damage (Figure 5):
  → 1200 - 1400 °C: localized core damage
  → 1800 - 2000 °C: extended core damage
  → 2600 - 2850 °C: total core destruction

- The extent of damage depends on the initial heat-up rate and the maximum temperature reached. Accident management measures which delay the core uncovery result in smaller initial heat-up rates of the core and, hence, in a reduced formation of liquid phases up to about 2600 °C (Figure 5).

- The present knowledge of early-phase core melt progression provides a better understanding of the physical and chemical processes contributing to the degradation of a reactor core with increasing temperature (for example, the TMI-2 accident) and provides a reasonable basis for code development and validation.

- For BWR core material behavior in severe reactor accidents, the use of other materials (B_4C/Zircaloy) instead of the present ones (B_4C/stainless steel) would result in a greater flexibility for accident management measures, because meltdown would be delayed in time and shifted to higher temperatures.

It can be summarized that the CORA experiments and single-effect investigations have contributed substantially to the understanding of the material behavior in

reactor accidents. The comparison of the out-of-pile CORA test results of material behavior with the results of in-pile experiments [2] as well as the results of the examinations of TMI-2 specimens, some of which were analyzed in the KfK Hot Cells [13], shows very good agreement. Moreover, the CORA experiments have provided new findings on damage initiation and propagation in LWR fuel rod bundles. These findings are of particular importance regarding possible accident management measures. The modelling of low-temperature liquefaction and quenching effects is not yet included in most computer codes.

Acknowledgements

The review of the manuscript by P. Bottomley (CEC/TU), T. Haste (AEA), and R.R. Hobbins (EG + G Idaho) is gratefully acknowleged.

References

[1] J.M. Broughton, P. Kuan, D.A. Petti; A Scenario of theThree Mile Island Unit 2 Accident, Nuclear Technology, Vol. 87 (1989) 34-53.

[2] R.R. Hobbins, D.A. Petti, D.J. Osetek, D.L. Hagrman; Nuclear Technology, Vol. 95 (1991) 287-306.

[3] S. Hagen, K. Hain: Out-of-pile Bundle Experiments on Severe Fuel Damage (CORA-Program), KfK 3677 (1986).

[4] P. Hofmann, S. Hagen, G. Schanz, A. Skokan: Reactor Core Materials Interactions at Very High Temperatures, Nuclear Technology, Vol. 87 (1989) 146-186.

[5] S. Hagen, P. Hofmann, G. Schanz, L. Sepold: Interactions in Zircaloy/UO_2 Fuel Rod Bundles with Inconel Spacers at Temperatures above 1200 °C (CORA-2 Experiments), KfK 4378 (1990).

[6] P. Hofmann, H.J.Neitzel, E.A. Garcia: Chemical Interactions of Zircaloy-4 Tubing with UO_2 Fuel and Oxygen at Temperatures between 900 and 2000 °C; Experiments and PECLOX Code, KfK 4422 (1988).

[7] P. Hofmann, M. Markiewicz: Compatibility Experiments between Inconel Spacer Grids and Zircaloy Cladding, KfK 4729 (in preparation).

[8] P. Hofmann, M. Markiewcz, J. Spino: Reaction Behavior of B_4C Absorber Material with Stainless Steel and Zircaloy in Severe LWR Accidents, Nuclear Technology, Vol. 90 (1990) 226-244.

[9] P. Hofmann, M. Markiewicz: Chemical Behavior of (Ag,In,Cd) Absorber Rods in Severe LWR Accidents, KfK 4670 (1990)

[10] S. Hagen, P. Hofmann, G. Schanz, L. Sepold: Behavior of (Ag,In,Cd) Absorber Material in Zircaloy/UO_2 Fuel Rod Simulator Bundles at High Temperatures (CORA-5 and CORA-12), KfK 4419 (in preparation).

[11] S. Hagen, P. Hofmann, G. Schanz, G. Schumacher, F. Seibert, L. Sepold; Influence of Reflood in the CORA Severe Fuel Damage Experiments, Heat Transfer and Fuel Behavior in Nuclear Reactor Accidents, 27th ASME/AICHE/ANS National Heat Transfer Conference, Minneapolis, July 28-31, 1991, USA. AIChE Symposium Series 283, Vol. 87, 120-129

[12] R.R. Hobbins, G.D. Mc Pherson; A Summary of Results from the LOFT LP-FP-2 Test, OECD/LOFT Final Event, ISBN 92-64-0339-4 (1991).

[13] H. Kleykamp, R. Pejsa; Chemical and X-Ray Diffraction Analysis on Selected Samples from the TMI-2 Reactor Core, KfK 4872 (1991)

Test No.	Max. Cladding Tempera-tures	Absorber Material	Other Test Conditions	Date of Test
2	≈ 2000°C	-	UO_2 refer., inconel spacer	Aug. 6, 1987
3	≈ 2400°C	-	UO_2 refer., high temperature	Dec. 3, 1987
5	≈ 2000°C	Ag, In, Cd	PWR-absorber	Febr. 26, 1988
12	≈ 2000°C	Ag, In, Cd	quenching	June 9, 1988
16	≈ 2000°C	B_4C	BWR-absorber	Nov. 24, 1988
15	≈ 2000°C	Ag, In, Cd	rods with internal pressure	March 2, 1989
17	≈ 2000°C	B_4C	quenching	June 29, 1989
9	≈ 2000°C	Ag, In, Cd	10 bar system pressure	Nov. 9, 1989
7	< 2000°C	Ag, In ,Cd	57-rod bundle, slow cooling	Febr. 22, 1990
18	< 2000°C	B_4C	59-rod bundle, slow cooling	June 21, 1990
13	≈ 2200°C	Ag, In, Cd	OECD/ISP; quench initiation at higher temperature	Nov. 15, 1990
29*	≈ 2000°C	Ag, In, Cd	pre-oxidized	April 11, 1991
31*	≈ 2000°C	B_4C	slow initial heat-up (≈ 0.3 K/s)	July 25, 1991
30*	≈ 2000°C	Ag, In, Cd	slow initial heat-up (≈0.2 K/s)	Oct. 30, 1991
28*	≈ 2000°C	B_4C	pre-oxidized	planned for 1992
10	≈ 2400°C	Ag, In, Cd	very high temperature, lower part of bundle in H_2O	planned for 1992
33*	≈ 2000°C	B_4C	dry core conditions, no steam flow	planned for 1992
27	≈ 2400°C	B_4C	very high temperature lower part of bundle in H_2O	
25	≈ 2000°C	B_4C	10 bar system pressure	
26	≈ 2000°C	B_4C	fast heatup, quenching	
24	≈ 2000°C	B_4C	steam-rich conditions, quenching	
32*	≈ 2000°C	Ag, In, Cd	quenching from the top	

Initial heat-up rate: ≈ 1.0 K/s; Steam flow rate, PWR: 6 g/s, BWR: 2 g/s; quench rate (from the bottom) ≈ 1 cm/s

* further proposed experiments

Table 1: CORA test matrix. Up to now 14 PWR and BWR related tests have been performed under different boundary conditions.

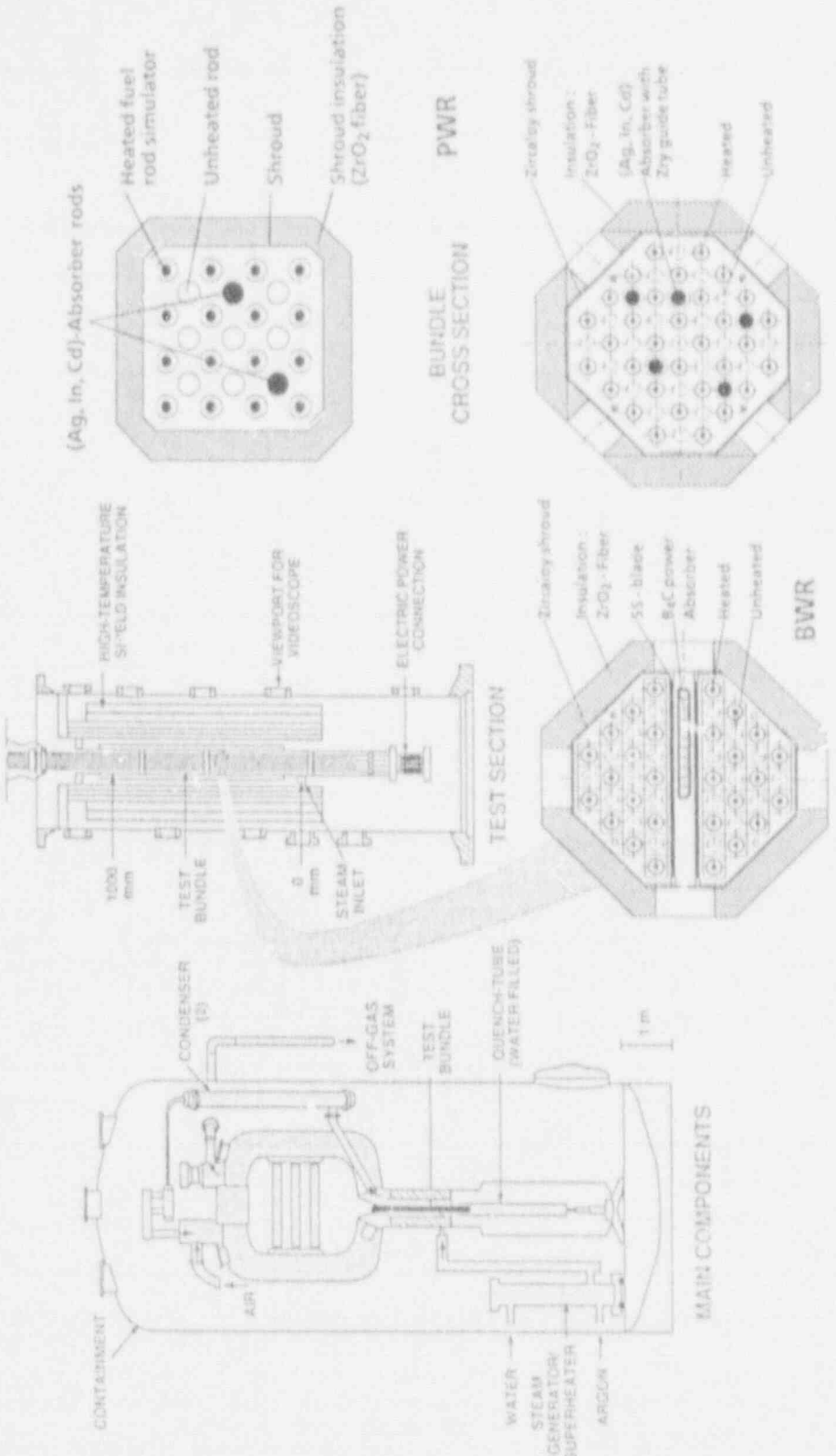

Figure 1: Main components of the CORA severe fuel damage test facility which serves to study the fuel element behavior up to 2400 °C. Bundle cross-sections with configuration of the heated and non-heated fuel rods and absorber materials for BWRs and PWRs (small and large bundle cross section).

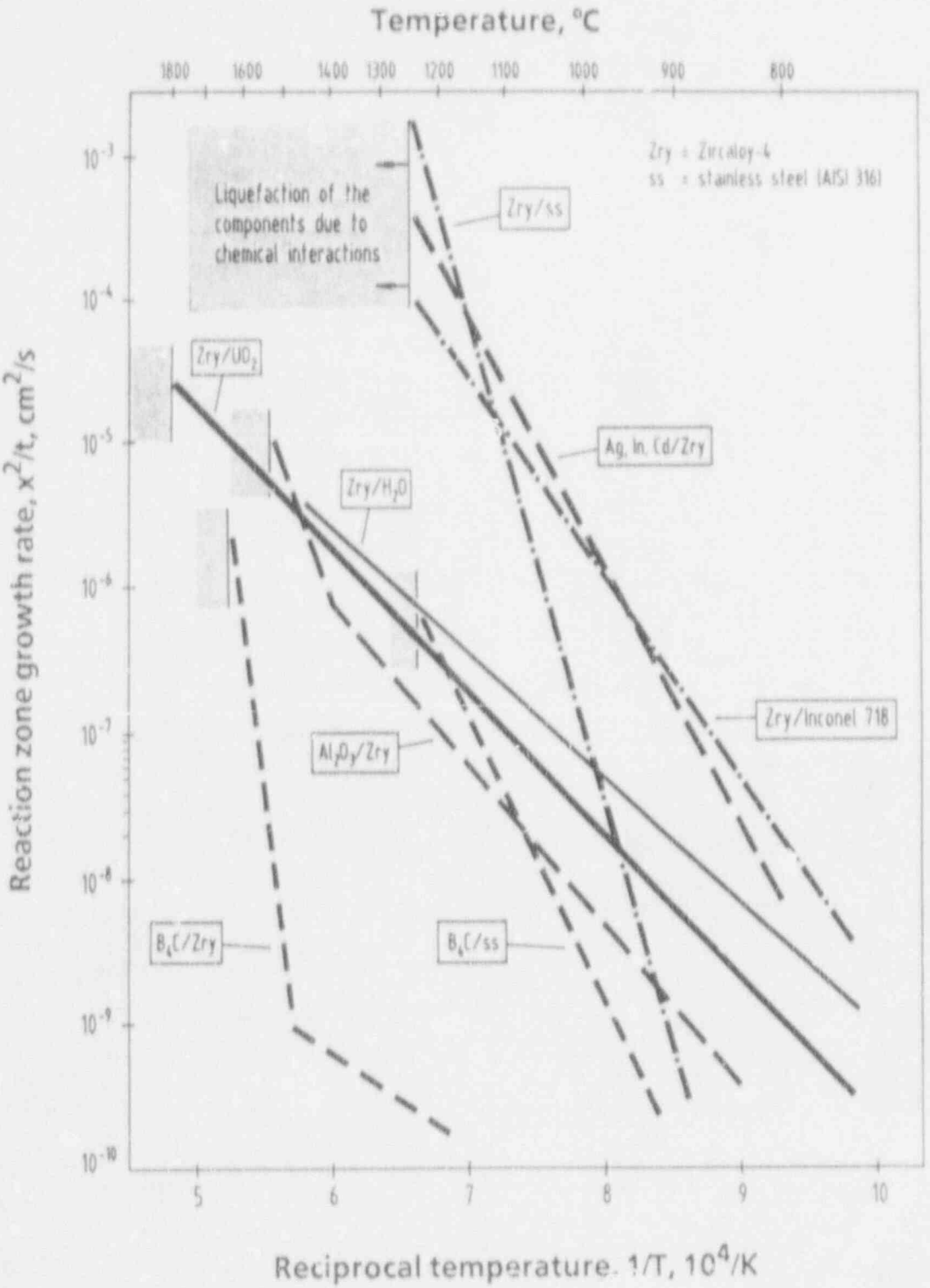

Figure 2: Comparison of the total reaction zone growth rates of different LWR reaction couples. There exists for each material couple a critical temperature above which a rapid and complete liquefaction of the specimens occurs.

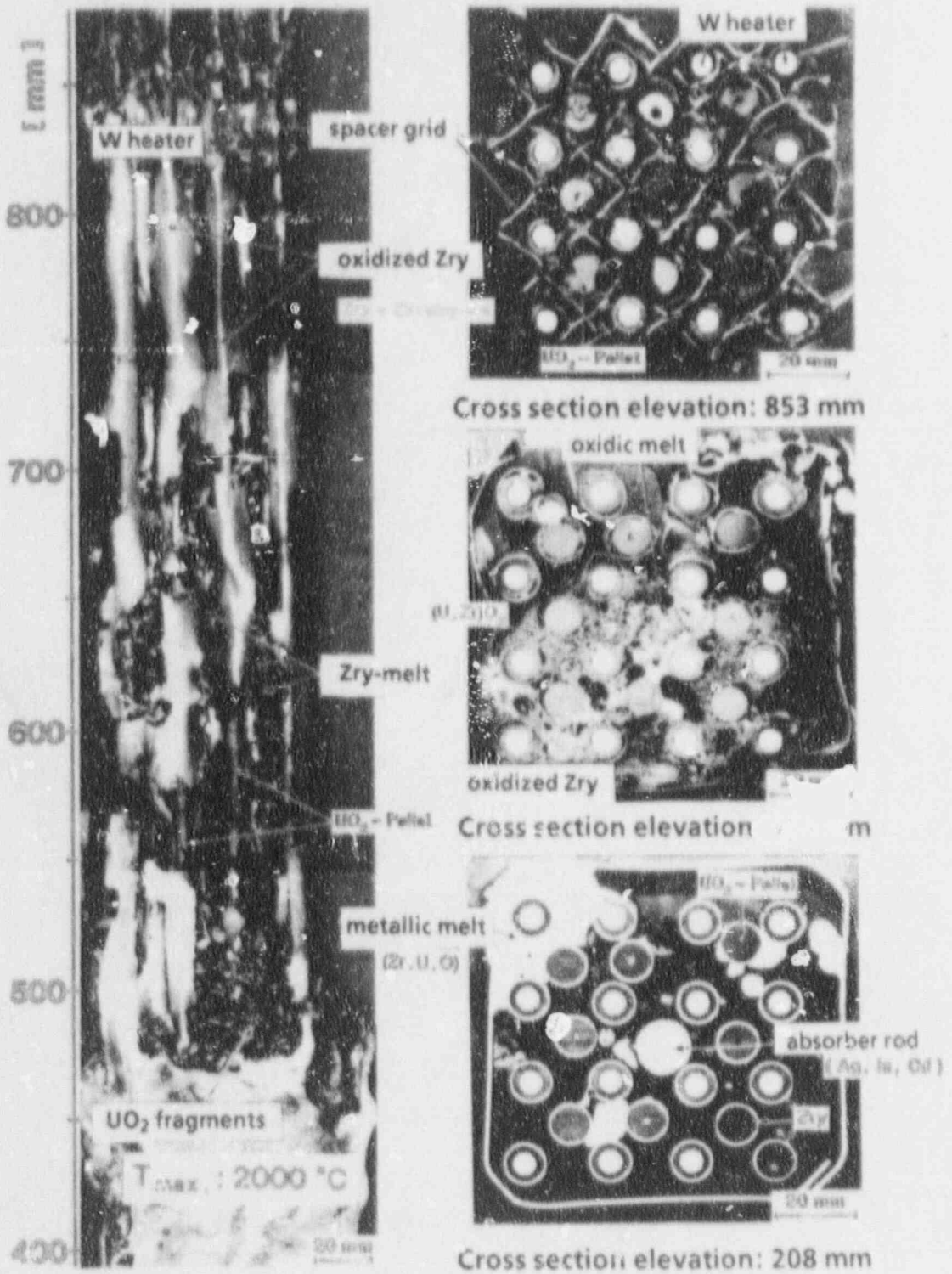

Figure 3: Post-test appearance of the simulated PWR bundle CORA-5 with one (Ag,In,Cd) absorber rod and Zircaloy guide tube. The maximum temperature in the bundle was about 2000 °C.

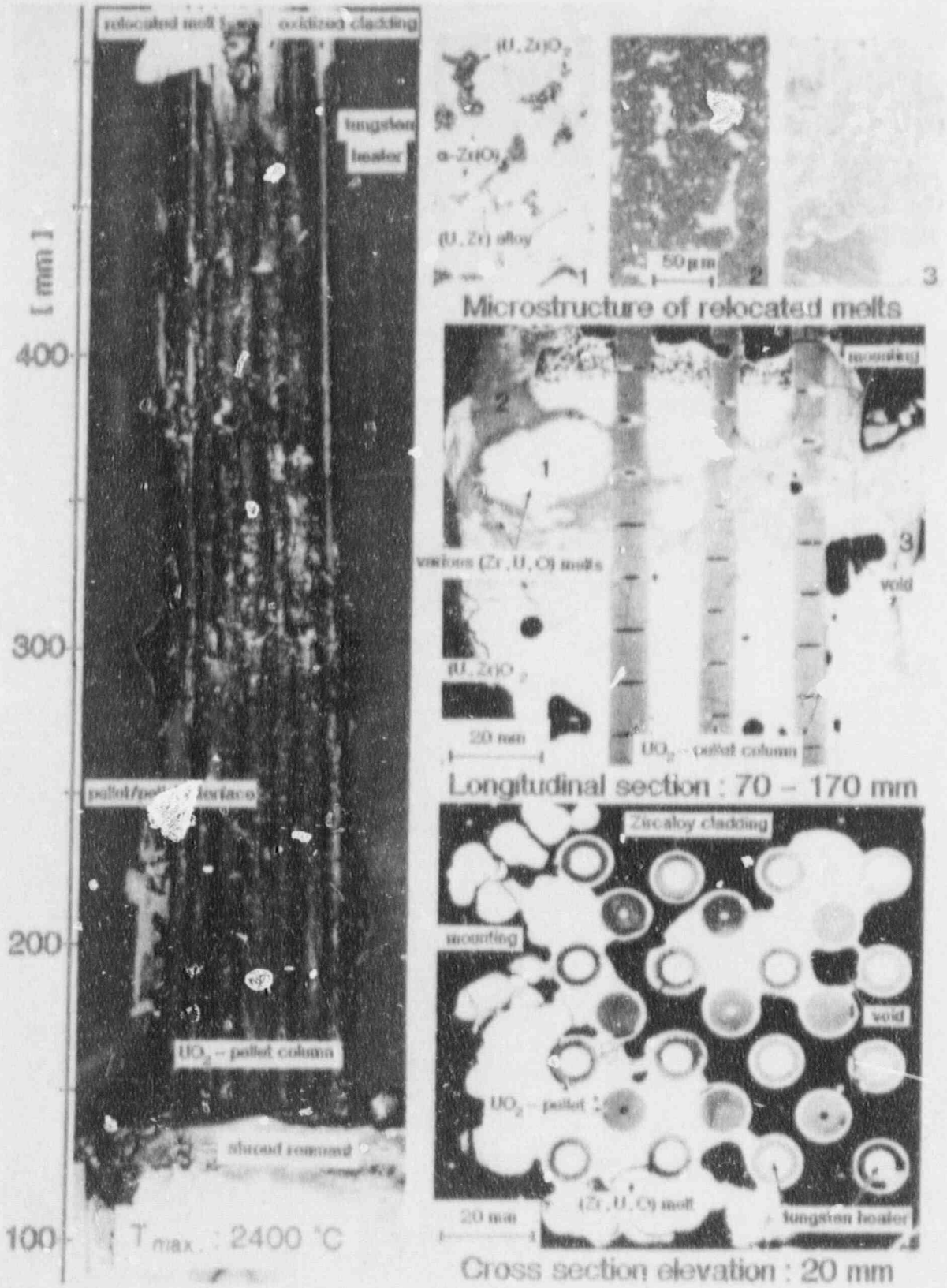

Figure 4: Post-test appearance of the simulated PWR bundle CORA-3 without absorber rods. The maximum temperature in the bundle was about 2400 °C.

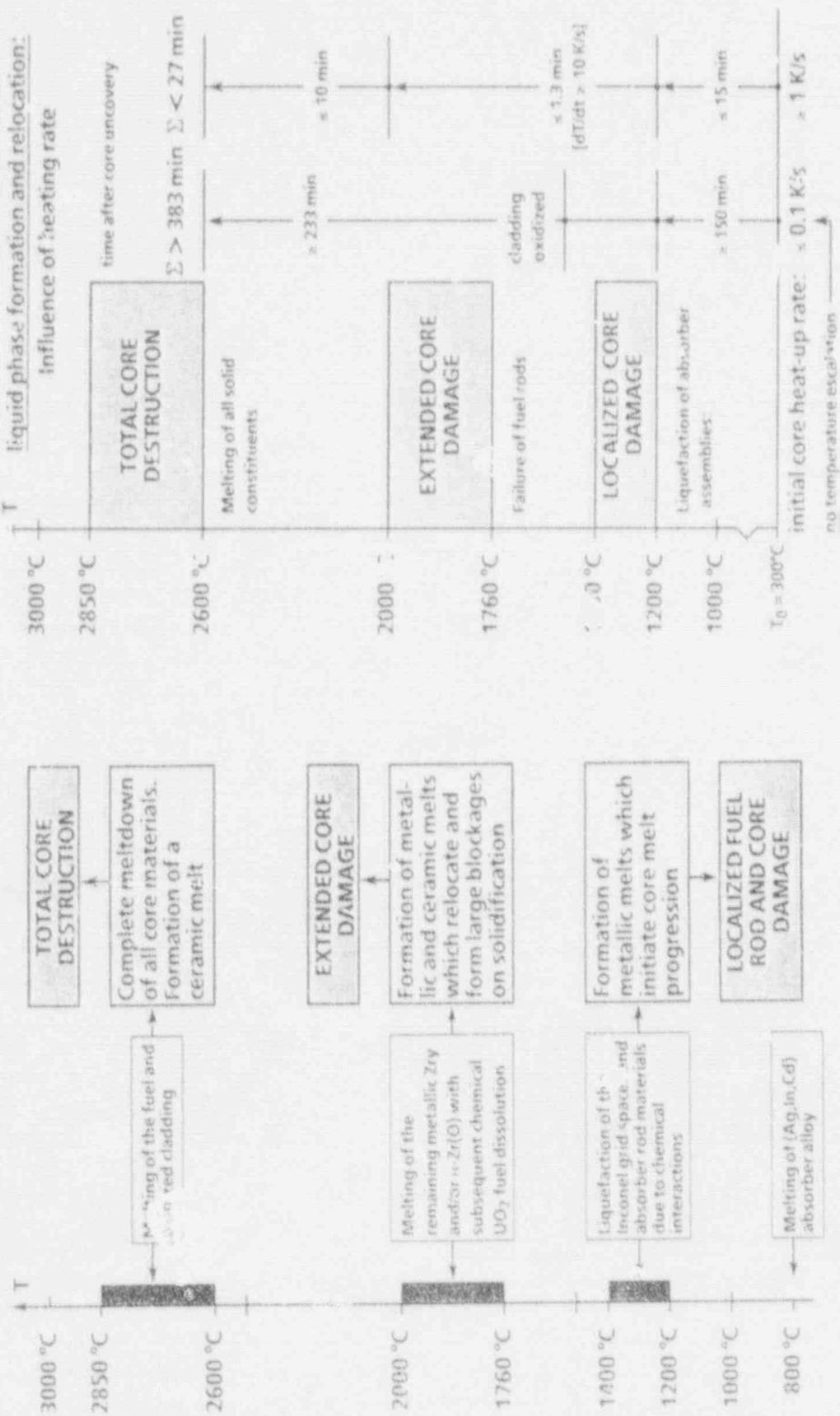

Figure 5: Temperature regimes for extended liquid phase formation in a severe reactor accident (lower picture) which depend on the initial heat-up rate of the core (upper picture). Small heat-up rates reduce drastically the amount of molten Zircaloy (1760 - 2000 °C) and give more time for possible accident measures.

Boiling Jet Modeling on IFCI – Preliminary Report

M.J. Rightley

Sandia National Laboratories

ABSTRACT

Simulations of the breakup and penetration of high temperature thermite jets into water have been performed using the integrated fuel-coolant interaction code, IFCI. The work to date has been directed towards assessing the model performance against data obtained from an experimental test series performed at Sandia. The tests, part of the EJET series, were extensively photographed to allow for direct digitization of the melt profile data thereby allowing a direct comparison of the IFCI predictions to the test data. This document is a preliminary report for Task 1, Molten Jet Model Evaluation, of the Molten Fuel-Coolant Interaction Program.

The IFCI simulation of test EJET-1, with initially saturated water, showed reasonable performance in predicting early time leading edge penetration rate and initial jet spreading as shown by comparisons of the molten thermite volume fraction. A transition to a bulk boiling temperature regime which was observed in both tests was not modeled adequately by IFCI. An attempt to simulate test EJET-0, with initially subcooled water, failed at very early times due to an automatic decrease in the time step to an unacceptable value caused by nonconvergence of the numerical algorithm. These preliminary assessment results suggest (1) the need to include the steam volume fraction in the data comparisons, (2) an improvement of the boiling model in IFCI to address the bulk boiling question and (3) use of a finer noding scheme to improve the spatial resolution of IFCI before the code is applied to addressing accident management concerns at reactor scale.

1. INTRODUCTION

1.1 Program Background

Postulated severe accidents in a nuclear reactor include the possibility of high temperature molten core materials contacting water and producing an explosive fuel-coolant interaction (FCI). The IFCI computer code (integrated fuel-coolant interactions) was developed as a tool to provide researchers with a best estimate tool to studies FCIs in reactor geometries. Since it was developed based on known physical laws and the results of available experiments, it can be used to aid in the interpretation of experimental results and to help study the phenomenological aspects of the experiments themselves.[1] [2]

A NRC program entitled "Molten Fuel-Coolant Interactions" (FIN #A1030) was developed to apply the IFCI code to study FCIs through an assessment of the code's performance against available experimental data and parametric analyses at reactor scale. Task 1 of this project involves an assessment of the boiling and fragmentation models in IFCI against the EJET series of boiling jet experiments performed at Sandia. This document is a preliminary report on the progress of the assessment of IFCI against the EJET tests as described in the work statement for this task in the NRC Form 189. It includes a comparison of the IFCI predictions of the breakup of the molten thermite jet in a saturated water test (EJET-1) and the results of a preliminary attempt to apply the code to a subcooled experiment (EJET-0).

1.2 Report Organization

The report is divided into three primary sections: IFCI input information, comparison results and a summary and future work section. The input information is included to provide an understanding of the nature of the process of setting up a "simulation" of an experiment on IFCI and it also provides suggestions for possible methods of improving the performance of the code without significant modifications. The results section presents the IFCI output and the experimental data and discusses the implications of the comparison results. Some time was expended in developing a "post-processing" technique that allows the experimental data and the IFCI data to be presented on the same plot. This method is briefly discussed based on its relevance to the comparison. Finally, the summary and future work section includes ideas for possible code improvements and plans for termination of the Molten Jet Model Evaluation task.

2. IFCI INPUT INFORMATION

This section presents the relevant information concerning the input variable values for the EJET simulations on IFCI. The differences in the input decks for specific tests are discussed in the results section.

2.1 Noding

For the initial attempts to simulate the boiling jet experiments on IFCI, a fairly coarse noding scheme was used. For the simulations discussed in this report, 15 axial nodes and 4 radial nodes were used to define the 2-D grid. Symmetry about the vertical axis was assumed (due to the two dimensional nature of IFCI). Consequently, the 15X4 noding covered a plane of dimensions 1.57 m height and 0.32 m width (which is the half width of the tank). Figure 1 illustrates the noding scheme.

It was anticipated that, if the results of the initial IFCI runs indicated a significant improvement would be achieved with a finer mesh, a new problem using a finer mesh would be run. The mesh illustrated in Figure 1 above, although coarse, still required over an hour run time on Sandia's Cray YMP to simulate 3 seconds of the EJET-1 test.

2.2 Boundary Conditions

The IFCI code is presently set up in such a way that, lacking a definition of the pressure along any boundary cells, the default is a solid boundary. Consequently, the input deck for the EJET simulations defined the inner ring cell at the "top" of the tank (axial cell 1, ring cell 1) as the inflow boundary and the outer ring cell at the top as the outflow boundary. All other boundaries were not specifically defined which forces them to be solid surfaces. The cell size was chosen to represent the size of the "mixer plate assembly"[3] allowing the outflow to occur along the outer annulus. The boundary condition at this location was defined as ambient pressure.

2.3 Initial Conditions

The initial conditions for the IFCI executions are concerned with the thermite jet entrance into the water tank through the jet orifice. For tests EJET-1 and EJET-0, the orifice size was 3.8 cm. The thermite inflow velocity was estimated from the photographic coverage of the tests to be 1 m/s (note that the thermite was released from a reaction crucible and fell 30 cm to the mixer plate assembly).[3] The initial temperature of the thermite was defined as 2700K.[4] The noding scheme used in the IFCI runs was defined such that the thermite jet entered the coolant tank through the inner ring cell at the top of the tank. The thermite used in the EJET tests consisted of 55% (by mass) iron and 45% alumina.

3. RESULTS AND COMPARISONS

The results of the IFCI simulations of tests EJET-1 and EJET-0 are presented in this section. Some discussion of the post-processing of the computer data is included since both sets of data (numerical and experimental) are presented on the same plot. An interpretation of the comparison between the two data sets, including indicated suggestions for code improvements, is given.

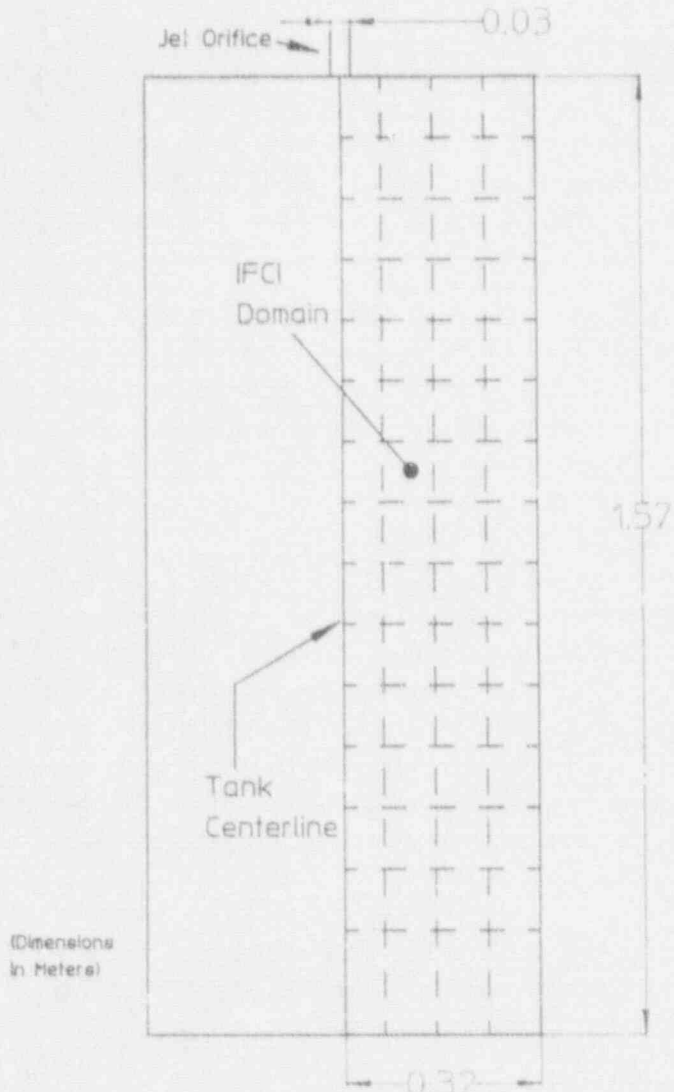

Figure 1. EJET Simulation Noding Scheme

3.1 EJET-1

3.1.1 Test Parameters and Description. The initial IFCI simulation was of test EJET-1 (the first test was named EJET-0). The second test was chosen due to the subcooled nature of the coolant in test EJET-0. It was anticipated that problems in the bulk boiling model in IFCI would cause a subcooled coolant simulation to be unsatisfactory. The coolant temperature for EJET-1 was 362K. As was mentioned

previously, the thermite was ignited in a reaction crucible and, at the appropriate time (i.e., when the molten products of the reaction melted through a 0.64 cm thick steel "burn through" plate of 12.7 cm diameter), introduced into the reservoir where the jet orifice was located.

A review of the high speed films of the test revealed that the thermite jet fragmented immediately upon contact with the water. The characteristic drop diameters were observed to be much less than the jet orifice diameter. Curves of the jet profile show that the mixture region expands to approximately twice the size of the jet orifice diameter.[3] At a time of approximately 1.3 seconds, the upper section of the jet (which is still glowing brightly) expands rapidly to fill the entire water chamber. The portion of the jet below this expansion region is still relatively narrow and has gradually lost its luminescence. The probable explanation for this is obtained by noting that posttest examination of thermite drops cooled in water show that the drop is radially stratified with a center of iron oxide (and possibly some unoxidized iron) and an outer shell of alumina. During the cooling phase, the outer surface of the drop (which is farthest from the exothermically reacting iron core) probably forms a thin crust of alumina which would "block out" the glow from the iron oxidation process (this situation would be aided by the probable change in the emissivity of the alumina upon phase transition). Bottom contact of this cooler leading edge of the jet occurs around 1.9 seconds. The glowing upper section of the jet "touches down" shortly thereafter (~1.2 s).

3.1.2 IFCI Data Output. Execution of the IFCI code produces data based on the 4 fluids simulated in the code. The separation of the fluids presents some difficulties in presenting the data for a quantitative comparison with the experimental data. A digitization technique is employed to obtain the profile of the jet from the high speed films of the test. When this data is scaled and corrected for photographic imprecision, the result is a profile that represents the location of the interface between the liquid water (fluid 2 in IFCI) and the mixture of the melt (fluid 4 is molten thermite) and the steam (fluid 1). Since IFCI presents its data in terms of the volume fraction of each fluid separately, some judgement must be made to allow direct comparison on a single plot.

For the initial comparisons performed for this study, the variable plotted against the experimentally measured melt profile is the product of the volume fraction and the density of the thermite ($\alpha\rho_{\text{fluid 4}}$). A direct comparison is provided by post-processing the IFCI data into a contour configuration in which the x and y axes are transformed from the discretized noding pattern to the spatial domain of the water chamber. The experimental data can then be overplotted in two dimensions after being translated to the x-y coordinates of the water chamber.

3.1.3 Comparison of Melt Profile Data to IFCI Data. The results of the post-processing data analysis are presented in Figures 2 through 7 for times (in seconds after initial melt/water contact) of 0.08, 0.7, 1.32, 1.94, 2.56 and 3.1, respectively. After 3.1 seconds, the melt had essentially expanded to fill the entire water chamber. The plots show the spatial location of the visible interface between the water and the melt/steam mixture as diamond shaped points. The IFCI data are presented as contours of the $\alpha\rho_4$ product with values of 10, 100 and, space permitting, 300 kg/m^3 labeled. Note that molten stoichiometric thermite has a density on the order of ~4000 kg/m^3, so the contours shown in the 3.1 second simulation are, at their maximum, approximately one order of magnitude below the value representing a volume fraction of unity.

The test data shown in the plots illustrate the initial jet spreading to twice the inlet diameter (Figure 2). Although the IFCI data shows a similar initial spreading characteristic, the contours that are observed to spread represent volume fractions on the order of 10^{-3} (Figures 3 and 4). However, any conclusions that might be drawn from this point must be deferred until similar plots of the steam volume fraction are obtained. Recall that the experimental melt profile data represent the visible interface between the water and the melt/steam mixture and, as such, some judgement is necessary to properly interpret the IFCI predictions. Certainly, some further study of this simulation concerning steam volume fractions is in order and will be addressed in the final report.

As is clear from looking at the plots (especially Figures 3, 4 and 5), the IFCI data is satisfactory in terms of predicting the leading edge penetration rate and the spreading of the jet *prior* to the rapid expansion that is first observed in the plots in Figure 4. This secondary rapid expansion of the jet, which is also observed in subcooled tests at relatively later times, is thought to be caused by a transition into the bulk boiling regime. (An unsuccessful attempt to model the subcooled test EJET-0 also seems to indicate that the bulk boiling model in IFCI is not correct.)

At times around 1.3 s, the IFCI model shows bottom contact of the lowest contours of $\alpha\rho_4$. The IFCI data appears to follow the leading edge of the test data closely, although a comparison of the contour labeled "100" and the leading edge of the data illustrates that the data appears to be "moving faster" than the IFCI predictions (see Figures 3, 4 and 5). The test data shows bottom contact some time before t=1.9s (Figure 5). Due to the size of the bulk boiling-associated rapid expansion of the thermite jet, it is difficult to observe any pile up of melt on the tank bottom. Figure 6 shows that the IFCI contour labeled "100" has already contacted the bottom and considerable pile-up has occurred. It is not clear from the data, however, that the expanded jet has reached the bottom at this time. In the judgement of the author, based on repeated viewings of the film records of the test, the wide section of the jet has not reached bottom and Figure 6 actually illustrates the pile up "meeting" the wide jet at some point above the water chamber floor. Figure 7 appears to verify this claim

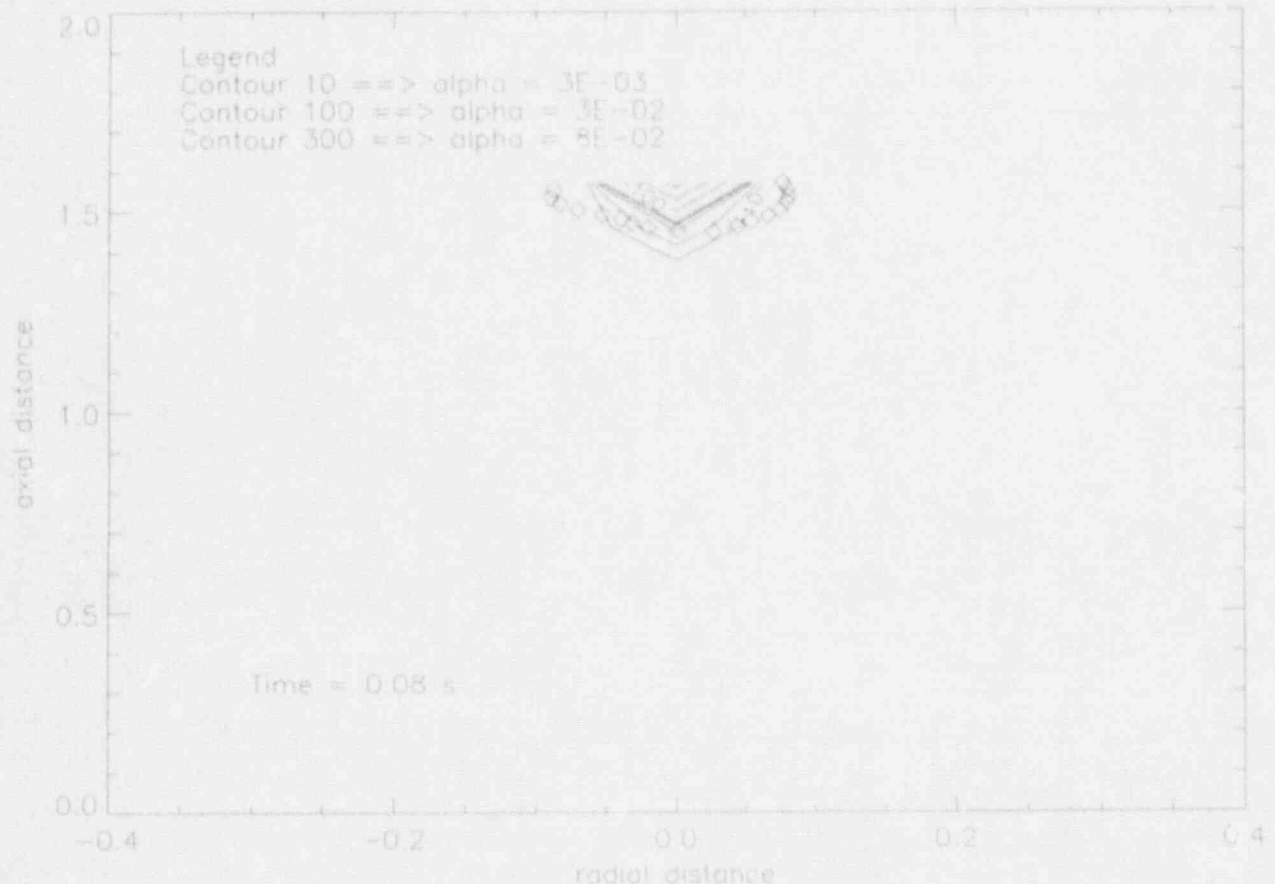

Figure 2. Predicted Vs. Measured Jet Breakup (t=0.08 s)

although the reason for the narrowing of the flow from t=2.6 s to t=3.1 s is unexplainable and probably is attributable to error in the data (collecting accurate data near the bottom of the tank at late time is difficult).

3.2 EJET-0

The basic experimental set up for the EJET-0 test is identical to that reported for EJET-1.[3] The primary difference is that EJET-0 was conducted with subcooled

Figure 3. Predicted Vs. Measured Jet Breakup (t=0.7 s)

water at a temperature of 303 K. The results are similar to EJET-1 including the lack of a coherent jet (implying rapid fragmentation), the almost immediate spreading of the jet to twice the orifice diameter and the secondary later time rapid expansion associated with a boiling transition. An important difference in the results (which is expected) is that the secondary rapid expansion occurs around 2.5 s compared to 1.3 s for the EJET-1 test supporting the hypothesis that the threshold and transition into the new boiling regime is water temperature driven.

Figure 4. Predicted Vs. Measured Jet Breakup (t = 1.32 s)

An IFCI simulation was set up to model the EJET-0 test. The input deck was identical to the EJET-1 input with the exception that the initial temperature of the water (fluid 2) was changed to the value measured in EJET-0. The execution attempt was unsuccessful and the program was terminated after a few time steps. The failure of IFCI to run with the same input deck but a decrease in the water temperature also implies that the boiling model in IFCI may be the culprit.

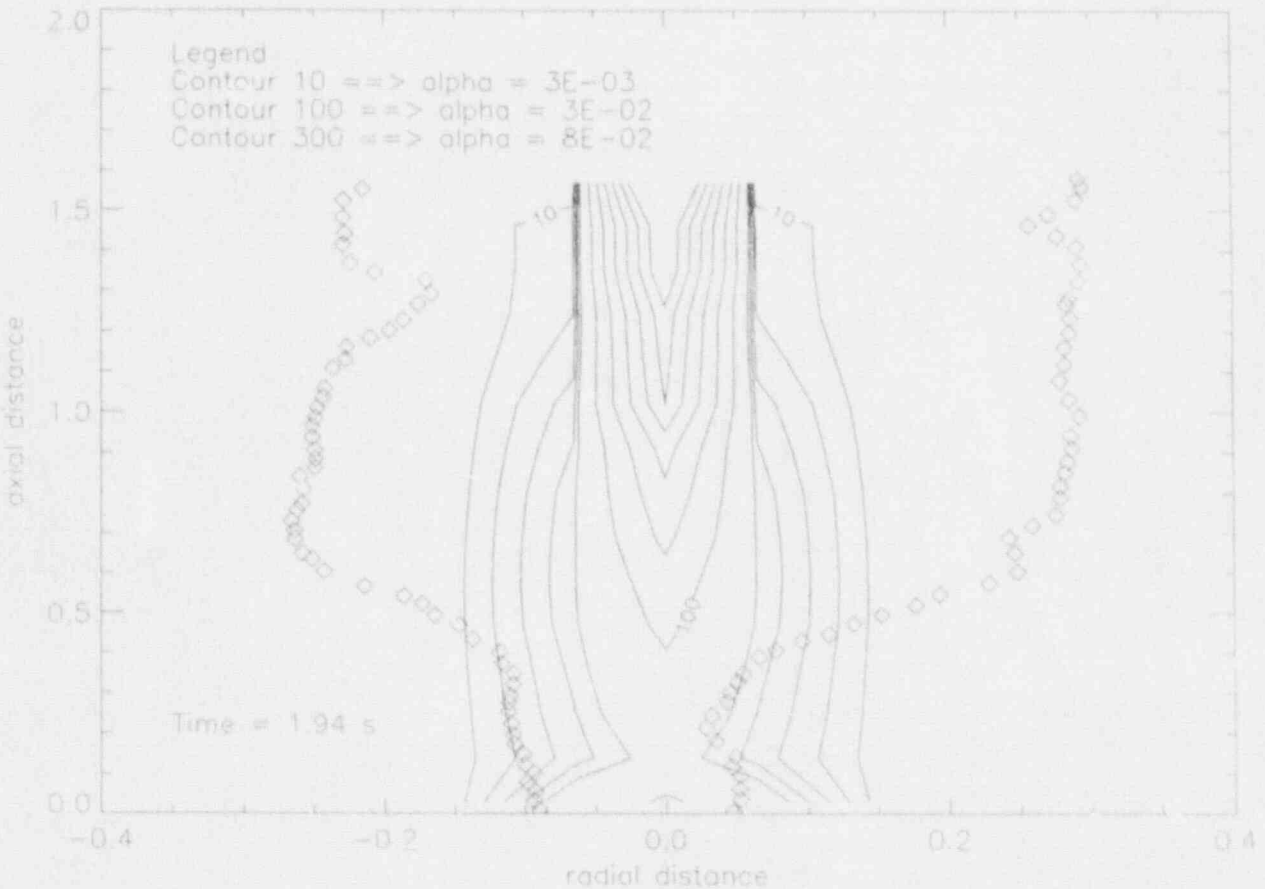

Figure 5. Predicted Vs. Measured Jet Breakup (t = 1.94 s)

4. SUMMARY AND PLANS FOR TASK TERMINATION

The computer code IFCI was used to model two tests of the penetration and breakup of a high temperature molten material (stoichiometric thermite) into a tank of water. The two tests were identical with the exception of the initial water temperature. The IFCI predictions appeared to reasonably simulate the early time behavior of the jet including the initial spreading and the rate of penetration of the leading edge. A

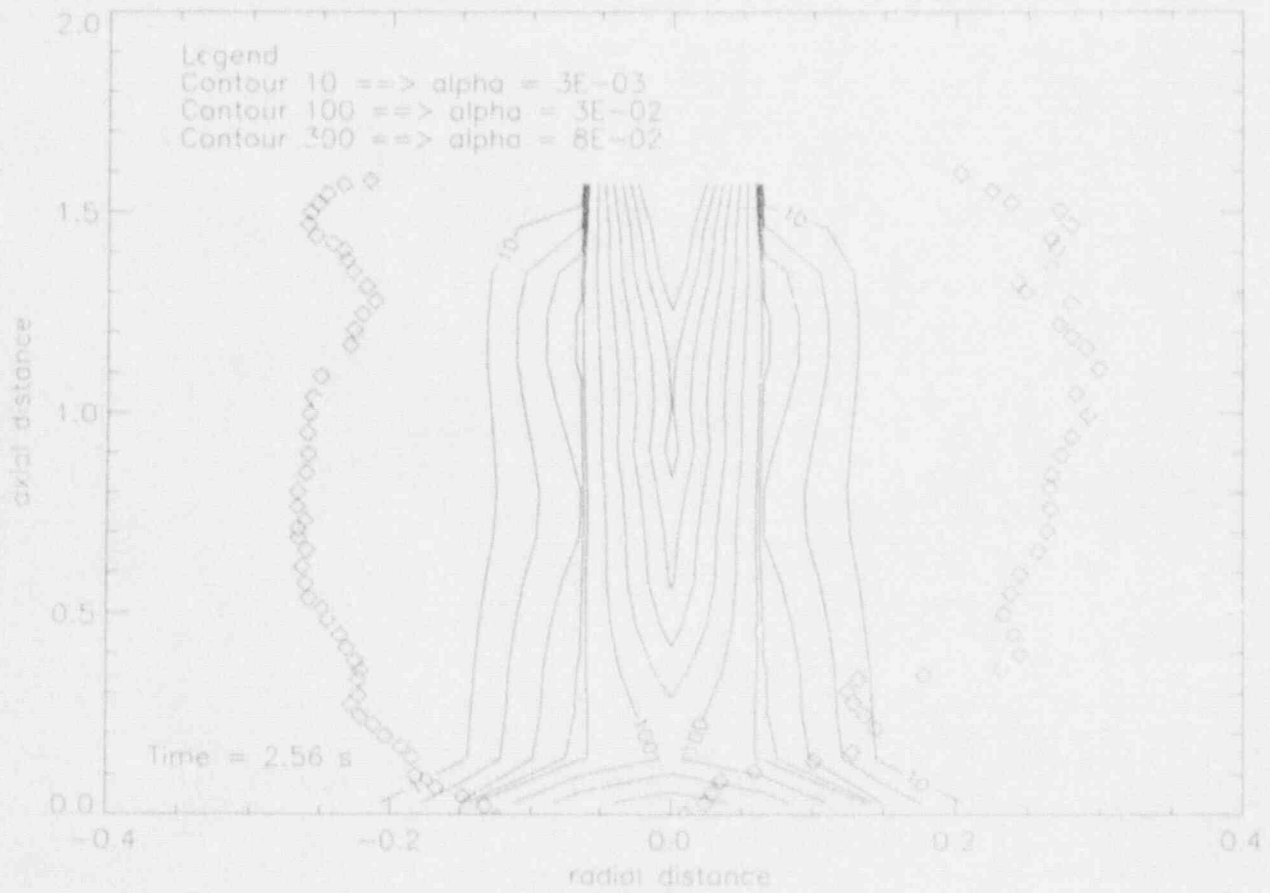

Figure 6. Predicted Vs. Measured Jet Breakup (t = 2.56 s)

phenomenon thought to be associated with the onset of a boiling regime transition (possibly from subcooled to bulk boiling) was observed in the photographic records of both tests at different times. This behavior was not observed in the IFCI data for the initially saturated water test (EJET-1). The IFCI simulation for EJET-0, in which the water was initially subcooled, failed at very early times due to an attempt to reduce the time step to an unacceptable value (IFCI will automatically reduce the time step to ensure that numerical errors remain below an acceptable level, or if the pressure

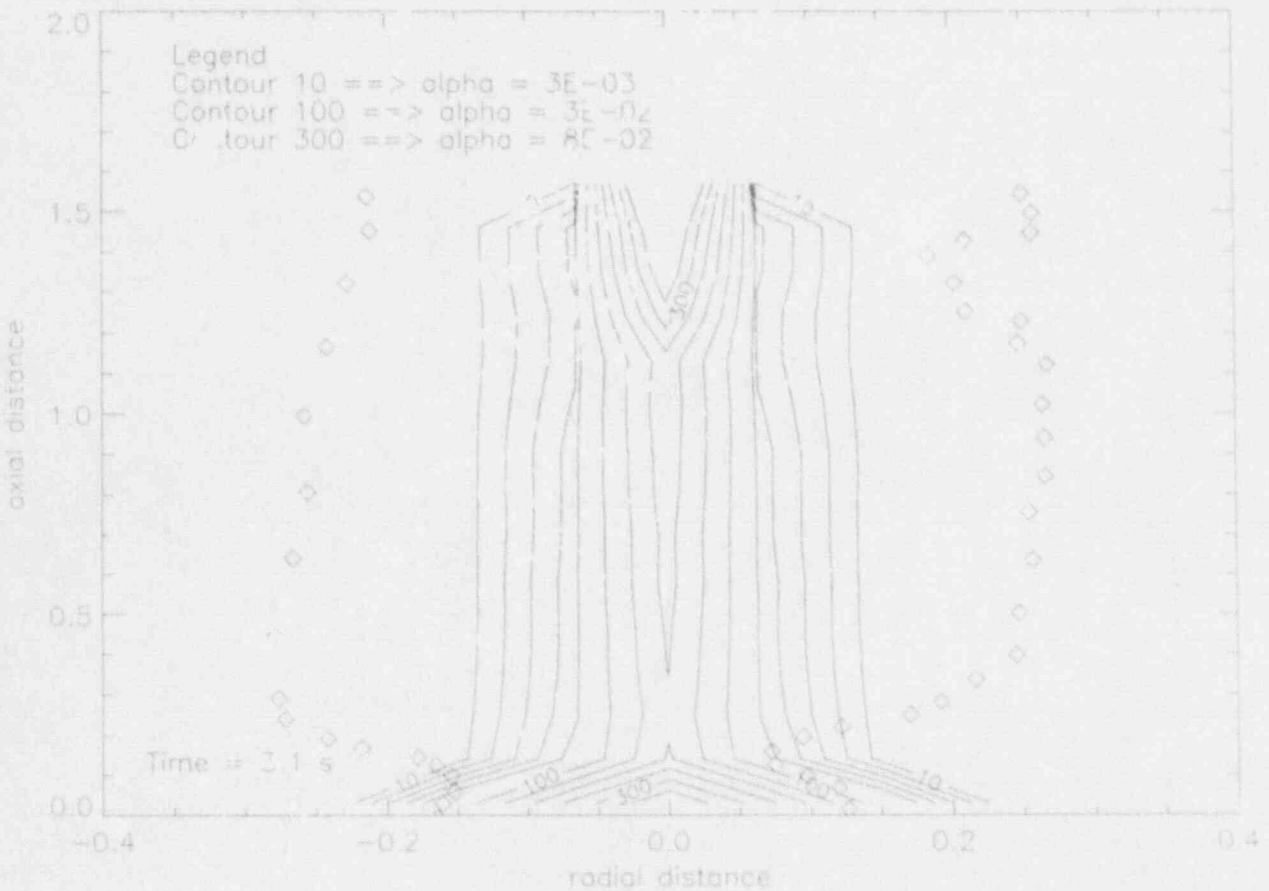

Figure 7. Predicted Vs. Measured Jet Breakup (t=3.1 s)

iteration in the fluids solution method fails to converge).

Prior to running simulations of the remaining two tests, EJET-2 and EJET-3, three points need to be addressed. The first concerns the choice of the molten thermite (fluid 4) as the IFCI output variable to be plotted against the test data. The volume fraction of the steam inside the "glowing" section of the jet is not directly obtainable from the test data. So, whether the visible interface recorded by the digitization is, in

fact, the boundary between the molten thermite and the water or is actually steam determined remains to be seen. Performing the same data analysis for the steam volume fraction (IFCI fluid 1) as was done for the thermite is warranted for the data taken from EJET-1. It is possible that a combination of the two fluids is required to completely address the extent of the jet mixture region.

Secondly, the apparent failure of IFCI to adequately model the transition into bulk boiling in EJET-1 and the total breakdown of the code for the EJET-0 simulation indicates that further study of the boiling models in IFCI is warranted.

Finally, for the simulations attempted to date, the noding scheme has been relatively coarse in order to assess the behavior of the model at minimum computational cost. A significant improvement in performance may be obtained by utilizing a finer mesh in critical areas of the numerical domain.

It appears that the simulation of the breakup of a high temperature molten jet in water is adequately modeled by IFCI. Further assessments of the code's performance against other codes (such as TEXAS, PM-ALPHA and THIRMAL) would be useful to confirm the performance of IFCI. When the bulk boiling model in IFCI has been corrected, the assessment of the code against the boiling jet tests will simply be a matter of "fine tuning" the code in preparation for the continuation of the total assessment of IFCI (i.e., subsequent tasks in the Molten Fuel-Coolant Interaction program).

REFERENCES

1. Young, M.F., 1987, *IFCI: An Integrated Code for Calculation of All Phases of Fuel-Coolant Interactions,* NUREG/CR-5084, SAND87-1048, Sandia National Laboratories, Albuquerque, NM, September.

2. Young, M.F., 1989, *"Application of the Integrated Fuel-Coolant Interaction Code to a FITS-Type Pouring Mode Experiment", Dynamics of Detonations and Explosions: Explosion Phenomena,* Edited by A.L. Kuhl, J.C. Leyer, A.A. Borisov, and W.A. Sirignano, Progress in Astronautics and Aeronautics, Vol. 134.

3. Marshall, B.W. Jr., and M. Berman, 1986, *An Experimental Study of Isothermal and Boiling Liquid Jets,* SAND86-2909C, Sandia National Laboratories, Albuquerque, NM.

4. Beck, D.F., 1988, *Melt Temperatures in Iron Oxide-Aluminum Thermites,* Memorandum to M. Berman, Sandia National Laboratories, August.

ADIABATIC EQUILIBRIUM MODELS FOR DIRECT CONTAINMENT HEATING

Martin M. Pilch

Severe Accident Phenomenology, 6422
Sandia National Laboratories
Albuquerque, New Mexico 87185

ABSTRACT

PRA studies are being extended to include a wider spectrum of reactor plants than was considered in NUREG-1150. There is a need for computationally simple models for Direct Containment Heating (DCH) that could be used for screening studies aimed at identifying potentially significant contributors to risk. This paper discusses two adiabatic equilibrium models that are candidates for the task. The first, a 1-cell model, places a true upper bound on DCH loads. This upper bound, however, often far exceeds reasonable expectations of containment loads based on best estimate CONTAIN calculations or experiment observations. In this paper, a 2-cell model is developed that largely captures the major mitigating features of containment compartmentalization, thus providing more reasonable estimates of the containment load. Predictions of the equilibrium models are compared with experiment data from the Limited Flight Path (LFP) test series conducted at Sandia National Laboratories.

1.0 Single-Cell Adiabatic Equilibrium Model

The single-cell adiabatic equilibrium model assumes that the entire containment volume can be treated as a single control volume in which there are no energy sinks. Failure of the lower head of the reactor pressure vessel (RPV) initiates melt ejection and blowdown of the reactor coolant system (RCS) into the reactor cavity. Blowdown gas adds both mass and energy to the containment atmosphere.

Some portion of the molten core material that is ejected from the RPV into the reactor cavity is assumed to be entrained from the reactor cavity and dispersed into the containment atmosphere; the remainder can be ignored in containment loads analyses of DCH. The metallic components of the dispersed corium are assumed to react completely with available steam, releasing energy to the debris and producing hydrogen. It is further assumed that the dispersed mass remains airborne indefinitely so that it can come to thermal equilibrium with the containment atmosphere.

The above processes will heat the containment atmosphere, often to the point at which steam can no longer inert the combustion of hydrogen. In this analysis, preexisting hydrogen, hydrogen in the blowdown gas, and hydrogen produced from metal/steam reactions in the containment are assumed to burn slowly to the extent that oxygen is available globally. Impulsive pressure loads due to possible hydrogen detonations are not considered.

Derivation of the single-cell model is being documented by Pilch and Allen [1990]. The relevant results are summarized here. Thermal equilibrium between airborne debris and the containment atmosphere,

$$\frac{\Delta U}{U^\circ} = \frac{\Delta P}{P^\circ} = \frac{\sum_i \Delta E_i}{U^\circ(1 + \psi)} \quad , \tag{1}$$

yields a simple, bounding expression for the DCH load. Here

ΔU	=	total internal energy gained by the containment atmosphere,
U°	=	initial internal energy of the entire containment atmosphere,
ΔP	=	pressure rise in the containment resulting from the DCH event,
P°	=	initial containment pressure,
ΔE_i	=	maximum energy that could be added to the containment atmosphere by the i^{th} process, and
ψ	=	heat capacity ratio.

The heat capacity ratio appears because at thermal equilibrium between airborne debris and the atmosphere the debris still carries sensible heat that is not available for containment pressurization. The heat capacity ratio is defined by

$$\psi = \frac{N_d C_d}{\left(N^\circ + N_b\right) C_v} \tag{2}$$

where

N_d	=	number of moles of debris participating in DCH,
C_d	=	molar heat capacity of debris,
N°	=	number of gas moles initially in the containment,
N_b	=	number of gas moles added to the containment by RCS blowdown, and
C_v	=	molar heat capacity of the containment atmosphere.

The molar inventory of the atmosphere and the RCS can be expressed in terms of containment and RCS initial conditions as

$$N^{o} = \frac{P^{o}V}{R_{u}T^{o}} \tag{3}$$

$$N_{b}^{o} = \frac{P_{RCS}^{o}V_{RCS}}{R_{u}T_{RCS}^{o}} \tag{4}$$

where

P^0, P^0_{RCS}	=	initial pressures in the containment and RCS, respectively,
V^0, V^0_{RCS}	=	volumes of the containment and RCS, respectively,
R_u	=	universal gas constant, and
T^0, T^0_{RCS}	=	initial gas temperatures in the containment and RCS, respectively.

The number of debris moles participating in DCH can be related to the initial number of debris moles in the RCS,

$$N_{d} = f_{disp}f_{eject}N_{d}^{o} \quad , \tag{5}$$

where

f_{eject}	=	fraction of melt initially in the RCS that is ejected into the reactor cavity
f_{disp}	=	fraction of melt ejected into the reactor cavity that is dispersed into the containment, and
N_d^0	=	moles of molten debris initially present in the RPV at the time of vessel breach.

DCH experiments and analyses [Pilch and Tarbell, 1985] suggest that virtually all molten material in the bottom of the RPV at the time of vessel breach is ejected into the reactor cavity (i.e., $f_{eject} \approx 1.0$). Experiments in the Zion, Surry, and Watts Bar geometries [Tutu et al., 1990; Tutu and Ginsberg, 1990] have failed to demonstrate that any cavity design will prevent dispersal of debris from the reactor cavity into the containment atmosphere for RCS pressures greater than about 4 MPa; consequently, $f_{disp} \approx 1.0$. This is contrary to subjective speculation by IDCOR [1985].

Four processes contribute to containment pressurization during DCH:

1. RCS blowdown,
2. exchange of debris thermal energy with the containment atmosphere,
3. chemical energy released by oxidation of metallic constituents of airborne core material by the containment atmosphere, and
4. combustion of hydrogen in the atmosphere.

Working expressions for these processes are discussed next.

The internal energy of the RCS is given by

$$\Delta E_b = \frac{P^o_{RCS} V_{RCS}}{\gamma - 1} \tag{6}$$

where

γ = C_p/C_v is the isentropic exponent of blowdown gas.

Virtually all this energy is convected into the containment during RCS blowdown.

The thermal energy contribution represents the total internal energy of airborne debris referenced to the initial temperature of the atmosphere

$$\Delta E_t = N_d \left[u_d\left(T^o_d\right) - u_d(T^o) \right] \tag{7}$$

where

u_d = molar internal energy of airborne debris,
T^0_d = initial temperature of airborne debris, and
T^0 = initial temperature of the containment atmosphere.

The specific internal energies are composition dependent,

$$u_d(T) = \sum_i f_{d,i} u_{d,i}(T) \tag{8}$$

where

$f_{d,i}$ = mole fraction of i^{th} species in the airborne debris, and
$u_{d,i}$ = molar internal energy of the i^{th} species in the airborne debris.

The chemical energy term accounts for the exothermic oxidation of the metallic components of airborne debris,

$$\Delta E_r = N_d \sum_j f_{d,j} \Delta h_{r,j} \tag{9}$$

where

$\Delta h_{r,i}$ = molar heat of reaction of the i^{th} component of the debris.

Two sources of oxidant in the containment atmosphere are oxygen and steam. The debris will preferentially oxidize with O_2 when available, and this is the more energetic reaction. If debris does react with steam, however, then hydrogen is produced that may subsequently combust with the available oxygen; in which case, the net energy release of the cycle is the same as if the debris burned with oxygen.

Reaction energies based on metal/steam reactions are recommended, provided the resulting hydrogen production is explicitly accounted for in the hydrogen combustion term. This facilitates comparison with experiments in which the atmosphere is inerted (no oxygen), but in which steam is available for reaction with the metal. There may be reactor applications when a similar situation arises. The energy contribution resulting from hydrogen combustion is given by

$$\Delta E_{H2} = N_{H2} \Delta h_{H2} \tag{10}$$

where

N_{H2} = total number of hydrogen moles in the containment atmosphere, and
Δh_{H2} = molar heat of reaction for hydrogen combustion.

The total amount of hydrogen available for combustion can be expressed as

$$N_{H2} = f_{H2} N^o + f_{H2,RCS} N^o_{RCS} + N_{H2,rxn} \tag{11}$$

where

f_{H2} = mole fraction of hydrogen initially in the containment atmosphere,
$f_{H2,RCS}$ = mole fraction of hydrogen in the RCS at the time of vessel breach, and
$f_{H2,rxn}$ = moles of hydrogen produced by metal/steam oxidation.

Global oxidant limitations for debris oxidation and hydrogen combustion generally do not exist for pressurized water reactor (PWR) containments, and they are not explicitly accounted for in this screening model. The magnitude of these energy terms will require adjustment should oxidant limitations arise in any other applications.

The earliest considerations of DCH [NRC, 1985] identified cavity water as a potential mitigator of DCH. Simple energy arguments support cavity water as a mitigator because energy absorbed in vaporizing water will not contribute to increased atmospheric temperature. Although

vaporized water adds moles of steam to the containment atmosphere leading to increased pressure, the resulting pressure rise would be considerably less than if all the energy went into heating the atmosphere. Consequently, cavity water is a potentially mitigating factor.

This simplistic energy argument does not reflect the kinetics of debris/water interactions. Experiments [Spencer et al., 1987; Allen et al., 1991b] have shown that cavity water can enhance debris dispersal from the cavity; however, the screening model already assumes nearly complete dispersal from the cavity for RCS pressures greater than 4 MPa. CONTAIN calculations [Williams et al., 1987] have indicated that efficient water interactions in the cavity can increase the peak pressure by as much as 20 percent compared to a dry scenario for a wide range of water masses (≤100 MT). Only modest increases in peak pressure and hydrogen production [Spencer et al., 1987; Henry et al., 1991; Allen et al., 1991b] have been observed in experiments. The latter already is accounted for fully in the equilibrium models. Analyses of these experiment results suggest that only a small fraction of the available water participates in the interactions. This conclusion is supported by other experiment observations [Tarbell et al., 1991] where violent debris/water interactions in the cavity expel the bulk of the water from the cavity as a slug. For these reasons, the neglect of cavity water in the screening model is judged to have minimal impact on predicted results.

2.0 Two-Cell Adiabatic Equilibrium Model

The two-cell adiabatic equilibrium model extends the previous results in order to capture part of the mitigating effects associated with containment compartmentalization, which prevents the efficient mixing of airborne debris with the entire atmosphere by confining the bulk of the debris to the subcompartment of the containment. Thermal equilibrium between debris and gas in the subcompartment retains more energy in the debris as unavailable for additional heating of the atmosphere. This effect is termed thermal saturation. Conceptual development of the model follows, as it has not been documented elsewhere.

The containment is divided into two volumes: upper dome and subcompartment. For a PWR, the subcompartment typically comprises the reactor cavity and the region generally located beneath the operating floor, bounded by the crane wall and the refueling canal wall. The upper dome comprises the remainder of the containment. Debris can be dispersed from a PWR cavity through two possible flow paths. The first flow path exists so that incore instrument guide tubes can have access to the lower head of the reactor pressure vessel. Debris dispersal through this path will enter the containment subcompartment.

A second path for debris dispersal is through an annular gap surrounding the reactor pressure vessel. Debris dispersed through this path enters the upper dome of the containment. The annular gap usually is filled partially with reflective insulation. The insulation is mostly void with layers of metal foil retained by thin sheet metal. The fate of the insulation under severe accident conditions is a matter of speculation. Some researchers argue that the insulation

will crumple up and restrict the flow path, while others argue that the insulation will be blown out of the way or compressed against the RPV, thus presenting the maximum flow area for debris dispersal. The analysis presented here allows for the possibility that both flow paths can exist.

The premise of the two-cell model is that DCH occurs independently in the subcompartment and the upper dome. The total energy imparted to the atmosphere is the sum of the subcompartment and upper dome contributions,

$$\Delta U = \Delta U_1 + \Delta U_2 = \frac{\sum_i \Delta E_{1,i}}{1 + \psi_1} + \frac{\sum_i \Delta E_{2,i}}{1 + \psi_2} \quad , \tag{12}$$

so that the resulting pressure rise is given by

$$\frac{\Delta U}{U^o} = \frac{\Delta P}{P^o} = \frac{\sum_i \Delta E_{1,i}}{U^o(1 + \psi_1)} + \frac{\sum_i \Delta E_{2,i}}{U^o(1 + \psi_2)} \tag{13}$$

where

ψ_1, ψ_2 = heat capacity ratio for the subcompartment and upper dome respectively, and

$\Delta E_{1,i}$; $\Delta E_{2,i}$ = maximum contribution of the i^{th} process in the subcompartment and the upper dome respectively.

On a containment-wide basis, ψ is usually a second order effect; but the local heat capacity ratio, ψ_1, could be very significant in the lower containment regions. Consequently, thermal saturation of a subcompartment has the potential to mitigate sigificantly containment loads. The local heat capacity ratios are defined by

$$\psi_1 = \frac{f_{al} N_d C_d}{\left(f_{vl} N^o + f_{al} N_b^o\right) C_v} \tag{14}$$

$$\psi_2 = \frac{(1 - f_{al}) N_d C_d}{\left[(1 - f_{vl}) N^o + (1 - f_{al}) N_b^o\right] C_v} \tag{15}$$

where

f_{V1} = fraction of the total containment volume occupied by the subcompartment, and
f_{a1} = fraction of the total flow area from the reactor cavity that communicates with the subcompartment.

The assumption here is that the debris and blowdown gas enter each cell in the same fractions as the flow areas. The HIPS-8C experiment [Pilch et al., 1988] lends partial credibility to this assumption.

Consider the contribution of RCS blowdown to the atmosphere energy. The total is the sum of the individual contributions for each cell

$$\Delta U_b = \frac{f_{a1}\Delta E_b}{1 + \psi_1} + \frac{(1 - f_{a1})\Delta E_b}{1 + \psi_2} \quad , \tag{16}$$

which, after some rearrangement, can be written as

$$\Delta U_b = \eta_b \frac{\Delta E_b}{1 + \psi} \quad , \tag{17}$$

where the efficiency is given by

$$\eta_b = f_{a1} \frac{1 + \psi}{1 + \psi_1} + (1 - f_{a1}) \frac{1 + \psi}{1 + \psi_2} \quad . \tag{18}$$

The thermal and chemical energy contribution can be developed in a simila. fashion since debris is also apportioned between the cells according to the flow areas. The results are

$$\Delta U_t = \eta_t \frac{\Delta E_t}{1 + \psi} \tag{19}$$

$$\Delta U_r = \eta_r \frac{\Delta E_r}{1 + \psi} \quad , \tag{20}$$

where $\eta_b = \eta_t = \eta_r$ are identical because all terms are flow-area weighted.

The contribution due to hydrogen combustion requires a little more care because preexisting hydrogen is apportioned between the cells by volume fractions, while hydrogen carried with the blowdown gas or formed by metal oxidation is apportioned by flow area fractions. The contribution due to hydrogen combustion is given by

$$\Delta U_{H2} = \eta_{H2} \frac{\Delta E_{H2}}{1 + \psi} \tag{21}$$

where

$$\eta_{H2} = \frac{f_{V1} f_{H2} N^o + f_{a1}\left(f_{H2,RCS} N^o_{RCS} + N_{H2,rxn}\right)}{f_{H2} N^o + f_{H2,RCS} N^o_{RCS} + N_{H2,rxn}} \frac{1 + \psi}{1 + \psi_1}$$
$$+ \frac{\left(1 - f_{V1}\right) f_{H2} N^o + \left(1 - f_{a1}\right)\left(f_{H2,RCS} N^o_{RCS} + N_{H2,rxn}\right)}{f_{H2} N^o + f_{H2,RCS} N^o_{RCS} + N_{H2,rxn}} \frac{1 + \psi}{1 + \psi_2} \tag{22}$$

In this formulation, it is assumed that sufficient oxygen exists to burn all hydrogen. Globally this may be true, but the assumption is suspect in the subcompartment. The more bounding result is favored for screening models. However, H_2 located in the subcompartment could be displaced into the upper dome where it could still burn.

The total containment response now can be written as

$$\frac{\Delta U}{U^o} = \frac{\Delta P}{P^o} = \frac{\sum_i \eta_i \Delta E_i}{U^o(1 + \psi)} , \tag{23}$$

or alternatively as

$$\frac{\Delta U}{U^o} = \frac{\Delta P}{P^o} = \eta_{eff} \left(\frac{\Delta P}{P^o}\right)_{1-cell} , \tag{24}$$

where the efficiency due to containment compartmentalization is given by the energy-weighted average of the individual process efficiencies

$$\eta_{eff} = \frac{\sum_i \eta_i \Delta E_i}{\sum_i \Delta E_i} \tag{25}$$

3.0 Comparison With Experiment Data

The LFP experiments [Allen et al., 1991a] provide useful data for assessing the utility of the adiabatic equilibrium models. In the LFP tests, the Surtsey vessel was divided into upper and lower compartments by a concrete slab placed in the path of dispersing debris. The relative size of the subcompartment was varied by positioning the concrete slab at various heights above the cavity exit. Large flow paths permitted easy gas flow between the cells. Virtually no debris was found above the slab; however, the annular gap around the RPV was not simulated in these experiments so that $f_{a1} = 1$. Furthermore, the containment atmosphere was inerted in these experiments, so the DCH contribution due to hydrogen combustion was eliminated. The tests employed a 1:10 linearly scaled reactor cavity representative of the Zion nuclear power plant.

Although the LFP tests simulate containment compartmentalization, they do not simulate any of the complex structures or equipment located in typical reactor subcompartments. Two additional tests, which provided detailed simulation of the Zion subcompartment structures, are added to the LFP data for model assessment. The first, SNL/IET-1 [Allen et al., 1991c] nominally represented a 1:10 linearly scaled mockup of the Zion containment; while the second, FAI/DCH-4 [Henry et al., 1991] nominally represented a 1:20 linearly scaled mockup of the same NPP. The containment atmosphere was inerted in both these tests, and the annular gap around the RPV was not simulated.

Figure 1 provides an assessment of the 1-cell equilibrium model. The axes represent the pressure increment (ΔP) normalized by the initial containment pressure (P^0). Figure 1 shows no correlation of the 1-cell model with the experiment data. Predicted pressure increments all exceed measured values, thus supporting the bounding nature of the 1-cell equilibrium model. Unfortunately, predicted values can exceed measured values by nearly an order of magnitude. Margins this large are likely to be of limited utility in most reactor analyses.

Figure 2 provides an assessment of the 2-cell equilibrium model. Experiment results are normalized by the pressure increment predicted by the 1-cell equilibrium model. In this manner, comparisons can be made on an efficiency basis. The lowest efficiencies typically occur for the smallest subcompartment volumes. For these cases, the 1-cell model overpredicts the pressure rise by nearly an order of magnitude. In comparison, the 2-cell model predicts pressures that exceed measured values by approximately a factor of 2, regardless of the degree of compartmentalization. Thus, the 2-cell model is favored strongly over the 1-cell model as a screening model.

Temptations to renormalize (tune) the two-cell model by this factor of 2 with the experiment data should be resisted for two reasons. First, the margin between model predictions and experiment data might be explained by kinetic arguments that pit heat and mass transfer rates against trapping rates. These kinetic arguments are potentially scale-dependent, resulting in a smaller margin at reactor scale.

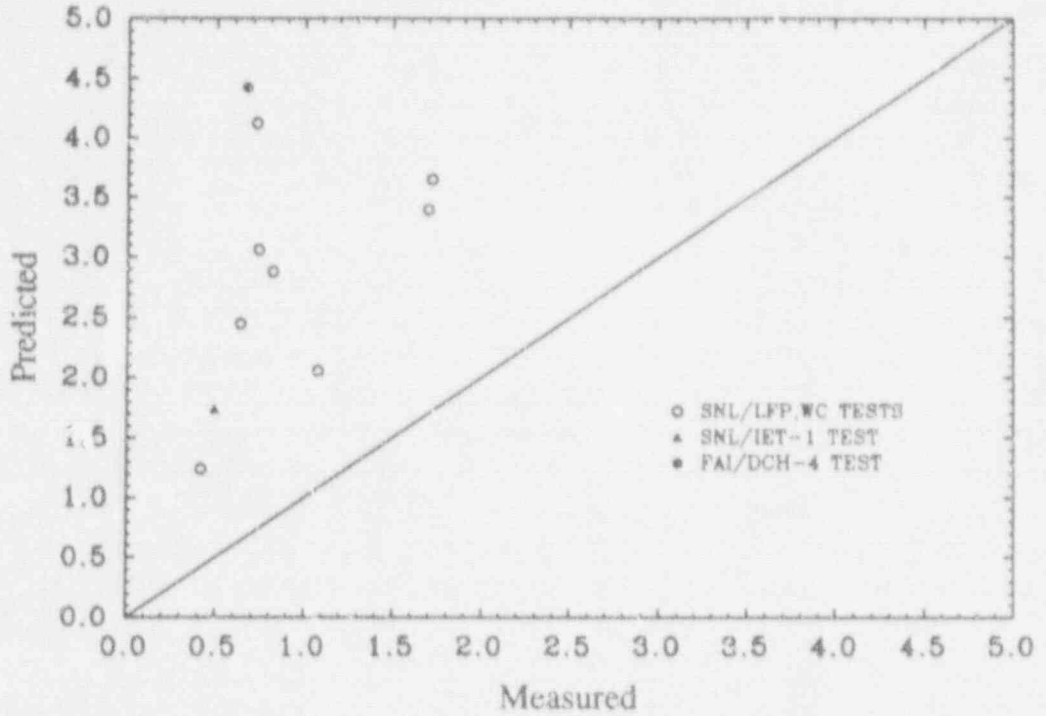

Figure 1. Comparison of Measured Pressure Increments (Delta P/ P^0)
With Predicted Pressure Increments Using the 1-cell Model

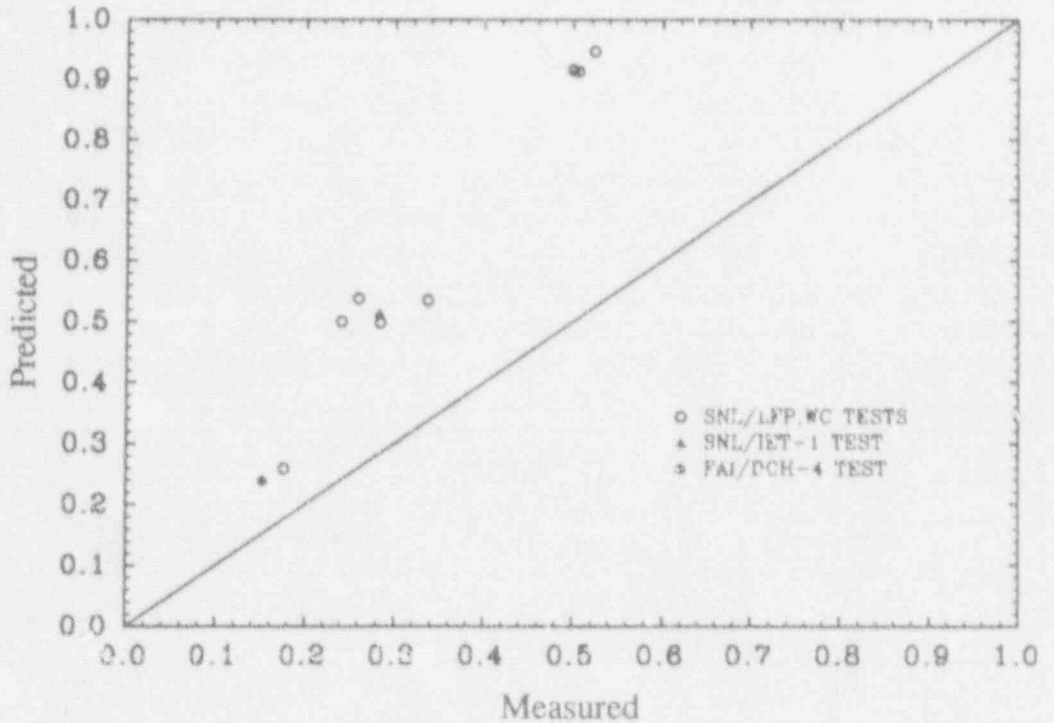

Figure 2. Comparison of Measured Efficiencies
With Predicted Efficiencies Using the 2-Cell Model

The second reason for caution is that the two-cell model may not be a rigorous bound to the DCH load in compartmentalized geometries. Although most model assumptions are selected to favor a bounding result, subtle kinetic arguments preclude such a strong assertion at this time. More complex integral effects experiments (which include the potential for hydrogen combustion) or numerical experiments using the CONTAIN code could lend more weight to the bounding nature of the 2-cell equilibrium model.

The apparent correlation shown in Figure 2 between the 2-cell model predictions and experiment measurements has important implications. The LFP tests [Allen et al., 1991a] employed only the crudest representation of containment compartmentalization, while the SNL/IET-1 test and the FAI/DCH-4 tests employed accurate and complex representations of the Zion subcompartment geometry. Yet all the tests apparently are correlated by the simple control volume representation inherent in the 2-cell model. This suggests that the plant specific details of subcompartment geometry are at most a second-order effect and that the dominate mitigating effect on debris/gas heat transfer is thermal saturation of the subcompartment atmosphere. Thus, DCH mitigation in compartmentalized geometries is predominantly a volume effect.

4.0 Reactor Analyses

The 2-cell equilibrium model is not intended to replace CONTAIN as the state-of-the-art best estimate tool for calculating DCH loads; however, the 2-cell model could be useful in PRA screening studies aimed at bounding the potential significance of DCH in a variety of reactor plants. This is illustrated with an application to the Zion reactor where typical initial conditions for a S2D accident (pump seal LOCA initiated by a station blackout) are given by P^0_{RCS}=6 MPa, M_{debris}=53 tonnes, and P^0=0.2 MPa with 4% preexisting hydrogen. Table 1 summarizes the results for two cases: one with hydrogen combustion and one without hydrogen combustion. Clearly, the potential combustion of hydrogen is a dominant contributor to the DCH load, and the 2-cell model treats hydrogen in a very bounding fashion (i.e., complete oxidation of the metallic component of dispersed debris and complete combustion of all hydrogen). Nonetheless, the probability of containment failure is reduced to nearly zero based on predictions of the 2-cell model; by comparison, the 1-cell model suggests that failure is virtually assured.

Table 1
Peak Containment Pressure (MPa)
for Zion Predicted by the Equilibrium Models

Model	Zion-S2D Without H_2 Combustion	Zion-S2D H_2 Combustion	Conditional Probability of Containment Failure
1-Cell Model	0.65	1.11	0.85
2-Cell Model	0.43	0.78	0.04

Simple DCH models could play an important role in bridging the gap between the complexity of phenomenological codes such as CONTAIN and the requirements of PRA analyses. PRA analyses of DCH are served better by a computationally efficient tool that returns peak containment pressure as a function of PRA-supplied initial conditions at the time of vessel breach. Best estimate computer codes are far too computationally burdensome to serve the need directly; however, a response surface fitted to computer generated data could serve as a surrogate for the phenomenological code in the PRA analyses. If phenomenological uncertainties exist, then the response surface can be sampled in a Monte-Carlo fashion to quantify the total uncertainty in peak containment pressure.

Response surface techniques have been applied successfully in other areas of NRC research (e.g., NRC, 1989), but they have not been applied to the DCH problem. One potential shortcoming of the technique is the difficulty in finding a suitable response surface that is applicable over the entire range of important parameters. Although not quantitatively accurate, simple phenomenologically based models, such as the 2-cell model or perhaps a 2-cell model with simple kinetic enhancements, can capture the major parameter sensitivities while preserving known phenomenological limits. The simple models can then be used as a seed for a more accurate response surface by fitting a candidate function to computer generated data that has been normalized by predictions of the simple model. In this manner, simple DCH models can be used to help bridge the gap between best estimate codes and PRA analyses by increasing the likelihood of finding a suitable response surface.

5.0 SUMMARY

Results of the 2-cell adiabatic equilibrium model clearly demonstrate that the inherent compartmentalization of reactor containments is a dominant mitigating factor for debris/gas heat transfer. DCH mitigation in compartmentalized geometries is predominantly a volume effect. Although viewed primarily as a bounding model, the 2-cell model could be a useful tool for PRA screening studies because it provides some discrimination as to the vulnerability of some plants to possible DCH loads. The model is computationally simple, and it has the potential to serve as a seed for a more complex phenomenologically based response surface describing DCH containment loads.

REFERENCES

M. D. Allen et al., 1991a, Experiments to Investigate the Effect of Flight Path on Direct Containment Heating (DCH) in the Surtsey Test Facility: The Limited Flight Path (LFP) Tests, NUREG/CR-5728, SAND91-1105, Sandia National Laboratories, Albuquerque, NM.

M. D. Allen, et al., 1991b, Experiments to Investigate the Effect of Water in the Cavity on Direct Containment Heating (DCH) in the Surtsey Test Facility, SAND90-1173 to be published, Sandia National Laboratories, Albuquerque, NM.

M. D. Allen, et al., Oct. 1991c, Quick-Look Report on the Integral Effects Test (IET-1) in the Surtsey Test Facility, Sandia National Laboratories, Albuquerque, NM.

R. E. Henry et al., 1991, "Direct Containment Heating Experiments in a Zion-Like Geometry," Seminar report, 26th National Heating Transfer Conference, Vol. 87.

IDCOR, July 1985, Technical Support for Issue Resolution, Technical Report 85.2, (Fauske & Associates).

NRC, 1985, Estimates of Early Containment Loads from Core Melt Accidents, NUREG-1079, U.S. Nuclear Regulatory Commission, Washington, DC.

NRC, 1989, Quantifying Reactor Safety Margins, NUREG/CR-5249, EGG-2552, U.S. Nuclear Regulatory Commission, Washington, DC.

M. Pilch et al., Sept. 1988, The Influence of Selected Containment Structures on Debris Dispersal and Transport Following High Pressure Melt Ejection from the Reactor Vessel, NUREG/CR-4914, SAND87-0940, Sandia National Laboratories, Albuquerque, NM.

M. Pilch and M. D. Allen, Dec. 1990, A Scaling Methodology for Direct Containment Heating With Application to the Design and Specification of an Experiment Program for Resolving DCH Issues, Draft for Comment Sandia National Laboratories, Albuquerque, NM.

M. Pilch and W. W. Tarbell, Sept. 1985, High Pressure Melt Ejection From a Reactor Pressure Vessel: The Discharge Phase, NUREG/CR-4383, SAND85-0012, Sandia National Laboratories, Albuquerque, NM.

B. W. Spencer et al., Mar. 1987, Hydrodynamics and Heat Transfer Aspects of Corium-Water Interactions, EPRI NP-5127, Argonne National Laboratory, Argonne, IL.

W. W. Tarbell et al., Mar. 1991, Pressurized Melt Ejection Into Water Pools, NUREG/CR-3916, SAND84-1531, Sandia National Laboratories, Albuquerque, NM.

N. K. Tutu et al., April 1990, Melt Dispersal Characteristics of the Watts Bar Cavity, Technical Report A-3024, Brookhaven National Laboratory, NY.

N. K. Tutu and T. Ginsberg, Oct. 1990, "A Letter Report on the Results of Melt Dispersal Experiments With Surry and Zion Cavity Models", Brookhaven National Laboratory, NY.

D. C. Williams et al., May 1987, Containment Loads Due to Direct Containment Heating and Associated Hydrogen Behavior: Analysis and Calculations with the CONTAIN Code, NUREG/CR-4896, SAND87-0633, Sandia National Laboratories, Albuquerque, NM.

RESULTS OF RECENT NUPEC HYDROGEN RELATED TESTS

K. Takumi and A. Nonaka, Nuclear Power Engineering Center
K. Moriya, Hitachi, Ltd.
J. Ogata, Mitsubishi Heavy Industries, Ltd.

ABSTRACT

NUPEC has started NUPEC Containment Integrity project entitled "Proving Test on the Reliability for Reactor Containment Vessel" since June, 1987. This is the project for the term of eleven years sponsored by MITI (Ministry of International Trade and Industry, Japanese Government). Based on the test results, computer codes are verified and as the results of analysis and evaluation by the computer codes, containment integrity is to be confirmed.
This paper indicates the results of hydrogen mixing and distribution test and hydrogen burning test.
The NUPEC tests conducted so far suggest that hydrogen will be well mixed in the model containment vessel and the prediction by the computer code is in excellent agreement with the data.
The NUPEC hydrogen burning test data is in good agreement with the FITS data at SNL that were obtained at the lower hydrogen concentration condition. New data bases have been added in the higher hydrogen concentration by the NUPEC data.

1. INTRODUCTION

A reactor containment vessel is important because it can hold radioactive materials when an accident occurs. Under present establishment permit, it is able to maintain integrity regarding internal pressure, temperature, flammable gas(hydrogen), etc. on the accident. In addition, it is able to maintain integrity even when a large amount of hydrogen gas is produced.
On the accident in the Soviet Union which occurred in April 1986, however, it was reported that a reactor containment vessel of sufficient performance had not been installed in that nuclear plant. In Japan, as a result, there occurred a fear among population, especially people living nearby nuclear power plants, that containment vessels used in Japan nuclear

reactors might not be sufficient necessarily.
Therefore, it is necessary to prove the integrity of reactor containment vessels and to calm the fear of population on the promotion of nuclear power generation.
In order to confirm the integrity of containment vessels under conditions which are assumed when a large amount of hydrogen is produced, hydrogen mixing and distribution test, and hydrogen burning test are conducted.
The hydrogen mixing and distribution tests are to investigate their behaviors in the containment vessel with multiple compartments representing a typical large dry containment of a PWR. The test vessel has a volume of 1,600m that is about 1/4th scale of an actual PWR containment vessel. Compartment number 25 in the test vessel is the same as that of actual plants. Helium gas is used for this test instead of hydrogen to avoid unexpected explosion.
Hydrogen burning tests are conducted at NUPEC with the objectives to investigate hydrogen burning phenomena including mitigation effect of steam, spray, and nitrogen inserting in a containment vessel and to confirm containment integrity against hydrogen burning. The hydrogen burning tests are conducted by using a small scale cylindrical vessel with 5m³ and a large scale spherical vessel with 270m³. In the small scale test, the effects of gases have been investigated in detail prior to the large scale test.

2 Hydrogen Mixing and Distribution Test

2.1 TEST FACILITY AND TEST CONDITIONS

The objective of this test is to investigate hydrogen distribution and mixing behavior in the containment with large volume and many compartments for the case of the relatively large amount of hydrogen production. Figure 1 and 2 show flow chart and test facility of hydrogen mixing and distribution test. The diameter and height of the test vessel are 10m and 20m respectively. Compartment number 25 in the test vessel is the same as that of actual plants. Figure 3 shows model compartment arrangement.
Having similar characteristic to hydrogen, helium is used for this test instead of hydrogen in order to avoid unexpected explosion. Equivalent hydrogen concentration in this test is less than 18%. The test facility has gas three supply systems that are helium supply system, cooling water supply system and steam supply system for simulating the burst of piping and blow down. Table 1 shows PWR mixing and distribution test conditions. For BWR only analysis is performed.

2.2 TEST RESULTS

Hydrogen mixing and distribution test was performed at Tadotsu Engineering Laboratory of NUPEC from 1989 to 1990. And additional test will be performed from 1991 to 1992.
Main test items are effect of natural circulation with helium injection, effect of density difference between helium and air, effect of steam injection, effect of spray water, etc.

Table 1 PWR Mixing and Distribution Test Conditions

	ITEMS	MIXING TEST CONDITIONS
1	HYDROGEN (HELIUM) CONCENTRATION	≦ 18 VOL %
2	STEAM CONCENTRATION	≦ 60 VOL %
3	WATER SPRAY FLOW	70 m³/h
4	HYDROGEN (HELIUM) FLOW	max. 0.12 kg/s
5	STEAM FLOW	max. 0.74 kg/s
6	COMPARTMENT	2 5
7	POSTULATED BREAK DOWN LOCATION	SG LOOP ROOM PRESSURIZER RELIEF TANK
8	INITIAL NITROGEN CONCENTRATION	ATMOSPHERIC
9	INITIAL OXGEN CONCENTRATION	ATMOSPHERIC
10	INITIAL PRESSURE	ATMOSPHERIC

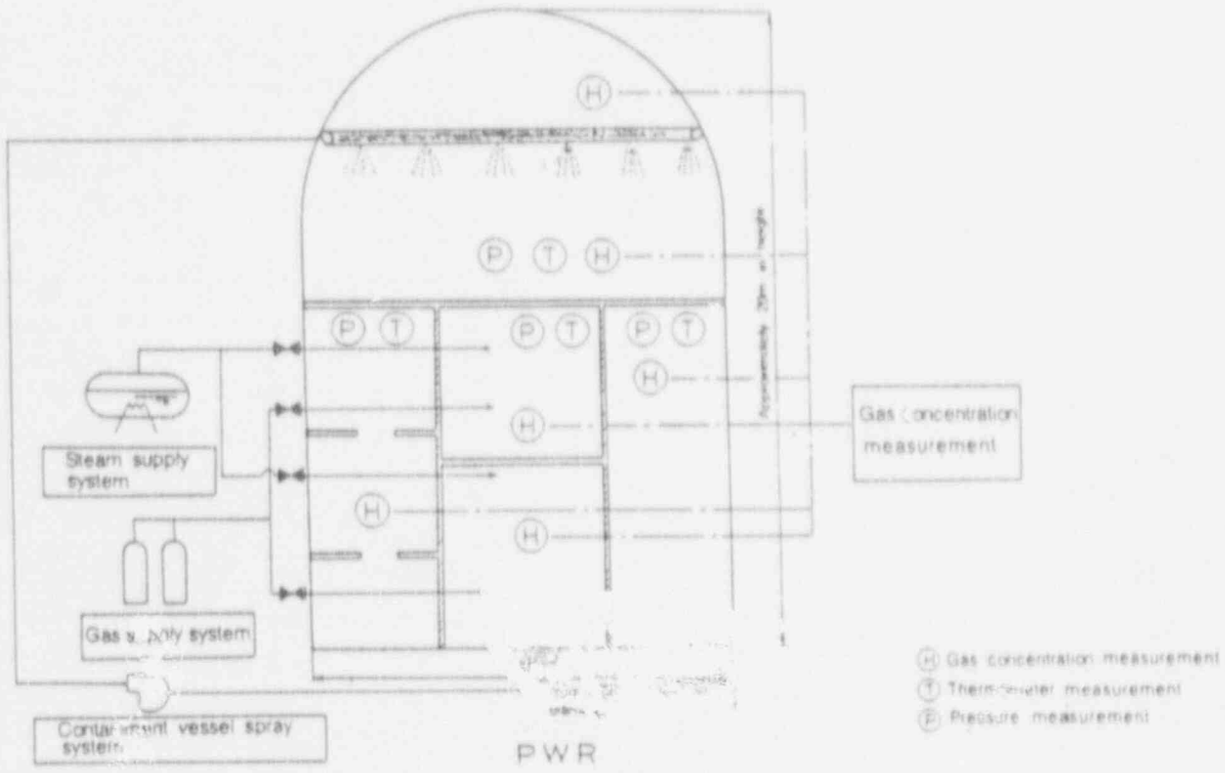

Figure 1 Flow Chart of Hydrogen Mixing and Distribution Test Facility

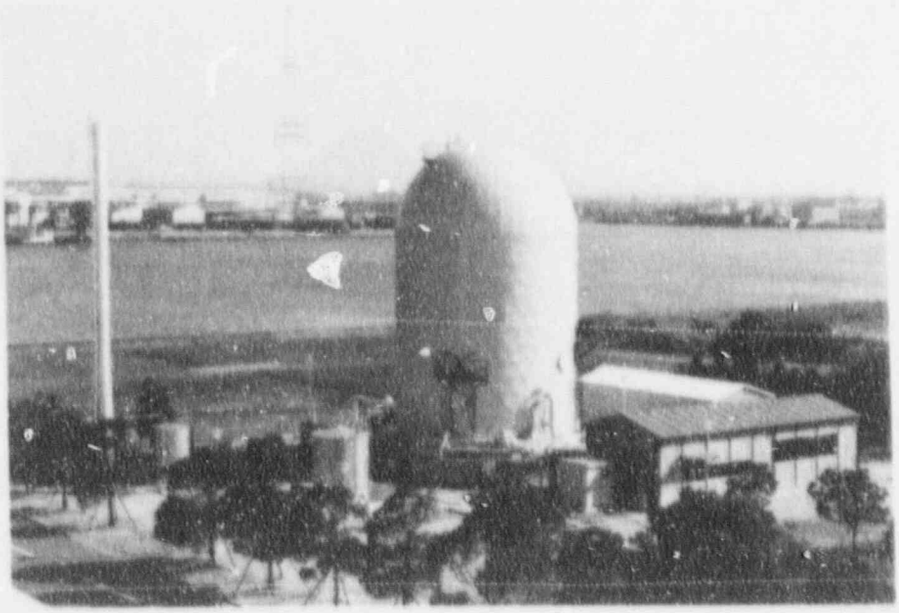

Figure 2 Test Facility of Hydrogen Mixing and Distribution Test

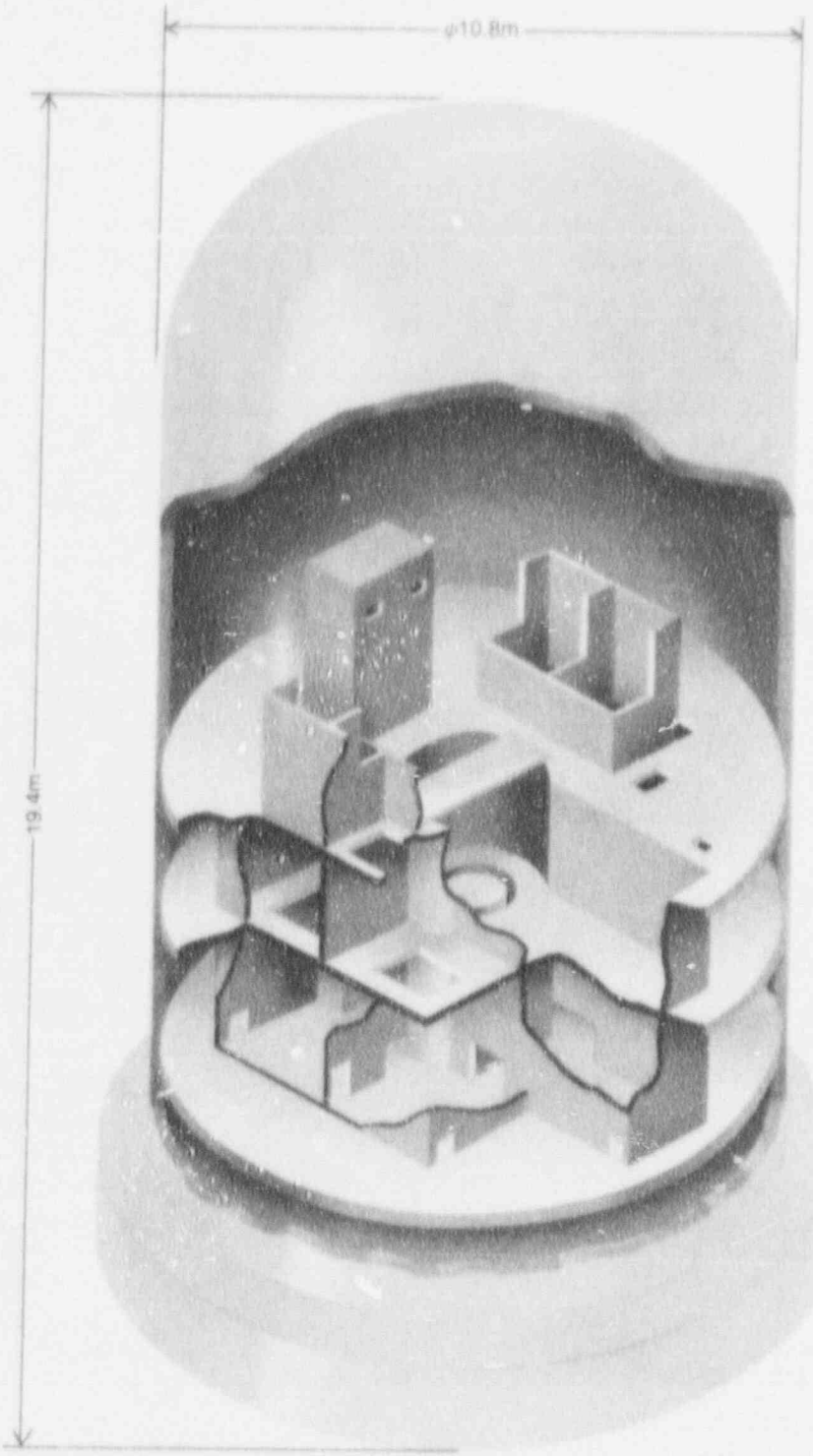

Figure 3 Model Compertment Floor Arrangement

3 Hydrogen Burning Test

3.1 TEST FACILITY AND TEST CONDITIONS

The objective of this test is to research hydrogen burning phenomena including mitigation effects of steam, spray, nitrogen inerting etc. in containment vessel and to confirm containment integrity for hydrogen burning. This test is composed of small scale test in 5m³ cylindrical vessel and large scale test in 270m³ spherical vessel.

Figure 4 and 5 show test vessel and test facility of small scale hydrogen burning test. The diameter of test vessel is 1.5m and its height is approximately 3.5m. The vessel design pressure 30kg/cm² was decided taking account of the postulated detonation. Figure 6 shows test vessel of large scale hydrogen burning test. The diameter of spherical test vessel is 8m. Test facility of large scale hydrogen burning test is now under construction at Takasago Engineering Laboratory of NUPEC.

The content of the small scale tests is as follows:

(1) Before large scale tests are conducted, basic data pertaining to the transitional areas among combustion, deflagration and detonation is accumulated to decide the scope of the large scale tests.

(2) Before large scale tests are conducted, the appropriateness of the measurement and data processing system is confirmed.

(3) Comparisons are made with data from the United States to make sure that the data is valid.

(4) In order to confirm the effectiveness of hydrogen combustion control, characteristic data is obtained.

(5) The flammable limit under nitrogen inerting condition is confirmed.

The content of the large scale tests is as follows:

(1) The effectiveness of compartments for hydrogen combustion is confirmed.

(2) Small scale and large scale test are conducted to confirm the effects of scale.

(3) The effectiveness of hydrogen combustion controls using blowdown steam, nitrogen and other diluents is confirmed.

(4) The flammable limit under nitrogen inerting condition is confirmed.

Table 2 and 3 show burning test conditions.

3.2 TEST RESULTS

Hydrogen burning test (small scale) was performed at Katstuta Engineering Laboratory of NUPEC from 1989 to 1990, and additional test will be performed from 1991 to 1992. Hydrogen

burning test (large scale) will be performed form 1992 to 1994. Main test items are effect of temperature, effect of pressure, turbulence effect, spray effect, distribution effect, concenration effect of gases etc. Figure 7 shows Iso-arrival time contour. Figure 8 shows typical temerature trenslent curve.

REFERENCES

(1) B. W. Marshall, Jr., "Hydrogen:Air:Steam Flammability Limits and Combustion Characteristics in the FITS Vessel", NUREG/CR-3468, Dec. 1984

Table 2 Small Scale Burning Test Coditions

	ITEMS	BWR	PWR
1	HYDROGEN CONCENTRAITON	≤ 70 vol %	≤ 20 vol %
2	STEAM CONCENTRATION	≤ 60 vol %	≤ 60 vol %
3	NITROGEN CONCENTRATION	≤ 97 vol %	ATMOSPHERIC
4	OXYGEN CONCENTRATION	≤ 10 vol %	ATMOSPHERIC
5	SPRAY FLOW RATE	≤ 15 m³/h	≤ 3 m³/h
6	INITIAL PRESSURE	ATMOSPHERIC	ATMOSPHERIC
7	COMPARTMENTS	———	———

Table 3 Large Scale Burning Test Coditions

	ITEMS	BWR	PWR
1	HYDROGEN CONCENTRAITON	≤ 70 vol %	≤ 18 vol %
2	STEAM CONCENTRATION	≤ 60 vol %	≤ 60 vol %
3	NITROGEN CONCENTRATION	≤ 97 vol %	ATMOSPHERIC
4	OXYGEN CONCENTRATION	≤ 10 vol %	ATMOSPHERIC
5	SPRAY FLOW RATE	≤ 64 m³/h	≤ 26 m³/h
6	INITIAL PRESSURE	ATMOSPHERIC	ATMOSPHERIC
7	COMPARTMENTS	———	———

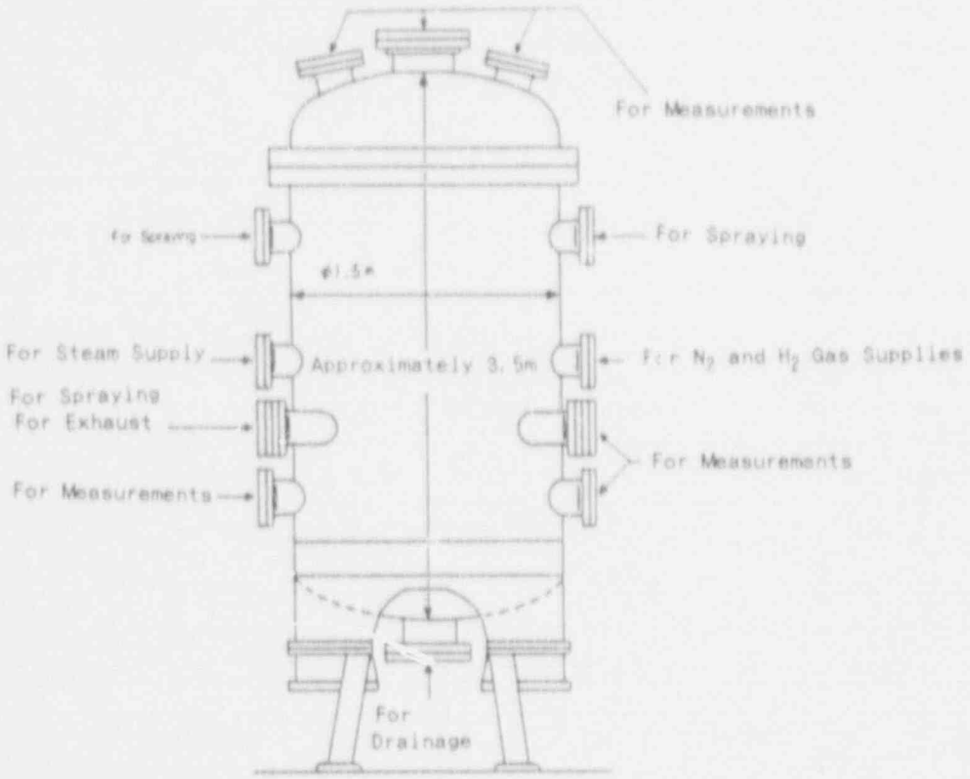

Figure 4 Test vessel of small scale hydrogen burning test

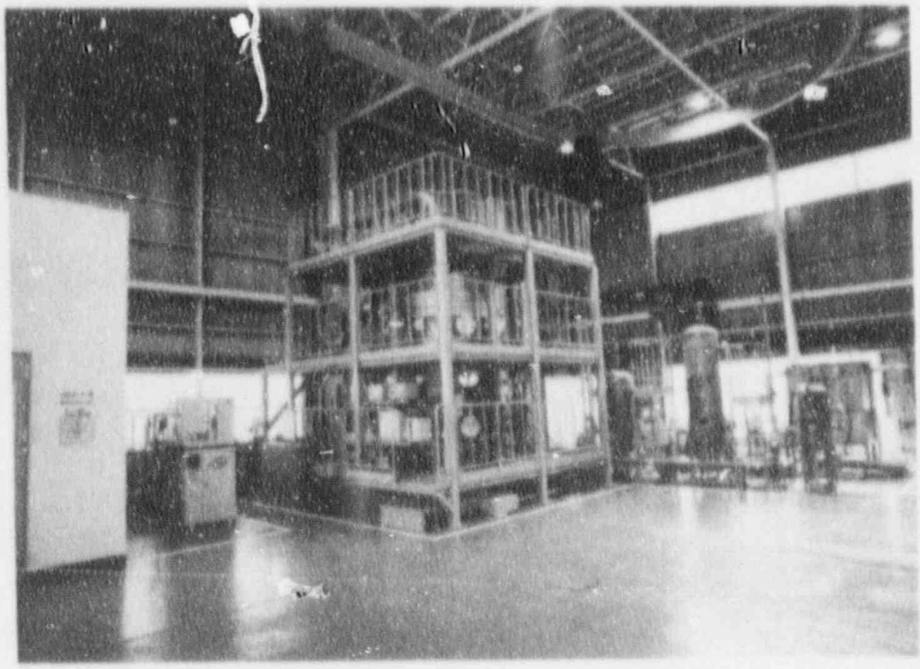

Figure 5 Test facility of small scale hydrogen burning test

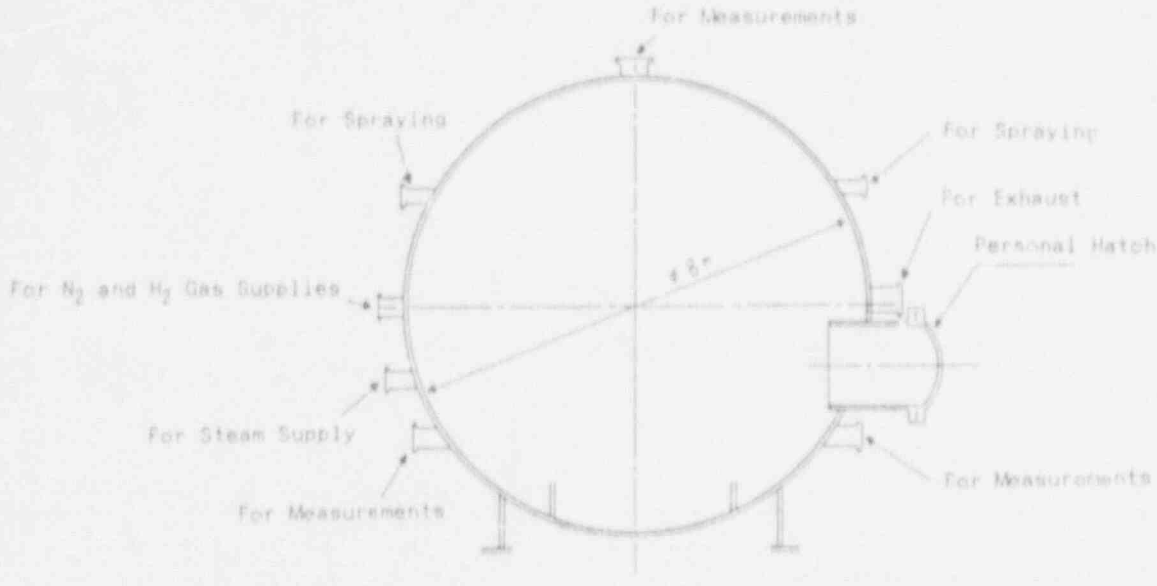

Figure 6 Test vessel of large scale hydrogen burning test

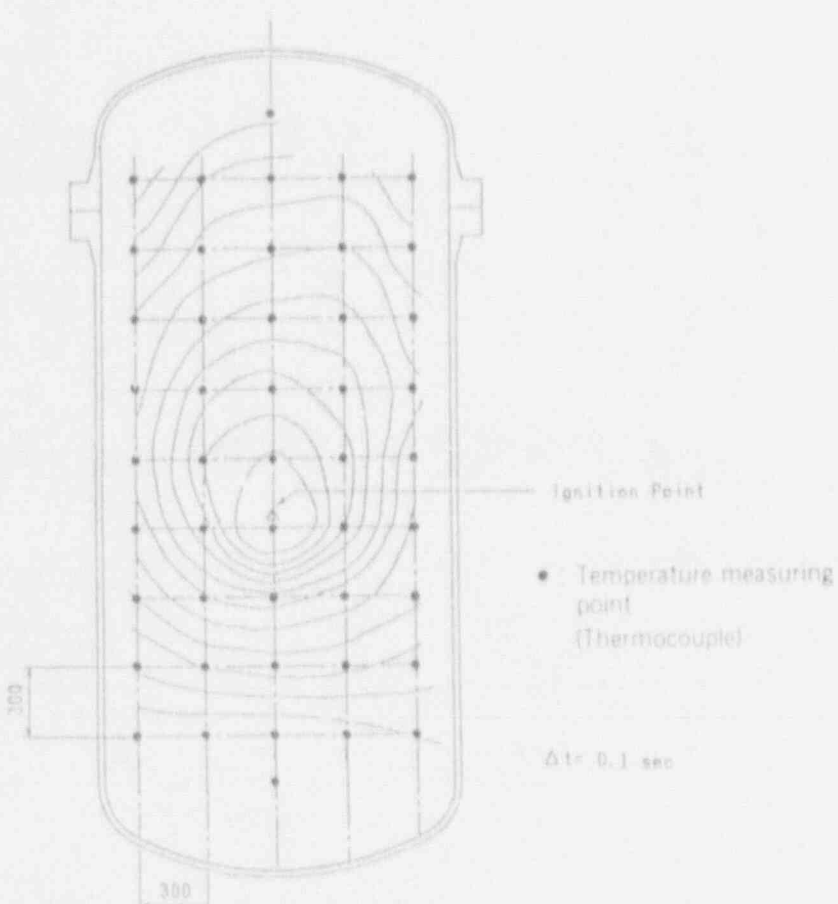

Figure 7 Iso-arrival Time Contour

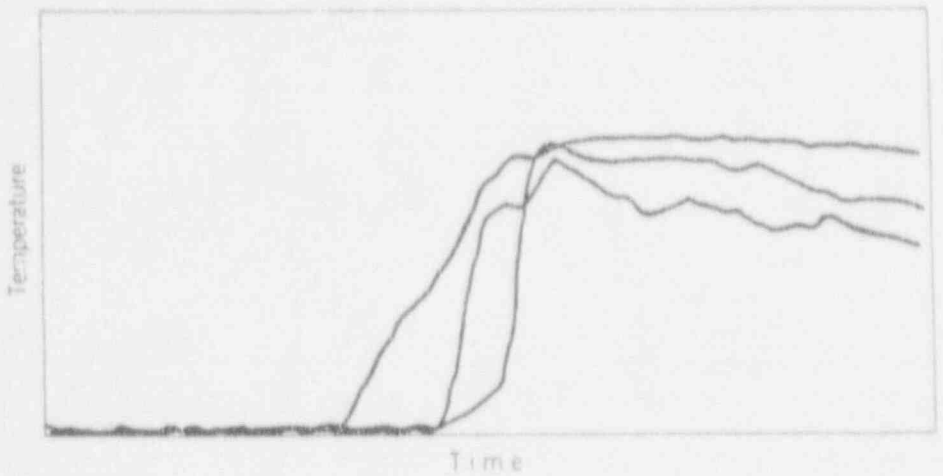

Figure 8 Typical temperature transient

COMPARISONS BETWEEN HDR-H_2-DISTRIBUTION EXPERIMENTS E11.2 AND E11.4

L. Wolf*, L. Valencia, H.-H. Wenzel**, R. Grimm**, K. Jansen**
Projekt HDR, Kernforschungszentrum Karlsruhe GmbH, Karlsruhe, FRG
**HDR, Karlstein, FRG
*Battelle-Europe, Frankfurt am Main, FRG

1. INTRODUCTION

The H_2-distribution and mixing experiments, designated as Test Group E11, performed in the HDR-facility /1-15/ combine the following features:

- large scale of the experimental facility
- high H_2-release rates
- superheated steam injection into the containment
- multi-compartment geometry with sufficiently large dome volume representation
- representative internal concrete and metal structures and surfaces
- energy transfer across the containment steel shell into a very high annular ring space of 50 m height
- multiple steam and H_2-injection phases
- different axial positions for H_2-releases
- examination of the efficiency of H_2-mitigating features including external dome spray as well as venting

The test group consisted of a total of eight different experiments addressing a wide spectrum of H_2-distribution and mitigation issues in severe accident containment atmospheres.

The paper focuses upon the specific E11.2 and E11.4 /1-4/ which both cover small break scenarios and a variety of mitigating measures. A gas mixture consisting of 85 vol% He and 15 vol% H_2 was used to examine the distribution and mixing behavior. The major differences between the experiments E11.2 and E11.4 concern primarily the axial break and gas release positions (E11.2: high; E11.4: low), the test duration and total energy input.

Fig. 1 presents an overview of the HDR-facility and the diverse subsystems used during the experiments E11.2 and E11.4 together with the positions of thermocouples and H_2-concentration sensors, measured results of which are presented and discussed in the following.

Fig. 2 shows schematic overviews of the experimental procedures exercised for the tests E11.2 and E11.4, respectively. Details and objectives of these procedures have been already presented in various reports and at a number of conferences /1-6, 10-12, 14-15/, including the 18th WRSM /7/.

As an outcome of intensive discussions and as a result of additional efforts by all of the participants in the aftermath of the two PHDR Blind Benchmark Exercises /4, 8/ (see Chapt. 3), PHDR/HDR was forced to perform recalibration tests /13/ on the external steam line originating at the neighboring coal-fired power station. These tests were performed for most parts with the original steam line, instrumentation and additional diverse and redundant instrumentation as depicted in Fig. 3.

The findings from these recalibration tests /13/ confirmed earlier speculations/suggestions by the computer code applicants that the PHDR-supplied steam mass flow was indeed too high. This is shown in Fig. 4 which compares the incorrect with the correct external steam mass flows indicating a substantial difference between both of them. Various measurement information and verification procedures were used to confirm the corrected steam mass flow, details of which are described in /13/.

2. COMPARISON BETWEEN THE EXPERIMENTAL RESULTS OF E11.2 AND E11.4

Figs. 5 through 10 present pairwise some major experimental results for pressures (Fig. 5), temperatures (Fig. 6), steam concentrations (Fig. 7), gas concentrations (Fig. 8), velocities at the 31 m position (Fig. 9) and temperatures in the annular gap between containment steel shell and secondary concrete shell (Fig. 10).

In order to comprehend the transient histories of the different quantities under consideration, Fig. 2 should be consulted to refer to the various experimental subphases. A detailed account for E11.2 was given in /7/.

A pairwise cross-comparison of the figures reveals among some similarities in the containment response, gross differences in the stratification and gas concentration distribution patterns, largely due to the axially differing break and release position (E11.2: high; E11.4: low).

As shown in Fig. 5, in both experiments, a maximum pressure of around 2 bar is reached at the end of the respective heatup periods as indicated in Fig. 2.

The different axial break/release positions lead to substantially different stratification patterns in both experiments as demonstrated in Fig. 6. Whereas for E11.2, a steep temperature gradient exists between the lower and upper parts of the containment, which cannot be equalized even by an additional steam release from the containment lower part, E11.4 is characterized by an almost homogeneous containment atmosphere except at positions below the break/release position. These differences have a major impact upon all other quantities as shown in the following figures.

The differences in the thermal stratification translate further into substantial differences in the steam concentration behavior as shown in Fig. 7. Again, for E11.2 the axial steam concentrations differs, about 100 vol % between top and bottom regions of the containment whereas E11.4 shows close to homogeneous steam concentration throughout the whole containment (bandwidth about 10 vol %) with the exception of the lowest containment part.

As a result of thermal and steam concentration gradients as well as the differences in impacts by the accident mitigation/management measures, such as external steam shell spraying, gas concentration histories for E11.2 and E11.4 show a totally different behavior. Whereas for E11.2, the gas concentration histories show extremely sensible responses as result of the various experimental subphases, such as steam addition, external spray, E11.4 is characterized by a nearly homogeneously distributed gas mixture throughout the whole extent of containment and over the total test time. Clearly, for E11.2 the steam "puff" from the lower part and especially the external dome steel shell spray have a dramatic effect upon the redistribution of the gas (He/H_2) whereas nothing similar can be observed during E11.4. As a result, close to the end of the test time, just prior to venting, a substantial gas concentration gradient remains for E11.2,

despite the broad variety of AMM exercised, whereas for E11.4 an even more homogeneous atmospheric state prevails. The comparison of both figures of Fig. 8 reveal the interesting observation that despite of the different histories both end states of the gas/hydrogen concentrations are the same (about 10 vol %) prior to venting.

Fig. 9 compares the velocities in the staircase and the spiral staircase close to the upper deck for E11.2 and E11.4, respectively. The sensor in the spiral case failed during E11.2 early in the heatup phase. Otherwise, the velocity traces clearly show the circulation pattern from the staircase towards the spiral staircase via the dome. Maximum velocities of about 2 m/s are reached at this axial position, respectively.

As the HDR-containment thermally interacts via the steel shell with the surrounding annular gap which was kept at a slightly subatmospheric pressure by a suction line, the major differences among the two experiments in containment atmospheric behaviors also translate into differences in the axial thermal gradients in the annular gap as shown in Fig. 10. It is worthmentioning that quite a large axial temperature gradient exists along the gap also for E11.4 although the inside is rather homogeneous. The temperature difference between bottom and dome reaches 70° C for E11.2 in the gap. It is apparent from these observations that the annular gap should/must be part of the computer model for analyzing containment accidents of the type examined by the Test Group E11.2.

It is evident from the aforementioned discussions and data comparisons that both experiments span a broad spectrum for the qualification and verification of the predictive capabilities of present containment analysis codes.

3. BLIND CODE ANALYSES - PHDR BENCHMARK EXERCISES

Because of the shift in emphasis from DBA-LOCA towards severe accidents, the HDR-experiments offered an excellent opportunity to test the predictive capabilities of present containment analysis codes with respect to H_2-distribution and mixing phenomena. Only blind computations form a sound basis for a qualified, stringent judgement. In order to minimize potential uncertainties introduced by the actual performance of the experiments, only blind post-test predictions could justify the substantial efforts by the participants.

The experiments E11.2 and E11.4, introduced in the foregoing were chosen as the specific tests for the two PHDR Benchmark Exercises.

The PHDR-Benchmark Exercise on E11.2 received widespread international attention with nine organizations from four countries participating with eight different computer codes. These included: CONTAIN, SNL, USA, and AEA, UK; COMPACT, NNC, UK; HECTR, VTT, Finland; MELCOR, AEA, UK; MAAP, FAI, USA; RALOC, GRS, FRG; and WAVCO, Siemens-KWU, FRG.

It is apparent from this list that the participating codes cover a broad spectrum of presently, world-wide known containment analyses tools for LWR-containment severe accident analyses.

The participation in the E11.4-Exercise decreased substantially and involved the following reduced set of codes: FATHOMS, BF, FRG; HECTR; VTT, Finland; MAAP, FAI, USA; RALOC, GRS, FRG; and WAVCO, Siemens-KWU, FRG.

All of the participating institutions received the same set of input data information and additional supplements as the evaluation process of the most important experimental initial- and boundary conditions evolved. However, no actual data of E11.2 or E11.4 characterizing the containment atmosphere were released prior to the same deadline of both PHDR-exercises. The computational results had to be provided in the PHDR-Standard Format for a large number of measurement positions for many different physical quantities.

After the deadline of both exercises, experiment E11.2, was selected as the open post-test, OECD-CSNI International Standard Problem No. 29 /4, 5/, now in progress with a deadline of January 1992. At the kickoff meeting of ISP 29 /4/, the experimental data of E11.2 were made publicly available and the institutions participating in the blind post-test PHDR-Benchmark Exercise on E11.2 received all of the experimental data on magnetic tape for their own use. In addition, each institution received a set of hard copy plots comparing data with the individual prediction. Both, magnetic tape data and comparison plots enabled the individual institutions to prepare presentations and reasonings at the international workshop of the PHDR-Benchmark Exercise /8/.

In view of the fact that ISP 29 is specified as an open standard problem, potential participants in ISP 29 were allowed to attend the workshop on E11.2 to optimize information transfer and minimize misconceptions.

The E11.2-participants unanimously decided during the workshop to publish the comparisons between data and predictions, provided, no quantitative reference is made to individual code results.

In the following, this paper strictly adheres to that decision.

4. COMPARISONS BETWEEN DATA AND CODE PREDICTIONS

In order to more easily comprehend the differences in the experimental results between E11.2 and E11.4 as well as the differences between predictions and data, the results for some major physical quantities are shown pairwise for the same positions in the containment in Figs. 11 through 15.

The following discussion is ideally supplemented by the experimental background outlined in Chap. 3.

Fig. 11 provides an overview of both the experimental pressure histories as well as of the comparisons with the code predictions. To everybody's surprise, the participating institutions overpredicted the experimental data by up to a factor of 4. This type of discrepancy in one of the controlling experimental parameters has never happened before in HDR-related exercises and resulted in speculations and controversies with respect to the reliability and quality of the experimental data as well as the input data for the computations provided by PHDR.

A quantitative comparison between the left and right parts of Fig. 11 reveals that the overpredictions are more severe for E11.4 than E11.2. Furthermore, the route for overpredictions already starts in the early phases of the experimental long-term heatup phase for E11.2 and despite some substantial underpredictions (too high energy transfer into structure) by most codes during the early stage. Surprisingly large are not only the deviations of the codes (one noticeable exception for E11.2) compared to the data but also the differences among the

code predictions for both E11.2 and E11.4. This suggests qualitatively that not only one single root-cause is respnsible for all of the differences shown but that combinations of different factors prevail for every individual code prediction.

Besides of the overpredictions, it is also of interest to look at the details of the predictive quality for the individual experimental phases outlined in Fig. 2. Concerning E11.2 and E11.4 the following observations can be made, including also the comparisons with the dome temperature as depicted in Fig. 12:

E11.2:

- The individual experimental phases: steam into R1805, overlapping steam and gas injections into R1805, steam into R1405 (low containment position) are predicted quite well as the detailed histories of computed pressure and temperature indicate.
- As the comparisons among the codes indicate many codes overemphasize the effects upon the pressure histories.
- The agreements are much better for the dome temperature both with respect to the absolute value as well as the details of the temperature histories.
- The subsequent experimental phase of natural cooldown after steam injection into R1405 has been predicted quite well by some of the codes; however, there are also grave discrepancies noticeable for at least half of the code results, predicting yet another pressurization with more or less steep pressurization gradient whereas in reality, the pressure curve shows a slight decline - as expected. Interestingly enough, the predicted temperatures do not show this peculiar behavior.
- The predictive quality for the subsequent phase of external steel dome spraying is difficult to qualify; all codes depressurize from more or less pronounced pressure peaks; some codes show good agreement with the temporal pressure history.
- The agreements with the measured temperature (Fig. 13) is much better.
- The following experimental phases of natural cooldown is predicted quite well by all codes both with respect of containment pressure as well as temperature; in fact it is surprising to see all codes to converge closely towards the data once they had "ventured" far out.

E11.4:

All of the aforementioned observations also hold for the prediction for this experiment. However:

- The deviations in predicted levels of pressures and temperatures compared with the data are much more pronounced; on the other hand, the predictive quality for the individual experimental phases and their details is seemingly better, although again in some cases striking differences in gradients are recognizable.
- Large differences prevail at the end of the final natural cooldown period in contrast to the observation made for E11.2.

From the sum of the observations listed above the following major conclusions can be drawn:

- All codes put too much energy into the containment atmosphere (one exception for E11.2); the amount differing among the participants.
- This effect is even more pronounced for E11.4 than E11.2.
- Some grave discrepancies and inconsistencies exist in the details.
- Some very good agreements exists in the predicted details, especially for E11.4.

Naturally, as it is known by now, all of the participating codes where equally affected by foremost:

- the incorrect external steam mass flow specified as input and
- the ommission by PHDR to specify the heat sink by the cooling lines to the sensors as one of the important input data.

However, as indicated by the wide spread of computational results, there must be additional sources for the differences among the code results as well as the code specific deviation from the experimental data curve.

Fig. 13 shows the comparisons between data and predictions for the transient gas distributions in the dome for E11.2 and E11.4. As is apparent from both figures gas distribution histories develop quite differently in both experiments mainly because of the different positions of break, steam and gas injections (high for E11.2, low for E11.4). This strongly affects heatup, stratification and gas distribution as already discussed in Chap. 2.

The code predictions show for

E11.2:

a) Selected nodalizations, models and codes are unable to predict the high gas concentration buildup as a result of the mitigative measure of external spray. Just to the contrary; besides of too low predicted concentration levels at the beginning of gas injection, the predicted gas concentrations sharply decrease, thereby showing just the opposite behavior than the experiment. When final peak concentrations are reached in the data, code results indicate minimum gas concentration. When measured concentration decreases, one the condensation potential at the dome shell ceased, predicted concentrations increase.
b) The differences among the codes' predictions are seemingly smaller than for the other quantities.
c) All codes underpredict the gas concentration at the end of the experiment.

These results are the more surprising considering the qualitative agreement in the dome temperature at the same position (compare Fig. 3 left), because of this as well as the fact that the external spray and low steam injection periods are much later than the heatup period, when the effect of the omitted heat sink is much less (compare Fig. 9 left), the heat sink issue cannot solely be made responsible for the deviations observed, rather other factors contribute also.

E11.4:

a) The differences between data and code predictions are seemingly smaller compared to E11.2.
b) The differences among the codes' results are about the same as those observed for E11.2.
c) Some pronounced deviations are noticeable for the external spray period.
d) For E11.4 the external spray does not result in such a dramatic gas concentration buildup as in E11.2; however, some codes predict more or less pronounced increases, while they did not for E11.2, when they should.
e) For the most part, all codes underpredict the gas concentration.

The somewhat improved tendency concerning agreement for most of the experimental time span is the more surprising in view of the dramatic and substantial differences in pressure and temperature, the latter at the same position.

Some of the peculiarities noted above can be explained in terms of the temperatures and gas concentrations at 12 m for E11.2 and E11.4 as shown in Figs. 14 and 15, respectively. The following findings evolve from these figures:

E11.2:

1) Comparing the experimental data curves between Figs. 12 and 14 (left), it is obvious that the containment atmosphere is clearly stratified, with the temperature at that position barely increasing despite the substantial energy input into the containment 10 m higher up (compare Chapt. 2, Fig. 6).
2) It is only during the steam injection period from the lower part that the temperature increases and decreases afterwards.
3) None of the codes predicted the stratification at this position.
4) Most predicted the temperature increase due to passing steam correctly; but one code even predicted a temperature decrease.
5) By comparing the predictions shown in Figs. 12 and 14 it is apparent that the codes predict nearly homogeneous temperatures between 40 m and 12 m.
6) The same can be said concerning the gas concentration shown in Fig. 15 (left). All codes more or less overpredict the gas concentration increase which is rather benign in the measurement.
7) Especially the injection period is substantially overpredicted by dramatic spikes when in reality the concentration is barely measurable. This indicates the drawbacks of lumped parameter codes and too coarse nodalization in this region of the containment, among other things.
8) With so much gas transported and distributed into the lower parts of the containment by the predictions, it is certainly difficult for the codes to calculate concentration increases at higher positions (40 m, compare Fig. 13) due to external spray and lower steam injection.
9) Some of these peculiarities were already noted during the T31.5 exercise but obviously did not enter the model considerations for E11.
10) Reasons for the computed homogenization could be nodalization, unrealistic recirculations, artificial mixing etc.

E11.4:

1) Experimentally, the containment atmosphere is not stratified but close to perfectly homogeneous, because of the low position of the injection port (compare Chapt. 2).
2) Qualitatively the codes predict this correctly (compare Figs. 3 and 5 right) albeit with the already mentioned deviations between data and predictions as well as among predictions.
3) Because of the homogeneous atmosphere, the agreements for the gas concentration between data and predictions are somewhat better than those observed for E11.2 and of about the same quality as already discussed for the position 40 m.
4) As before, some codes overpredict the external spray effect to the same extent as for the 40 m position.

In general, it is obvious that experiment E11.4 is much better suited than E11.2 for code success because of its homogeneous features.

As discussed during the workshop /8/ and schematically shown in Figs. 16 and 17 other possible sources of uncertainties introduced directly or indirectly into the PHDR input data specifications affecting more or less the codes' results are:

- leaks developing at the interfaces between steel shell and hatches etc. under hot, pressurized long-term conditions; however an additional leak test at HDR (cold) proved that the HDR-containment is leak-tight for the condition of the leak test
- errors in the experimental determination of mass flow rates, which unfortunately for the exercises proved to be true
- additional, unspecified fraction of inside steel shell exposed to direct steam access, e.g. additional condensation, because of past deterioration of insulation material between concrete and steel due to high level shaker experiments simulating earthquake excitations
- unknown water ingress into porous concrete structures because of deteriorated wall plaster and paint peeled off because of thermal, blasting, and jet impact by previous HDR-experiments of different kinds in the past
- deviations of the thermal physical properties of the concrete structures compared to the specified input data because of anisotropic rebar distributions in different parts of the HDR-structures
- errors/uncertainties in specifying the purging of the annular gap
- RPV insulation

With the help of the recalibration tests and a coarse specification of the additional cooling lines heat sinks, the primary causes for most of the differences between data code predictions have been resolved by now. However, the differences among the code predictions can only be explained by additional sources of uncertainties which have been introduced by the code user into the model and/or are inherently embedded in the computer codes themselves by virtue of assumptions, physical models, correlations and numerical methods.

During the workshop /8/ the following list of potential contributors for the deviations was assembled, which is also presented in Fig. 17 in a more condensed format:

- neglect of energy transfer across the steel shell into and across the annular gap by specifying isothermal or adiabatic boundary conditions
- too coarse nodalization schemes not representative of the real flow
- the coarse nodalization schemes at the release levels chosen from past experience simulating LOCA processes but not suitable for following plume - like behavior of light gases injected into a post-accident containment atmosphere
- too low energy transfer rates into internal structures, resulting in too high energies remaining in the containment atmosphere for pressure built-up
- present deficiencies in simulating counter-current flow phenomena through vents in the context of lumped parameter codes and the basis of available correlations
- artificial mixing induced by the lumped-parameter method
- too much mixing and resultant homogenization introduced by wrong nodalization schemes
- not fully tested, patched on inclusion of gravity terms into typical LOCA-containment codes
- user errors introduced in collapsing the 72-room PHDR data files into computational models with lower numbers of control volumes to decrease computational expenditure
- wrong assumptions for specifying vent flow coefficients
- errors introduced in modelling internal structures

This list is not necessarily complete as more insights will evolve through the ISP 29 and other, additional open post-test computations, such as the one with the GOTHIC-Code /16, 17/ discussed in the following chapter.

5. OPEN GOTHIC-CODE ANALYSES OF E11.2 AND E11.4

5.1 GENERAL FATHOMS AND GOTHIC FEATURES

FATHOMS, developed by NAI, USA, is an extension of the well-known code COBRA-NC, is a state-of-the-art computer program used for transient thermal hydraulic analyses of multiphase systems in complex geometries. It solves the conservation equations for mass, momentum, and energy for multicomponent, two-phase flow. FATHOMS is a FORTRAN code that can be operated on computers ranging from PC's and low-end workstations to mainframes and supercomputers.

CAPP is a completely graphics and menu driven pre/postprocessor for setting up the input for FATHOMS, running the calculations, and selecting and obtaining graphical output from the analysis. It allows for fast, flexible creation and modification of computational models, while greatly reducing the possibility of errors in the input.

The finite volume approach used in FATHOMS allows modeling in one, two, or three dimensions as well as lumped parameter modeling. Combining lumped parameter noding with multidimensional noding within a single problem is permitted using FATHOMS' versatile noding approach. FATHOMS models the interdependent behavior of three separate flow fields (8-equation model):

- Continuous liquid
- Steam and noncondensable gas mixture
- Liquid droplets

Concentrations of up to eight noncondensable gases are tracked. FATHOMS solves for the temperature distribution in solid conductors and has models for fluid to solid and interfacial heat transfer that cover the entire range of flow regions.

More recently, FATHOMS has been further expanded into a full 9-equation model (3 fluids) completely accounting for a fully separated drop model. Under EPRI sponsorship now it has been renamed to GOTHIC /16, 17/. A nuclear plant utility working group, consisting of 20 mostly American utilities, has been assembled with the objective to apply for and obtain a NRC-license for GOTHIC for containment LOCA-analyses, equipment qualifications and the like. These efforts involve diverse applications of GOTHIC to real plant applications, as well as stringent quality assurance programs concerning the code including a vast diversity of verifying computations covering all known containment experiments.

5.2 FATHOMS GOTHIC MODEL OF THE E11.2 AND E11.4 HDR-EXPERIMENTS

In designing the FATHOMS/GOTHIC computational model for the E11.2 and E11.4 experiments the following considerations were kept in mind:

(1) To keep model development costs down, a single model should be used for both experiments with about the same degree of accuracy without the need for rezoning.
(2) Because of the axial differences in major release positions for E11.2 and E11.4, sufficient detail had to be factored into the model at both release levels.
(3) From the outset it was clear that the annular gap plays an important role in the energy

transfer path; therefore additional attention was paid to model it properly by also accounting for possible asymmetries in the containment flow paths, e.g. staircase and spiral staircase. To account for this, considerations were given not only to the axial extent of the gap, but also to its azimuthal noding.

(4) From the T31.5 exercise it was known that the large dome space may affect the gas concentration markedly and that gas concentration gradients may develop over its appreciable height. In addition, because the mitigative feature of the external spray was to be examined during both experiments, the impact of which upon the containment internal atmosphere was not known a priori, it was decided to use a true two-dimensional model for the dome region coupled to the lumped-parameter representation of the rest of the HDR-containment.

(5) Because 24 h (E11.2) and 54 h (E11.4) problem times had to be covered for the very complex HDR-multicompartment geometry, a compromise had to be made between computational expenditure and scientific curiosity.

The final features of the FATHOM3-model accounting for the considerations given above are listed in Figs. 18 and 19. Accordingly, the model contained the following major features:

- 41 lumped-parameter nodes for the inside of the containment below the dome space
- 6 truly two-dimensional subspaces for the dome
- 9 lumped-parameter nodes for the outside annular gap with one node covering the upper dome, two times four nodes representing staircase and spiral staircase sides, respectively
- 97 flow path junctions inside the containment
- 10 flow path junctions in the annular gap
- 54 heat structures representing concrete walls inside the containment
- 47 heat structures representing metallic structures inside the containment
- 43 heat structures representing the steel shell, which shows that special attention was paid to this energy transfer path right from the outset.

Because from previous experiments it was known that the Uchida-correlation may somewhat underpredict heat transfer during long-term heatup, it was amplified by a factor of three.

The steel shell was simulated as a plate heated/cooled from both sides. Special care was given to simulate the external spray.

To account for deteriorated insulation between concrete and steel shell, it was assumed that the steel shell comes in contact with the steam also at these locations. On the other hand, the associated concrete structures were only modeled as one-sided heat conductors.

With the model features listed above, the following computation times were achieved on the workstation APOLLO DN 10000:

- Test E11.2, problem time: 24 h, computation time: 4.2 h
- Test E11.4, problem time: 54 h, computation time: 21.6 h

The same model as described above has been used for the open GOTHIC-predictions with some readjustments as noted below.

5.3 COMPARISONS BETWEEN DATA, BLIND FATHOMS AND OPEN GOTHIC PREDICTIONS

The following changes were introduced for the open post-test predictions by GOTHIC Vers. 3.4 for rerunning E11.2:

1. Correct external steam mass flow for heatup as shown in Fig. 4
2. Heat sink capability by cooling lines
3. Containment steel shell modeling according the PHDR specification accounting for concrete and insulation
4. Heat transfer to internal structures according to the Uchida-correlation (no amplification)
5. Heat transfer coefficient from steel shell to annular gap, h = 5 $W/m^2 K$
6. No air exchange in annular gap

The changes made for the E11.4 open post-test prediction were as follows:

A. Same changes 1-4, as above
B. Heat transfer coefficient from steel shell to annular gap, h = 25 W/m^2K
C. Air exchange in annular gap accounted for.

The following figures, Figs. 20 through 33 show pairwise arranged the comparisons of E11.2 and 11.4 with respect to the data, blind FATHOMS- and open GOTHIC-code predictions, respectively.

Without going into many details, the comparisons show the following:

I. Correcting the external steam mass flow and accounting for the heat sinks by the cooling lines, together with the other items listed above substantially improve the agreements between data and GOTHIC-predictions.

II. The improvements are especially noteworthy and consistent for all quantities and positions for E11.4 including the gas concentrations and velocities, with only some minor differences remaining.

III. For E11.2, the improvements, especially for the pressure, some temperatures, some steam concentrations and velocities, are remarkable but not to the extent as observed for E11.4, which is not surprising in view of the stratification.

IV. Despite of noticeable improvements in predicting the stratification pattern for E11.2, there is still need for further improvements.

V. Especially worthmentioning is, that despite of the improvements in all predicted quantities, the post-test predicted H_2-concentrations remained about the same as for the blind prediction (for which the lower initial peaks were caused by coarse sampling for post-processing purposes). Top region H_2-concentrations are still too low; bottom region H_2-concentrations remain too high.

VI. The agreements for the velocities are acceptable to excellent.

VII. The physical models for most AMM seem to work quite satisfactory.

Possible causes for the remaining differences, especially for E11.2, are listed in Fig. 17.

Because of the very special GOTHIC-features (multi-dimensional, mixed dimensions) and the code's numerical efficiency, it is hoped that the deviations which may be attributed to the plume-like release behaviors, amplified by the top break position, can be resolved.

ISP 29 constitutes an opportunity for such an improved computation.

6. OVERALL CONCLUSIONS AND RECOMMENDATIONS

From qualitative and comparative evidence presented in the foregoing the following conclusions emerge:

I. Large-scale facility data are needed for code qualification and verification.
II. Long-term containment processes indicate quite different energy partitioning patterns than what can be extrapolated from past experience from typical DBA-LOCA atmospheres.
III. Therefore, previous data bases are partially unsuitable for reliably covering and solving present containment issues.
IV. Because of the importance of computational tools in this area containment facilities are also needed in the future to provide close to realistic data. The importance of this contribution has been highlighted by virtue of the blind post-test PHDR-Benchmark Exercises again.
V. The value of performing blind exercises to obtain a realistic picture of present code/users capabilities cannot be rated high enough, as the foregoing discussions show, even when controversies arise.
VI. The predictive qualities of containment analyses codes have been possibly overrated in the past, especially considering long-term effects.
VII. On the other hand, the question arises whether for real systems and/or those being designed sufficient informations can be provided to the extend necessary as needed to obtain acceptable computational results (heat sources, sinks).
VIII. Long-term effects are characterized by extreme sensitivities which pose stringent requirements for lumped-parameter codes not previously anticipated.
IX. Given the stringent objectives of design goals for mitigative measures as well as advanced containment systems (passive heat removal) great care should be exercised by applying code and nodalization strategies stemming from the past and presently available. Therefore, there remains the explicit need for additional experimental data.
X. Other areas of containment analyses, such as fire analyses, have already succeeded in applying local multi-dimensional discretizations coupled to the common lumped-parameter approach, thereby solving counter-current and plume rise flow phenomena. This know-how has not been transferred yet to the thermal-hydraulic issues but is readily available now.
XI. The total set of international experiments (LACE, F2 (12), VANAM, HDR) and the associated exercises altogether reveal commonalities and drawbacks with respect to the abilities of codes which have not been either fully fed back to and/or taken up by the code developers and users.

ACKNOWLEDGEMENT

The German Federal Ministry of Research and Technology (BMFT) fully supports the HDR-Safety Program and made the execution of the Test Group E11 possible. It provided experiments E11.2 and E11.4 to the international community for participation in the PHDR blind post-test Benchmark Exercise as well as for the OECD/CSNI International Standard Problem No. 29. We gratefully acknowledge the participation of a larger number of international institutions.

REFERENCES

/1/ Valencia, L.; Wolf, L.: Hydrogen Distribution Experiments, E11.1-E11.5, Preliminary Design Report, PHDR Working Report No. 10.003/89, March 1989

/2/ Wenzel, H.-H.; Grimm, R.; Löhr, L.: H_2-Distribution Experiments, HDR-Test Group CON, Experiment E11.2, Data Report (In German), PHDR-Working Report No. 10.010/89, Aug. 1-3, 1989

/3/ Wenzel, H.-H.; Grimm, R.; Löhr, L.: H_2-Distribution Experiments, HDR-Test Group CON, Experiment E11.4, Data Report (In German), PHDR-Working Report No. 10.013/89, Aug. 27-30, 1989

/4/ International Working Group and ISP-29 Kickoff Meeting on E11.2/4, ISP29, PHDR/KfK, June 19-20, 1990

/5/ Karwat, H.: OECD International Standard Problem: OECD-CSNI-ISP29: Distribution of Hydrogen Within the HDR-Containment Under Severe Accident Conditions - Task Specifications -, July 1990

/6/ Valencia, L.; Wolf, L.: Overview of First Results on H_2-Distribution Tests at the Large-Scale HDR-Facility, 2nd Intl. Conf. on Containment Design and Operation, Toronto, Oct. 14-17, 1990

/7/ Wolf, L.; Valencia, L.: Large-Scale HDR-Hydrogen Mixing Experiments - Test Group E11 - 18th WRSIM, Rockville, MD, USA, Oct. 22-24, 1990

/8/ International Working Group Meeting on E11, PHDR, Kernforschungszentrum Karlsruhe GmbH, Nov. 29-30, 1990 (presentations, papers and notes exchanged)

/9/ Tuomisto, H.; Hytönen, Y.; Valencia, L.: Application of HDR-Experiments E11.2 and 4 to Demonstrate Effectiveness of External Spray Cooling for Loviisa Containments, 14th Status Report of PHDR/KfK, Dec. 12, 1990, Contribution No. 2, pp. 99-128, PHDR-Working Report 05.48/90

/10/ Valencia, L.; Wolf, L.: Experimental Results of the Large-Scale HDR Hydrogen-Mixing Experiments E11.2 and E11.4, CEC/Water-Cooled Nuclear Power Plants, Brussels, Belgium, March 4-8, 1991

/11/ Wolf, L.; Valencia, L.: Results of the PHDR Computational Benchmark Exercises on Hydrogen Distribution Experiments E11.2 and E11.4, ibid

/12/ Wolf, L.; Holzbauer, H.: Comparisons of FATHOMS Blind and Open Post-Test Predictions With the Experimental Data of HDR-H_2-Mixing Tests E11.2 and E11.4, ibid

/13/ Wenzel, H.-H., Wolf, L.; Valencia, L.; Bader, H.-J.; Grimm, R.; Jansen, K.: Quality Considerations of Major Direct and Indirect Measured Quantities [illegible] the Experiments of Test Group E11 - Examinations of Measurement Errors and [illegible]s of Measurements for Energy and Mass Balances for the H_2-Mixing Experiments Demonstrated on the Basis of Experiment E11.2 (ISP 29), PHDR-Working Report No: 10.025/91, June 1991

/14/ Valencia, L.: Hydrogen Distribution Tests at the Large-Scale HDR-Facility, SMiRT-11, Seminar No. 4: Containment of Nuclear Reactors, Shanghai, VR China, Aug. 14-16, 1991

/15/ Valencia, L.: Hydrogen Distribution Test Under Severe Accident Conditions at the Large-scale HDR-Facility, SMiRT-11, Tokyo, Japan, Aug. 18-23, 1991, Paper J11/1

/16/ Merilo, M.; George, T.L.: Thermohydraulic Analysis of Containments, Numerica, Simulation, Montreal, Canada, 1990

/17/ George, T.L.; Thurgood, M.J.; Wiles, L.E.; Wheeler, C.L.; Merilo, M.: Containment Analysis With GOTHIC, Heat Transfer Conf., Portland, Oregon, USA, July 1991

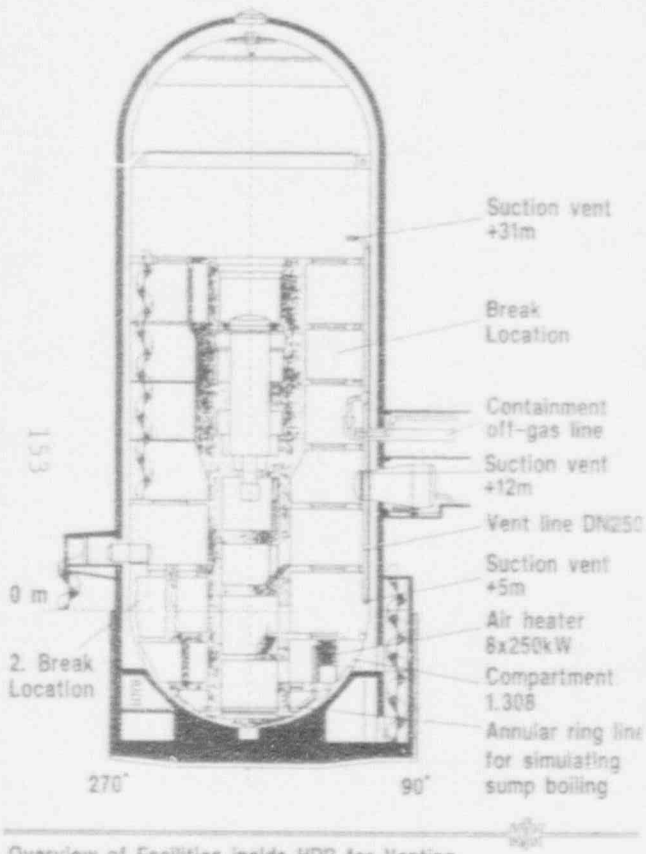

Overview of Facilities inside HDR for Venting, Atmospheric Heating and Sump Boiling

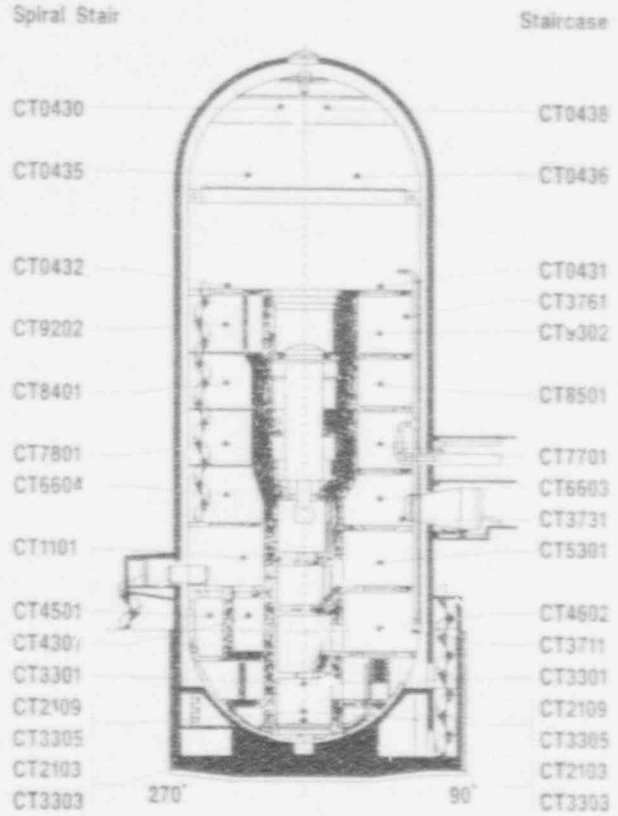

Positions of Thermocouples Along Major Flow Paths

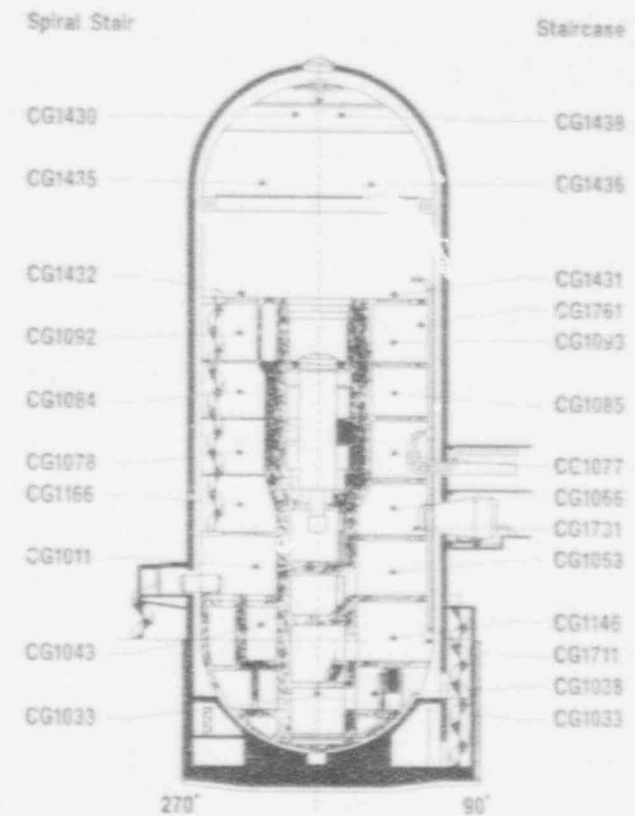

Positions of Gas Concentration Sensors

Fig. 1: HDR-Facility and Distributions of Thermocouples and H_2-Concentration Sensors

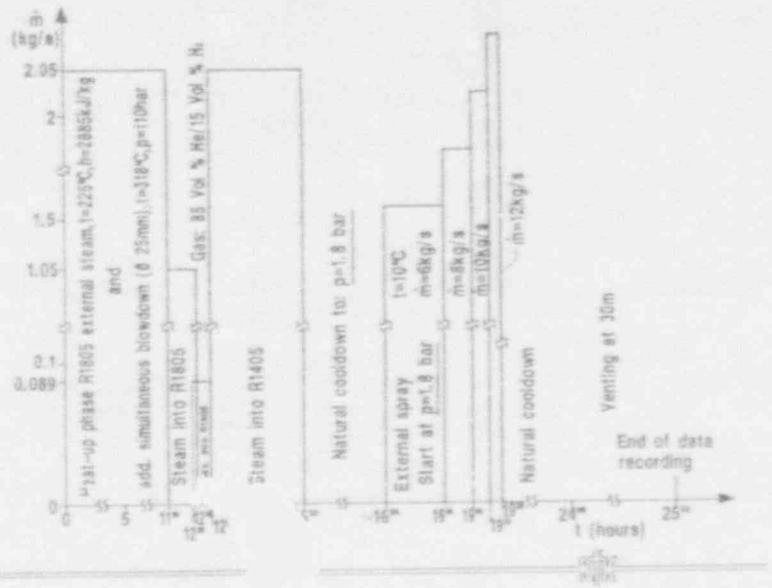

Fig. 2: Experimental Procedure for E.

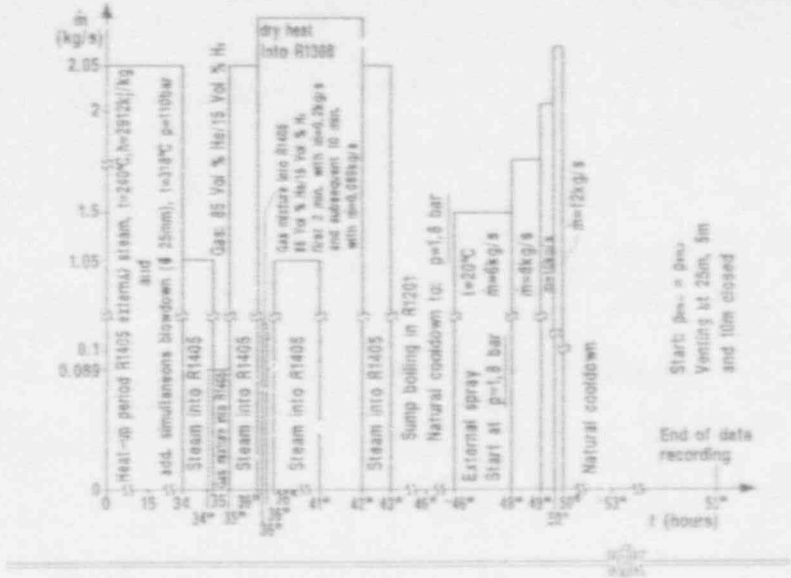

Experimental Procedure for E11.4

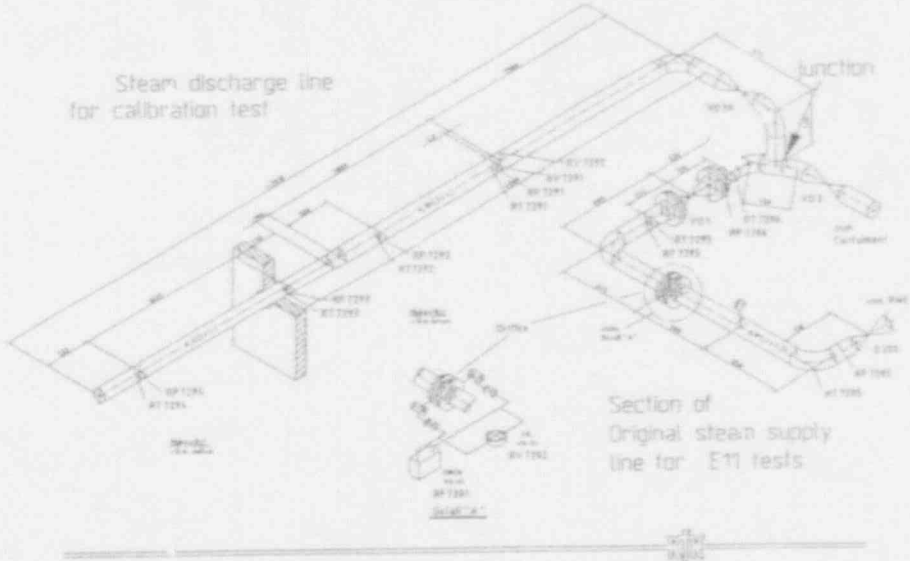

Fig. 3: Steam Lines and Measurements for Calibration Tests

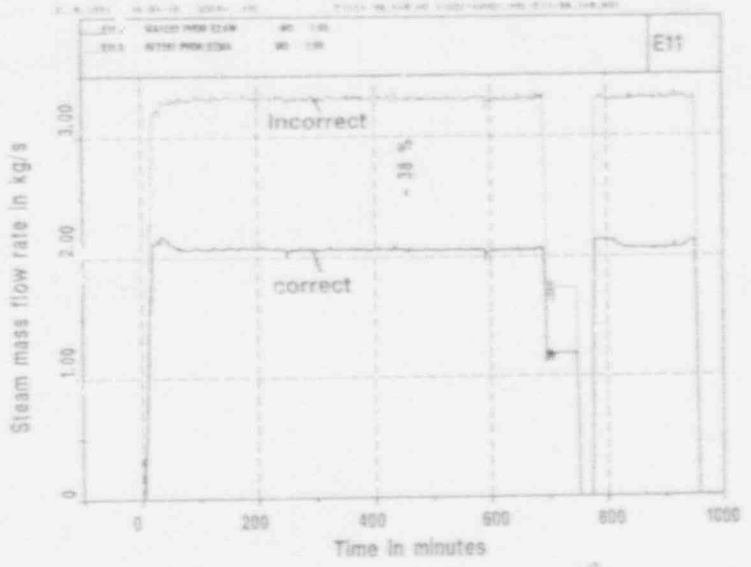

Fig. 4: Comparison of "new" MA7202 and "old" RF7201 external steam mass flow rate, test E11.2

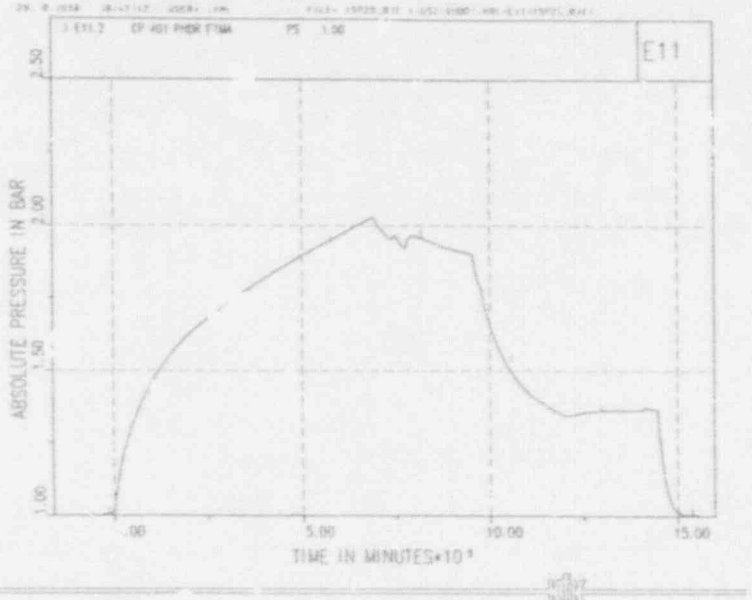

Fig. 5: Containment Pressure, Test E11.2

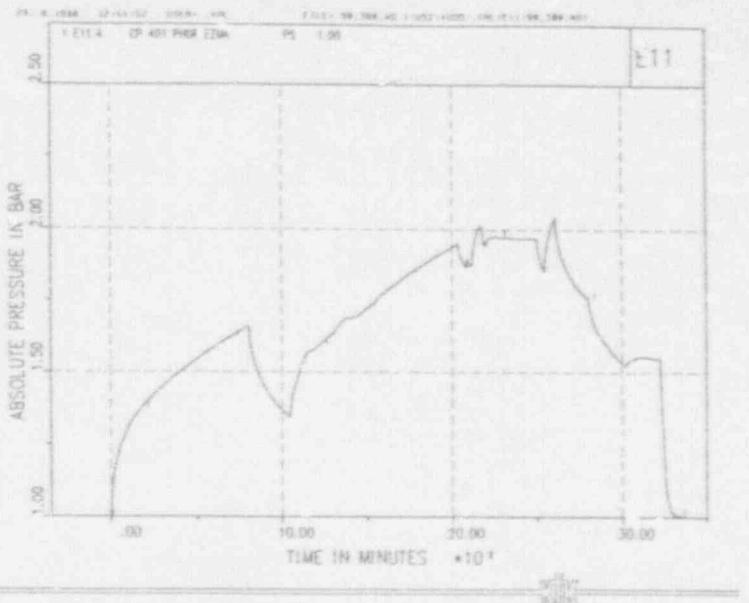

Containment Pr_ssure, Test E11.4

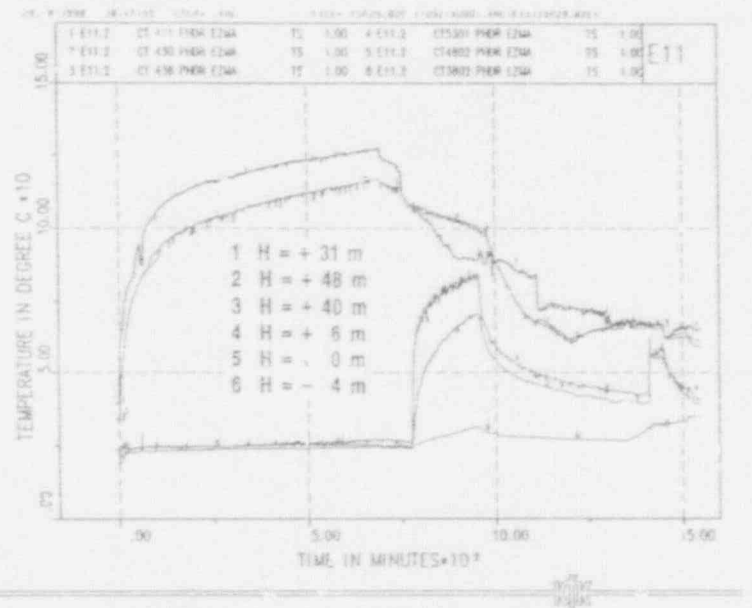

Fig. 6: Temperatures along Staircase, Test E11.2

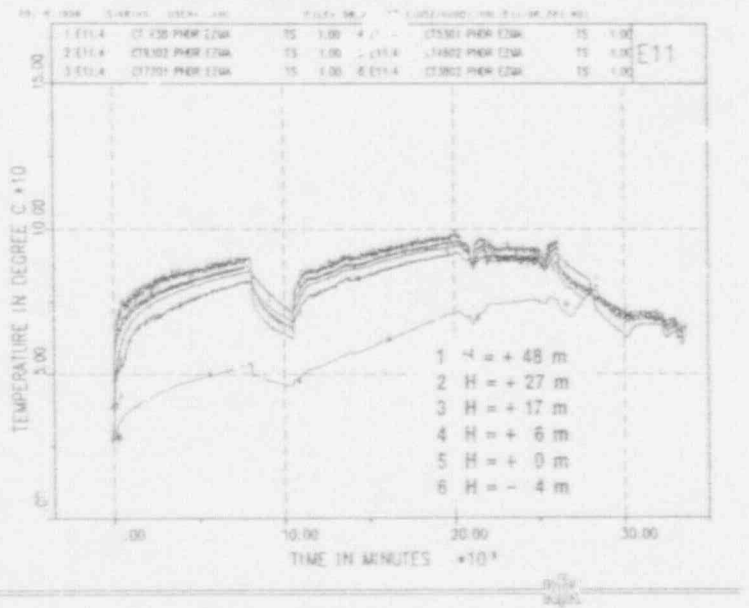

Temperatures along Staircase, Test E11.4

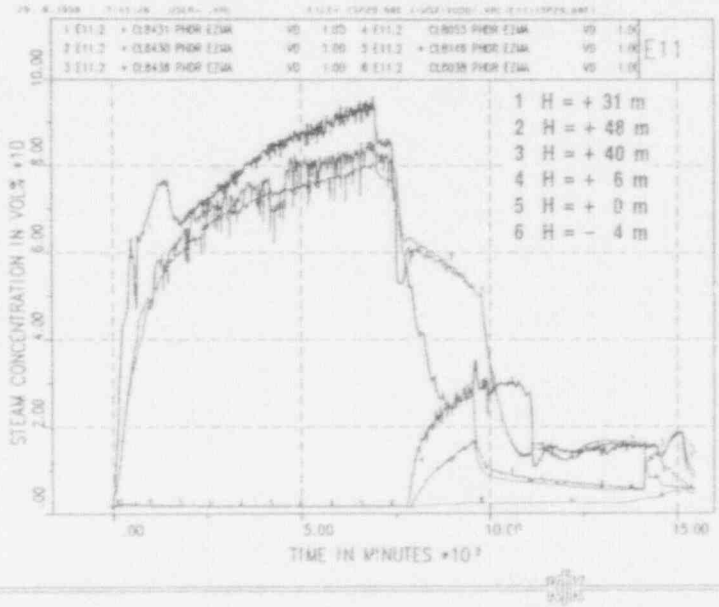

Fig. 7: Steam Concentrations along Staircase, Test E11.2

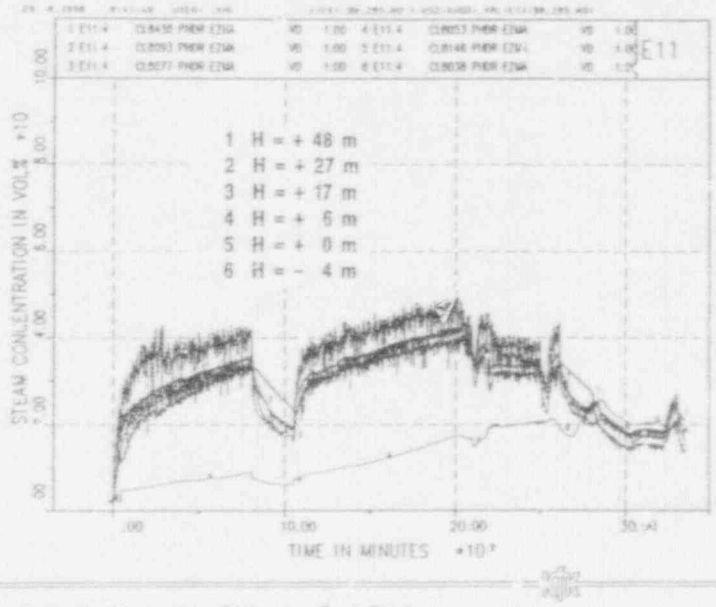

Steam Concentrations along Staircase, Test E11.4

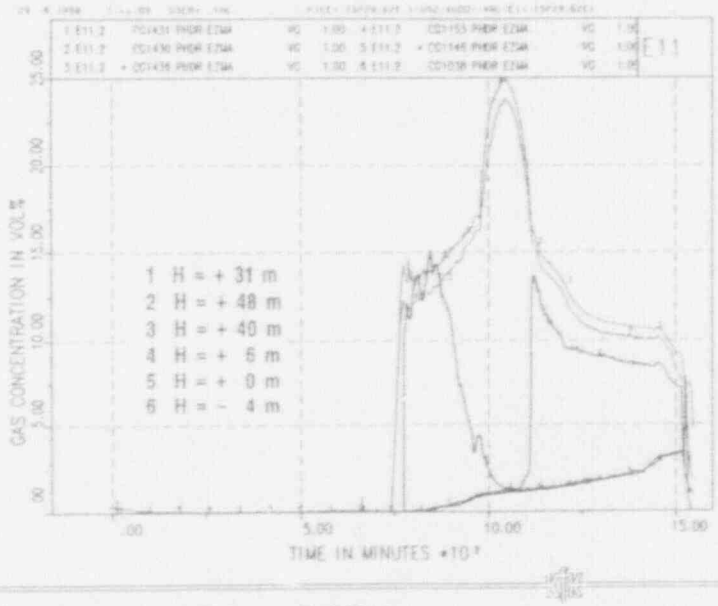

Fig. 8: Gas Concentrations along Staircase, Test E11.2

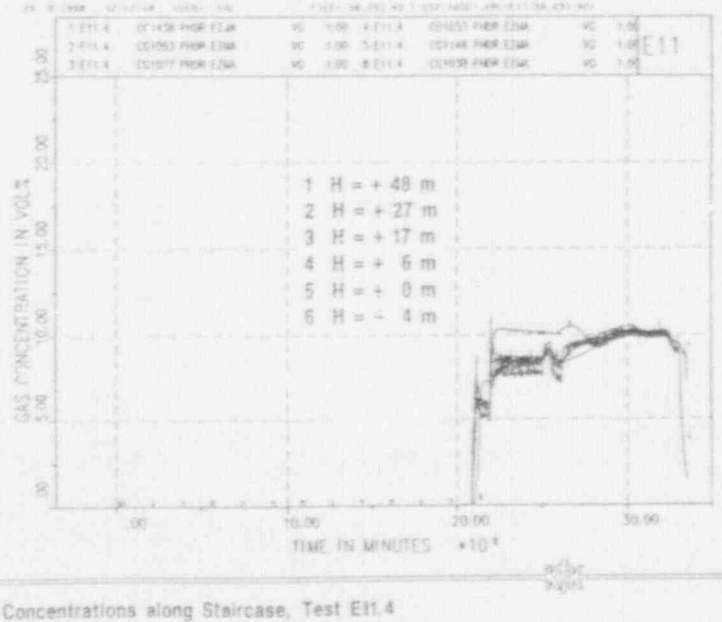

Gas Concentrations along Staircase, Test E11.4

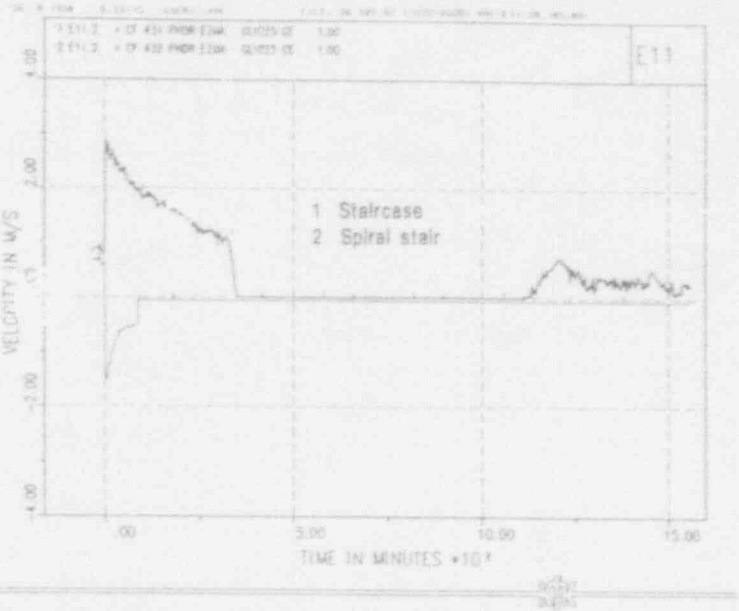

Fig. 9: Velocities at 31 m (Staircase 81° and Spiral Stair 270°), Test E11.2

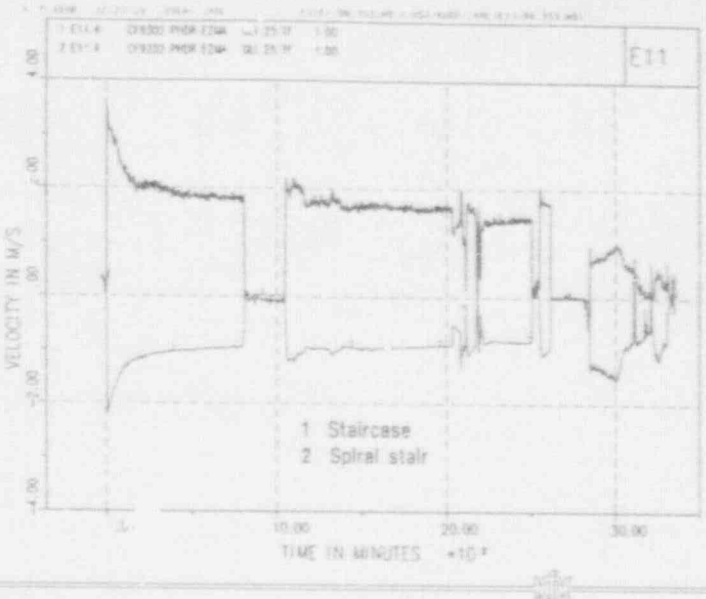

Velocities at 25 m (Staircase 81° and Spiral Stair 270°), Test E11.4

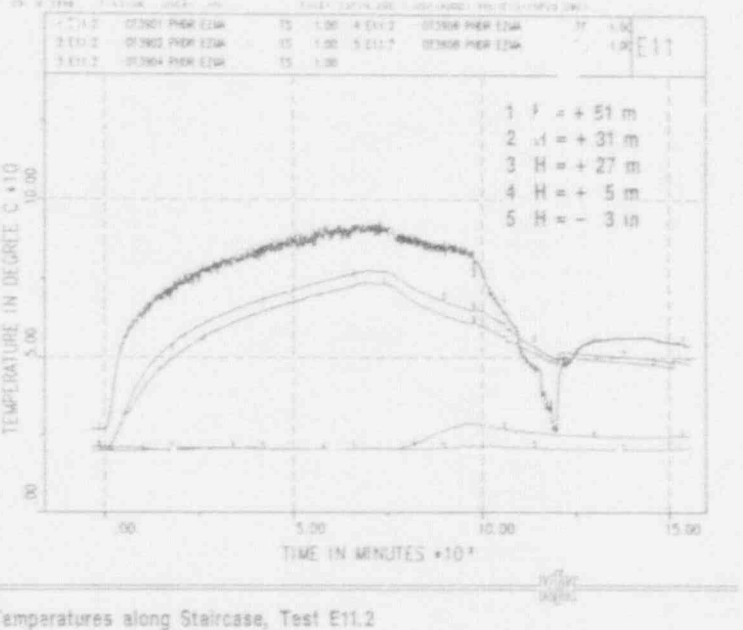

Fig. 10: Gap Temparatures along Staircase, Test E11.2

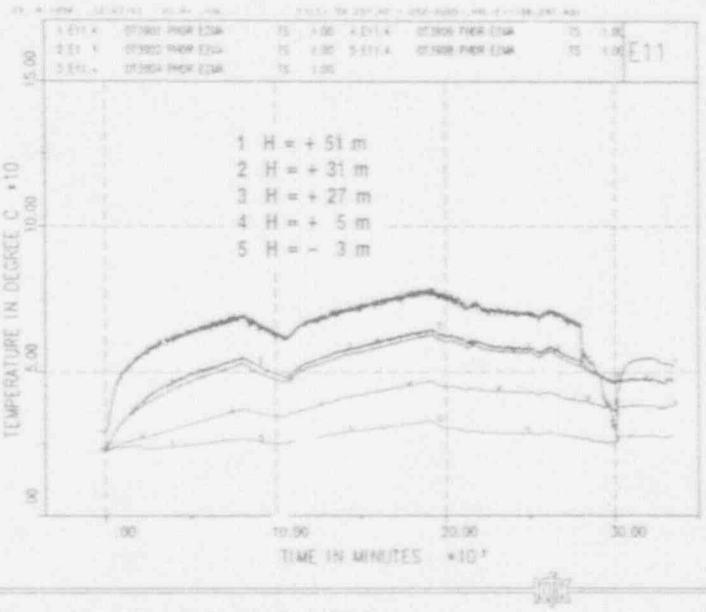

Ga, Temperatures along Staircase, Test E11.4

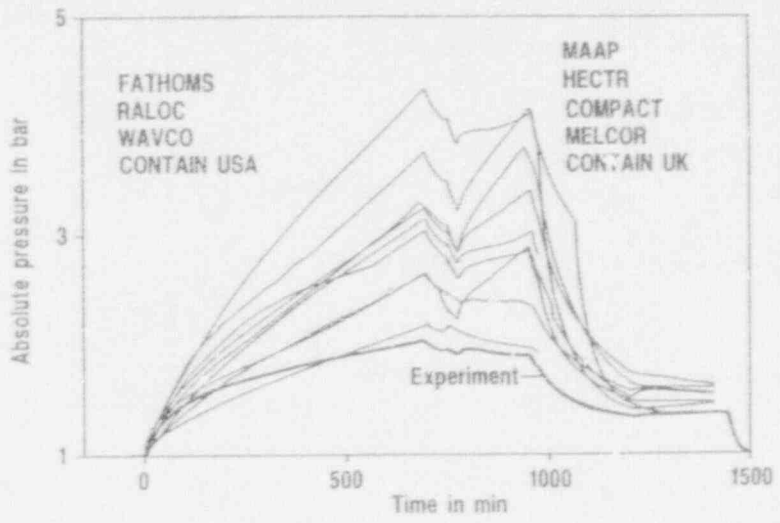

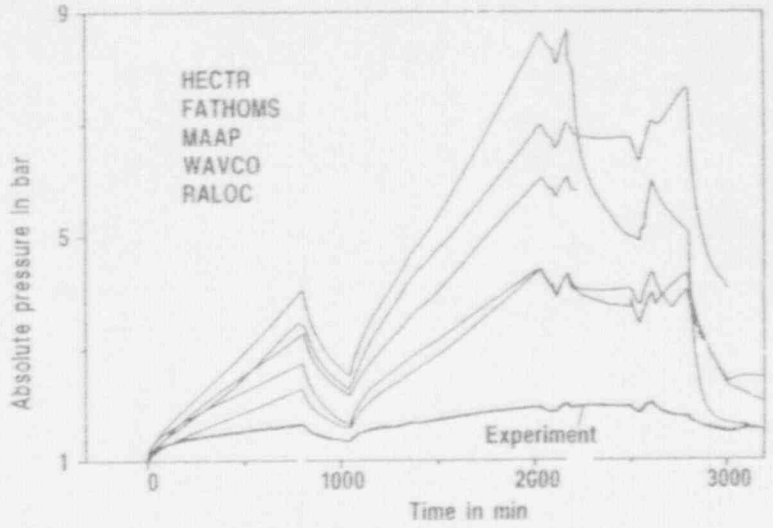

Fig. 11: E11.2 (left), E11.4 (right) - Data vs. Code Predictions for Containment Pressures

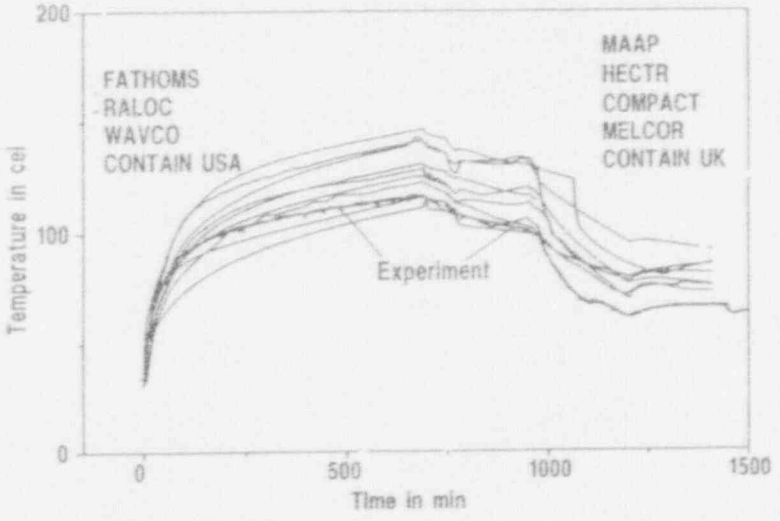

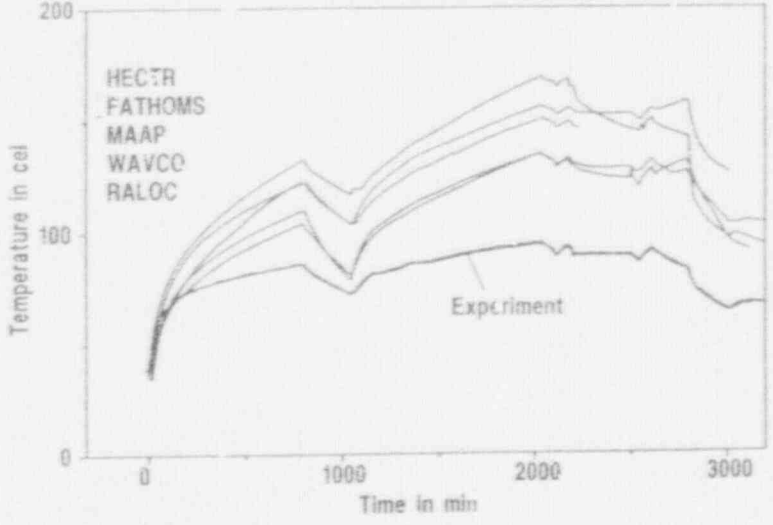

Fig. 12: E11.2 (left), E11.4 (right) - Data vs. Code Predictions for Temperature in Dome Region at 40 m

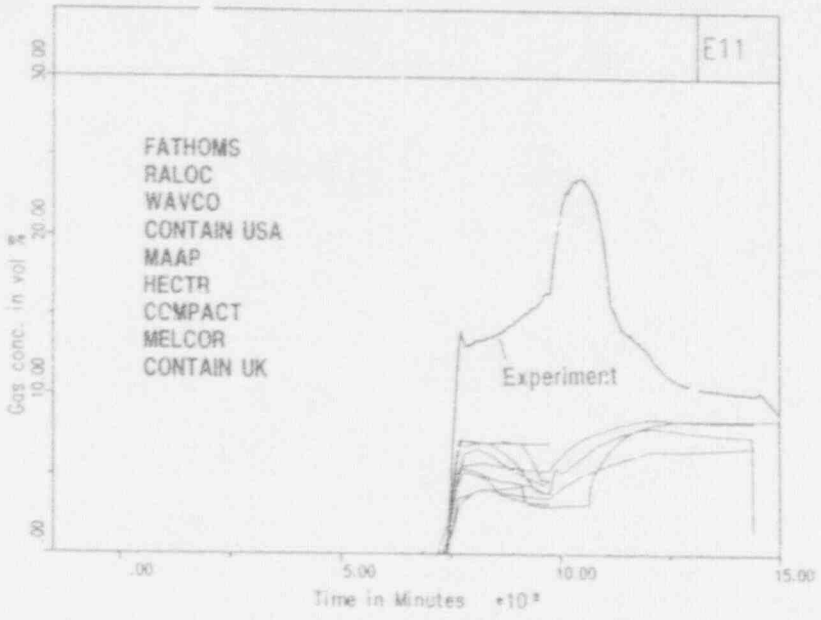

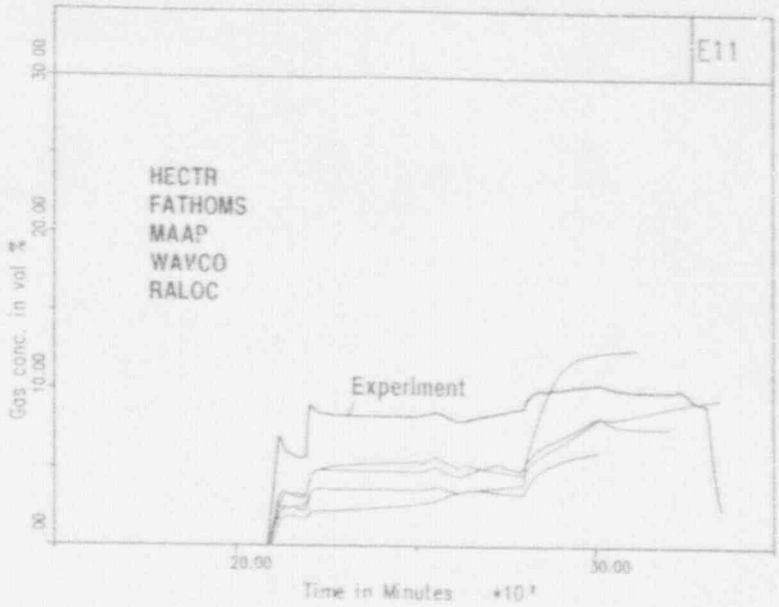

Fig. 13: E11.2 (left), E11.4 (right) - Data vs. Code Predictions for Gas Concentrations in Dome Region at 40 m

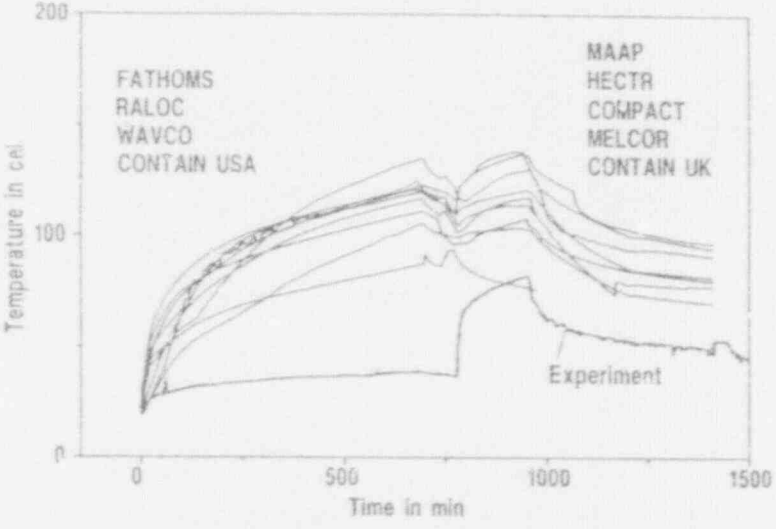

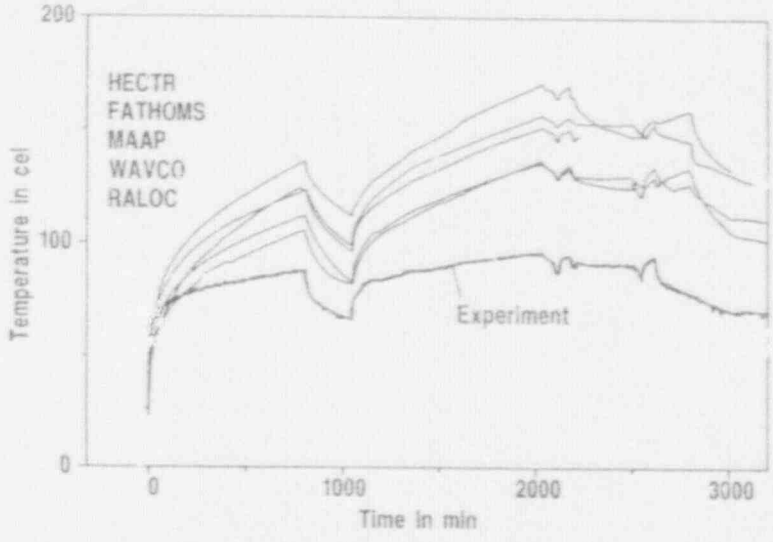

Fig. 14: E11.2 (left), E11.4 (right) - Data vs. Code Predictions for Temperatures at 12 m

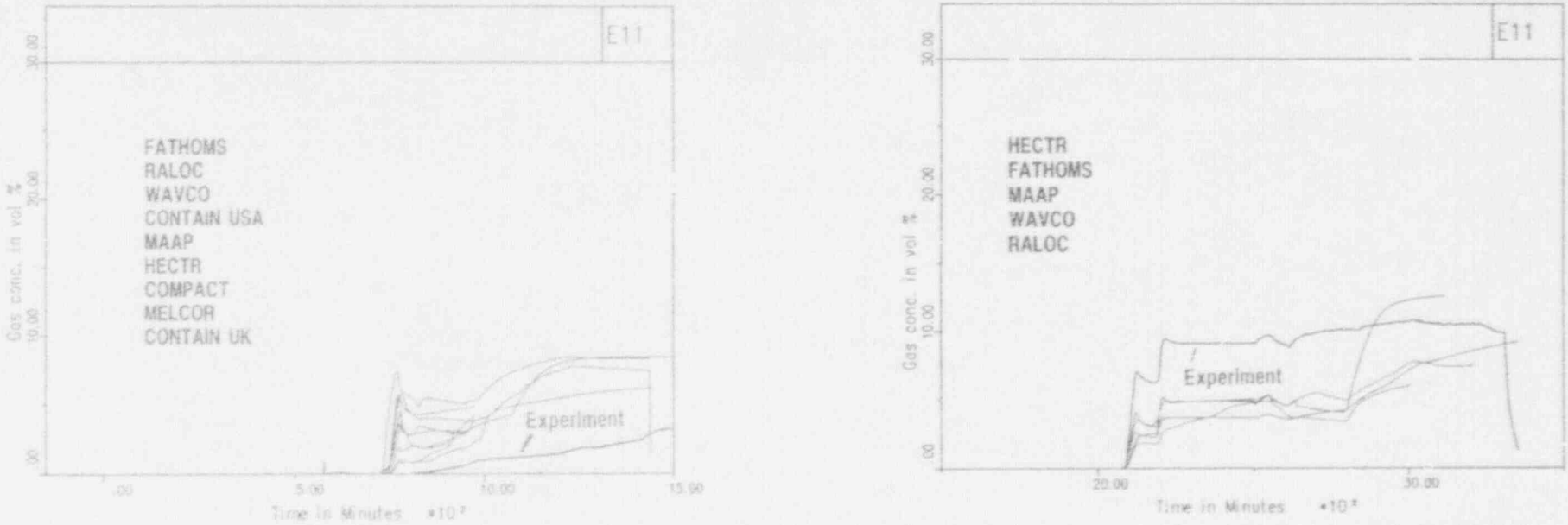

Fig. 15: E11.2 (left), E11.4 (right) - Data vs. Code Predictions for Gas Concentrations at 12 m

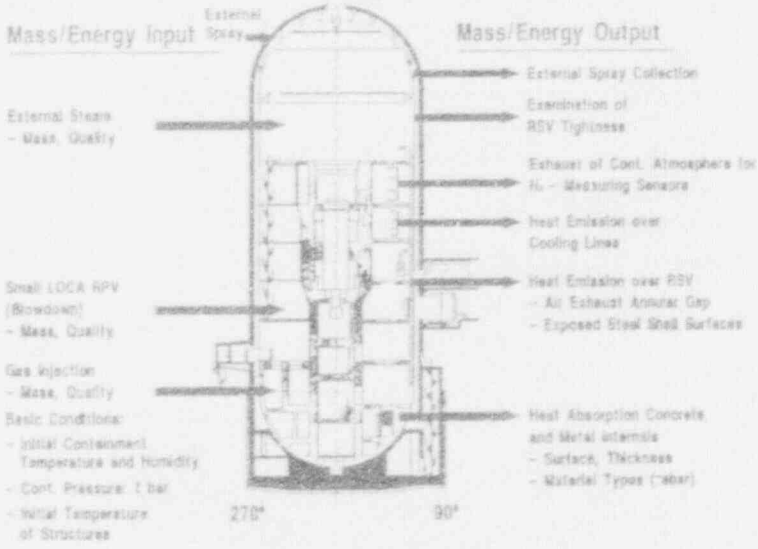

Fig. 16: Input Data for Code Predictions

- Nodalization
- Realistic Modelling for Long Term
- Accounting for all Heat Sources and Sinks
- Boundary Conditions
- Energy Partioning
- Heat Transfer During Stratification
- Artificial Mixing
- Counter-Current Flows
- Multi-Dimensional Effects
- Physics of AMM

Fig. 17: Issues of Uncertainties by Code Predictions

Nodalisation

1.) Control Volumes

Containment	41	Lumped Parameter Nodes
	1	(Dome) 2 - dimensional with 6 Subnodes
Annular Gap	9	Lumped Parameter Nodes

2.) Flowpath Junctions

Containment	97
Annular Gap	10

3.) Heat Structures

Concrete Walls	54
Metallic Structures	47
Steel Shell	43

Fig. 18: Summary of FATHOMS Nodalization

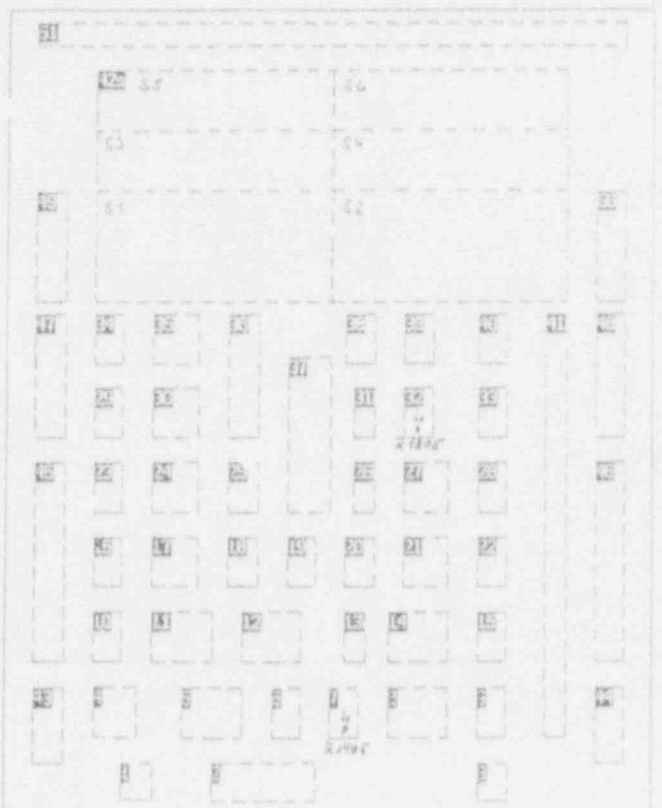

Fig. 19: Control Volume Nodalization of HDR

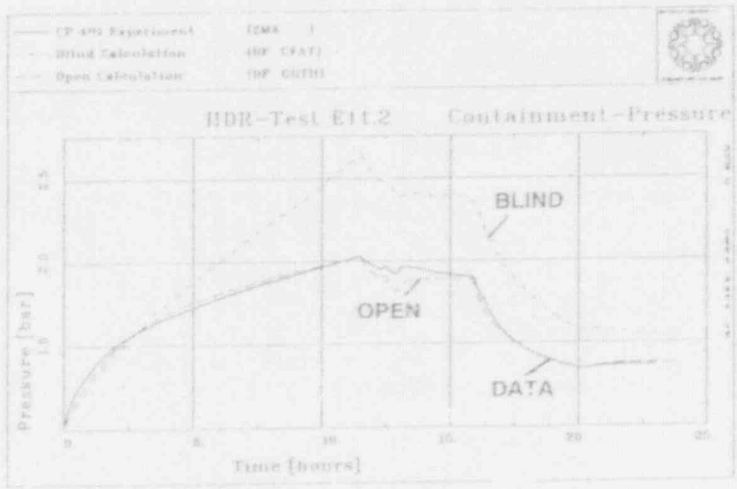

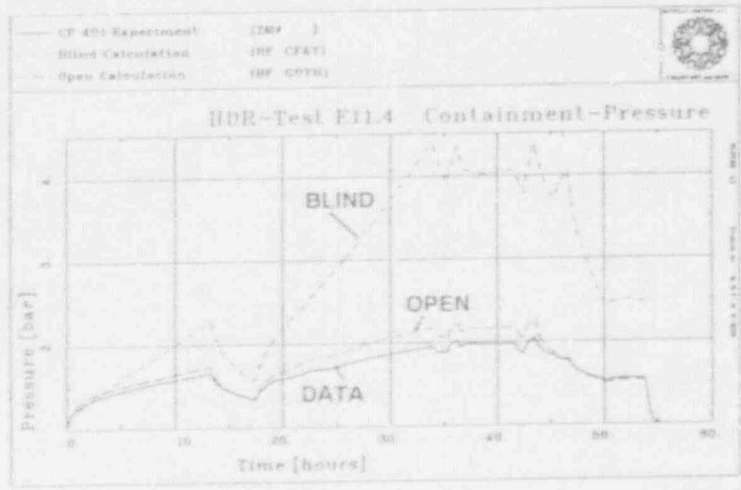

Fig. 20: Comparisons Between Data, blind FATHOMS and open GOTHIC-Predictions

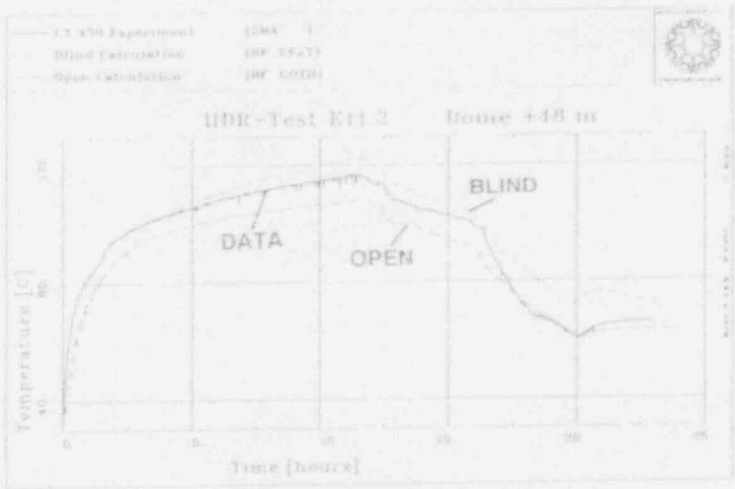

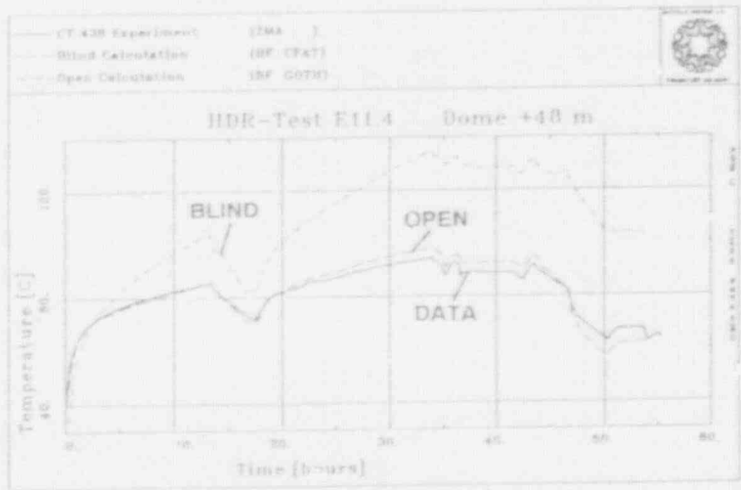

Fig. 21: Temperatures; Comparisons Data, FATHOMS, GOTHIC

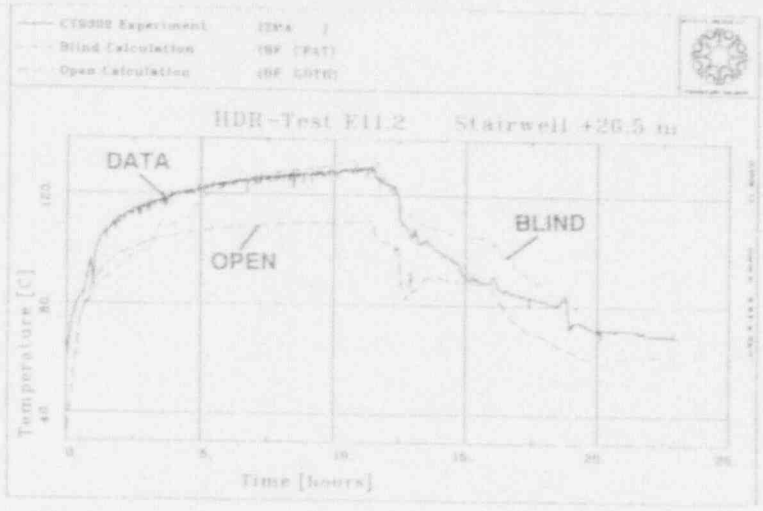

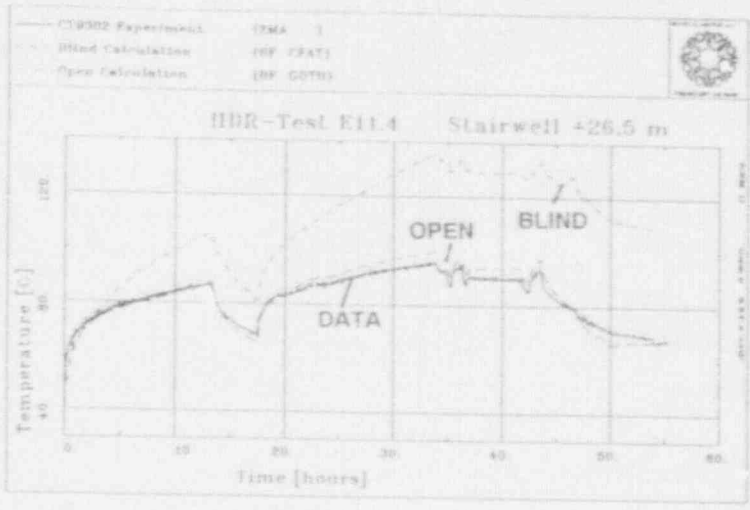

Fig. 22: Temperatures; Comparisons Data, FATHOMS, GOTHIC

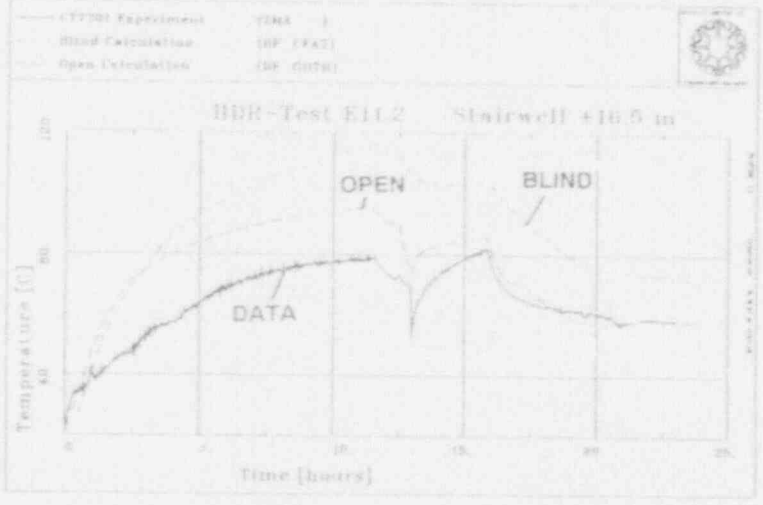

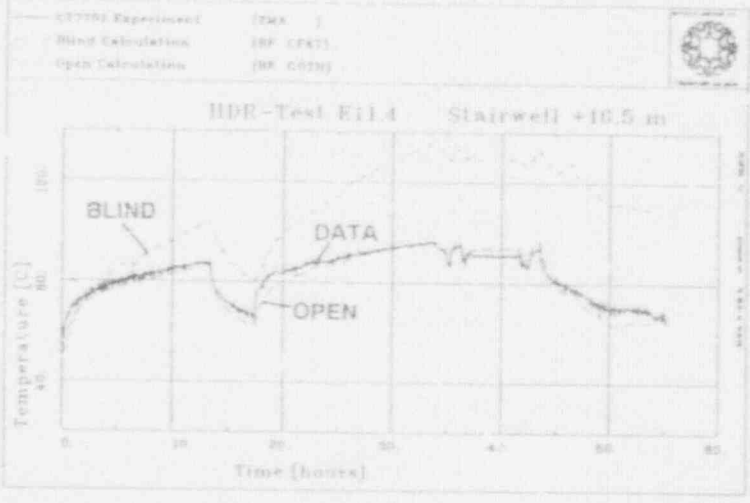

Fig. 23: Temperatures; Comparisons Data, FATHOMS, GOTHIC

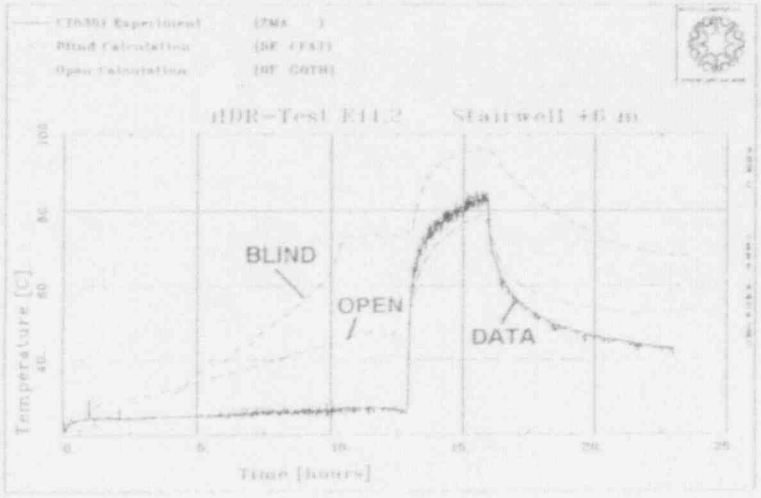

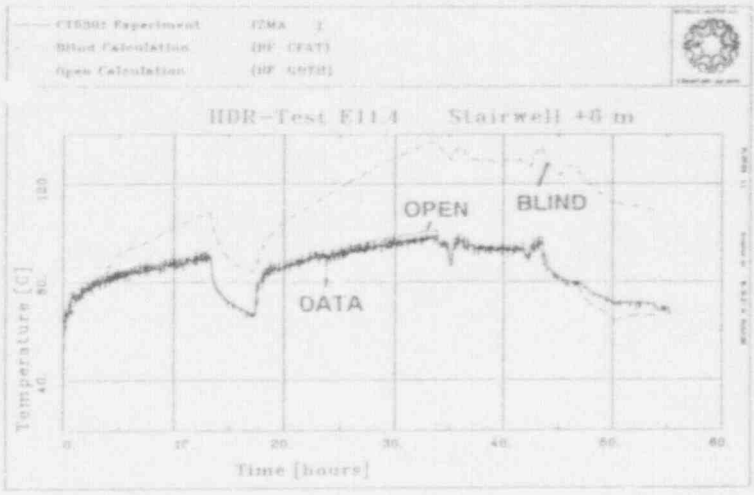

Fig. 24: Temperatures; Comparisons Data, FATHOMS, GOTHIC

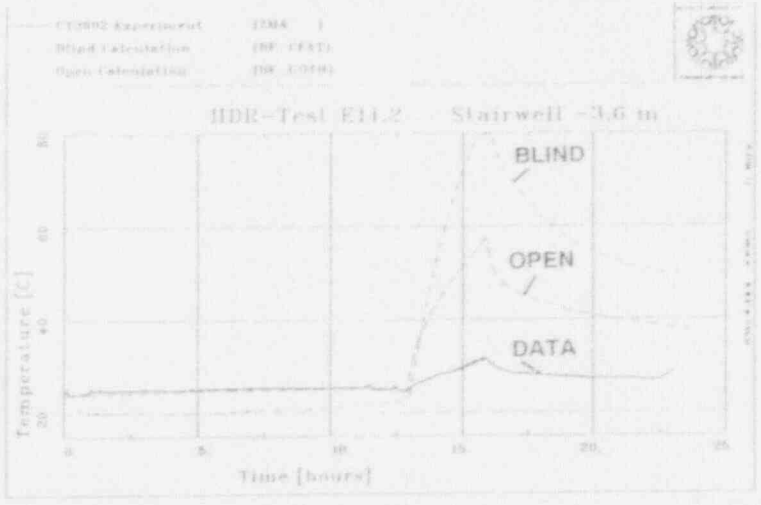

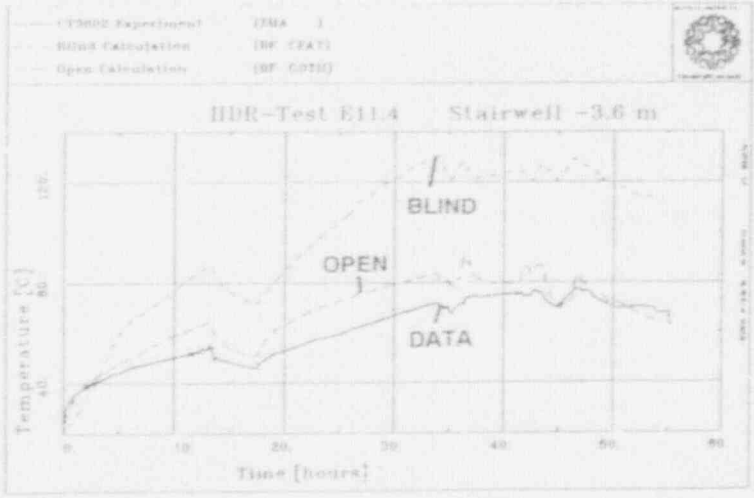

Fig. 25: Temperatures; Comparisons Data, FATHOMS, GOTHIC

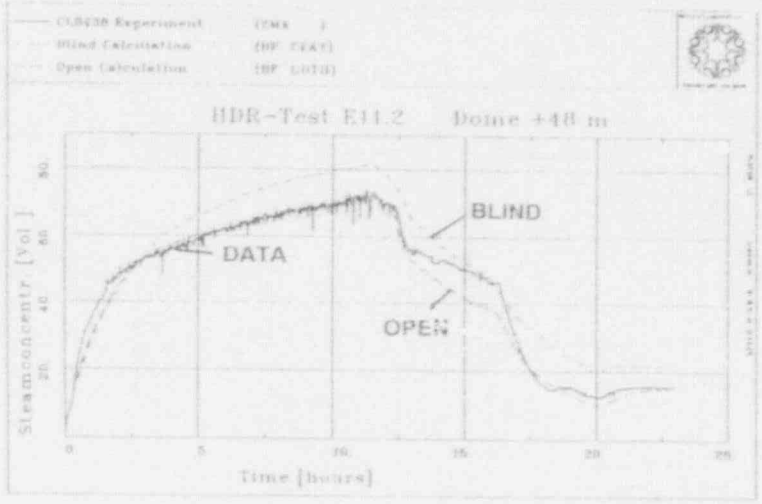

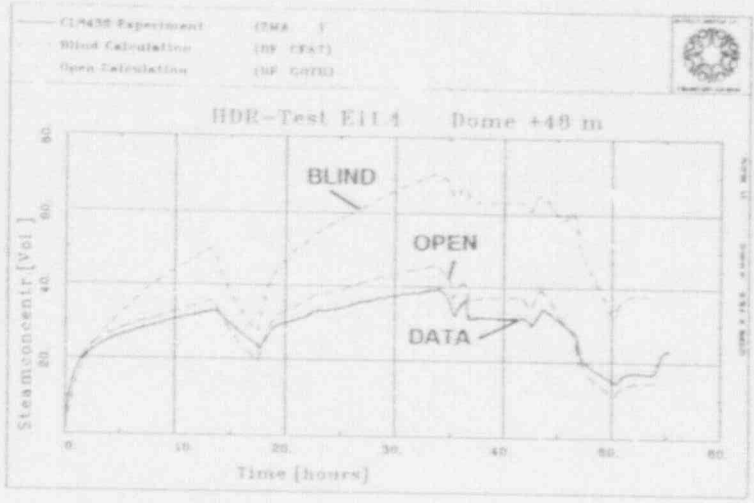

Fig. 26: Steam Concentrations; Comparisons Data, FATHOMS, GOTHIC

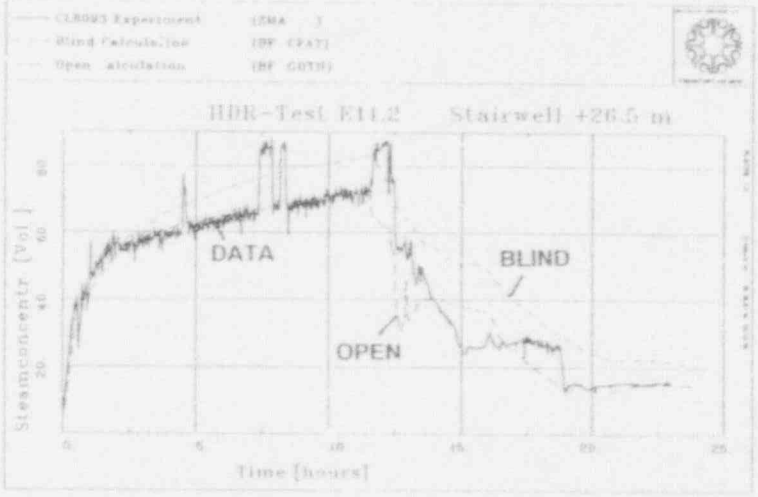

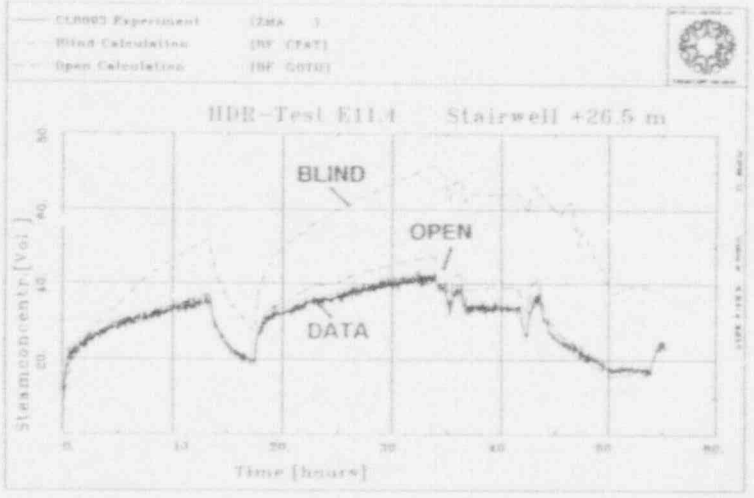

Fig. 27: Steam Concentrations; Comparisons Data, FATHOMS, GOTHIC

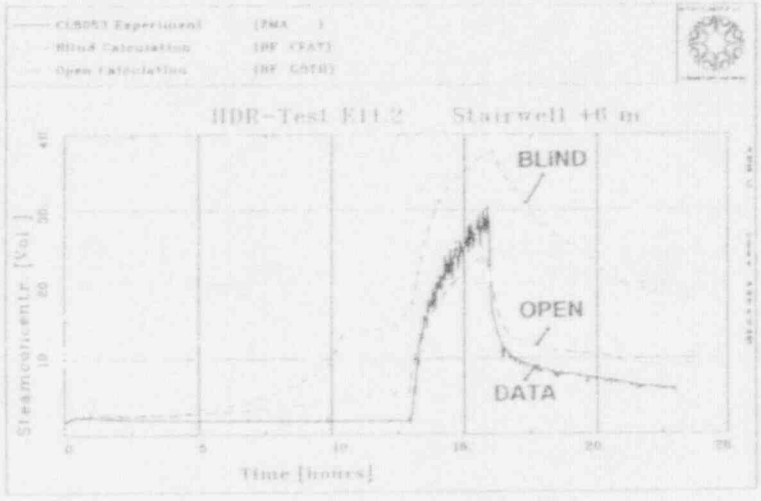

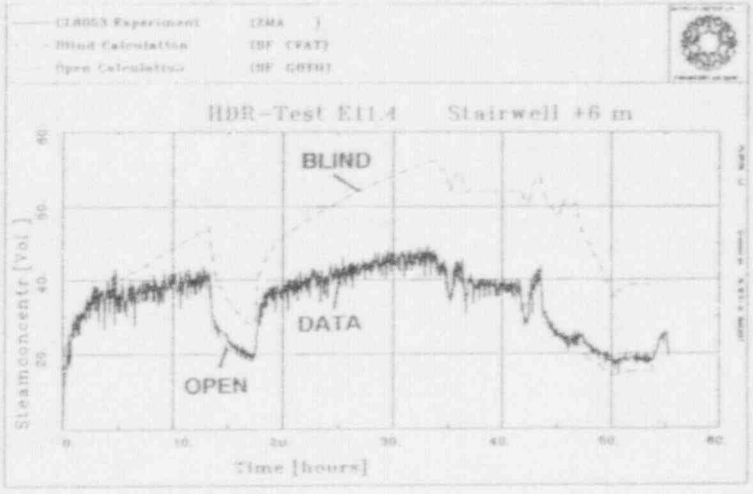

Fig. 28: Steam Concentrations; Comparisons Data, FATHOMS, GOTHIC

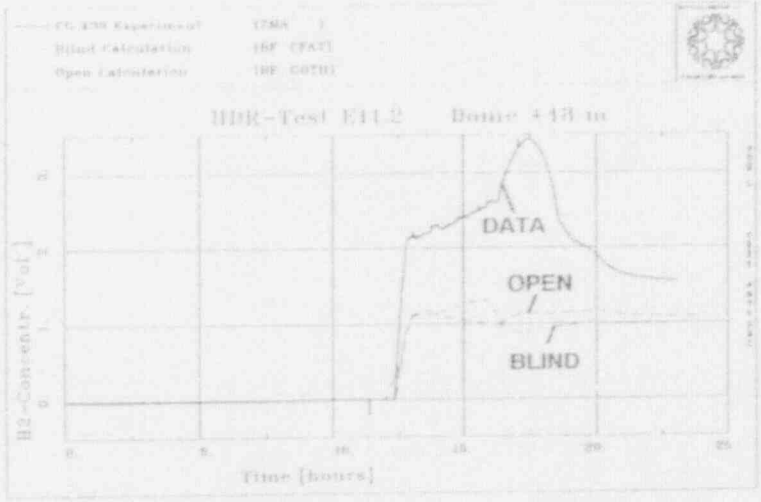

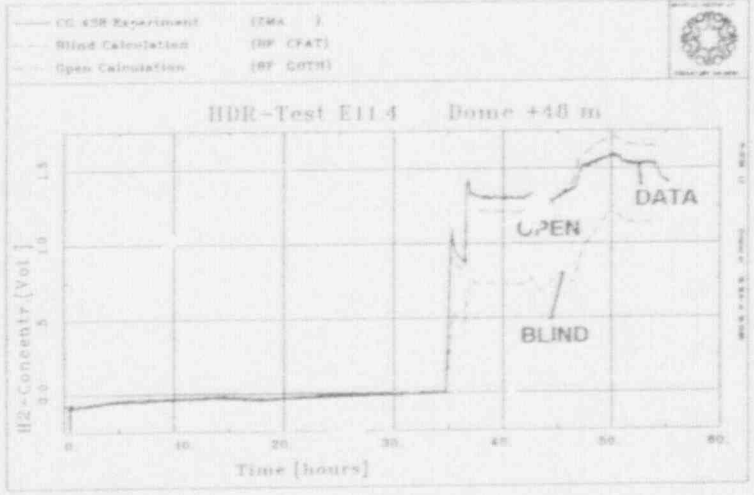

Fig. 29: H_2-Concentrations; Comparisons Data, FATHOMS, GOTHIC

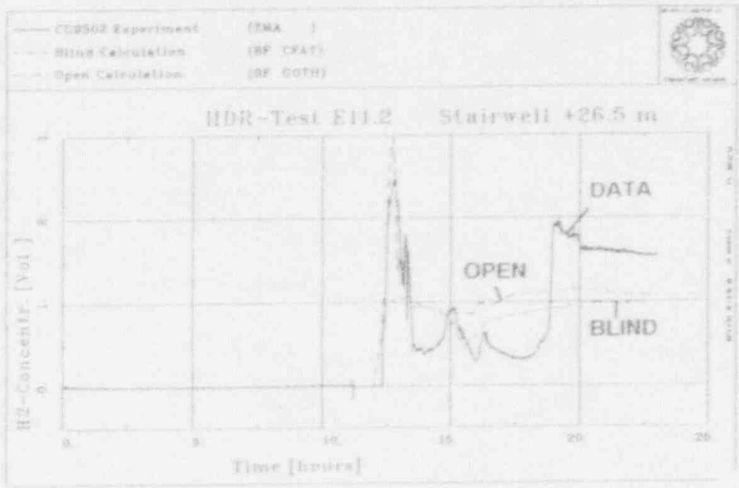

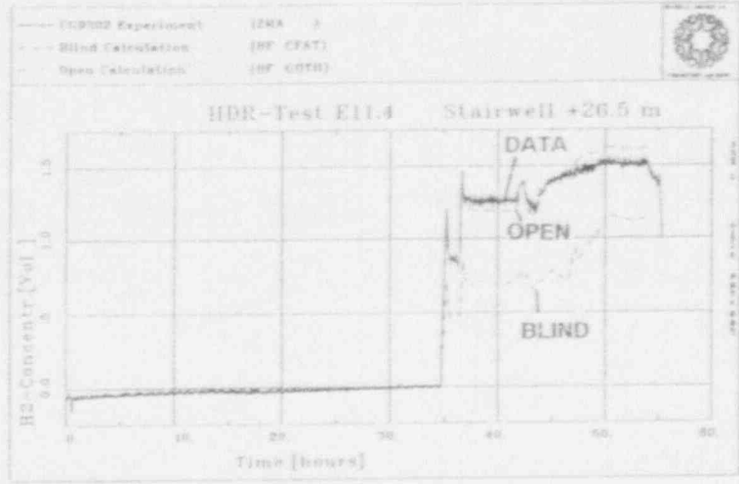

Fig. 30: H_2-Concentrations; Comparisons Data, FATHOMS, GOTHIC

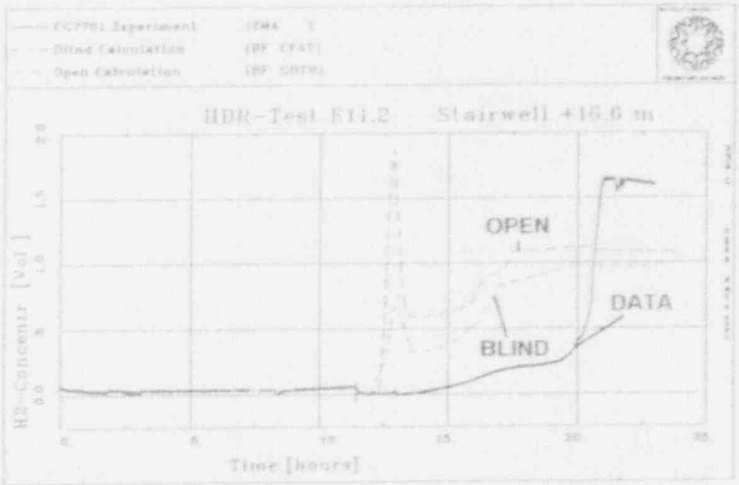

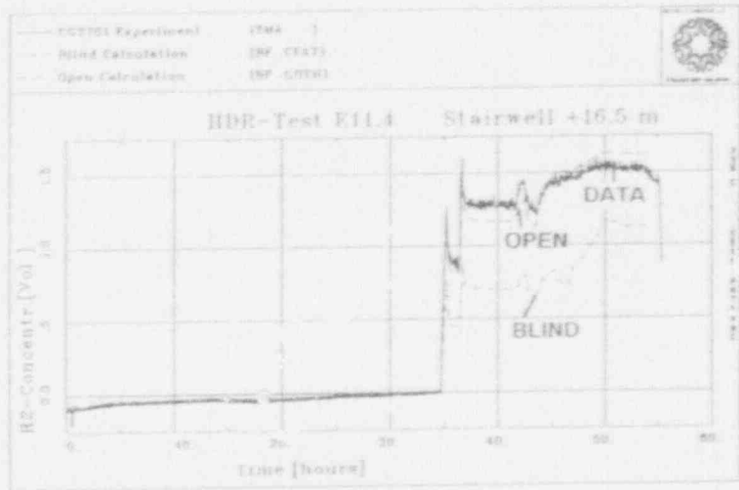

Fig. 31: H_2-Concentrations; Comparisons Data, FATHOMS, GOTHIC

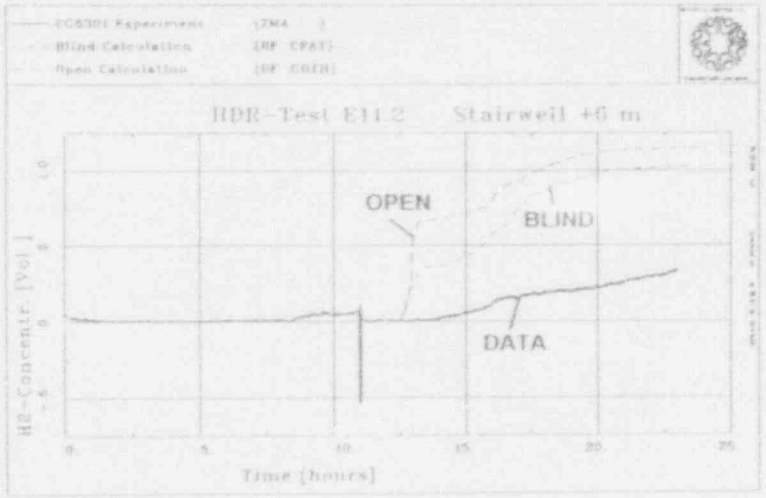

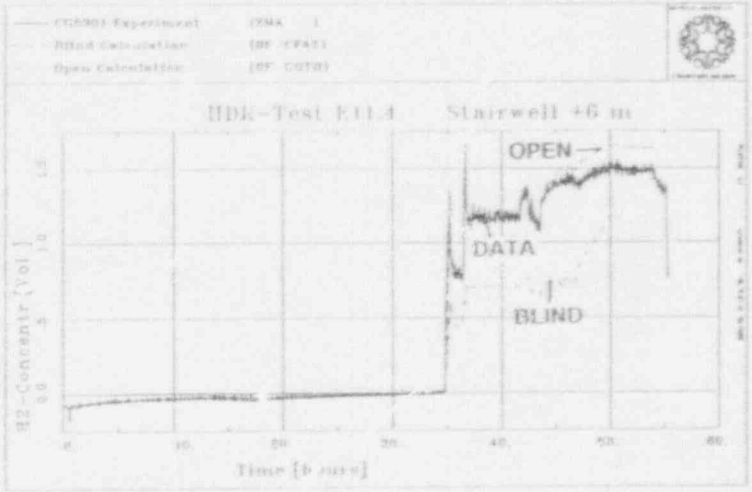

Fig. 32: H_2-Concentrations; Comparisons Data, FATHOMS, GOTHIC

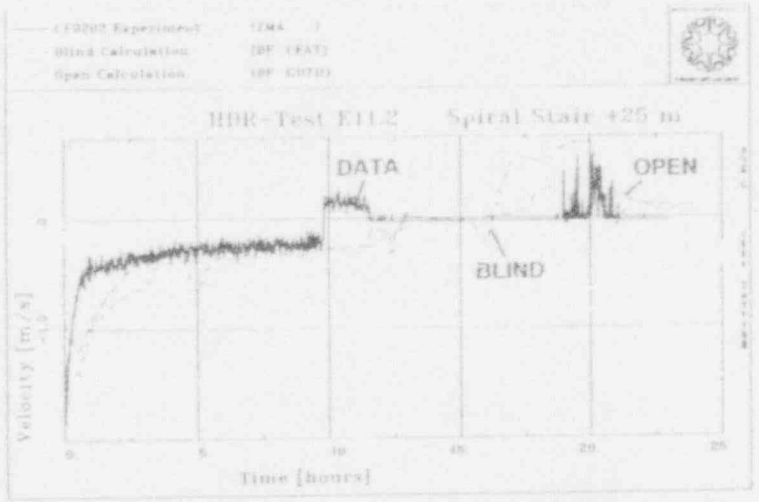

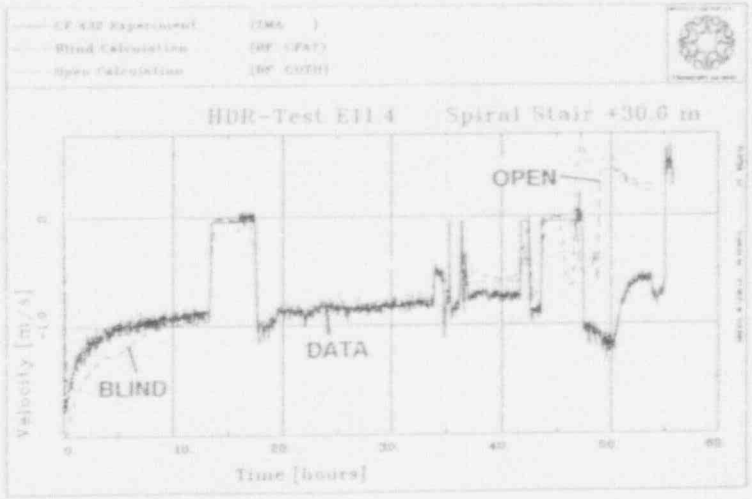

Fig. 33: Velocities; Comparisons Data, FATHOMS, GOTHIC

MOST LIKELY FAILURE LOCATION DURING SEVERE ACCIDENT CONDITIONS[a]

J. L. Rempe and C. M. Allison
Idaho National Engineering Laboratory
EG&G Idaho, Inc.
P.O. Box 1625
Idaho Falls, Idaho 83415

ABSTRACT

This paper describes preliminary results from an analysis in which finite element calculation results are used in conjunction with analytical calculation results to predict failure in different LWR vessel designs during a severe accident. Detailed analyses are being performed to investigate the relative likelihood of a BWR vessel and drain line penetration to fail during a wide range of severe accident conditions. Analytically developed failure maps, which were developed in terms of dimensionless groups, are applied to consider geometries and materials occurring in other LWR vessel designs.

Preliminary numerical analysis results indicate that if ceramic debris relocates within the BWR drain line to a distance below the lower head, the drain line will reach failure temperatures before the vessel fails. Application of failure maps for these debris conditions to other LWR geometries indicate that in-vessel tube melting will occur in either BWR or PWR vessel designs. Furthermore, if this melt is assumed to fill the entire penetration flow area, the melt is predicted to travel well below the lower head in any of the reference LWR penetrations. However, failure maps suggest the result that ex-vessel tube temperatures exceed the penetration's ultimate strength is specific to the BWR drain line because of its material composition and relatively large effective diameter for melt flow.

1. INTRODUCTION

The mode and timing of reactor vessel lower head failure has a controlling effect on subsequent consequences during a severe accident. Because of uncertainties related to the nature of vessel failure, the U.S. Nuclear Regulatory Commission (NRC) is sponsoring a lower vessel head research program to investigate plausible modes of reactor vessel failure to determine (a) which modes have the greatest likelihood of occurrence during a severe accident and (b) the range of core debris and accident conditions that lead to these failures.[1] All major types of U.S. light water reactor (LWR) vessels are being considered, and both high- and low-pressure conditions are being addressed for each reactor type. The research program includes analytical and finite element

---

a. Work supported by the U.S. Nuclear Commission, Office of Nuclear Regulatory Research, under DOE Contract No. DE-AC07-76ID01570.

calculations. In addition, high temperature creep and tensile data for predicting vessel structural response were obtained.

This paper describes results from one aspect of this research program in which results from finite element thermal response calculations are used with results from analytical calculations to predict which failure location is more likely in different LWR designs. Preliminary results from an on-going two-dimensional thermal and structural response for a boiling water reactor (BWR) penetration and vessel are reported and compared with results from analytical models. Then, analytical models are used to consider penetrations in other LWR vessel designs.

1.1 Objectives and Problem Description

Several major questions related to vessel failure require detailed analyses. Detailed thermal and structural response calculations are being performed within the NRC Lower Head Failure Research Program. Primary objectives of the thermal calculations, which are discussed within this paper, are to (a) assess the relative importance of thermal fronts created by the debris in a vessel penetration and upon the vessel lower head; (b) assess the sensitivity of thermal response to debris composition, porosity, and heat removal from the lower head and drain line; (c) provide input to the structural response analyses; and (d) provide input to subsequent consequence analysis codes by specifying the fraction of the debris that is molten at the time of vessel failure. Although these objectives require detailed numerical techniques, results from a limited number of numerical calculations can be used in conjunction with analytical results to obtain general conclusions related to the nature of lower head failure.

Detailed calculations described within this paper center upon a BWR vessel and its drain line penetration. A BWR design was selected because of design information availability. A schematic of the BWR 4 vessel and drain line is shown in Figure 1. The vessel is composed of SA533 Grade B, Class I steel. The lower head is somewhat thicker (0.20 m) than the sidewalls (0.16 m) so that it can be penetrated by 185 control rod guide tubes, 55 instrument tubes, and the drain line tube. A support skirt, which is composed of SA302 Grade B steel, is attached to the lower head. Surrounding the lower head and support shirt is reflective insulation composed of layered stainless steel, 7.6 cm thick.

Analyses in this paper focus upon the drain line because initial studies indicate that this penetration is more likely to fail than other locations within BWR vessels. The drain line penetration is located in the bottom of the reactor vessel, six inches off the centerline. It directs flow to the reactor water clean-up system to aid in the removal of suspended solids, provide a temperature measurement of water in the bottom head area, and minimize cold water stratification in the bottom head area. The portion of the drain line analyzed in this study consists of the SA105 Class II carbon steel nozzle and the SA106 Grade B mating pipe. A schematic of the drain line penetration is also shown in Figure 1. The pipe extends two feet vertically below the vessel before connecting to an elbow joint.

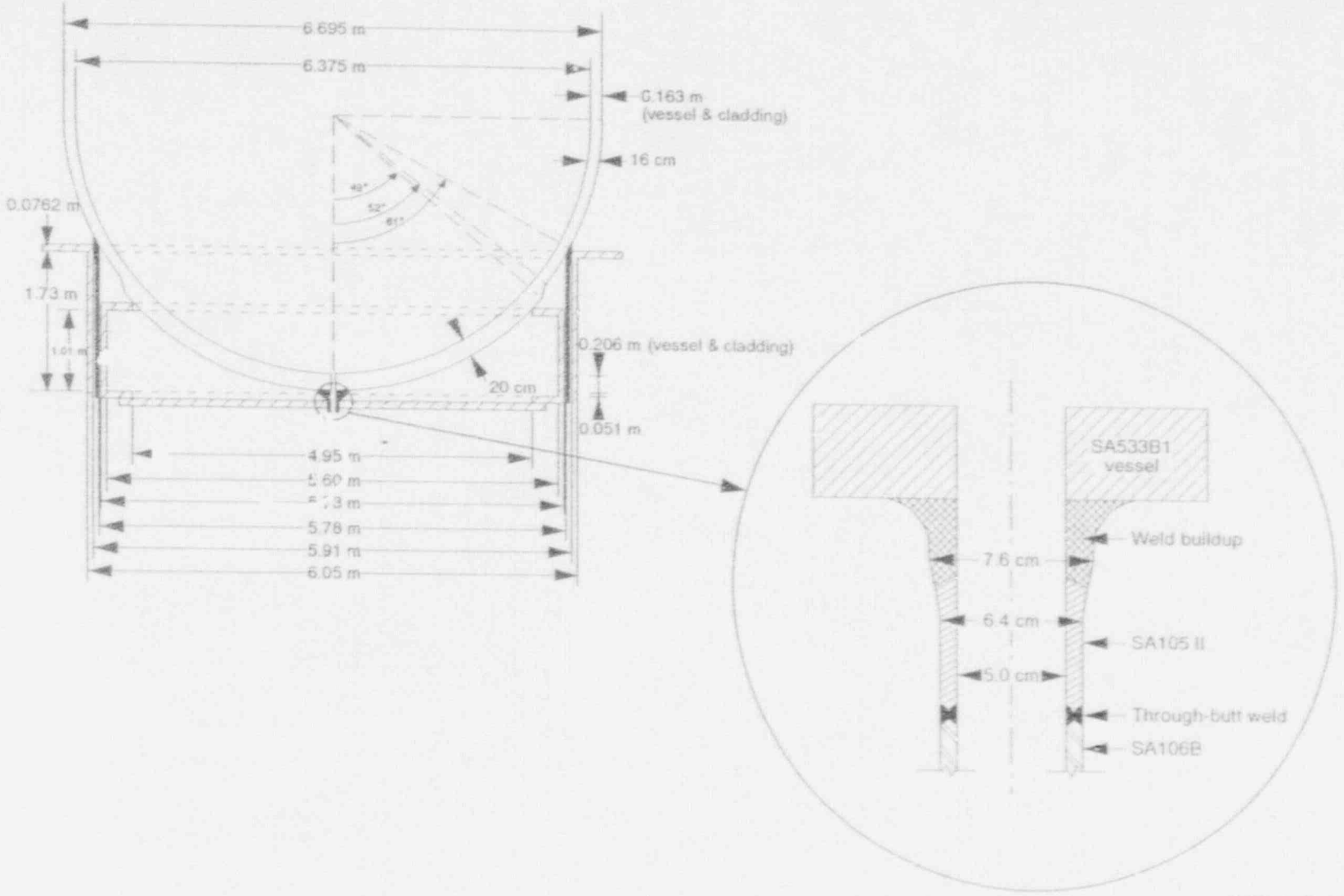

Figure 1. Typical BWR vessel and drain line configuration.

A preliminary study indicates that the drain line penetration is the region most likely to fail for the following reasons:

- Primary stresses (those caused by system pressures) are estimated to be low in the vessel and the drain line. Therefore, failure is most likely to occur at elevated temperatures from the reduction in strength.

- Drain line thickness (0.7 cm) is much less than the vessel lower head thickness (20.0 cm). Thus, if debris relocates onto the lower head and into the drain line, the drain line may be susceptible to reaching failure temperatures more rapidly than the vessel.

- Once high temperatures are reached, drain line material is more susceptible to high temperature failure than the vessel or other BWR penetration material. The drain pipe material, SA106 Grade B, is not recommended for use above 811 K.[2] The ultimate strength of SA106 is 238 MPa at 811 K[3] whereas the ultimate strength of the vessel material, SA533B, is over 350 MPa at the same temperature.

- Although BWR instrument tube walls are thinner than the drain line, the drain line has a larger effective diameter for melt flow. Furthermore, the drain nozzle is directly open to relocating corium melt and no in-vessel structure melting is required for melt penetration.

1.2 Two-Dimensional Thermal Response Model

A two-dimensional finite element analysis is being performed using the COUPLE thermal analysis model in Version 3.0 of the SCDAP/RELAP5 code.[4] Although not discussed in this paper, detailed structural analysis for the vessel will be performed using the ABAQUS code.[5]

Separate analytical closed-form solutions to evaluate heat transfer from debris to the penetration tube and the vessel are available. However, a two-dimensional finite element numerical solution is needed to simultaneously evaluate the relative importance of the thermal fronts transmitted from the debris through the drain line and through the vessel lower head. SCDAP/RELAP5 offers a number of advantages over most two-dimensional heat transfer codes because it simulates reactor thermal-hydraulic conditions, fuel liquefaction and relocation, time- and composition-dependent debris pool formation, and natural convection from a pool of molten debris.

Since a primary objective of this analysis is to determine vessel and penetration thermal response, a simplified RELAP hydrodynamic model was used with a detailed COUPLE model (the finite element conduction heat transfer model in SCDAP/RELAP5) of the debris, vessel, and drain line configuration. As shown in Figure 2, two representative RELAP circuits were used to represent the hydrodynamic conditions through the vessel and through the reactor building cavity. The first loop includes an eight subvolume "pipe" component (volumes 70-01 through 70-08) to model the heat removal from the debris to coolant in the vessel. Liquid in the first subvolume (volume 70-01) is in contact with the

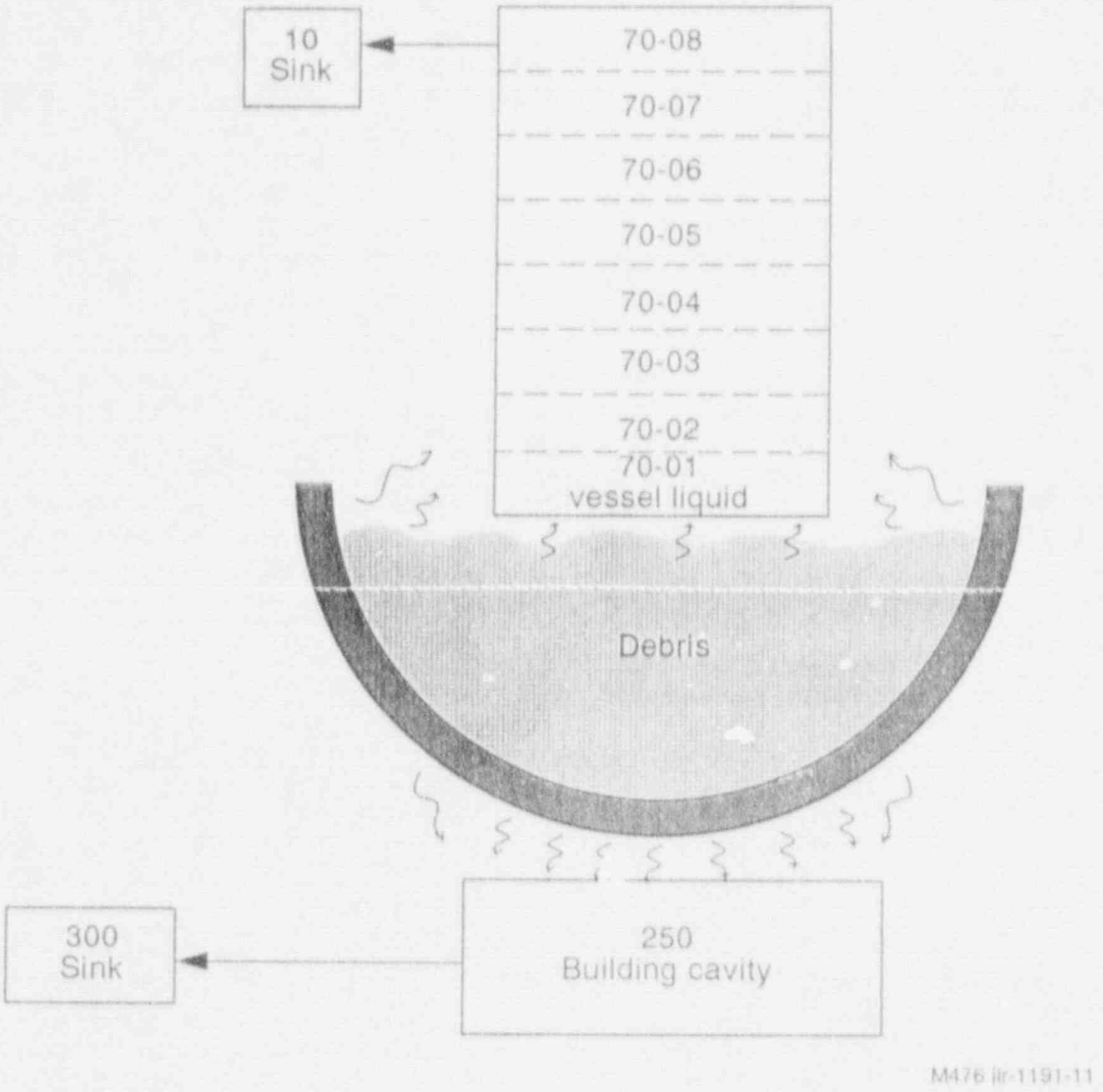

Figure 2. RELAP hydrodynamic model used for modeling BWR vessel and drain line penetration.

vessel inner surface and the debris, which is assumed to relocate into the lower head and the penetration at the beginning of the transient. As vapor is generated within this volume, it travels upward (from volumes 70-01 to 70-08). Pressure remains constant within the reactor vessel by allowing excess steam to exit to a time-dependent "sink" component (volume 10). The second loop is included to model the heat removal from the vessel outer surface to the reactor building cavity (volume 250). Pressure within the reactor building cavity remains constant by allowing excess vapor to exit to a time-dependent "sink" component (volume 300).

Figure 3 and Figure 4 illustrate the COUPLE models for the debris/vessel and debris/vessel/drain line configurations. Models were constructed in r-z geometries, axisymmetric with respect to the center of the vessel or with respect to the penetration tube. Only a portion of the vessel was modelled in the drain line mesh (Figure 4). The maximum radial width of this mesh was selected to correspond to half of the distance between the center of the drain line and the center of the nearest penetrations in a BWR lower head (7.62 cm). The axial length was based on the distance traveled by the melt before it solidified within the drain line pipe and the maximum expected debris height. Up to four types of materials are included in the models. Both meshes contain carbon steel for the vessel and drain line; a null material for the debris-to-vessel and debris-to-drain line gaps; and a debris mixture, consisting of UO_2, stainless steel, zircaloy or zirconium oxide, and B_4C. In addition, the mesh for the drain line contains Inconel for the vessel liner. Accuracy requirements for mesh nodalization precluded the inclusion of this thin liner in the global vessel mesh. As discussed in Reference 6, the insulation present around the outside of the vessel will not impede water from contacting the vessel if the containment is flooded. Hence, the outer boundary conditions for the vessel and drain line can be simulated by applying the appropriate convective heat transfer coefficient. Sensitivity studies were used to confirm that the nodalization scheme and the timesteps chosen for these calculations performed were adequate.

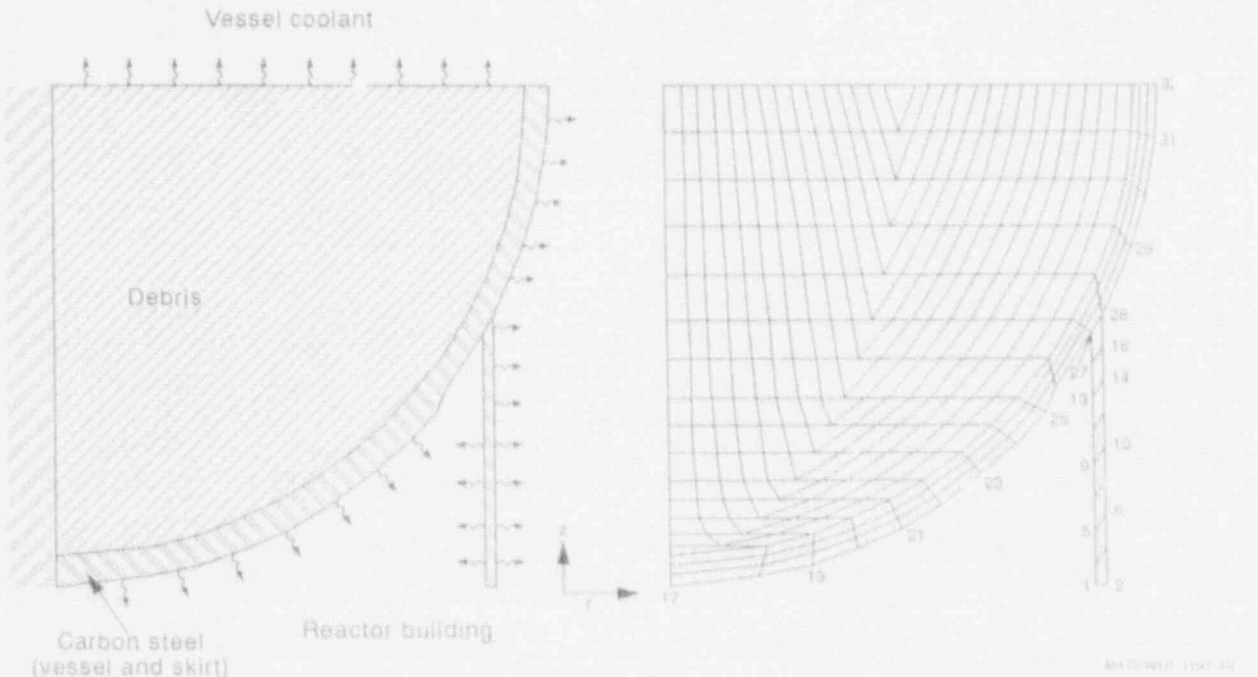

Figure 3. COUPLE mesh nodalization scheme and boundary conditions for BWR vessel thermal analysis.

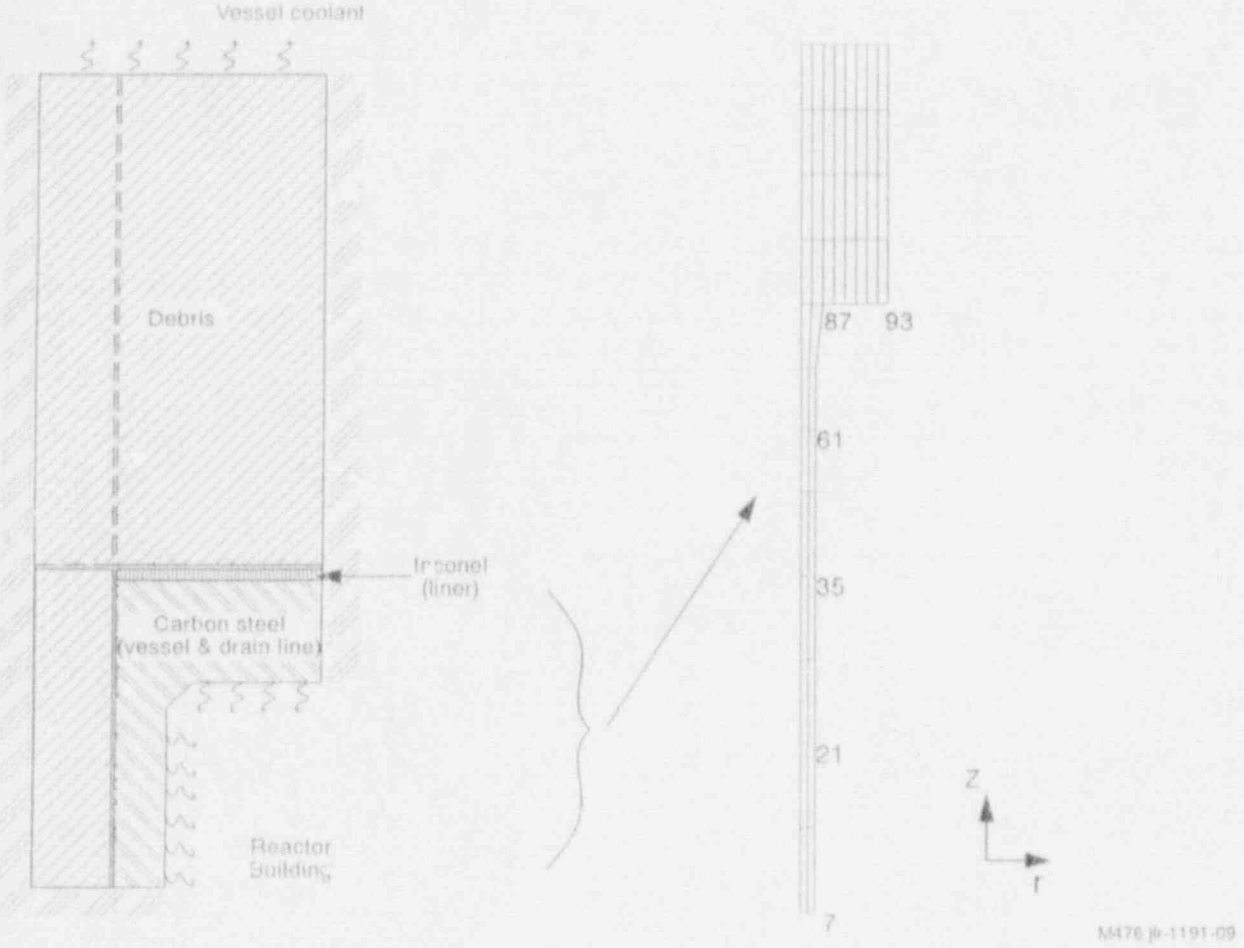

Figure 4. COUPLE mesh nodalization scheme and boundary conditions for BWR drain line thermal analysis.

Boundary conditions for each of the COUPLE meshes are also illustrated in Figure 3 and Figure 4. Heat is convected away from the top surface of the debris to the coolant in vessel subvolume 70-01. For the vessel calculations, heat is convected along the vessel outer surface (along the surface with nodes 17 through 32) and the vessel support skirt surfaces (surfaces with nodes 1 through 16) to the containment building. An adiabatic boundary condition is assumed at the center of the axisymmetric mesh. For the drain line calculations, heat is convected from the drain line and vessel outer surface (along the surfaces with nodes 7, 21, 35, 61, and 87 through 93) to the containment building. Adiabatic boundary conditions are assumed at the outer surface of the mesh, the lower edge of the drain pipe, and at the center of the axisymmetric mesh.

The rate of heat transfer from the debris region to the vessel and drain line is a strong function of the conditions at the interface between the debris and structure. The modeling of this heat transfer is simulated by including a gap between these materials. The gap heat transfer coefficient is divided into two regimes for solidified and liquefied debris. For the solidified debris

regime, the heat transfer coefficient is based upon a user-specified value that is based upon parameters, such as the debris and structure surface roughness.[7] In the liquefied debris regime, a gap heat transfer coefficient is calculated based on the rate of heat transfer through the thermal boundary layer between the liquefied debris and the structure in contact with the liquefied debris.[8] Radiative and convective heat transfer from the vessel to the stainless steel insulation is modeled by using an effective conductivity for the air between these structures.

Table 1 summarizes input assumptions and parameters used for base case calculations. Three types of debris beds are considered: a uniform debris bed that is primarily metallic (Case I); a uniform debris bed that is primarily ceramic (Case II); and a layered debris bed with metallic debris near the vessel and ceramic debris on top (Case III). These compositions were selected to envelope the possible BWR debris bed compositions during severe accidents. Sensitivity studies are being performed to consider the effects of parameters

Table 1. Input assumptions for thermal analysis

Parameter	Case I	Case II	Case III	
			Layer 1	Layer 2
Corium mass, kg				
UO_2	1200	10[illegible]00	1200	108000
Zircaloy	17804	---	17804	---
Zircaloy in ZrO_2	---	9370	---	9370
B_4C	330	174	330	174
SS	4666	2456	4666	2456
Total, kg	24000	120000	24000	120000
Relocation time period, s	5000	5000	5000	5000
Corium temperature, K	2100	2700	2100	2700
Power density, MWt/m^3	0.1	0.4	0.1	0.4
Water inventory, kg	88000	260000		0
Water temperature (saturated), K	433	559		433
System pressure, MPa	0.62	7.0		0.62
Drain line/vessel temperature, K	433	559		433
Reactor building temperature, K	373	373		373

such as debris decay heat, debris porosity, debris particle size, debris-to-surface gap resistance, reactor coolant pressure, and heat transfer conditions on the outer surface of the drain line and vessel. In this paper, results will only be reported for base Case II.

In Case II calculations, it is assumed that 50% of the corium mass relocates to the lower head. Although all of the control rods and structural materials are assumed to be included in the core debris, they represent a small fraction of the total corium mixture, which consists primarily of UO_2. Most metallic components are assumed to be oxidized. This scenario is more similar to the debris relocation postulated to have occurred during the TMI-2 event and has been postulated to occur during long term BWR station blackout events. During this event, loss of control air or dc power precludes the opening of the safety relief valves, so that coolant within the vessel causes molten material to form blockages above the core plate. When the core plate fails, the corium relocates as a fully molten mass into the lower plenum.

Other assumptions utilized within these calculations are summarized below:

- *Material Thermal Properties.* Corium thermal properties, such as specific heat, density, thermal conductivity, latent heat of fusion, fusion temperature, and viscosity of the corium are calculated in SCDAP/RELAP5 based upon the debris composition. Structural material thermal properties are also calculated in SCDAP/RELAP5 using temperature dependent functions. Before performing these calculations, carbon steel thermal properties (enthalpy, conductivity, and density) in SCDAP/RELAP5 were updated using data in Reference 1. However, it should be noted that these updated thermal properties of carbon steel are extrapolated for temperatures above 900 K.

- *Corium Porosity and Particle Size.* For Case II, a liquid debris with 0.0 porosity is assumed. However, on-going sensitivity studies are considering porosities ranging from 0.0 (corresponding to liquid) to 0.7 (corresponding to upper values observed in the TMI-2 debris).

- *Debris Relocation Time.* The debris is assumed to relocate during the first 5000 seconds of the transients simulated in Cases I and II. The relocation time for the multilayer debris simulated in Case III is based upon calculations described in Reference 9.

- *Melt Plug Distance within the Penetration Tube.* In selecting a proper drain pipe length that the melt could travel before solidification or the melt "plug" distance, it must first be established that the melt could enter the drain pipe, which is filled with reactor coolant. Applying the Taylor wavelength criteria for two fluids with unequal densities,[10] it can be established that molten debris will penetrate any tube with a diameter larger than 0.5 cm.

  Although detailed numerical calculations may provide an exact distance that the melt could penetrate a tube filled with water, it was decided to bound possible distances by neglecting the resistance and cooling from water

within the tube. The melt plug distance selected was 0.66 m. This plug distance was calculated using analytical expressions for a condition where conduction heat transfer dominated (using the model proposed by Epstein in Reference 11) and for a condition where turbulent heat transfer dominated (using the model proposed by Ostensen and Jackson in Reference 12). Although plug distances for both methods were greater than 1.0 m, preliminary analyses indicated that hot spots within the drain line occurred nearer to the vessel/drain line interface. Hence, the mesh was truncated at 0.66 m, and an adiabatic boundary condition was applied to the lower edge of the tube and debris.

- *Solid Debris to Vessel and Drain Line Thermal Contact.* The results reported in this paper assume a solid debris-to-vessel and debris-to-drain line heat transfer coefficient of 500 W/m^2K. However, the value of this heat transfer coefficient is being varied from 500 to 10,000 W/m^2K. Upper and lower bounds for this heat transfer coefficient were calculated based upon the debris-to-vessel gap thickness, the debris and vessel surface roughness, system pressure, and system temperature.[7]

- *Heat Removal from Vessel Outer Surface.* Results reported in this paper assumed that heat is removed from the vessel via natural convection and radiation. However, heat removal conditions on the vessel outer surface are also being varied to consider cases when the vessel is subjected to flooded cavity conditions.

1.3 Analytically-Developed Failure Map Models

In predicting the potential for tube and vessel failure based upon thermal response, several key questions can be answered by applying failure maps that were developed in Reference 1.

- Is the temperature and mass of the debris sufficient to induce in-vessel tube melting?

- Will the melt penetrate below the vessel?

- Will the tube fail ex-vessel?

Failure maps are used to predict failure for other penetration and vessel geometries subjected to the debris conditions input for the BWR drain line and vessel calculations.

The application of analytical methods is simplified if debris conditions and reactor geometries are viewed in terms of key parameters and dimensionless groups, such as the key geometrical dimensionless parameters listed in Table 2. The parameters in Table 2 emphasize some key geometrical differences between LWR vessel and penetration designs. For example, a BWR lower head is relatively thicker than a PWR lower head. These groups also illustrate that a Westinghouse instrument tube is one of the thickest LWR penetrations with one of the smallest flow areas and that a BWR drain line has a relatively high flow area compared to other LWR penetrations.

Table 2. Key geometrical LWR dimensionless groups

Parameter	General Electric			Babcock & Wilcox	Combustion Engineering	Westinghouse
Vessel Radius/thickness	13.1[illegible]			17.48	19.73	15.71
Penetration[a]	DN	IT	C/R	IT	NA[b]	IT
Outer radius/inner radius	1.28	1.31	1.23	1.71	NA	4.13
Effective flow diameter/outer diameter	0.78	0.67	0.43	0.52	NA	0.24
Tube cross-sectional area/ effective flow area	0.64	0.93	1.84	2.47	NA	16.06

a. Penetrations include a GE BWR drain line nozzle (DN); a G[illegible], B&W PWR, and Westinghouse PWR instrument tube (IT); and a GE BWR control rod guide tube (CR).

b. Representative Combustion Engineering plant considered does not have any lower head penetrations.

2. RESULTS

As discussed in Section 1.2, three types of debris beds are considered for base case analyses in these calculations. Final results for each of the base cases and sensitivity analyses are documented in Reference 1. Base case results for Case II, which considers vessel and drain line response following relocation of a ceramic debris at a vessel pressure of 7.0 MPa, are discussed in Section 2.1. Calculational results are then applied to failure maps to predict the response of other LWR vessel designs in Section 2.2.

2.1 Numerical Results for Base Case Ceramic Debris (Case II)

In base Case II, approximately 120000 kg of ceramic debris is assumed to relocate as a liquid within 5000 seconds to the lower head. Temperature profiles at 0.5 and 1 hour are shown in Figure 5 and Figure 6. Peak debris temperatures are predicted to occur near the center of the debris bed.

During the time that the debris is relocating to the lower head, heat is predicted to be primarily transferred from the debris bed to the coolant (Volume 70 in Figure 2), although some heat is also transferred to the reactor building cavity outside the vessel (Volume 250 in Figure 2). For example, at one hour, 91% of the heat is transferred to the vessel coolant. Figure 7 shows peak debris temperature predictions for base Case II. As shown in Figure 7, peak debris and vessel temperatures remain below 2500 K for the first two hours, although these temperatures are increasing because of decay heat. Since the solidus temperature for this eutectic is around 2700 K, the relocated debris remains solid during the time this transient is modeled.

Numerical results indicate that drain line melting occurs within 0.6 hours, but vessel temperatures remain below 1400 K during the two hours that the transient was evaluated. Peak vessel temperatures are predicted to occur near

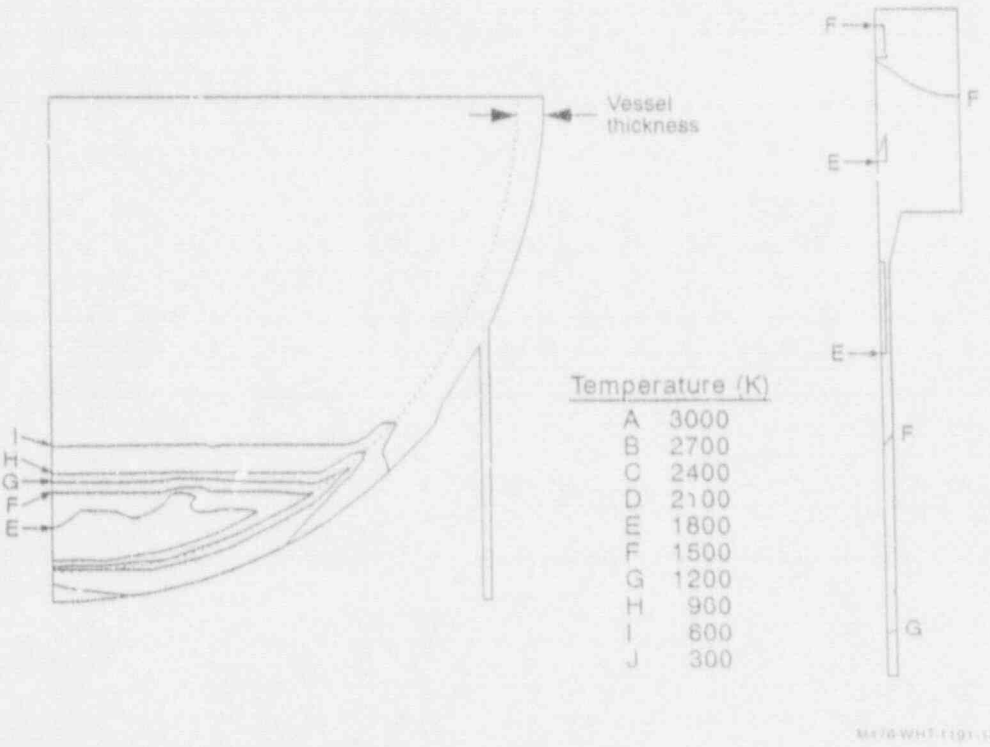

Figure 5. Vessel and drain line thermal response for base Case II at 0.5 hours.

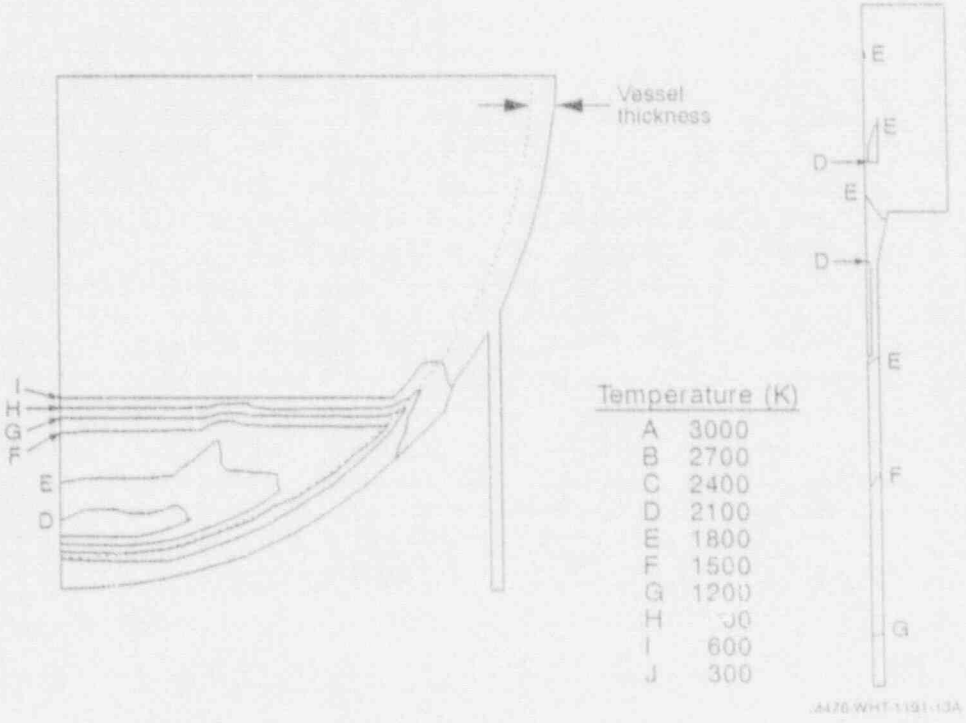

Figure 6. Vessel and drain line thermal response for base Case II at 1 hour.

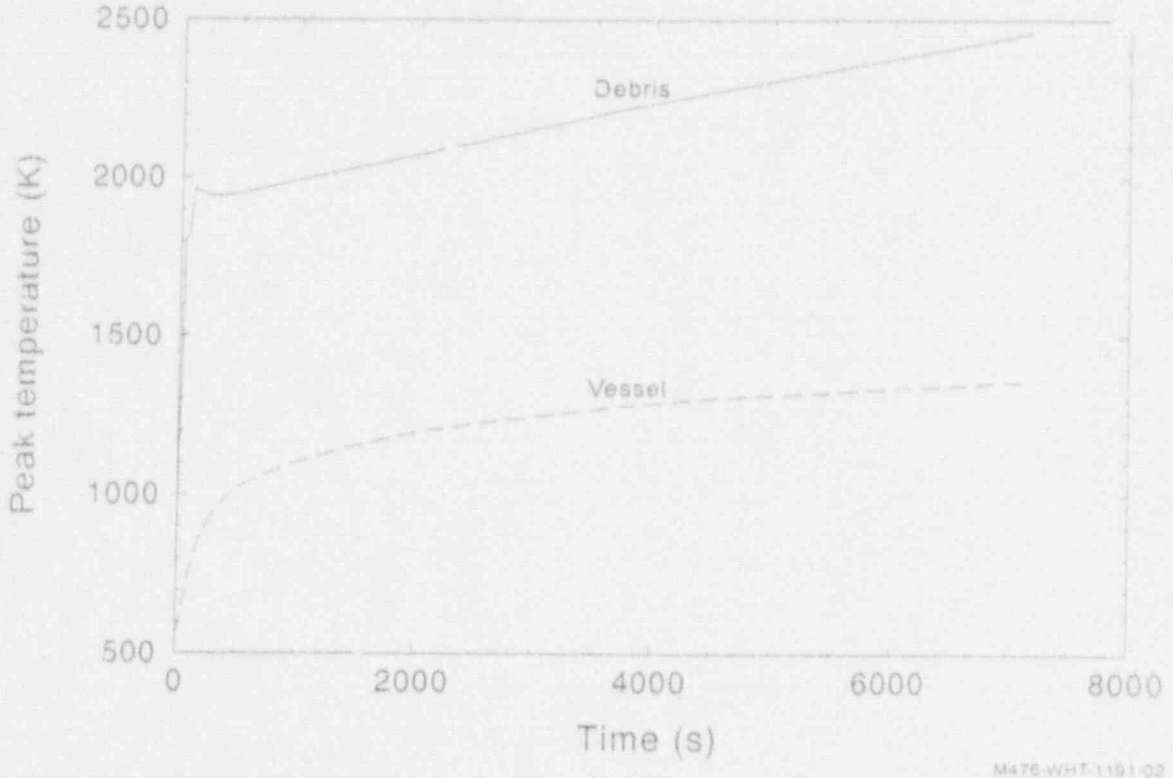

Figure 7. Peak debris and vessel temperatures for base Case II analysis.

the bottom of the vessel at the debris/vessel interface, and peak drain line temperatures are predicted to occur at a location (~14 cm) below the outer surface of the vessel lower head.

2.2 Application to Analytical Model Predictions

As discussed in Section 1, a final objective of this analysis is to extrapolate numerical calculation results to other debris conditions and geometries using analytically-developed failure maps (a detailed description of failure map development is found in Reference 1). Results are presented as responses to the key questions discussed in Section 1.3.

Is the temperature and mass of the debris sufficient to induce in-vessel tube melting?

The drain line does not contain any in-vessel structure that must be attacked by the debris before melt exits the vessel. However, in-vessel tube melting is of interest in considering the potential for melt to enter instrument tube and control rod penetrations.

Figure 8 is a failure map for predicting the potential for debris heat capacitance to induce tube failure. The abscissa for points in this failure map is the mass ratio of the tube material to the debris material that relocates to

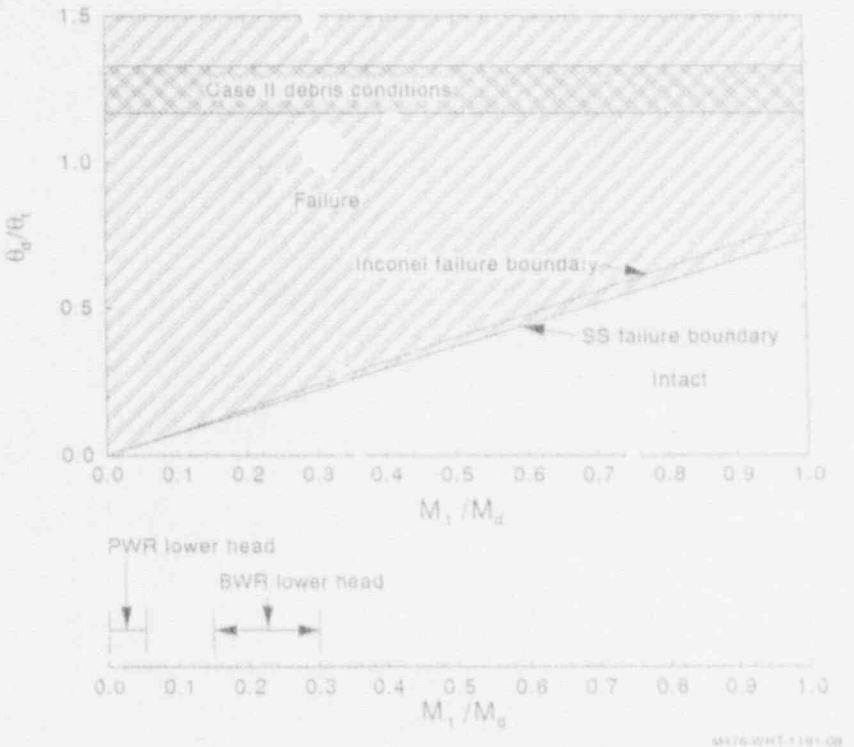

Figure 8. Failure map for determining requirements for in-vessel tube melting.

the lower head (M_t/M_d), and the ordinate for points is the ratio of the effective debris to tube temperature ratio (θ_d/θ_t), which are defined by the following equations:

$$\theta_d = T_d(0) - T_{mp/t} + \frac{L_d}{c_{pd}}; \qquad \theta_t = T_{mp/t} - T_t(0) + \frac{L_t}{c_{pt}}$$

where T(0) represents the initial temperature, $T_{mp/t}$ represents the tube melting point, L represents the latent heat of fusion, and c_p represents the specific heat capacity for the debris or tube material (denoted by the subscripts d or t). The failure region is separated from the intact region by lines that are dependent upon the tube material composition (note that only Inconel and stainless steel are considered on this map, since there are no drain line in-vessel structures). These lines were obtained by applying energy conservation to debris that relocates around vessel penetrations, which simplifies to

$$\frac{\theta_d}{\theta_t} = \frac{c_{pt} M_t}{c_{pd} M_d} \quad .$$

The lower axis in Figure 8 illustrates the range of tube to debris mass ratios that occur in PWR and BWR lower heads. Ranges are presented in this figure since the ratios are highly dependent upon the location within the lower head penetration configuration (i.e., whether along the periphery or the central

region of the reactor vessel). Figure 8 contains a cross-hatched horizontal bar that corresponds to Case II debris bed/tube effective temperature ratios. As indicated in Figure 8, this cross-hatched region falls within the failure region for tube-to-debris mass ratios found in PWR and BWR designs. Hence, tube melting is predicted to occur in both BWR and PWR lower heads for the highly ceramic base Case II debris bed compositions considered.

Will the melt travel through the penetration to a distance below the lower head?

Reference 1 discusses the methodology used to predict the distance that the melt will travel in a penetration before it solidifies. As discussed within Reference 1, melt penetration distances are highly dependent upon whether conduction or turbulent heat transfer dominates heat transfer between the melt and the tube. Some of the parameters identified in Reference 1 for predicting penetration distance, X_p, of a melt at a specified temperature through a tube at an initial temperature are shown in Figure 9 and include the distance required for the melt to travel till it has gone beyond the lower head, l_p; the effective diameter for melt flow within a tube, d_e; and the Peclet number for the debris, Pe_d, which is a function of the melt velocity, v_d, melt thermal diffusivity, α_d, and d_e.

Figure 10 contains a map for predicting melt penetration distance. This map is developed in terms of the dimensionless Peclet number and the ratio of the predicted melt penetration distance, X_p, to the tube effective diameter, d_e. The large horizontal bar contains bounding values for the ratio of the distance that the melt must travel through different LWR penetrations so that it is below the lower head, l_p, to the tube effective diameter for melt flow, d_e. The two curves in Figure 10 represent penetration distances predicted for ceramic flows using the bulk freezing model (in which turbulent heat transfer is assumed to dominate)[12] and the conduction model (in which conduction heat transfer is assumed to dominate).[11] As discussed in Reference 1, molten debris is predicted to travel much longer distances if conduction heat transfer dominates since the crust that is assumed to form along the wall retards heat transfer between the tube and the molten debris.

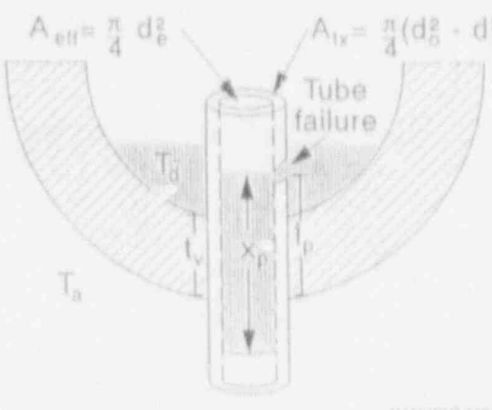

Figure 9. Geometry of tube and vessel configuration for developing melt penetration and ex-vessel tube failure maps.

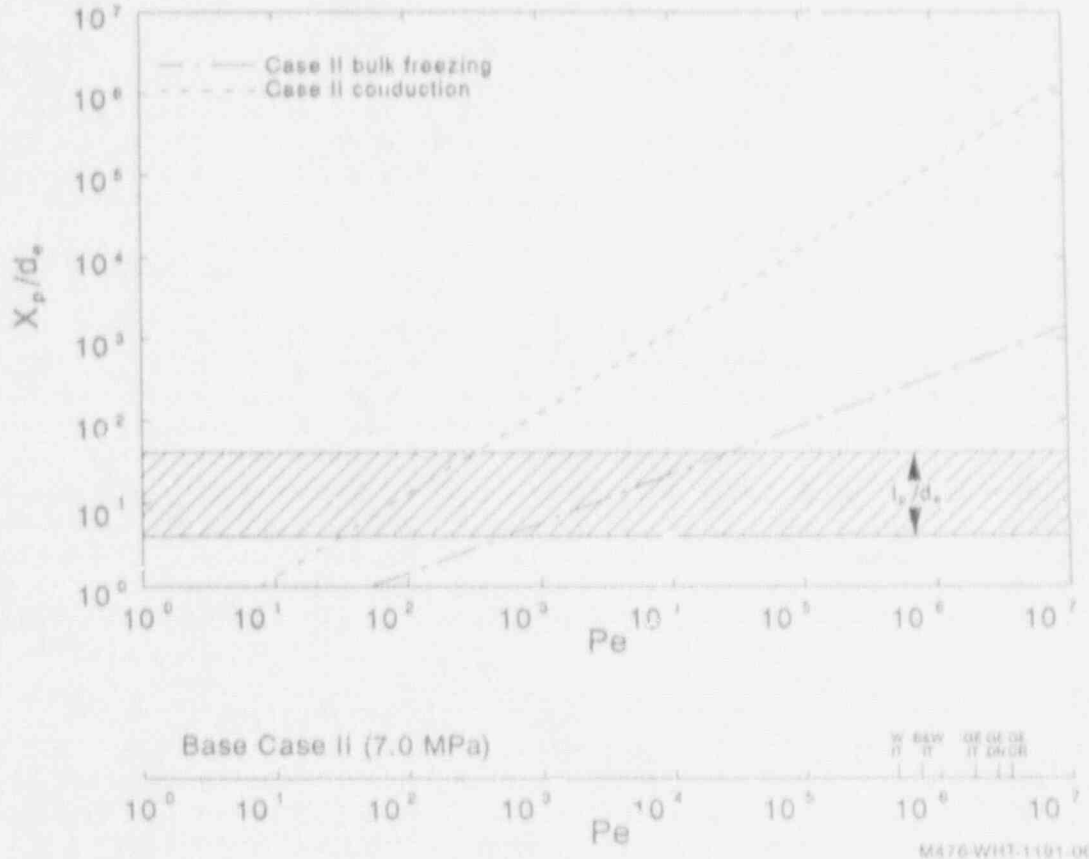

Figure 10. Comparison of melt penetration distances assuming full effective diameter flow.

Lower axes in Figure 10 are marked to indicate Peclet numbers calculated for base Case II debris conditions and various penetrations found within LWR lower heads: a GE BWR instrument tube (GE IT), a BWR drain line nozzle (GE DN), a GE BWR control rod guide tube (GE CR), a Westinghouse PWR instrument tube (W IT), and a B&W PWR instrument tube (B&W IT). As indicated on these axes, higher Peclet numbers (and thus longer melt distance predictions) occur for penetrations with larger effective diameters (e.g., a GE control rod guide tube and a GE drain line).

As shown in Figure 10, the melt is predicted to travel distances significantly longer than the bottom of the lower head if the melt follows conduction model predictions. Even if the melt behaves according to bulk-freezing model predictions, the melt is predicted to travel below the lower head for the penetrations considered.

Will ex-vessel tube failure occur?

In Figure 11 is shown a failure map for predicting tube equilibrium temperature using a heat balance. The abscissa for points in this map is the ratio of the tube cross sectional area, A_{xx}, to the tube effective area for melt flow, A_{eff}, as defined in Figure 9. The ordinate for points in this map is the

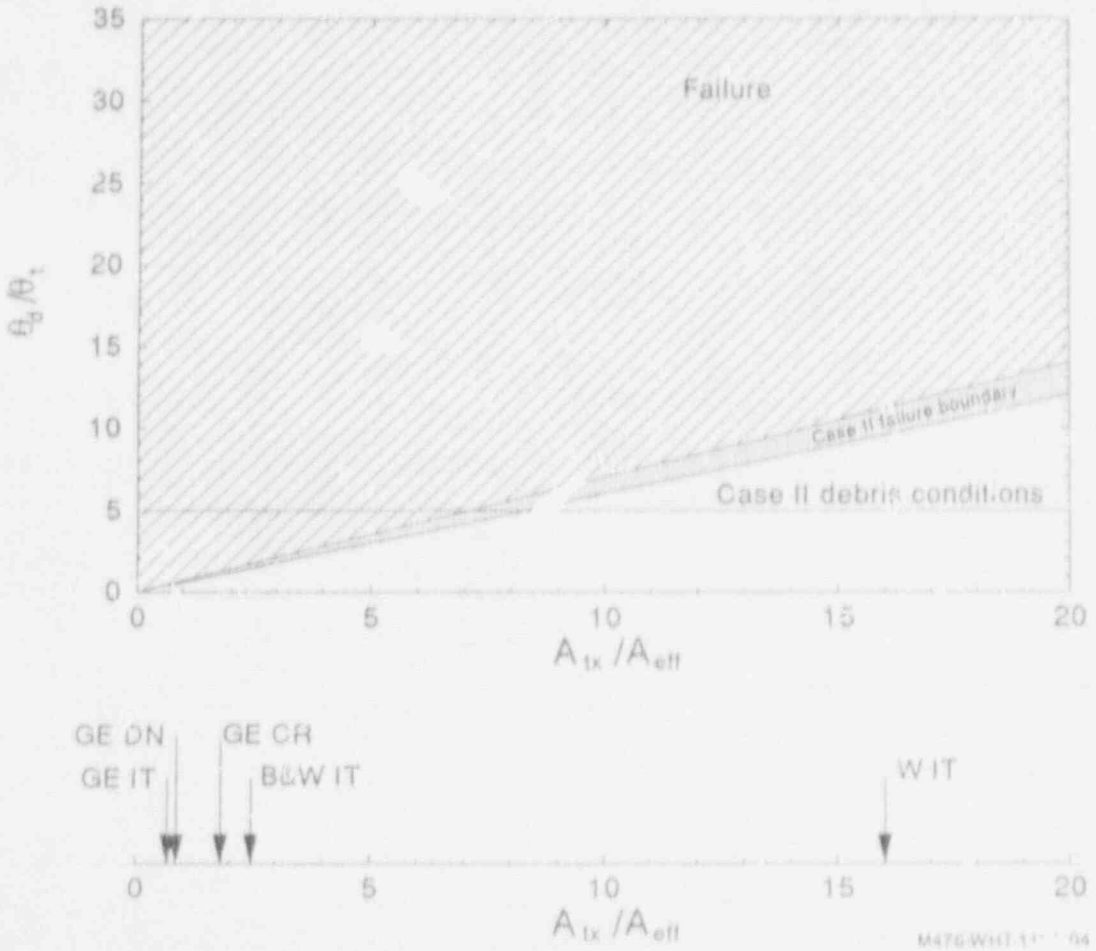

Figure 11. Failure map obtained from heat balance between tube and debris.

ratio of the effective debris to tube temperature ratio, which are given by the following equations:

$$\theta_d = T_d(0) - T_{f/t} + \frac{L_d}{c_{pd}}$$

$$\theta_t = T_{f/t} - T_t(0) \quad .$$

where $T_{f/t}$ represents the tube failure temperature, which is the temperature where the tube material's ultimate strength decreases to zero.

In this map, the failure region is separated from the intact region by lines that are dependent upon the debris composition and the tube material. These lines

were obtained by applying energy conservation to debris that relocates into the penetrations, which simplifies to

$$\frac{\theta_d}{\theta_t} = \frac{A_{tx}}{A_{eff}} \frac{c_{pt}\,\rho_t}{c_{pd}\,\rho_d} \quad .$$

The lower axis in Figure 11 illustrates the range of area ratios that exist in LWR penetration [illegible]uming that the debris fills the entire cross-section of area available for [illegible]flow). The axis emphasizes the point that PWR instrument tubes have relat[illegible]hick walls and relatively low areas available for melt flow.

Consistent with the numerical results for Case II, the failure map indicates that the drain line will fail if subjected to this debris composition. However, the map also indicates that the Westinghouse penetration tube would remain intact if subjected to base Case II ceramic debris.

Figure 12 contains a failure map for predicting tube failure by considering debris decay heat and radiation heat transfer to the reactor containment building. The abscissa for points in this map is the ratio of the tube [illegible]ective

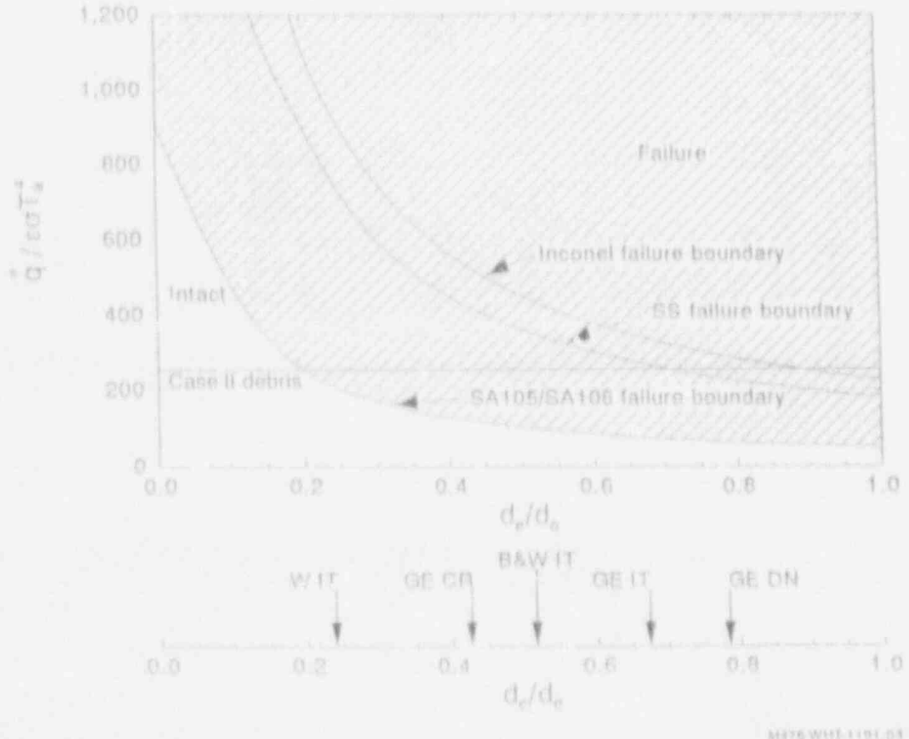

Figure 12. Failure map obtained considering debris decay heat and radiation to containment.

diameter for melt flow to the tube outside diameter (see Figure 9). The ordinate for points in this map is the ratio of the debris heat flux (q_d) to the tube emissivity (ϵ), the Stefan Boltzmann constant (σ), and the containment temperature (T_c). In this map, the failure region is separated from the intact region by lines that are dependent upon the tube material. Note that the failure region for SA105/SA106 steel is considerably larger than that for Inconel or stainless steel, because the temperatures at which the ultimate strength for Inconel or stainless steel go to zero (~1450 K for Inconel and ~1370 K for stainless steel) are considerably higher than for SA105/SA106 steel (~1000 K).

The lower axis in Figure 12 illustrates the range of diameter ratios that exist in LWR penetrations (assuming that the debris fills the entire cross-section of area available for melt flow). This axis emphasizes the point that drain line penetrations have a considerably larger effective diameter for melt flow than other LWR penetrations.

Consistent with numerical results for base Case II, this failure map also indicates that the drain line will fail if subjected to either of these debris compositions. However, this map also indicates all of the other LWR penetrations will remain intact if subjected to Case II ceramic debris. Thus, the BWR drain line penetration is more likely to fail than other penetrations because of its material composition and geometry.

3. CONCLUSIONS

A study is being performed to assess the two-dimensional thermal and mechanical response of a BWR drain line penetration and vessel when subjected to relocated debris for a wide range of accident conditions. Results to date from these calculations indicate that the drain line will reach failure temperatures before the vessel fails if subjected to base Case II ceramic debris conditions. Two-dimensional results are in agreement with results obtained with analytically-developed failure maps for the base case ceramic (Case II) debris conditions.

Application of failure maps to other LWR geometries indicate that in-vessel tube melting will occur following Case II debris relocation in any of the BWR and PWR vessel designs considered. Furthermore, tube melt is predicted to travel distances well below the lower head for base case debris conditions in any of the reference PWR penetrations (Westinghouse instrument tubes, B&W instrument nozzles, GE control rod guide tubes, GE instrument tubes, and GE drain line penetrations were considered). However, failure maps suggest that the result that ex-vessel tube temperatures exceed the penetration's ultimate strength is specific to the BWR drain line because of its material composition and relatively large effective diameter for melt flow.

4. REFERENCES

1. J. L. Rempe et al., *Light Water Reactor Lower Head Failure Analyses*, NUREG/CR-5642 (Draft), EGG-2618, December 1991.

2. United States Steel, *Steels for Elevated Temperature Service*, ADUSS 43-1089-05, December 1974.

3. American Society of Mechanical Engineers, "Boiler and Pressure Vessel Code," Section III, Division I, Appendix I, Table I-3.1, 1989.

4. C. M. Allison and E. M. Johnson (ed.), *SCDAP/RELAP5/MOD2 Code Manual, Volumes 1, 2, and 3*, NUREG/CR-5273, EGG-2555, September 1989.

5. Hibbitt, Karlsson & Sorenson, Inc., ABAQUS User's Manual, Version 4.8, Providence, RI, 1989.

6. R. E. Henry et al., "Cooling of Core Debris within the Reactor Vessel Lower Head," Annual Meeting of the American Nuclear Society, Orlando, Florida, June 2-6, 1991.

7. J. Garnier, *Ex-Reactor Determination of Thermal and Contact Conductance*, NUREG/CR-0330, April 1979.

8. F. Mayinger et al., *Examination of Thermal-Hydraulic Processes and Heat Transfer in a Core Melt*, BMFT RS 48/1, 1976, Institute für Verfahrenstechnik der T.U. Hanover.

9. S. A. Hodge, J. C. Cleveland, and T. S. Kress, *External Flooding of a BWR Reactor Vessel as a Late Accident Mitigation Strategy*, ORNL/NRC/LTR-91/0, August 1991.

10. F. J. Moody, *Introduction to Unsteady Thermofluid Mechanics*, New York: John Wiley & Sons, 1990.

11. M. Epstein, "Heat Conduction in the UO_2-Cladding Composite Body with Simultaneous Solidification and Melting," *Nuclear Science and Engineering*, *51*, 1976, pp. 310-323.

12. R. W. Ostensen and J. F. Jackson, *Extended Fuel Motion Study*, ANL-RDP-18, July 1973.

ON THE PREDICTION OF STEAM EXPLOSIONS ENERGETICS

by

T. G. Theofanous, S. Angelini*, R. Buckles and W. W. Yuen*
Center for Risk Studies and Safety
Department of Chemical and Nuclear Engineering
University of California, Santa Barbara
Santa Barbara, CA 93106

Abstract

The quantitative aspects of "premixing" and rate of "fragmentation" in steam explosions are addressed. For "premixing" the experiments are focused on the water-depletion phenomenon predicted to occur within the two-dimensional, three-phase, transient mixing zone of a high temperature melt poured into a pool of coolant. These experiments are scaled to yield similar water-depletion regimes as expected in the lower plenum of the reactor vessel. The first, preliminary, results are consistent with numerical predictions. For "fragmentation" the experiments are focused on observing single exploding melt drops in a steady, elevated pressure field, prototypic of an escalated explosion. The first, preliminary, data demonstrate the interplay between the "thermal" and "hydrodynamic" components of the fragmentation-driving mechanism(s), and provide the promise that on such a basis appropriate constitutive laws can be made available for the numerical computation of the escalation and propagation of steam explosions.

1. INTRODUCTION

Several analytical/numerical tools are now available to compute the "premixing," and once a trigger has been supplied, the "propagation" of steam explosions (Medhekar et al. 1989). The "premixing" computations are useful in defining the range of consistencies (volume-fraction distribution of melt, steam, and water) possible for given initial and boundary conditions, and this has been used in conjunction with a conservative treatment of energy conversion (thermodynamically ideal) to estimate upper bounds on the energetics of such explosions (Theofanous et al. 1987). This work emphasized the importance of verifying these predictions experimentally, and the major component of the present effort is to fulfill this need.

The "escalation" and "propagation" calculations are useful in characterizing what premixtures, under given triggers, can support detonations and in providing estimates of resulting pressures. In particular, large scale mixing zones evolve into highly non-uniform, highly voided configurations, and such propagation calculations have indicated significant effects on the explosion propagation dynamics and peak pressures reached (Medhekar et al. 1989). The basic feature in these computations is the fine scale fragmentation (and mixing with the surrounding coolant), which is responsible for providing the pressure feedback necessary to develop the explosion, or rather its rate as modelled in terms of the "driving" parameters. It is known that this "driving"

* Also with the Department of Mechanical Engineering, UCSB

of fragmentation will have "thermal" and/or "hydrodynamic" components, but the data needed to delineate these regimes are not yet available. Most calculations make use of data (and related formulations) from the hydrodynamic regime—i.e. obtained under isothermal conditions. On the other hand, it is known that single drops can thermally explode, given a sharp pressure pulse (a trigger). What is needed is fragmentation-rate data in a sustained pressure field, as in the "reaction" zone of a propagating explosion, with the pressure level and melt temperature being the parameters. Such observations, of course, are not possible in a real explosion; however, the condition can be simulated in a hydrodynamic shock tube and a single drop that can be observed in the fine detail that is necessary. The second component of this effort is to fulfill this need.

Our basic analytical tools are PM-ALPHA and ESPROSE for the premixing and propagation calculations, respectively. The corresponding experimental facilities are MAGICO and SIGMA. In this presentation we include a description of the experimental facilities, related instrumentation, and a set of initial experimental results, which have just been obtained (preliminary, therefore). An indication of the future experimental program is also provided.

2. PREMIXING EXPERIMENTS

The basic idea for this experiment is to test the 3-fluid formulation (field equations and constitutive laws) in PM-ALPHA by isolating the melt particle size effects; this is done by using fixed size, solid particles instead of a melt. Once this is done, one could then approach the process of breakup, as it would occur with melt pours, with all other parts of the model fixed. The point is that the various degrees (varying in space and time) of particulation in an experiment cannot be measured directly (and the relevant breakup processes are not well understood yet), but they could possibly be inferred, once all other parts of the model have been verified experimentally. In all other respects the experiments are intended to simulate premixing in the lower plenum of a pressurized water reactor.

As already mentioned, the key "figure of merit" in premixing results is the space-time distribution of the three fluids in the mixing zone: melt, steam, and water. Thus local volume fraction measurements are needed in a 2-dimensional, hostile (very high temperatures), and highly transient environment. This experimental difficulty is responsible for the absence (until now) of relevant data in this area. A great deal of the present effort has been devoted to overcoming this obstacle, which eventually we did with the development of FLUTE (Angelini et al. 1991).

In the experiment mm-size hot steel spheres are poured, in tens-of-kilogram quantities, into a pool of saturated water. The interaction is followed by high-speed video equipment and local measurements of the volumetric liquid (water) concentration (using FLUTE). Similarity to reactor conditions is obtained by using a 1/8-scale geometrically similar lower plenum and choosing particle sizes, initial temperatures, and pour rates that produce (numerically, using PM-ALPHA) similar water depletion (voiding) patterns as in the reactor. The experiments reported here were run with 9 kg of 1.5 mm steel particles at initial temperatures of 993 and 1073 K. Future experiments will explore in detail particle size and temperature, pour diameter, pour area density, and internal structures in the lower plenum.

A schematic of the experimental facility (called MAGICO) is shown in Figure 1. Once in the "core" region the particles are suddenly released into the lower plenum by aligning the holes in the two "core support" plates as shown. A view of the facility in operation is given in Figure 2.

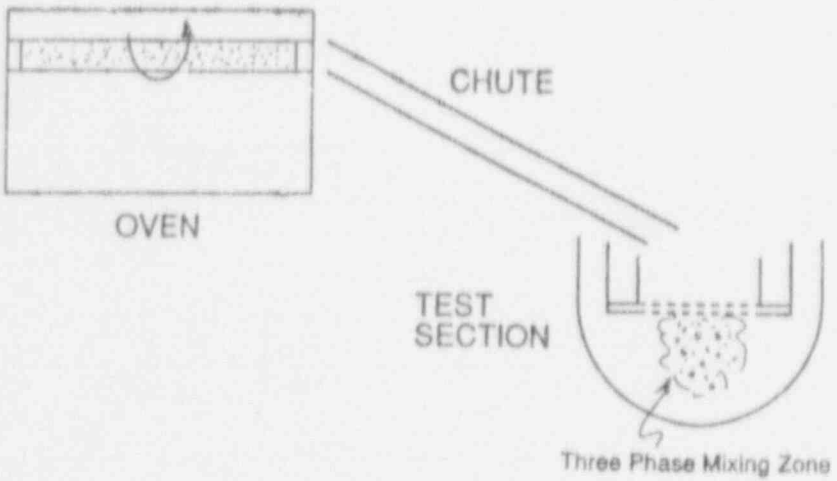

Figure 1. Schematic of the MAGICO experiment.

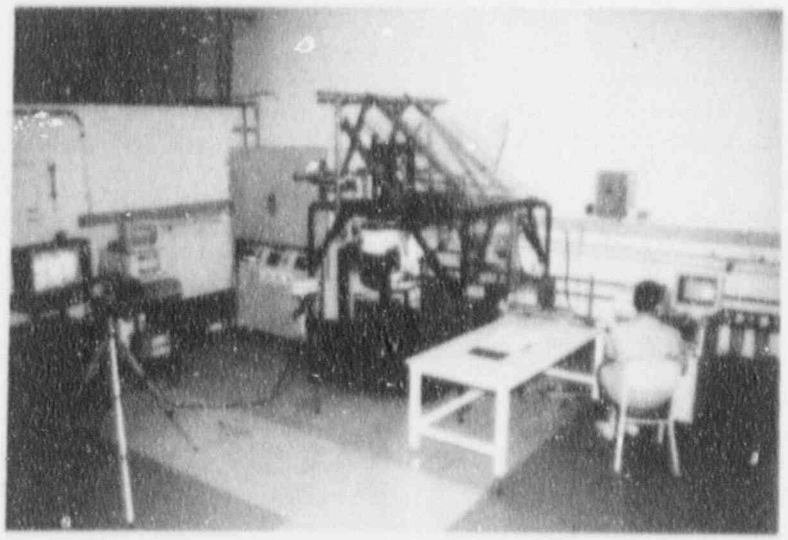

Figure 2. The MAGICO experiment in operation.

The first experimental data, from shake-down runs #8 and #16 are shown together with PM-ALPHA predictions in Figures 3, 4 and 5. In Figures 3 and 4 the average void fraction in the premixing zone was obtained from the observed water level change in the pool. In Figure 5 the transient void fraction measured is at a position of 5 cm below the initial water level along the test section vertical axis. It is noteworthy that these are *a priori* predictions, using the standard features of PM-ALPHA code, as already published (Medhekar et al. 1989). Also, it should be noted that the data in Figure 5 were obtained with the original version of FLUTE, capable of rates up to only 150 Hz (hence the rough character of the signal). A new version now coming on line will provide rates of up to 100,000 Hz, and thus the possibility of simultaneous measurements in

2 or 3 different locations still at adequately high rates (to essentially continuous signal). These experiments provide the first experimental demonstrations of the water-depletion phenomenon in premixing, as originally conjectured by Henry and Fauske (1981) and subsequently quantified by Amarasooriya and Theofanous (1987).

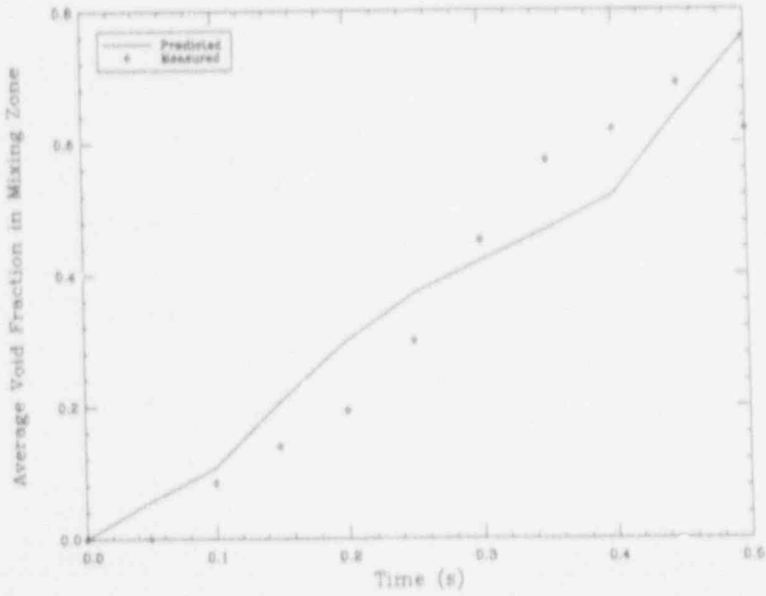

Figure 3. Comparison of measured and predicted average void fraction transients, in the mixing zone, for shake-down run #8 in MAGICO. Steel particles, 1.5 mm, at 993 K.

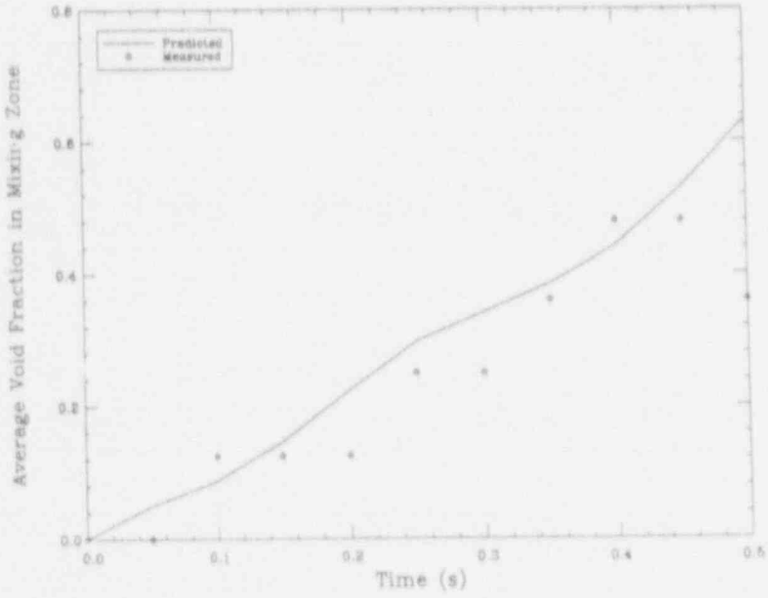

Figure 4. Comparison of measured and predicted average void fraction transients, in the mixing zone, for shake-down run #16 in MAGICO. Steel particles, 1.5 mm, at 1075 K.

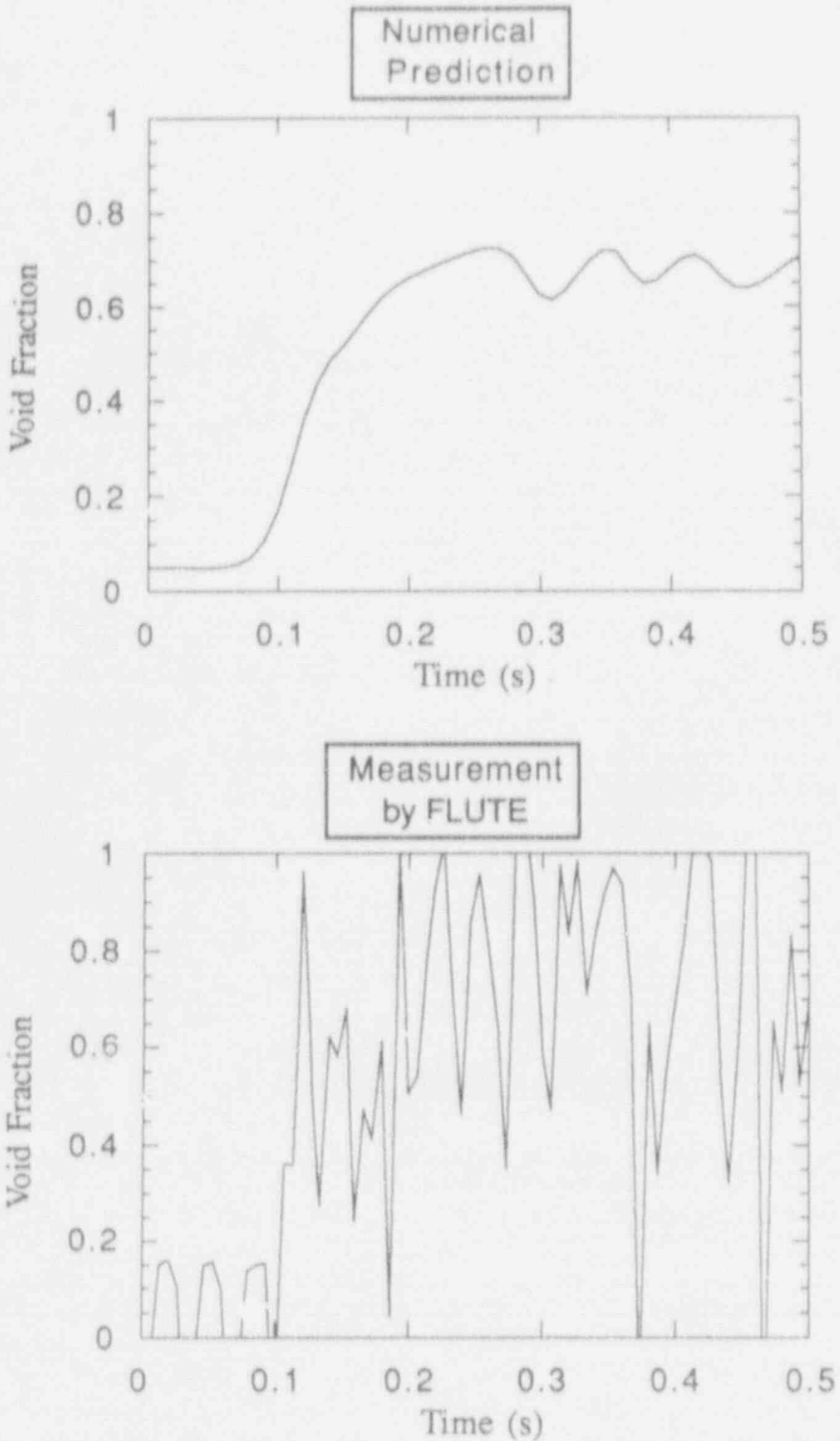

Figure 5. Comparison of measured and predicted local (5 cm below the initial water level on the centerline) void-fraction transients for shake-down run #8 in MAGICO.

3. FRAGMENTATION EXPERIMENTS

The basic idea for this experiment is to create, in a shock tube, the pressure field of a propagating steam explosion, such that exploding single melt drops can be observed under the relevant conditions. From such detailed observations fragmentation rates can be determined and on this basis appropriate, generally valid, constitutive laws be formulated. Such formulations will, in turn, allow rational investigations of the detonation phenomena, and addressing such issues as "pressure cutoff," role of void fraction in mitigating/limiting explosions, and peak detonation pressures in large scale explosions with reactor materials.

The shock-tube facility (called SIGMA) is shown in Figure 6. The cross section is 5 cm square, and it can provide pressure waves of up to 100 MPa and 2.5 ms duration. The melt drop generator releases single molten metal drops of precisely controlled mass (currently 1g) and temperatures (currently up to 1,000 °C but we are working toward even higher temperatures). The generation of the pressure wave is synchronized with the drop release such that the shock-drop impact occurs within the view of a small window, and there is still enough time to observe the fragmentation process, for time delays of up to 2.5 ms following the initial impact. The progression of fragmentation is obtained from flash X-ray radiographs obtained at different delay times, following impact, in a series of repeat runs (with all other conditions kept the same). Besides, the final debris is collected to determine the fragment size distribution and the rate of cooling (from metallographic examinations).

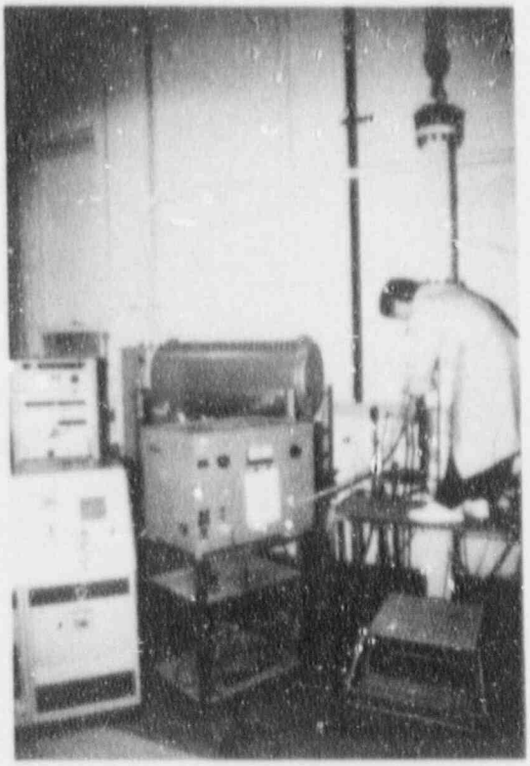

Figure 6. A view of the SIGMA facility.

Here we report some initial runs, using 1g tin drops at 800 °C under 6.6 or 20 MPa pressure waves (Figure 7). Also, we have some previous data with molten tin at 425 °C under 20 MPa (Figure 8) and previously obtained a rather detailed set of data with mercury droplets, isothermal conditions (Figure 9) and pressure waves up to 50 MPa. In future experiments we also will consider the effects of coolant void fraction and elevated initial pressure.

From these figures we see three significantly different fragmentation regimes. First, in the isothermal runs (Figure 9), we observe a gradual development of a downstream cloud from a diminishing-in-size "lumped" mass. The low-temperature tin experiments (Figure 8), at early times show a similar behavior, but at 2 ms the mass distribution is quite different. Finally, the high-temperature tin drops (Figure 7) at high pressures are similar also, but at 6.6 MPa exhibit a still different behavior. Here the drop seems to explode (fragment) up and against the flow. Clearly, many more runs are necessary to fully elucidate these "thermal" vs "hydrodynamic" mechanisms and to quantify respective regimes.

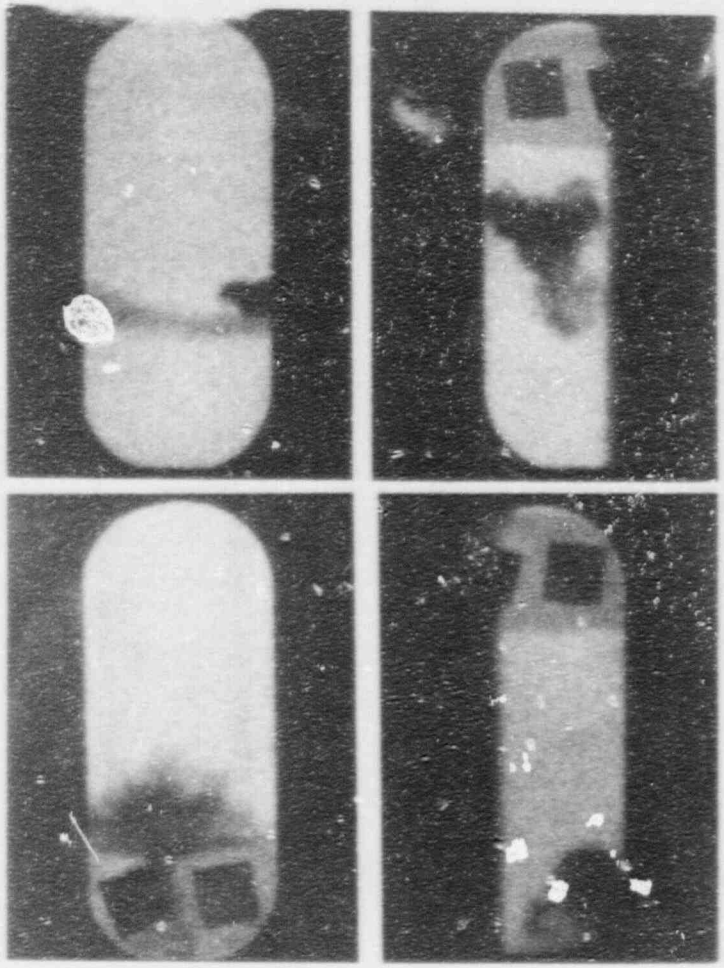

Figure 7. Fragmentation of a molten tin drop at 800 °C under 6.6 and 20 MPa pressure waves and with delay times of 1, 1, 1.5 and 2 ms.

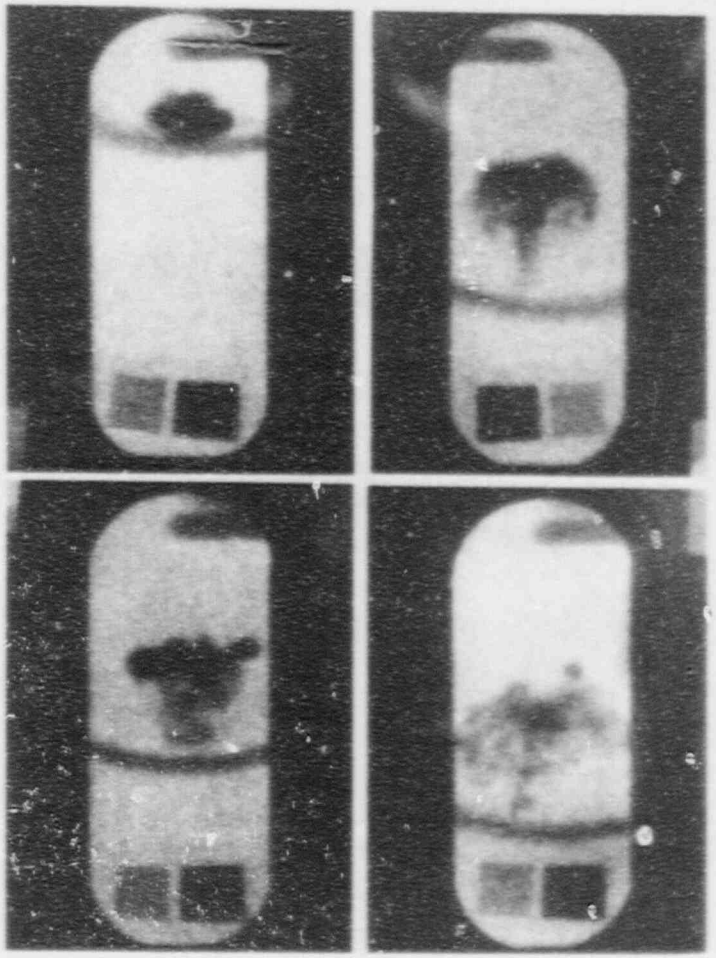

Figure 8. Fragmentation of a molten tin drop at 425 °C under 20 MPa pressure waves and with delay times of 0.5, 1.5, 1.6 and 2 ms.

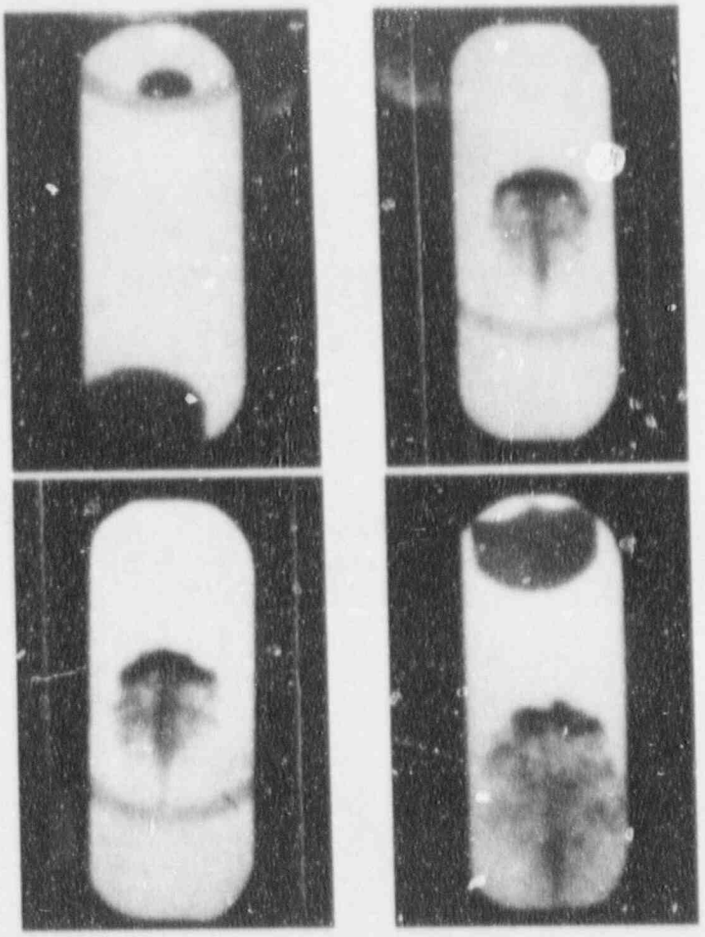

Figure 9. Fragmentation of a mercury drop at isothermal conditions under 33 and 50 MPa pressure waves and with delay times of 0, 1.3, 1.5 and 2 ms.

4. CONCLUSIONS

This is a predominantly experimental program addressing important needs in (a) verifying the 3-field treatment of premixing, as in PM-ALPHA, and (b) providing applicable experimental data for the kinetics of fragmentation in propagating explosions. From the initial experimental data available at this time we can conclude the following:

1. Major experimental challenges, in both areas, have been successfully met, and the facilities/instrumentation are ready for production runs.
2. The water-depletion phenomenon, in premixing, has been experimentally demonstrated, and comparisons with PM-ALPHA predictions are very promising.
3. The interplay between "thermal" and "hydrodynamic" fragmentation regimes under proper explosion escalation/propagation conditions has been experimentally demonstrated, and a new theoretical description accounting for this interplay appears to be required (it is to be developed once the data base is sufficient).

5. REFERENCES

1. Amarasooriya, W.H. and T.G. Theofanous 1987, "An Assessment of Steam-Explosion-Induced Containment Failure. Part III: Expansion and Energy Partition," *Nuclear Science and Engineering*, **97**, 296-315 .

2. Angelini, S., W.M. Quam, W.W. Yuen and T.G. Theofanous 1991, "FLUTE: FLUorescent tEchnique for Two-Phase-Flow Liquid-Fraction Measurements," To appear in Proceedings 1991 ANS Winter Meeting, San Francisco, CA. Nov. 1991.

3. Henry, R.E. and H. K. Fauske 1981, "Required Initial Conditions for Energetic Steam Explosions," *Fuel-Coolant Interactions, HTD-V19*, American Society of Mechanical Engineers.

4. Medhekar, S., W.H. Amarasooriya and T.G. Theofanous 1989, "Integrated Analysis of Steam Explosions," Proceedings Fourth International Topical Meeting on Nuclear Reactor Thermal-Hydraulics, Karlsruhe, FRG, Oct. 10-13, 1989, Vol. 1, 319–326.

5. Theofanous, T.G., B. Najafi and E. Rumble 1987, "An Assessment of Steam-Explosion-Induced Containment Failure. Part I: Probabilistic Aspects," *Nuclear Science and Engineering*, **97**, 259-281.

SCDAP/RELAP5/MOD3 Code Development and Assessment[a]

C. M. Allison, C. H. Heath, L. J. Siefken, J. K. Hohorst
Idaho National Engineering Laboratory

ABSTRACT

The SCDAP/RELAP5 computer code is designed to describe the overall reactor coolant system (RCS) thermal-hydraulic response, core damage progression, and fission product release and transport during severe accidents. The code is being developed at the Idaho National Engineering Laboratory (INEL) under the primary sponsorship of the Office of Nuclear Regulatory Research of the U.S. Nuclear Regulatory Commission (NRC). The current version of the code, SCDAP/RELAP5/MOD3, was created in January, 1991 and reflects the merger of SCDAP/RELAP5/MOD2.5 damage progression and fission product transport models with RELAP5/MOD3 system thermal-hydraulics models. Systematic assessment of modeling uncertainties is currently underway. This paper describes the results of that assessment. Results presented include (a) a summary of important results from code-to-data comparisons , (b) estimates of modeling and experimental uncertainties, and (c) proposed model improvements to resolve the deficiencies identified in the assessment.

Introduction

The SCDAP/RELAP5 computer code is designed to describe the overall reactor coolant system (RCS) thermal-hydraulic response, core damage progression, and fission product release and transport during severe accidents up to the point of reactor vessel or system failure. The code is being developed at the Idaho National Engineering Laboratory (INEL) under the primary sponsorship of the Office of Nuclear Regulatory Research of the U.S. Nuclear Regulatory Commission (NRC). The code also includes models developed by the U.S. Department of Energy.

Status

SCDAP/RELAP5/MOD3 was created in January, 1991. A systematic code developmental assessment effort is now underway for both the RELAP5/MOD3 thermal-hydraulic models and the SCDAP early phase damage progression models. The results of the assessment will be described in new volume being added to the code manual draft NUREG/CR reports[1]. This volume, with the addition of new RELAP5/MOD3 volumes[2] describing the system thermal-hydraulics models will be be issued as draft NUREG/CR reports this fall. A total of ten volumes will be issued with six volumes describing the systems thermal-hydraulics models - theory, models and correlations

[a]Work supported by the U.S. Nuclear regulatory Commission, Office of Research, under DOE Contract No. DE-AC07-76ID01570.

used, numerics, developmental assessment, and user guidelines and four volumes describing damage progression and fission product models - theory, material properties, developmental assessment, and user guidelines.

Code Capabilities

SCDAP/RELAP5/MOD3 is the result of merging RELAP5/MOD3 with SCDAP and TRAP-MELT2[3] models from SCDAP/RELAP5/MOD2.5. The RELAP5 models calculate the overall RCS thermal-hydraulics, control system interactions, reactor kinetics, and the transport of noncondensible gases, fission products, and aerosols. The SCDAP models calculate the damage progression in the core structures, the formation, heatup, and melting of debris, and the creep rupture failure of the lower head and other RCS structures. The TRAP-MELT models calculate the deposition of fission products upon aerosols or structural surfaces; the formation, growth, or deposition of aerosols; and the evaporation of species from surfaces.

These models are explicitly coupled at each time step as shown in Figure 1. RELAP5 models provide thermal-hydraulic boundary conditions to the SCDAP and TRAP-MELT models, the SCDAP models describe the source terms for heat and mass transfer from the structures including fission product release and hydrogen production, and the TRAP-MELT models describe the mass transfer of fission products or aerosols carried in the fluid or deposited on walls. Surface-to-surface radiation heat transfer within the core region is modeled using an enclosure model developed for SCDAP[4]. A radiation model developed specifically for RELAP5 heat structures is used outside the core.

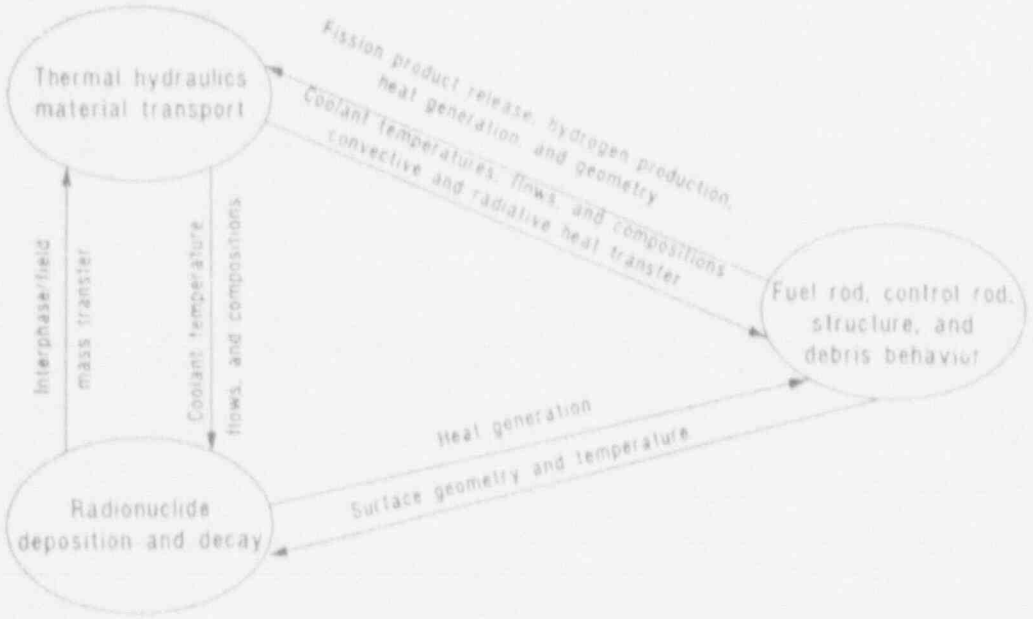

Figure 1 - Coupling Between RELAP5 System Thermal-hydraulic Models, SCDAP Damage Progression Models, and TRAP-MELT2 Fission Product Models.

All of the capabilities of RELAP5/MOD3 have been maintained to describe the response of the RCS during accident initiation and the severe accident portions of the accident. The hydrodynamics model uses a one dimensional, nonhomogeneous, nonequilibrium, two-fluid approach. Multidimensional flow for low flow rate or natural circulation conditions can be modeled through a simplified crossflow junction option. In this option, the full two-fluid model equations are applied in the primary flow direction while simplified equations, neglecting virtual mass and cross-product momentum fluxes, are applied in the secondary flow directions. Comparisons of the model against full three-dimensional two-fluid models in TRAC[5] and a special version of RELAP5 being developed for DOE[6,7] show good agreement for predicted flow patterns while requiring significantly less computer time.

The code uses representative structures to model the core during the early phases of an accident. Specific representative structures include (a) UO_2-Zircaloy fuel rods, (b) Ag-In-Cd, stainless steel clad control rods with surrounding Zircaloy guide tubes, (c) B_4C, stainless steel clad control rods/blades, and (d) a generic structural model which is used to represent BWR channel boxes and other structures subject to oxidation and melting. The code also includes a fuel rod model with a central tungsten heater element designed specifically for electrically heated experiments. RELAP5 heat structures can also be used to model those structures where oxidation and melting can be neglected. These representative structures incorporate models to treat (a) one-dimensional (radial) and two-dimensional (radial and axial) heat conduction, (b) oxidation, (c) nuclear heat generation, (d) fission product release (fuel rods only), and (e) changes in geometry including cladding deformation and rupture (fuel rod models only), fragmentation, liquefaction, and melt relocation.

Lumped parameter and detailed porous body structure models are used to bound the core and vessel behavior during the latter phases of an accident[8]. The lumped parameter models are used in the core region to treat the formation of loose rubble beds or cohesive beds of previously liquefied material. The lumped parameter designation is used because it is assumed that rubble within a given thermal-hydraulic volume is at a single temperature and of a uniformly mixed composition. The detailed porous body model accounts for time dependent accumulation of debris, two-dimensional heat conduction within a debris bed and associated vessel structures, and creep rupture of those structures. The composition, porosity, and other debris characteristics can vary throughout the debris bed for the detailed model. Although an arbitrary mesh can be defined for the detailed model, the mesh spacing is typically significantly smaller than an associated thermal-hydraulic volume so that gradients in the bed can be resolved. The detailed model can be used anywhere in the system. Both the lumped parameter and detailed models treat the internal dryout and quenching of rubble beds, formation and growth of molten pools, surrounding crust failure and associated melt relocation. Fission product release and oxidation of a limited set of materials is considered for the detailed model. Debris beds can be formed as a result of (a) the significant disruption of representative core structures, such as the

fragmentation or melt down of representative fuel rods, (b) the relocation of molten material from a molten pool, and, in the case of the detailed model, (c) user defined debris beds and structures.

The fission product behavior models use a combination of four basic approaches. The aerosol and fission product deposition models were derived from TRAP-MELT2[3], while the fission product release is modeled using a theoretical model developed by Rest[9] to treat the release of Xe, Kr, Cs, I, and Te from solid fuel and an empirical model, CORSOR-M[10], to treat less volatile fission products. Ag-In-Cd aerosol formation is modeled using a model developed by Lorenz[11].

Code Assessment

The systematic assessment of modeling uncertainties in SCDAP/RELAP5 code is currently underway. This assessment includes (a) the evaluation of code-to-data comparisons using stand-alone SCDAP and SCDAP/RELAP5, (b) the estimation of modeling and experimental uncertainties, and (c) the determination of the influence of those uncertainties on predicted severe accident behavior.

The evaluation of code-to-data comparisons includes a summary of historical code-to-data comparisons[12] using the tests and code versions identified in Table I. The ongoing SCDAP/RELAP/MOD3 code-to-data comparisons are focused on those experiments that cover the early phases of the accident as listed on Table II. As shown in Figure 2, these code-to-data comparisons cover a wide range of scales both in terms of the

Table - Summary of Historical Code-to-Data Comparisons.

Experiment	Temperature	Ballooning	Early Deformation	Oxidation, H Production	F.P. Release	Late Deformation	Thermal-hydraulics
PBF SFD-ST	S	S	-	S	S	S	-
PBF SFD 1-1	S	S	-	S	S	S	S
PBF SFD 1-3	SR-2	SR-2	SR-2	SR-2	SR-2	SR-2	-
PBF SFD 1-4	SR-1	SR-1	-	SR-1	SR-1	SR-1	-
OECD LOFT LP-FP-2	SR-1	SR-1	-	SR-1	-	-	SR-1
CORA-7	SR-2.5	-	-	SR-2.5	-	SR-2.5	-
DF-1	S	-	S	S	-	S	-
DF-4	SR-2	-	-	SR-2	SR-2	SR-2	-
TMI-2	SR-1	SR-1	SR-1	SR-1	-	SR-1	SR-1
FLHT-2,-4	S	S	S	S	S	-	S
Other		S	S	S			

Key

S = SCDAP
SR-1 = SCDAP/RELAP5/MOD1
SR-2 = SCDAP/RELAP5/MOD2
SR-2.5 = SCDAP/RELAP5/MOD2.5

Table II - On-going Code-to-Data Comparisons.

Problem Type	Experiment
Integral-Effects Problems:	
1. Fission driven bundle boildown, heatup, ceramic melting	PBF SFD-ST, SFD 1-1 SFD 1-3, SFD 1-4
2. Fission driven bundle boildown, heatup, metallic melting	NRU FLHT-5, FLHT-6
3. Fission driven bundle heatup in steam	ACRR DF-4
4. Decay heat driven core heatup, ceramic melting	LOFT FP-2
5. Electrical heat driven bundle heatup and metallic melting with slow cooling	CORA 2,3,5,7,9,16,18
6. Electrical heat driven bundle heatup and metallic melting with quenching	CORA 12,17
Separate-Effects Problems	
1. Rod bundle and rupture during LOCA	To be determined

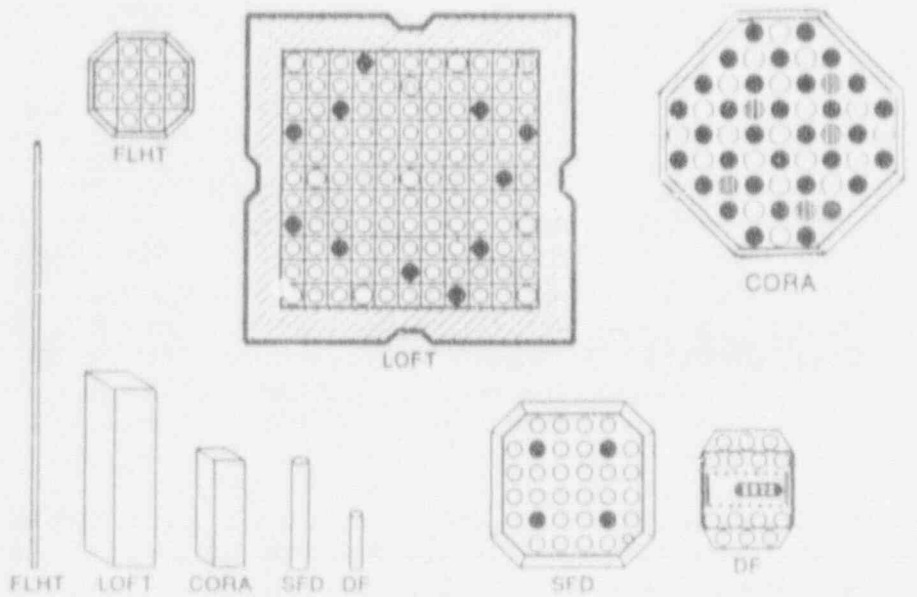

Figure 2 - Relative Scales of Different Experimental Bundles.

number of rods and axial length. Table III gives a more detailed description of the important characteristics of these tests.

Table III - Key Experimental Conditions for Code Assessment Experiments.

Test/ Accident	Fuel Irradiation	Control Materials	Spacer Grids	Steam Input	No. Rods/ Length	Heating Method	System Pressure (MPa)
DF-1	Trace	None	Inconel	Limited	9/0.5 m	Fission	0.28
DF-2	Trace	None	Inconel	Limited	9/0.5 m	Fission	1.72
DF-3	Trace	Ag-In-Cd	Inconel	Limited	8/0.5 m	Fission	0.62
DF-4	Trace	B_4C	Inconel	Limited	14/0.5 m	Fission	0.69
SFD-ST	Trace	None	Inconel	Excess	32/0.9 m	Fission	6.9
SFD 1-1	Trace	None	Inconel	Limited	32/0.9 m	Fission	6.8
SFD 1-3	30 GWd/tU	None	Inconel	Limited	28/0.9 m	Fission	6.85/4.7
SFD 1-4	30 GWd/tU	Ag-In-Cd	Inconel	Limited	28/0.9 m	Fission	6.95
CORA[a]	None	Ag-In-Cd/ B_4C	Inconel +Zry	Variable	18-57/1.0 m	Electric	0.2-1.0
FLHT-1	Trace	None	Inconel	Excess	12/4.0 m	Fission	1.38
FLHT-2	Trace	None	Inconel	Limited	12/4.0 m	Fission	1.38
FLHT-4	1-30 GWd/tU 10-Trace	None	Inconel	Limited	11/4.0 m	Fission	1.38
FLHT-5	1-30 GWd/tU 10-Trace	None	Inconel +Zry	Limited	11/4.0 m	Fission	1.38
LOFT FP-2	0.45 GWd/tU	Ag-In-Cd +H_3BO_3	Inconel	Excess	100/1.7 m	Decay	1.1
TMI-2	3 GWd/tU	Ag-In-Cd +H_3BO_3	Inconel	Excess	36.816/ 4.0 m	Decay	5-15

a. CORA test matrix includes 15 tests

The evaluation of code-to-data comparisons using SCDAP and SCDAP/RELAP5 indicated that the calculations performed with SCDAP/RELAP5, and to a lesser extent SCDAP, described the important features of each experiment. However, the assessment identified several important modeling improvements, incorporated during successive releases of SCDAP and SCDAP/RELAP5, that considerably improved the agreement between calculation and experiment. These included the merger of SCDAP with RELAP5 and the addition of the new models for double sided oxidation, fuel dissolution, and axial heat transfer.

The overall code-to-data comparisons for SCDAP/RELAP5 indicated that estimated variation between calculated and measured results was as follows[12]. The thermal response, including variations in timing as well as magnitude, could typically be predicted within ± 20 % with a few outliers in the ± 40 % range. Figures 3 and 4 show comparisons of calculated and measured temperatures for experiments using representative

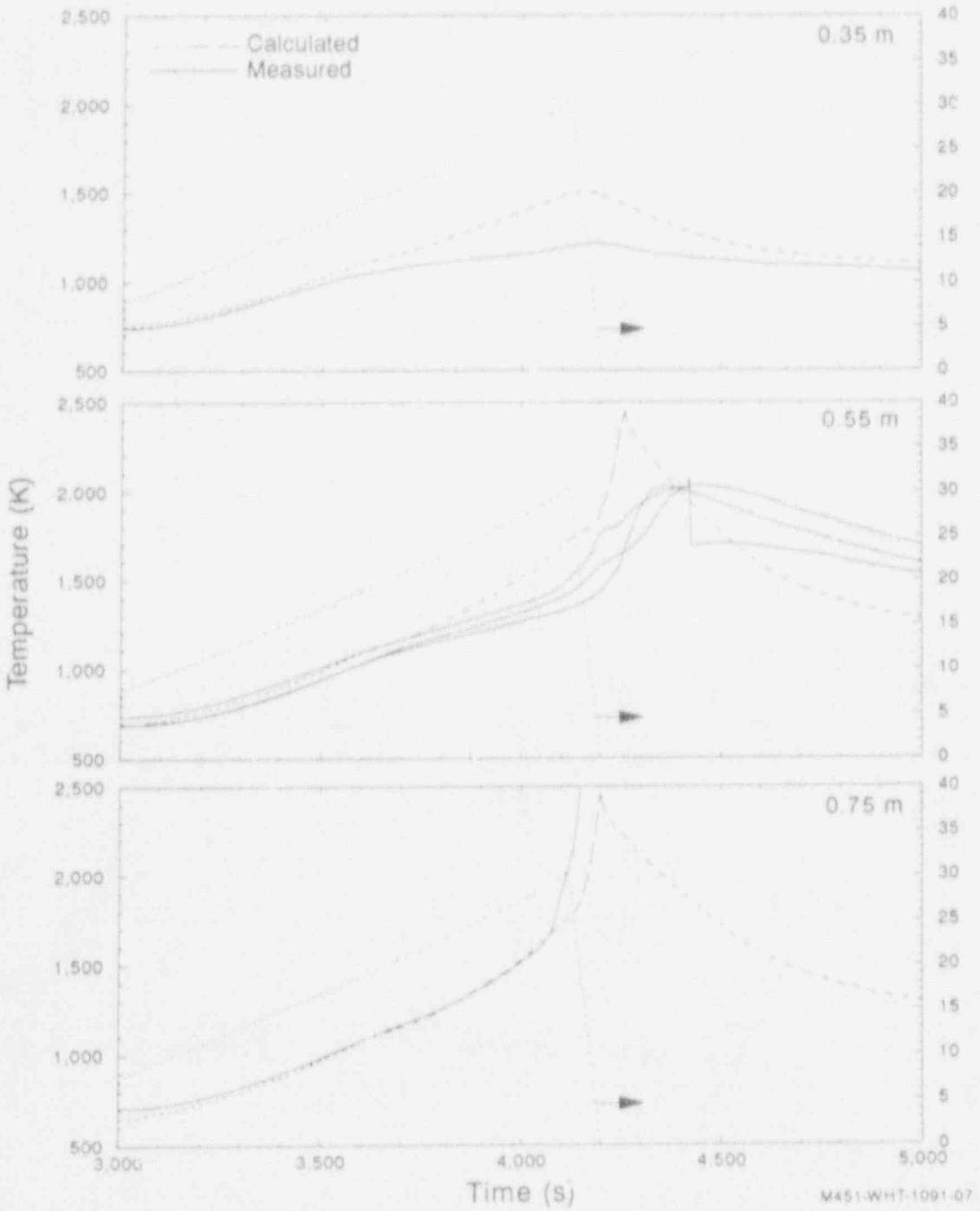

Figure 3 - Calculated and Measured Fuel Rod Cladding Temperatures for the CORA-7 PWR Bundle Heatup and Melting Test.

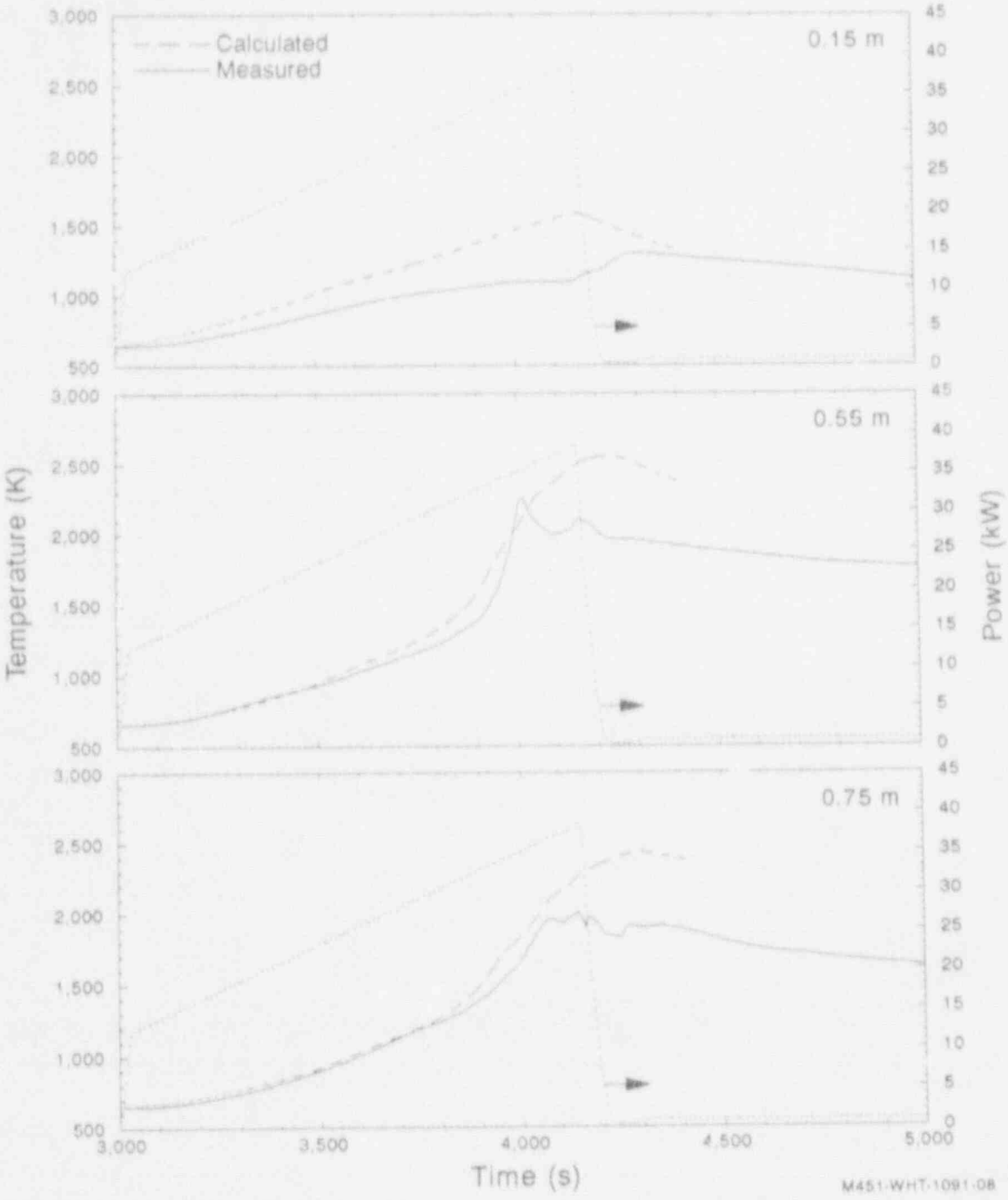

Figure 4 - Calculated and Measured Fuel Rod Cladding Temperatures for the CORA-18 BWR Bundle Heatup and Melting Test.

PWR and BWR bundles. Figure 5 shows calculated fuel rod temperatures for representative tests plotted versus measured temperatures at the same time and position. The ballooning and rupture could typically be predicted to a few percent. The hydrogen production had the worst overall agreement, particularly during bundle reflood, with a variation up to a factor of two.

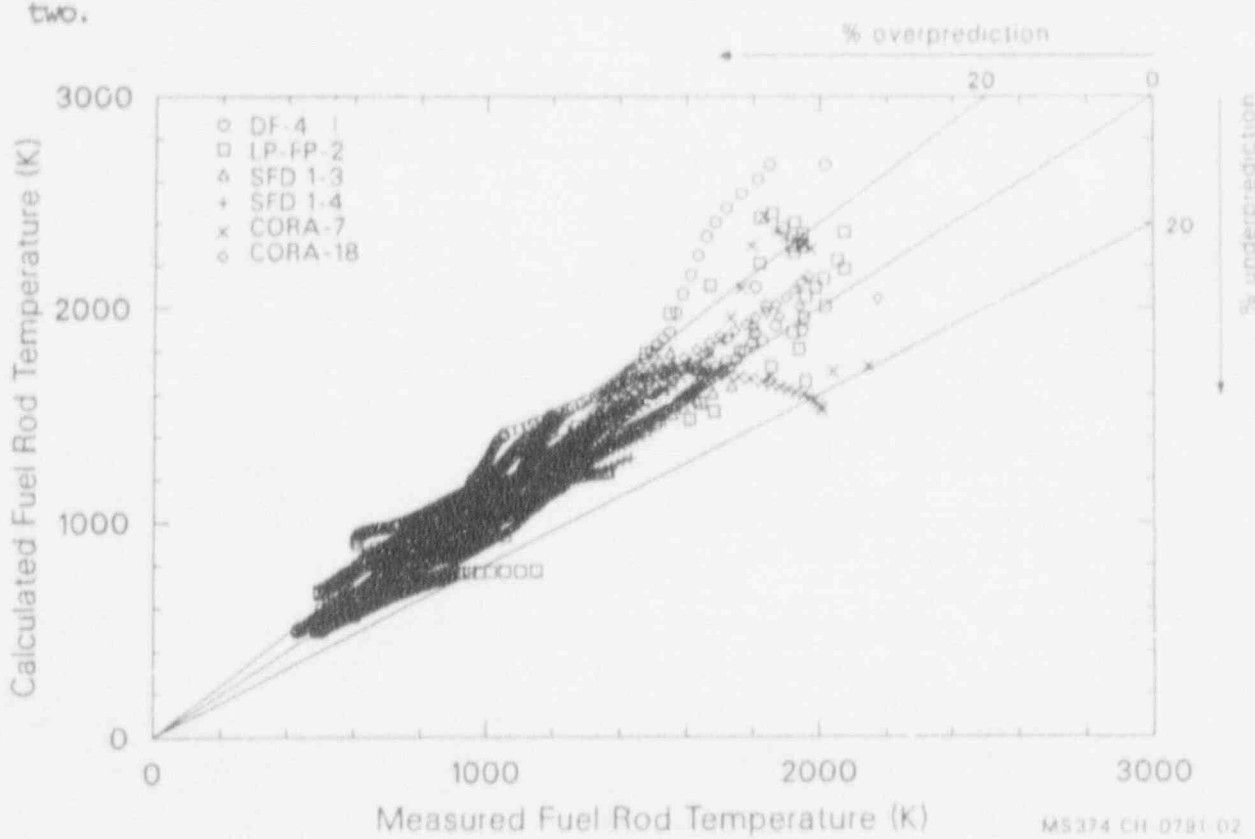

Figure 5 - Overall Variation Between Calculated and Measured Fuel Rod Cladding Temperatures.

Sensitivity studies using SCDAP/RELAP5 indicated that the variations between SCDAP/RELAP5 calculations and experiments were due equally to uncertainties in (a) experimental conditions or results and (b) modeling important processes. Uncertainties in radial heat losses, power, flow conditions, hydrogen production measurements, and peak temperature estimates were dominant contributors for experimental conditions or results. Figure 6 shows the variation in calculated cladding temperatures for the SFD 1-4 experiment for a systematic variation in test conditions within their estimated uncertainties[13]. In this experiment, variations in radial heat losses due to a estimated degradation in the zirconia insulation around the bundle due to the ingress of steam changed peak bundle temperatures by 400-500 K. Dominant modeling uncertainties were the initial relocation of liquefied fuel rod material, flow diversions due to changes in geometry, multi-dimensional flow patterns in the upper plenum region, and oxidation once the initial bundle geometry was lost. Figure 7 shows the variation in calculated cladding temperatures for the

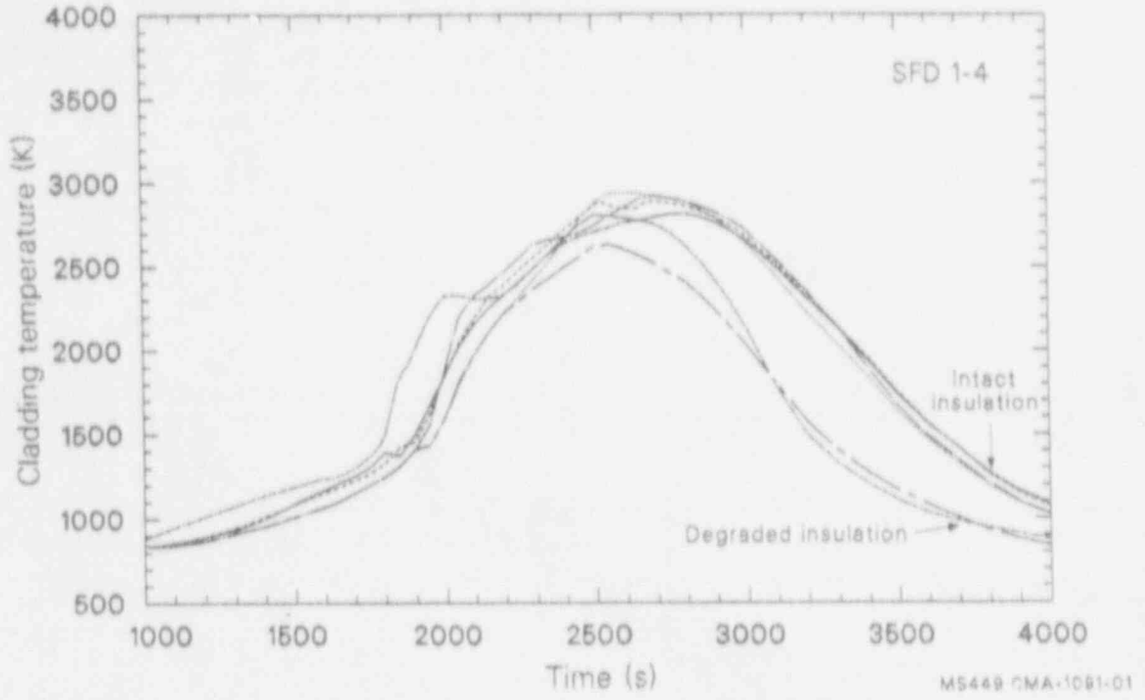

Figure 6 - Variation in Calculated Fuel Rod Temperatures for SFD 1-4 Due to Experimental Uncertainties.

SFD 1-4 experiment for a systematic variation within estimated modeling uncertainties. The potential variation in the initiation of melt relocation starting at a peak bundle temperature at two extremes from 2150 K to 2650 K caused a comparible variation in the peak bundle temperatures.

Variations in predicted and actual thermal-hydraulic response of the experimental systems - (a) liquid level and dryout times for temperatures below 1000 K, (b) local flow perturbations due to cross flows from outer assemblies or flow diversions from damaged bundles, and (c) radial heat losses, due to both experimental and modeling uncertainties had a dominant influence on the overall variation between experiment and calculation. User guidelines are being developed to minimize the influence of these uncertainties in modeling the thermal hydraulic features of these facilities.

Ongoing Model Improvements

Six specific damage progression model deficiencies were identified in code-to-data comparisons - (a) influence of ballooning upon flow and subsequent heatup, (b) oxidation of the inside of unpressurized fuel rod cladding, (c) the oxidation of relocating material or material that has formed a cohesive blockage, (d) additional hydrogen during reflood, (e) the porosity of frozen melt and the relocation of ceramic fuel rod

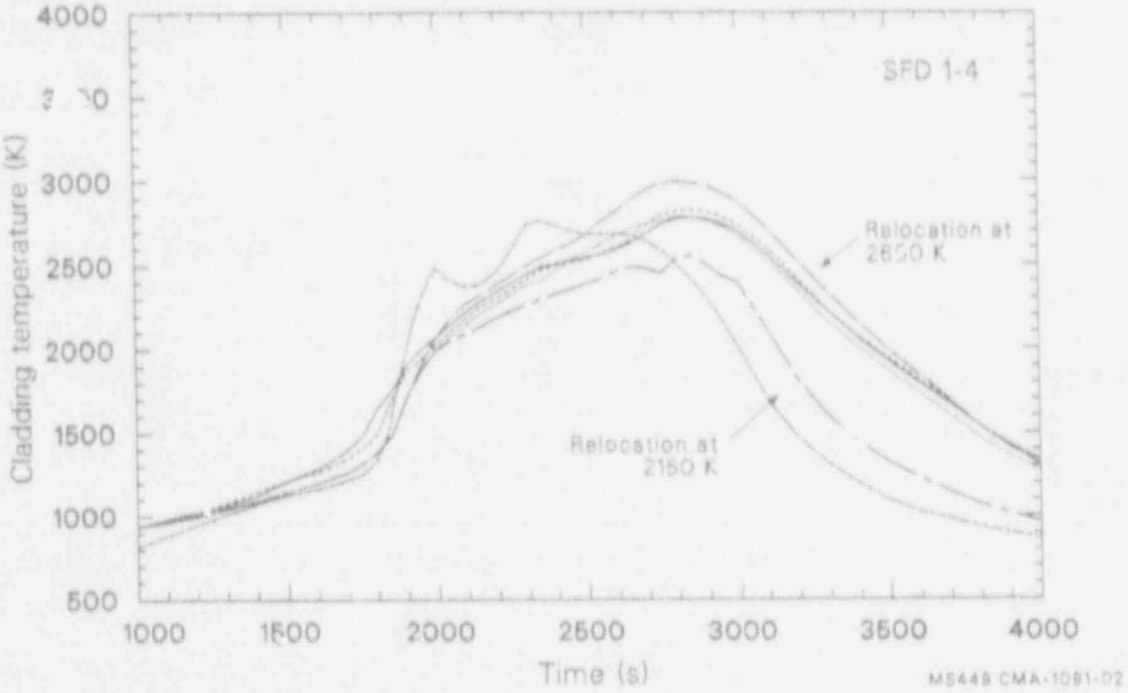

Figure 7 - Variation in Calculated Fuel Rod Temperatures for SFD 1-4 Due to Modeling Uncertainties

material, and (f) the interaction occurring between bundle materials and complex flow of rivulets and droplets. A model development effort to resolve these deficiencies is currently underway.

References

1. RELAP5/MOD3 Code Manual, Edited by C. M. Allison, C. S. Miller, N. L. Wade, Draft NUREG/CR-5535, EGG-2596, June 1990.
2. SCDAP/RELAP5/MOD3 Code Manual, Edited by C. M. Allison, E. C. Johnson, Draft NUREG/CR-5273, EGG-2555, September 1990.
3. H. Jordan and M. R. Kuhlman, TRAP-MELT2 User's Manual, NUREG/CR-4205, BMI-2124, May 1985.
4. M. S. Sohal, "A Radiation Heat Transfer Model for the SCDAP Code", ASME Winter Annual Meeting, New Orleans, 1984.
5. P. D. Bayless and C. A. Dobbe, Calculation of Reactor Vessel Steam Recirculation Using the RELAP5 and TRAC Computer Codes, EG&G Report.
6. R. A. Riemke, "RELAP5 Multi-Dimensional Constitutive Models", 1991 RELAP5/TRAC-B International Users Seminar, Baton Rouge, November 4-8, 1991 (Proceedings available through EG&G).
7. K. E. Carlson, "Addition of Three Dimensional Modeling", 1991 RELAP5/TRAC-B International Users Seminar, Baton Rouge, November 4-8, 1991 (Proceedings available through EG&G).
8. L. J. Siefken and C. M. Allison, "Models for Calculating the Progression of Reactor Core and Vessel Damage During Severe Accidents, Commission of the European Communities Report on Nuclear Science and Technology, Transactions of Two International Seminars on the

Mathematica`/Mechanical Modelling of Reactor Fuel Elements, edited by K. Lassmann, 1991.
9. J. Rest, "The Coupled Kinetics of Grain Growth and Fission Product Behavior in Nuclear Fuel under Degraded-Core Accident Conditions", Journal of Nuclear Materials, 131, 1985, pp. 291-302.
10. M. R. Kuhlman, et al., CORSOR User's Manual, NUREG/CR-4173, BMI-2122, March, 1985.
11. R. A. Lorenz, et al., "Fission Product Source Terms for the Light Water Reactor Loss-of-Coolant Accident", Nuclear Technology, 46, 1979.
12. C. M. Allison, et al., SCDAP/RELAP5 Assessment: Review of 198j-1990 Assessments of Damage Progression Models, EGG-EAST-9400, January 1991.
13. D. A. Petti, et al, Power Burst Facility (PBF) Severe Fuel Dmage Tests 1-4 Test Results Report, NUREG/CR-5163, EGG-2542, April 1989.

MAIN SAFETY ISSUES RELATED TO IPSN SEVERE ACCIDENT RESEARCH

C. LECOMTE

IPSN (INSTITUTE FOR NUCLEAR PROTECTION AND SAFETY)

DPEI (DEPARTMENT FOR THE PROTECTION OF ENVIRONMENT AND INSTALLATIONS

FRANCE

ABSTRACT

IPSN has developed a rationale for accident studies which involves both analytical and crisis strategies. The operational aim to provide as high as possible prevention of damage for installations and environment is fulfilled during accidental and post-accidental phases through development of crisis tools and analysis of emergency plans. Further research will provide still more detailed insight into release prevention capabilities and environment recovery techniques.

1 - INTRODUCTION

The work performed at IPSN concerning accident studies on nuclear installations is focused on the characterization of accidental sequences with three major aims :

- prevention ;

- mitigation ;

- dimensioning and optimisation of counter-measures.

As criteria to optimize all efforts made to improve nuclear safety so as to prevent environmental consequences, the effects of radioactive dispersal in the environment must be quantified as function of internal and external radioactive products transfers. This effort involves the development of both detailed, analytical tools for safety studies, and crisis tools specifically designed for on time evaluations.

2 - INTERNAL PLANT BEHAVIOR CHARACTERIZATION

2.1 - ANALYTICAL METHODS

The ESCADRE system is the french code system used by IPSN, as technical support to the french safety authorities, for the overall analysis of severe accident sequences liable to occur on pressurized water reactors. Its main objective is to determine, qualitatively and quantitatively, the potential source term to the environment in case of severe accident. It also allows to study the efficiency of various preventive or mitigative measures.

In order to fulfill this goal, it is necessary to predict quantitatively the fission products location, at any time and for every containment failure modes.

For this, the thermohydraulics properties of the carrier fluid which governs fission product phenomena have to be computed, either for the circuits, either for the containment.

Then, the fission products caracteristics - i.e. the physical and chemical properties - are computed at each stage from the core to the containment and to the environment.

ESCADRE is validated by numerous analytical studies related to containment and fission product behaviour ; it will be further qualified by the results of the global experiments performed in the PHEBUS FP facility at IPSN with a large international cooperation.

The organization scheme of the ESCADRE system is represented on Figure 1. The different codes belong to two distinct categories :

- thermalhydraulics codes :

  * VULCAIN for the primary circuit thermalhydraulics and core degradation ; VULCAIN also calculates the fission products release during core degradation ;

  * JERICHO for containment thermalhydraulics ; JERICHO calculates pressure, temperature, atmosphere composition in the containment, from mass and energy flowrates coming from the other modules ; it can also describe hydrogen deflagration phenomena ;

  * ECROUL is a module based on mass and energy balances which can derive the time between a given core degradation state and the beginning of corium-concrete interaction ;

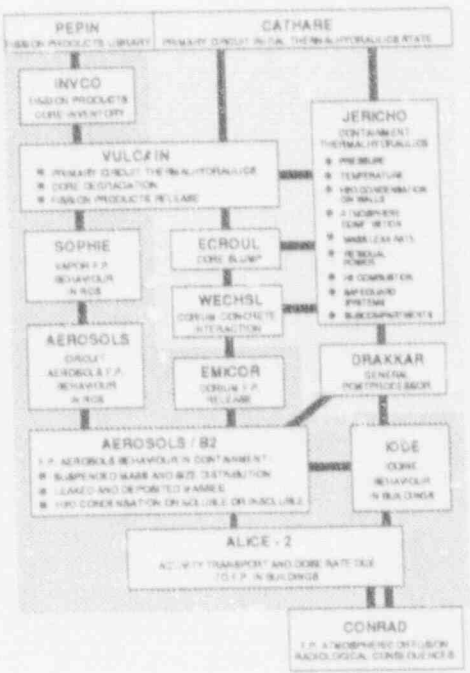

Figure 1 : Organization of the code system ESCADRE

* WECHSL calculates corium-concrete interaction and the resulting gas and energy flowrates to the contain-ment ;

- fission product codes :

* VULCAIN, already mentioned, for which fission products release and core thermalhydraulics are strongly coupled ;

* SOPHIE, which stands for vapor fission product behavior in the pipes ;

* AEROSOLS CIRCUIT, concerning the specific depletion of aerosols in pipes (prima. or secondary circuit, safety injection lines) ;

* AEROSOLS/B? which calculates the behavior of aerosols in the containment ;

* IODE, which is devoted to the chemistry of iodine compounds under radiation in the containment.

Finally, the code ALICE can evaluate the activity transport and the dose rate due to the fission products in different buildings, as a function of time.

As mentioned earlier, the ESCADRE code system is an operational tool aimed at predicting main parameters describing the potential "source term" in case of severe accident ; the strategy adopted by IPSN has been to develop an engineer code, the degree of detail in the modelisation being adapted to both the final needs and the possibility of obtaining pertinent data from the experiments, given the general instrumentation limitations.

So far, the code system ESCADRE has helped to prepare a number of experiments, from the results of which it derives further data.

Besides this, the main applications of the ESCADRE system in the frame of safety studies involve :

- characterization of selected core-melt sequences, from the point of view of containment and fission products behavior ;

- parametric studies in order to identify the more significant parameters for source term evaluation ;

- identification of the potential effects of operator actions ;

- prioritization and assessment of new Accident Management Measures ;

- technical basis for emergency planning implementation ;

- reference calculations for crisis tools development.

2.2 - CRISIS TOOLS

During an hypothetical crisis, IPSN, as technical support to the french safety authorities (DSIN/Direction for the Safety of Nuclear Installations), would be in charge of the evaluation of the situation in order to forecast its development, mainly in terms of releases in the environment.

For that purpose, the IPSN Emergency Technical Center (CTC for "Centre Technique de Crise", in French) is organized round a management unit receiving analysis data from two working parties, one studying the situation within the damaged plant (Plant Assessment Unit) and the other concerned with assessing the radiological consequences of the accident (Radiological Consequence Unit, discussed in § 3.1).

In the Plant Assessment Unit, the experts have to make an operational synthesis of the available informations, which implies the identification of erroneous informations and the discrepancy between essential and subordinate informations ; doing so, they elaborate a diagnosis and a prognosis of the situation, which is periodically confronted, through a phone conference network, to the evaluations of the ... s.

The work of the Plant Assessment Unit is supported by the use of the tools ... d in the frame of the SESAME project.

In a **first step**, a ... ive assessment is made ... entify the state of the ... afety barriers ; this qualitative diagnosis is elaborated by monitoring a set of about 100 measurements, picked out among all the data transmitted from the affected plant to the IPSN CTC.

The evaluation is made easier by use of the expert system ALADIN, developed by IPSN ; this system gives informations on safety systems availability ; it contains both a documentation function - description of the electrical supply of the systems - and a simulation function - investigation of the consequences of a fault on an electrical supply or a component -.

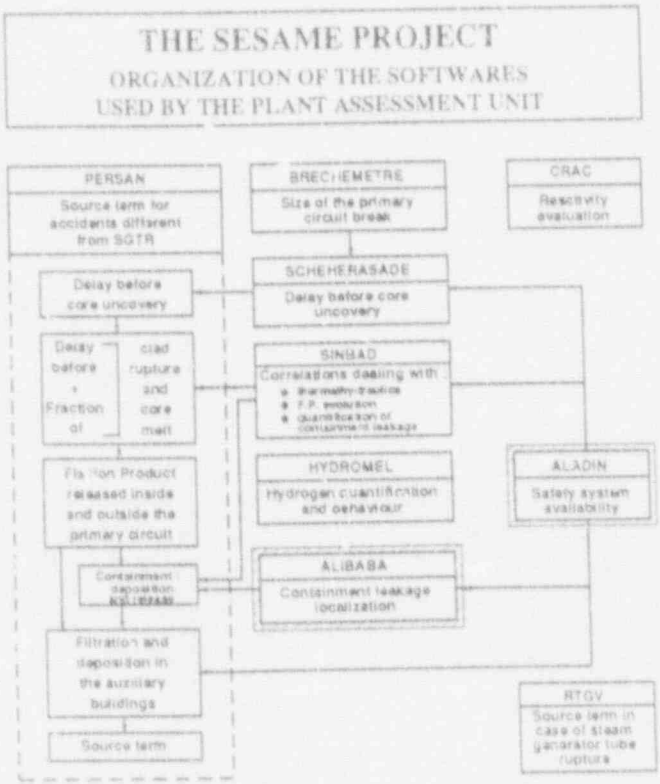

Figure 2 : Organization of the SESAME tools

The **second step** is a quantitative approach : in this step, the Emergency Teams try to give some quantitative answers about the state of the safety functions (subcriticality, core cooling, confinement efficiency) and the margins to critical states.

In order to answer these questions, specific tools have been developped in the frame of a project entitled SESAME : the organisation of these tools is described in Figure 2.

In the origin, these tools consisted mainly of correlations and reports, that have enabled the progressive development of softwares running on PCs or work stations.

All these tools have common features, which are user-friendliness, flexibility, fast execution. They use realistic assumptions and physical laws ; a systematic qualification is performed through comparison with reference codes, which also allows the identification of their validity domain.

These tools can be classified according to three main groups :

- thermal hydraulics :

The "BRECHEMETRE" sofware makes an evaluation of the size of the primary break by means of a mass balance on the primary circuit and a comparison with a critical flow correlation issued from the french CATHARE code.

An other way to estimate the break size is to use the "SINBAD" software which allows to compare the pressure evolution in the containment with scenarios precalculated with the ESCADRE system. "SINBAD" also includes correlations and calculations on core and RCP behavior.

The "SCHEHERASADE" software calculates the evolution of the liquid inventory in the primary circuit by means of mass and energy balances. The delay before core uncovery can thus be estimated.

- fission products behavior :

The expert system "ALIBABA" provides an early diagnosis of containment leakage and identifies the position of the leakage. This diagnosis is elaborated from radioactivity measurements in the auxiliary buildings and from informations on containment isolation valves.

The "SINBAD" software which has already been mentioned includes also correlations for estimation of core residual power, core residual activity and flow rate through the containment leaks.

The "PERSAN" software collects the data from "ALADIN", "SCHEHERASADE", "ALIBABA" and "SINBAD" to calculate the evolution of fission products within the RCP, the containment, the leakpaths and the auxiliary buildings.

Finally, the "RTGV" software calculates fission products releases in case of steam generator tube rupture without core degradation.

- other softwares :

The "HYDROMEL" software is used to study the behavior of hydrogen in the containment by calculating the position of the containment atmosphere in the

Shapiro diagram ; if combustion is found possible, corresponding pressure and temperature loads c[illegible] calculated.

The margin to criticality is approximately evaluated by the "CRAC" software which performs a reactivity balance in the core.

2.3 - ACCIDENT MANAGEMENT MEASURES

During an hypothetical emergency situation, the utilities would apply operational means including design basis and ultimate measures and application of the "Internal Emergency Plan" (PUI for "Plan d'Urgence Interne").

Procedures to cope with an accident involve the I (Incidental), A (Accidental), H (Complementary) and U (Ultimate) measures ; a further level of reflexion is provided by the GIAG (Guide for Intervention in case of Severe Accident) which supports the reflexion of the national crisis teams.

All these procedures and guidelines are validated by numerous studies and experiments.

Besides these technical measures, a specific organisation has been defined and is regularly tested to ensure an adequate management of the plant accident situation for the short-term period (a few days) ; it defines the respective roles and responsabilities of all partners. The organisation of the utility is described by the PUI - Internal Emergency Plans-.

A three-step PUI exists for each site and is initiated by the head of the plant whenever an accident occurs ; the different steps of the PUI are initiated either on radiological criteria, either depending on the application of procedures from a pre-established list.

The goals of the emergency organization established by the PUI are as follows :

- decisions and implementation of relevant actions for reactor and environment protection ;

- collection of useful informations for the diagnosis/-prognosis of the accident ;

- information of the administration.

Special emergency teams are constituted to fulfill these goals.

As technical support of the Safety Authorities, IPSN is in charge of Internal Emergency Plans analysis ; following points are systematically investigated :

- operationality of the organization ;

- quality insurance of the documents ;

- compatibility with the technical basis -"source-term"-, as defined by the safety authorities ;

- on site crisis preparedness.

3 - RADIOACTIVE RELEASES IN THE ENVIRONMENT

3.1 - PREDICTION OF RELEASES

After the first phase of an accident, the goals and means of the ETC would change. Given the potential "source term" from the installation, the radioactivity dispersal in the environment can then be predicted both by detailed codes and crisis tools. The CONRAD system is operational to predict the dispersal itself, while the CART project will produce a data base of relevant parameters for the countries surrounding nuc'ear sites.

The prediction of radiological consequences makes use of predicted releases (see § 2.2) ; it also needs the knowledge of meteorogical data, which are available from three main ways :

- meteorological parameters from the damaged site ;

- "METEOTEL" images ;

- connection with the computers of the meteorological office.

Atmospheric dispersion and dose calculations for the near field (some tens of km) are made with the CONRAD system ; three methods are used, all based on Doury's standard deviations :

- set of operational graphs of atmospheric transfer coefficients ;

- classical bi-gaussian plume model ;

- gaussian puff model integrated in the SIROCCO code.

For long distances (up to some hundreds of km), the SIROCCO-LD code has been developed, on the same physical basis as SIROCCO. The puffs follow the meteorological trajectories which are generated each hour.

For all these methods, a computerized graphical treatment allows to superimpose isovalue curve (for concentration, dose, ...) on maps showing the distribution of population, rivers, road or railway network.

3.2 - PROTECTION OF THE POPULATION

These results are essential to determine the adequate counter-measures for the protection of the population and the environment, as they are planned in the so-called "Particular Intervention Plans" (PPI for "Plans Particuliers d'Intervention").

The goal of a PPI on a nuclear site is to forecast and organize relevant short-term measures to protect the population out of the considered nuclear site.

The elaboration of the PPI requires the definition of one or more conventional "source terms" which represent the potential releases originating from the installations on the site.

The definition of these "source terms" relies on the realistic evaluation of the more serious accidents liable to occur on the installations considered. Counter-measures which have to be foreseen result from the dispersal of these "source terms" and from the sanitary effects which could eventually be induced, taking into account radiological/toxicological recommendations in a french or international frame.

3.3 - CHARACTERIZATION OF ENVIRONMENTAL IMPACT

The prediction of environmental consequences during a crisis would also be a guide line to elaborate the measurement strategy for the impact of releases in the environment, both for accidental and post-accidental phases.

After an hypothetical radioactive release, the ground, the population, the vegetation and the water bodies can be contaminated.

The optimisation of measurement actions (e.g. sampling, airborne measurements, dose to the population, ...) results from the radiological calculations as combined with cartographic data, as cited in § 3.1.

4 - REHABILITATION OF THE ENVIRONMENT

Concerning this latter phase, rehabilitation of contaminated environment is the purpose of the "Post-Accidental action Plan" (PPA). The technical actions to be undertaken are based on the results of predictions and measurements ; their efficiency is studied by the experimental program named RESSAC, adressing soil and plant radionucleide transfers and contamination removal techniques. This program is performed in cooperation with the European Community Commission.

Main objectives of the RESSAC program may be described as follows :

- determination of intervention priorities :

This action is based on cartographic data banks, including soil occupation and known vulnerabilities. Special mention has to be made for underground water levels. Specific enquiries can be performed.

- evaluation of nucleïde behavior in soils and plants :

Analytical as well as global experimentations are performed in order to evaluate radionucleïde migration in soils and plants ; realistic agricultural practices are investigated, including for example the use of fertilizing additives. Global experiments are performed with the POLYR oven, which produces

representative aerosols from UO_2 and structural material ; within the frame of the european cooperation, soil samples (about 1 m^3) taken from selected european nuclear sites will be studied and realistic agricultural and meteorological conditions will be simulated.

- choice of operational intervention strategies :

The techniques which are investigated are the interception by specific vegetals (cultures/trees) and the possibilities of soil removal, for example by mechanical means.

- treatment of wastes.

The evaluation of the volume of wastes generated is made for each technique.

5 - CONCLUSIONS

IPSN has developed a rationale for accident studies which involves both analytical and crisis strategies. The operational aim to provide as high as possible prevention of damage for installations and environment is fulfilled during accidental and post-accidental phases. Further research will provide still more detailed insight into release prevention capabilities and environment recovery techniques.

6 - REFERENCES

/1/ "CEA Analytical Activities : HEVA, PITEAS, Mini-containments", C. LECOMTE, G. LHIAUBET, Communication at the first PHEBUS FP Seminar, Cadarache, June 1991.

ACKNOWLEDGMENTS :

The author is very much endebted to MM. MANESSE, MAIGNE, CHAULIAC, CROUZET, LHIAUBET, who provided a lot of material to prepare this paper.

Recent Development and Results from Severe Accident Research In Japan

K. Soda, J. Sugimoto, N. Yamano, K. Shiba
Department of Fuel Safety Research
Japan Atomic Energy Research Institute
Tokai-mura, Ibaraki-ken, Japan

SUMMARY

An overview on Japanese activities of severe accident research is presented, covering various fields and topics of experimental investigation on severe accident phenomena such as fuel damage and melt progression, fission products release and transport, and component and containment integrity. The current status of analytical investigation on severe accident is also described in the fields of the level-1 and level-2 PSA studies, code development and assessment activities. The basic considerations on accident management is summarized.

1. INTRODUCTION

In the procedure of nuclear power plant licensing in Japan, the safety examination on basic design is performed based upon the relating laws and guidelines whose requirements on safety design are prescribed within the design basis accident. Accordingly, the severe accident issues are not involved in the current licensing procedures. In recent years, however, it became widely recognized that severe accident research is important to understand the safety tolerance of the system in detail and also to investigate how to improve the accident management measures.

As a background for the safety examination of a particular design of a nuclear power plant or for the examination of its operational safety, PSAs on a reference plant similar to the particular design are being performed, and the results are being taken into account as reference materials for the safety evaluation. In this sense, severe accident research is a useful support for the safety licensing procedure.

Within the Government authorities, the Nuclear Safety Commission (NSC) has initiated a discussion of severe accident issues and the interim report was released in 1991. The position of NSC on severe accident is summarized as follows;

(1) The knowledge of severe accident is one of the most important basis for the formulation of safety design criteria, siting criteria, and guideline for emergency planning.
(2) Plant operator should have knowledge of severe accident and reflect it upon the plant management so as to be able to cope with properly even in cases of beyond design basis accident.
(3) Industry and research organizations should perform severe accident research of which purposes are;
    * To identify phenomena associated with a severe accident,
    * To develop analytical tools for source term analysis,
    * To estimate a risk and safety margin of plant, and

* To evaluate measures to prevent and mitigate severe accident by design and/or accident management.

In accordance with the NSC's recommendation, the Government's Annual Plan on Reactor Safety Research gives an emphasis on severe accident research as one of the top-prioritized reactor safety research /1/. The Japan Atomic Energy Research Institute (JAERI) is the primary Government research organization pursuing severe accident research experimentally and analytically /2/. In addition, demonstration tests are conducted at the Nuclear Power Engineering Center (NUPEC) with an emphasis on quantification of the safety tolerance of a nuclear power plant in conditions beyond the design basis. Industries are making progress in quantifying risks of nuclear power plants in Japan.

2. CURRENT STATUS OF SEVERE ACCIDENT RESEARCH IN JAPAN

2.1 Experimental Studies

2.1.1 Melt Progression

In-Vessel

Experimental investigation of in-vessel melt progression in Japan relies largely on the international research collaboration involving a large scale experiment such as the Cooperative Severe Accident Research Program (CSARP) and the TMI-2 R & D Program in U.S.A., the CORA experiment in Germany, the LOFT program of OECD and the PHEBUS program in France. Analyses of such experimental data have provided us insights into how core melt progresses during a severe accident.

To better understand and interpret the data of the large scale experiments, fuel damage experiment was performed at JAERI by using the Nuclear Safety Research Reactor (NSRR) which is capable of performing a test simulating reactivity initiated accident (RIA) conditions as well as transient conditions. Recent experiments at NSRR included high temperature flooding experiment by using the test capsule illustrated in Fig. 1. Failure of the cladding caused by flooding was correlated with oxidation of the cladding material as shown in Fig. 2 /3/.

Interactions of fuel, control rod and core component materials have been studied to supplement the large scale experiment. The apparatus used for this purpose is shown in Fig. 3. Reaction rates of various combinations of core materials were experimentally measured as shown in Fig. 4 /4/. The TMI-2 debris samples were received and the examination has been initiated since spring of 1991.

Mechanism of vessel failure due to the attack of molten core to the reactor vessel still remains with a large uncertainty. The TMI-VIP program is expected to provide useful information to reduce the uncertainty. Structural analysis of the reactor vessel was performed at JAERI to interpret the data obtained in the TMIVIP program as shown in Fig. 5. Results showed that the stress concentration near the instrument nozzle might have caused the crack near the nozzle /5/.

Ex-Vessel

Ex-vessel melt progression after the vessel failure plays an important role in determining timing of the containment failure and quantifying source terms. Problems arising during the ex-vessel melt progression include core-

concrete interaction and melt coolability in a containment. Hydrogen generation and burn in the containment are also affected by the ex-vessel melt progression.

The Assessment of Loads and Performance of Containment in a Hypothetical Accident (ALPHA) program at JAERI focuses on the ex-vessel melt progression, especially core-concrete interaction and molten core coolability in a containment in which steam explosion may have an influence on the integrity of a reactor vessel and a containment. Schematic diagram of the ALPHA test facility is shown in Fig. 6 and the major capability of the facility is summarized in Table 1. Recent experiment of molten metal and water interaction resulted in steam explosion. Energy conversion ratio was estimated from data as less than 1.0 % /6/. Future experiments will include steam explosion at high pressure and cooling of molten core by water pool or water spray.

2.1.2 Fission Product Release and Transport

Fission product release and transport have been studied at JAERI from the view point of supplementing the large scale integral experiment data such as those obtained from the CSARP program and the PHEBUS FP program.

Formation of organic iodine in the radiation field is experimentally studied with the small test apparatus at JAERI. Recent result showed the effect of organic compound on formation of organic iodine as shown in Fig. 7 /7/. Basic reaction kinetics of iodine, cesium and tellurium with component materials such as Fe, Ni and Cr are investigated by using the apparatus illustrated in Fig. 8. Future test is planned at JAERI to fabricate a test assembly with which fission product release from a damaged fuel will be investigated at high temperature of 2800^{o}C under various conditions ranging from oxidized to reduced environment.

As was pointed out by the PSA studies at JAERI, pool scrubbing efficiency is one of the dominant factors influencing source term evaluation. Therefore the experimental facility for pool scrubbing investigation (EPSI) shown in Fig. 9 was fabricated at JAERI to quantify the efficiency. Experiment results indicate as shown in Fig. 10 that pool scrubbing is extremely effective to remove fission products even at elevated temperature and pressure /8/.

NUPEC is planning a test program of radioactive material trapping in the leakage path of a containment such as electric penetration assembly (EPA) and an equipment hatch. In this test, iodine trapping effect in the leakage path will be investigated under simulated severe accident conditions. The test program consists of a bench scale test for surveying controlling parameters which affect the efficiency of trapping iodine in the leak path and a large scale test for confirming and evaluating iodine trapping effect in an actual component used in a nuclear power plant.

2.1.3 Components and Containment Integrity

Integrity of a containment has become focus of attention especially since the Chernobyl accident showed important roles of a containment, namely containing radioactive materials not to be released to the environment. It is anticipated during a severe accident that mechanical and thermal loads might be resulted from ex-vessel phenomena such as steam explosion, hydrogen burn, over-pressure and over-temperature exceeding the design limit.

Effects of dynamic and static pressure increase exceeding the design limit has been studied at JAERI by the finite element analysis code. The

result indicated that a containment will maintain its integrity even if the pressure reaches 4 to 5 times of the design pressure as shown in Fig. 11 for a PWR steel containment /9/. Similar result was obtained for a BWR steel containment /10/. The predicted result by JAERI of the 1/6 scale reinforced concrete containment vessel (RCCV) experiment at the Sandia National Laboratories (SNL) is shown in Fig. 12 in which the first yielding zones were in good agreement with experimental results /11/.

Leak rate tests at high pressure and temperature have been carried out as a part of the ALPHA program at JAERI to characterize the failure mechanism of the penetrations for instrument cables and power cables. Experiments conducted so far show no leakage resulting from high pressure /12/, but a potential leakage may occur due to the high temperature in the containment.

A proving test program on containment integrity is promoted by NUPEC. In the program are included hydrogen mixing and distribution tests, hydrogen burning tests, and tests to failure of a steel containment vessel (SCV) and a prestressed concrete containment vessel (PCCV). Failure tests of a containment due to over-pressurization of SCV and PCCV are in preparation in which the scales of these tests are 1/10 th scale for SCV with 1/5 thickness and 1/6 th scale for PCCV.

2.1.4 Accident Management

Accident management has become an important issue in terms of prevention and mitigation of a severe accident. For the prevention phase of accident management, the utilities have set up operational procedures to terminate an accident early enough so that the accident never goes into a severe accident. Experimental and analytical studies have been also made for this aspect to prove and propose methods of accident management.

ROSA-V program planned at JAERI focuses on accident management during a transient and accidents. Experiments will be conducted to demonstrate the effectiveness of methods of accident management by using the 1/48 scale large test facility simulating a PWR. ALPHA program pays an attention to the ex-vessel phase of accident management such as terminating further core degradation by adding water on top of molten core material and mitigating consequences of a severe accident by scrubbing and/or filtering.

2.2 Analytical Studies on Severe Accident

2.2.1 Recent PSAs for LWR Plants

Level 1 PSA

Probabilistic Safety Assessment (PSA) is recognized as the convincing tool to support the deterministic method to assess the balance of design and assist regulatory activities of nuclear power plants. From this point, the preparation and application of PSA methodologies are under way with collaboration among the government organizations and industries.

Among the governmental organizations, JAERI has been developing a methodology of PSA while the Japan Institute of Nuclear Safety (JINS) of NUPEC has been conducting level-1 and level-2 PSAs for typical Japanese BWRs and PWRs /13/. The evaluations of 1,100 MWe-class BWR-5 with MARK II containment and 1,100 MWe-class four loop PWR with a large dry steel containment were completed in 1989.

The initiating events selected for the level-1 PSA at JINS were limited to

the internal events such as a loss of coolant accident (LOCA) and abnormal operational transients during high power operation. In this study, the data base of component failure rates was mainly composed of the IREP and the LER data while the data on the emergency diesel generator failure rate and recovery rate of failed off-site power were based on Japanese experiences.

The result of the JINS PSA showed that the total mean core damage frequency (CDF) for the BWR is about 2.0×10^{-7}/Reactor Year (RY). The upper 5% value is 4.9×10^{-7}/RY and the lower 5% value is 8.9×10^{-9}/RY. Corresponding error factor is 7.4. Among the initiating events, LOCAs have contribution of 83% to the total CDF and the secondary side break, steam generator tube rupture (SGTR), and other events have 7%, 5%, and 5%, respectively.

The reevaluation for the 1,100 MWe-class BWR and PWR is ongoing using the revised data base which includes more domestic data on the component failure rates based on the operational experiences. Two year program has started of surveying the possibility of core damage occurrence during the maintenance activities at the plant shutdown state.

Level 2 PSA

JAERI has developed its original source term code package which consists of the THALES code for severe accident progression analysis and the ART code for fission product release and transport analysis. The validity of the code package was examined through comparisons with experimental results or benchmarked against detailed analysis codes. Recent improvement of the code package includes an integration of THALES and ART into the THALES-2 code and addition of new models.

The THALES-2 code was applied to a source term calculation for some severe accident sequences in BWR with Mark-II containment. The analysis results indicated that the retention of fission products in the reactor coolant system would be strongly affected by revaporization and that the effects of the revaporization on the source terms are dependent on the timing of the containment failure and the structure temperature in the reactor coolant system /14/. Code comparison exercise was carried out at JAERI for MELCOR and STCP. It revealed that melt progression models influences release fractions of fission products as seen in Fig. 13.

Level-2 PSA at JINS follows the JINS level-1 PSA. Containment event trees were developed, considering physical phenomena influencing on fission product release timing and the recovery of failed safety systems. Dominant accident sequences were analyzed using the Source Term Code Package (STCP) and point-estimated values of fission product release frequency and source term were obtained for each release category. The result shows that the dominant accident sequences concerning fission product release frequency are not necessarily the same as those for the core damage frequency.

2.2.2 Code Development and Assessment

Code Development has been primarily pursued at JAERI and verification and assessment of the codes have been extensively done. In order to verify, models of the THALES code package, the detailed mechanistic codes have been developed for benchmark calculation. The mechanistic codes have been also used for experimental analysis. Such codes include MUFLAR, HOLN and REMOVAL.

MUFLAR is a two-dimensional core wide analysis code which was used

for analyzing core damage progression /15/. HORN is the code which is capable of predicting chemical forms of fission products along the release path of fission products /16/. REMOVAL is the aerosol analysis code which has been validated against the LACE experiments /17/.

Assessment of the integrated code such as SCDAP/RELAP5 and MELCOR has been carried out by applying to reactor situation such as the TMI-2 accident /18/. Large scale tests such as PBF/SFD, CORA and PHEBUS/SFD were also used for code assessment. An example of the CORA experiment analysis is shown in Fig. 14.

Participation in the international standard problem (ISP) exercise organized by the Committee of Safety of Nuclear Installations (CSNI) of OECD has become one of the important activities for the code assessment. JAERI has participated in ISPs of the TMI-2, CORA, BETA, HDR and PHEBUS experiments.

2.2.3 Accident Management Strategies

In the accident management, various measures will be involved including operational procedures, special equipments, and communications. Many of these have to be prepared primarily by the owners of nuclear power plants in coordination with the basic safety considerations of the regulatory body. From this point of view, the Japanese utilities have been making a lot of effort, for instance to provide emergency procedures.

As to the operational procedures for accidents, the electric utilities have already partly proceeded to the symptom-based procedure to cope with the unexpected events which has not been described in the event-based operational procedures during accidents. Operators are expected to use the symptom-based procedure when the event is beyond or not under control of the event-based procedures. The addition of symptom-based procedure brings flexibility to the operators, and the preparation of authorized recovery procedure against the error following the event-based procedure surely contributes to the reduction of work load.

Analytical investigation of accident management was performed by using STCP and RELAP5/SCDAP at JAERI with emphasis on effectiveness of intentional depressurization /19/ and also on reflooding of damaged core /20/. Intentional depressurization was found effective to prevent a direct containment heating (DCH) if the rate of depressurization is equivalent to opening more than two PORVs simultaneously as shown in Fig. 15. It was also found that amount of hydrogen generation during reflooding of damaged core depends on the timing of the reflooding initiation as in Fig. 16. There seems to exist a optimum timing to minimize hydrogen generation during reflooding.

Findings from such analyses will be further investigated experimentally to confirm and quantify the effectiveness of accident management scheme. For this purpose, experiment facilities such as ALPHA, ROSA-V and EPSI will be utilized.

3. SUMMARY

Severe accident research is promoted by the Government research organization to understand phenomena associated with severe accidents and to quantify the safety tolerance of a nuclear reactor under extreme conditions. Experimental and analytical studies have been conducted at JAERI and other organizations in Japan.

Experimental studies include in-vessel and ex-vessel melt progression, fission product release and transport, components and containment integrity, and accident management. Recent achievements have increased our knowledge of severe accident phenomena and reduced uncertainties of some of phenomena. Results are expected to be reflected into modeling improvement and development.

Analytical studies include PSA, code development and assessment, and accident management evaluation. The THALES-2 code package is JAERI's primary tool for source term evaluation of a nuclear power plant. Result of application of THALES-2 code to a nuclear power plant identified key parameters which influences source term.

Severe accident research will be continued until a closure of severe accident issues has been achieved. It is also common agreement that the an international cooperation is truly indispensable for effectively conducting experiments and analysis, since the severe accident is the common issue among the countries and its investigation can be promoted effectively by sharing information and resources.

REFERENCES

/1/ Nuclear Safety Commission, "Five Year Program of Safety Research for Nuclear Installations (FY 1991-1995)", September 1991.

/2/ JAERI, "Progress of Nuclear Safety Research - 1990", JAERI, Tokaimura, Ibarakiken, Japan, July 1990.

/3/ Katanishi, S. et al., "Quenching Degradation In-Pile Experiment on Oxidized Fuel rod in the Temperature Range of 1000°C to 1260°C", (To be published in Nuclear Engineering and Design).

/4/ Otomo, T. and Uetsuka, H., "Interaction of Core Component Materials at High Temperature - (3) B_4C Stainless Steel Interaction", Proc. 1991 Fall Meeting of AESJ, D26, Oct. 15-18, 1991, Fukuoka, Japan, (in Japanese).

/5/ Hashimoto, K. et al., "Thermal Response Analyses of the Three Mile Island Unit 2 Reactor Pressure Vessel", Trans. SMiRT-11, Aug. 1991, Tokyo, Japan.

/6/ Sugimoto, J. et al., "ALPHA (Assessment of Loads and Performance of Containment in a Hypothetical Accident) - Melt Drop Steam Fxplosion Experiment -", Proc. 1991 Fall Meeting of AESJ, D20, Oct. 15-18, 1991, Fukuoka, Japan, (in Japanese).

/7/ Naritomi, M. et al., "Batch-type Tests on Formation of Volatile Iodine Species from Aqueous Iodine under Cobalt 60 Gamma-Rays Irradiation", Proc. Third OECD/CSNI Iodine Chemistry Workshop in Reactor Safety, September 11-13, 1991, Tokaimura, Ibarakiken, Japan. (To be published)

/8/ Hashimoto, K. et al., "High Pressure Pool Scrubbing Experiment for a PWR Severe Accident", Proc. ANS International Topical Meeting on Safety of Thermal Reactors, July 22-25, 1991, Portland, U.S.A.

/9/ Isozaki, T. et al., "Structural Analysis of Japanese PWR Steel Containment Vessel Under Internal Pressure Loading", Nucl. Eng. & Des., 126, 387-393(1991).

/10/ Isozaki, T. et al., "Structural Analysis of a Japanese BWR Mark-I Containment Under Internal Pressure Loading", Nucl. Eng. & Des., 104 365-370(1987).

/11/ Kimura, H. and Soda, K., "Structural Analysis of the RCCV Under Extreme

Static and Dynamic Loading", Proc. the Second International Conference on Containment Design and Operation, October 14-17, 1991, Toronto, Canada.
/12/ Yamano, N. et al., "Scoping Test of Penetration Leakage Tests in the ALPHA Program", Proc. 1990 Fall Meeting of AESJ, F42, Oct. 2-5, 1991, Sendai, Miyagiken, Japan. (in Japanese).
/13/ Kondo, S. and Abe, K., "Comparison of Analytical Models and Calculated Results of Source Term Evaluation Codes", Proc. OECD/CSNI Workshop on Applications and Limitations of PSA, September 4-6, 1990, Santa Fe, U.S.A.
/14/ Kajimoto, M. et al., "Development of THALES-2, A Computer code for Coupled Thermal-Hydraulics and Fission Product Transport Analyses for Severe Accident at LWRs and Its Application to Analysis of Fission Product Revaporization Phenomena", Proc. ANS International Topical Meeting on Safety of Thermal Reactors, July 22-25, 1991, Portland, U.S.A.
/15/ Tanabe, F. et al., "Development of a Two-Dimensional Core-Wide Heat-Up Code MUFLAR and Its Application to Analysis of TMI-2 Core Damage Behavior", Proc. Second International Topical Meeting on Nuclear Power Plant Thermal Hydraulics and Plant Operation, April, 1986, Tokyo, Japan.
/16/ Uchida, M. et al., "A Computer Code to Analyze the Gas-Phase Transport of Fission Products in Reactor Cooling System Under Severe Accidents", JAERI-M 86-158, November 1987.
/17/ Yamano, N. and Soda, K., "Multicompartment Analysis of Aerosol Behavior in the Thermal-Stratified Containment", Proc. OECD/CSNI Workshop on Aerosol Behavior and Thermal-Hydraulics in the Containment, CSNI Report No. 176, November 26-28, 1990, Fontenay-aux-Roses, France.
/18/ Golden, D. W. et al., "Summary of the Three Mile Island Unit 2 Analysis Exercise", Nuclear Technology, 87(1), 326-333(1989).
/19/ Soda, K. et al., "Intentional Depressurization of the Primary and Secondary Circuits as an Accident Mitigation Measure", Proc. OECD/CSNI Specialist Meeting on Intentional Coolant System Depressurization, CSNI Report No. 158, June 12-14, 1989, Garching, Germany.
/20/ Hidaka, A. et al., "Hydrogen Generation during Reflooding of Degraded Core as an Accident Management Measure", Proc. Workshop on Hydrogen Behavior and Mitigation in Water-Cooled Nuclear Power Reactors, March 4-8 , 1991, Brussels, Belgium.

Table 1. Major Dimensions and Capabilities of ALPHA

Volume	50	m^3
Height	5.7	m
Diameter	3.9	m
Design Pressure	2	MPa
Design Temperature	250	^oC

Table 2. Summary of Experimental Conditions

Pressure	: 0.1 - 1.6 MPa
Melt mass	: 10 - 20 kg
Melt composition	: Thermite (iron oxide +aluminum)
Estimated melt temperature	: about 2750 K
Water temperature	: 285.7 - 293 K
Water mass	: 778 - 1,000 kg
Height above water	: 3.5 m

Table 3. Summary of Steam Explosion Experiment

Run No.	Melt Mass (kg)	Pressure (Mpa)	Explosion (Y/N)	Comment
STX001	10	0.1	N	
STX002	20	0.1	Y	Data Acquisition Trouble
STX003	20	0.1	Y	
STX004	20	0.1	Small	Dispersion Device
STX005	20	0.1	Y	Transparent Vessel(T.V.)
STX006	20	0.1	N	Dispersion Device, T.V.
STX007	20	1.6	N	High Pressure, T.V.

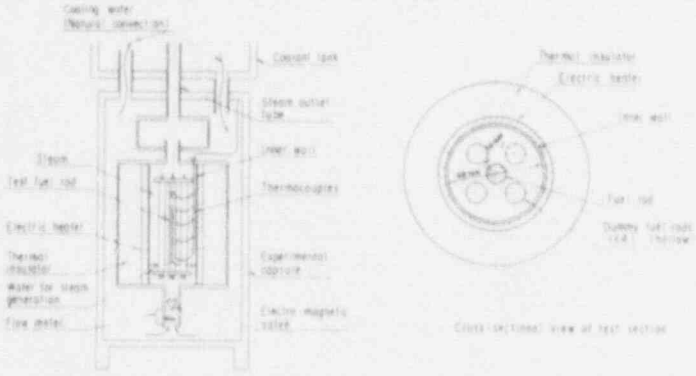

Fig. 1. Schematic of High-Tempeature Flooding Capsule

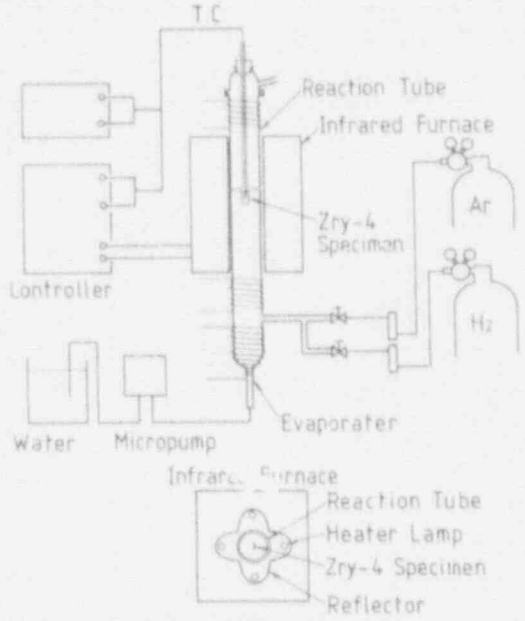

Fig. 3. Fuel Component Interaction Test Apparatus

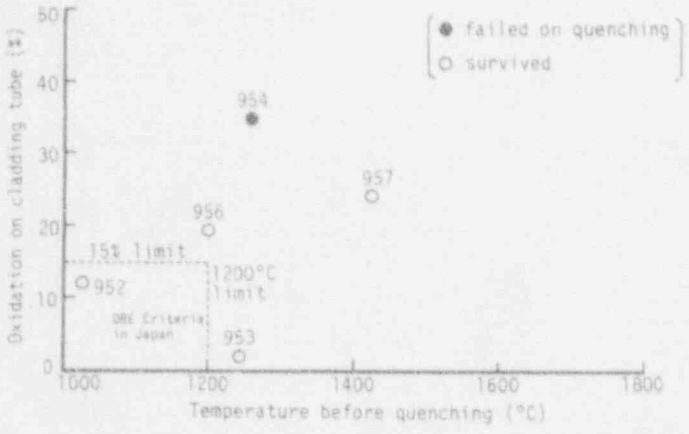

Fig. 2. Failure Map of High Temperature Flooding Tests

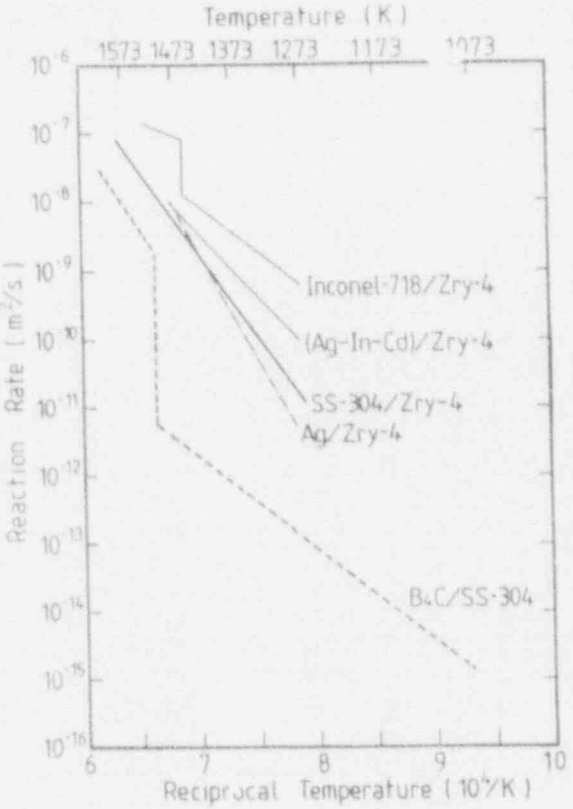

Fig. 4. Reaction Rates of Interactions of Component Materials Interaction

(a) Temperature distribution

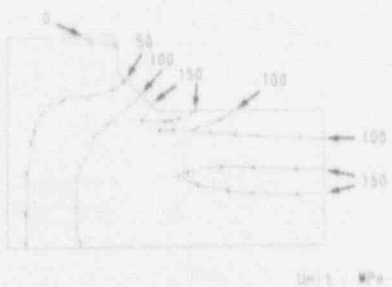

(b) Stress distribution

Fig. 5. Structural Analysis of the T?I-2 Vessel Bottom Head

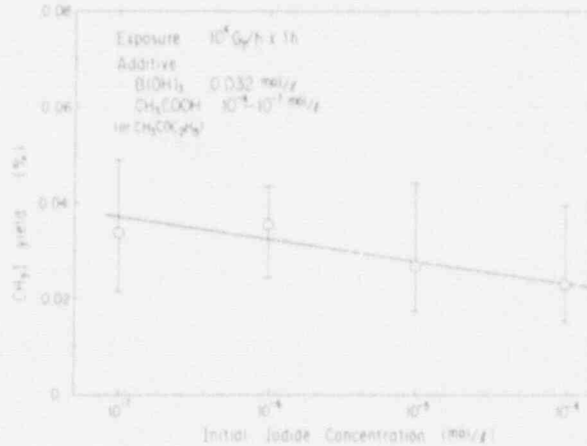

Fig. 7. Effect of Organic Compounds on Formation of Organic Iodine

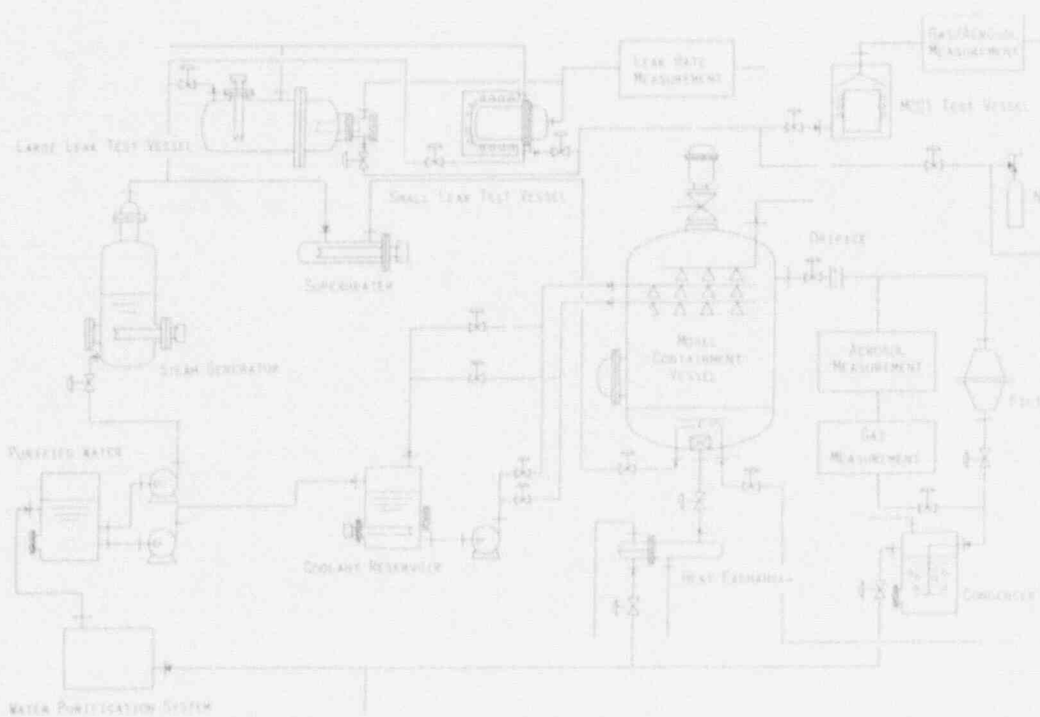

Fig. 6. Schematic Diagram of ALPHA

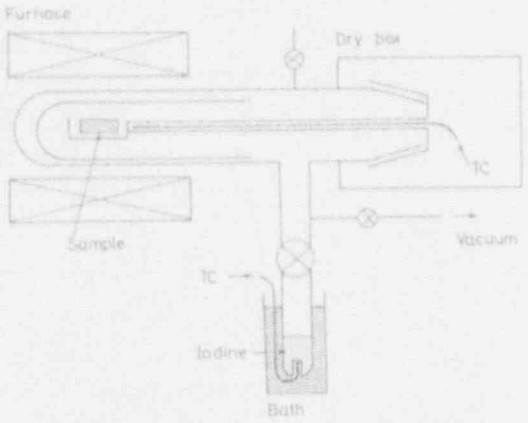

Fig. 8. Schematic Diagram of the Test Apparatus for Reaction Kinetics Experiment

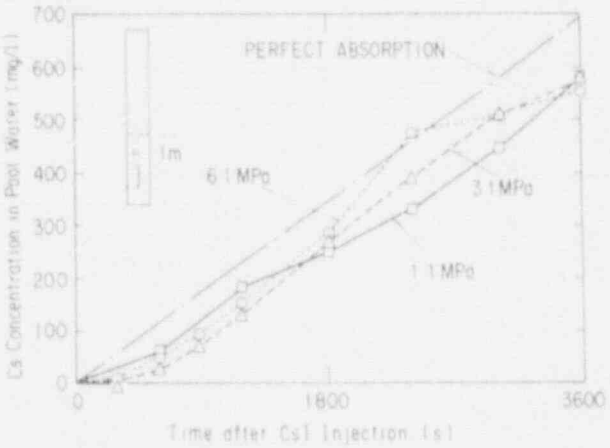

Fig. 10. Effect of Pressure on Efficiency of Pool Scrubbing

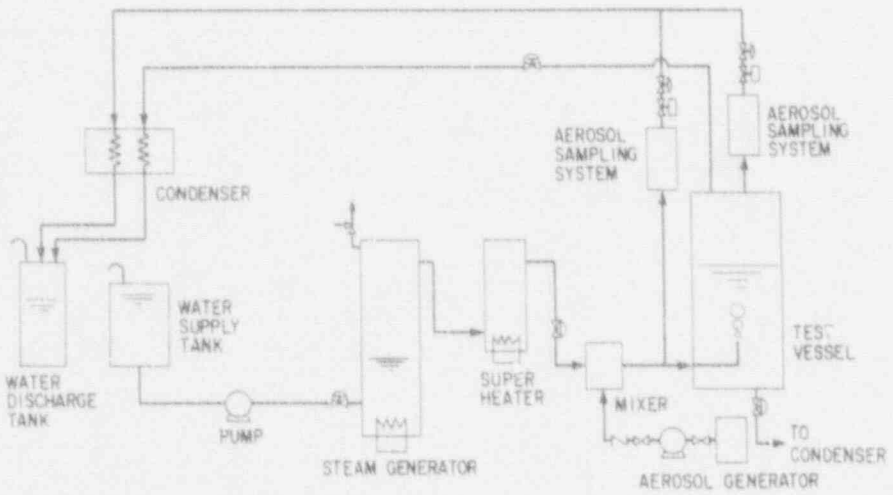

Fig. 9. Schematic Diagram of EPSI

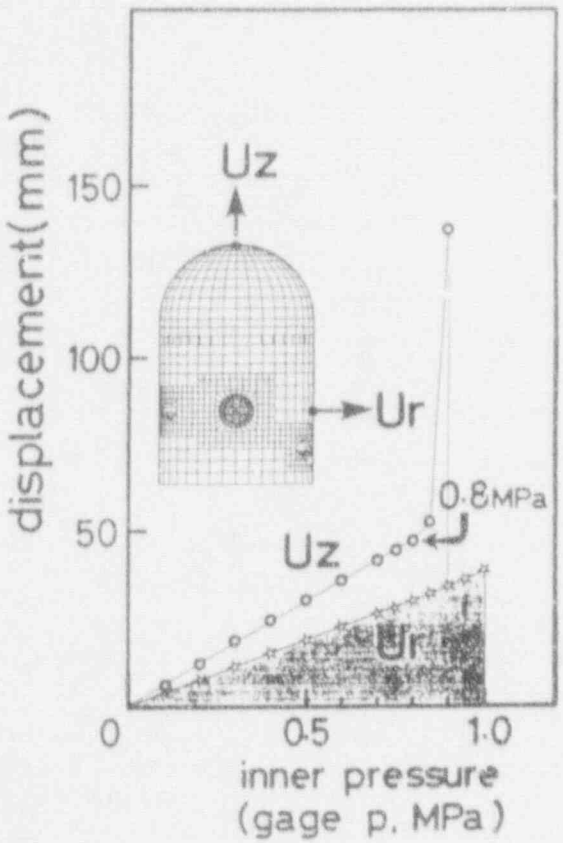

Fig. 11. Displacement of a PWR Steel Containment Vessel Under Extreme Inner Pressure Loading

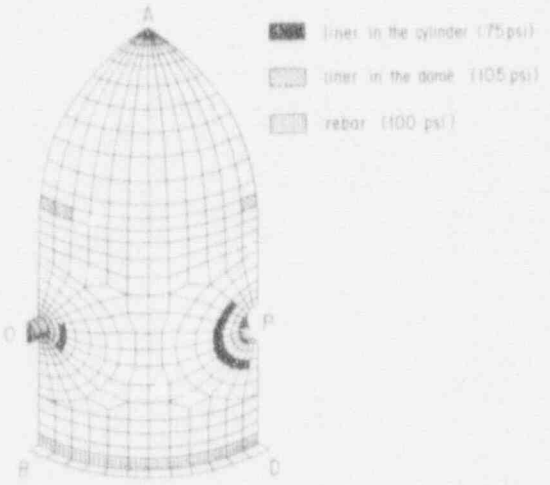

Fig. 12. Predicted Yielding Zones for the 1/6 SNL RCCV Experiments

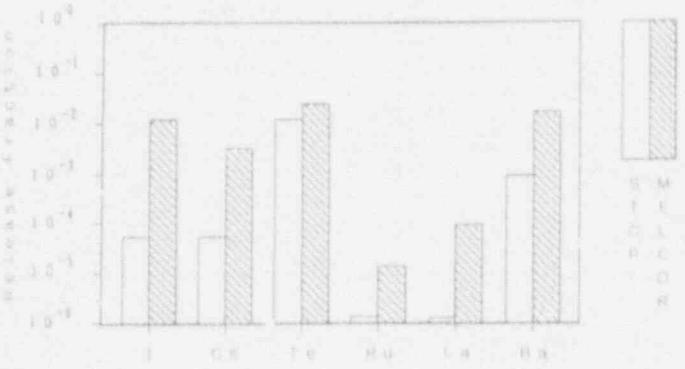

Fig. 13. Comparison of Release Fractions of Fission Products Calculated by MELCOR and STCP

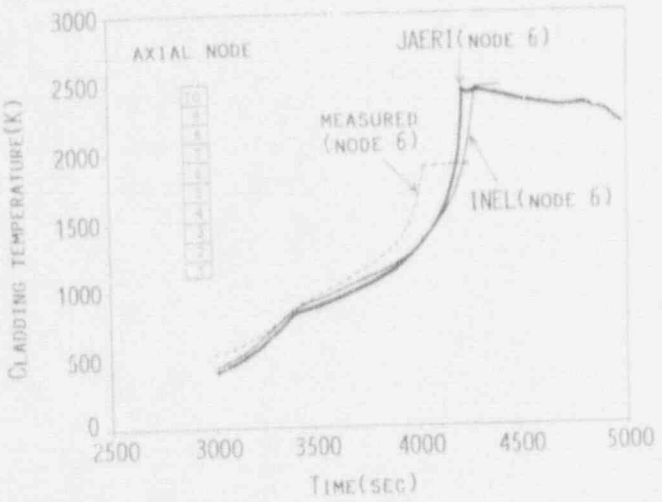

Fig. 14. Simulator Rods Temperature in CORA-2 Experiment

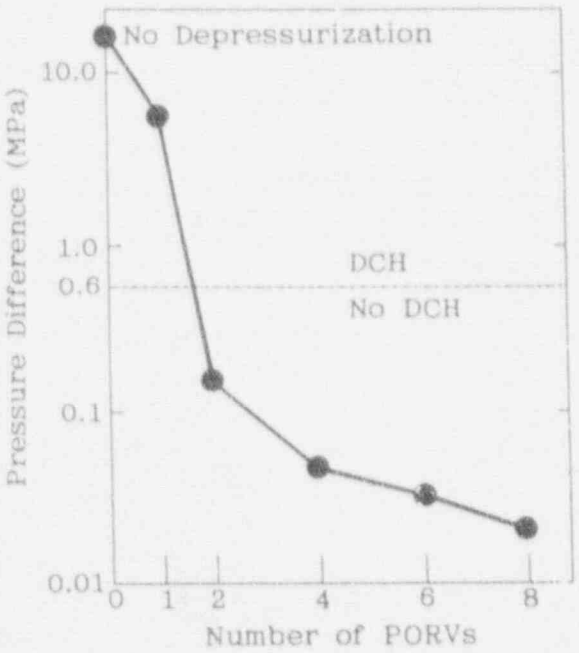

Fig. 15. Pressure Difference Between Primary Coolant System and Containment at RPV Melt-through

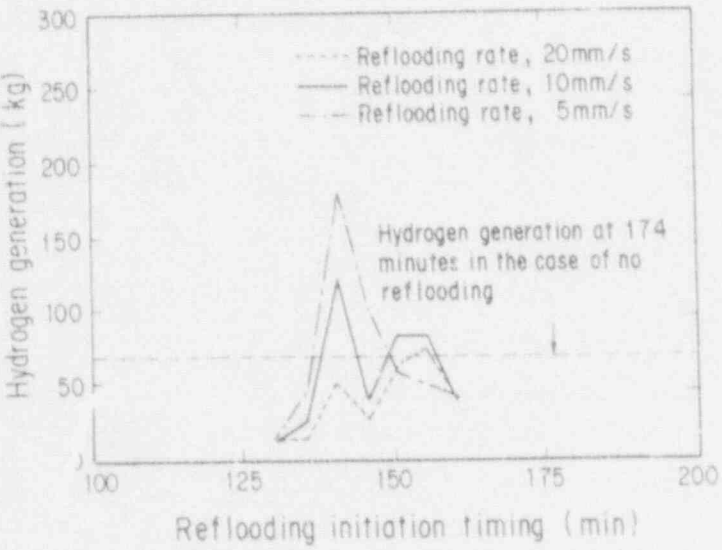

Fig. 16. Effect of Core Reflooding Initiation Timing on Hydrogen Generation

CORE-CONCRETE INTERACTIONS WITH OVERLYING WATER POOLS

E. R. Copus
Sandia National Laboratories
Albuquerque, New Mexico

ABSTRACT

An inductively heated experiment, WETCOR-1, was executed as part of the NRC research program to study and evaluate core debris coolability by overlying water pools. A 35 kg charge material of 80 w/o Al_2O_3 - 20 w/o CaO was heated to melting at 1850K within a 32 cm diameter tungsten annulus heated to 2100K. Ablation of a limestone-common sand concrete basemat was allowed to begin and water at 293K was then added continuously at 60 liters per minute. Both power and water flow were terminated after a 30 minute test period. The main observations from the WETCOR-1 test were that there was an initial period of vigorous melt-water interaction which lasted for 1-2 minutes and was replaced by a relatively stable crust-water geometry with substantially reduced rates of energy transfer to the overlying water. These rates of energy transfer were insufficient to either quench the melt or to discontinue the pre-established meltpool-concrete ablation process.

INTRODUCTION

One of the most important phenomenological issues in the progression of severe accidents after the reactor vessel has failed is whether or not the plant can be brought to a stable condition which avoids the threat to containment integrity, whether by basemat penetration or by containment pressurization. The most commonly available mechanism for removing heat from discharged melt in LWR containments is water addition. The DOE, industry, and the NRC are all now working to develop and evaluate design criteria to address core debris coolability by water pools. The WETCOR experimental program being performed at Sandia National Laboratories is part of the NRC effort to address this issue which is identified as issue L5 under the revised Severe Accident Research Plan. These tests are intended to compliment and augment the ACE/MACE program sponsored by EPRI. Technically, the NRC approach will differ from the basic approach in the MACE tests by including heating of the experiment perimeter to reduce crust attachment and support and thus promote conditions which might lead to bulk freezing. This is accomplished by inductively heating a 32 cm diameter tungsten annulus which is filled with molten oxide mixtures of Al_2O_3, ZrO_2, CaO, and SiO_2 at temperatures of 1800 - 2400K and then flowing subcooled water onto the melt. The WETCOR tests are also designed to answer two additional questions: These are (1) Is oxidic debris more or less coolable than the metallic debris studied in the SWISS test series? (2) What are the limits of coolability in terms of the debris depth, the debris power,

and the debris composition? WETCOR-1 was performed using a different oxidic debris type and under different boundary conditions than either the SWISS tests or the MACE tests in order to focus on the first question. The remaining WETCOR tests will focus on conditions which will address the second question.

WETCOR-1 TEST

WETCOR-1 was executed on September 5, 1991. The test goals were to observe and record the initial simultaneous interactions among molten oxide debris, a concrete basemat, and an overlying water pool. The charge materials for the test were 34 kg of an oxide powder mixture composed of 79 w/o Al_2O_3 - 15 w/o CaO - 4 w/o SiO_2 - 1 w/o Fe_2O_3 with a density of 2.54 g/cc (75% dense). The concrete material for the test was limestone - common sand with a density of 2.34 and a composition of 36 w/o SiO_2 - 32 w/o CaO - 22 w/o CO_2 (as $CaCO_3$) - 5 w/o H_2O. The test procedure was to heat and melt the charge at 1850K, hold a tungsten wall temperature of 2100K, allow 2 cm of ablation to establish the concrete interaction, and then add water at 60 lpm. The water addition was continued for thirty minutes and then the experiment was terminated by turning off the input power.

A schematic diagram for the WETCOR test apparatus is shown in Figure 1. Overall crucible dimensions were 60 cm in diameter and 100 cm in height. The inner tungsten sleeves contained the charge material and had an inside diameter of 32 cm, a height of 18 cm, and a thickness of two centimeters. The concrete basemat was 40 cm in diameter and 40 cm deep. This entire apparatus was contained in a stainless vessel which was continuously purged with air at a rate of 1500 liters per minute and vented through a gravel filter so as to dilute and contain all of the aerosol effluents. Instrumentation for the test was designed to measure the debris temperature, the crucible sidewall temperatures, the heat flux to the overlying water pool, the concrete ablation rate, the approximate gas release rates and composition, and the approximate aerosol release rates and compositions. In addition, there was video coverage of the meltpool surface so that the initial debris-water interactions could be observed.

OBSERVATIONS

The main purpose for performing the WETCOR-1 test was to ascertain whether or not melt-coolant interactions were unstable for extended times during the initial interaction period. Long-lived instabilities might allow for extended periods of very high rates of heat transfer which would result in relatively rapid bulk freezing with very little interaction with the concrete basemat. Extraordinary effort was made in the design and execution of the WETCOR-1 experiment to extend the time for unstable melt-coolant interaction and thus promote a bulk quenching process. This included the use of heated tungsten sidewalls to reduce heat flux-limiting crusts, the use of oxide materials with relatively high specific heats to maximize melt surface temperatures, and the use of a concrete basemat with

an established high gas production rate to increase melt mixing and crust breakup. In addition, the power input to the melt was held to relatively low levels and the meltpool height was relatively shallow. The main observations from the WETCOR-1 test were that there was indeed an initial period of vigorous melt-water instability but that this period only lasted for 1-2 minutes and was replaced with a relatively stable crust-water geometry with substantially reduced rates of energy transfer to the overlying water.

The total energy to the overlying water pool was quantified by measuring the temperature rise in a water supply which was flowing constantly at 60 liters per minute. Initial energy removal rates were 300 kJ/s. These rates steadily dropped to 60 kJ/s after a few minutes and then were relatively constant for the remainder of the test. This total energy must be partitioned among the crucible wall surface area, the tungsten surface area and the meltpool surface area to obtain heat flux information. A quantitative estimate of the energy transfer rates from the debris surface to the water pool is 1.5 MW/m^2 initially with an exponential drop to .4 MW/m^2 at 8-10 minutes and times thereafter. These rates of energy transfer were insufficient to either quench the melt or to discontinue the pre-established meltpool-concrete ablation process.

A comparison of the WETCOR-1 result to previous experiments and analysis indicates that no new dominant phenomenology has been identified and that these results are comparable to those for the FRAG, SWISS, and MACE tests. In each of these previous tests there have been only short periods of high energy release, the concrete ablation process has continued, and stable crusts have formed which limited the upward heat flux to .3-.8 MW/m^2. None of these tests have defined the regime of coolability.

Our next goal is to analyze the extensive data return from the WETCOR-1 test and to compare these results to the data return from the MACE program sponsored by EPRI. Future WETCOR tests will be designed to focus on defining and bounding the limit of debris coolability by varying the debris depth, the debris power, and the debris composition.

REFERENCES:

R.E. Blose, J.E. Gronager, A.J. Su-Antilla, and J.E. Brockmann, "SWISS: Sustained Heated Metallic Melt/Concrete Interactions with Overlying Water Pools", NUREG/CR-4727, SAND85-1546, Sandia National Laboratories, Albuquerque, N.M., 1987

W.W. Tarbell, D.R. Bradley, R.E. Blose, et al., "Sustained Concrete Attack by Low Temperature, Fragmented Core Debris", NUREG/CR-3024, SAND82-2476, Sandia National Laboratories, Albuquerque, N.M., 1987

B.W. Spencer, M. Fischer, M.T. Farmer, and D.R. Armstrong, "MACE Scoping Test Data Report", MACE-TR-D03, Argonne National Laboratory, Argonne, IL., 1991

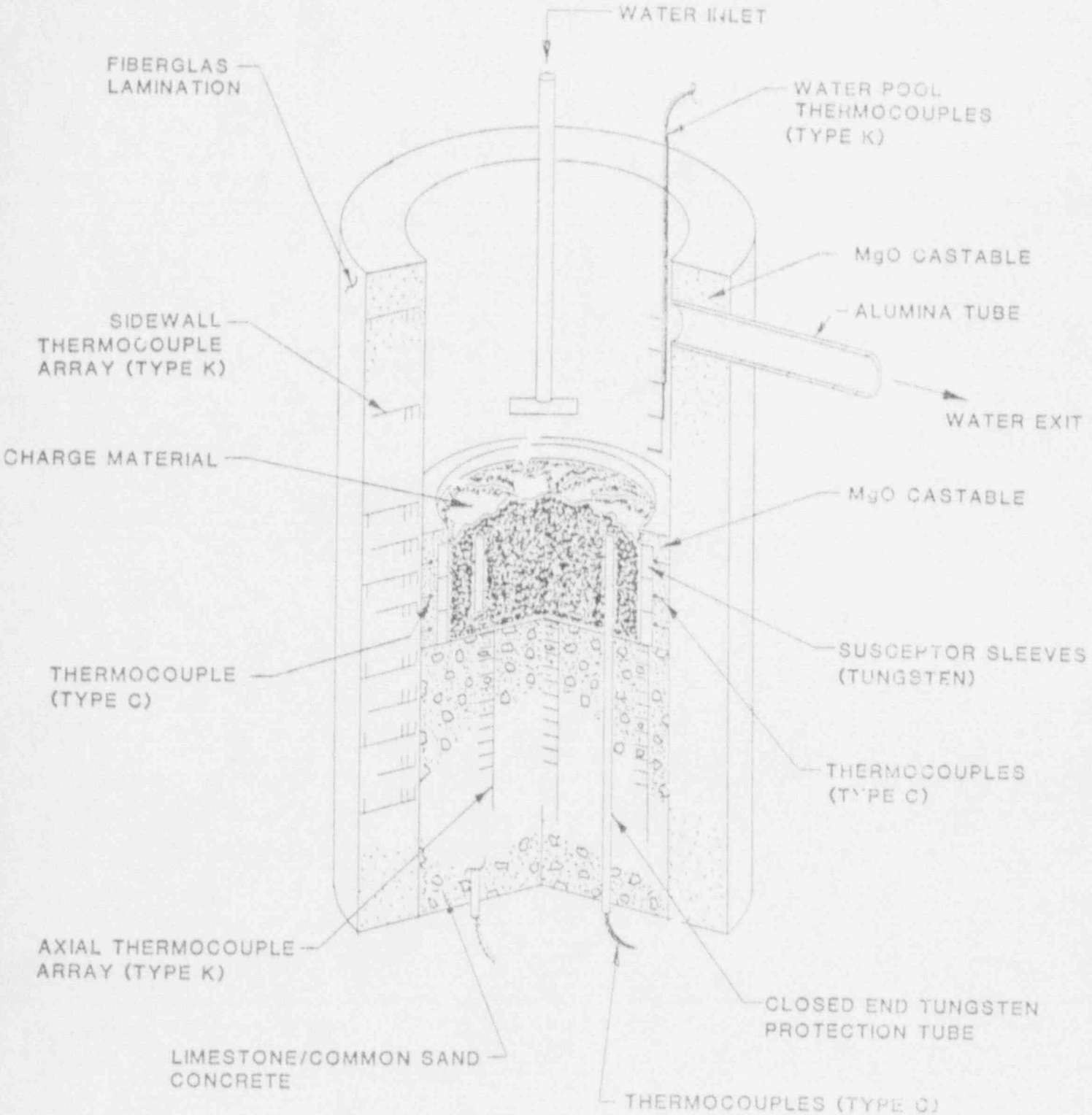

INTERACTION CRUCIBLE WITH SUSCEPTOR SLEEVES
AND CHARGE MATERIAL INSTALLED

PARAMETER EFFECTS ON MOLTEN DEBRIS SPREADING AND COOLABILITY

F. J. Moody
K. M. Fruth
R. Muralidharan

GE Nuclear Energy

ABSTRACT

The spreading, cooling, and freezing of molten core debris on a horizontal surface during a postulated severe accident are important considerations which influence the containment thermal response. This study describes theoretical models for predicting the time-dependent spreading geometry of molten core debris on a horizontal floor, and several associated cooling responses. It was found that corium discharge from a doorway tends to have a spreading angel of about 52 degrees when surface tension is negligible. Simplified heat transfer models are employed to estimate local freezing and mounding of flowing corium, which can diminish its coolability. Effects of metal/oxide stratification and voids on the hot spot temperature also are included. It is shown that when corium arrives at a wall, the resulting hot spot temperature is reduced if the wall slopes away from the corium.

NOMENCLATURE

A	Area
c	Specific heat
D	Diameter, Doorway width
E	Energy
e_{L-s}	Heat of solidification
F	Force
g	Acceleration of gravity
g_o	Newton's constant in $F = Ma/g_o$
H	Corium depth
h	Convective heat transfer coefficient
h_r	Equivalent radiation coefficient
k	Thermal conductivity
M	Mass
P	Pressure
Q	Volume flow rat
q	Heat transfer rate
q''; q'''	Heat flux; Volumetric heating rate
R, r	Radius
T	Temperature
t	Time
$\underline{V} = u\underline{i} + v\underline{j}$	Velocity; u, v components
x, y, z	Displacement coordinates
$( )_c$	Concrete
$( )_i$	Initial value

$( )_s$	Steel; Slab
$( )_\infty$	Ambient value
V	Volume
α	Void fraction; Thermal diffusivity
δ	Plate thickness
ϵ	Small parameter
β	Angle
σ	Surface tension
ρ	Density
τ	Response time

INTRODUCTION

Coolability of flowing debris is largely determined by the spreading configuration, as described by its time-dependent surface area and depth. If freezing occurs at the frontal edge of flowing debris, it may be sufficiently immobilized to prevent its contacting exposed containment boundaries. However, local mounding or piling up of debris could reach a depth at which decay and chemical heating cannot be removed by available cooling mechanisms, resulting in progressive, localized concrete degradation.

An important aspect of molten debris spreading is its pattern as it emerges from the pedestal doorway in a Mark I containment. Various analyses, including those by Kazimi [1], Spencer [2], and Moody [3] were done to help understand various aspects of corium spreading. Experiments by Greene [4] and Henry [5] demonstrate several parameter effects on the flow and freezing configurations of molten simulants.

Available programs for tracking and the spread of flowing debris are based on an assumed spreading angle. The MELTSPREAD [2] computer program has been structured to include all of the anticipated phenomena of molten corium spreading, and it appears that it can be upgraded as new understanding develops. The phenomena treated by MELTSPREAD include spreading, puddling, cooling to the freezing temperature, freezing, remelting, interaction with concrete, convective cooling from the top surface, and internal heat generation. This code is not fully verified at this time.

One difficulty in using or developing a multi-phenomena, complex computer simulation of postulated severe accidents is that the effects of various accident parameters are often obscured. Simplified theoretical models usually can provide an understanding or insight into how a given parameter affects some aspect of an accident.

This study employs a simplified method-of-characteristics formulation to predict the unsteady spreading pattern prior to arrival at a containment boundary. Additional analyses provide approximate models to estimate: how far molten debris can spread before immobilization by freezing and subsequent mounding; the effect of gaseous void fraction; the effect of metal/oxide stratification on the vertical temperature profile; and the effect of sloping angle on the hot spot of an embedded wall when molten debris arrives.

The simplified models are offered only for help in understanding individual parameter effects on selected severe accident responses.

MOLTEN DEBRIS SPREADING ON A FLOOR

Figure 1 shows a two-dimensional spreading configuration where molten core debris discharges through a doorway of width D_o onto a horizontal floor. Open channel theory [6] yields a critical discharge Froude number of $V_o/\sqrt{gy_o} = 1.0$, so that a volume flow rate Q_o corresponds to the discharge elevation and velocity

$$y_o = \left(\frac{Q_o^2}{gD_o^2}\right)^{1/3} \tag{1}$$

$$V_o = \sqrt{gy_o} = \left(\frac{gQ_o}{D_o}\right)^{1/3} \tag{2}$$

Liquid spreading on a floor is driven by gravity, and restrained by both viscosity and surface tension. The reciprocal Reynolds number $\nu/y_o V_o$ for a liquid corium depth of several millimeters or more is less than 0.0004, and can be neglected. The puddle depth, y_σ, determined by equal hydrostatic pressure and surface tension forces, is given by

$$y_\sigma = \sqrt{\frac{2ng_o\sigma}{\rho g}}\ , \quad n = \begin{cases} 1, \text{ Moderate Wetting} \\ 2, \text{ Nonwetting} \end{cases} \tag{3}$$

When the spreading front reaches a depth y_σ, it stops getting thinner as it spreads.

A mass conservation and momentum formulation for the spreading configuration in Fig. 1 is based on a model for one-dimensional hydrostatic waves in a channel of variable width $b'(x',t')$, to accommodate lateral spreading [7], [8]. The lateral spreading rate of a flowing liquid requires one additional describing equation, taken as the open channel result, $Db'/Dt' = \sqrt{gy'}$. The full set of equations for a LaGrangian system which moves with the liquid is expressed in the nondimensional form,

$$\text{Mass:} \qquad \frac{Dy}{Dt} + \frac{y}{b}\frac{Db}{Dt} + y\frac{\partial V}{\partial x} = 0 \tag{4}$$

$$\text{Momentum:} \qquad \frac{DV}{Dt} + \frac{\partial y}{\partial x} = 0 \tag{5}$$

$$\text{Spreading:} \qquad \frac{Db}{Dt} = 2\sqrt{y} \tag{6}$$

where the variables are

$$b = \frac{2b'}{D_o}, \quad y = \frac{y'}{y_o}, \quad V = \frac{V'}{V_o}, \quad x = \frac{x'}{D_o}, \quad t = \frac{V_o}{D_o} t', \tag{7}$$

and the total (substantial) derivative operator is given by

$$\frac{D}{Dt} = \frac{\partial}{\partial t} + V \frac{\partial}{\partial x} \tag{8}$$

Boundary conditions are given by

$$x = 0, \; V = 1, \; y = 1, \; b = 1 \tag{9}$$

and initial conditions correspond to

$$t = 0, \; V = 1, \; y = 1, \; b = 1 \tag{10}$$

Equations (4) - (6) are cast into characteristic forms [7].

Right (+) and Left (-) Traveling Disturbances

$$\frac{dy}{dt} \pm \sqrt{y} \frac{dV}{dt} + \frac{2\zeta\sqrt{y}}{b} = 0, \text{ on } \frac{dx}{dt} = V \pm \sqrt{y} \tag{11}$$

Fluid Particle Path

$$\frac{db}{dt} - 2\sqrt{y} = 0 \quad , \text{on } \frac{dx}{dt} = V \tag{12}$$

If surface tension is zero, the advancing front resembles a classical dam break problem where $y_f = 0$. However, the advancing front cannot be less than the puddle depth of Eq. (3), which would remain constant. In either case, $dy/dt = 0$ at the front. Moreover, $y/b \approx 0$ since the depth y is generally much smaller than the width b. It follows from the right moving disturbance of Eq. (11) that the frontal velocity remains constant for the cases of zero or nonzero surface tension. The value of frontal velocity can be obtained by first integrating the right traveling disturbance of Eq. (11) as

$$\int_1^{y_o} \frac{dy}{\sqrt{y}} + \int_0^{V_f} dV + \int_0^t \frac{2y}{b} dt = 0$$

Letting $t \to 0$, the frontal velocity is

$$V_f = 2(1 - \sqrt{y_o}) \tag{13}$$

Equation (13) also can be obtained from the Riemann solution for simple waves with propagation in one direction only [7]. The frontal velocity of Eq. (13) describes a boundary in the t,x solution field shown in Fig. 2.

Most corium pours will result in a sufficiently high y_o that $V_f \approx 2.0$ is a reasonable simplification, and surface tension does not dominate the spreading front velocity or profile. The case for negligible surface tension, with a critical Froude number discharge, results in the single time-dependent profile solution shown in Fig. 3. The forward flow is supercritical. The elevation profile also is shown in Fig. 3.

Water spreading experiments in a 1/10 scale facility were reported by Theofanous [9], and several profiles are shown in Fig. 4. Calculations in the present study are based on a sudden outpouring of molten debris at the critical Froude number with fixed depth in the doorway. Water pours in the experiments would have spread from the doorway at a variable discharge rate until the discharge level reached its steady value. However, the qualitative comparison appears to bear a good resemblance. Moreover, the method of characteristics solution can be easily modified to include a time-dependent pour from the doorway.

The steady state profile for an unbounded floor is obtained by setting all the partial derivatives with respect to time equal to zero in Eqs. (4), (5), and (6). The resulting equations,

$$V \frac{dy}{dx} + \frac{y}{b} V \frac{db}{dx} + y \frac{dV}{dx} = 0 \tag{14}$$

$$V \frac{dV}{dx} + \frac{dy}{dx} = 0 \tag{15}$$

$$V \frac{db}{dx} = 2 \sqrt{y} \tag{16}$$

can be integrated to give steady profiles of b, y, and V as functions of x. The calculated results show that the spreading angle is about 52 degrees when surface tension is negligible. It follows that the assumption of 45 degrees used in the MELTSPREAD program is reasonably supported by this analysis. No far wall boundary conditions are included in the present analysis.

BASIC HEAT TRANSFER MODELS [10, 11, 12]

Theoretical models for tracking the two-dimensional spreading of molten core debris on a surface involves the mechanics of a gravity driven fluid. However, cooling of the liquid and phase change to the solid may impose both local flow restraints or regional boundaries which immobilize the flow. Therefore, the vertical depth of a corium layer may become uneven, causing local hot spots or other regions which are noncoolable, resulting in extensive concrete attack, and containment pressurization by gas release and chemical heating. Several heat transfer models are summarized next to display effects of various parameters on corium temperatures.

Unsteady Conduction with Heat Generation

Heat conduction in a multidimensional region with volumetric heat generation q''' is governed by [10]

$$T_t = \alpha \nabla^2 T + \frac{q'''}{\rho c} \tag{17}$$

The heat generation term is useful for corium temperature estimates when decay or chemical heat is present, and the heat transfer is conduction-dominated.

Unsteady Cooling of Flowing Liquid Layer

The cooling of a layer of fluid flowing at velocity u with depth H, uniform width, and internal volumetric heat generation q''', based on uniform vertical temperature, negligible conduction in the flow direction, and surface heat flux q_s'' is obtained from energy conservation in the form

$$T_t + uT_x + \frac{q_s''}{\rho CH} = \frac{q'''}{\rho c} \tag{18}$$

Equation (18) applies to corium layers having either rapid conduction thermal response, or internal mixing which maintains local temperature uniformity.

Lumped Thermal Regions

When the internal temperature of a region is approximately uniform, a lumped heat transfer model of volume V and surface area A yields

$$T_t = - \frac{q_s''}{\rho c} \frac{A}{V} + \frac{q'''}{\rho c} \tag{19}$$

which is useful in estimating the thermal response of hot corium layers.

Surface Cooling

If a hot system is cooled by convection, the heat flux is expressed by

$$q'' = h (T - T_\infty) \tag{20}$$

where the convection coefficient h can be modified to include radiation effects by adding [10]

$$h_r = \zeta(\varepsilon) \left[\frac{\sigma (T^4 - T_\infty^4)}{(T - T_\infty)} \right] \tag{21}$$

The term $\zeta(\varepsilon)$ depends on geometry and emissivity, ε. A small object in a large enclosure has $\zeta = \varepsilon$, which can range from about 0.2 to 0.6, depending on the radiation boundary materials.

THERMAL RESPONSE TIMES

Thermal response times encountered in postulated severe accident conditions are useful in determining which cooling modes and models are expected to dominate various heat transfer configurations. Each case below gives a brief description of the phenomenon, the temperature transient form, and the thermal response time.

Convection Cooling

A closed region of uniform temperature T(t) in contact with a convective environment cools according to

$$\frac{q/A}{h\,(T_i - T_\infty)} = \frac{T - T_\infty}{T_i - T_\infty} = \exp\,(-t/\tau_h) \tag{22}$$

$$\tau_h = \frac{\rho c H}{h}, \text{ layer, depth } H \tag{23}$$

Internal Heat Conduction

Heat transfer from an object of characteristic dimension L could be controlled by internal conduction, based on the classical analysis of a slab [10], which gives the surface temperature,

$$\frac{T - T_\infty}{T_i - T_\infty} = A_1 \exp\,(-t/\tau_\alpha) + \ldots \tag{24}$$

$$\tau_\alpha = \frac{4L^2}{\alpha\pi^2}\,; \quad L = H, \text{ layer} \tag{25}$$

Insulated Hot Layer on a Thick Slab

A molten layer of thickness H and initial temperature T_i is suddenly placed in contact with a thick slab at T_∞, where outer surfaces are insulated. The molten layer without internal heating provides the boundary condition $dT/dt = -q''/\rho cH$ from Eq. (19) with $q''' = 0$, for which

$$\frac{T - T_\infty}{T_i - T_\infty} = e^{t/\tau}\ \mathrm{erfc}\ (t/\tau)^{1/2} \tag{26}$$

$$\tau = 1.7 \frac{H^2}{\alpha_s} \left(\frac{\rho c}{\rho_s c_s}\right)^2 \qquad (27)$$

Melting or Freezing

A region of pure substance initially at temperature T_i with melting temperature T_m, could have a surface heat flux limited by either conduction, $K (T_m - T_i)/L$, or convection, $h (T_m - T_i)$. If the heat flux is equated to the rate of phase change, $h_{LS} V_n \rho$, where V_n is the velocity of the phase change front, the freezing or melting response time is

$$\tau = \frac{L}{V_n} = \left\{ \begin{array}{ll} \dfrac{L^2 \rho h_{LS}}{K (T_i - T_m)} & \text{conduction limited} \\ \dfrac{L \rho h_{LS}}{h (T_i - T_m)} & \text{convection limited} \end{array} \right\} \qquad (28)$$

HEAT TRANSFER DURING CORIUM SPREADING ON A FLOOR

An estimate of response times is useful in determining which phenomena dominate a particular transient. Selected responses are summarized below, based on example parameters in Appendix 1 for y of 1.0 cm.

Internal conduction through corium layer (25)

$$\tau_{conduction} = \frac{1}{\alpha} \left(\frac{2y}{\pi}\right)^2 \simeq 3 \text{ s} \qquad (29)$$

Enhanced film boiling convection to overlying water (23)

$$\tau_{convection} = \frac{\rho c_p y}{h} \simeq 72 \text{ s} \qquad (30)$$

Conduction to concrete (27)

$$\tau_{concrete} = \frac{y^2}{\alpha_c} \left(\frac{\rho c_p}{\rho_c c_{pc}}\right)^2 \simeq 324 \text{ s} \qquad (31)$$

Freezing by water, limited by internal conduction (28)

$$\tau_{freezing} = \frac{y^2 \rho h_{LS}}{K (T_i - T_f)} \simeq 7 \text{ s} \qquad (32)$$

Freezing by water, limited by convection to water (28)

$$\tau_{freezing} = \frac{y\rho h_{Ls}}{h\,(T_f - T_\infty)} \simeq 22\ s \qquad (33)$$

This set of example parameters shows that while spreading, convection to water dominates both cooling and freezing. Concrete heat transfer does not play a strong role during the initial spread, and internal conduction across the spreading layer is fast enough to consider uniform local temperature across the depth.

Equation (18) for flow in a channel of uniform width with the surface heat transfer r - of Eq. (20) and the conditions,

$$\left.\begin{array}{ll} \text{incoming boundary} & T\,(o,t) = T_i \\ \text{initial temperature} & T\,(x,o) = T_\infty \end{array}\right\} \qquad (34)$$

yield the solution

$$T^*\,(x^*,t^*) = \pi_1\,(1 - e^{-t^*}) + e^{-x^*}\left\{1 - \pi_1\left[1 - e^{-(t^* - x^*)}\right]\right\} H_s\,(t^* - x^*) \qquad (35)$$

with

$$T^* = \frac{T - T_\infty}{T_i - T_\infty}\ ,\ x^* = \frac{h}{\rho c y V}\,x\ ;\ t^* = \frac{h}{\rho c y}\,t\ ;\ \pi_1 = \frac{q'''y}{(T_i - T_\infty)h} \qquad (36)$$

where H_s is the Heaviside unit step, which is 1.0 for positive values of its argument, and otherwise is zero. Temperature of the advancing corium front corresponds to $x = Vt$, or $t^* = x^*$, for which Eq. (35) yields

$$T^*_{front} = e^{-x^*} + \pi_1\,(1 - e^{-x^*}) \qquad (37)$$

The corium front temperature is graphed in Fig. 5 for corium entering at T_o with volumetric heat generation. Other parameter effects included are the corium density, specific heat, convective heat transfer coefficient, the flowing depth and velocity, and the distance traveled. It is seen that the corium front will be cooled as it flows for values of the parameter $q'''Y/h\,(T_o - T_\infty) < 1.0$. Consider a case where corium enters at the liquidus temperature, $T_o = 2600°K$, with internal heat generation $q''' = 4\ Mw/m^3$ which includes both zirconium reaction and radioactive decay. Use of additional properties of Appendix 1 in Fig. 5 show that when the front travels a distance $x = 3$ m across the ex-pedestal floor to the shell, its temperature drops to

2288°K for an enhanced film boiling coefficient of h = 390 W/m^2-K. If nucleate boiling occurred with h = 60,000 W/m^2-K, the corium front would reach the 2100°K solidus temperature before it traveled 5 cm. Therefore, there are ranges of accident parameters which would result in corium freezing before it reached the shell.

If a downward vertical corium jet spreads radially at uniform depth y on a horizontal concrete surface with cooling by an overlying water layer and negligible heat generation, Eq. (18) becomes

$$DE \frac{\partial T}{\partial t} + \frac{a}{r} \frac{\partial T}{\partial r} + b\,(T - T_\infty) = 0 \tag{38}$$

where

$$a = \frac{Q_o}{2\pi y} \; ; \quad b = \frac{h}{\rho c_v y} \tag{39}$$

Initial and boundary conditions are given by

$$IC \quad T(r,0) = T_\infty, \qquad \text{(before flow begins)} \tag{40}$$

$$BC \quad T(0,t) = T_i \tag{41}$$

A solution for temperature in the spreading layer is

$$\frac{T(r,t) - T_\infty}{T_i - T_\infty} = \exp\left(-\frac{\pi h r^2}{\rho c_v Q_o}\right) H_s\left(t - \frac{\pi y r^2}{Q_o}\right) \tag{42}$$

Eq. (42) shows that the temperature is a function of r only, behind the advancing front, which proceeds according to $t = \pi y r^2/Q_o$, or

$$r_F = \sqrt{\frac{Q_o t}{\pi y}} \tag{43}$$

The temperature profile generated behind r_F does not depend on the depth y (as long as the assumption of uniform T across the depth is valid). Increased h or decreased Q_o would cause a steeper temperature reduction in the radial direction. If the example parameters of Appendix 1 are used, it is found that the freezing temperature is reached at the front when it reaches a radius

$$r_F = 2.7 \text{ m}$$

Suppose that the front stops moving when freezing begins, and forms a dam for continued pour to overflow. A slow flow would continue to freeze at the same r_F, according to Eq. (42). This model does not show whether the freezing would extend radially inward or outward from the point of initial frontal freezing.

A variation in the heat transfer model is employed when the dam forms to determine if freezing and mounding, or continued flowing of the corium would occur. Figure 6 shows corium flow into the puddled region of radius r_F with heat transfer from the top surface. If the convective heat transfer rate is based on an average temperature $\bar{T}$, energy conservation yields

$$\frac{d\bar{T}}{dt} = \frac{1}{y}\left[\frac{Q_o}{\pi r_F^2}(T_i - \bar{T}) - \frac{h}{\rho c_v}(\bar{T} - T_\infty)\right] \tag{44}$$

Note that the layer temperature rises ($d\bar{T}/dt > 0$) or falls ($d\bar{T}/dt < 0$), depending on the sign of the bracketed term. The value of r_F for $d\bar{T}/dt = 0$ is, therefore,

$$r_F = \left[\frac{Q_o \rho c_v}{\pi h}\frac{(T_i - \bar{T})}{(\bar{T} - T_\infty)}\right]^{1/2} ; \quad \frac{d\bar{T}}{dt} = 0 \tag{45}$$

A larger value of r_F would cause continued cooling of the layer. If $\bar{T}$ is set equal to $T_f = 2100$ K,

$$r_F = 2.88 \text{ m}$$

which is close to the results of Eq. (43) for the parameters of Appendix 1. It follows that a slightly greater r_F corresponds to a lower average temperature $\bar{T}$, and $d\bar{T}/dt < 0$, or continued cooling. In other words, the corium would tend to build a frozen mound (probably lifting a top surface crust) inside the radius r_F. The total pour, therefore, is expected to remain within an approximate radius r_F, given by Eq. (45) with $\bar{T} \leq T_f$. A higher pour rate Q_o extends r_F ultimately to the floor limits, for which uniform shallow spreading would be expected.

The pour rate for which the corium would cover a floor of about 10 m radius, based on Eq. (45) with $\bar{T} = T_f$, and the other parameters of Appendix 1, would be

$$Q_o = 0.1 \text{ m}^3/\text{s}$$

CORIUM-WALL CONTACT TEMPERATURE

If a layer of corium of depth H and temperature T_i arrives at a wall of thickness δ and temperature T_∞, continuous heat transfer across the interface results in a contact temperature between T_i and T_∞. Equation (17) was solved

in both the corium and wall of Fig. 7 for which the short term solution yields the classical result [1]

$$\frac{T_c - T_\infty}{T_i - T_\infty} = \left(1 + \frac{k_s}{k}\sqrt{\frac{\alpha}{\alpha_s}}\right)^{-1} \tag{46}$$

based on constant specific heat of both materials. The case of a pure substance with phase change [11] increases the contact temperature about 100°K for the parameters of Appendix 1. Diffusion in a steel wall of the geometry in Fig. 7 causes immediate reduction of the contact temperature, quickly achieving the contact boundary condition $-kHT_x = k_s \delta T_{sx}$. The conduction response time of Eq. (29) for a 3.0 cm thick steel plate wall and 1.0 cm corium depth is 7 s, after which the contact temperature approaches

$$\frac{T_c - T_\infty}{T_i - T_\infty} = \left(1 + \frac{\delta}{H}\frac{k_s}{k}\sqrt{\frac{\alpha}{\alpha_s}}\right)^{-1} \tag{47}$$

or about 864 K, based on an arriving temperature of $T_i = 2600$ K.

Equations (46) and (47) are based on constant specific heat of corium. Since corium is not a pure substance, its temperature changes during solidification. An equivalent specific heat was obtained by employing the heat of fusion in the definition of specific heat, which gave

$$c = \left(\frac{\partial e}{\partial T}\right)_p = \frac{e_{l,s}}{T_{liq} - T_{sol}} = 0.5 \text{ J/gm-K} \tag{48}$$

This value of specific heat is essentially equal to the corium value of Appendix 1.

QUASI-STEADY CORIUM TEMPERATURE

The corium depth will continue to increase in a bounded region while discharge is occurring. The temperature profile will approach the steady state whenever the cooling rate exceeds the energy addition rate by mass flow and internal heating. If corium is added at volume rate Q, the energy addition rate is $E^+ = \rho c Q (T_i - T_\infty)$. If it is spread over area A to a depth H, the internal heating rate is $q'''AH$. If cooling is by convection at an approximate flux $q = hA (T_i - T_\infty)$, and internal conduction is not limiting, the conditions for quasi-steady temperature are $q > E^+ + q'''AH$, and $\rho cH/h > H^2/\pi^2\alpha$, or

$$\frac{H^2}{\pi^2\alpha} < \frac{\rho cH}{h} < \left(\frac{HA}{Q} - \frac{q'''A\,H^2}{h\,(T_i - T_\infty)\,Q}\right) \tag{49}$$

A corium layer of about 20 cm depth satisfies the quasi-steady conditions of Eq. (49) for a corium rate of 0.3 m^3/min, enhanced film boiling, a floor area of about 130 m^2, and about 1.0 Mw/m^3 decay heat generation.

STEADY CORIUM TEMPERATURE PROFILE

The quasi-steady temperature profile in a layer of corium of depth H and internal heating q''' is governed by Eq. (17) with $T_\tau = 0$ and $\nabla^2 T = d^2T/dy^2$. If the layer is insulated at the bottom, and cooled by convection at the top,

$$T(y) - T_\infty = \frac{q'''H}{h} + \frac{q'''}{2k}\,(H^2 - y^2) \tag{50}$$

with the maximum temperature at the bottom,

$$T(0) - T_\infty = \frac{q'''H}{h}\left(1 + \frac{Hh}{2k}\right) \tag{51}$$

A corium depth of 20 cm with $q''' = 1.0\ MW/m^3$ and enhanced film boiling yields the maximum temperature T(0) = 1540 K. If gas bubbling occurred, stirring the layer so that the effective k increased substantially, T(0) would be reduced to about 870 K.

CORIUM, EMBEDDED PLATE HOT SPOT

Liquid corium rises on an embedded plate of thickness δ, insulated on the outside as shown in Fig. 8. The bottom corium surface also is insulated and the top is cooled by convection. Excess heat transfer goes to the plate, which acts like a fin. Therefore, the steady form of Eq. (17) is solved with the additional plate boundary condition,

$$T_{ss}\,[x\,(y),y] + \left(\frac{k}{k_s\delta}\right)\,T_z\,[x\,(y),y] = 0 \tag{52}$$

If the plate profile is described by

$$x = \varepsilon y \tag{53}$$

where ε is small, a regular perturbation of the form

$$T\,(x,y) = \sum_{n=0}^{\infty} \varepsilon^n T_n\,(x,y) \tag{54}$$

n=0 yields an eigenvalue problem for θ=0, which gives the vertical plate solution. The n = 1 solution gives the linearized slanted plate solution. The plate hot spot temperature T(0,0) is given in Fig. 8 for the example parameters $hH/k = 2.7$ and $kH/k_s\delta = 4$. It is seen that a plate which slants outward from the corium has a lower hot spot temperature than a vertical or inward-sloping plate.

CORIUM STRATIFICATION

The steady form of Eq. (17) was applied to cases where the corium was stratified with UO_2 settled to depth H_1 and molten metal of depth H_2 was on top, as shown in Fig. 9. The ratio of homogenized-to- stratified corium maximum temperatures is

$$\frac{[T(0) - T_\infty]_h}{[T(0) - T_\infty]_s} = \frac{\frac{1}{2}\left(\frac{H_1}{H_2} + 1\right)^2 \frac{hH_2}{k_2} + \frac{k_1}{k_2}\frac{H_1}{H_2} + 1}{\left(\frac{k_1}{k_2}\frac{H_1}{H_2} + 1\right)\left(1 + \frac{hH_2}{k_2} + \frac{1}{2}\frac{hH_1}{k_1}\right)} \tag{55}$$

Stratification is not likely if gas is bubbling through the corium from concrete releases. However, gas bubbling is expected to raise the internal heat generation rate and the temperature by reacting chemically with corium metals. A typical case for $q''' = 1.0$ Mw/m^3 decay heat in stratified UO_2 on the bottom has a hot spot temperature about 75% of that resulting from a bubbling mixture with $q''' = 4$ Mw/m^3 decay plus chemical heating in a homogenized layer.

THE EFFECT OF VOIDS

The collapsed depth of corium is H with the steady temperature of Eq. (50). If bubbling caused a void fraction of α, the swollen depth H_α, k_α, and q'''_α would correspond to

$$H_\alpha = \frac{H}{(1-\alpha)} \; ; \quad k_\alpha = k(1-\alpha); \quad q'''_\alpha = q''' (1-\alpha) \tag{56}$$

for which the ratio of maximum temperatures at y = 0 for a swollen and collapsed depth is

$$\frac{[T(0) - T_\infty]_\alpha}{[T(0) - T_\infty]} = \frac{1 + \frac{hH}{2k}\frac{1}{(1-\alpha)^2}}{1 + \frac{hH}{2k}} \tag{57}$$

Equation (57) shows that higher voids increases the maximum temperature. A void fraction of 10% increases the maximum temperature by about the same percentage for a collapsed corium depth of 20 cm. However, the presence of voids implies continuous mixing of corium, which increases the effective conductivity k, thereby causing the maximum temperature to approach its value without voids.

SUMMARY

Simplified theoretical models are summarized in this work to predict: the spreading angle of molten core debris flowing from a doorway onto a horizontal floor; the temperature profile of spreading debris; and the effect

of metal/oxide stratificiation, voids, and embedded wall slope on the hot spot temperature.

The predicted spreading angle is about 52 degrees if surface tension is negligible. Parameter effects on the hot spot temperature are displayed by graphs and equations which include heat transfer properties of the metal and oxide, convective heat transfer coefficients, corium depth, spreading velocity, pouring rate, and concrete properties.

REFERENCES

1. Kazami, M. S. (1989), "On the Liner Failure Potential in Mark-I Boiling Water Reactors," Nuclear Science and Engineering.

2. Spencer, B. W. (1991), "Meltspread-1 Code and Application to Mark I Containment Melt Through," Presentation to Working Group 3--Melt Spreading Under Water, January 9, 1991.

3. Moody, F. J., et. al. (1988), "Mark I Drywell Shell Temperature Response in a Severe Accident," Proc. 16th Water Reactor Safety Information Meeting, October 24-27.

4. Greene, G. A., et. al. (1988), "Experimental Studies on Melt Spreading, Bubbling Heat Transfer, and Coolant Layer Boiling," Proc. 16th Water Reactor Safety Information Meeting, October 24-27.

5. Henry, R. E., (1988), "Mark I Containment Experiments," U.S. NRC Mk I Containment Workshop, February 24-26.

6. White, F. M., Fluid Mechanics, 2nd Ed., McGraw-Hill, New York, 1968.

7. Moody, F. J., Introduction to Unsteady Thermofluid Mechanics, Wiley Interscience, 1990.

8. Fruth, K. M., "Spreading Flow of Molten Corium on a Horizontal Surface," M.S. Project Report, Mechanical Engineering Department, University of California at Berkeley, 1990.

9. Theofanous, T. G., et. al. "The Probability of Liner Failure in a Mark I Containment," NUREG/CR-5423, 1989.

10. Kreith, F., Principles of Heat Transfer, 3rd Ed., IEP-A Dun-Donnelley Publisher, N.Y., 1976

11. Carslaw, H. S., and Jaeger, J. C., Conduction of Heat in Solids, 2nd Ed., Oxford, 1959.

12. Moody, F. J., "First Order Analyses of Molten Corium Heat Transfer," 1989 National Heat Transfer Conference Proceedings, Philadelphia.

APPENDIX I

Example Severe Accident Parameters

Corium	$k = 30$ W/m-K	$T_{liq} = 2600$ K
	$\rho = 9000$ kg/m^3	$T_{sol} = 2100$ K
	$c = 0.48$ J/gm-K	$\sigma = 1.0$ N/m
	$e_{l-s} = 250$ J/gm	$\alpha = 0.07$ cm^2/s
	$\nu = (6.7)10^{-7}$ m^2/s	$Q_o = 0.00833$ m^3/s (slow pour)
Steel	$k_s = 50$ W/m-K	$\alpha^s = 0.14$ cm^2/s
	$\rho^s = 8000$ kg/m^3	$c^s = 0.46$ J/gm-K
Concrete	$k^c = 1.3$ W/m-K	$\alpha^s = 0.0068$ cm^2/s
	$c^c = 0.835$ J/gm-K	$\rho^c = 2300$ kg/m^3
Water	$\rho^w = 1000$ kg/m^3	$c^c = 4.17$ J/gm-K
	$\alpha^w = 0.11$ cm^2/s	$\mu^{pw} = (1.13)10^{-3}$ N-s/m^2
	$k^w = 0.6$ W/m-K	$v^w_{fg} = 1.7$ m^3/kg
	$h^w_{fg} = 2453$ kJ/kg	$h = 390$ W/m^2-K

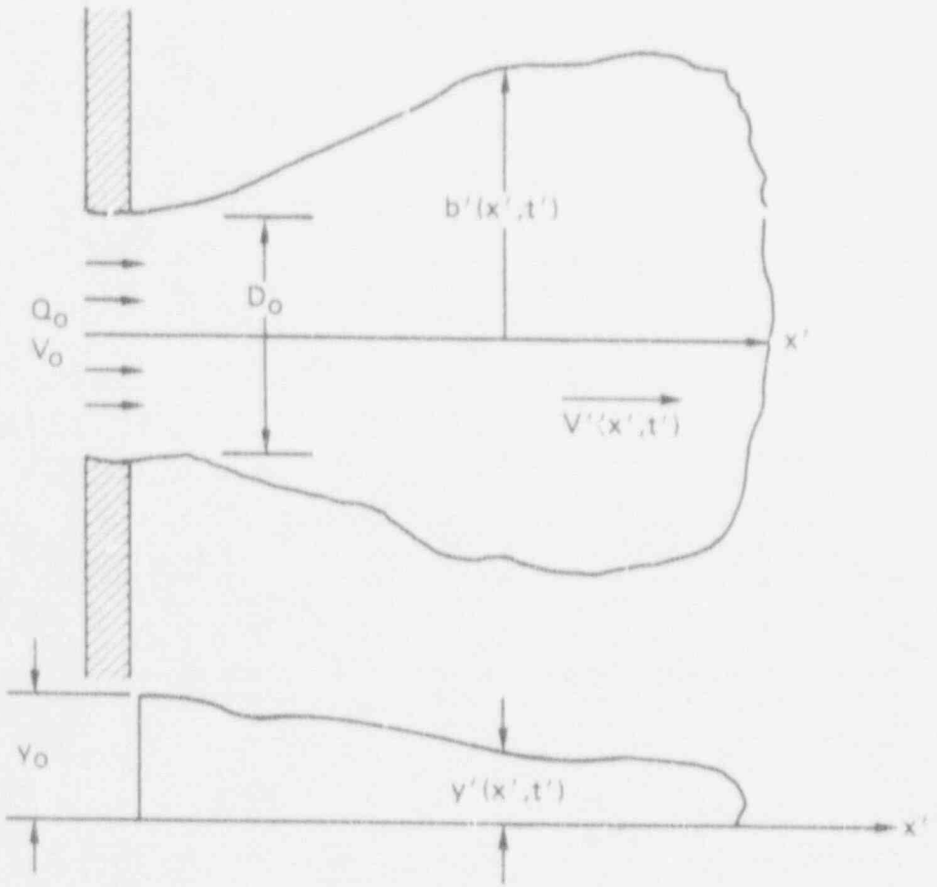

Fig. 1. Molten Debris Spreading on a Floor

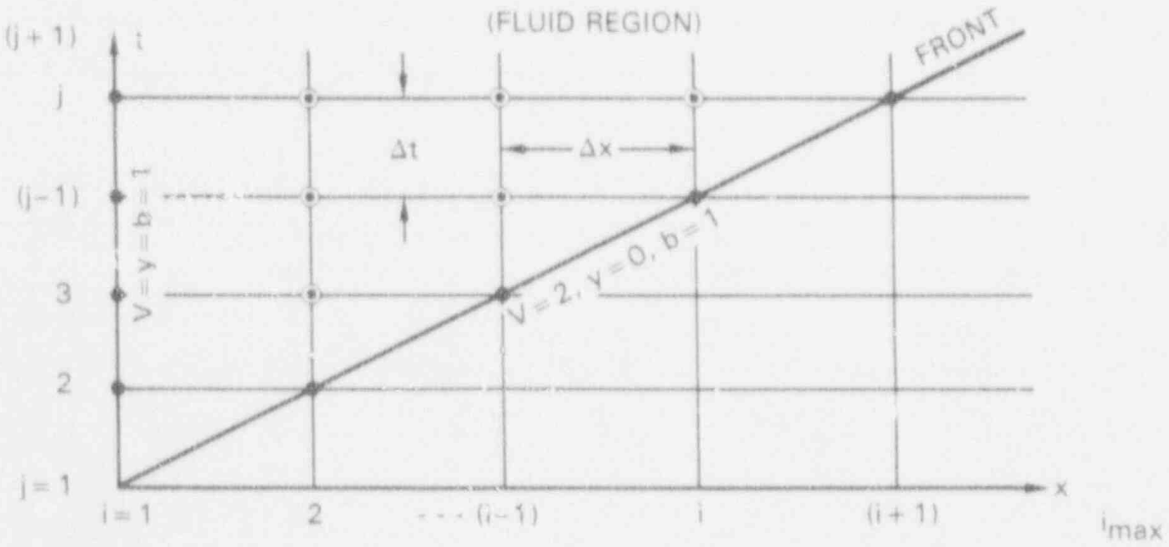

Fig. 2. Solution Field

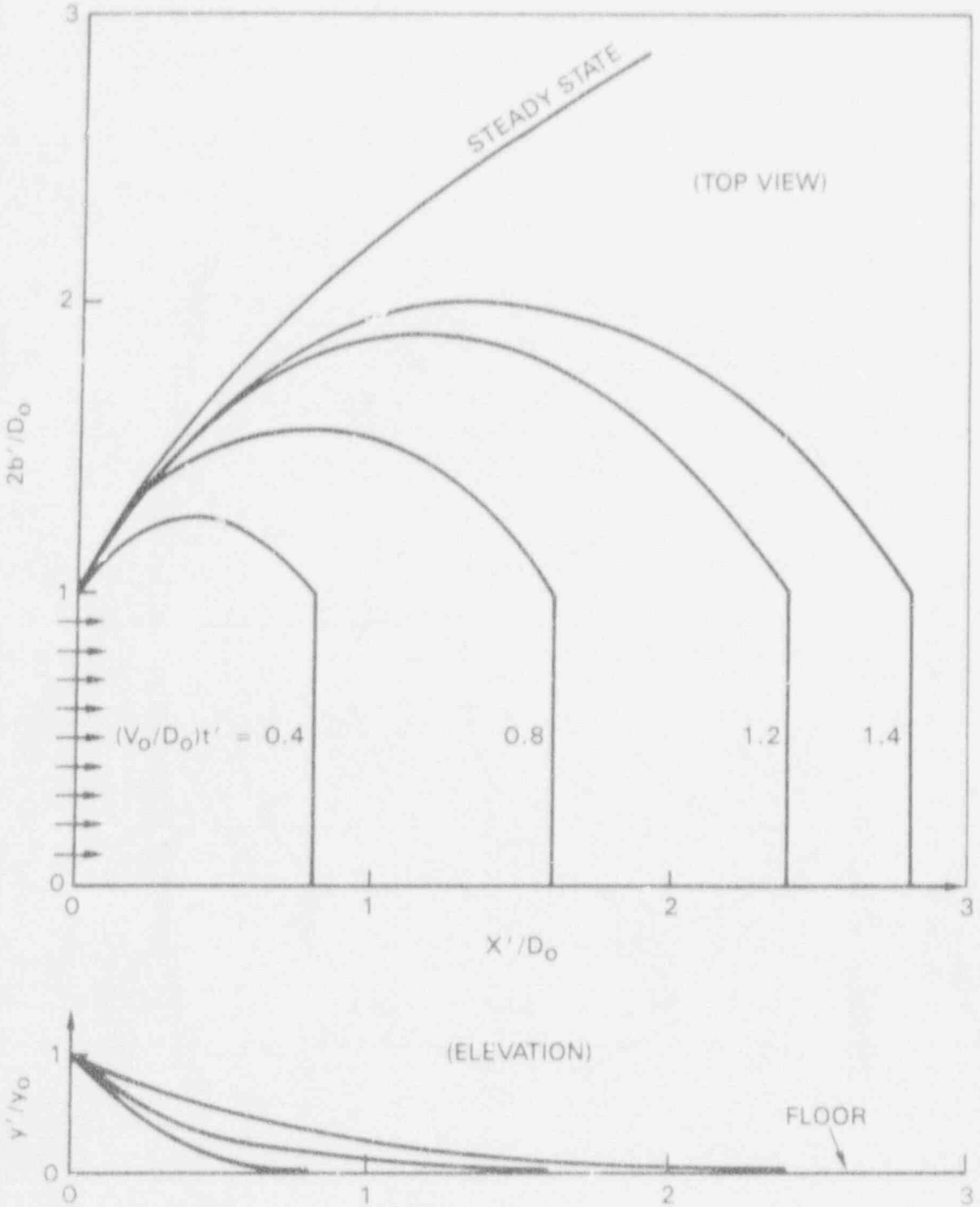

Fig. 3. Corium Spreading Profiles

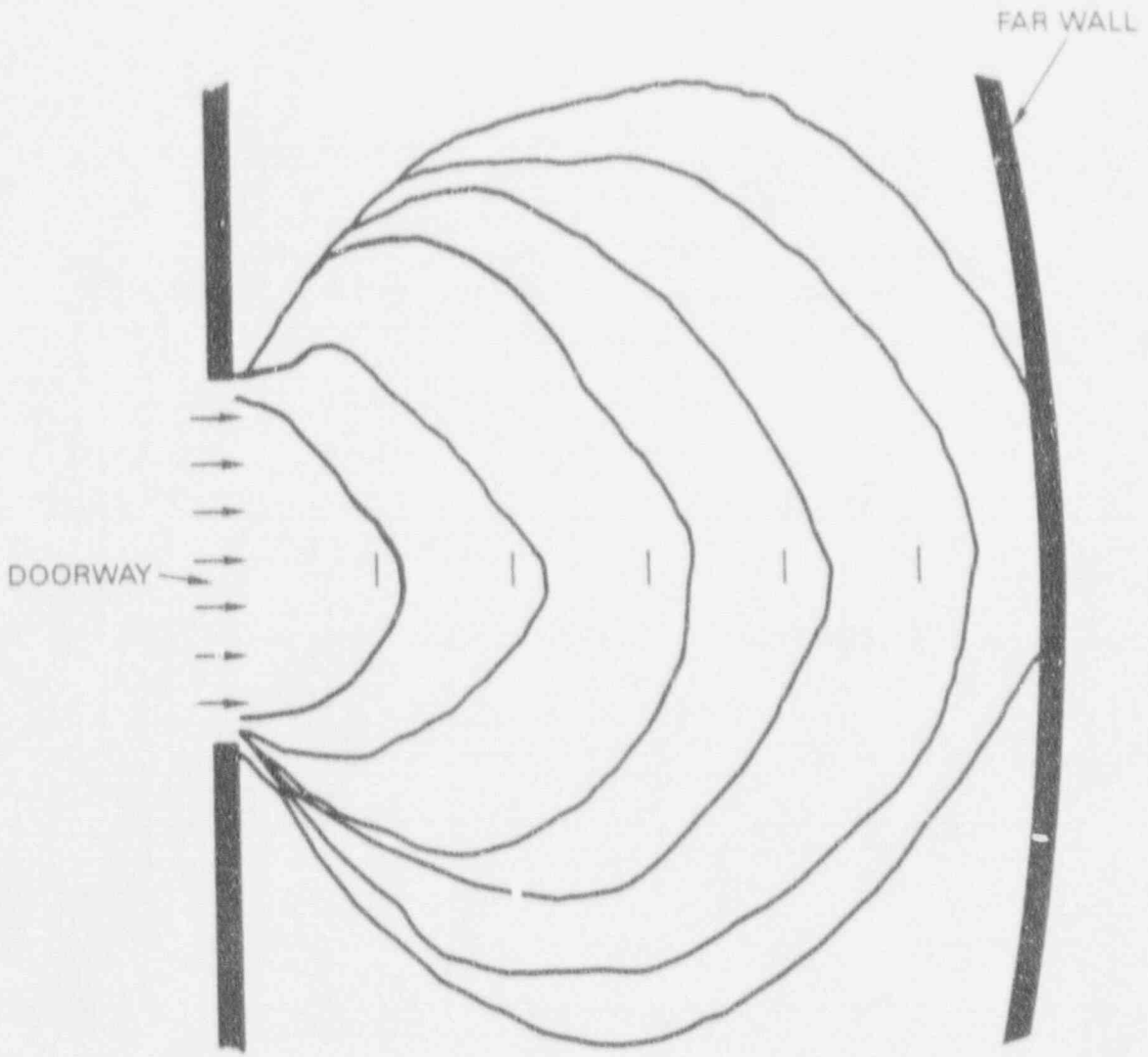

Fig. 4. Early Water Spreading Profiles (Theofanous, 1989)

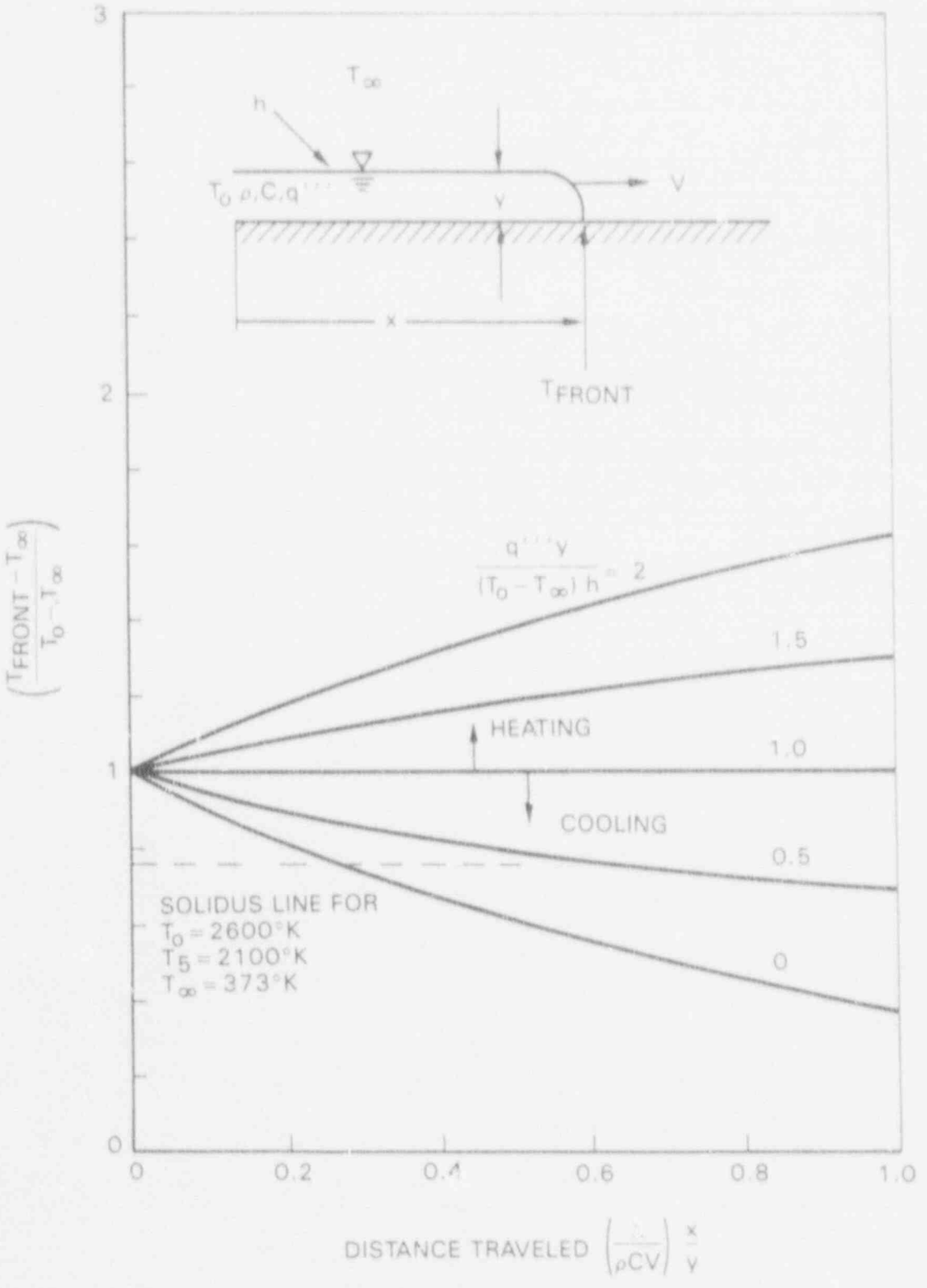

Fig. 5. Corium Advancing Front Temperature

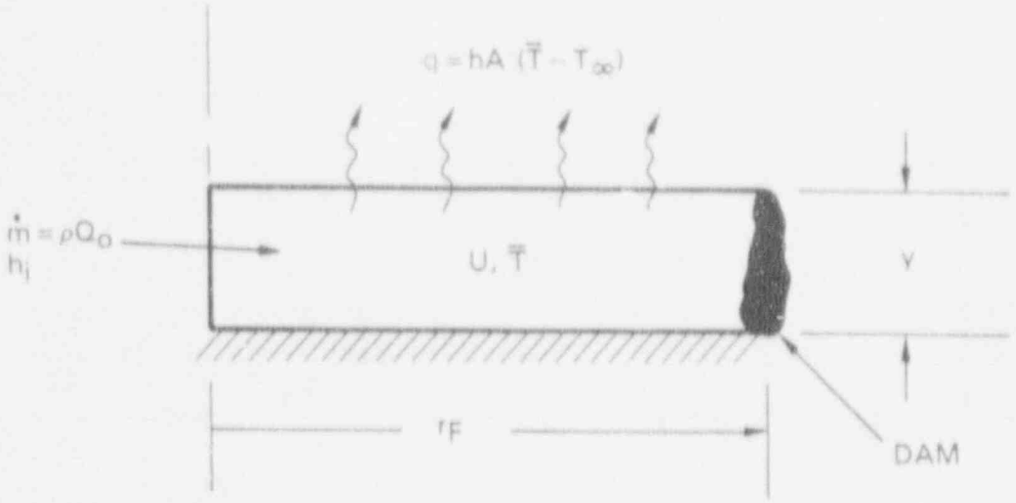

Fig 6. Model to Predict Corium Mount Buildup

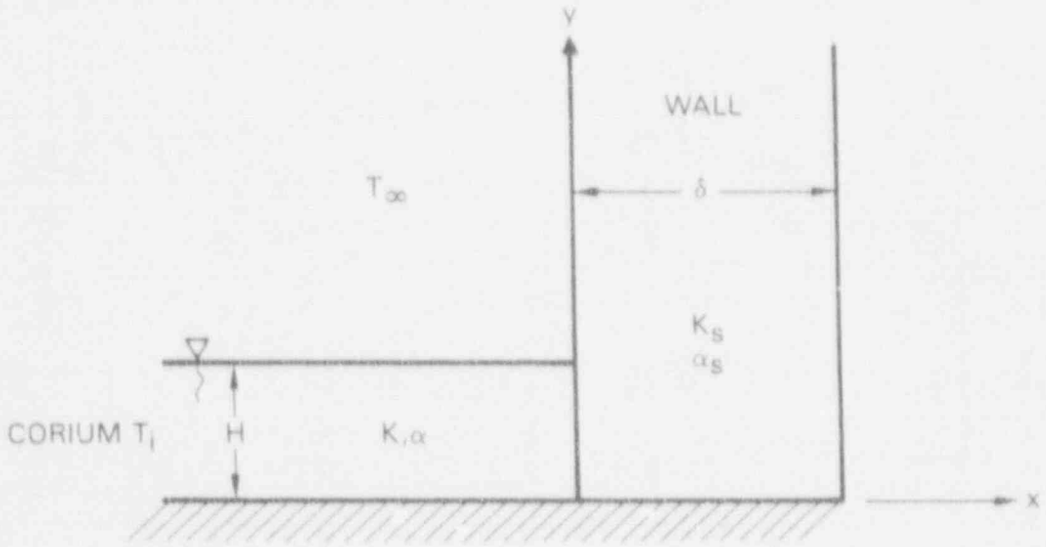

Fig. 7. Model for Contact Temperature

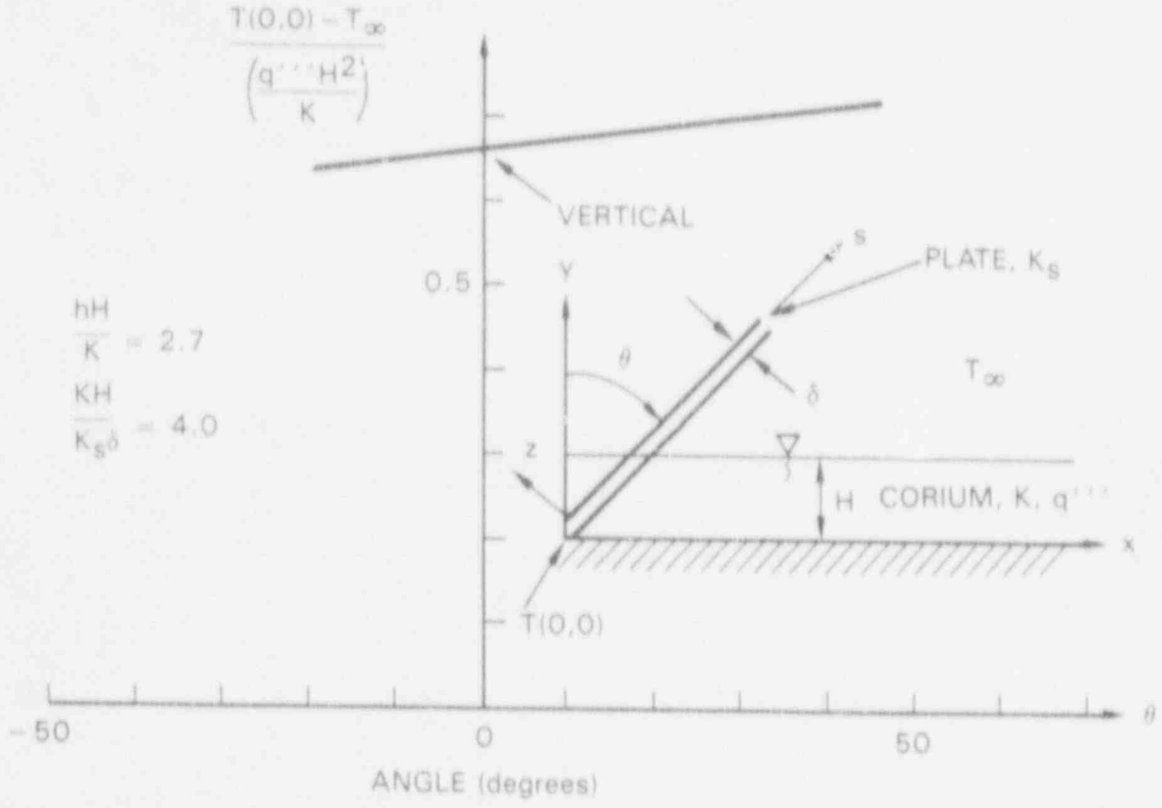

Fig. 8. Maximum Temperature, Corium and Slanted Plate

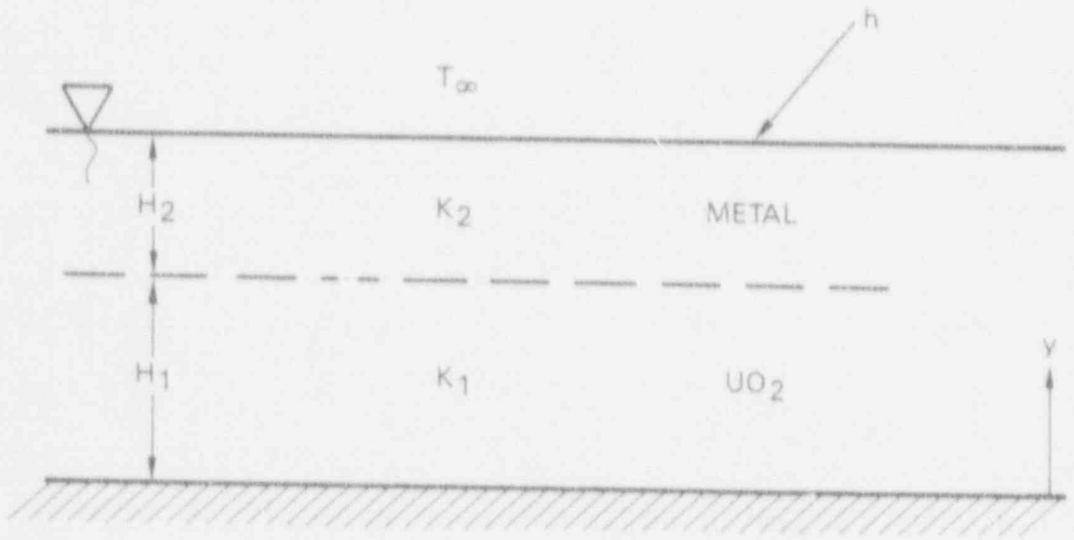

Fig. 9. Stratification Model for Corium Maximum Temperature

ANALYSES OF CORIUM SPREADING IN MARK I CONTAINMENT GEOMETRY*

by

J. J. Sienicki, C. C. Chu and M. T. Farmer
Engineering Development Laboratories
Reactor Engineering Division
Argonne National Laboratory
Argonne, IL 60439

ABSTRACT

An assessment of melt spreading in the Mark I system has been carried out using the MELTSPREAD-1 computer code together with supporting analyses. Application of MELTSPREAD-1 confirms the calculation of shell survival in a wet containment for the most probable melt release conditions from NUREG/CR-5423. According to MELTSPREAD-1, a dry containment also may not be threatened by melt spreading. This reflects the heat losses undergone by the melt in the process of spreading to the shell conservatively neglected in NUREG/CR-5423. However, there exist parameter ranges outside the most probable set where shell failure may be calculated. Accounting for the breakup and quenching of melt relocating through a deep layer of subcooled water also conservatively neglected in NUREG/CR-5423 can reduce the set of parameter variations for which containment failure is calculated in the wet case.

INTRODUCTION

Studies of the risks associated with U. S. Mark Boiling Water Reactors (BWRs) have focused attention on postulated severe accidents involving core melt, core material migration into the reactor vessel lower plenum, vessel lower head failure, and melt release into the containment. Of major interest is whether or not core and structural materials can accumulate inside the pedestal and relocate horizontally under the influence of gravity, or spread, all the way to contact the containment shell and cause shell failure. In the Peach Bottom 2 and 3 Mark I units, the spreading melt is free to exit the pedestal through a single doorway to enter the annular region between the pedestal and containment shell (Figure 1). Although the containment shell is located only 2.6 meters (8.6 feet) from the doorway, the spreading melt will be subjected to significant heat losses as the result of upward heat transfer to overlying water and downward heat transfer to underlying concrete. Heat removal from the spreading material will tend to lower its temperature and promote freezing. Assessment of the potential for melt to spread to the shell and to cause shell failure thus requires the calculation of a number of interrelated physical processes.

An assessment of the containment shell conditional failure probability in the event of melt release into the drywell has been carried out by Theofanous et. al. in NUREG/CR-5423 (1989) using a probabilistic framework. While NUREG/CR-5423

*Work sponsored by the United States Nuclear Regulatory Commission, Office of Nuclear Regulatory Research, Division of Systems Research under FIN No. L11351.

presents an extensively documented and methodical treatment of the shell vulnerability problem as well as providing approaches and solutions for many of the processes involved, a simplified treatment of melt spreading was employed.

In particular, for rapid melt release rates, NUREG/CR-5423 applied results from one-tenth scale simu[illegible] material experiments utilizing water as the spreading fluid. These results [illegible] include the effects of melt freezing nor thermal and chemical interactions wi[illegible]ither the underlying concrete or overlying water that would be present during spreading in the actual Mark I system. For slow melt release rates, melt was simply postulated, in a parametric fashion, to spread over a specified portion of the drywell floor area.

A computer code, MELTSPREAD-1, has been developed at Argonne National Laboratory under Electric Power Research Institute (EPRI) sponsorship to calculate the transient spreading of core and structural materials inside reactor containments (Farmer, Sienicki and Spencer, 1990). MELTSPREAD-1 incorporates models for the basic processes involved in the spreading of reactor materials over a steel or concrete substrate. The code currently accounts for: gravity-driven flow; melt freezing, immobilization, and remelting; concrete heatup, decomposition, and gas release; concrete melting, entrainment, and intermixing with the spreading melt; enhancement of heat transfer to overlying water or underlying concrete due to sparging decomposition gases; chemical oxidation of melt metallic constituents; spreading of melt over previously spread material; and two-dimensional heatup of the shell due to forced convection and impingement heat transfer from spreading melt adjacent to the shell.

There were numerous conservatisms in the approach used in NUREG/CR-5423 to calculate the melt spreading and containment shell heatup behavior. In general, the conservatisms can be grouped into three categories. First, there are the conditions of melt release from the reactor vessel following failure of the vessel lower head. Currently, the various in-vessel codes and models predict a wide spectrum of melt release conditions, particularly with regard to melt release rate. In NUREG/CR-5423, the wide variations in the calculated melt delivery rates were treated by defining two widely differing "scenarios." The first, Scenario I, is based on results obtained from then-current MAAP calculations and assumes a rapid initial release of mainly oxidic core melt materials followed by a slow long-term release of mainly oxidic materials. In Scenario II, based upon Oak Ridge model calculations, the release consists of a more gradual initial release of mainly molten stainless steel and zirconium metals followed by a somewhat slower long-term release of mostly oxides. A second type of conservatism involves the interactions that the melt undergoes while relocating downward from the reactor vessel to the pedestal floor. The conditions of melt arriving upon the pedestal floor may be quite different from the conditions of melt release at the reactor vessel due to the effects of melt interactions with the principally control rod drive-related structure located below the reactor vessel as well as water residing on the drywell floor. The effects of such interactions were conservatively neglected in NUREG/CR-5423. The third type of conservatism involves the melt spreading dynamics which conservatively ignored heat loss processes (to overlying water and the concrete substrate) during spreading.

The objectives of the present work are to evaluate the conservatisms made in the probabilistic assessment of NUREG/CR-5423 and determine the major sensitivities to parameter variations in melt release conditions and melt

spreading phenomena. In addition to the application of MELTSPREAD-1, supporting analyses involving the compilation of BWR melt release conditions and calculations of below-vessel interactions are carried out.

BWR MELT RELEASE CONDITIONS

Table 1 shows melt release conditions for Scenarios I and II corresponding to the most probable values determined from NUREG/CR-5423. Various in-vessel accident progression analyses predict release conditions different from those in Table 1. In order to determine the extent by which specific melt release conditions differ from those selected in NUREG/CR-5423, the results of in-vessel analyses were compiled and documented. For the initial release phases of Scenarios I and II, Figures 2 and 3 present the comparison of model and code predictions versus the most probable values from NUREG/CR-5423. Three calculations are represented in these figures: (i) a MAAP 3.0B Rev. 6.05 calculation for a BWR-3 subjected to the simultaneous loss-of-offsite power and loss-of-injection contributed by J. R. Gabor (Gabor, Kenton & Associates); (ii) an APRIL Mod 3 calculation for a BWR-4 ATWS sequence received from M. Z. Podowski (RPI); and (iii) a recent ORNL model calculation for a short term station blackout in the Peach Bottom BWR-4 units contributed by S. A. Hodge (ORNL).

Aside from differences in the mass released during the initial phase, the melt superheat and release rate calculated with MAAP 3.0B both exceed the most probable values for Scenario I from NUREG/CR-5423 by a significant amount (Figure 2). The extent of in-vessel zirconium oxidation predicted by MAAP 3.0B is also much lower than the most probable value from NUREG/CR-5423 (Figure 3). In contrast, APRIL Mod 3 predicts a lower release rate and zero superheat relative to NUREG/CR-5423 but a similar extent of in-vessel oxidation. APRIL Mod 3 also predicts a greater proportion of metal in the released melt mixture than assumed in Scenario I. This reflects the inclusion in the released material of melted-in, above-core stainless steel structure calculated by APRIL but not considered in NUREG/CR-5423. MAAP 3.0B also predicts the presence of stainless steel constituents in the released melt not included in the melt composition assumed for Scenario I. The results of the recent ORNL model calculation are in fairly close agreement with the most probable values from Scenario II with the exception of the superheat of the released melt constituent phases.

ANALYSIS OF BELOW-VESSEL INTERACTIONS

An analysis of the effects of below-vessel melt-structure and melt-water interactions was carried out. The analysis accounts for the progression of phenomena involved in the relocation to the floor of a corium jet released from a single localized failure in the lower head: melt jet interception by a below-vessel structural member; freezing-induced melt retention within the structure (Figure 4); dripping of melt drops off of the structure; breakup and quenching of the drops in the water layer on the floor; meltthrough of the intervening structural member by jet impingement heat transfer; as well as the breakup and quenching of the subsequently unimpeded melt jet in the water layer (Figure 5). Also calculated are the consequences of the melt-water interactions upon the occurrence and timing of melt jet impingement-induced heatup and meltthrough of the carbon steel sump cover plates located beneath the vessel at the drywell floor elevation. Melt-jet water interactions were calculated using the recently upgraded THIRMAL code developed at Argonne (Wang, Blomquist, and Spencer, 1989). The breakup of drops dripped form the structure is predicted based upon Taylor

instability processes.

For an initially 15 centimeter diameter jet corresponding to the most probable melt release conditions of Scenario I from NUREG/CR-5423, the jet splashes in the structure for the first 30 seconds. Of the 106000 Kilograms released in the 189 second long initial release phase, 6500 Kilograms freezes in the structure during the 30 second splashing stage and 10400 Kilograms falls into the water as drops that break up into smaller droplets that largely freeze to form particulate. Thereafter, melt enters the water layer as a coherent jet calculated to undergo significant partial erosion and freezing but a portion of the melt still impinges upon the sump covers in a jet mode. At 52 seconds, localized plate meltthrough allows the melt remaining in the form of a jet to enter the sump region such that melt impinges upon the sump floor. At the end of the initial release phase, 43700 Kilograms of molten corium has filled the sumps, another 28200 Kilograms has arrived as molten droplets or melt jet, and 27600 Kilograms has arrived as solid particulate. In the 8800 second long-term release phase of Scenario I that involves release rates nearly two orders of magnitude lower than the initial phase, the jet is calculated to initially break up and freeze completely in the water layer. However, the extent of quenching and breakup progressively decrease as a moundlike accumulation of frozen corium develops beneath the vessel and the local effective water depth decreases.

For Scenario II, a negligible mass is calculated to be retained in the structure. Following the 15 second long period of splashing in the structure, the mainly metallic melt jet undergoes partial erosion in the water layer but still impinges on the sump covers causing cover plate meltthrough at 420 seconds. At the end of the 12000 second initial release phase, 38700 Kilograms of molten material has filled the sumps, another 113000 Kilograms has arrived as molten droplets or jet, and 72000 Kilograms has arrived as particulate. The melt jet is calculated to be initially completely broken up and solidified during the subsequent 13000 second long secondary release phase. However, material accumulation effects again ultimately decrease the extent of quenching and breakup.

Thus, melt-water interactions are not calculated to be effective in completely breaking up and freezing the melt released in either Scenarios I or II. However, partial breakup and quenching are predicted such that the released materials arrive as a liquid-solid slurry having a reduced temperature.

MELTSPREAD-1 ANALYSIS APPROACH

To meet the objectives of the present study, a large number of cases were defined summarized in Tables 2 through 4. Cases 1 through 4 correspond as closely as possible to the spreading scenarios addressed in NUREG/CR-5423. These calculations employ the reference melt release conditions representing most probable values from NUREG/CR-5423 (Table 1). Both Scenarios I and II as well as wet and dry containments are calculated. These calculations provide a prediction of shell heatup for conditions similar to NUREG/CR-5423 but using a detailed mechanistic analysis tool (MELTSPREAD-1) that is largely independent of the methodology followed in NUREG/CR-5423. Consistent with the approach followed in NUREG/CR-5423, the calculations include the effects of meltthrough of the sump cover plates and melt collection in the sump volume but neglect melt retention

in the below-vessel structure as well as quenching of the melt as it passes through water on the pedestal floor.

Cases 5 through 41 comprise a sensitivity study for Scenarios I and II. The purpose of the sensitivity study is to determine where the major sensitivities to parameter variations in melt release conditions and melt spreading phenomenlogy lie. Having identified what conditions or modeling assumptions to vary, special attention has been devoted to determining the range within which the value of a particular variable may lie or, at least, the lower or upper end of the range. The intent here is to preclude the calculation of variations that lie outside of physically realistic bounds and, at the same time, understand the relationship of the assumed variation relative to the realizable range. For each pertinent case, the range or either the upper or lower end of the range is included in Tables 3 and 4. Also, the basis for each particular variation is given. For most of the uncertainties examined, only one variation is performed. The present study does not go so far as to delineate the dependency of the spreading behavior upon a particular variable throughout the possible range. In fact, it might be desirable to determine such dependencies for the more sensitive variables at a later date.

Melt is assumed to relocate from the reactor vessel as a single circular jet having a diameter of 15 centimeters (6.0 inches). Due to the effects of melt jet impingement-induced heat transfer, the jet locally melts through the sump covers. Prior to the local meltthrough time, all of the arriving materials collect upon the cover plates. Following meltthrough, the jet penetrates through the hole in the covers and collects inside the sump region. For those cases incorporating the effects of below-vessel interactions, a portion of the melt is assumed to be eroded from the jet to form droplets and particles that continue to accumulate as a slurry on the remaining intact part of the plates. When the sumps are completely filled up, meltthrough of the cover plate thickness sandwiched between the melt in the sump and overlying corium is assumed to immediately occur and the plate carbon steel is added to the material accumulated inside the sump region.

The configuration of the Peach Bottom 2 and 3 Mark I units is assumed for all calculations. MELTSPREAD-1 calculates the spreading of materials through a one-dimensional spreading geometry. Figure 4 shows the nodalization scheme employed for all cases except Cases 13 and 19 that examine the sensitivity to speculation about "tunneling" from the pedestal doorway to the shell and are carried out using the nodalization shown in Figure 5. Inside the pedestal, radial mesh cells are defined concentric with the centrally located jet impingement point. The first four nodes correspond to a radial representation of the rectangular sump region having the same total volume contained by the sumps.

SCENARIO I REFERENCE CASE

Figures 6 through 9 illustrate the calculated spreading behavior for the Scenario I wet containment reference case (Case 1). In the spreading profiles (Figure 6), the horizontal axis represents the distance along the one-dimensional spreading pathway through which materials spread inside the drywell. In particular, zero distance is equivalent to the center of the cylindrical pedestal and a distance of 20 meters corresponds to the rear of the drywell annulus behind the doorway. Plotted on each figure are the calculated local elevation of the

substrate plus immobilized material layers, the actual melt height (with gas sparging-induced level swell effects), the collapsed melt height (without level swell effects included), and the temperature of spreading melt. By 10 seconds, the melt that impinges upon the center of the sump cover plates has spread over the plate area as well as the surrounding concrete pedestal floor and has just flowed through the thickness of the pedestal doorway. The melt temperature has decreased to oxide liquidus a short distance from the jet impingement zone and continues to decrease from the liquidus to a value somewhat above the oxide solidus over the extent of the pedestal and doorway. Between the liquidus and solidus, the melt is assumed in MELTSPREAD-1 to consist of a liquid-solid slurry in which solid particles are intermixed with the molten metal phase (i.e., molten zirconium) and remaining liquid oxide. At 16 seconds, the impinging melt jet locally melts through the sump covers creating a circular hole through the cover plates. Beyond this time the impinging jet passes through the hole eroded through the plate thickness and the released melt collects inside the sump region. However, the surrounding portion of the sump covers is still intact and the melt that has previously collected atop the covers and pedestal floor continues to spread. By 20 seconds, freezing of the oxides at the leading edge of this spreading melt has resulted in immobilization of the leading edge material and formation of a "dam" immediately outside the doorway. At 57 seconds, the sump volume becomes filled with two-phase corium resulting in meltout of the cover plate thickness and incorporation of the melted plate steel into the melt. As melt released from the vessel continues to collect in the sump region, the melt layer above the sumps increases and intermittently exceeds the height of the immobilized material adjacent to and in the pedestal doorway. Melt overflows the immobilized layer and spreads to about half the distance from the pedestal to the shell by 70 seconds. By 100 seconds, the height of melt continuing to collect in the sumps significantly exceeds that of the surrounding immobilized material such that significant flow over the immobilized layers is calculated. The advance of the spreading front involves successive cycles of melt flow over previously immobilized material, melt flow over bare concrete beyond the immobilized material, freezing at the leading of edge of the spreading melt, and continued melt flow over the newly immobilized material at the leading edge. In this manner, melt first reaches and contacts the containment shell at 110 seconds. By 160 seconds, material is calculated to have spread over 73 square meters of the drywell. A plan view showing the extent of melt spreading at this time is presented in Figure 7. This turns out to be the maximum extent of material spreading that is calculated by MELTSPREAD-1. The spreading melt is calculated to have undergone a significant reduction in temperature by the time that it reaches the containment shell. This is illustrated by Figure 8 that shows the time dependent temperature of melt (that has not been immobilized or frozen) and the collapsed depths of melt as well as immobilized material in the node immediately adjacent to the shell impingement point. The melt that first reaches the shell at 110 seconds is rapidly frozen contributing an immobilized layer about 1.5 centimeters in depth atop the underlying concrete. However, melt rapidly overflows the immobilized layer increasing the total collapsed material depth to 12 centimeters at 210 seconds shortly after the completion of the initial rapid release phase. The oxide phase of this melt is subsequently frozen and immobilization takes place at about 285 seconds. The temperature of the melt adjacent to the containment shell is initially just slightly greater than the oxide solidus temperature. However, the temperature rises to a value 155 degrees Kelvin above the solidus at 393 seconds. The temperature boundary condition for convective heat transfer from the melt to the crust formed on the containment shell is taken equal to the temperature of the slurry initially contacting the

shell. The calculated containment shell inner surface temperature at various elevations above the original concrete floor substrate is shown in Figure 9 for the first 1000 seconds. The shell inner surface temperature at heights of 3.2 to 4.6 centimeters above the concrete is calculated to attain a local maximum of 1420 degrees Kelvin at 280 seconds. This is well below the assumed carbon steel melting temperature of 1811 degrees Kelvin. After the oxide melt adjacent to the shell freezes, the temperature is calculated to continue to rise to 1490 degrees Kelvin at about 950 seconds due to thermal conduction effects.

Following the completion of the initial rapid release phase at 189 seconds, the melt release rate falls dramatically from 560 to 7 Kilograms per second and the upper surface attains a more or less uniform elevation in the drywell region outside of the sumps. In this region, the continuing heat losses result in melt immobilization such that the oxide material outside the sumps undergoes freezing. Melt located in the outer part of the sump region is also calculated to immobilize. However, the central node of the sumps into which the melt draining from the reactor vessel is added remains above the solidus throughout the calculation. Thus, the MCCI in this region is calculated to continue with the melt in a bulk slurry state. The gradual release and collection of melt at 7 Kilograms per second is accompanied by a much reduced spreading potential. The melt spreads only a short distance before being immobilized and frozen due to heat loss effects. In the calculation, the immobilization of melt atop previously immobilized material gives rise to a growing wall of frozen material retaining melt in the central part of the sump. MELTSPREAD-1 calculates that this damlike wall of frozen material and the MCCI pool upper surface continue to grow until reaching the 0.7 meter water depth. The resulting local absence of heat losses to water results in an increase in the penetration of melt that flows down the central wall outer surface and over previously immobilized material in the pedestal. By 9000 seconds when the melt release from the vessel permanently ceases, melt released during the long-term phase is calculated to penetrate as far as part of the way through the pedestal doorway. However, this prediction is not completely realistic because a retaining wall of immobilized material is not likely to remain stable. In particular, MELTSPREAD-1 calculates that the material in the inner part of the wall layer thickness undergoes remelting. At 8000 seconds, a maximum temperature of 3530 degrees Kelvin is calculated inside the wall retaining the central MCCI zone. This reflects the inability of the heat transfer mechanisms to remove the energy generated by decay heating inside the thick layer. The problem here is that once melt is immobilized, the immobilization criteria currently programmed into MELTSPREAD-1 do not permit material comprising the immobilized layer to commence flowing again until the temperature of the uppermost substrate heat transfer node rises above the relevant solidus. Thus, while nodes below the uppermost one have remelted, the material remains immobilized. In reality, the physical phenomena associated with internal remelting of a previously frozen layer are currently uncertain. If the immobilized material contains sufficient porosity, then the melt formed might be continuously and immediately released to spread at a gradual rate consistent with decay heating-induced melting. On the other hand, a central cavity of superheated melt might form that is released suddenly. This situation would be analogous to the formation and release of an in-core molten pool surrounded by thick crusts that has been postulated for the Three Mile Island Unit 2 accident.

SCENARIO II REFERENCE CASE

Case 2 is the reference case for Scenario II that involves melt release at only 19 Kilograms per second in the initial phase and 11 Kilograms per second in the long-term phase. The initial release in Scenario II involves a mainly metallic zirconium-stainless steel mixture with a low proportion of oxides followed by the release of mostly uranium and zirconium oxides in the long-term phase. Only a very small mass of melt is released and immediately frozen atop the sump cover plates before localized jet impingement-induced meltthrough of the sump covers is calculated at 11 seconds. The initial release stage thus effectively involves melt collection inside the sump region until it becomes filled at 1080 seconds. Gas release from the sump concrete substrate and sparging of the melt pool in the sumps causes the melt upper surface to temporarily rise to a greater height than the surrounding pedestal floor. Part of this melt spreads to about halfway between the pedestal doorway and the containment shell (Figure 10) and freezes. However, the depth of this frozen layer does not exceed a maximum of 1.1 centimeter calculated at the leading edge. The continued collection of melt inside the sumps causes the pool upper surface to permanently rise above the surrounding floor. However, at the low release rate the melt overflowing the sump boundary is immobilized due to heat transfer to water and the substrate after traveling only a short distance inside the pedestal. This gives rise to the formation of a retaining wall of largely frozen metal above the outer portion of the sump region and the surrounding pedestal floor. This wall serves to contain an increasing level of melt inside the central portion of the sumps. Thus, the behavior here is analogous to that predicted during the long-term release phase of Scenario I in that the formation of a moundlike accumulation beneath the reactor pressure vessel consisting of an annular wall and molten central cylinder is calculated. The height of the mainly metallic mound rises to essentially the 0.7 meter water depth before further melt radial penetration beyond the pedestal commences by 6000 seconds. Temperatures inside the immobilized retaining wall are calculated to locally rise above the solidus temperature of the metal phase. However, the temperatures do not exceed the metal liquidus and, in fact, remain closer to the solidus. For example at 12000 seconds, a peak temperature of 1700 degrees Kelvin is calculated relative to the solidus and liquidus temperatures of 1610 and 1810 degrees Kelvin, respectively. This is a very different situation than in Scenario I where temperatures hundreds of degrees above the material liquidus were calculated. The principal difference here is the lower decay heat source of the mainly metallic mixture initially released in Scenario II relative to the predominantly oxidic composition that is released throughout Scenario I. After the retaining wall height reaches the water depth, melt continues to collect in the central MCCI pool region, overflow the surrounding wall of immobilized metal, and flow down the wall outer surface to spread inside the pedestal. By 10000 seconds, melt is calculated to have spread through the doorway. When the initial release phase that involves mostly metallic melt ends at 12000 seconds, material has spread roughly halfway between the pedestal doorway and the containment shell.

Since the superheat of the released melt remains constant in time, the temperature of the released mainly oxidic melt in the long-term release phase is much higher than the mainly metallic melt in the initial phase. The height of the MCCI pool continues to rise as the retaining wall continues to grow by the freezing of oxide atop the previously immobilized metal. The oxide melt spreads over the frozen metal and eventually reaches the containment shell at 15400 seconds. This results in the presence of an immobilized layer adjacent to the

shell having a depth of 2 centimeters (Figure 11). The resulting shell thermal transient is characterized by a peak shell temperature of about 900 degrees Kelvin (Figure 12). Although the released melt is mainly oxidic, the higher melt temperature results in melting of the underlying immobilized metal substrate over which the melt spreads. Entrainment and intermixing of the melted metal with the oxide produces a metal-oxide mixture in which the metal becomes the dominant phase. Thus, the material that contacts the shell is actually a predominantly metallic mixture having a temperature between the metal phase liquidus and solidus temperatures. The mixture in this regime is a slurry consisting of frozen oxide, frozen metal, and liquid metal. The metal-oxide slurry spreads over previously immobilized material in the drywell resulting in formation of a thick immobilized layer 30 to 40 centimeters thick that extends to beyond the containment shell by 22000 seconds. The maximum spreading extent is attained at 21000 seconds and corresponds to the same spreading extent calculated for the Scenario I reference case. Over a 1000 second interval, the material depth adjacent to the shell rises from to 36 centimeters. The shell thermal transients associated with the repeated contacts with the spreading melt and subsequently immobilized material are characterized by a peak shell temperature of 1230 degrees Kelvin at 21100 seconds.

Melt release from the reactor vessel ceases at 25000 seconds. The temperatures within the frozen layer inside the drywell annulus generally lie below the metal phase solidus. Thus, the layer next to the containment shell represents a stable configuration in which the internal heat generation is removed by upward heat transfer to overlying water and downward heat transfer into the concrete substrate. In contrast, MELTSPREAD-1 also calculates the growth of a 1.7 meter high, mainly oxidic retaining wall inside the pedestal near the termination of melt release. Temperatures as high as 3100 degrees Kelvin are calculated inside this wall. As discussed for Scenario I, this type of configuration in which highly superheated molten material is indefinitely treated as immobilized is not realistic.

SENSITIVITY ANALYSES

In order to reveal the extent of sensitivities to parameter variations, several figures of merit have been employed to compare the various cases. The most important ones are the maximum floor area covered by the spreading melt (i.e., the "spreading area"), the maximum depth of material adjacent to the containment shell, the maximum temperature of material next to the shell, and the maximum shell temperature rise attained. These figures of merit for all of the cases are included in Tables 5 and 6 that summarize the major results for Scenarios I and II, respectively. For reference, key floor areas inside the Peach Bottom 2 and 3 containments are presented in Table 12.

The sensitivity of the maximum spreading area for the Scenario I variations is also shown in Figure 13a. Here the percent change in the spreading area relative to the reference case (Case 1) is plotted versus the extent by which each particular condition or modeling assumption is varied with respect to the possible range of the parameter. Specifically, the extent of variation is defined as

$$e = \begin{cases} \dfrac{x - x_{ref}}{x_{max} - x_{ref}}, & \text{if } x \geq x_{ref} \\ \dfrac{x - x_{ref}}{x_{ref} - x_{min}}, & \text{if } x < x_{ref} \end{cases}$$

where

e = extent of variation,

x = value of variable assumed in calculation,

x_{ref} = value of variable assumed in reference case,

x_{max} = maximum possible value of variable,

x_{min} = minimum possible value of variable.

A positive extent of variation generally corresponds to an increase in a variable (e.g., an increase in the molten superheat of the released melt). A negative extent of variation generally represents a decrease (e.g., a decrease in the melt-to-substrate heat transfer coefficient). The objective of a plot such as Figure 16a is to attempt to compare sensitivities on an approximately equal footing with regard to the maximum extent over which a particular variation represents a realistic uncertainty or conservatism.

The only case found to significantly reduce the calculated spreading area for Scenario I is the assumption of an immobilization criterion based upon a maximum slurry solid volume fraction of 0.6. For the reference melt composition of Scenario I, freezing of the oxide phase nominally immobilizes the melt at a solid volume fraction of approximately 0.8. This reduction in spreading area is highly significant as it totally precludes melt from reaching the containment shell. Increases in the melt spreading area are most sensitive to the assumptions of a more metallic melt composition representative of the inclusion of above-core stainless steel and lower retention in the sump volume. The inclusion of above-core steel results in the melt metal phase volume fraction exceeding that of the oxide phase. Thus, melt immobilization requires the freezing of the metallic phase in addition to the oxide enhancing the spreading penetration. Elimination of retention in the sump volume effectively increases the melt mass/volume spreading on the floor thereby increasing the area covered before the additional spreading melt immobilizes.

Figure 13b shows the maximum depth of material (spreading plus immobilized) calculated immediately adjacent to the shell. A greater peak depth does not, in general, correlate with a lesser spreading extent. This is a consequence of the transient nature of the spreading processes. Figure 13c shows the changes in the maximum temperature of melt adjacent to the containment shell. Plotted here is the change in the temperature difference between the peak melt temperature and the oxide phase solidus temperature. The maximum melt temperature next to the shell is most sensitive to lower sump retention and lower downward heat transfer.

Figure 13d shows the sensitivities of the maximum containment shell inner surface temperature for Scenario I. Specifically, the percent change in the shell temperature rise above the initial temperature is plotted. Three variations are calculated to result in shell meltthrough: zero sump retention, lower downward heat transfer, and a lower spreading angle representative of a tunneling flow between the doorway and shell. The assumption of a stable crust formation freezing mode results in a shell inner surface temperature above the carbon steel melting temperature. However, only surface melting is calculated; melting does not extend into the shell thickness. As discussed earlier, eliminating retention in the sump effectively increases the mass of spreading material and eliminates intermixing with the melt pool in the sump giving rise to greater melt depths and melt temperatures next to the shell. Decreasing the downward melt-to-concrete heat losses also raises the temperature of melt arriving at the shell, decreases the erosion of the sump and drywell floors, reduces melt retention in the enlarged sump cavity, and decreases enhancement of the melt viscosity due to entrainment of eroded concrete slag. Decreasing the spreading angle increases the spreading layer depth and velocity between the doorway and shell that has the net effect of increasing both the depth and temperature next to the shell. The assumption of stable crust formation results in the calculation of a greater melt temperature arriving at the shell due to lower heat losses in the presence of a crust as well as lower viscosities due to reduced concrete slag entrainment. In general, the calculation of shell melting correlates with significant increase in the melt temperature next to the shell. Significantly, the shell temperature is calculated not to rise above melting for the case of a dry containment.

Figure 14 show the sensitivities determined for Scenario II. The maximum melt spreading area is most sensitive to the immobilization criterion; for this variation melt never reaches the shell. Significant reductions in the maximum spreading area are also obtained for the assumption of zero decay heat, lower melt superheat, lower sump retention, rapid chemical reactions, lower upward heat transfer, and lower downward heat transfer. The calculation of a smaller extent of spreading when the heat losses are decreased at first seems counter-intuitive. Decreasing the heat losses increased the maximum spreading area for Scenario I. However, Scenario II involves the spreading of mainly oxidic melt over immobilized metallic material. Decreasing the downward heat losses reduces the remelting of underlying metal thereby decreasing the extent of intermixing of entrained metal into the melt. This results in a greater solid oxide volume fraction in the spreading melt tending to decrease the penetration. Shorter penetrations in turn enhance the formation of thicker layers of immobilized material. It is observed that the cases for which the smallest extent of spreading is calculated are also those resulting in the largest material depth immediately adjacent to the containment shell. In none of the cases is the shell temperature predicted to exceed the carbon steel melting threshold.

Finally, Figure 15 shows the sensitivities for Scenario I for all of the cases that include the effects of melt-structure and melt-water interactions during relocation from the vessel to the pedestal floor. These cases are more realistic than those discussed previously because the previous calculations largely ignored the realistic interaction effects. The four variations encompassed in Figures 15 are those that previously resulted in the calculation of shell inner surface temperatures that exceed the shell steel melting temperature. It is observed that the below-vessel interactions (principally melt breakup and quenching while falling through the water layer) have a mitigative

effect on the calculation of shell melting for two out of the four variations. This reflects the partially solidified slurry composition and lower temperature of the arriving melt.

CONCLUSIONS

The following major conclusions are drawn from the results of the MELTSPREAD-1 analyses:

i) MELTSPREAD-1 confirms the calculation of shell survival in a wet containment for the most probable release conditions from NUREG/CR-5423. The containment shell temperature is calculated to remain below the carbon steel melting temperature of 1810 degrees Kelvin. In particular, peak shell temperatures of 1490 and 1230 degrees Kelvin are obtained for Scenarios I and II, respectively, at a shell location directly facing the doorway. Despite the many differences in melt release conditions and spreading behavior, similar maximum extents of spreading (i.e., maximum spreading areas) are calculated for the two scenarios. The drywell floor area is not completely covered by the spread melt; less than half of the drywell annulus is covered.

ii) According to MELTSPREAD-1, a dry containment may not be threatened by melt spreading. For the most probable release conditions from NUREG/CR-5423, peak shell temperatures of 1570 and 1650 degrees Kelvin are calculated for Scenarios I and II, respectively. The difference from NUREG/CR-5423 reflects the effects of heat losses and the reduction in temperature undergone by the melt as it spreads to the containment shell in the MELTSPREAD-1 calculations. These effects were conservatively neglected in NUREG/CR-5423. However, it should be cautioned that the sensitivities to parameter variations in a dry containment have not been examined as they have for a wet containment.

iii) There exist parameter ranges within which shell failure may be calculated in a wet containment. Shell inner surface temperatures that exceed the melting temperature are calculated only for Scenario I and for those four variations relative to the reference case that involve the assumptions of no retention in the pedestal sumps, a downward convective heat transfer coefficient reduced by 50 percent, tunneling flow between the pedestal doorway and shell instead of spreading, and a stable crust freezing mode as opposed to bulk slurry freezing. In the latter case, only transient melting at the shell inner surface is calculated; melting does not extend into the shell thickness.

iv) The inclusion in the analysis of the realistic effect of below-vessel melt-structure and melt-water interactions conservatively neglected in NUREG/CR-5423 can reduce the set of parameter ranges for which shell failure is calculated. In particular, shell inner surface temperatures exceeding the melting temperature are calculated for the assumptions of minimal retention in the sumps and a reduced downward heat transfer coefficient. The principal effect is the breakup and quenching of released melt in a deep layer of subcooled water. This transforms the released melt into a slurry with a reduced temperature. The below-vessel interactions were found not to significantly influence the maximum spreading extent.

v) The maximum extent of spreading and the containment shell temperature are more sensitive to parameter variations in the melt spreading phenomena than to melt release conditions. Within the range of uncertainty in the melt

immobilization criterion, the spreading melt is calculated not to even reach the shell. In particular, the assumption of melt immobilization at a slurry solid volume fraction of 0.6 results in a maximum spreading area of 35 square meters in both Scenarios I and II relative to a value of 39 square meters corresponding to shell contact and a spreading area of 73 square meters in the reference case calculations.

ACKNOWLEDGEMENTS

This work was sponsored by the United States Nuclear Regulatory Commission, Office of Nuclear Regulatory Research, Division of Systems Research under FIN No. L11351. The authors gratefully appreciate the assistance of F. Eltawila, C. E. Tinkler, and A. Notafrancesco. The authors are also indebted to B. W. Spencer for interesting discussions on the definition and presentation of sensitivity cases as well as for reviewing the manuscript, and J. R. Gabor (GKA), M. Z. Podowski (RPI), and S. A. Hodge (ORNL) for providing the results of in-vessel analyses. Results of the calculations were plotted by exchange student A. Ratsirahonana, CEA, Cadarache. The paper was typed by L. J. Ondracek.

REFERENCES

1. Farmer, M. T., Sienicki, J. J., and Spencer, B. W., "The MELTSPREAD-1 Computer Code for the Analysis of Transient Spreading in Containments," Sixth Proceedings of Nuclear Thermal Hydraulics, 1990 ANS Winter Meeting, Washington, DC, November 11-16, 1990, p. 21, American Nuclear Society, La Grange Park (1990).

2. Farmer, M. T., Sienicki, J. J., and Spencer, B. W., "CORQUENCH: A Model for Gas Sparging-Enhanced, Melt-Water, Film Boiling Heat Transfer," Sixth Proceedings of Nuclear Thermal Hydraulics, 1990 ANS Winter Meeting, Washington, DC, November 11-16, 1990, p. 35, American Nuclear Society, La Grange Park (1990).

3. Theofanous, T. G., Amarasooriya, W. H., Yan, H., and Ratnam, U., "The Probability of Liner Failure in a Mark-I Containment (Draft)," NUREG/CR-5423, July 1989.

4. Wang, S. K., Blomquist, C. A., and Spencer, B. W., "Modeling of Thermal and Hydrodynamic Aspects of Molten Jet/Water Interactions," ANS Proceedings 26th National Heat Transfer Conference, Vol. 4, pp. 225-232, Philadelphia, PA, August 6-10, 1989.

5. Wang, S. K., Blomquist, C. A., and Spencer, B. W., "Interfacial Instability Leading to Bubble Departure and Surface Erosion During Molten Jet/Water Interaction," ANS Proceedings 26th National Heat Transfer Conference, Vol. 4, pp. 31-38, Philadelphia, PA, August 6-10, 1989.

Table 1. MELT RELEASE CONDITIONS OBTAINED FROM NUREG/CR-5423

	Scenario I		Scenario II	
	Initial Release	Long-Term Release	Initial Release	Long-Term Release
Mass Released, Kg	106000	63800	224000	123000
Volume Released, m^3	12.5	7.5	30	15
Melt Release Rate, Kg/s	70-560	7	18.7	7
Melt Composition, wt%				
Zr	18	18	24	2
Fe	-----	-----	45	9
Cr	-----	-----	10	0
Ni	-----	-----	5	0
ZrO_2	11	11	6	24
UO_2	71	71	10	65
Initial Superheat of Released Melt, K	37	37	87	87
Density, Kg/m^3	8500	8500	7480	8210

Table 2. MELTSPREAD 1 REFERENCE CASE CALCULATIONS

Case No.	Scenario	Cavity Condition	Remarks	Basis
1	I	Wet	Includes meltthrough into sump region	NUREG/CR-5423
2	II	Wet	Includes meltthrough into sump region	NUREG/CR-5423
3	I	Dry	Includes meltthrough into sump region	NUREG/CR-5423
4	II	Dry	Includes meltthrough into sump region	NUREG/CR-5423
5	I	Wet	Includes meltthrough into sump region, retention in below-vessel structure, and melt quenching while falling through water	Analysis of below-vessel interactions
6	II	Wet	Includes meltthrough into sump region, retention in below-vessel structure, and melt quenching while falling through water	Analysis of below-vessel interactions

Table 3. MELTSPREAD-I SENSITIVITY STUDY FOR SCENARIO I; VARIATIONS ARE PERFORMED RELATIVE TO CASE 1

Case No.	Variation	Possible Range of Variable or Extreme Value	Basis
7	Increase initial superheat from 37 to 250 K	250 K	MAAP calculation
8	Increase initial release rate from 560 to 1120 Kg/s	1120 Kg/s	MAAP calculation
9	Decrease oxidized Zr percentage from 31 to 3%	3%	MAAP calculation
10	Change melt composition from 18 wt % Zr - 11 wt % ZrO_2 - 71 wt % UO_2 to 22 wt % Zr - 17 wt % Fe - 1 wt % ZrO_2 - 60 wt % UO_2		MAAP calculation
11	Change melt composition to 19 wt % Zr - 44 wt % SS - 21 wt % ZrO_2 - 16 wt % UO_2		APRIL Mod 3 calculation including release of above-core stainless steel
12	Change concrete composition from limestone-common sand to siliceous	Siliceous	Relationship between gas release and concrete type
13	Decrease spreading angle between doorway and shell from 90 to 0 degrees	0 degrees	Speculation about "Tunneling"
14	Decrease temperature boundary condition for melt-to-shell heat transfer from the liquidus to the solidus	Liquidus to solidus	Freezing range
15	Decrease immobilization solid volume fraction from 1.0 to 0.6	0.5 to 1.0	Data on flow of binary metallic alloys and particle-liquid mixtures
16	Change melt freezing mode from bulk freezing to crust freezing	Crust freezing	Existing data on freezing of flowing melts
17	Ignore decay heat	0	Lower bound on internal heating
18	Hold decay heat constant at initial value rather than use a variable decay heat	Initial value	Initial value provides an upper bound on internal heating
19	Raise extent of completion of chemical reactions from variable to 100 percent	100 percent	Upper bound on completion
20	Lower extent of completion of chemical reactions from variable to zero	0	Lower bound on completion
21	Ignore impingement contribution to melt-to-shell heat transfer	Ignore contribution	Lower bound on impingement
22	Multiply heat transfer coefficient for upward melt-to-water heat transfer by a factor of 0.5	0.4 to 1.0	Estimate of effects of crusting at upper surface
23	Multiply heat transfer coefficient for downward melt-to-substrate heat transfer by a factor of 0.5	0.5 to 1.0	Estimate of concrete slag effects
24	Ignore meltthrough into sumps		Lower bound on sump retention
38	Decrease spreading angle between doorway and shell from 90 to 0 degrees; Include retention in below-vessel structure and melt quenching while falling through water	0 degrees	Speculation about "Tunneling"; Analyses of below-vessel interactions
39	Change freezing mode from bulk freezing to crust freezing; Include retention in below-vessel structure and melt quenching while falling through wa	Crust freezing	Existing data on freezing of flowing melts; Analyses of below-vessel interactions
40	Multiply heat transfer coefficient for downward melt-to substrate heat transfer by a factor of 0.5; Include retention in below-vessel structure and melt quenching while falling through water	0.5 to 1.0	Estimate of concrete slag effects; Analyses of below-vessel interactions
41	Ignore meltthrough into sumps; Include retention in below-vessel structure and melt quenching while falling through water		Lower bound on sump retention; Analyses of below-vessel interactions

Table 4. MELTSPREAD-1 SENSITIVITY STUDY FOR SCENARIO II; VARIATIONS ARE PERFORMED RELATIVE TO CASE 2

Case No.	Variation	Possible Range of Variable or Extreme Value	Basis
25	Decrease initial superheat from 85 to 5 K	0 K	Oak Ridge model calculation
26	Increase release rate from 18.7 to 85 Kg/s	85 Kg/s	Local maximum from NUREG/CR-5423
27	Change melt composition to 17 wt % Zr + 54 wt % Fe + 12 wt % Cr + 6 wt % Ni + 4 wt % ZrO_2 + 7 wt % UO_2		APRIL Mod 3 calculation predicting addition of 94000 Kg of above-core stainless steel
28	Change concrete composition from limestone-common sand to siliceous	Siliceous	Relationship between gas release and concrete type
29	Decrease spreading angle between doorway and shell from 90 to 0 degrees	0 degrees	Speculation about "Tunneling"
30	Decrease temperature boundary condition for melt-to-shell heat transfer from the liquidus to the solidus	Liquidus to solidus	Freezing range
31	Decrease immobilization solid volume fraction from 1.0 to 0.6	0.4 to 1.0	Data on flow of binary metallic alloys and particle-liquid mixtures
32	Ignore meltthrough into sumps		Lower bound on sump retention
33	Ignore decay heat	0	Lower bound on internal heating
34	Raise extent of completion of chemical reactions from variable to 100 percent	100 percent	Upper bound on completion
35	Ignore impingement contribution to melt-to-shell heat transfer	Ignore contribution	Lower bound on impingement effects
36	Multiply heat transfer coefficient for upward melt-to-water heat transfer by a factor of 0.5	0.4 to 1.0	Estimate of effects of crusting at upper surface
37	Multiply the heat transfer coefficient for downward melt-to-substrate heat transfer by a factor of 0.5	0.5 to 1.0	Estimate of concrete slag effects

Table 5. RESULTS OF MELTSPREAD-1 CALCULATIONS FOR SCENARIO I

Case No.	Variation	Max. Spreading Area, m^2	Time of Max. Spreading Area, s	Time Melt First Contacts Shell, s	Maximum Material Depth Adjacent to Shell, cm	Time of Maximum Material Depth Adjacent to Shell, s	Max. Melt Temp. Adjacent to Shell, K	Max. ΔT Relative to Solidus[a], K	Time of Max. Melt Temp. Adjacent to Shell, s	Max. Shell Inner Surface Temp., K	Time of Max. Shell Inner Surface Temp., s	Shell Melt-through Predicated (Time of Melt-through, s)
1	Reference Case	73	150	110	12	219	2325	155	193	1489	950	No
3	Dry Containment	106	150	26	9	198	2356	186	123	1567	223	No
5	Include Below-Vessel Interactions	73	190	50	11	238	2315	145	192	1323	1150	No
7	Higher Superheat	73	150	93	13	208	2330	160	150	1468	950	No
8	Higher Release Rate	95	100 <t< 150	15	17	95	2318	148	102	1390	1300	No
9	Higher Metallic Zirconium Content	95	170	109	12	268	2310	140	193	1467	920	No
10	More Metallic Composition	84	150 <t< 200	104	13	198	2294	124	190	1487	261	No
11	Include Above-Core Steel	117	180	62	0	268	1786	206[b]	197	1650	222	No
12	Siliceous Concrete	95	150 <t< 200	110	10	218	2366	196	184	1287	265	No
13	Lower Spreading Angle	95	200	106	15	251	2355	185	193	2197	205	Yes (352)
14	Lower Shell Crust Freezing Temperature	73	150	110	12	220	2325	155	193	1493	210	No
15	Lower Immobilization Solid Fraction	35[c]	-----	-----	-----	-----	-----	-----	-----	-----	-----	No
16	Crust Dominated Freezing	84	150 <t< 200	118	11	234	2365	195	195	1999	241	No[d]
17	Zero Decay Heat	73	150 <t< 200	112	12	221	2320	150	194	1400	900	No
18	Constant Decay Heat	84	150 <t< 200	111	12	283	2338	168	196	1523	900	No
19	Faster Chemical Reactions	84	150 <t< 200	110	11	271	2324	154	200	1455	750	No
20	Slower Chemical Reactions	73	150 <t< 200	112	12	220	2314	144	186	1450	1039	No
21	Lower Shell Impingement Heat Transfer	73	150	112	12	220	2314	144	186	1748	1046	No
22	Lower Upward Heat Transfer	95	100 <t< 150	102	10	200	2343	173	135	1547	29	No
23	Lower Downward Heat Transfer	106	100 <t< 150	21	8.7	244	2435	265	185	2333	194	Yes (340)
24	Lower Sump Retention	117	100	16	10	91	2569	399	99	2404	105	Yes (228)
30	Lower Spreading Angle with Below-Vessel Interactions	84	150 <t< 200	47	15	125	2345	175	194	1479	1131	No
39	Crust Dominated Freezing with Below-Vessel Interactions	73	190	50	12	264	2317	147	193	1311	1298	No
40	Lower Downward Heat Transfer with Below-Vessel Interactions	106	190	148	3.3	149	2424	254	188	2228	198	No[d]
41	Lower Sump Retention with Below-Vessel Interactions	50	100 <t< 150	50	38	504	2180	110	75	1810	200	Yes

a) Oxide phase solidus nominally considered.
b) Metal phase solidus.
c) Melt calculated not to reach containment shell.
d) Only shell inner surface exceeds melting temperature; melting does not extend into shell thickness.

Table 6. RESULTS OF MELTSPREAD-1 CALCULATIONS FOR SCENARIO II

Case No.	Variation	Max. Spreading Area, m^2	Time of Max. Spreading Area, s	Time Melt First Contacts Shell, s	Maximum Material Depth Adjacent to Shell, cm	Time of Maximum Material Depth Adjacent to Shell, s	Max. Melt Temp. Adjacent to Shell, K	Max. ΔT Relative to Solidus[a] K	Time of Max. Melt Temp. Adjacent to Shell, s	Max. Shell Inner Surface Temp., K	Time of Max. Shell Inner Surface Temp., s	Shell Melt-through Predicated (Time of Melt-through, s)
2	Reference Case	73	21000	15400	38	21300	1770	180	20900	1232	21100	No
4	Dry Containment	106	8000	6530	26	17500	1689	79	7550	1654	7750	No
6	Include Below-Vessel Interactions	84	3450	3400	18	18600	1676	67	18600	1092	3400	No
25	Lower Superheat	50	2410	2400	76	21600	1673	63	2400	1294	20500	No
26	Higher Release Rate	62	2000	1710	43	2810	1665	55	2210	1607	2840	No
27	Include Above-Core Steel	62	19500	15900	42	19800	1672	62	19500	1473	19800	No
28	Siliceous Concrete	50	17000	16300	73	17400	1625	15	17300	1628	25000	No
29	Lower Speading Angle	62	20000	15400	50	22400	1698	88	19500	1435	20200	No
30	Lower Shell Crust Freezing Temperature	79	19000	15400	30	19000	1676	76	18800	1181	18800	No
31	Lower Immobilization Solid Fraction	35[b]	24300	-----	-----	-----	-----	-----	-----	-----	-----	No
32	Lower Sump Retention	50	12000	9630	71	13200	1640	30	12000	1039	11000	No
33	Zero Decay Heat	39	16000	15800	1	15800	1610	0	15800	1004	15800	No
34	Faster Chemical Reactions	50	18000	15400	25	21000	1632	22	19800	1062	19500	No
35	Lower Shell Impingement Heat Transfer	50	18000	15410	12	19100	1632	22	19100	1070	18100	No
36	Lower Upward Heat Transfer	50	14000	13300	50	20500	1648	38	25000	1068	25000	No
37	Lower Downward Heat Transfer	50	17000	15800	70	19100	1669	59	18800	1400	25000	No

a) Metal phase solidus nominally considered.
b) Melt calculated not to reach containment shell.

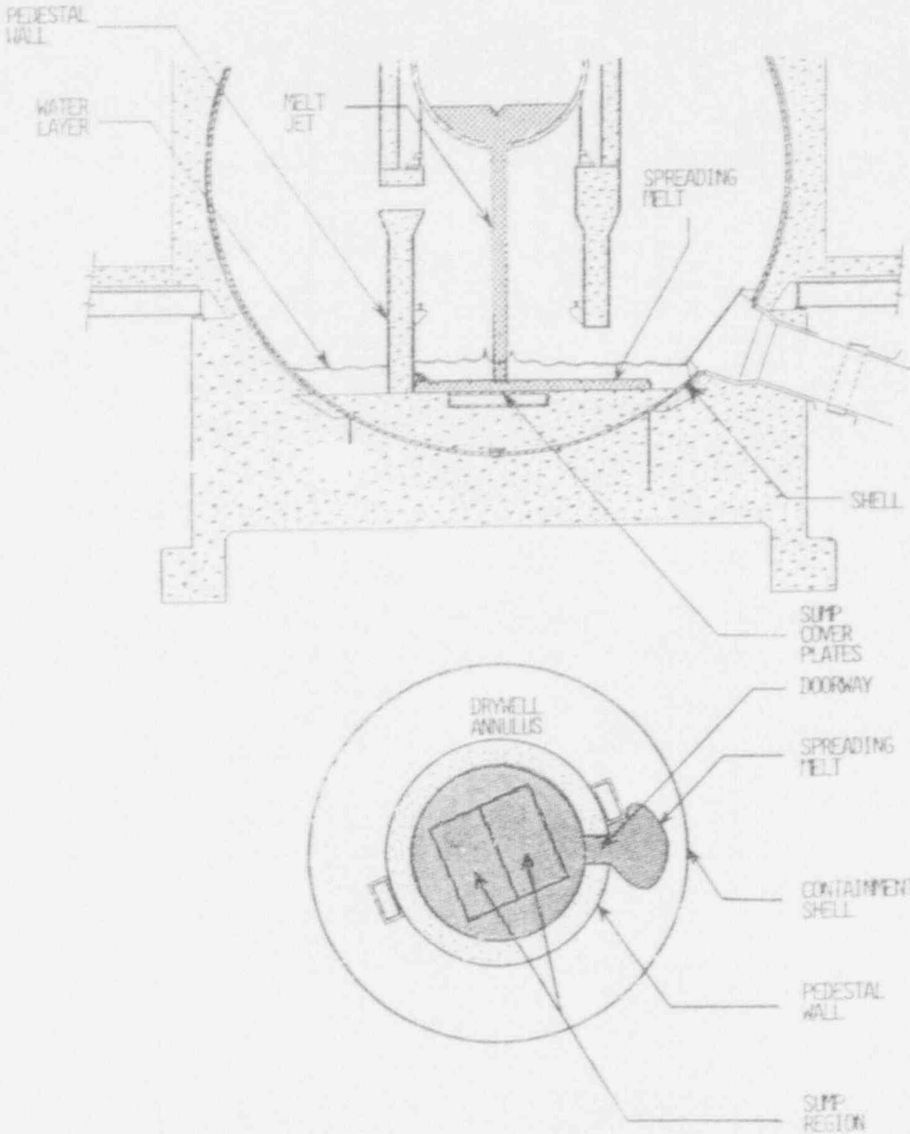

Figure 1. Illustration of Melt Spreading Inside Mark I Containment.

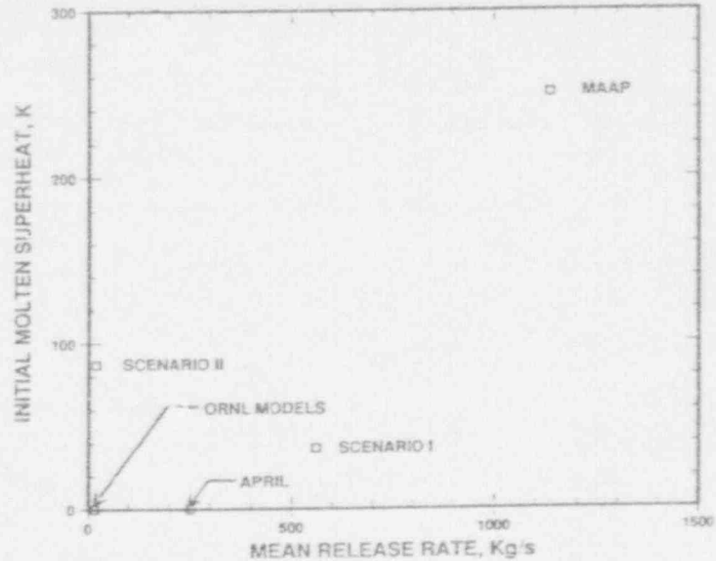

Figure 2. Comparison of Melt Superheat and Release Rate for Initial Release Phase.

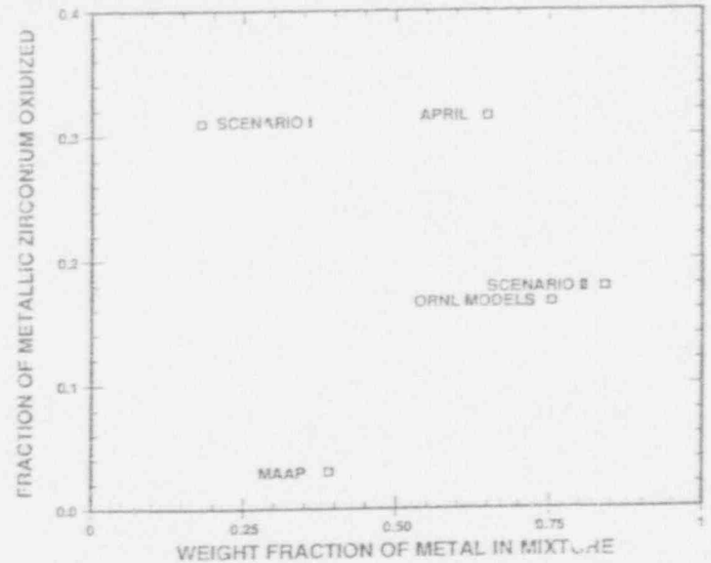

Figure 3. Comparison of In-Vessel Zirconium Oxidation Extent and Metal Content for Initial Release Phase.

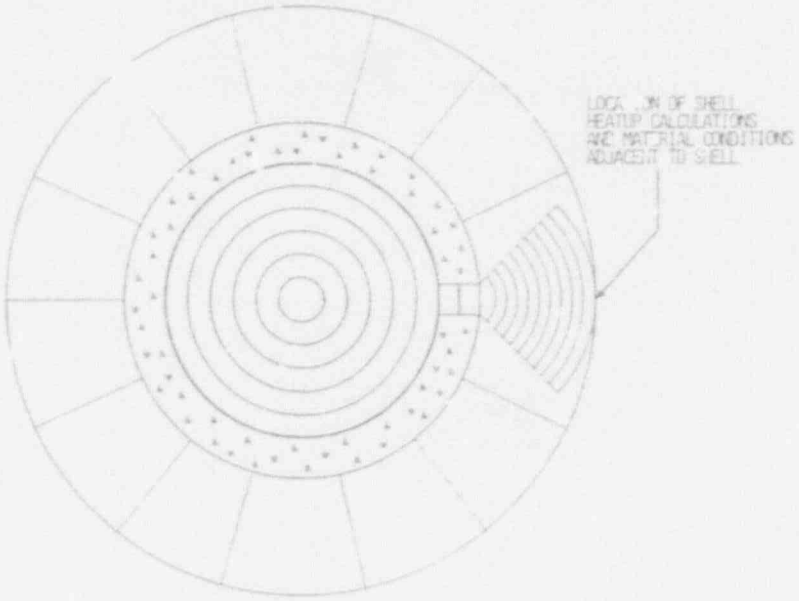

Figure 4. Spreading Channel Nodalization for Reference Cases.

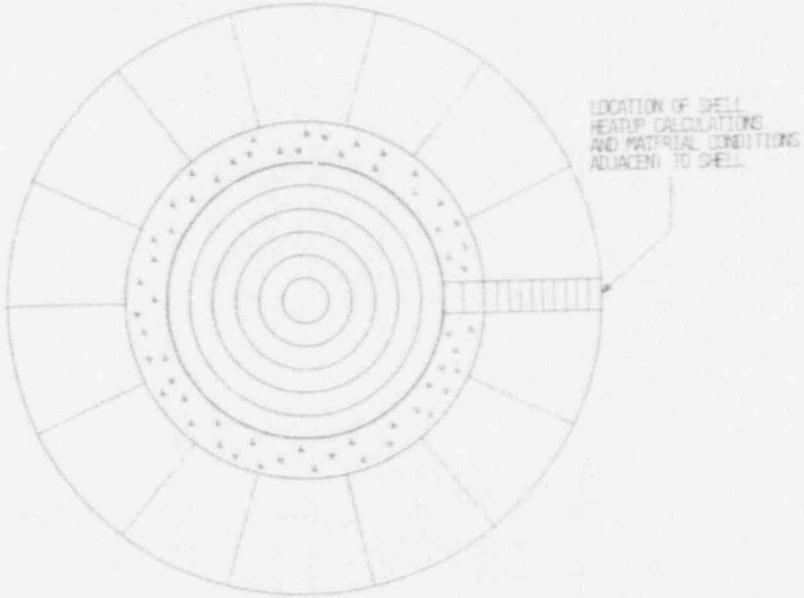

Figure 5. Spreading Channel Nodalization for Investigation of Tunneling Flow Effects.

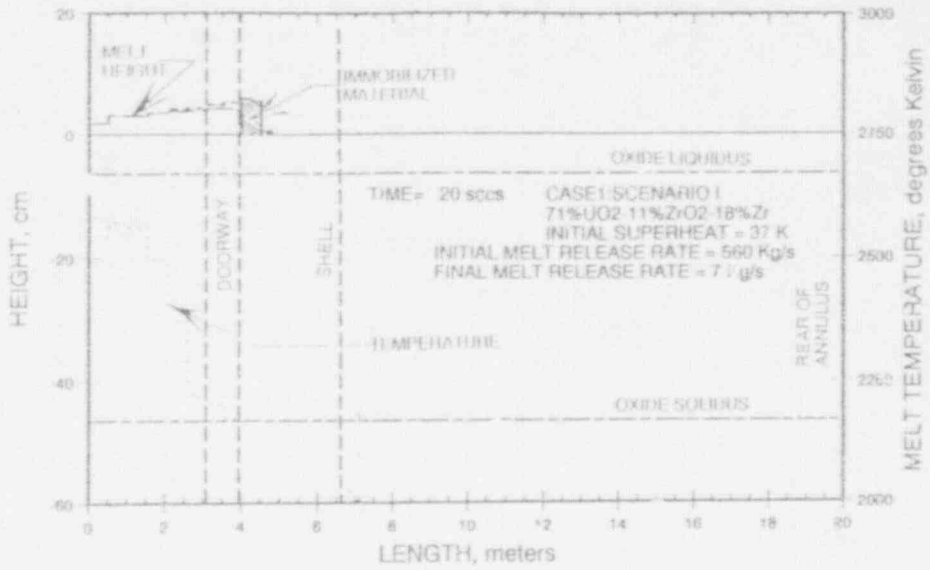

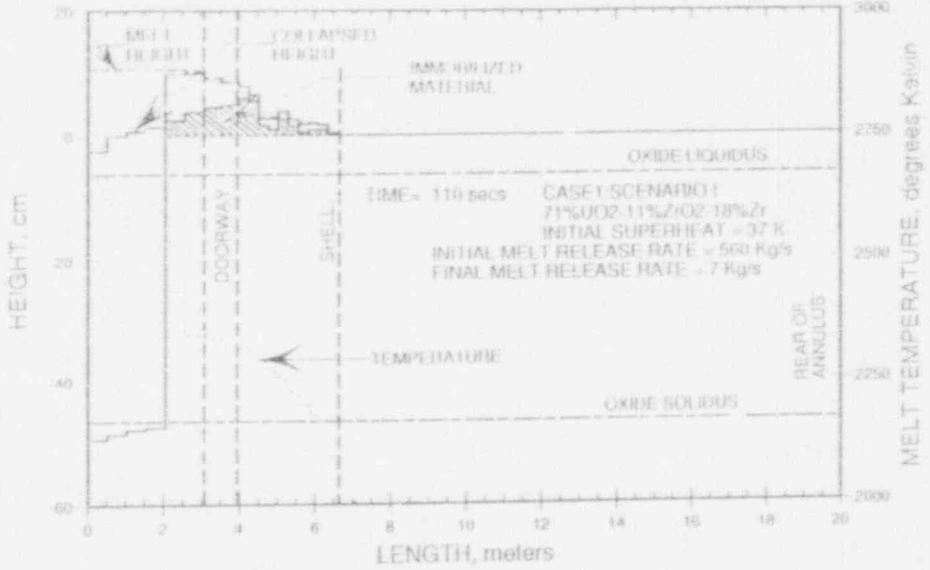

Figure 6. Spreading Profiles for Scenario I Wet Reference Case.

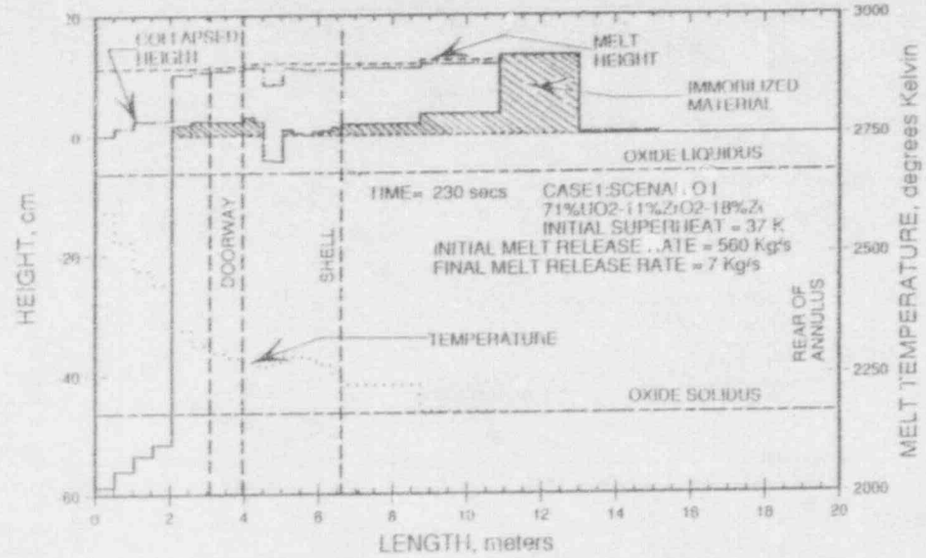

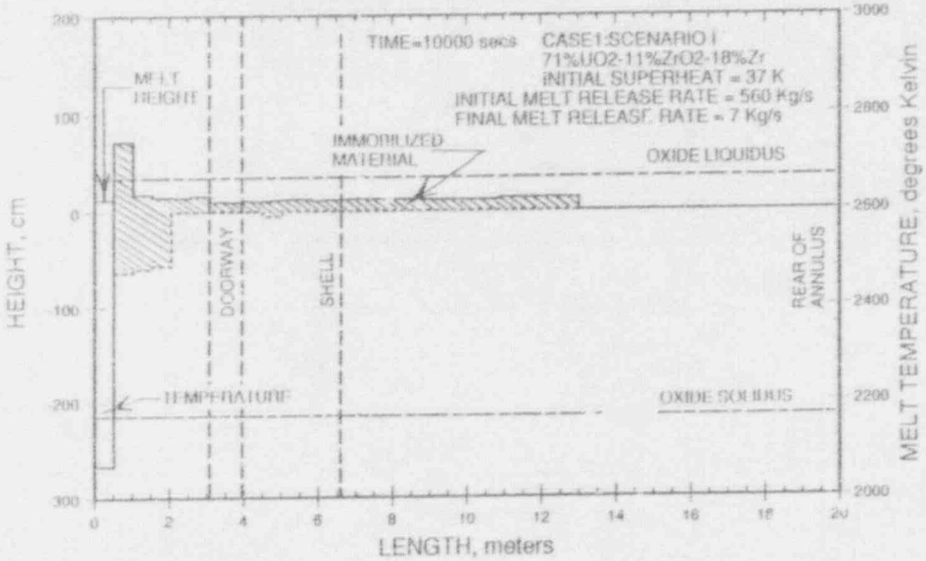

Figure 6. Spreading Profiles for Scenario I Wet Reference Case.

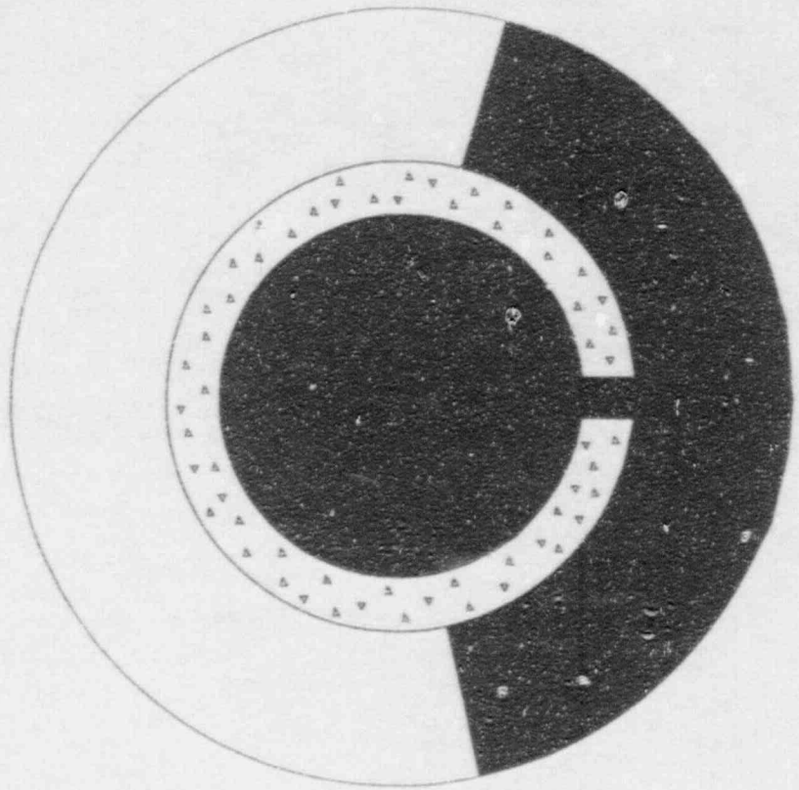

Figure 7. Maximum Spreading Extent for Wet Containment Reference Cases.

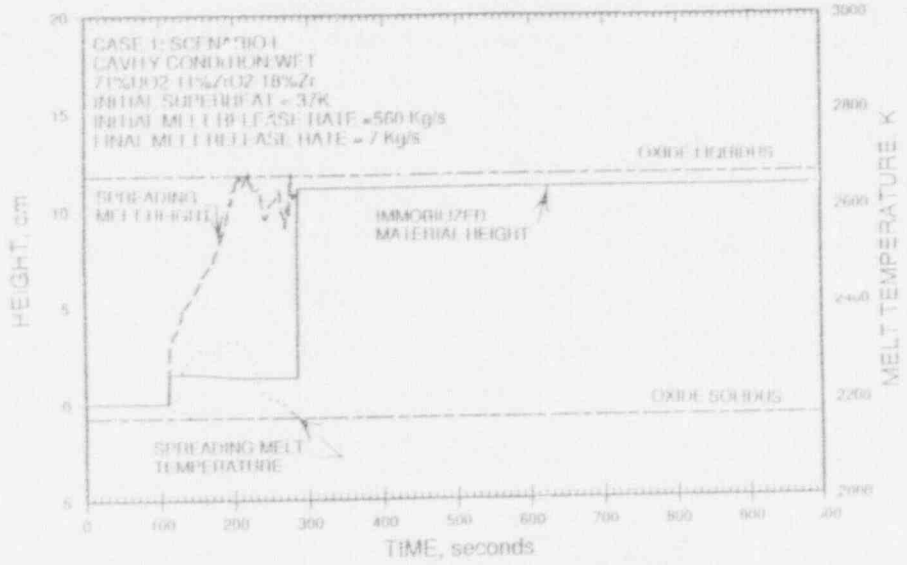

Figure 8. Material Depth and Melt Temperature Adjacent to Shell for Scenario I Wet Reference Case.

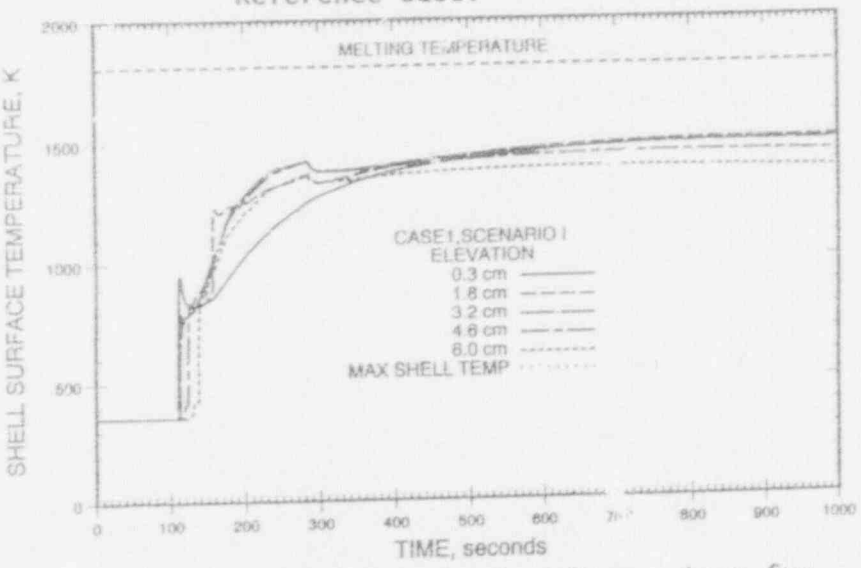

Figure 9. Shell Inner Surface Temperature for Scenario I Wet Reference Case.

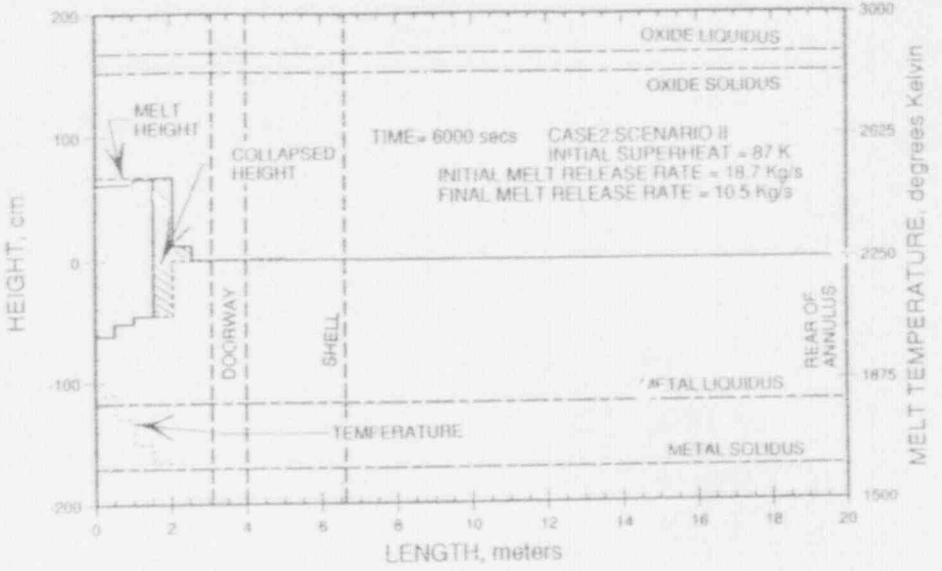

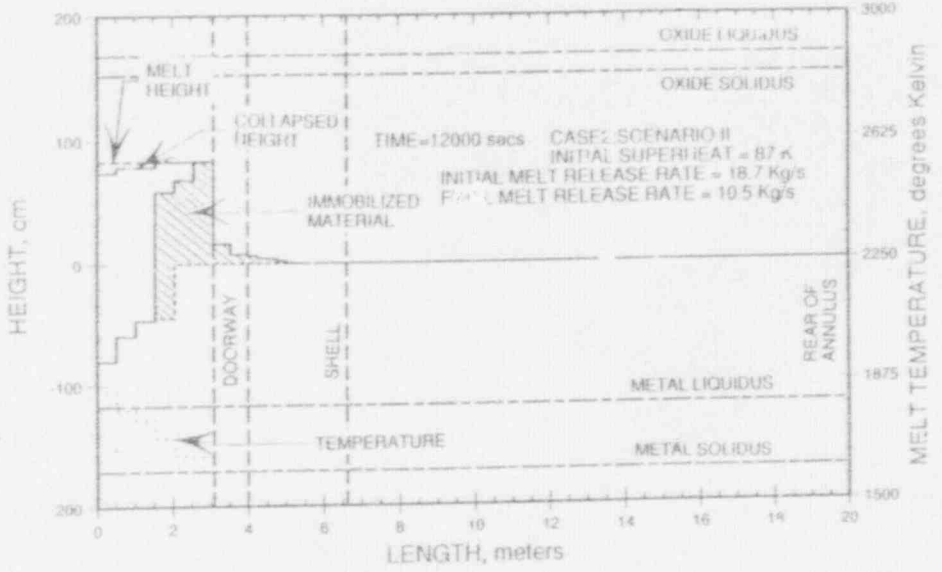

Figure 10. Spreading Profiles for Scenario II Wet Reference Case.

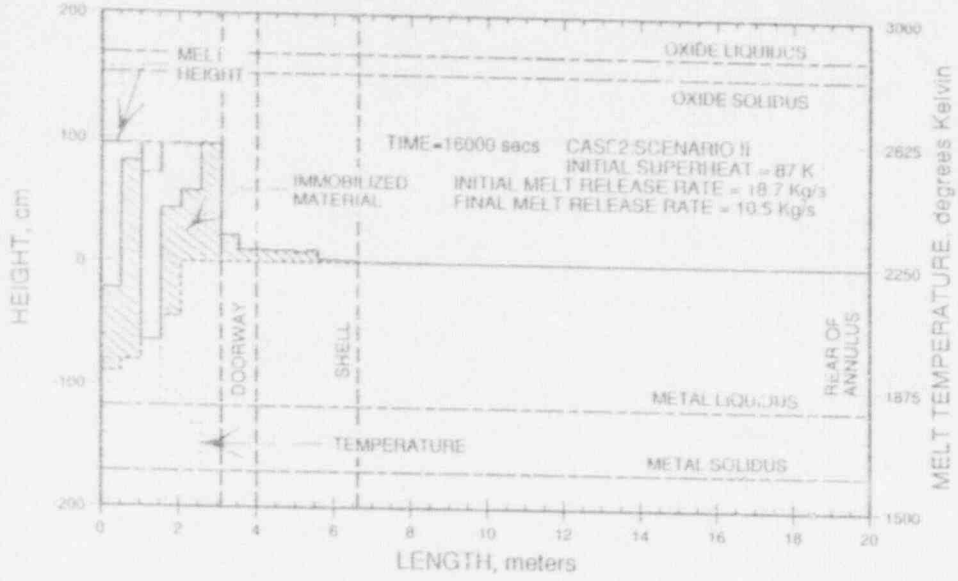

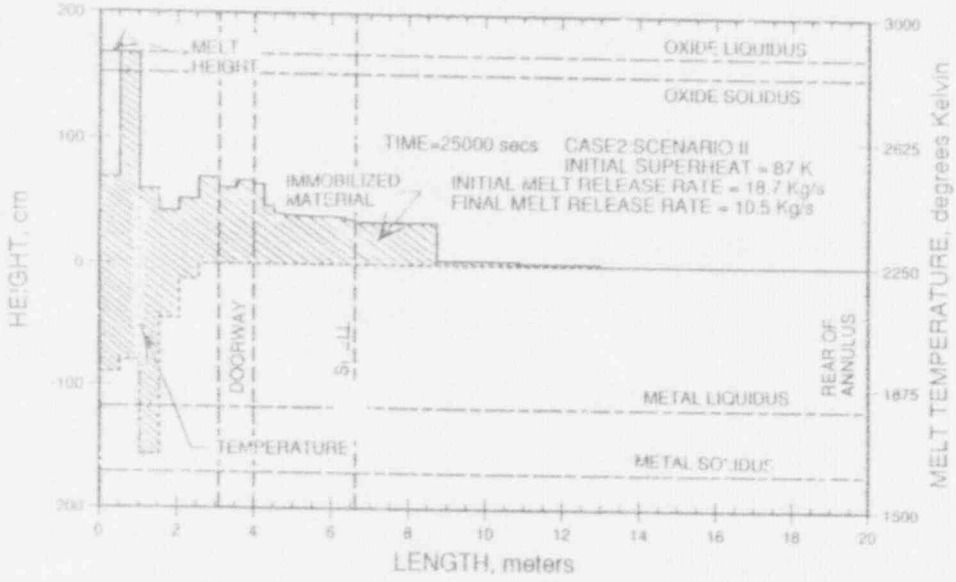

Figure 10. Spreading Profiles for Scenario II Wet Reference Case.

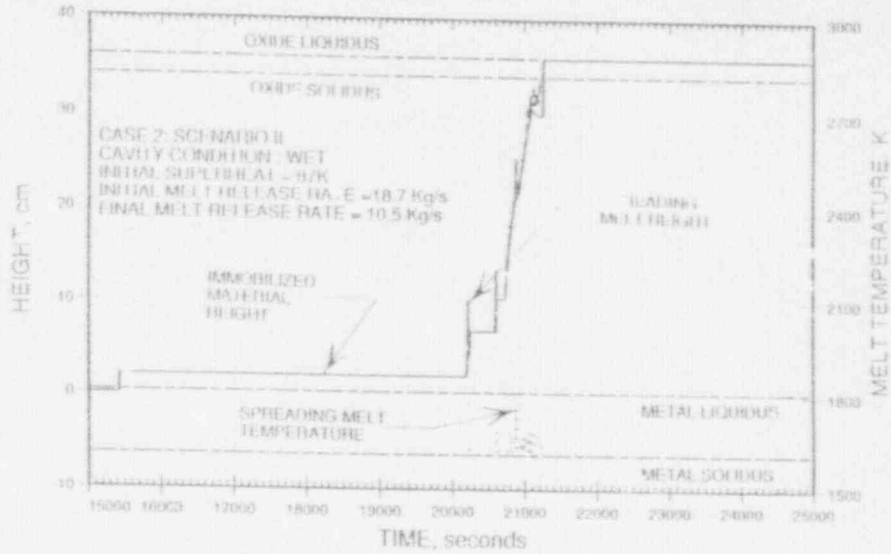

Figure 11. Material Depth and Melt Temperature Adjacent to Shell for Scenario II Wet Reference Case.

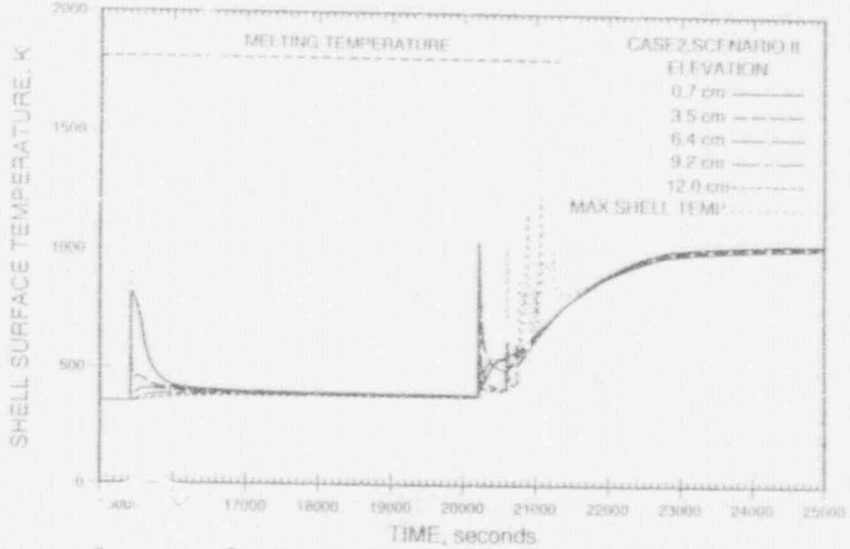

Figure 12. Shell Inner Surface Temperature for Scenario II Wet Reference Case.

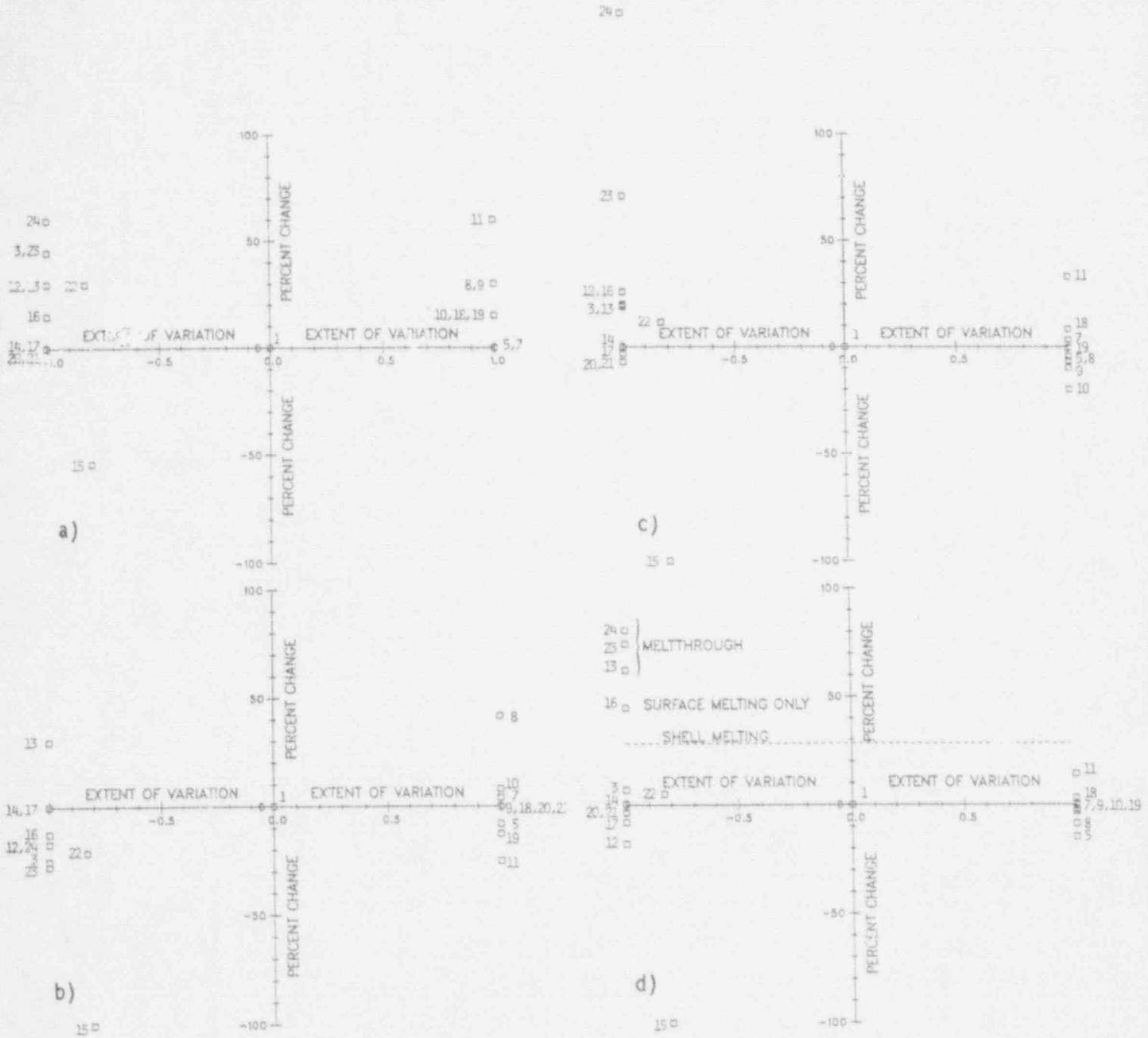

Figure 13. Sensitivities for Scenario I: a) Maximum Melt Spreading Area; b) Maximum Material Depth Adjacent to Shell; c) Difference Between Maximum Melt Temperature and Solidus Adjacent to Shell; and d) Maximum Shell Inner Surface Temperature Rise.

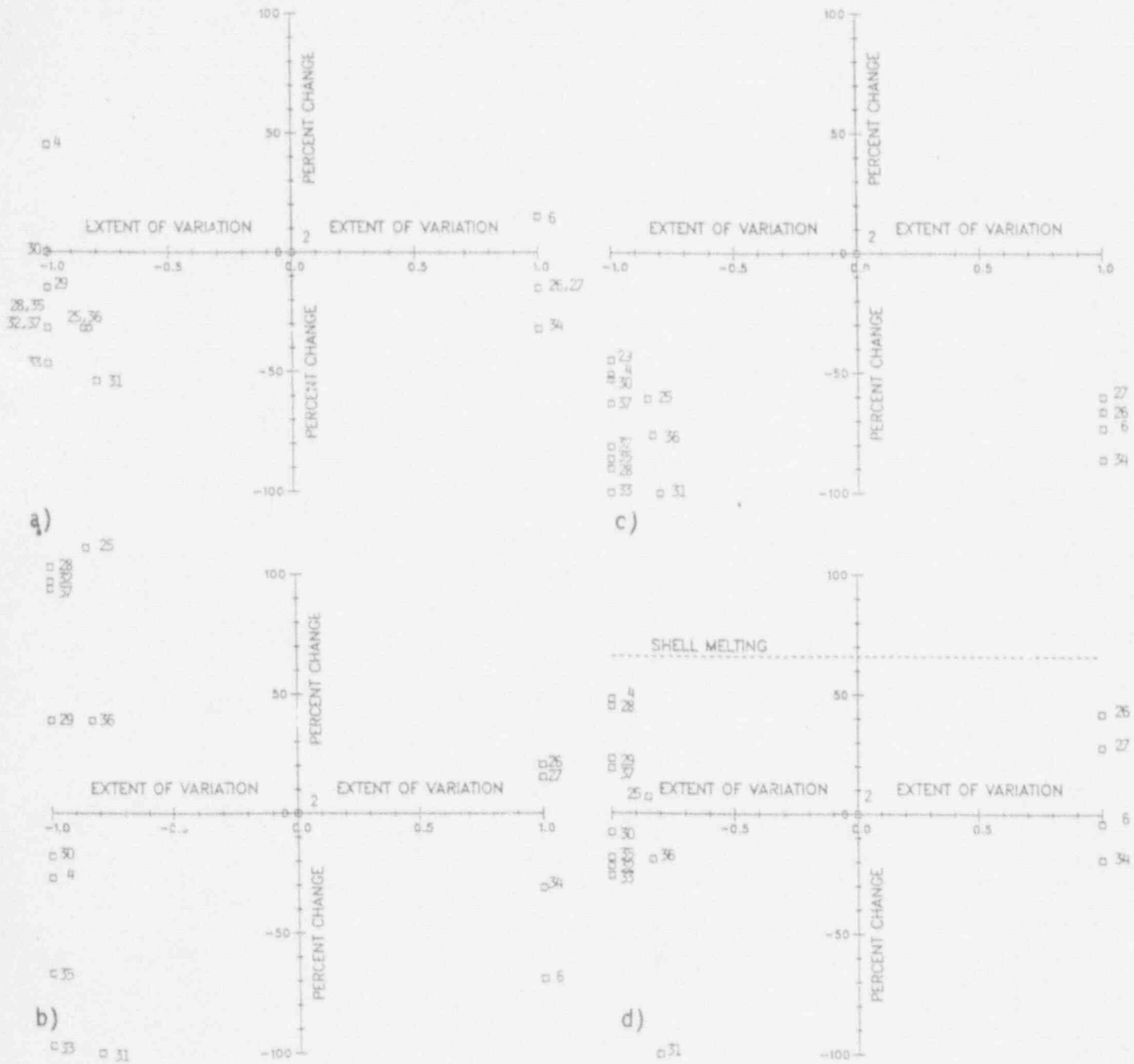

2-Reference Case
4-Dry Containment
6-Include Below-Vessel Interactions
25-Lower Superheat
26-Higher Release Rate
27-Include Above-Core Steel
28-Siliceous Concrete
29-Lower Spreading Angle
30-Lower Shell Crust Freezing Temperature
31-Lower Immobilization Solid Fraction
32-Lower Sump Retention
33-Zero Decay Heat
34-Faster Chemical Reactions
35-Lower Shell Impingement Heat Transfer
36-Lower Upward Heat Transfer
37-Lower Downward Heat Transfer

Figure 14. Sensitivities for Scenario II: a) Maximum Melt Spreading Area; b) Maximum Material Depth Adjacent to Shell; c) Difference Between Maximum Melt Temperature and Metal Phase Solidus Adjacent to Shell; and d) Maximum Shell Inner Surface Temperature Rise.

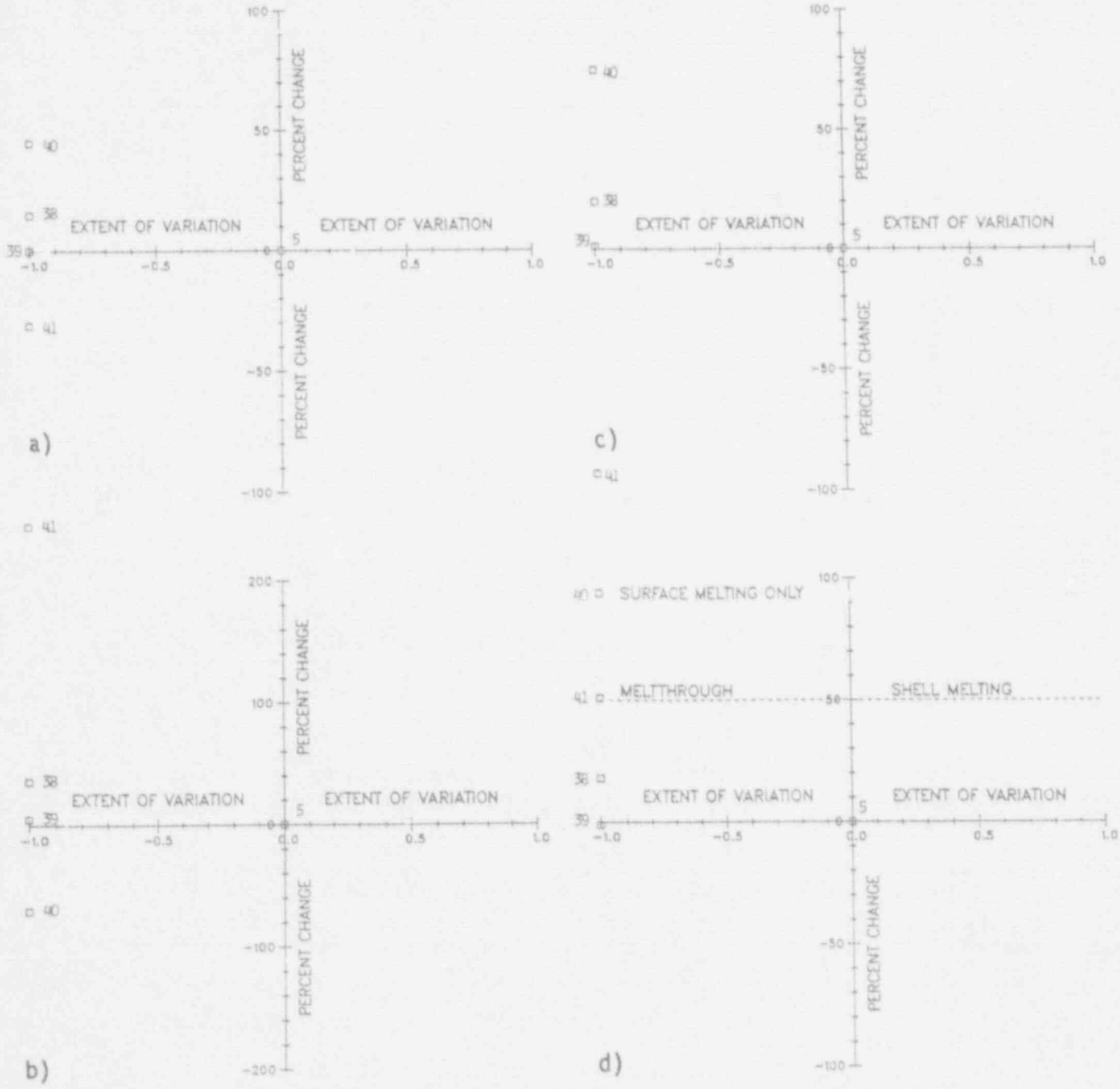

Figure 15. Sensitivities for Scenario I with Below-Vessel Interaction Effects: a) Maximum Melt Spreading Area; b) Maximum Material Depth Adjacent to Shell; c) Difference Between Maximum Melt Temperature and Solidus Adjacent to Shell; and d) Maximum Shell Inner Surface Temperature Rise.

ACE PROJECT PHASES C & D:

ACE/MCCI AND MACE TESTS

by

B. R. Sehgal
Electric Power Research Institute
3412 Hillview Avenue
Palo Alto, CA 94303
(415) 855-2719

and

B. W. Spencer, D. H. Thompson, J. K. Fink and M. T. Farmer
Argonne National Laboratory
9700 S. Cass Avenue
Argonne, IL 60439
(708) 972-4758

ABSTRACT

Programs of experiments and related analysis are underway at Argonne National Laboratory investigating the interaction of molten core material with concrete and its coolability. The major objectives are: 1) obtain data on fission product release during MCCI; and 2) investigate the conditions for successful cooling and stabilization of core melt attacking the concrete basemat.

The fission product release tests have been completed, and data analysis is in progress. The experiments will be analyzed by several groups to validate the various MCCI codes, e.g., CORCON and VANESA, WECHSL and MAAP-DECOMP.

A scoping melt attack and coolability experiment (MACE) involving the addition of water atop an ongoing MCCI has been performed. A facility to conduct larger scale tests is currently being constructed, and two additional tests are planned to be completed before the end of CY91.

This paper will describe the progress of the MCCI and the MACE testing programs in the ACE project.

I. INTRODUCTION

The evaluations of the risks of U.S. nuclear power plants have focused attention on postulated beyond-design-basis accidents[1] in which core melting occurs and fission products are released. In certain prescribed scenarios, the molten core materials (corium) are calculated to flow into the lower head region of a BWR or a PWR pressure vessel (as occurred at TMI-2), and thereafter, at some point in time, cause failure of the vessel lower head. The accumulated corium is then discharged into the BWR pedestal region or the PWR containment cavity (which did not occur at TMI-2), and the ex-vessel phase of the accident begins.

The interaction of corium with the concrete basemat results in the release of substantial quantities of combustible (H_2; CO), noncondensible gases which pressurize the containment. If the corium-concrete interaction continues for a long time (tens of hours) and heat removal and pressure reduction measures (e.g., through venting) fail, containment integrity and basemat penetration are of concern. Fission products will be released if and when the containment fails; although in this case, the release is much less than that in the case of early containment failure, because of the depletion of aerosol source with time. Basemat penetration is also of serious concern, although the environmental effects are very much site-specific.

The gases produced during the molten corium concrete interaction (MCCI) sparge through the molten corium, undergoing chemical reactions and carrying volatile fission product compounds and other materials to the containment atmosphere. The metals Zr, Cr, Ni, Fe react with the gases exothermically to release substantial

amounts of energy which supplements the decay heat generation in the melt. The vaporized materials after emerging from the corium melt will form an aerosol source as they condense in the containment atmosphere.

The magnitude, content, and physical chemical character of the MCCI fission product aerosol sources are extremely important in estimating the source term and the risks from the LWR postulated accidents. The magnitude of the releases of refractory fission products e.g., La, Ba, Sr, Ce, which may occur during MCCI, have been an issue. There have been substantial differences in the predicted releases of these materials obtained from the various severe accident codes e.g., MAAP,[2] MELCOR,[3] CORCON,[4] and VANESA.[5]

A very important related issue is that of melt coolability and termination of the ex-vessel progression of the accident. Clearly, if the melt can be cooled and a heat transport cycle established, a long term safe stable state may be achieved and containment integrity assured. Virtually all LWRs have the ability to add water to reactor containment, although in some instances such capability may be of ad-hoc nature. SECY 88-147,[6] which requires the implementation of a Severe Accident Management Program, recognizes the beneficial effects of water addition to cool the molten corium pool. The advanced LWR program also has prescribed long term melt coolability and stabilization as a utility requirement for both the AP600 (Westinghouse) and the SBWR (General Electric) designs.

II. PREVIOUS WORK

Extensive research has been conducted to understand, model, and predict the dynamics of the attack of molten corium on concrete. This research consists of experiments performed at various scales with simulant and real materials and the development of state of the art codes e.g., CORCON,[4,7,8] WECHSL,[9] and DECOMP-MAAP.[2] The major MCCI test series performed so far i.e., BETA,[10] SURC,[11] HS,[12] and TURC[13] investigated the thermal hydraulic aspects of the MCCI i.e., the concrete spatial ablation rates and the gas and the aerosol generation rates. Except for one recent SURC test, these tests did not measure the release of the refractory fission products during the MCCI.

The melt coolability experimentation has not been as extensive as that for the MCCI. Sandia National Laboratory performed the FRAG[14] and the SWISS[15] tests, which employed, respectively hot steel balls and steel melt interacting with concrete and cooled by water from above. In these small scale experiments a crust developed which inhibited the transfer of heat from the melt to water, and long term melt coolability was not achieved. In addition to these experiments, Greene,[16] Theofanous,[17] and Kazimi[7] have conducted coolability experiments using simulant materials and gas injection. There is a dearth of models describing melt coolability due to lack of data and understanding, and presently there is a considerable divergence of opinion on the feasibility of quenching a large, deep molten corium pool.

III. ACE PROJECT

The advanced containment experiments (ACE) project is a cooperative research project funded by the countries and organizations shown in Table 1 and managed by Electric Power Research Institute (EPRI). The project consists of four phases: phase A, already completed, obtained data on the decontamination of aerosol sources that may be found in the containment after a severe accident using prototypic filter designs; phase B about to be completed, obtained data on the iodine transport and partitioning in the containment during prolonged residence; phases C and D described further in this paper, have obtained or will obtain data respectively on the fission product release during MCCI and the coolability and quenchability with water of a melt interacting with concrete.

Table 1. Status of ACE Participation

Organization
1. VTT, Finland
2. PSI, Switzerland
3. ENEA, Italy
4. CEA, France CEA, + JRC ISPRA
5. KEMA, The Netherlands
6. AEA, United Kingdom
7. OH, Canada
8. GRS,* FRG
9. UNESA,* Spain
10. Kurchatov, USSR
11. ABB-ATOM, SKI, Sweden
12. JAERI, Japan
13. AEC, Republic of China
14. VEIKI, Hungary
15. ININ, Mexico
16. Tractebel, Belgium
17. U.S. EPRI DOE NRC W

*Lead organization.

+Special dissemination rights proposed.

The experimental programs conducted in the ACE Project have been of relatively large scale in order to obtain data which could be applied directly for prototypic accident evaluations. This is particularly true for phases A, B, and C. For instance in phase C, about 300 Kg of prototypic corium material containing representative inactive refractory fission product compounds is heated to melt temperatures of 2500 K and reacted with concrete. In this way, the appropriate thermal and chemical environment is achieved in a relatively large interaction zone so that the aerosol release data obtained can be applied to the prototypic accident situations. Similar care is being exercised to limit the effect of scaling distortions in the conduct of the melt attack and coolability experiments (MACE).

IV. ACE PHASE C: MCCI PROGRAM

The phase C of the ACE Program addressing fission product release occurring during a molten core concrete interaction (MCCI) is being conducted at Argonne National Laboratory. A series of integral-type accident simulations is being performed to investigate the thermal-hydraulic and chemical processes of MCCIs and to expand the data base on release of low volatility refractory material fission products for further development and validation of MCCI/fission product release codes. The objectives of the ACE MCCI/fission product release research are to:

1. measure the releases of low-volatility fission product species during the MCCI stage of a postulated severe LWR accident,

2. measure the physical and chemical character of the aerosols generated from the MCCI,

3. measure the thermal hydraulic aspects of the interaction, including concrete ablation rate,

4. analyze the data obtained in the tests to enable comparisons with code predictions, and

5. support code comparison activities among ACE consortium members.

Real reactor materials are utilized in the ACE MCCI tests to investigate early aggressive interaction and longer term erosion of reactor basemat concrete by core melt material. Both the core melt material, termed "corium", and the concrete basemat in these tests are contained within a water cooled test apparatus. Direct electric heating is used to initiate core melt and maintain internal heat generation during the sustained interaction of the melt with the basemat. Unsintered or sintered, but unmelted, corium adjacent to the water cooled walls of the test apparatus serves as an insulating envelope to contain the melt within the apparatus. Interaction of the corium with the basemat is one-dimensional; predominant heat transfer processes from the internally heated core melt material are vertically upward and downward.

The facility for conducting the ACE MCCI/fission product release tests includes a confinement cell, test apparatus, power supply, gas/aerosol diagnostics system, water cooling system, ventilation/exhaust system and data acquisition system. The test apparatus, shown in Figure 1, consists of water cooled copper panels which form the four walls enclosing the concrete basemat and the corium. Tungsten rod electrodes form two inner walls of the apparatus and are connected near the top of the corium volume by tungsten wire coils for starting a test. An insulated and water cooled plenum and lid fit on top of the test apparatus. The lid contains ports for gas sampling and for video recording the melt surface.

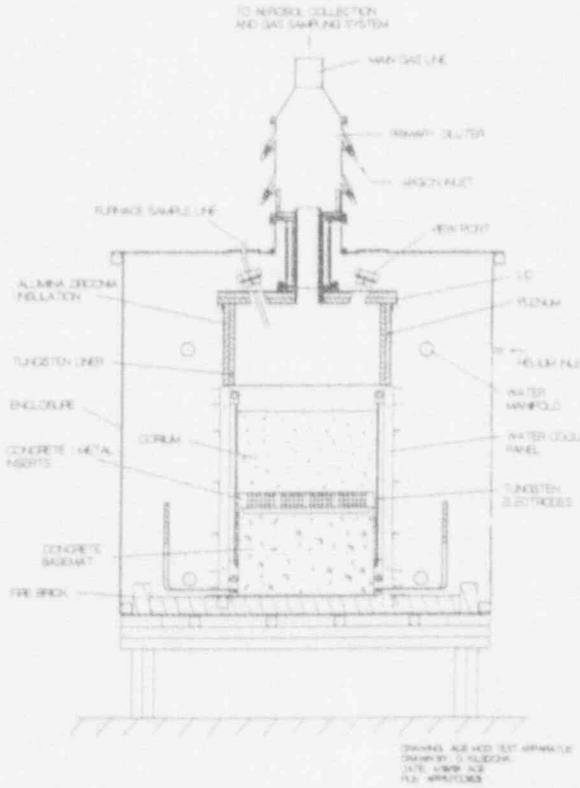

Figure 1. ACE MCCI Test Apparatus.

The gas/aerosol diagnostics system was designed to accommodate sampling equipment recommended by an international group of aerosol experts. The system, shown in Figure 2, transports, dilutes, samples, and filters the off gas/aerosol stream drawn from the test apparatus. Argon gas delivered to the primary diluter in the aerosol system main line above the test apparatus dilutes the aerosol concentration and cools the hot gas from the MCCI. A helium atmosphere is maintained within the enclosure surrounding the test apparatus. The helium flow rate to the en-

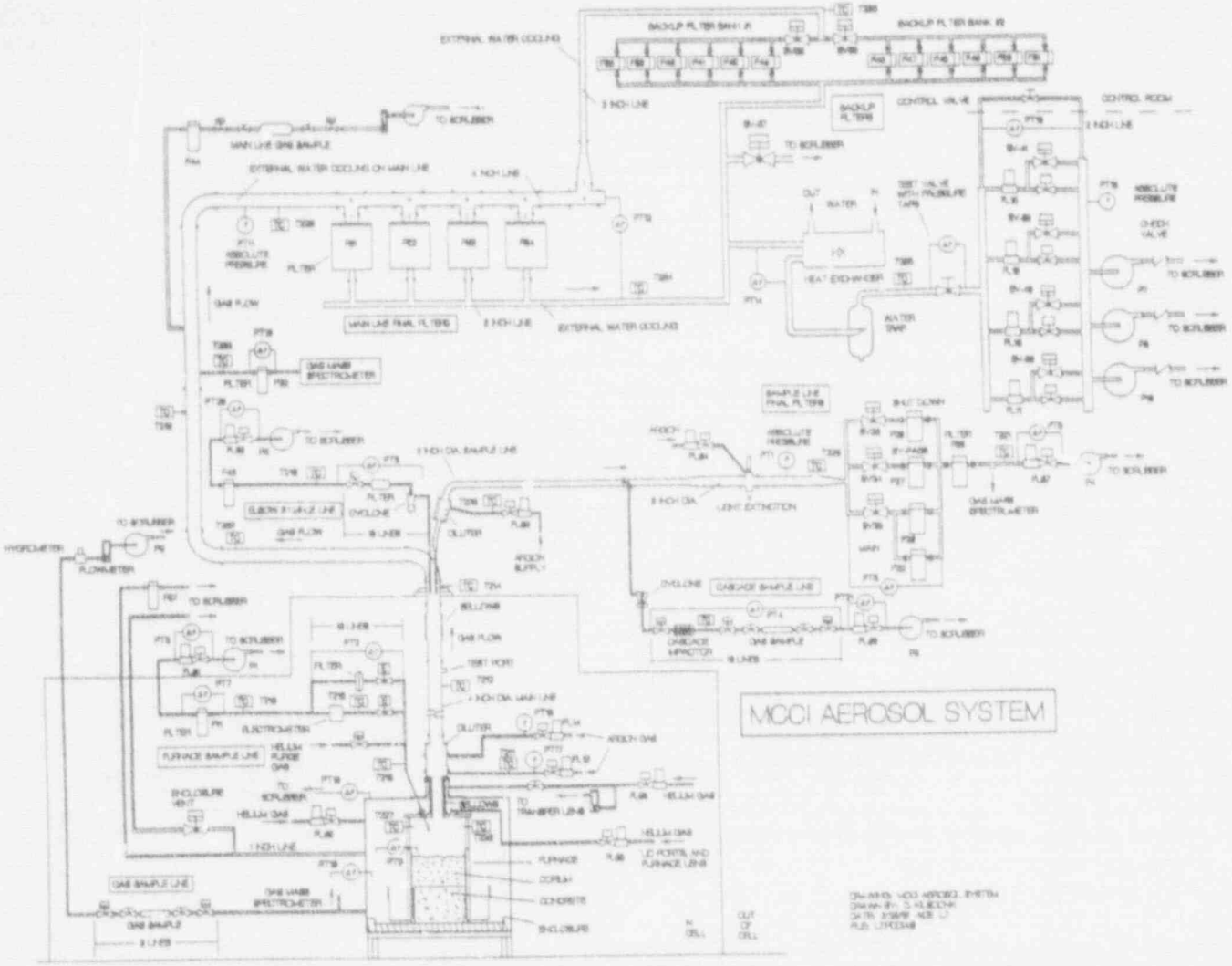

Figure 2. ACE MCCI Gas/Aerosol Diagnostics System.

closure exceeds the predicted peak off-gas production rate. Most of the helium is drawn into the aerosol system until off gassing begins. Off gas produced during melt interaction with the basemat displaces part of the helium drawn into the aerosol system. The displaced helium is vented from the enclosure.

The aerosol concentration variation with time is determined with a light extinction system and from a series of ten cyclones followed by filters which sequentially sample the aerosol throughout a test. The cyclones and filters are also used to characterize the ratio of large to small particles as well as variation in composition with time. A series of ten impactors provides the particle size distribution of the respirable fraction. The change in gas composition with time is obtained from an on-line mass spectrometer. Gas and water migration downward through the concrete during the test are determined by a hygrometer sampling gas drawn from beneath the concrete basemat and from the analysis of gas samples collected beneath the basemat. The composition of the aerosol released is determined by analysis of multiple samples of material collected on filters, impactors and cyclones, and deposits from the aerosol system piping.

Eight tests in the ACE MCCI test matrix are listed in Table 2. Each test was performed with 300 Kg of corium and a 200 Kg concrete basemat having a surface area of 2500 cm^2. The corium contains UO_2, ZrO_2, stainless steel oxides or zirconium and stainless steel, plus nonradioactive fission product simulants (BaO, La_2O_3, SrO, CeO_2, etc.) and control rod material. Appropriate ratios of fuel to structural materials are used for pressurized and boiling water reactor cores. The initial degree of in-vessel oxidation of the zirconium is one of the test parameters. Absorber material is silver plus indium for PWRs, boron carbide for BWRs. Fission product simu-

Table 2. ACE MCCI/Fission Product Release Tests Test Conditions

Corium composition will be determined from specific Code Cases:

- Oxides from in-vessel: UO_2, ZrO_2, Fe_2O_3, Cr_2O_3, NiO
- Oxides from early ex-vessel ablation: CaO, SiO_2
- Metals: Zr OR Zry, Fe, Cr, Ni, Ru-steel alloy
- Fission products: La_2O_3, BaO, SrO, CeO_2

Test No.	Concrete Type (1)	Net Heat Generation W/Kg UO_2	Corium Mixture	Initial Zr Oxidation, %	Absorber Material
L5	L/S	350	BWR	100	
L2	S	350	PWR	70	
L1	L/S	350	PWR	70	
L6	S	350	PWR	30	Ag, In
L4	S	250	BWR	30	B_4C
L7	L/S	250	BWR	30	B_4C
L3	L/S	350 (2)	PWR	30	Ag, In
L8	L/L	350(2)	PWR	70	Ag, In

Note: (1) concrete type:

L/S = limestone/common sand concrete plus rebar
S = siliceous concrete plus rebar
L/L = limestone/limestone concrete plus rebar

(2) reduced power operation after Zr is fully oxidized to represent longer term corium-concrete interaction

lants are included in the corium at concentrations higher than found in reactor plants to improve detectibility in the aerosol. Metal in the corium is located in concrete/metal inserts directly above the basemat to preclude early oxidation. Tests are being performed using four types of concrete: limestone/common sand, limestone/limestone, siliceous, and serpentine/ordinary structural concrete. Aggregate, sand, concrete mix designs, and reinforcing rod details for siliceous and serpentine/ordinary structural concrete were provided by consortium members Germany and the USSR, respectively. Other concretes are based on US reactor construction mixtures. Two-hour decay heat levels are used to achieve target melt temperatures of about 2500 K. A reduction in decay heat level after metal oxidation is complete is included in the test matrix to address the longer term stages of MCCI.

The melt appears to be thoroughly mixed by gas sparging in the ACE MCCI tests. No crust development has been observed on the melt surface; a thin film has been seen to develop, then disappear, in a periodic manner. Foaming of the melt has been encountered. Upward off gas transport is less than the gas and water content of the various concrete tested. A substantial fraction of the gas and water migrate downward into and through the basemat.

Over 200 channels of data are logged at a five-second frequency during a test. Thermal-hydraulic results, such as ablation rate, melt temperature, off gas composition, and superficial gas velocity as a function of time are processed from the recorded test data.

Multiple samples of aerosol and solidified melt are collected for chemical analysis after each test. From the aerosol samples, overall aerosol composition is determined. Total release fraction of each element and release fraction as a function of time are calculated. Aerosol samples are also characterized by electron microscope examination. The United Kingdom, a consortium member, is performing depth profiling and other analyses of individual aerosol particles to determine aerosol formation mechanisms and chemical speciation.

Results of the ACE MCCI tests indicate that the aerosol is composed primarily of concrete decomposition products. The aerosol released varies in concentration, composition and form depending on the type of concrete being ablated and the metal fraction in the melt. Aerosol concentrations in the off gas have varied by two orders of magnitude. Measured releases of the low volatility fission product elements, such as Ba, Ce, La, and Sr, have been consistently lower than those predicted by VANESA 1.01.[5] Because the fission product releases thus far have been low, the original test matrix has been reduced by deleting Test L3.

ACE consortium members are developing new codes,[8] modifying VANESA, and applying other chemical equilibrium codes such as SOLGASMIX[18,19] to fission product release from MCCIs. Results of calculations with new and existing codes are being compared with experimental results. Blind posttest code calculation comparisons with experimental releases are underway for two experiments to evaluate the codes. Analysts from eight countries are participating in these calculations.

Blind post-test comparisons are also being done with thermal hydraulic codes. Comparisons of the thermal hydraulic results of these experiments with existing thermal hydraulic codes such as CORCON-mod2, CORCON as modified at the University of Wisconsin,[8] and WECHSL,[9] a German code, indicate that further code developments may be needed.

V. ACE PHASE D: MACE PROGRAM

Phase D of the ACE program is being carried out at Argonne National Laboratory to investigate the quenching of a corium pool interacting with a concrete basemat when water is flooded atop the MCCI zone. This program addresses a key accident management question which relates to the efficacy of water addition to terminate corium attack on the basemat and stabilize the accident situation, assuming the existence of a water reflux cycle. The Melt Attack and Coolability Experiment (MACE) program will investigate whether melt quench can be achieved under MCCI conditions and whether there are practical limits to achieving quench, such as the depth of the corium pool. The results are thereby also important in the safety approach for future containment designs.

The key importance of the Phase C data lies in characterizing the aerosol releases and their fission product content. Emphasis of Phase D, on the other hand, is to examine the thermal-hydraulic processes of melt-water interaction which ultimately determine whether sufficient energy is extracted from the melt so that the concrete attack is stooped and whether a permanently coolable debris configuration is formed. To put the MACE program into perspective, it is the melt quench (solidification) stage of the process that is being investigated. The tests will terminate when, and if, quench is achieved such that the solidified debris can be characterized afterward from the standpoint of coolability. As is the case for water attenuation of aerosol releases, there is a large international database that already exists relating to the coolability of solidified debris. What is needed from the MACE program is a determination of the processes that lead, or fail to lead, to transformation of the corium melt undergoing intensive interaction with basemat concrete into a layer of solidified debris together with characterization of that debris.

The ACE Consortium approved the Stage 1 test matrix shown in Table 3 for the current series of tests. This matrix contains a small scale scoping test M0 (~100 Kg corium melt) and two large scale tests (~400 Kg corium melt). When concluded, the results of these three tests will be analyzed and a determination will be made whether additional tests are warranted (Stage II experimentation) and what should be the scale of additional tests. The MACE facility is being constructed to accommodate even larger scale tests of ~1000 Kg corium melt if deemed necessary.

Table 3. MACE Stage I Test Matrix

Test No.	Concrete Type	Corium Composition	Melt Depth (cm)	Size (cm)	Water Addition	Pressure (bar)	Parameter Investigated
M0	*L/S	Oxidic + 30% Zr	15	30 x 30	Immediately after MCCI	1	Scoping Test (Completed 8/89)
M1	L/S	Oxidic + 30% Zr	25	50 x 50	Immediately after MCCI	1	Scaling
M2	Siliceous	Oxidic + 30% Zr	25	50 x 50	Immediately after MCCI	1	Different concrete

*L/S - Limestone/common sand

An important aspect of the MACE program development has been attention to scale effects. Scale was not a significant issue for the MCCI tests of Phase C inasmuch as the thermal, physical, and chemical processes contributing to the aerosol formation and its fission product content are of a local nature, driven by concrete decomposition effects whose characteristic length scale was small compared to the 50 cm lateral expanse of the melt layer. The materials, temperature, and melt layer depth of 15 cm (collapsed pool height) used in those tests are representative of real reactor conditions. Moreover it was observed that crusting of the top of the pool was not a significant factor. When observed at all, the crust was thin, cracked (floating), and of only temporary duration before disappearing into the bulk of the agitated melt, as alluded to in the previous section. However, this crusting behavior may be different when water is added which may introduce a scale effect. Certain models of the mode of quenching are based on formation and growth of a corium crust at the melt-water interface as heat is extracted from the top of the melt layer via the overlying water. If this crust becomes sufficiently strong over the lateral expanse of the test section, it may become physically stable and, owing to heat conduction limitation, may preclude complete pool quench. This is deemed unlikely in the reactor case owing to the very large expanse of reactor cavity or pedestal regions. EPRI is sponsoring a companion program at the University of Wisconsin-Madison which aims to address crust strength and related scale dependency. Alternatively, if melt quenching is found to be dominated by melt/crust interfacial mixing with water such that heat extraction occurs via a bulk cooling mode for this gas sparging-driven system, then the process becomes scale independent and there should be no need for tests larger than the current 50 x 50 cm (400 Kg) size.

The small-scale scoping test M0 was performed in August 1989. The objectives of this early test were:

1) determine the viability of the ACE Phase C DEH experiment approach for the MACE experiments, and

2) obtain early information about the melt-water interaction process to aid in planning the future, larger scale tests and to guide early modeling approaches.

The overall experiment apparatus used for M0 is illustrated in Fig. 3. The corium internal heat generation is provided by direct electric heating (DEH) using the same approach as described for Phase C experiments. However, for the coolability testing, the apparatus was provided with a water delivery/makeup system and a large and a small steam quench tank as well as an off-gas measurement and cleanup line. The test section is a thick-walled heat capacity design rather than cooled-wall design required for Phase C. For M0, the sidewalls as well as basemat were limestone-common sand concrete. The initial corium mass was 109 Kg consisting of 67% UO_2, 13% ZrO_2, 4% Zr plus concrete decomposition products. The test section was vented at the top by a 15-cm diameter duct which carried steam and the gaseous products of concrete decomposition first to a small quench tank, sized for high resolution measurement of modest heat transport rate, and secondly to a large quench tank to extract any residual heat particularly in the event of very large heat transport rates. The vertical height of the test section was 1.5 m above the top of the 30-cm tall basemat. This height permitted large level swell of both the melt pool and overlying water without significant carryover of liquid. Any offgas not condensed or dissolved in overlying water was ducted through a flowmeter, filter, and entered the containment cell ventilation system consisting of HEPA filters and building stack. Instrumentation featured a video recording system viewing down atop one-quarter of the melt surface as well as flowmeter and thermocouple systems to diagnose quench rate and system cooldown upon water addition, energy balance, concrete ablation, and melt zone temperature (high temperature thermocouples used in Phase C).

To initiate the experiment the corium powders were melted at an internal heat generation of 1.4 kw/Kg UO_2, about three times the nominal decay heat level at two hours into an accident for a PWR. When concrete ablation reached 1.2 cm into the basemat according to the centerline TC, it was visually observed that the top of the melt layer was molten without crust in the central zone. (However, a bridge of sintered crust material remained along the electrode walls, anchored to the electrode tops, and covering roughly half the melt surface.) The gas sparging superficial velocity is estimated to have been 3.5 cm/sec based on the concrete ablation rate. Water flow was initiated via two wiers along the tops of the two walls adjacent to the electrode walls. The water temperature was 22°C, and the addition rate was 10 ℓ/s up to a water pool depth of nominally 50 cm. Makeup flow was designed to maintain the 50 cm pool depth.

The video showed that at the onset of injection the water was extraordinarily agitated and boiled up from steam formation as the pool attempted to form, albeit the high water subcooling. Test data depicting energy extraction from the melt is shown in Fig. 4. This data has been corrected for transient cooling of structural members by the injected water. The initial vigorous quench stage extracted ~44 MJ energy from the melt pool during the first three minutes of interaction; the heat flux related to the test section cross section was 3.5 MW/m^2. Assuming the melt pool was at liquidus temperature at the start of quench (due to an anomaly, the melt pool TC's did not record melt temperature until several minutes later) and using a nominal heat of fusion of 0.3 MJ/Kg for the corium, the quench during the first three minutes was capable of extracting the heat of solidification from the entire melt mass

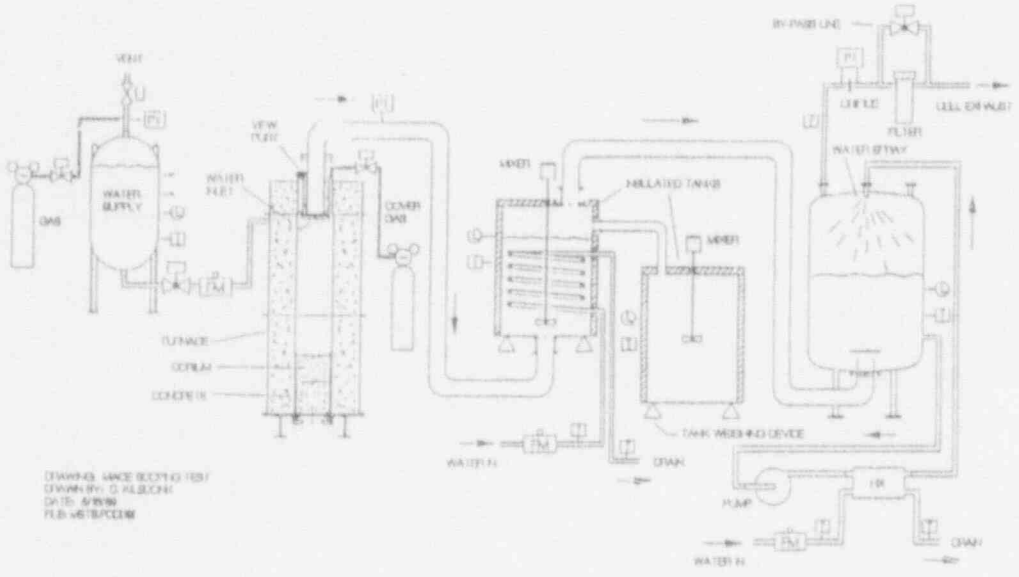

Figure 3. Experiment Apparatus for MACE Scoping Test (M0).

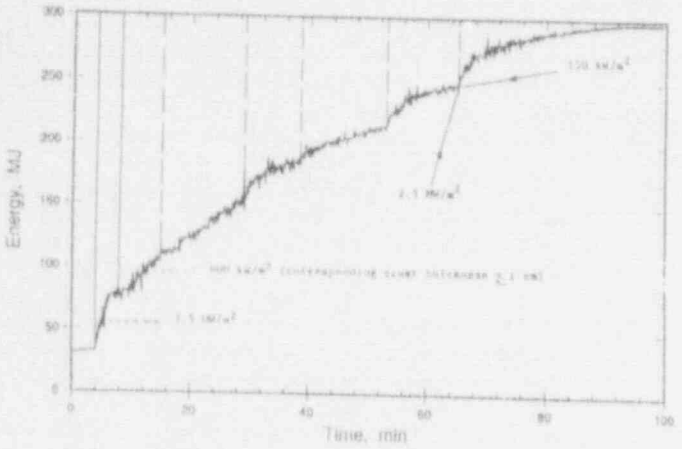

Figure 4. Upward Heat Extraction from Corium Pool.

even accounting for continued internal heat generation. This would have rendered the corium mass completely solidified from a uniform bulk cooling viewpoint, albeit still at very high temperature. Alternatively, the measured energy extraction could have completely quenched (to water T_{sat}) about 30% of the melt mass based on ΔE ~1.3 MJ/Kg, leaving unaffected the remaining 70%. Neither of these extreme cases depicts reality, but it is apparent that the energy extraction during the initial interaction resulted in a significant cooling transient which would at least have resulted in slurry formation. The heat extraction during the next five minutes became very small. It is likely that a surface crust formed atop the melt layer during this period. Subsequently there was a prolonged period of heat extraction at ~0.6 MW/m^2. This period was periodically punctuated by pressure-driven dispersal of melt through a volcanic-like fault in the crust. These eruptions caused periodic jumps in the heat extraction of as much as 22 MJ as the ejected melt was quenched in the overlying water.

The test was eventually ended by shutting off the power at ~80 minutes after initial water injection, at a time when all the available cooling water inventory had been boiled off. Basemat erosion proceeded steadily during the course of the test at ~1.3 mm/min; ablation depth was about 12 cm at termination. The melt temperature was ~1600 K at that time. After surface dryout, prior to shutdown, the video revealed a clear picture of the debris surface which consisted of quenched particles. During this period a final eruption event occurred in the field of view. This event was clearly visible owing to the absence of overlying water. Melt droplets were dispersed upward through a volcanic-like vent in the surface. The droplets were ejected presumably by blowdown of gaseous concrete decomposition products accumulated in the volume between the remaining basemat and the crust. Following gas blowdown, additional melt was observed to benignly pour forth from the vent hole and flow across the debris surface until the source was exhausted. This may be evidence of a melt boilup or foaming process within the cavity-volume which transported melt directly in contact with the underside of the crust.

No evidence of this postulated boilup or foaming was found when the test section was later visually examined and dissected. The pretest and posttest configurations are illustrated in Fig. 5. The upper debris region consisted of a particle bed of 3 to 4 cm depth. The particles were generally well formed spheres loosely sintered together presumably formed as a result of dispersion and quench in the overlying water followed by settling into a bed. The characteristic particle size was ~0.8 cm dia. The total mass of loose debris was 10.1 Kg. The particle bed was resting atop a dense crust layer whose thickness ranged from 2 to 5 cm. This crust was anchored to the tops of the tungsten electrodes, perhaps an outgrowth of the original partial crust observed in the video at that elevation prior to water injection. An additional 12.5 Kg debris was present in the crust. Hence about one-quarter of the original corium mass was contained in the crust and debris layers by the end of the test. The remaining melt was collapsed and solidified in a 12 cm layer at the bottom of the crucible. The cavity measured about 15 cm in height.

Figure 5. Cross-Sectional Illustration of the Test Section as Viewed From the West Before and After the Experiment.

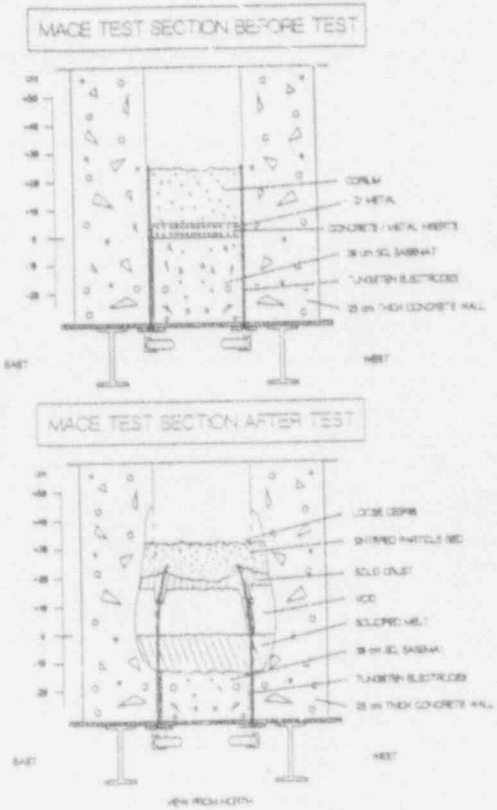

The MACE scoping test successfully demonstrated that the ACE/DEH method of quasi-steady internal heat generation is a viable approach for conducting the MACE test series. However, it is not clear that the results obtained in the scoping test can be readily applied to the reactor system. The results, of course, indicated that quench was not achieved and would not have been achieved even if the test had run longer. Following the initial cooling transient when the water was first added, the quasi-steady energy balance indicated about 35% of the internally generated heat went downward into concrete ablation vs 65% upward into overlying water; by the end of the test the split was about 55% vs 45%. Clearly, upward heat transport in this test was being diminished by the presence of the crust and debris layers which were growing thicker with time.

Interpretation and application of the M0 test results to the reactor system are very uncertain. A partial crust existed even prior to water injection where sintered corium was anchored to the tungsten electrodes. That crust was the nucleus for the bridge crust which existed throughout the test, allowing upward gas escape only via one or more discrete vent holes. The apparatus for the current tests will increase the lateral span from 30 to 50 cm and will do away with intrusive electrodes to avoid precursor crust anchoring. Also, the wall material will be MgO which will be heated above the corium freezing temperature prior to start of the test to further avoid crusting. The low gas sparging rate achieved during the initial MCCI stage in M0 as well as the nonprototypic high power level will be corrected in upcoming tests.

The new MACE apparatus is essentially the same as that employed for the M0 test except for the increases in size to 50 cm x 50 cm and modifications which implement lessons learned from M0. The project is currently in a stage of intense construction activity to satisfy requirements that M1 and M2 be conducted prior to the end of this calendar year.

Acknowledgements

The authors gratefully acknowledge all the members of the ACE Technical Advisory Committee who have provided advice and guidance on the conduct of the experiments. They also acknowledge Drs. Walt Lowenstein, Richard Vogel, Ian Wall, Frank Rahn, and Al Machiels of EPRI who have been, at various times, helpful in organizing the ACE Program, together with Drs. Farouk Eltawila and Charles Tinkler of USNRC and Dr. Walter Pasadag of USDOE. Dr. Manfred Fisher of Siemans, Inc., has been a German participant at ANL in the MACE program whose efforts have been particularly helpful. Key participants in the ANL experiment team include Donn Armstrong, Dennis Kilsdonk, and Robert Aeschlimann. This manuscript was prepared for publication by Lois Ondracek.

REFERENCES

1. B. R. SEHGAL and J. J. GARREY, "Degraded Core Accidents - An Overview," Proc. Int. Mtg. Light Water Reactor Severe Accident Evaluation, Cambridge, Massachusetts, August 28 - September 1, 1983, American Nuclear Society, 1983.

2. R. E. HENRY and M. G. PLYS, "MAAP 3.0B-Modular Accident Analysis Program for LWR Power Plants. Vols. 1 and 2 EPRI Report NP-7071-CCML (Nov. 1990) and R. E. HENRY, "A Model for Core-Concrete Interactions," Proc. Int. Mtg. on LWR Severe Accident Evaluation, Cambridge, MA, paper 12.10 (August 28 - September 1, 1983); and M. G. PLYS and M. A. McCARTNEY, "A Mechanistic Model for Core-Concrete Interactions and Fission Product Release in Integrated Accident Analysis," Draft ARSAP Report (June 1988).

3. R. M. SUMMERS, et. al., "MELCORE 1.8.0: A Computer Code for Nuclear Reactor Severe Accident Source Term and Risk Assessment Analysis," NUREG/CR-5531, SAND90-0364 (Jan. 1991).

4. R. K. COLE, D. P. KELLEY, and M. A. ELLIS, "CORCON-MOD2: A Computer Program for Analysis of Molten-Core/Concrete Interactions," U.S. Nuclear Regulatory Report NUREG/CR-3920, SAND84-1246 (1984).

5. D. A. POWERS, J. E. BROCKMAN, A. W. SHIVER, "VANESA: A Mechanistic Model of Radionuclide Release and Aerosol Generation during Core Debris Interactions with Concrete," U.S. Nuclear Regulatory Report NUREG/CR-4308, SAND85-1370 (1985).

6. U.S. Nuclear Regulatory Commission, "Integration Plan for Closure of Severe Accident Issues," SECY88-147 (1988).

7. M. LEE and M. S. KAZIMI, "Modeling of Molten Corium-Concrete Interaction " EPRI NP-5403 (September 1987) and L. S. Kao and M. S. Kazimi, "Thermal-Hydraulics of Core/Concrete Interactions in Severe LWR Accidents," Report MITNE-276 Massachusetts Institute of Technology (June 1989), to be published as an EPRI NP Report.

8. J. K. NORKUS and M. L. CORRADINI, "Modeling of Molten-Core/Concrete Interactions: Fission Product Release," Proc. Intl. Conf. on Thermal Reactor Safety, Avignon, France, October 2-7, 1988 and to be published as an EPRI NP report.

9. M. REIMANN and W. A. MURFIN, "The WECHSL Code: A computer Program for the Interaction of Core Melt with Concrete," Karlsruhe Report KfK-2890 (1981).

10. H. ALSMEYER, "BETA-Experiments in Verification of the WECHSL Code: Experimental Results on the Melt-Concrete Interaction," Nuclear Engineering and Design 103, 115-125 (1987). Also see H. ALSMEYER, et. al., "Beta Experimental Results on Melt/Concrete Interactions: Silicate Concrete Behavior," Proceedings of the Committee on the Safety of Nuclear Installations (CSNI) Specialists Meeting on Core Debris-Concrete Interactions, EPRI NP-5054-SR (February 1987).

11. D. R. BRADLEY and E. R. COPUS, "Significant Results from SURC-3 and SURC-3A Experiments," presented at 15th Water Reactor Safety Meeting, National Bureau of Standards, Gaithersburg (October 16-30, 1987); and E. E. R. Copus, et. al., "Core-Concrete Interactions Using Molten Steel with Zirconium on a Basaltic Basemat: The SURC-4 Experiment," NUREG/CR4994, SAND87-2008, R3, R5, R7 (August 1987); and M. LEE and R. A. BARI, "International Standard Problem No. 24, ISP-24, SURC-4 Experiment on Core-Concrete Interactions," Restricted CSNI Report No. 155 (December 1988).

12. E. R. COPUS and D. R. BRADLEY, "Interaction of Hot Solid Debris with Concrete," NUREG/CR-4558, SAND85-1739 (1986).

13. J. E. GRONAGER, A. J. SUO-ANTTILA, D. R. BRADLEY, and J. E. BROCKMAN, "TURC1: Large-Scale Metallic Melt-Concrete Interaction Experiments and Analysis," NUREG/CR-4420, SAND85-0707 R5, R7 (January 1986); and J. E. GRONAGER, A. J. SUO-ANTTILA, and J. E. BROCKMAN, "TURC2 and TURC3: Large-Scale $UO_2/ZrO_2/Zr$ Melt-Concrete Interaction Experiments and Analysis", NUREG/CR-4521, SAND86-0318 R5, R7 (June 1986).

14. W. W. TARBELL, D. R. BRADLEY, R. E. BLOSE, J. W. ROSS, and D. W. GILBERT, "Sustained Concrete Attack by Low-Temperature, Fragmented Core Debris," NUREG/CR-3024, SAND82-2476 R3, R4 (July 1987).

15. R. E. BLOSE, J. E. GRONAGER, A. J. SUO-ANTTILA, and J. E. BROCKMAN, "Sustained Heated Metallic Melt/Concrete Interactions with Overlying Water Pools," NUREG/CR-4747, SAND85-1546 R3, R4, R7 (July 1987).

16. G. A. GREENE, C. FINFROCK, and S. B. BURSON, "Phenomenological Studies on Molten Core-Concrete Interactions," Nucl. Eng. and Design 108, 167-177 (1988).

17. T. G. THEOFANOUS and M. SITO, "An Assessment of Class 9 (Core-Melt) Accident for PWR Dry-Containment Systems," Nucl. Eng. and Design 66, 301-332 (1981).

18. G. ERIKSSON, "Thermodynamic Studies of High Temperature Equilibria XII. SOLGASMIX, A Computer Program for Calculation of Equilibrium Compositions in Multiphase System," Chemical Scripta 8, 100-103 (1975).

19. T. M. BESMANN, "SOLGASMIX-PV, A Computer Program to Calculate Equilibrium Relationships in Complex Chemical Systems," Oak Ridge National Laboratory Report ORNL/TM-5775 (1977).

THE INTEGRAL EFFECTS TEST (IET-1) IN THE SURTSEY TEST FACILITY

Michael D. Allen
Richard O. Griffith
Martin M. Pilch
Robert T. Nichols

Sandia National Laboratories
Albuquerque, NM

ABSTRACT

The first experiment of the Integral Effects Test (IET-1) series was conducted to investigate the effects of high pressure melt ejection (HPME) on direct containment heating (DCH). A 1:10 linear scale model of the Zion reactor pressure vessel (RPV), cavity, instrument tunnel, and subcompartment structures were constructed in the Surtsey Test Facility at Sandia National Laboratories (SNL). The RPV was modelled with a melt generator that consisted of a steel pressure barrier, a cast MgO crucible, and a thin steel inner liner. The melt generator/crucible had a semi-hemispherical bottom head containing a graphite limitor plate with a 3.5 cm exit hole to simulate the ablated hole in the RPV bottom head that would be formed by tube ejection in a severe nuclear power plant (NPP) accident. The reactor cavity model contained 3.48 kg of water with a depth of 0.9 cm that corresponded to condensate levels in the Zion plant. A steam driven iron oxide/aluminum/chromium thermite was used to simulate HPME.

A relatively small steam explosion occurred in the cavity during IET-1. Steam blowthrough entrained debris into the Surtsey vessel resulting in a peak pressure increase in Surtsey of 98 kPa. The Surtsey vessel had been previously inerted with N_2. The total debris mass ejected into the Surtsey vessel was 43 kg. The hydrogen concentration was 3.1 mol.% in the vessel at equilibrium. The concentration measured inside the subcompartment structures immediately following HPME transient was 20.7 mol.% H_2.

INTRODUCTION

The Surtsey Test Facility at SNL is used to perform scaled experiments that simulate a high-pressure melt ejection (HPME) accident in a NPP. These experiments are designed to investigate the phenomena associated with direct

containment heating (DCH). High-temperature, chemically reactive melt is ejected by high-pressure steam into a 1:10 linear scale model of a reactor cavity. Debris is entrained by the steam blowdown and ejected into the Surtsey vessel, where the effect of subcompartment structures, water in the cavity, and hydrogen generation can be studied.

IET-1 was the first in a series of experiments using a small scale model of the Zion Nuclear Generating Station. The purpose of this test and the Argonne National Laboratory (ANL) counterpart test was to investigate possible scale distortions in DCH phenomena between NPP scale and experiment scale. The IET-1 test at SNL was conducted at 1:10 linear scale, whereas ANL counterpart tests will be performed at 1:40 scale. Results of these experiments will allow assessment of scaling methodologies proposed by the SASM-TPG and by SNL.

EXPERIMENT DESCRIPTION

A composite view of the Surtsey vessel, the HPME delivery system, and the subcompartment structures used in the IET-1 experiment is shown in Figure 1. An exploded view of the subcompartment structures is also shown in this figure. In IET-1, 1:10 linear scale models of the Zion reactor pressure vessel (RPV), cavity, instrument tunnel, and subcompartment structures were constructed.

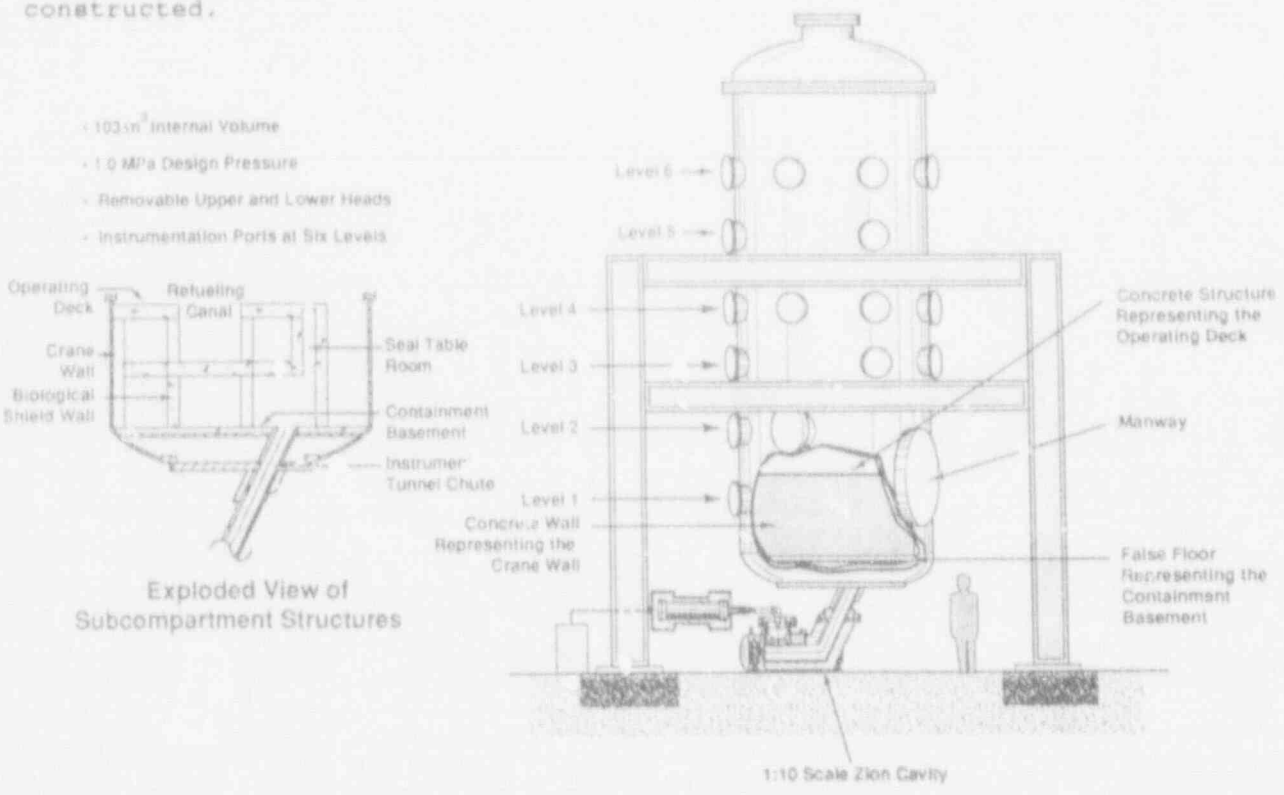

Figure 1. Surtsey vessel, high-pressure melt ejection system, and subcompartment structures used in the IET-1 experiment.

A melt generator that consisted of a steel pressure barrier, a cast MgO crucible, and a thin steel inner liner (Figure 2) modelled the RPV. The melt generator/crucible had a semi-hemispherical bottom head containing a graphite limitor plate with a 3.5 cm exit hole to simulate the ablated hole in the RPV bottom head that would be formed by tube ejection in a NPP severe accident.

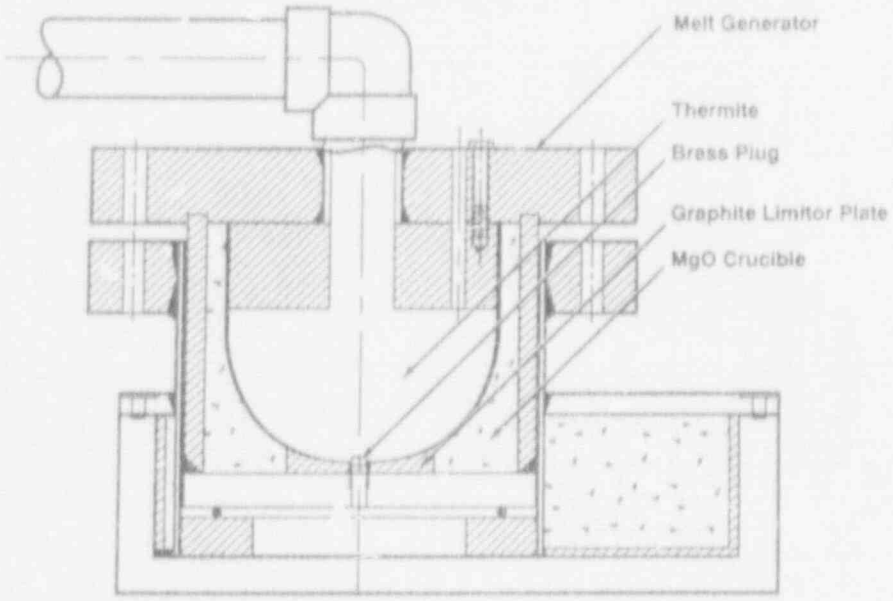

Figure 2. Melt generator and MgO crucible used in the IET-1 experiment.

The cavity used in the IET-1 test was a 1:10 linear scale model of the Zion reactor cavity that was designed to withstand internal pressures of 1000 psi with a safety factor of 4 (Figure 3). The inclined portion of the instrument tunnel entered the bottom head of Surtsey at a 26° angle from vertical, as it does in Zion. A false concrete floor was constructed in the Surtsey vessel. In the ANL facility the inclined portion of the instrument tunnel was 2.7 times the correct scaled length of the Zion instrument tunnel exit because of limited clearance between the melt generator an test vessel.

The subcompartment structures included 1:10 linear scale models of the crane wall, four steam generators, four reactor coolant pumps (RCP), the seal table opening, the seal table room, the biological shield wall, the refueling canal, the radial beams and the gratings at the RCP deck, and the operating deck (Figure 4). Figure 5 shows an isometric view of the subcompartment structures in Surtsey with a 90° section cut out. The freeboard volume inside the subcompartment structures was 4.65 m^3, and the freeboard volume in the Surtsey upper dome was 85.15 m^3 for a total freeboard volume of 89.8 m^3 in the Surtsey vessel (Table 1). The steam generators, reactor coolant pumps, and gratings were made of steel and the other structures were constructed of reinforced

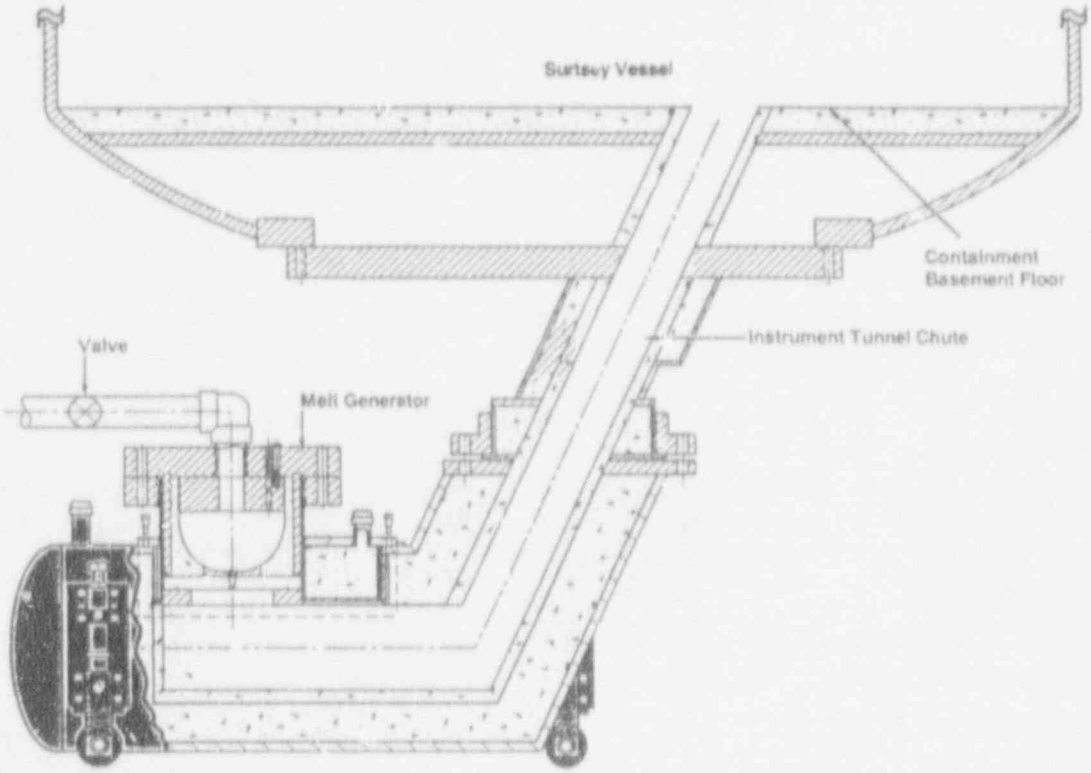

Figure 3. Schematic of the 1:10 linear scale model of the Zion reactor cavity.

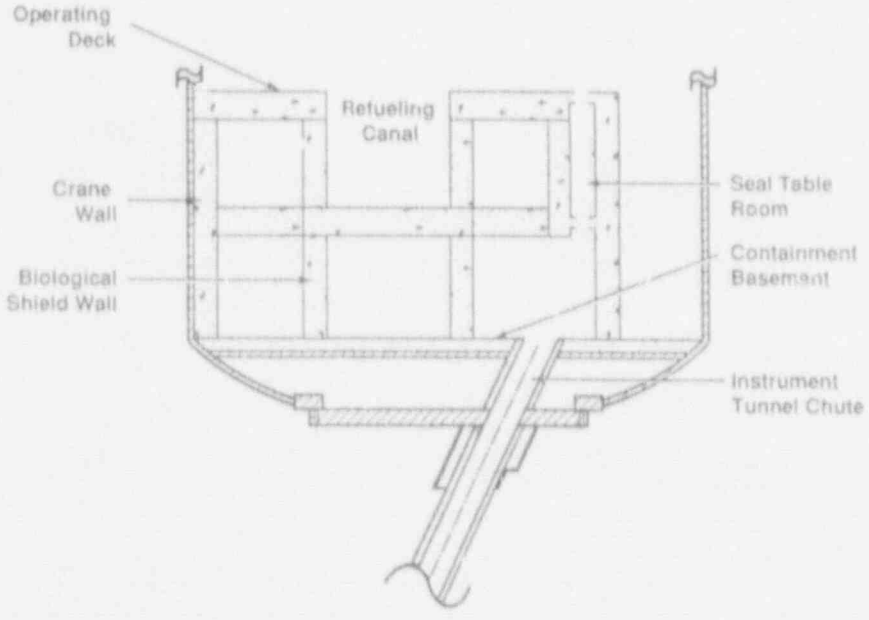

Figure 4. Subcompartment structures inside the Surtsey vessel.

concrete. All of the structures were painted with an epoxy paint similar to the paint used in actual NPPs.

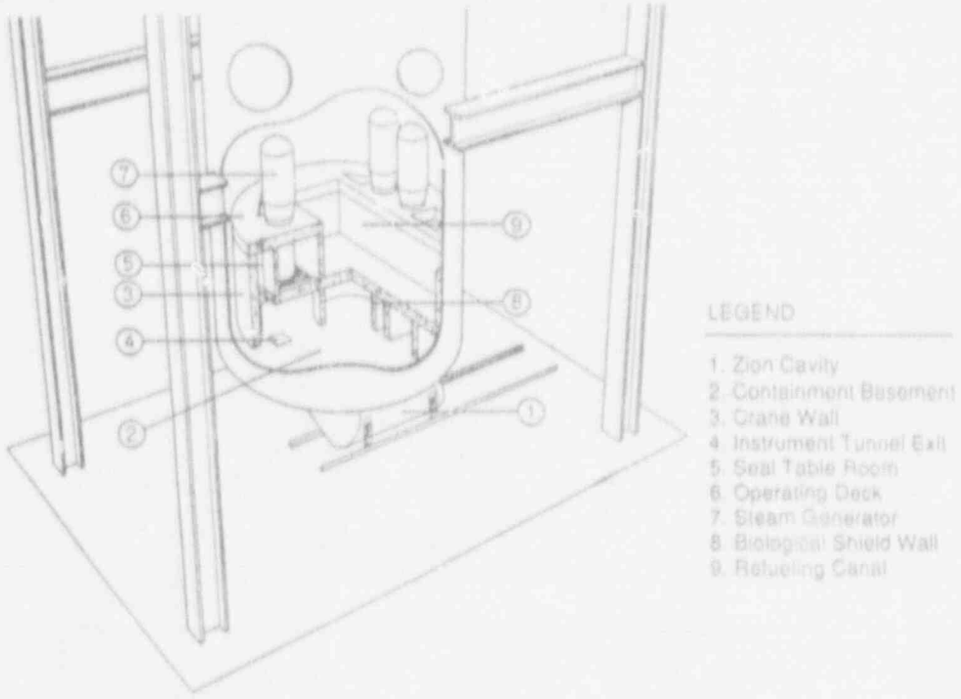

Figure Subcompartment structures inside the Surtsey vessel.

The steam accumulator tank was pressurized to ≈6.4 MPa with superheated steam. After the pressurization sequence, the iron oxide/aluminum/chromium thermite mixture was ignited remotely with a braided wire fuse placed on top of the compacted thermite. After the reaction was initiated, the heat generated by the thermite reaction caused the pressure in the crucible to rise. This pressure increase verified that the thermite reaction had started, and signaled the operator to open the valve separating the steam accumulator tank and the molten thermite in the melt generator. This brought superheated steam into contact with the molten thermite. Upon contacting and failing a fusible brass plug at the bottom of the crucible, the molten thermite in the crucible was expelled by high-pressure steam into the cavity.

Zero time for HPME was set by the data acquisition system as the time at which the melt failed the brass plug and entered the cavity. This event was signaled by a photodiode located at the melt plug exit. When the hot melt burst through the brass plug, the intense light emitted from the melt caused the photodiode to emit a signal that was used to mark the initiation of the HPME.

Initial Conditions

The IET-1 test was conducted with the following initial conditions: (1) the melt simulant was 43 kg of iron oxide/aluminum/chromium powder; (2) the driving gas was ≈440 moles of superheated steam (≈600 K) at an absolute pressure of 7.1 MPa; (3) the initial absolute pressure in the Surtsey vessel was ≈0.2 MPa of relatively pure nitrogen (>99.96 vol.% N_2); (4) the cavity was a 1:10 linear scale model of the Zion reactor cavity; and (5) the cavity contained 3.48 kg of water that was 0.9 cm deep. The initial conditions of the IET-1 experiment are listed in Table 1.

Measurements and Instrumentation

The most significant variables measured in the Integral Effects Tests (IET) are: (1) the increase in pressure in the Surtsey vessel, (2) the number of moles of hydrogen generated by the reaction of metallic debris with steam driving gas and water in the cavity, (3) the debris temperature as it struck the concrete structure, (4) the debris interaction times, (5) the debris particle size, (6) the mass of debris recovered from the Surtsey vessel, and (7) the cavity pressure. The instrumentation and techniques used to make these measurements are described in the sections below.

		IET-1
Thermite composition (kg)		
	iron oxide	29.260
	chromium	4.650
	aluminum	9.090
Total mass (kg)		43.000
Final hole diameter (cm)		3.5
Driving pressure at plug failure (MPa)		7.1
Moles of steam driving gas (moles)		440
Cavity water (kg)		3.48 (0.9 cm deep)
Initial absolute pressure in Surtsey (MPa)		0.20
Initial gas composition in Surtsey (mol.%)	N_2	99.96
	O_2	0.03
Freeboard volume inside subcompartment structures		4.65 m^3
Freeboard volume in Surtsey upper dome		85.15 m^3
Total freeboard volume inside Surtsey		89.8 m^3

Table 1. Initial conditions for the IET-1 experiment.

Pressure Measurements

Six pressure transducers, two each at levels 1, 3, and 5 (Figure 1), were used to measure the pressure in the Surtsey vessel in the IET-1 experiment. These transducers were mounted in tapped holes in instrument penetration ports in the sides of the Surtsey vessel and had their sensing ends protected with steel turnings. Pressure transducers were also used to measure the gas pressure in the accumulator tank, in the crucible above the thermite, in the sealed reactor cavity, in the subcompartment structures, and in the seal table room. These devices were metal-diaphragm, strain gauge-type pressure transducers (Model 141-1, Precise Sensor, Inc., Monrovia, CA). The two pressure transducers used to measure pressure in the cavity were embedded in the concrete walls of the round section of the cavity under the melt generator, and were piezoelectric-type gauges with a range of 0-6.9 MPa. Data from the peizoelectric pressure transducers were recorded with an FM recorder.

The data acquisition system recorded data from the pressure transducers at a rate of 1400 data points per second from the time of thermite ignition to about 60 seconds following the HPME transient.

Temperature Measurements

Following the HPME transient, the gas temperatures in the Surtsey vessel were measured with five aspirated thermocouple assemblies. An aspirated thermocouple assembly consisted of three bare, type-K thermocouples mounted in an anodized aluminum tube. One of each of these assemblies was installed through instrumentation ports at levels 1, 3, and 5 (Figure 1). To sample gas from inside the subcompartment structures, a thermocouple assembly was also installed through the refueling canal wall just above the radial concrete beam on the same side as the instrument tunnel exit. Another thermocouple assembly was installed through the crane wall into the seal table room. Each tube was opened with a solenoid-operated valve that was actuated remotely by a signal from the photodiode under the melt plug immediately after the HMPE transient.

The temperature of the driving gas in the steam accumulator tank was measured using two type-K thermocouples that extended through the accumulator shell and were secured in place using pressure-tight fittings. Measurements from these thermocouples were important because the measured temperature and pressure in the accumulator tank were used to calculate the number of moles of steam driving gas.

A thin-foil graphite calorimeter was embedded in the crane wall directly in the flight path of the debris to measure the debris contact temperature as it impacted the structure. Two other thin-foil graphite calorimeters were embedded in the containment basement floor between the chute exit and the biological shield wall. Each graphite calorimeter consisted of a 1-mm thick graphite disk with a diameter of 25.4 mm. Each graphite disk had a type-S thermocouple attached to the backside of the disk and was set in a ceramic holder that was embedded in the concrete structure.

Data points from the thermocouples were recorded by the data acquisition system at a rate of 10 per second prior to thermite ignition. Just prior to thermite ignition, the data acquisition system was switched to the fast data acquisition mode in which data points were recorded at a rate of 1400 per second.

Gas Composition

Ten pre-evacuated 500-cm^3 gas grab sample bottles were used to collect samples from the vessel at the following locations: a background sample at level 4 just prior to ignition of the thermite; three gas grab sample bottles located at levels 2, 4, and 6 were opened remotely for 10 seconds at 2 minutes after the HPME; three gas grab sample bottles at levels 2, 4, and 6 were opened manually for 10 seconds at ≈30 minutes after the HPME; and three gas grab sample bottles that had their inlet inside the subcompartment structures were opened 2 s after the HPME and remained open for 5 s. In addition, two gas grab samples were taken from the cavity following the HPME by opening bottles attached to the cavity; one was opened as the HPME was initiated and remained open for 2 s, and the other was opened at 0.5 s following the HPME and remained open for 2 s. The gas samples were analyzed using gas mass spectroscopy by Battelle Pacific Northwest Laboratories in Richland, WA.

Posttest Debris Recovery

The total mass dispersed into the Surtsey vessel and the mass in specific locations were determined by a very careful posttest debris recovery procedure. The following measurements were made: (1) mass of the molten debris in the cavity and inclined portion of the instrument tunnel; (2) mass on the horizontal surfaces outside the subcompartment structures; (3) mass on the vertical surfaces outside the subcompartment structures; (4) mass recovered from the floor inside the structures; (5) mass recovered from the horizontal surfaces other than the floor inside the structures; (6) mass recovered from the vertical surfaces inside the structures; (7) mass recovered from the doorways inside the structures; (8) mass recovered from the seal table room; (9) mass recovered from the rooms adjacent to the seal table room; and (10) mass recovered from the melt generator/crucible.

Debris Velocity

Breakwires were placed across the opening from the containment basement to the seal table room. When the debris front severed the breakwire, a timing signal was recorded by the data acquisition system. The breakwire was intended to give timing information on entry of debris into the seal table room.

In the IET-1 experiment, the Surtsey was purged with nitrogen in order to perform the tests in an atmosphere that was almost oxygen free (i.e., ≈0.03 mol.% O_2). This virtually eliminated metal/oxygen reactions in the Surtsey atmosphere and preserved hydrogen produced by steam/metal reactions so that hydrogen production could be accurately measured.

EXPERIMENT RESULTS

Blowdown History

Figure 6 shows the blowdown history of the IET-1 experiment. In the experiment, the accumulator tank (volume = 0.29 m^3) was pressurized with superheated steam to ≈6.4 MPa. The free volume in the crucible and in the 10-cm diameter pipe above the crucible was purged with nitrogen. After the thermite was ignited, the valve separating the accumulator and the molten thermite was opened, and the crucible free volume pressurized because of the heat from the reaction. Figure 6 indicates that steam was in contact with the molten thermite for ≈4.5 s prior to the HPME. The horizontal line across Figure 6 shows that the steam driving gas pressure at the initiation of the HPME was 7.1 MPa.

The steam pressure in the accumulator was 6.4 MPa before the valve between the accumulator and the melt generator was opened, the steam temperature was 598 K, and the total steam volume in the accumulator was 0.29 m^3. These data were used to determine the number of moles of steam driving gas using the specific volume of steam from standard thermodynamic tables. The number of moles of steam driving gas in the IET-1 test was 440.

Figure 6 shows the steam blowdown from the accumulator in the IET-1 experiment. The steam blowdown was complete in ≈4 seconds. In previous tests with a final hole diameter of 3.5 cm (i.e., WC-1, LFP-1B, LFP-2A, and LFP-8A), the steam blowdown lasted ≈3 seconds [Allen et al. 1991a; Allen et al. 1991b].

Pressure Measurements

Pressure transducers were used to measure the pressure increase in the Surtsey vessel, in the cavity, in the seal table room, and in the subcompartment structures because of the HPME transient. The following sections describe the results of the pressure measurements.

Surtsey Vessel Pressure

Figure 7 shows the absolute pressure measured at level 3 in the Surtsey vessel versus experiment time. This figure has a horizontal dotted line across the graph to show the initial pressure in Surtsey prior to the HPME transient. The initial absolute pressure was ≈0.2 MPa as listed in the table of initial conditions (Table 1). This figure also has a horizontal dotted line across the graph at the peak pressure caused by the HPME. The pressures measured at levels 1, 3, and 5 with other pressure transducers in the Surtsey vessel because of the HPME transient were virtually identical. The pressure increase in the IET-1 experiment was 0.098 MPa.

Cavity Pressure

Figure 8 shows the cavity pressure and vessel pressure versus experiment time for the IET-1 experiment. This figure shows a relatively small peak just after the HPME began. This peak was because of gas expansion caused by hot

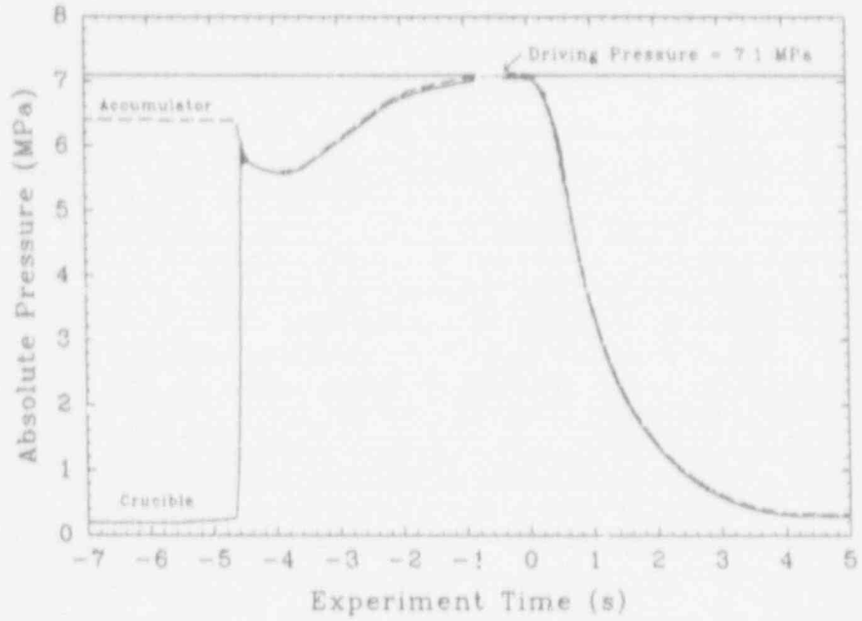

Figure 6. Blowdown history of the IET-1 experiment.

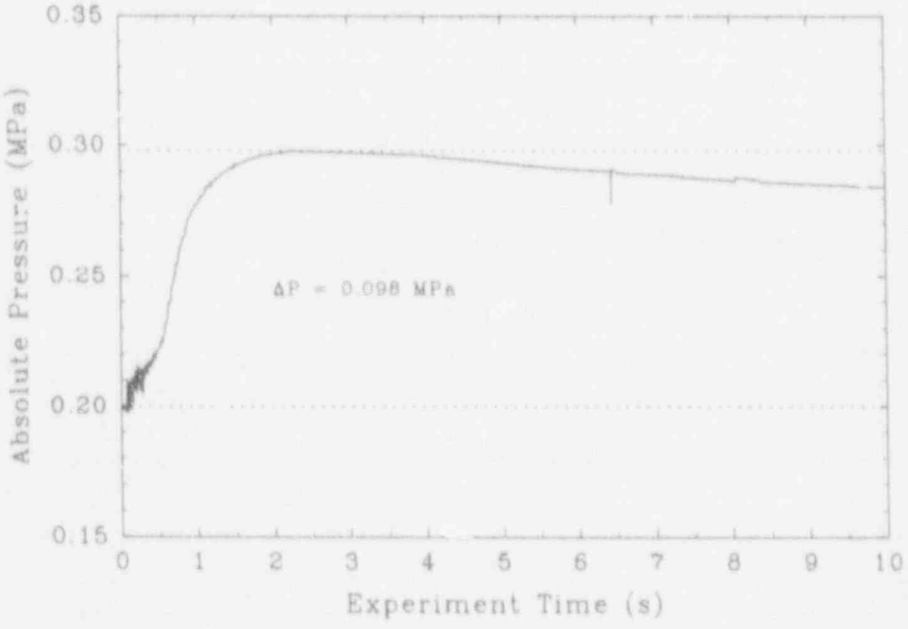

Figure 7. Vessel pressure measured at level 1 versus time in the IET-1 experiment.

thermite entering the cavity. The second peak, which occurred at ≈0.06 s and had a magnitude of ≈1.4 MPa, was a relatively small steam explosion. The third broad peak, which occurred between 0.4 and 0.8 s, was due to thermite entrainment from the cavity. At 0.4 s steam blowthrough occurred and debris was accelerated out of the cavity by the high-velocity steam, which resulted in a higher pressure in the cavity than in the Surtsey vessel. In previous Surtsey experiments with a 3.5 cm exit hole and a dry cavity (LFP-1A, LFP-2A, LFP-8A, and WC-1) [Allen et al. 1991b], the debris entrainment interval was on the order of 1 s. Differences in the debris ejection observed in IET-1 and earlier Surtsey tests are probably due to the new melt generator/crucible design used in IET-1.

Figure 9 is a plot of the cavity pressure measured with three transducers for an experiment time of 0 to 0.2 s. These transducers were installed in the cavity to measure the pressure due to possible steam explosions. There was a small steam explosion in the cavity at 0.06 s with a magnitude on the order of 1.4 MPa. It is hypothesized that these sensors recorded a single steam explosion. The small steam explosion observed in IET-1 was similar to the steam explosions observed in the WC-2 experiment. There is some indication from the graphite calorimeter data that the steam explosion ejected some debris into the subcompartment structures before steam blowthrough entrained debris from the floor of the cavity.

Pressure Measured Inside the Seal Table Room

Figure 10 shows the pressure measured in the seal table room and the pressure measured in the Surtsey vessel plotted against experiment time. Clearly, the pressure measured in the seal table room follows the pressure measured in the cavity (Figure 8). There is a small pressure peak that corresponds to hot thermite entering the cavity. Then there is a large, sharp peak that is probably the result of the steam explosion in the cavity. There is also a broad pressure peak between 0.5 and 0.8 s that corresponds to the debris ejection from the cavity.

These same data are plotted for an experiment time of 0 to 0.2 s in Figure 11. The steam explosion registers on the pressure transducers in the seal table room and in the Surtsey vessel. The pressure differential across the seal table room walls caused some damage to the seal table room. The seal table room was separated from the crane wall on one side and also had a large crack in the inner wall. In addition, the concrete plug in the seal table room ceiling was violently ejected into the upper dome of Surtsey.

Pressure Measured Inside the Subcompartment Structures

Figure 12 shows the pressure measured inside the subcompartment structures and the pressure measured in the Surtsey vessel for an experiment time of 0 to 1 s. The steam explosion that occurred at ≈0.06 s apparently caused a shock wave in the subcompartment structure. The pressure measured inside the subcompartment structures follows the pressure measured in Surtsey after about 0.1 s. There is no differential pressure between the structures and Surtsey because of the debris ejection that occurred between 0.4 and 0.8 s. Thus

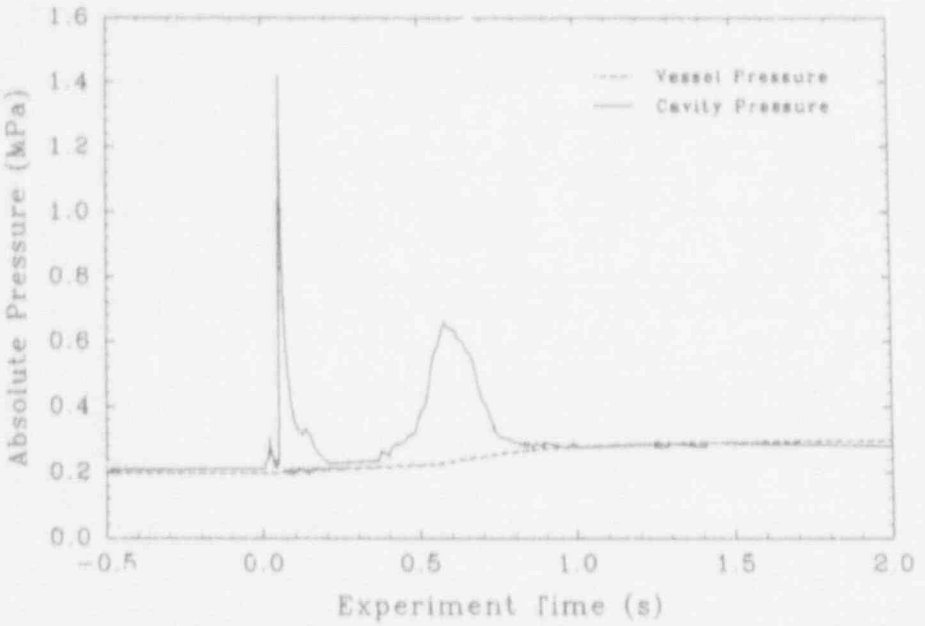

Figure 8. Cavity and vessel pressure versus time for the IET-1 experiment.

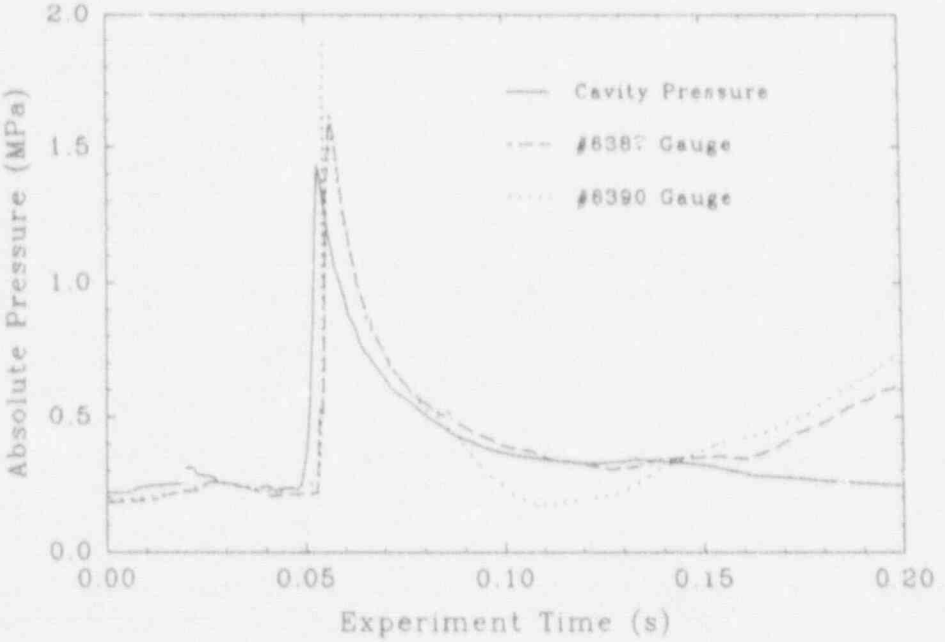

Figure 9. Cavity pressure in the IET-1 experiment showing a steam explosion at 0.05 s.

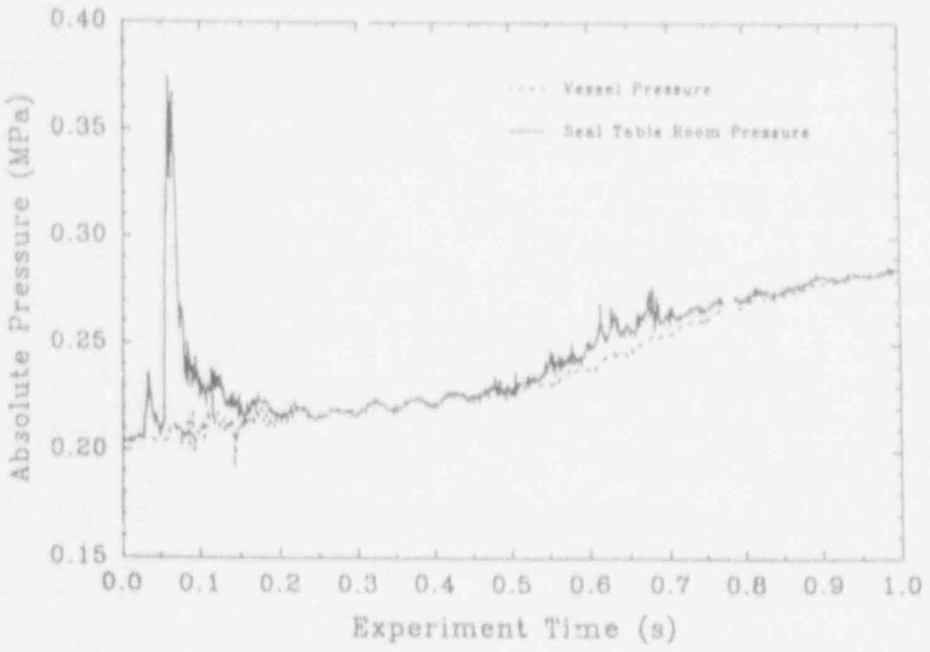

Figure 10. Seal table room and vessel pressure versus experiment time in the IET-1 experiment.

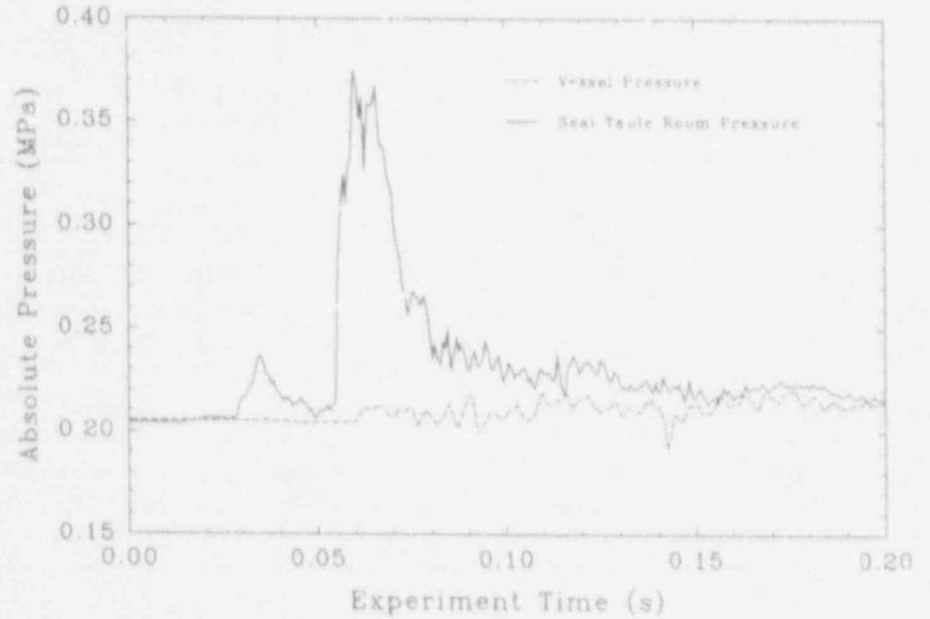

Figure 11. Seal table room and vessel pressure plotted for an experiment time of 0 to 0.2 s in the IET-1 experiment.

there was no differential pressure across the walls of the structures except from the steam explosion. All of the pressure transducers showed an oscillatory behavior after the steam explosion that damped out after approximately 2 s. The shock wave from the steam explosion may have caused the Surtsey vessel to resonate.

Gas Temperature Measurements

Figure 13 shows the gas temperatures at the Surtsey vessel walls measured with aspirated thermocouples at levels 1, 3, and 5 (Figure 1). The gas temperatures measured at levels 1 and 3 in the Surtsey vessel were substantially higher than the temperatures measured at level 5. In IET-1, the highest gas temperature was measured at level 3, and the second highest was measured at level 1. The gas temperature was higher at level 3 than at level 1 because there was a direct path for debris ejected from the seal table room to flow past level 3. Level 1 was below the operating deck and thus there was no direct path for debris to flow past the aspirated thermocouple at that level. The gas temperature at level 5, which is relatively high in the vessel, was barely above the ambient temperature. This is an indication that not much debris was ejected into the upper dome of the vessel.

Figure 14 shows the gas temperature in IET-1 measured inside the subcompartment structures with an aspirated thermocouple. The gas temperature reached a peak of ≈1180 K at an experiment time of 0.9 s. The aspirated thermocouples in the seal table room were destroyed by direct contact with molten debris. Figures 15 and 16 show the measured temperatures in the triangular vent spaces above the 1A and 1D RCPs plotted against time. If a person stands in the center of the structures and looks toward the instrument tunnel exit, then the 1A RCP vent space is on the left-hand side. The 1D RCP vent space is diagonally across the operating deck from the 1A vent space. Figure 15 shows the temperature in the 1A vent space plotted against experiment time. The peak temperature was 430 K at ≈1 s. Figure 16 shows that the temperature in the 1D vent space reached a peak of 340 K at ≈17 s.

Debris Temperature Measurements

Figure 17 shows the debris contact temperatures for IET-1 at the surface of the concrete structure measured with three thin-foil graphite calorimeters: one embedded in the crane wall just under the seal table room directly in the path of the debris, and two in the containment basement floor between the exit to the instrument tunnel and the biological shield wall. Figure 17 shows that the calorimeter in the crane wall was quickly destroyed by the debris plume. The calorimeter embedded in the containment basement floor near the instrument tunnel exit reached a peak temperature of 600 K in ≈8 s, and the calorimeter embedded in the containment basement floor near the biological shield wall reached a temperature of 1225 K at ≈16 s.

Gas Composition Measurements

Ten gas grab samples were taken from the Surtsey vessel. The hydrogen concentrations measured in these gas grab samples are listed in Table 2. A

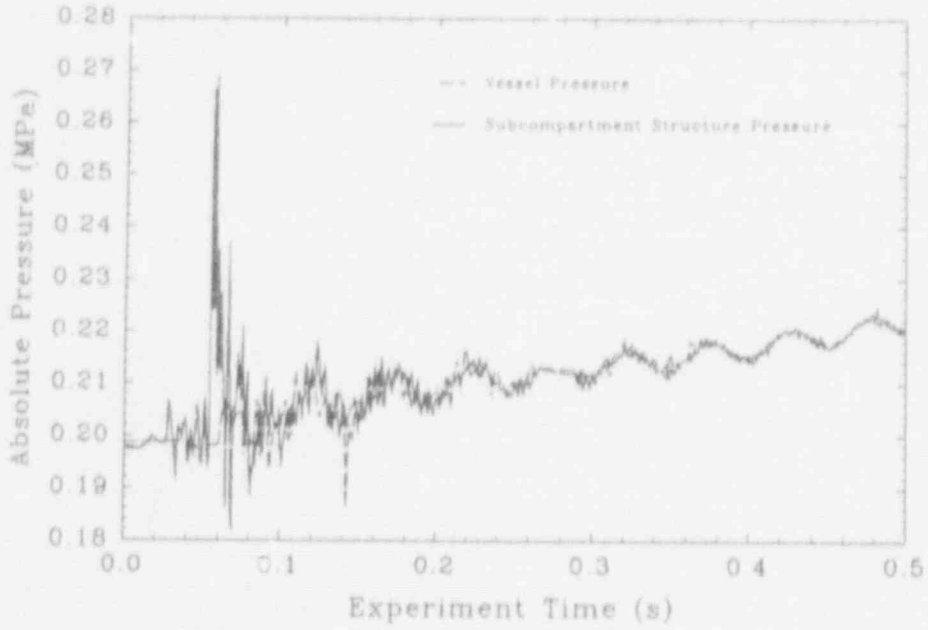

Figure 12. Absolute pressure inside the cubcompartment structures in the IET-1 experiments.

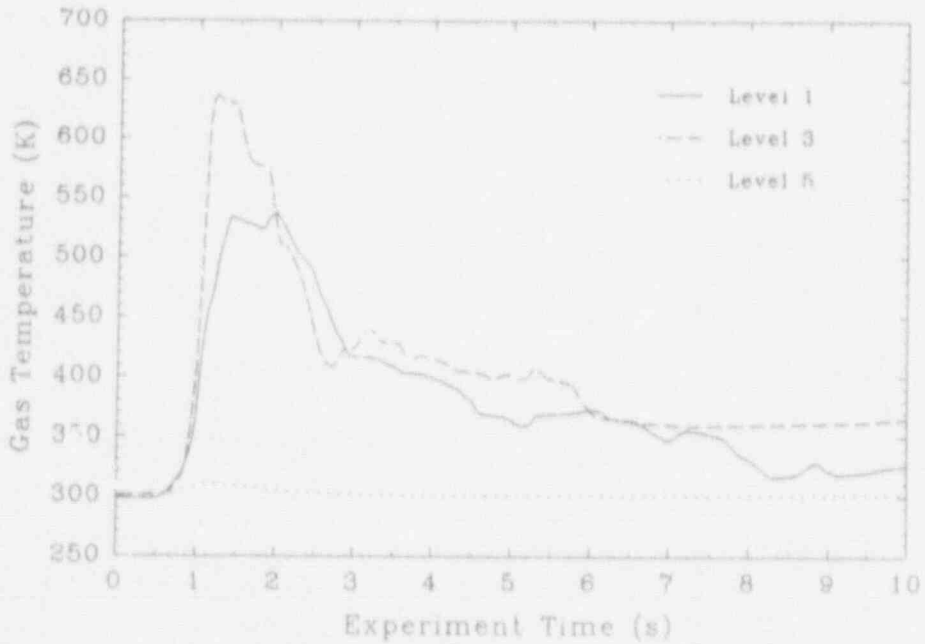

Figure 13. Gas temperatures measured in Surtsey with aspirated thermocouples in the IET-1 experiment.

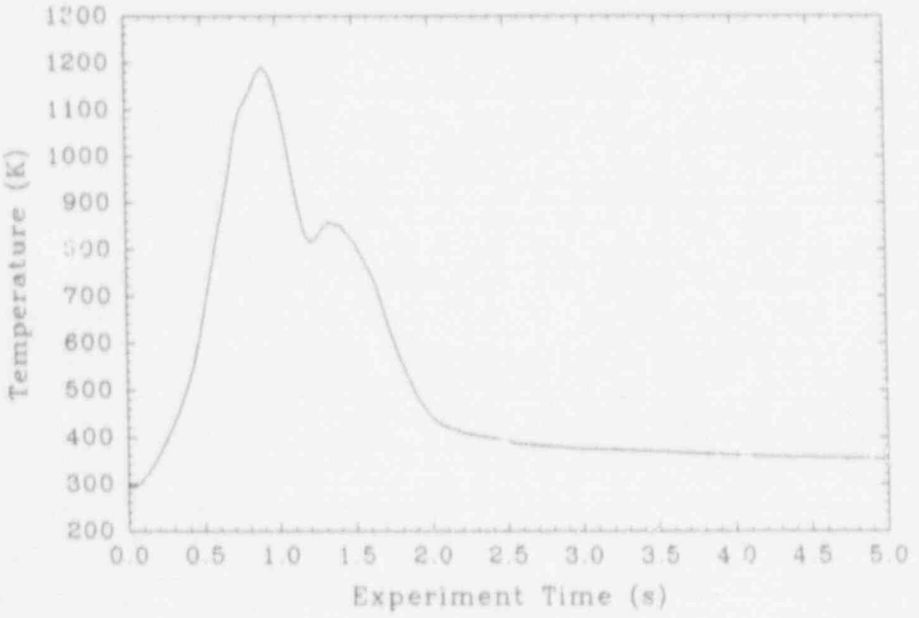

Figure 14. Gas temperature inside the subcompartment structures in the IET-1 experiment.

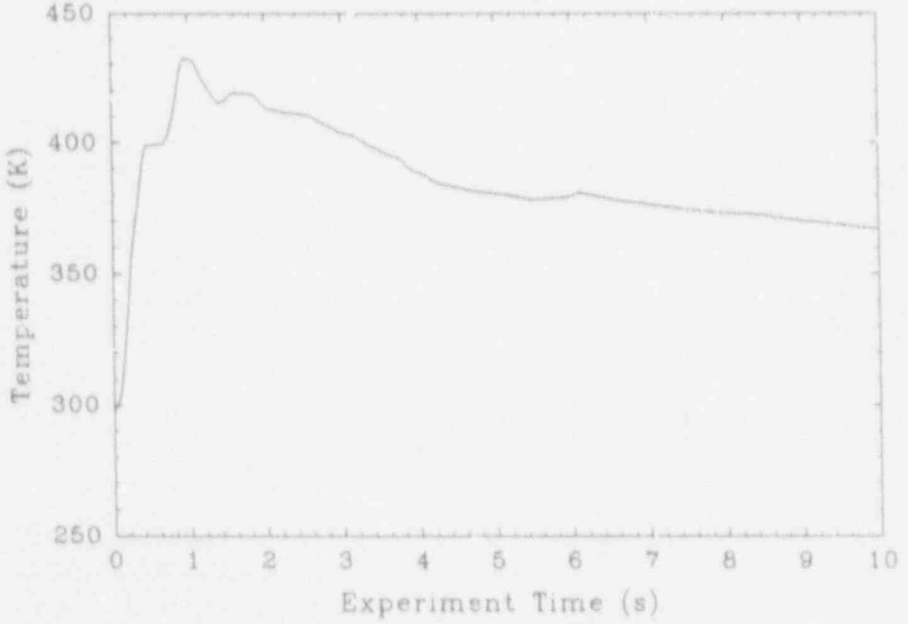

Figure 15. Temperature history in the triangular vent space above reactor coolant pump 1A in the IET-1 experiment.

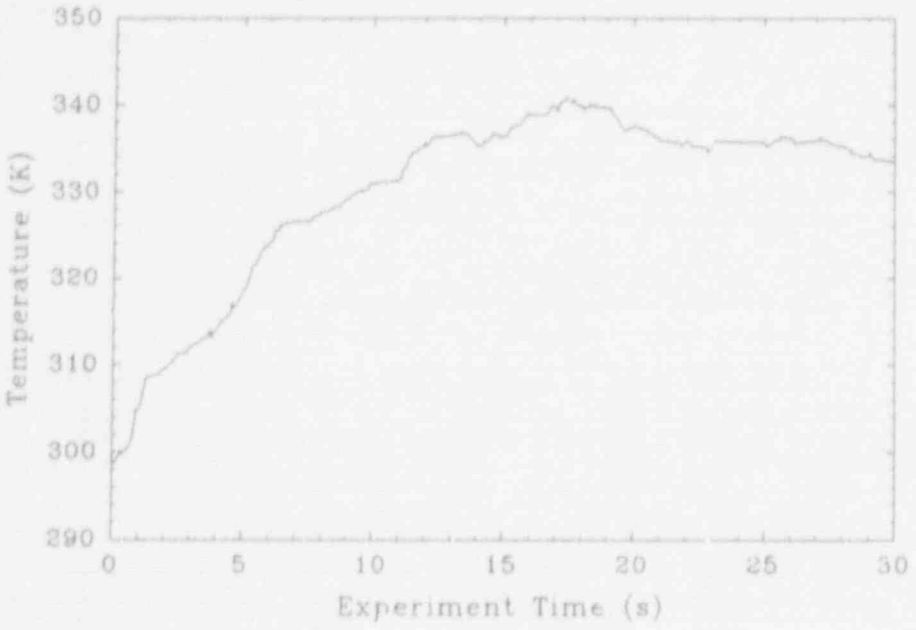

Figure 16. Temperature history in the triangular vent space above reactor coolant pump 1D in the IET-1 experiment.

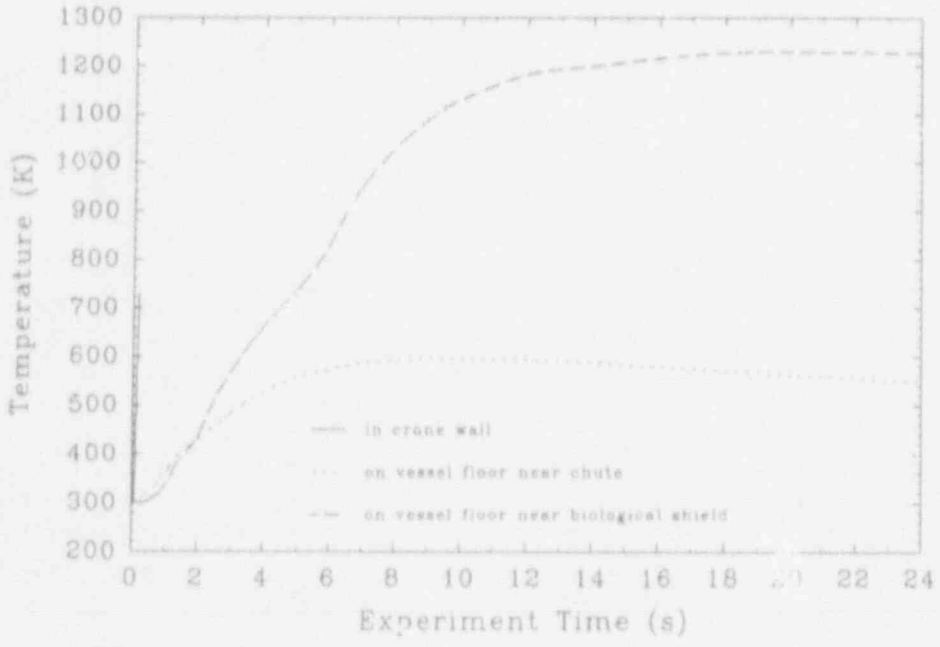

Figure 17. Debris temperature in the IET-1 experiment.

background sample bottle located at level 4 of the vessel was opened for 10 s prior to ignition. The measured background oxygen concentration was 0.03 mol.%. The results of all samples taken from the vessel outside the subcompartment structures at times greater than 2 minutes after the HPME transient are in excellent agreement. At equilibrium the hydrogen concentration was at 3.108 mol.% ± 0.029. The gas composition results

Location	Start Time wrt HPME → Duration		Hydrogen Concentration (mol.%)
Background	-20 s → 10 s	H_2 O_2	< 0.01 0.03
Cavity Cavity	0.0 s → 2 s 0.5 s → 2 s		36.5 13.0
Inside Structures	2 s → 5 s 2 s → 5 s 2 s → 5 s		20.5 20.8 20.9
Level 2 Level 2	2 min → 10 s 30 min → 10 s		3.07 3.10
Level 4 Level 4	2 min → 10 s 30 min → 10 s		3.09 3.13
Level 6 Level 6	2 min → 10 s 30 min → 10 s		3.11 3.15
Mean[1] Standard Deviation[1]			3.108 0.029

[1] Mean and standard deviations were computed for all of the samples taken outside the subcompartment structures in the Surtsey vessel after the HPME.

Table 2. Hydrogen concentrations measured in the IET-1 experiment.

indicate that two minutes after the HPME transient the hydrogen concentration was uniform everywhere in the vessel.

Three gas grab samples were taken from inside the subcompartment structures. These bottles were opened at 2 s after the initiation of the HPME and were closed 5 s later. These three samples were in excellent agreement, averaging 20.7 mol.% H_2. This indicates that there were high H_2 concentrations inside the subcompartment structures soon after the HPME.

Two gas grab samples were taken from the cavity in the IET-1 experiment. The results of these samples indicate that there are high hydrogen concentrations in the cavity during the HPME transient (36.5 and 13.0 mol.% H_2).

Debris Recovery Summary

Debris in the Surtsey vessel was recovered from four basic locations: (1) from inside the subcompartment structures, (2) from the Surtsey vessel outside the structures, (3) from the cavity and instrument tunnel chute, and (4) from the crucible. Table 3 gives the debris recovery summary of the IET-1 experiment. The total molten mass available for dispersal into the vessel is usually about 20% greater than the initial iron oxide/aluminum/chromium thermite charge due to the melting of the inner wall of the crucible, vaporization of the fusible brass plug, ablation of concrete in the cavity, and oxidation of metallic debris [Allen et al. 1991a]. Table 3 indicates that ≈86% of the molten debris in the cavity was dispersed into the vessel in IET-1.

	Mass (kg)
Initial thermite charge	43.000
- Debris inside structures	38.030
- Debris outside structures	4.980
Total debris recovered from Surtsey	43.010
Total debris recovered from cavity and chute	7.060
Total debris recovered from crucible	4.540
Total mass recovered[1]	54.610

[1] The molten mass available for dispersal into the vessel is usually about 20% greater than the initial iron oxide/aluminum/chromium thermite charge due to melting of the inner wall of the crucible, vaporization of the fusible brass plug, ablation of concrete in the cavity, and oxidation of metallic debris by steam.

Table 3. Debris recovery summary for the IET-1 experiment.

The debris plume apparently impacted the crane wall and the concrete ceiling near the seal table. Some of the debris was deflected to the containment basement floor, and some of the debris entered the seal table room. Of the 38.03 kg recovered from within the subcompartment structures, 9.775 kg was in the seal table room. The concrete plug in the ceiling of the seal table room (i.e., in the operating floor) had been violently ejected and had impacted a tank in the upper dome of the Surtsey vessel. A video taken from a port in the upper head of the Surtsey vessel shows that debris was ejected through the opening in the ceiling of the seal table room into the upper dome of Surtsey.In addition, some debris was ejected through the three doorways in the crane wall, around the steam generators, and through the triangular vent spaces above the reactor coolant pumps.

Debris Velocity

breakwires installed across the opening in the floor of the seal table room were intended to measure the time that the leading edge of the debris plume

entered the seal table room. The breakwires were severed at 0.06 s, possibly by the shock wave from the steam explosion. It appears to be difficult to measure debris velocities in experiments with short flight paths and water in the cavity.

Energy Balance

The scaling analysis code developed by M. Pilch, QUICK-DCH, used a single-cell equilibrium model to perform an energy balance on the IET-1 experiment. Based on the actual IET-1 initial conditions, QUICK-DCH indicated that the blowdown added 6.44 MJ to the Surtsey vessel, steam/metal reactions could contribute as much as 34.2 MJ, and that debris/gas heat transfer could contribute as much as 94.9 MJ. Ignoring the presence of water in the cavity, QUICK-DCH predicted that the total possible amount of energy that could be added to the Surtsey vessel due to the HPME could be as much as 135.5 MJ. Based on this energy input, the single-cell equilibrium model in QUICK-DCH predicted a peak pressure increase in the Surtsey vessel of 0.443 MPa. The experimentally measured peak pressure increase in the vessel was 0.098 MPa. These results indicate that the total thermal efficiency of DCH in the IET-1 experiment was approximately 22%.

The presence of water in the cavity during the IET-1 experiment provided a potential heat sink in the system, since some portion of the thermal and chemical energy in the debris would be used to vaporize the water. In the WC-2 experiment [Allen et al. 1991b], the experimental results indicated that less than 15% of the water initially present in the cavity was vaporized, despite the fact that the thermite in that experiment contained approximately 5 times the amount of energy necessary to vaporize all of the water that was present. The result suggested that water was ineffective as a heat sink. Furthermore, the HIPS tests with water in the cavity suggest that the bulk of the water was ejected as a slug prior to debris dispersal [Tarbell et al. 1991], and that the water did not exhibit the same degree of fragmentation as the debris as a result of gas blowdown. In the IET-1 experiment, the thermite contained approximately 17 times the amount of energy necessary to vaporize all of the water that was present in the cavity. However, the actual amount of water that was vaporized cannot be determined without repeating the IET-1 experiment without water in the cavity.

COMPARISON TO PRETEST PREDICTIONS

Pretest predictions were performed with CONTAIN 1.12, the NRC's best-estimate computer code for the integrated analysis of light water reactor (LWR) severe accident containment phenomena [Williams 1991]. For the best-estimate model, the steam supply system, cavity, subcompartment regions, and upper regions were subdivided into 14 CONTAIN cells. The cell locations may be described as follows:

Cell 1: steam accumulator
Cell 2: melt generator

Cell 3: horizontal body of the cavity
Cell 4: chute connecting cavity body to Surtsey vessel
Cell 5: basement, vicinity of chute exit
Cell 6: basement, clockwise from chute exit
Cell 7: basement, counterclockwise from chute exit
Cell 8: lower level, behind crane wall
Cell 9: basement, portions further from chute exit
Cell 10: seal table room
Cell 11: pump deck level, near side
Cell 12: pump deck level, far side
Cell 13: upper region of Surtsey, near side
Cell 14: upper region of Surtsey, far side

A more detailed description of the cell locations in the CONTAIN model of IET-1 can be found in the letter report to the NRC describing the pretest calculations [Williams 1991]. The initial conditions assumed for the CONTAIN IET-1 analysis are listed in Table 4.

A number of critical assumptions and approximations were made in developing the CONTAIN model of the IET-1 experiment. One important approximation is in the area of debris chemistry. CONTAIN 1.12 includes models for the reaction of iron and zirconium with both steam and oxygen. However, chromium and aluminum chemistry are not currently modeled. As a result, the effects of aluminum and chromium in the melt were simulated using the zirconium chemistry model in CONTAIN. A calculated amount of zirconium, 7.626 kg, was selected to replace the aluminum and chromium present in the thermite. This mass of zirconium had the same potential for hydrogen generation as the chromium-aluminum mixture that was actually present in the melt. To account for the fact that the gross exothermic energy release from this mass of zirconium was far greater than the exothermic energy release from the aluminum and chromium that was actually present, the enthalpy of the ZrO_2 reaction product in the code was artificially enhanced by 2.1868 MJ/kg. The details of this procedure and a more complete justification are provided in the IET-1 pretest letter report.

In the CONTAIN model, the molten debris was introduced into the cavity cell as a time-dependent debris source term. The total amount of debris injected into the cavity was assumed to be the entire debris inventory of the melt generator. However, the timing of the debris injection was based on a GASBLOW2 calculation for the conditions of the IET-1 experiment. The time dependence of the debris source from the GASBLOW2 calculation was simply normalized to produce the desired total amount of debris ejection. Because CONTAIN does not currently have the capability to model fuel-coolant interactions, the water present on the cavity floor was introduced into the cavity over the first 0.2 seconds of the debris entrainment process as steam with the enthalpy of liquid water. Based on the WC-2 experiment, only 15% of the initial water inventory in the cavity was introduced into the cavity in this way. It was assumed that the remaining water did not effectively participate in the vaporization process.

CONTAIN 1.12 has a number of models available for simulating the trapping process, with the most mechanistic being the time-of-flight/Kutateladze (TOF/KU) model. The TOF/KU model determines the time-of-flight for the debris to impact with the first structure in a cell, and then uses a Kutateladze criteria to determine if the debris remains trapped on the surface or rebounds

Melt generator (m)	
Final hole diameter	0.035
Lower head radius	0.2
Melt composition (kg)	
Al_2O_3	16.056
Cr	4.648
Al	0.596
Fe	21.699
TOTAL	43.000
Melt temperature (K)	2500
Steam driving gas	
Temperature (K)	550
Pressure (MPa)	6.2
Accumulator volume (m^3)	0.29
Melt generator volume (m^3)	0.45
Vessel atmosphere	
Pressure (MPa)	0.20
Temperature (K)	300
Composition (mol.%):	
N_2	99.95
O_2	0.05
Water in cavity (kg)	3.4

Table 4. Initial conditions for the CONTAIN IET-1 analysis.

from it. If the debris does not adhere on the first impact, a time-of-flight is calculated for the debris to impact with a second structure in the cell. If the debris fails to adhere on this impact, it is allowed to fall to the floor of the cell through a gravitational fall time (GFT) model. The TOF/KU model was used in the analysis of the IET-1 experiment. A more detailed discussion of its application is presented in the pretest letter report.

A number of CONTAIN runs were made in the pretest IET-1 analysis effort. A detailed discussion of these calculations is presented in the IET-1 letter report. In the base case CONTAIN run, the debris particle size was assumed to be 0.82 mm. The predicted peak pressure increase in the Surtsey vessel was 0.0704 MPa, and the predicted steam-to-hydrogen conversion efficiency was 30.1%. In the IET-1 experiment, the measured peak pressure increase was 0.098 MPa, and the measured steam to hydrogen conversion efficiency was 51%.

SUMMARY

Table 5 summarizes the results of the IET-1 test.

In the IET-1 experiment, iron oxide/aluminum/chromium thermite was used as a corium melt simulant. Forty-three kg of molten thermite was ejected by slightly superheated steam at 7.1 MPa through the hole in the graphite limitor plate. Steam blowthrough entrained the molten debris into the Surtsey vessel, which had been pre-inerted with nitrogen (≈0.03 mol. O_2) to 0.20 MPa.

In the IET-1 experiment, the cavity initially contained 3.48 kg of water, which corresponds to condensate levels in the Zion plant. There was a small steam explosion (≈1.4 MPa) shortly after the beginning of the HPME. This steam explosion apparently ejected a slug of hot water (and possibly some debris) from the cavity into the subcompartment structures. The video shows violent ejection of debris from the subcompartment structures, probably through the hole in the ceiling of the seal table room; some of this debris impacted the upper dome of Surtsey. The peak pressure increase measured in the Surtsey vessel was 0.098 MPa. Analyses of the gas grab samples indicated that 223 moles of H_2 were produced by the HPME and that there were high hydrogen concentrations in the cavity and in the subcompartment structures early in the transient.

	IET-1
Driving pressure at plug failure (MPa)	7.1
Time from ignition to HPME (s)	7.3
Time steam was in contact with thermite prior to HPME (s)	4.5
Moles of H_2O driving gas (moles)	440
Cavity water (moles)	193
Moles of H_2 produced (moles)	223
ΔP due to the HPME (MPa)	0.098

Table 5. Summary of the results of the IET-1 experiment.

REFERENCES

Allen et al., 1991a, *Experiments to Investigate the Effect of Flight Path on Direct Containment Heating (DCH) in the Surtsey Test Facility: The Limited Flight Path (LFP) Tests*, NUREG/CR-5728, SAND91-1105, Sandia National Laboratories, Albuquerque, NM.

Allen et al., 1991b, *Experiments to Investigate the Effect of Water in the Cavity on Direct Containment Heating (DCH) in the Surtsey Test Facility*, SAND91-1173, to be published, Sandia National Laboratories, Albuquerque, NM.

Tarbell et al., 1991, *Pressurized Melt Ejection into Water Pools*, NUREG/CR-3916, SAND84-1531, Sandia National Laboratories, Albuquerque, NM.

Williams, D. C., 1991, "Pretest Calculations for the First Integral Effects Experiment (IET-1) at the Surtsey and CWTI DCH Experimental Facilities, Rev. 1," Letter Report to the U. S. Nuclear Regulatory Commission, August 23, Sandia National Laboratories, Albuquerque, NM.

IODINE CHEMICAL FORMS IN LWR SEVERE ACCIDENTS*

E. C. Beahm, C. F. Weber, T. S. Kress, and G. W. Parker
Chemical Technology Division
Oak Ridge National Laboratory
Post Office Box 2008
Oak Ridge, Tennessee 37831-6221

ABSTRACT

Calculated data from seven severe accident sequences in light-water reactor plants were used to assess the chemical forms of iodine in containment. In most of the calculations for the seven sequences, iodine entering containment from the reactor coolant system was almost entirely in the form of CsI with very small contributions of I or HI. The largest fraction of iodine in forms other than CsI was a total of 3.2% as I plus HI. Within the containment, the CsI will deposit onto walls and other surfaces, as well as in water pools, largely in the form of iodide (I^-). The radiation induced conversion of I^- in water pools into I_2 is strongly dependent on pH. In systems where the pH was controlled above 7, little additional elemental iodine would be produced in the containment atmosphere. When the pH falls below 7, it may be assumed that it is not being controlled, and large fractions of iodine as I_2 within the containment atmosphere may be produced.

1. INTRODUCTION

This study attempts to re-examine the chemical form of iodine in containment, focusing on two major effects: the form entering from the reactor coolant system (RCS) and actions that may produce volatilization within the containment. The results are based on quantitative (calculated) results of seven severe accident sequences for light-water reactor (LWR) nuclear power plants, which are listed in Table 1. These sequences represent a wide range of conditions that are significant risks; each sequence was evaluated by the Source Term Code Package (STCP) and documented in previous U.S. Nuclear Regulatory Commission (NRC) reports.[1,2] Note that this analysis does not address the ultimate disposition of various species, only the likelihood of their formation or presence in the gas phase. Thus, the effects of deposition or various engineered safety features are not considered.

The primary motivation of this study is to re-evaluate the basis for Regulatory Guides 1.3[3] and 1.4[4] which state that:

1. 50% of the maximum iodine inventory of the reactor core is released to the primary reactor containment; 25% is available for leakage; and

---

*Research sponsored by the Office of Nuclear Regulatory Research, U.S. Nuclear Regulatory Commission, under Interagency Agreement DOE 1886-8058-4B with the U.S. Department of Energy under contract DE-AC05-84OR21400 with Martin Marietta Energy Systems, Inc.

Table 1. LWR accident sequences evaluated

Plant	Reactor type	Accident	Accident type	Documentation*
Grand Gulf	BWR — Mark III	TC (ATWS)	High pressure	BMI-2104, Vol. III
		TQUV (No makeup water)	Low pressure	BMI-2104, Vol. III
Peach Bottom	BWR — Mark I	TC2 (ATWS)	High pressure	NUREG-4624, Vol. I
		AE (LOCA, no ECCS)	Low pressure	BMI-2104, Vol. II
Sequoyah	PWR — ice condenser	TBA	Low pressure	NUREG-4624, Vol. II
Surry	PWR — large containment	TMLB' (Station blackout)	High pressure	BMI-2104, Vol V
		AB (LOCA, no ECCS) (Station blackout)	Low pressure	BMI-2104, Vol. V

*See refs. 1 and 2 for complete reference description.

2. of this 25% available for leakage, 91% is in the form of elemental iodine, 5% is in the form of particulate iodine, and 4% is in the form of organic iodide.

Iodine is assumed to enter containment in the forms and amounts stated above with neither physical nor chemical changes occurring in containment. However, present knowledge may not support this distribution of iodine forms and the static state throughout the duration of an accident.

It is anticipated that a more realistic representation of the chemical speciation of fission product iodine would likely result in a large proportion of particulate iodine (CsI), with smaller fractions of gaseous iodine (HI or I). In addition, a continuous revolatilization of molecular iodine would occur within containment and would include some small complement of organic iodine.

2. CHEMICAL FORMS OF IODINE ENTERING CONTAINMENT FROM THE REACTOR COOLANT SYSTEM

The chemical forms of iodine in the RCS are closely tied to the chemical forms of cesium as governed by the following reactions:

$$CsI + H_2O \rightleftharpoons CsOH + HI \qquad \text{and} \tag{1}$$

$$CsI + H_2O \rightleftharpoons CsOH + I + \frac{1}{2}H_2 \ . \tag{2}$$

Equation (1) is the reverse of an acid-base reaction and, thus, is unlikely to proceed unless one or both products are removed. Reactions of CsOH with other materials in the RCS will tend to lower the partial pressure of CsOH. Such reactions will shift the equilibrium to the right and enhance the formation of HI. At temperatures in excess of 1800 K and at low hydrogen pressures, atomic iodine is the favored product of the reaction between CsI and H_2O, as shown in Eq. (2). Thus, in general, iodine chemical forms other than CsI are favored when steam pressures are much greater than cesium hydroxide pressures.

2.1 DATA MANIPULATION AND CALCULATIONAL TECHNIQUES

In order to evaluate the chemistry in the RCS, it is necessary to specify the thermodynamic conditions under which reactions would occur and a measure of the time span over which such conditions hold. Required quantities are temperature, pressure, volume, and molar inventories of constituent species H_2, H_2O, I, and Cs within each control volume. This evaluation has been undertaken for each of the accident sequences in Table 1 using data from the STCP calculations.[12] See ref. 5 for a complete description of the data manipulations and calculational procedures.

Another necessary quantity is the mean residence time (τ) for flow through a control volume. Figure 1 shows this quantity for each of the two control volumes above core in the Surry TMLB' sequence. A mean residence time greater than 1 s is usually sufficient to attain equilibrium for regions with a sufficiently high temperature. In Fig. 1, this condition holds for both volumes, although control volume 1 approaches this limit briefly at about 30 min.

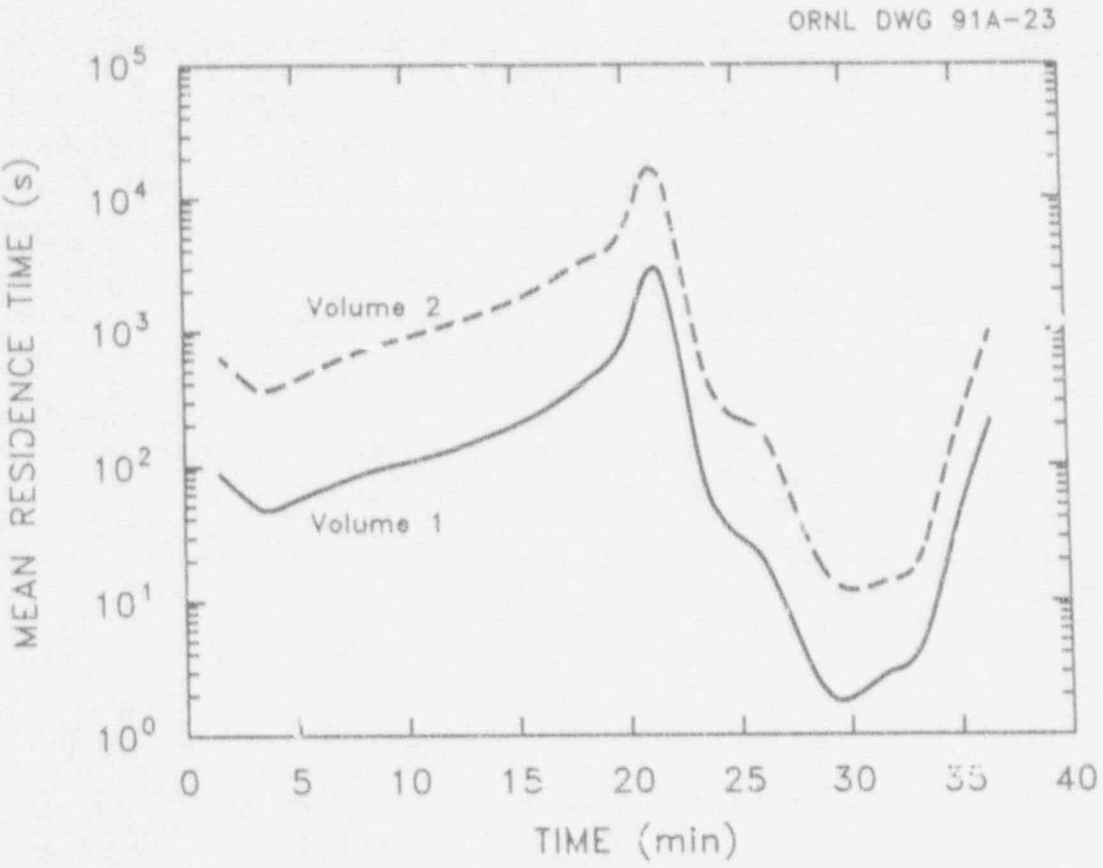

Fig. 1. Mean residence time in volumes above core for Surry TMLB'.

Fission products released from the core will undergo changes in temperature and concentration as they pass through regions of the RCS. A chemical kinetic model used 20 reactions to determine the control volume where an equilibrium of the iodine, cesium, hydrogen, and steam species becomes "frozen." This means that the temperatures and concentrations of species in subsequent control volumes are not sufficient to reach an equilibrium in the mean residence time available. Separate equilibrium calculations were run, using the FACT system,[6] to obtain the final distribution of iodine species.

2.2 OVERALL RESULTS OF CALCULATIONS

In six of seven calculations, the iodine was almost entirely in the form of CsI; the contribution of I or HI was less than 0.1% of the overall percentage of iodine. These calculations considered only reactions involving cesium, iodine, hydrogen, and water. They covered a wide range of temperatures, hydrogen concentrations, steam concentrations, and fission product concentrations. Reactions with other RCS materials were not included in these calculations, but their effects were investigated with scoping or bounding calculations as described in Sects. 2.3 and 2.4.

During the second half of the Surry AB sequence, there is a period during which temperatures in the core region are in excess of 2000 K, and subsequent volumes of the upper grid

plates and guide tubes are at temperatures of only 500 K. Because of this, equilibrium compositions in the core region would be "frozen" in by the rapid decrease in temperature. For this sequence, the overall iodine distribution was 2.8% as I and 0.4% as HI, with the remainder as CsI. Thus, a total of 3.2% as I plus HI was the largest fraction of iodine in a form other than CsI in this study.

2.3 REACTION OF CsOH WITH SURFACES

Of the possible reactions of CsOH in the RCS, the reaction with structural surfaces is the most amenable to evaluation. Johnson et al.[7] have studied the deposition of CsOH on oxidized stainless steel surfaces. They used the following simple expression to relate the thermodynamic activity of CsOH to the surface concentration:

$$a = 0.5 \exp\left\{\left(98.5 - \frac{3.84 \times 10^4}{T}\right)(x - 0.28)\right\}, \qquad x < 0.28, \tag{3}$$

where a and x are the surface activity (atm) and concentration (mg/cm^2), respectively. The reaction of interest with stainless steel may be written as

$$\text{CsOH (surface)} \rightleftharpoons \text{CsOH (gas)} . \tag{4}$$

Thermochemical data obtained from the FACT system[6] give the respective equilibrium constants for the reactions in Eqs. (1) and (4) as

$$K_1 = \frac{P_{CsOH}}{P_{H_2O}} \frac{P_{HI}}{P_{CsI}} = \exp\left(-1.407 - \frac{1.626 \times 10^4}{T}\right), \tag{5}$$

$$K_4 = \frac{P_{CsOH}}{a} = \exp\left\{1.189 \times 10^1 - \frac{1.500 \times 10^4}{T}\right\}, \qquad 900 \le T \le 1263 . \tag{6}$$

Calculations using Eqs. (3), (5), and (6), together with mass balances on cesium and iodine, indicate that the amount of HI formed due to the CsOH surface reaction is less than 0.6% for each of the accident sequences studied. This is because P_{CsOH} must be very small if the ratio P_{HI}/P_{CsI} is large enough to be significant. However, if P_{CsOH} is very small, then so is x: hence, very little surface reaction could occur.

2.4 OTHER REACTIONS OF CsOH

Other reactions of CsOH may also remove it from the vapor phase, but there is generally a lack of information on the amounts and locations of other reactants. Several cesium borates may form in the reaction of CsOH with boric acid or boron oxide, which are introduced into the RCS as coolant additives. For example, the formation of cesium metaborate ($CsBO_2$) may occur by the following reaction:

$$CsOH + HBO_2 \rightleftharpoons CsBO_2 + H_2O \quad . \tag{7}$$

If sufficient metaboric acid (HBO_2) were available, it could result in a lowering of the vapor pressure of CsOH.

Two simulated core-melt tests were run by the present authors to assess boric acid volatility and the potential for vapor interactions with CsI. Two different sized simulant fuel bundles were used—nominally 1 and 10 kg. The smaller, 1 kg, fuel simulant bundle consisted of 12 zirconium tubes (10.16-cm long) with 0.247-kg end caps, 0.093-kg stainless steel grids, 0.0185-kg Inconel grids, and 0.585-kg UO_2 pellets. There were no added Cs or I species in the small bundle test. The test was performed by inductively heating the fuel bundle while injecting feed water containing 2000-ppm boric acid into the bottom of the bundle. In this test, it was found (see Table 2) that during the lower temperature heating steps up to 1600°C, ~10% of the boron transported through the bundle and was captured downstream as boron oxide. As the temperature was increased to partial melting of the bundle, the collected B_2O_3 decreased. This decrease was attributed to increased reactivity of the boron oxide with the hot fuel and clad oxides.

Table 2. Simulated core melt tests conducted in the ORNL 1-kg facility. Boric acid addition to water injected below the bundle

Heating step	Total boron present[a] (g)	Boron collected as B_2O_3	
		Filter (%)	WASH (%)
A (1600°C)	0.034	10.37	0.0
B (1800°C)	0.088	5.5	0.68
C (2400°C)	0.142	0.024	0.009

[a]As boric acid in water used for steam generation.

The composition of the 10-kg fuel bundle is shown in Table 3. Note that in this test, CsI was added to 12 of the 60 simulant fuel rods in a limited region near the bundle centerline. Excess cesium was not added.

The 10-kg test was conducted at a bundle centerline temperature limit of 1600°C which was reached in ~30 min and maintained for an additional 30 min. During this time, 365 mL of boric acid solution containing 3.83 g of H_3BO_3 was added to the steam generator porous media below the fuel bundle. Hydrogen release measured 326 L, which would be equivalent to 72% conversion of the water and ~30% reaction of the Zircaloy in the bundle.

Analytical results from X-ray diffraction showed that white solids observed plated out on the quartz chimney were nearly pure CsI with no detectable B_2O_3. Chemical analysis of the washings

Table 3. Composition of 10-kg fuel bundle

Item	Weight[a] (g)
60[b] — Zircaloy tubes	2181.0
120 — Zircaloy end caps	503.6
3 — Stainless steel grids	342.0
1 — Inconel grid	112.0
4 — Stainless steel supports and screws	58.5
2 — Stainless steel lifts and screws	9.0
UO_2 pellets	(N.W.) 7464.0 (E.W.) 6739.9
UO_2 powder	(N.W.) 1201.9 (E.W.) 1059.5
$SrCO_3$	3.00
$BaCO_3$	4.05
La_2O_3	2.28
Eu_2O_3	0.21
Sm_2O_3	1.12
CeO_2	4.87
Mo	4.70
Te	0.82
Ru	5.16
CsI[c]	0.85

[a]N.W. = net weight; E.W. = uranium element weight.

[b]Twelve of these tubes each had three horizontal slits 0.010-in. wide × 1-in. long, 120° apart in their midsection.

[c]CsI mixed with 300-g UO_2, rare earths, and metal powders was added to the 7 in. section of the 12 tubes.

from the system indicated that nearly half of the CsI had vaporized and that no boron containing materials were present. This complete failure to find any B_2O_3 downstream of the bundle was somewhat unexpected since the 1-kg test had resulted in some penetration of boron oxide. It is likely that the extra length of the 10-kg system prevented penetration by the reaction of B_2O_3 with ZrO_2. A sample analysis of a white oxide (a thin ring of mixed ZrO_2 and B_2O_3) in a very highly refractory solid solution on the oxidized clad surface was estimated to account for about one-third of the total boron added. The remainder of the boron oxide appeared to be associated with the porous ZrO_2

steam generator base at the bottom of the bundle. A test scrubber that had been operated continuously on a diverted part of the hydrogen/steam flow showed no evidence of volatile (non-particulate) iodine.

Similar results were subsequently obtained in a test with silver vaporized in a 10-kg bundle containing Ag-In-Cd alloy control rod simulants. In this later case, cadmium vapor was observed downstream, but the silver did not penetrate out of the bundle—presumedly because of interactions with Zircaloy.

Based on these results, it is highly likely that boric acid covaporized from residual water below the core in severe accidents will be tied up by the Zircaloy in the lower regions of the core and not be available airborne to affect the chemical form of the released iodine.

2.5 REVAPORIZATION OF CsI AS A SOURCE OF HI

There has been speculation that the fission product aerosols, CsI and CsOH, deposited onto the RCS surfaces under high pressure accident sequence conditions could revaporize due to heatup from their radioactive decay and from the system thermal hydraulics to become re-released into containment. Most analyses of this have considered the re-released material to remain as CsI and have focused only on the extent and timing of the revaporization. If, however, the CsOH portion of the deposited material were not available for revaporization and the revaporized CsI "saw" only steam, the question then becomes, what portion of the CsI that is revaporized gets converted to HI by the reaction in Eq. (1). To attempt to bound this, the Oak Ridge study made the following assumptions:

1. The temperature of revaporization was 1000 K (the general temperature at which equilibrium is frozen). The CsI vapor pressure was held constant according to the value predicted from the FACT system equation

$$P_{CsI} = \exp\left[\frac{-2.021 \times 10^4}{T} + 1.307 \times 10^1\right]. \qquad (8)$$

2. The steam pressure varied in time the same as in the seven accident sequences (this was an arbitrary choice and is not intended to imply that revaporization is continuous throughout an accident sequence rather than being later in time).

3. No CsOH was present [except that made via the reaction in Eq. (1)].

4. No H_2 was present.

The integration was carried out over each sequence until an amount of CsI had been revaporized that was equivalent to the total amount of iodine released in the sequence (i.e., all of the iodine was equivalently on the surface at the start of a sequence at a location where the temperature was 1000 K).

The result of this calculation was that the largest conversion of CsI to HI in any of the sequences was 3.8%. This indicates that revaporization is not likely to produce significant amounts of volatile forms of iodine under these conditions. However, an equivalent calculation should be made for possible sequences that may have air ingress at times simultaneous with revaporization.

2.6 SUMMARY OF IODINE CHEMICAL FORMS IN THE RCS

Iodine entering containment from the RCS should be predominantly in the form of CsI. The examination of Cs-I-H_2O-H_2 interactions for seven accident sequences gave a maximum of 3.2% iodine as I plus HI, with the remainder as CsI. There are some uncertainties in the reactions of $CsOH$ with oxides and in the revaporization of CsI that produce uncertainties to the extent in which iodine may exist in a form other than CsI. Cesium needs to be removed from reactions involving iodine if very much iodine is to be in a form other than CsI.

Based on this analysis, the chemical forms of iodine entering containment from the RCS may reasonably be described as a maximum of 5% as elemental iodine and HI, with not less than 1% as either elemental iodine or HI. The remaining ≥95% would be CsI.

3. PROCESSES THAT ALTER THE CHEMICAL FORMS OF IODINE IN CONTAINMENT

3.1 RADIOLYSIS

In the presence of radiation, the equilibrium formation of I_2 from I^- is strongly dependent on pH and less dependent on temperature and concentration. Ignoring the last two effects, this dependence can be written as

$$F(pH) = \textit{equilibrium fraction} = \frac{[I_2]}{[I_2] + [I^-]} , \tag{9}$$

where [x] is concentration of I_2 or I^- (g-atom/L). Data from Lin,[9] as shown in Fig. 2, illustrate this effect for several initial concentrations and pH values using solutions that were at ambient temperature and had been irradiated for 1 h at 4.5 Mrad/h. The final pH values were not indicated but probably decreased slightly because no mention is made of buffering in the experiment. The values of pH >6 may not be quantitatively useful since the very small conversion fractions are probably incorrect due to measurement error. As seen in Fig. 2, F is near 0 for pH >7 and near 1 for pH <2 but experiences a drastic change in the range 3 < pH < 4. This can be effectively modeled by the functional form

$$F = [1 + e^{\alpha\ pH + \beta}]^{-1} , \tag{10}$$

that was fit to Lin's data using nonlinear least squares, yielding $\alpha = 1.72$, $\beta = -6.08$.

If the pH is maintained sufficiently high through buffering or addition of sufficient basic material, very little conversion will occur. In this case, most iodine remains dissolved as I^-. A quantitative treatment is more difficult. Lin's data generally indicate less than 1% conversion at

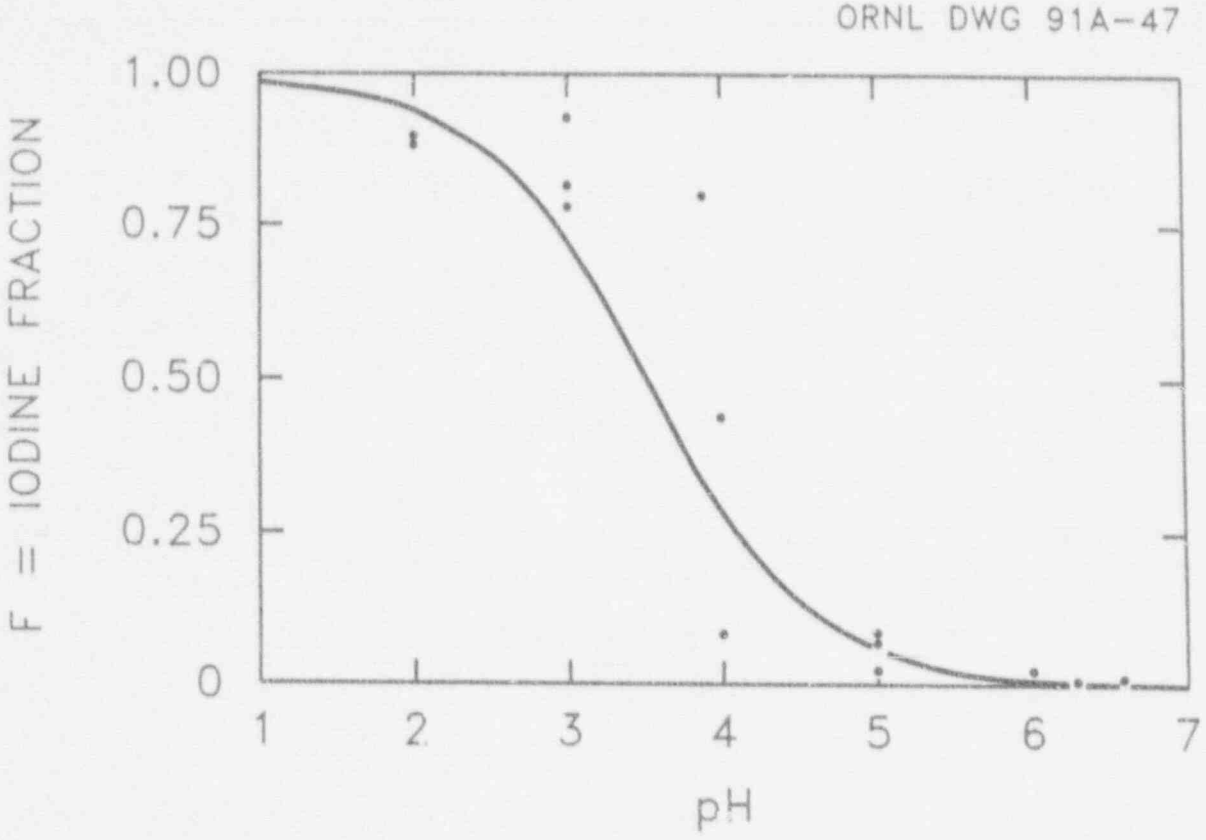

Fig. 2. Radiolytic conversion of I^- to I_2 [data from C. C. Lin, *J. Inorg. Nucl. Chem.* **42**, 1101 (1980)].

pH = 7. This value declines as the total iodine concentration decreases. ORNL data indicate that for a dose rate of 0.35 Mrad/h and an iodine concentration of 10^{-4} mol/L, conversion was 0.003% after 4 h of irradiation and 0.03% after 24 h. The last value, 0.03%, has been used in the present work.

If the pH level is not deliberately controlled, it may decrease sufficiently to allow considerable conversion of I^- to I_2. The primary mechanism is radiolytic generation of nitric acid. If the pH is neutral initially, then this effect soon dominates, resulting in

$$[H^+] = 10^4 \, g(HNO_3) \, \frac{E_{dep}}{V_L N_a} \, , \tag{11}$$

where

$[H^+]$ = concentration of H^+ (mol/L),
$g(HNO_3)$ = rate of HNO_3 production due to irradiation (molecules/100 eV),
E_{dep} = total energy deposition due to fission product decay (MeV),

V_L = volume of water (L), and
N_a = 6.022×10^{23} (molecules/mol).

ORNL measurements of pH change and nitrate ion formation at 30°C gave:

$$g(HNO_3) = 0.007 \text{ molecules/100 eV} . \tag{12}$$

This relationship is based on radiation absorption by the aqueous phase. The actual mechanism for the formation of nitric acid is not known. It may occur in the aqueous phase, in the gas phase, or at the gas-surface interface.

The energy deposition over a time, Δt, is

$$E_{dep} = \dot{E}_{dep}\, \Delta t = \Delta t \sum m_j\, \dot{e}_j , \tag{13}$$

where

Δt = time (h),
$\dot{E}_{dep}$ = total energy deposition rate (MeV/h),
m_j = mass of nuclide group j in pool (g), and
$\dot{e}_j$ = energy deposition rate per unit mass of nuclide group j (MeV/s · g).

A grouping of fission products and actinides compatible with that used in STCP accident studies was selected and is shown in Table 4. The specific energy deposition rate $\dot{e}_j$ for each group was determined from a detailed analysis of Browns Ferry [a large boiling-water reactor (BWR) with Mark I containment] accident sequences using the ORIGEN2 code.[10,11] These group energy deposition rates for the Browns Ferry BWR are assumed applicable to all plants and sequences considered in the present study.

The group masses (m_j) are obtained by multiplying the total core inventory ($\bar{m}_j$) by the estimated fractional release into containment:

$$m_j = f_j\, \bar{m}_j . \tag{14}$$

Total core inventories for the plants are those identified in previous reports.[1,2] Various estimates of the fractional releases f_j can be obtained from a study by Nourbakhsh.*

Finally, Δt in Eq. (13) is the time needed to reach the approximate steady state. In general, the first phase of an accident can be considered to reach steady state in 10 to 15 h; the latter is the time value used for Δt in this work. Combining Eqs. (10) through (13), the fractional conversion takes the form

$$F = \left[1 + e^{\beta}[H^+]^{-\frac{\alpha}{\ln 10}}\right]^{-1} = \left[1 + 5.55 \times 10^{13} \left(\frac{V_L}{E_{dep}}\right)^{0.747}\right]^{-1} . \tag{15}$$

*H. P. Nourbakhsh, presentation to NRC staff, October 4, 1990.

Table 4. Nuclide groupings and group-specific energy deposition rates

Group index, j	Characteristic element	Included nuclides	Energy deposition rate, $\dot{e}_j \times 10^{-13}$ (MeV/s · g)
1	I	I, Br	111.2
2	Cs	Cs, Rb	1.006
3	Te	Te, Se	3.497
4	Sr	Sr	7.879
5	Ba	Ba	2.348
6	Ru	Ru, Tc, Rh, Mo	1.706
7	Ce	Ce, Pu, Np	0.407
8	La	La, Am, Cm, Y, Pr, Nd, Pm, Sm, Eu, Zr,[a] Nb	6.523
9	Xe	Xe, Kr	0.721

[a]Includes only fission products.

Thus, when pH is not controlled, fractional conversion is directly dependent on the liquid volume (V_L) in which radiolysis occurs; the energy deposition E_{dep}, which itself depends on the amounts of radioactive species in water; and the time (Δt) allowed for radiolysis processes to reach steady-state conditions.

3.2 GAS-LIQUID PARTITIONING

The equilibrium distribution of a single volatile specie such as I_2 is represented by the partition coefficient:

$$P = \frac{[I_2\ (aq)]_{eq}}{[I_2\ (g)]_{eq}} \quad . \tag{16}$$

This quantity is inversely related to the Henry's Law constant K (i.e., $P = 1/K$) and should not be confused with the overall iodine partition coefficients often used in reactor safety studies. In this study partition coefficients for I_2 were calculated from the equation.

$$\log_{10} P = 6.29 - 0.0149\ T \quad . \tag{17}$$

This relationship gives the experimental value reported by Eguchi et al.[12] and by Sanemasa et al.[13] at 298 K. Extrapolation of the experimental results of these investigators to 373 K yielded a partition coefficient of 3. Furrer et al.[14] reported a calculated partition coefficient at 373 K of 9. Some of the data used in his calculation were based on estimated parameters. Equation (17) gives a partition coefficient of 5.3 at 373 K, a reasonable average of these values.

Even though it may take considerable time to approach such equilibration in a large system such as a reactor containment, Eq. (16) can still be used to estimate I_2 volatility. In fact, instant equilibration is a conservative assumption since considerable holdup could be expected in real-life situations.

3.3 GAS-PHASE REACTIONS: FORMATION OF ORGANIC IODIDES

The process of converting I_2 into organic iodides (chiefly CH_3I) is still not fully understood. Postma and Zavodoski[15] reviewed production rates from about 70 containment tests and determined that the asymptotic steady-state conversion to CH_3I was

$$\% \ I_2 \text{ converted} = 0.19 \ C_{mo}^{-0.26} , \tag{18}$$

where C_{mo} = initial I_2 concentration (mg/m^3). In a more recent review, Beahm et al.[16] described the steady-state organic iodide concentration (mg iodine/m^3) using the form

$$C^* = 0.0189 \ C_{mo}^{0.82} \tag{19}$$

in place of Eq. (18). This equation was based on containment experiments performed with irradiated fuel rather than simulated materials, resulting in a percent conversion somewhat greater than that obtained from simulant materials (cf Fig. 4, ref. 17). By converting units to g-atom/L, Eq. (19) can be rewritten as

$$[CH_3I] = \beta \ [I_2]^{0.82} , \tag{20}$$

where $\beta = 0.0189 \ (10^6 \cdot MW)^{-0.18}$, MW being the molecular weight of I. For MW = 130, then $\beta = 6.55 \times 10^{-4}$, which indicates that generally less than 1% of gaseous iodine will be organic.

3.4 OVERALL BEHAVIOR

As described in the previous sections, the distribution of species throughout the gas and liquid phases can be estimated from models for three basic processes: radiolytic conversion of I^- to I_2 in water, evaporation of I_2, and gas-phase formation of organic iodides. Defining the desired quantities as concentration variables (g-atom/L),

$$C_1 = [I_2(aq)], \qquad C_2 = [I_2(g)], \qquad C_3 = [I^-(aq)], \qquad C_4 = [CH_3I(g)] , \tag{21}$$

Eqs. (16), (9), and (20) can be rewritten as

$$C_1 = PC_2 , \quad C_3 = \frac{(1 - F)}{F} \ C_1 , \quad \text{and} \quad C_4 = \beta \ C_2^{0.82} . \tag{22a,b,c}$$

In addition, the total iodine inventory N_T (g-atom) is equal to the initial I^- entering the containment, and remains constant throughout the distribution process:

$$N_T = V_L (C_1 + C_3) + V_g (C_2 + C_4) \quad . \tag{22d}$$

These four equations, (22a) through (22d), can be solved in a straightforward manner to obtain the four unknown concentrations in Eq. (21).

Because organic iodide is such a small part of the total, it is helpful to examine the distribution behavior without considering organic iodide. By ignoring Eq. (22c), it is possible to combine and rearrange Eqs. (22a), (22b), and (22d) to get

$$\frac{N_2}{N_T} = \left(1 + \frac{V_L P}{V_g F}\right)^{-1} \quad , \tag{23}$$

where $N_2 = V_g C_2$ = g-atom of I_2 in gas. Equation (23) is a convenient expression of the fraction of iodine that is volatilized. (Consideration of organic iodide will increase this fraction very slightly.) For the case of uncontrolled pH, substitution of Eq. (15) into Eq. (23) yields

$$\frac{N_2}{N_T} = \left\{1 + \frac{V_L P}{V_g}\left[1 + 5.55 \times 10^{13}\left(\frac{V_L}{E_{dep}}\right)^{0.747}\right]\right\}^{-1} \quad . \tag{24}$$

Equations (23) and (24) are in particularly convenient form to quickly estimate iodine volatility.

3.5 CALCULATIONAL RESULTS AND DISCUSSION

The analysis described in this section has been applied to each of the seven accident sequences mentioned in Table 1. The gas volumes used for BWRs include all primary containment space, although it may sometimes be appropriate to use only wetwell airspace, depending on sequence considerations. The various data and the quantities calculated from them are described for each accident sequence in ref. 5.

The conversion data of Lin[9] were taken at a dose rate of 4.5 Mrad/h—in the range of PWR rates. The data taken at ORNL are generally in the range of BWR dose rates (i.e., 0.35 to 0.6 Mrad/h). Both sets of data indicate that conversion is dominated by pH effects. In this study, two scenarios were evaluated: (1) control of pH above 7 and (2) uncontrolled pH with resulting drops below 7 due to nitric acid formation. For this calculation, it was not necessary to specify the material that was used to control the pH at 7 or above.

If the pH is controlled so that it stays above 7, the system of equations (22) is solved to yield the species distributions in Table 5. These results indicate a small production of volatiles for PWRs but virtually none for BWRs. Such results are strongly dependent on the aqueous conversion fraction of $F = 3 \times 10^{-4}$, which represents a best estimate of the maximum from ORNL data. Thus, if pH is maintained at 7 or above, only a small additional amount of I_2 is expected in the gas phase of PWR systems.

Table 5. Distribution of iodine species for pH controlled above 7

Plant	Accident	Fraction of total iodine (%)[a]			
		I_2(g)	I_2(L)	I^-(L)	CH_3I(g)
Grand Gulf	TCγ	0.05	0.03	99.92	0.001
	TQUVγ	0.01	0.03	99.96	0.0003
Peach Bottom	AEγ	0.002	0.03	99.97	0.0001
	TC2γ	0.002	0.03	99.95	0.0004
Sequoyah	TBA	0.21	0.03	99.97	0.004
Surry	TMLB'γ	1.9	0.03	98.0	0.03
	ABγ	2.3	0.03	97.5	0.03

[a]Assuming an equilibration time of Δt = 15 h.

If the pH falls below 7, a system for controlling pH is not being used and the decreased pH results in a larger fraction of aqueous I^- being converted to I_2. Evaporation of this volatile species to maintain equilibrium partitioning will result in greater atmospheric I_2. This, in turn, yields higher organic iodide concentrations. Results for this case are shown in Table 6 for the equilibrium species distributions. As expected, the levels of airborne volatiles are much higher than in the controlled case, indicating almost complete conversion for PWRs.

Table 6. Distribution of iodine species for uncontrolled pH

Plant	Accident	Fraction of total iodine (%)[a]			
		I_2(g)	I_2(L)	I^-(L)	CH_3I(g)
Grand Gulf	TCγ	24.1	13.9	61.8	0.20
	TQUVγ	6.0	16.6	77.7	0.05
Peach Bottom	AEγ	1.6	20.5	77.9	0.01
	TC2γ	10.1	16.7	73.2	0.06
Sequoyah	TBA	67.3	9.6	22.6	0.40
Surry	TMLB'γ	97.2	1.5	0.7	0.60
	ABγ	97.7	1.2	0.6	0.60

[a]Assuming an equilibration time of Δt = 15 h.

The gaseous I_2 fraction is considerably higher in PWRs than in BWRs because the large water volumes in the latter both lower the dose rate and retain greater quantities of dissolved I_2. This last effect also depends on the gas volume and the ratio of gas to liquid volumes. It is ironic that the relatively small gas space in the Peach Bottom reactor (generally a safety liability) permits noticeably less evaporation than other reactors, resulting in the lowest gaseous I_2 fractions.

The other principal effect is due to temperature—the I_2 partition coefficient changes markedly over the range of temperatures used. This effect of temperature is most noticeable in the BWR sequences where different sequences at the same plant show large differences in the airborne I_2 fraction. Thus, an increase in containment temperature (at the gas-liquid interface) from 60 to 115°C produces nearly an order of magnitude increase in the airborne fraction.

The organic iodide is present in PWRs at about 0.5% of core inventory. In BWRs, this concentration is closer to 0.1%. The I_2 generated by the radiolytic conversion of I^- dominates the amount released as I_2 from the RCS. Further, based on the equilibrium assumption, the presence of some I_2 already airborne will result in less evaporation of I_2 formed radiolytically. Hence, for the case of uncontrolled pH, the cumulative total is well represented by the equilibrium amount formed within containment.

4. TECHNICAL FINDINGS

This study assumed that iodine forms in containment can be delimited by an examination of the seven severe accident sequences in LWR plants, along with an evaluation of associated processes. The associated processes include the deposition of CsOH on RCS surfaces and the effects of radiolysis. The issue is the chemical form of iodine that may be produced in the RCS and in containment—not the ultimate disposition of the various chemical forms. For example, it is likely that much of the gaseous I_2 in containment would be removed by engineered safety features or would deposit on painted or metal surfaces.

4.1 ASSESSMENT OF IODINE CHEMICAL FORMS IN THE RCS

The maximum iodine as I plus HI calculated for the seven severe accident sequences is 3.2%. Iodine in all forms other than I, HI, and CsI is estimated to be less than 1%. Although this analysis only considered seven sequences at four plants, it is reasonable to consider that a maximum of 5% of the iodine would be present as elemental iodine and HI for all accident sequences. A minimum value would not be expected to be less than 1%. The remaining 95% of the iodine would be as CsI.

The gaseous forms of iodine that entered containment from the RCS were given in terms of both elemental iodine and HI, which are related by the reaction

$$I + \frac{1}{2}H_2 \rightarrow HI. \qquad (25)$$

Lower temperatures and higher hydrogen pressures tend to favor HI over I, with the opposite conditions favoring I over HI.

The major uncertainty is the extent to which CsOH will react with oxide materials and reduce its vapor pressure. If the reaction of CsOH is to have a major impact on the iodine chemical forms, most of it (certainly more than 90%) must be fixed at a very low vapor pressure.

4.2 ASSESSMENT OF IODINE CHEMICAL FORMS IN CONTAINMENT

The production of I_2 in containment will be directly related to the pH levels of the water pools. Failure to control the pH at or above 7 could result in a dramatic increase in atmospheric I_2. Essentially all of the I_2 could become gaseous in the PWRs without pH control. For BWRs, as much as 25% of the core inventory could become gaseous. However, maintaining the pH above 7 results in negligible volatilization.

5. REFERENCES

1. J. A. Gieseke et al., *Radionuclide Release Under Specific LWR Accident Conditions*, BMI-2104, Battelle Columbus Laboratories, 1984.

2. R. S. Denning et al., *Radionuclide Release Calculations for Selected Severe Accident Scenarios*, NUREG/CR-4624 (BMI-2139), Battelle Columbus Laboratories, 1986.

3. U.S. Nuclear Regulatory Commission, Regulatory Guide 1.3, "Assumptions Used for Evaluating the Potential Radiological Consequences of a Loss-of-Coolant Accident for Boiling Water Reactors," June 1974.

4. U.S. Nuclear Regulatory Commission, Regulation Guide 1.4, "Assumptions Used for Evaluating the Potential Radiological Consequences of a Loss-of-Coolant Accident for Pressurized Water Reactors," June 1974.

5. E. C. Beahm, C. F. Weber, and T. S. Kress, *Iodine Chemical Forms in LWR Severe Accidents*, NUREG/CR-5732, draft report for comment, Martin Marietta Energy Systems, Inc., Oak Ridge Natl. Lab., 1991.

6. FACT, a copyrighted product of THERMFACT Ltd., 447 Berwich Ave., Mount-Royal, Quebec, Canada, H3R 1Z8.

7. I. Johnson, M. K. Farahat, J. L. Settle, I. D. Arntzen, and C. E. Johnson, *Downstream Behavior of Volatile Iodine, Cesium, and Tellurium Fission Products*, EPRI NP-6182, January 1989.

8. G. W. Parker, "Chemistry of Nuclear Reactor Accidents: Problems and Progress," p. 2-1, *Proc. Symp. Chemical Phenomena Associated with Radioactivity Releases During Severe Nuclear Plant Accidents*, ed. S. J. Niemczyk, NUREG/CP-0078, June 1987.

9. C. C. Lin, "Chemical Effects of Gamma Radiation on Iodine in Aqueous Solutions," *J. Inorg. Nucl. Chem.* 42, 1101 (1980).

10. A. G. Croff, *ORIGEN2 — A Revised and Updated Version of the Oak Ridge Isotope Generation and Depletion Code*, ORNL-5621, Union Carbide Corp., Nucl. Div., Oak Ridge Natl. Lab., July 1980.

11. C. F. Weber, *Calculation of Absorbed Doses to Water Pools in Severe Accident Sequences*, ORNL/CSD/TM-274, Martin Marietta Energy Systems, Inc., Oak Ridge Natl. Lab., 1991.

12. W. Eguchi, M. Adachi, and M. Yoneda, *J. Chem. Eng. Jpn.* **6**, 389 (1973).

13. I. Sanemasa, T. Kobayashi, C. Y. Piao, and T. Deguchi, *Bull. Chem. Soc. Jpn.* **57**, 1352 (1984).

14. M. Furrer, K. C. Cripps, and R. Gubler, *Nucl. Technol.* **70**, 290 (1985).

15. A. K. Postma and R. V. Zavodoski, *Review of Organic Iodide Formation Under Accident Conditions in Water-Cooled Reactors*, WASH-1233, U.S. Atomic Energy Commission, 1972.

16. E. C. Beahm, W. E. Shockley, and C. L. Culberson, *Organic Iodide Formation Following Nuclear Reactor Accidents*, NUREG/CR-4327, Martin Marietta Energy Systems, Inc., Oak Ridge Natl. Lab., 1985.

CALCULATION OF FUEL PIN FAILURE TIMING UNDER LOCA CONDITIONS[a]

K. R. Jones, N. L. Wade, L. J. Siefken, M. Straka, K. R. Katsma

ABSTRACT

The objective of this research was to develop and demonstrate a methodology for calculation of the time interval between receipt of the containment isolation signals and the first fuel pin failure for loss-of-coolant accidents (LOCAs). Demonstration calculations were performed for a Babcock and Wilcox (B&W) design (Oconee) and a Westinghouse (W) 4-loop design (Seabrook). Sensitivity studies were performed to assess the impacts of fuel pin burnup, axial peaking factor, break size, emergency core cooling system (ECCS) availability, and main coolant pump trip on these times. The analysis was performed using a four-code approach, comprised of FRAPCON-2, SCDAP/RELAP5/MOD3, TRAC-PF1/MOD1, and FRAP-T6. In addition to the calculation of timing results, this analysis provided a comparison of the capabilities of SCDAP/RELAP5/MOD3 with TRAC-PF1/MOD1 for large-break LOCA analysis. This paper discusses the methodology employed and the code development efforts required to implement the methodology.

The shortest time intervals calculated between initiation of containment isolation and fuel pin failure were 11.4 s and 19.1 s for the B&W and W plants, respectively. The FRAP-T6 fuel pin failure times calculated using thermal-hydraulic data generated by SCDAP/RELAP5/MOD3 were more conservative (earlier) than those calculated using data generated by TRAC-PF1/MOD1.

1. INTRODUCTION

A licensing basis for nuclear reactors has been the loss-of-coolant accident (LOCA), with an assumed instantaneous release of fission products from the fuel into the containment. Certain equipment performance requirements, such as rapid closure of containment isolation valves, have been required to facilitate compliance with 10 CFR Part 100[1] regarding offsite radiological consequences. These fast closure times have placed a burden on valve design and maintenance.

The objective of this research was to develop a viable methodology for

---

a. Work supported by the U.S. Nuclear Regulatory Commission, Office of Nuclear Regulatory Research, under DOE Contract No. DE-AC07-76ID01570.

calculation of the timing of the earliest fuel pin cladding failure, relative to the containment isolation signal, for LOCAs. The calculation was expected to show that certain isolation valves do not have to be closed as rapidly as now required, thus permitting more realistic licensing requirements.

In order to meet this objective, a calculational methodology was developed employing the FRAPCON-2[2], SCDAP/RELAP5/MOD3[3], and FRAP-T6[4] computer codes. Demonstration calculations were performed, applying this methodology to two plant designs, a Babcock and Wilcox (B&W) design analyzed using an Oconee plant model and a Westinghouse (W) 4-loop design analyzed using a Seabrook plant model. Sensitivity studies were performed involving varied break sizes, fuel pin burnups, and axial peaking factors.

These calculations represent the first application of SCDAP/RELAP5/MOD3 and were performed using a preliminary version of the code, prior to completion of the code assessment efforts. In order to evaluate the adequacy of SCDAP/RELAP5/MOD3, a single TRAC-PF1/MOD1[5] calculation was performed, duplicating the worst-case SCDAP/RELAP5/MOD3 calculation for the Seabrook analysis. This calculation consisted of a complete, double-ended, offset-shear break of a cold leg, without pumped emergency core cooling systems (ECCS) and assuming that the main coolant pumps continued operating.

This paper summarizes the methodology developed for these calculations and the results obtained from two demonstration calculations.

2. METHODOLOGY

A four-code approach, utilizing FRAPCON-2, SCDAP/RELAP5/MOD3, TRAC-PF1/MOD1, and FRAP-T6, was adopted for the analysis. This approach provided a defensible calculational methodology for performing the analyses, incorporating a fully assessed calculational path, using FRAPCON-2, TRAC-PF1/MOD1, and FRAP-T6, and a parallel path, utilizing FRAPCON-2, SCDAP/RELAP5/MOD3, and FRAP-T6.

The FRAPCON-2[2] code was developed to calculate the steady-state response of light water reactor (LWR) fuel rods during long-term burnup. It calculates the temperature, pressure, deformation, and failure histories of a fuel rod as functions of time-dependent fuel rod power and coolant boundary conditions.

The FRAP-T6[4] code was developed to predict the performance of LWR fuel rods during operational transients and hypothetical accidents. It obtains initial fuel rod conditions by reading a file created by the FRAPCON-2 code and calculates all of the phenomena that influence the transient performance of fuel rods, with particular emphasis on temperature and deformation of the cladding.

Both FRAPCON-2 and FRAP-T6 have been thoroughly assessed over a range of normal burnups;[6-9] however, they have not been assessed for analysis of high-burnup fuel (>35 GWd/MTU). Results obtained for exposures above 35 GWd/MTU are in general agreement with expected trends. In addition, it is not anticipated

that high-burnup fuel pins (>35 GWd/MTU) would be operating at power levels that would cause them to fail earlier than lower-burnup pins.

The SCDAP/RELAP5/MOD3[3] code was developed for best-estimate transient simulation of LWR coolant systems under severe accident conditions, as well as large- and small-break LOCAs. It is currently under development, and a preliminary version (cycle 7B) was used for the analyses.

The TRAC-PF1/MOD1 code[5] was developed for transient simulation of LWR coolant systems during large-break LOCAs. Version 14.3U5Q.LG was used for this analysis. This version was frozen in 1987 by the U.S. Nuclear Regulatory Commission for use in the code scaling, applicability, and uncertainty evaluation (CSAU) study.[10] A broad assessment effort has been completed, which has demonstrated that the code is capable of addressing the entire large-break LOCA scenario (blowdown, refill, and reflood). Appendix III of the CSAU report[10] provides an extensive list of assessment reports applicable to this code.

SCDAP/RELAP5/MOD3 was chosen as the primary thermal-hydraulic code for the analysis, since it provides a considerable cost savings over TRAC-PF1/MOD1 for calculation of system thermal-hydraulic response under LOCA conditions. SCDAP/RELAP5/MOD3 is a relatively fast-running code that can execute from a workstation platform, as opposed to TRAC-PF1/MOD1, which requires a mainframe platform. A wide range of sensitivity cases were analyzed using SCDAP/RELAP5/MOD3 to assess the impact of break size, ECCS availability, and main coolant pump trip on the fuel failure timing. However, due to the lack of code assessment for SCDAP/RELAP5/MOD3, a supplemental TRAC-PF1/MOD1 calculation, duplicating the case resulting in the shortest time to pin failure, was run to provide an evaluation of its accuracy.

The calculational methodology using SCDAP/RELAP5/MOD3 is illustrated in Figure 1. In these calculations, FRAPCON-2 was used to calculate the burnup-dependent fuel pin initial conditions for FRAP-T6; FRAP-T6 was used to calculate the initial steady-state fuel pin conditions for SCDAP/RELAP5/MOD3; SCDAP/RELAP5/MOD3 was run to obtain the system thermal-hydraulic boundary conditions, consisting of the fuel pin power distribution and thermodynamic conditions of the coolant channel; and FRAP-T6 was used to calculate the transient fuel pin behavior.

The supplemental calculation utilizes a similar methodology with the exception that SCDAP/RELAP5/MOD3 is replaced by TRAC-PF1/MOD1, as illustrated in Figure 2. Initialization of burnup-dependent variables for the TRAC-PF1/MOD1 fuel components is not necessary, since the code does not have a fuel performance model. However, a comparison of initial stored energy calculated by TRAC-PF1/MOD1 to that calculated by FRAP-T6 indicated reasonable agreement.

A significant software development effort was conducted to implement the chosen methodology. This effort included conversion of the FRAPCON-2 and FRAP-T6 codes to portable FORTRAN 77 to allow execution on a 32-bit-based UNIX workstation, and the creation of interface codes to link the thermal-hydraulics codes to FRAP-T6. In addition, advanced graphics capabilities were added to the FRAP-T6 code. These capabilities include interfacing to the Nuclear Plant

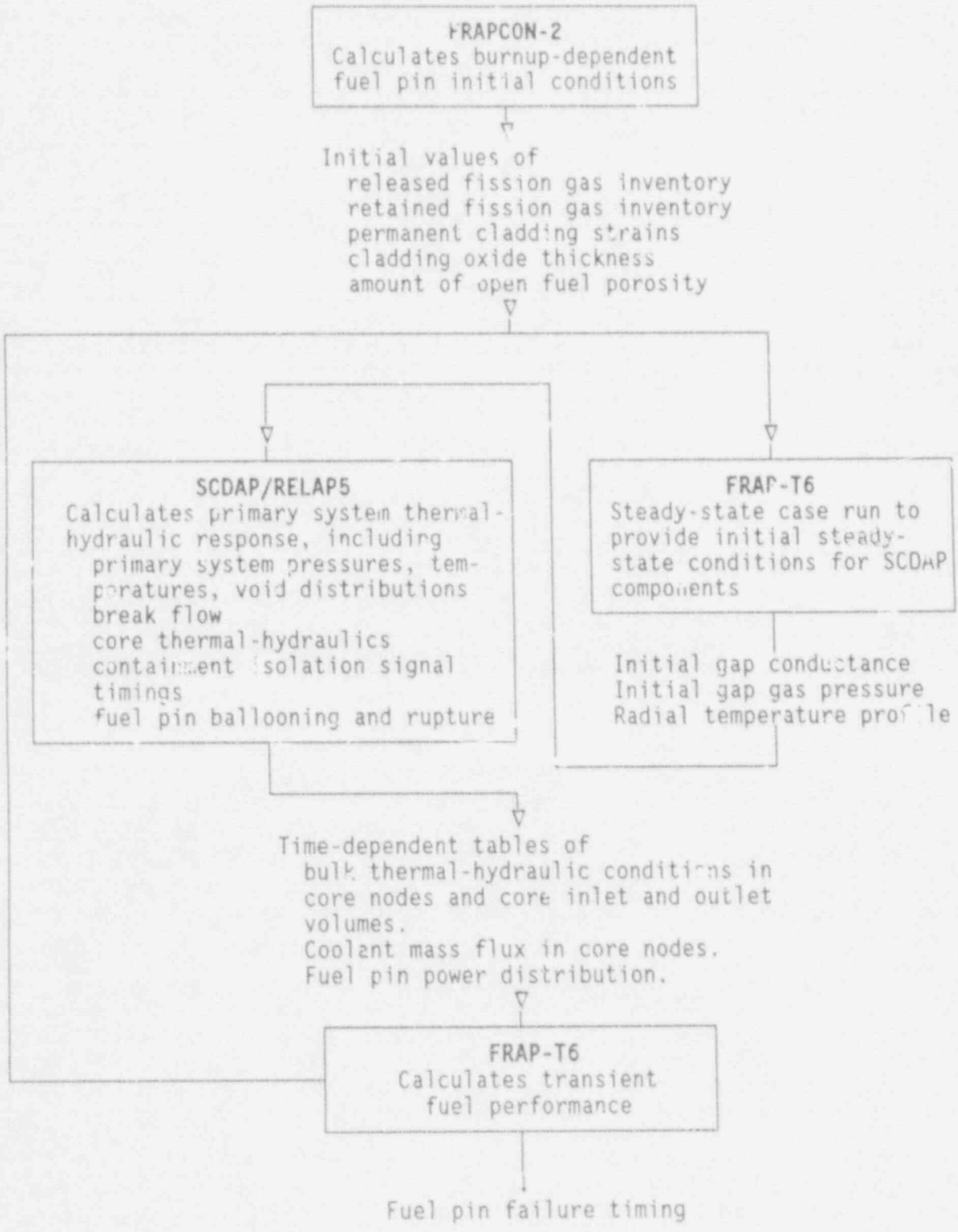

Figure 1. Flow chart of methodology using SCDAP/RELAP5/MOD3 thermal-hydraulic data.

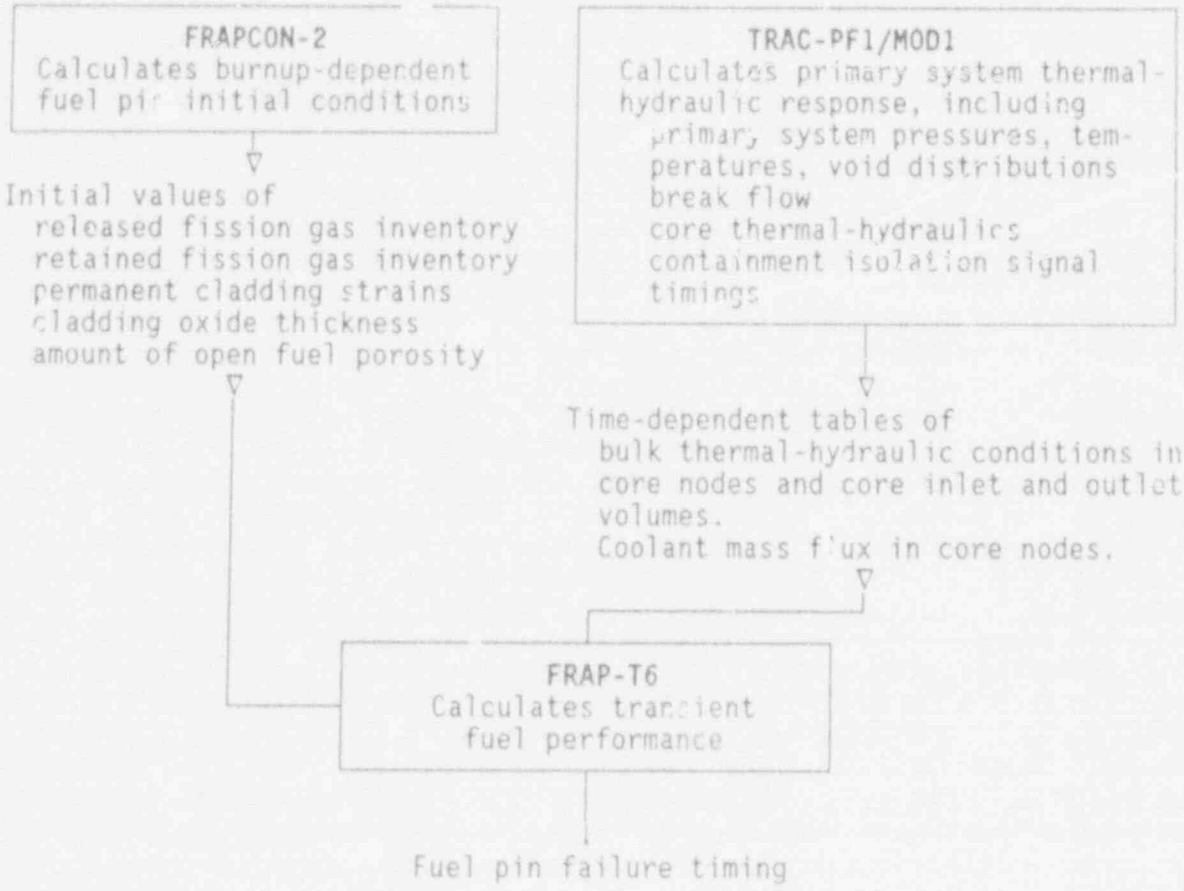

Figure 2. Flow chart of methodology using TRAC-PF1/MOD1 thermal-hydraulic data.

Analyzer (NPA)[11] and the GRAFITI[12] graphics packages. The NPA software is an advanced interactive graphics package that provides an animated display of the fuel rod behavior during program execution. The GRAFITI package provides a presentational graphics capability.

3. MODEL DEVELOPMENT

The calculations were performed assuming an equilibrium core operating at 102% core thermal power. Similar core nodalization was used for the SCDAP/RELAP5/MOD3 and TRAC-PF1/MOD1 models, with the exception that the core bypass was lumped into the outer core region in the TRAC-PF1/MOD1 model. This nodalization consisted of a detailed three-channel core model with nine axial nodes, simulating hot channel, central, and outer regions of the core. The hot channel included four fuel assemblies. The total power generated in the hot

channel was assumed to be governed by the technical specification enthalpy rise hot channel factor.

The Seabrook SCDAP/RELAP5/MOD3 model used for this analysis was adapted from a RELAP5/MOD2 deck created for station blackout transient analysis of the Seabrook nuclear power plant.[13] The Oconee SCDAP/RELAP5/MOD3 model was derived from a RELAP5/MOD2 model created for evaluation of operational safety at B&W plants.[14] Several modifications were required to produce the models needed for this analysis. These included the addition of a detailed 3-channel, 9-axial-node core model, describing the hot channel and the central and outer core region; point kinetics modeling; SCDAP modeling; a simplified containment model; and a detailed downcomer model.

A simplified containment model, consisting of a single RELAP5 volume with heat conductors representing steel and concrete surfaces, provided a fairly rough estimate of containment response. A more detailed treatment of containment response would require the use of a containment analysis code. For Seabrook, results indicate that the containment isolation signal from the pressurizer low pressure trip trails the signal received from high containment pressure by only about 3 s. Due to the approximate nature of the containment pressure calculation, the pressurizer low pressure trip time was used to determine the containment isolation signal time. For Oconee large-break cases, the containment isolation signal from the reactor coolant system (RCS) low pressure trip trails the signal received from high containment pressure by only about 0.02 to 0.28 s; the RCS low pressure trip time was used to determine the containment isolation signal time. For the small-break cases, the high containment pressure trip trails the low RCS pressure trip by about 5 s; the high containment pressure trip was used to determine the time of containment isolation.

The Seabrook TRAC-PF1/MOD1 model used for this analysis was derived from a TRAC-PF1/MOD1 model utilized for the CSAU study.[10] The modifications for this analysis included renodalization of the core region from five to nine axial nodes, describing the hot channel and the central and outer core region, removal of pumped ECCS, modification of the core power distribution, and replacement of containment pressure and decay heat boundary conditions. Boundary conditions for containment pressure and total core power history were obtained from the corresponding SCDAP/RELAP5/MOD3 calculation.

The FRAPCON-2, FRAP-T6, and SCDAP fuel pin models were developed specifically for this analysis. A single fuel pin design was modeled for each plant type analyzed. These fuel designs included the Mk-B9/10 design for the Oconee analysis and the W 17x17 standard fuel design for the Seabrook analysis. Reactor-specific fuel data were obtained either from the fuel vendor or the appropriate Final Safety Analysis Report.[15,16] The basic design parameters for each fuel type are summarized in Table 1.

The results generated by this analysis are dependent on the specific fuel design parameters, such as initial helium fill inventory, fuel pellet dimensions,

Table 1. Summary of fuel design characteristics

Characteristic	B&W Mk-B9/10	W 17x17 standard
Pin lattice	15x15	17x17
Fuel pins per assembly	208	264
Fuel pellet OD (in.)	0.370	0.3225
Cladding ID (in.)	0.377	0.329
Cladding OD (in.)	0.430	0.374
Plenum length (in.)	8.394	6.479
Initial fuel stack height (in.)	140.595	144.0
Fuel enrichment (wt. % ^{235}U)	3.5	3.1

cladding dimensions, and plenum volume. Fuel pin failure times can be expected to vary with both fuel design and reactor design.

4. SENSITIVITY STUDIES

Using SCDAP/RELAP5/MOD3, sensitivity studies were performed for each reactor type to identify the break size resulting in the shortest time to pin failure. The large-break spectrum analyzed consisted of double-ended, offset-shear breaks of a cold leg, with break sizes corresponding to 100%, 90%, 75%, and 50% of the full design basis analysis (DBA) cold leg break area (200% of the cold leg cross-sectional area). For these cases, the break modeling consisted of restarting a steady-state calculation with a percentage of the flow area from each side of a cold leg junction redirected into the containment volume. The junction control flag for an abrupt area change was turned on for each break junction. The break model for the 6-in.-diameter, small-break LOCA consisted of a trip valve located between the cold leg and the containment at the same location used for the large-break case.

The large-break spectrum was run without any pumped ECCS available. The large-break cases resulting in the shortest time to pin failure were also run with pumped ECCS available, to determine the impact of ECCS on pin failure timing. The accumulators were assumed to be available for all cases.

The base analysis did not incorporate a concurrent loss of offsite power. As a result, the reactor coolant pumps are assumed to continue operation throughout the transient. Sensitivity cases were run using the worst-case break size, both with and without pumped ECCS, to determine the impact of tripping the RCS pumps at time zero.

For each set of large-break transient thermal-hydraulic conditions generated by SCDAP/RELAP5/MOD3, a series of 16 FRAP-T6 cases were run to determine fuel pin failure times for a range of fuel pin peak burnups and axial power peaking factors, up to and including the heat flux hot channel factor. A fundamental assumption governing this methodology is that the hot channel thermal-hydraulic conditions generated by SCDAP/RELAP5/MOD3 do not vary significantly for changes in hot pin axial power profile. In each case, the total fuel pin power, integrated over the length of the pin, is governed by the enthalpy rise hot channel factor and is therefore independent of the axial peaking factor applied.

For each small-break SCDAP/RELAP5/MOD3 calculation, a preliminary matrix of four FRAP-T6 cases was executed. These cases correspond to the highest burnup and peaking factor for each reactor. Since no fuel pin failure was observed prior to 393 s for Oconee and 600 s for Seabrook (at which time code failure was encountered in SCDAP/RELAP5/MOD3), no additional FRAP-T6 cases were run.

FRAP-T6 is a best-estimate code; however, a set of evaluation models, including the NUREG-0630[17] ballooning model, are available as options that can be used to perform calculations of fuel rod behavior that can satisfy most criteria specified in 10 CFR, Part 50, Appendix K.[18] The evaluation models include the areas of mechanical deformation and rupture, thermal-hydraulic boundary conditions, initial conditions, and material properties of fuel and cladding. The 16-case FRAP-T6 matrix was repeated for the worst-case break size (100% DBA) using the evaluation model options.

In addition to the cases described above, the 16-case FRAP-T6 matrix for the worst-case break size for the Seabrook reactor (100% DBA) was run using thermal-hydraulic boundary condition data provided by TRAC-PF1/MOD1.

5. RESULTS

The results of the timing analysis of PWR fuel pin failures are summarized below. Sections 5.1 and 5.2 describe the accident scenarios considered and the fuel pin failure results obtained from FRAP-T6 using thermal-hydraulic boundary conditions calculated by SCDAP/RELAP5/MOD3 and TRAC-PF1/MOD1, respectively.

5.1 Results Generated Using SCDAP/RELAP5/MOD3

The thermal-hydraulic results calculated by SCDAP/RELAP5/MOD3 for the worst-case LOCA for Oconee are illustrated in Figure 3. Core thermal power drops off rapidly in response to core voiding. Falling pressurizer pressure lags the drop in system pressure, due to choking in the surge line. Starting at about 30 s, collapsed reactor water level begins a gradual recovery as flow from the accumulators begins to reach the core. The containment isolation trip setpoints were exceeded at 0.6 and 3.7 s for Oconee and Seabrook, respectively. An additional 2-s delay to account for instrument response times was assumed for each plant for calculating the containment isolation times.

The hot channel thermal-hydraulic conditions generated by each

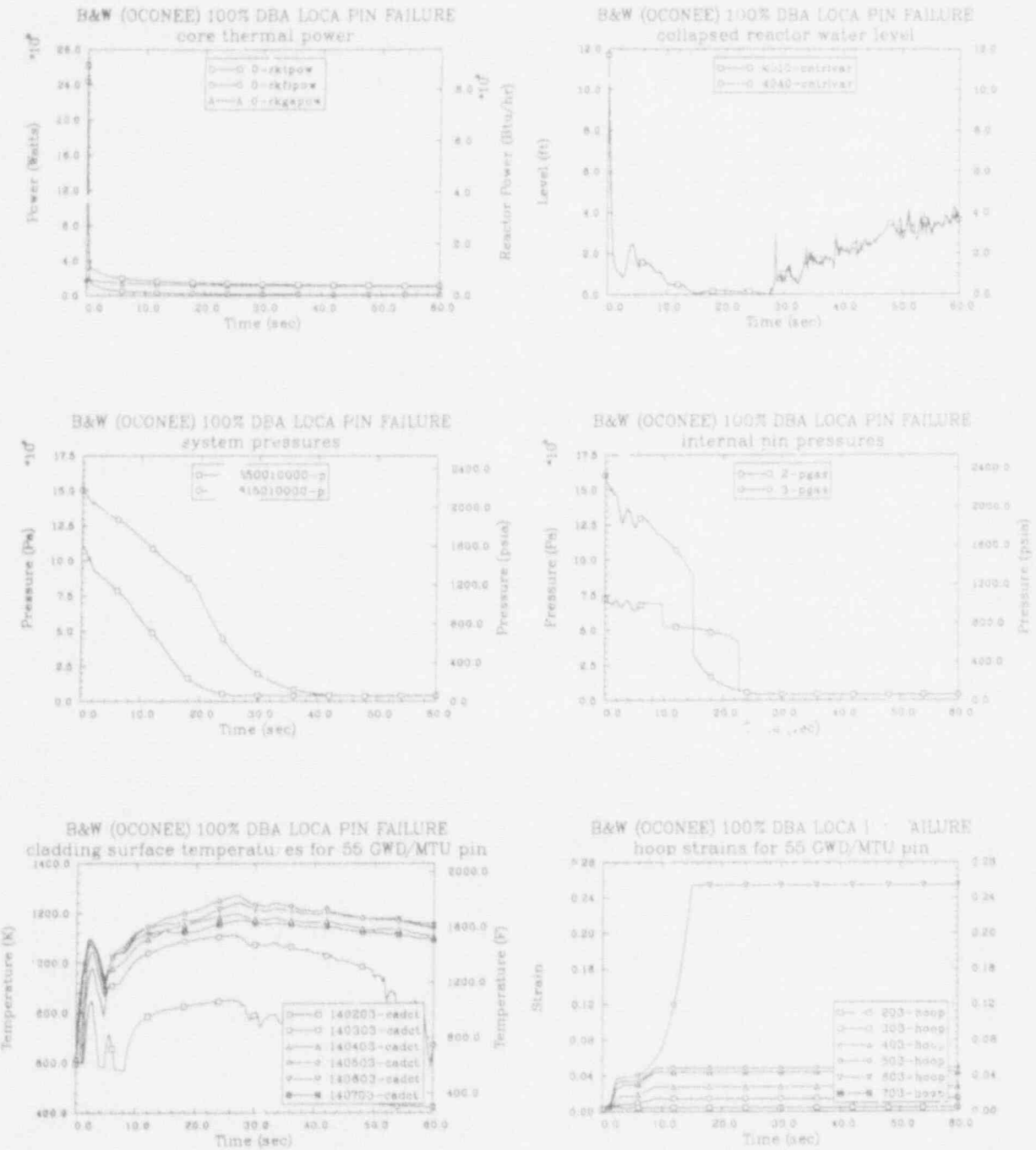

Figure 3. Plots of the transient results generated by SCDAP/RELAP5/MOD3 for a complete double-ended offset shear LOCA for Oconee.

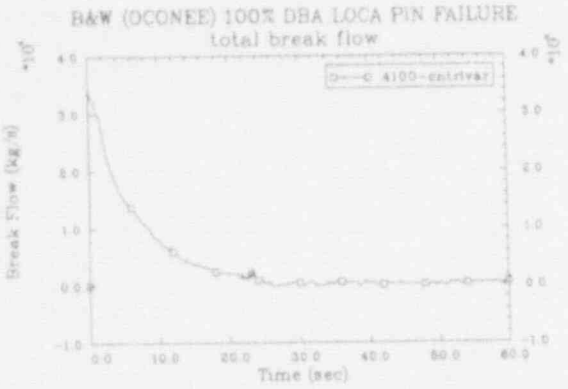

Variable	Description
SCDAP/RELAP5/MOD3 Variables:	
0-rktpow	Total core thermal power (W)
0-rkfipow	Total core fission power (W)
0-rkgapow	Total core decay heat (W)
4010-cntrlvar	Hot channel collapsed reactor water level (m)
4040-cntrlvar	Core-average collapsed reactor water level (m)
550010000-p	Reactor upper head pressure (Pa)
615010000-p	Pressurizer dome pressure (Pa)
2-pgas	Internal pin pressure for 5 GWD/MTU pin (Pa)
3-pgas	Internal pin pressure for 55 GWD/MTU pin (Pa)
14nn01-cadct	High-burnup fuel pin cladding temperature for node nn (^{o}K)
nn03-hoop	High-burnup fuel pin cladding hoop strain (dimensionless)
4100-cntrlvar	Total break flow (kg/s)
702000000-mflowj	Total accumulator flow (kg/s)

Figure 3. (continued)

SCDAP/RELAP5/MOD3 run were used to provide boundary conditions for FRAP-T6, which calculated fuel pin failure times for a matrix of fuel pin exposures and peaking factors. The fuel pin failure times calculated by FRAP-T6 for the worst-case LOCA are summarized in Tables 2 and 3 for Oconee and Seabrook, respectively. In cases where no fuel pin failure was predicted, the values given in the tables correspond to the transient time at the end of the calculation, prefixed by a "greater than" symbol (>). The failure nodes are indicated by the numbers in parentheses; nodes are numbered from 1 at the bottom of the core to 9 at the top.

Table 2. FRAP-T6-calculated hot fuel pin failure time (s) and locations as a function of burnup and peaking factor (pf) for a complete, double-ended, offset-shear LOCA for Oconee.

Burnup/pf	5 GWd/MTU	20 GWd/MTU	35 GWd/MTU	55 GWd/MTU
2.63	22.7 (5)	20.3 (4)	18.0 (4)	13.0 (4)
2.4	> 60.0	25.3 (4)	19.7 (4)	14.1 (4)
2.2	> 60.0	34.8 (4)	23.9 (4)	16.4 (4)
2.0	> 60.0	>60.0	33.8 (4)	22.5 (4)

Table 3. FRAP-T6-calculated hot fuel pin failure time (s) and locations as a function of burnup and peaking factor (pf) for a complete, double-ended, offset-shear LOCA for Seabrook.

Burnup/pf	5 GWd/MTU	20 GWd/MTU	35 GWd/MTU	50 GWd/MTU
2.32	29.1 (5)	29.7 (5)	27.7 (5)	24.8 (4)
2.2	34.4 (5)	36.7 (5)	35.8 (5)	32.5 (4)
2.0	44.5 (4)	48.4 (4)	43.6 (4)	43.6 (4)
1.8	> 60.0	> 60.0	> 60.0	> 60.0

The transient fuel pin performance results calculated by FRAP-T6 are shown in Figures 4 and 5 for Oconee and Seabrook, respectively. Initially, the fuel pin internal pressures drop gradually as the fuel pin plenum temperatures drop and ballooning of the cladding occurs. A sudden drop in fuel pin internal pin pressure to the system pressure is observed when the fuel pin failure criterion (failure probability > 0.5) is reached.

The fuel cladding surface temperatures rise rapidly during the first few seconds, as the fuel rod surface heat flux is reduced due to core voiding. Fuel cladding temperatures peak at about 1100 K, then decline over the next few

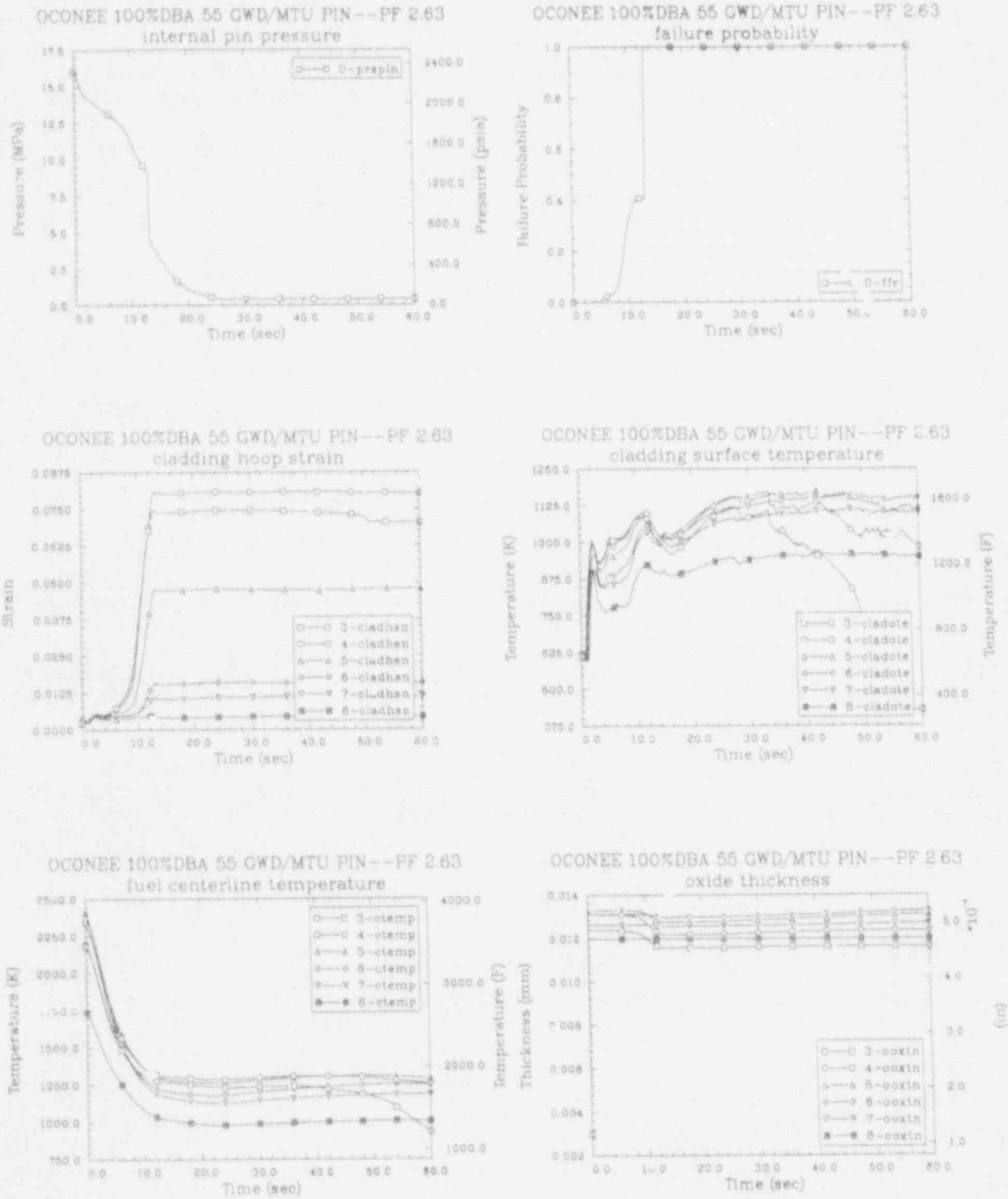

Figure 4. FRAP-T6 transient fuel performance results for an Oconee hot channel hot pin, peaking factor 2.63, 55 GWd/MTU burnup, using SCDAP/RELAP5/MOD3 thermal-hydraulic boundary condition data.

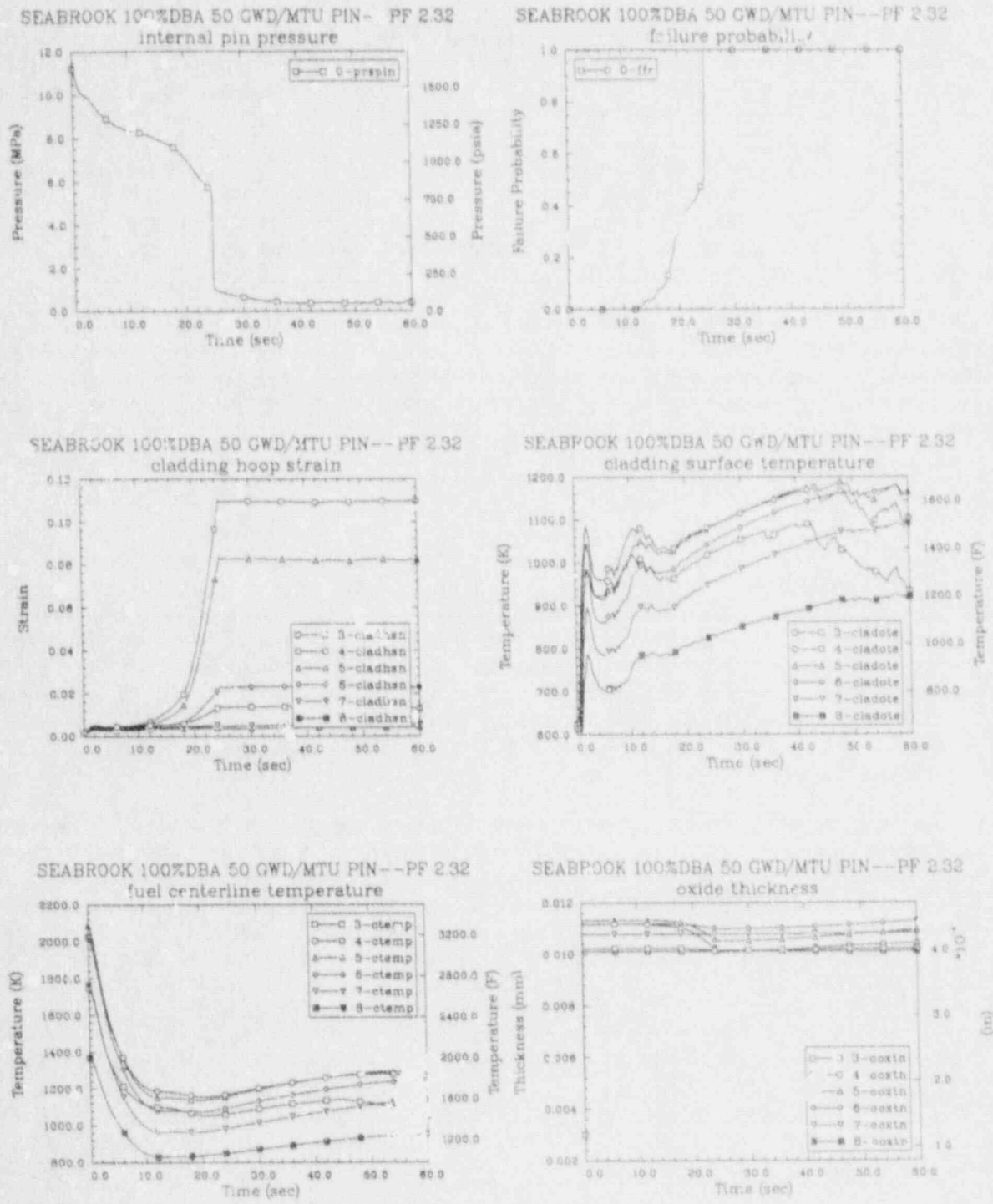

Figure 5. FRAP-T6 transient fuel performance results for a Seabrook hot channel hot pin, peaking factor 2.32, 50 GWd/MTU burnup, using SCDAP/RELAP5/MOD3 thermal-hydraulic boundary condition data.

seconds as the fuel gives up its stored energy and fuel pellet temperatures drop due to the reduced power generation. Eventually, the reduced heat transfer at the cladding surface produces a steady rise in cladding and fuel pellet temperatures. This temperature rise continues until water from the accumulators (and the pumped ECCS, if available) makes its way into the core region.

The zircaloy cladding undergoes a phase change starting at about 1050-1090 K and ending at about 1250 K. As a result of this phase change, the material properties of the cladding change rapidly over this temperature range. In each case, pin failures were calculated to occur during this phase transition prior to reaching a temperature of 1250 K.

The fuel centerline temperatures calculated by SCDAP/RELAP5/MOD3 for both the Oconee and Seabrouk models are in fairly close agreement with those calculated by the best-estimate models of FRAP-T6. The Seabrook results also indicate good agreement between SCDAP/RELAP5/MOD3 and FRAP-T6 cladding surface temperatures; however, for Oconee, SCDAP/RELAP5/MOD3 tends to overpredict cladding surface temperatures in comparison to those calculated by FRAP-T6. These differences are attributed to the different heat transfer correlations used in the two codes.

The fuel pin failure times calculated by SCDAP/RELAP5/MOD3 do not, in general, correlate well with those calculated by FRAP-T6. Except for the Oconee 100% DBA LOCA cases, the fuel pin failure times calculated by SCDAP/RELAP5/MOD3 tend to be longer than those calculated by FRAP-T6. This discrepancy increases significantly as the break size is reduced. A fairly good agreement is obtained between the two codes for the 100% DBA Oconee cases, both with and without pumped ECCS. However, fuel pin failure times calculated by SCDAP/RELAP5/MOD3 are about half of those calculated by FRAP-T6 for the two 100% DBA Oconee cases run with main coolant pump trip.

The observed deviations between FRAP-T6 and SCDAP fuel pin failure times can be traced, at least in part, to the difference in the cladding strains calculated by the two codes. In SCDAP, a step change in cladding strain was encountered at each axial node of the low-exposure fuel pins at around 10 s for each large-break LOCA case for both the Oconee and Seabrook fuel pins. This step change in cladding strain was also calculated for the Seabrook high-exposure fuel pin. The cladding deformation model does not appear to be properly taking strain rate effects into account. The step change in cladding strain produces a step decrease in internal fuel pin pressure. As illustrated by the plots of internal pin pressure calculated by SCDAP/RELAP5/MOD3 (see Figure 3), the step decrease in pressure early in the transient results in a delayed time to fuel pin rupture. SCDAP/RELAP5/MOD3 overpredicts the axial extent of cladding deformation, which results in an underprediction of internal pin pressures and an overprediction of the time to fuel pin failure.

The minimum time to fuel pin failure for Oconee, calculated with the FRAP-T6 best-estimate models, is 13.0 s for the 100% DBA case without RCS pump trip. This time was not affected by availability of pumped ECCS. The minimum time to fuel pin failure calculated by FRAP-T6 for Seabrook is 24.6 s for the 100% DBA case without ECCS available. Overall, the results generated by FRAP-T6 are

consistent with expected trends. Pin failure times shortened as peaking factors, burnups, and break areas were increased.

The earliest pin failure times calculated for Oconee are significantly shorter than those calculated for Seabrook. The shorter failure times can be directly attributed to the higher linear heat generation rate and the larger fuel pin diameter in Oconee, which results in higher initial stored energy. In addition, the failure times calculated for Oconee are stronger functions of burnup than those reported for Seabrook. The pin failure times calculated for Seabrook are only weak functions of burnup, with only about 5 s separating the pin failure times over the range of burnups.

Several parameters affecting fuel pin failure times vary as a function of exposure, including cladding creep, fuel and cladding material properties, internal gas pressure, and gap conductance. The fuel pin failure times calculated for Seabrook generally increase between 5 and 20 GWd/MTU and then decrease to the shortest pin failure time at 50 GWd/MTU. The increase in fuel pin failure time between 5 and 20 GWd/MTU can be attributed to the decrease in stored energy over this period, resulting from cladding creep and increased gap conductance. After 20 GWd/MTU, the fuel pin internal pressure becomes the dominant factor affecting the fuel failure timing.

The stored energy calculated for Oconee does not vary with exposure to the same extent as observed in the Seabrook analysis. Fuel pin failure times for Oconee are dominated primarily by the internal pin pressure, resulting in a stronger dependence on exposure.

As anticipated, no fuel pin failures are predicted for the small-break cases during the first 60 s of the calculation. The small-break cases without pumped ECCS was subsequently extended to 393.0 s (at which time code failure occurred) for Oconee and to 1800.0 s for Seabrook, with no fuel failures predicted by either SCDAP/RELAP5/MOD3 or FRAP-T6.

3.2 Supplemental TRAC-PF1/MOD1 Calculation

Figure 6 compares the transient results generated by SCDAP/RELAP5/MOD3 and TRAC-PF1/MOD1. The plots illustrate a good comparison of break flow and resulting system depressurization. The TRAC-PF1/MOD1 calculation reaches the low pressurizer pressure setpoint at 3.84 s, only 0.11 s later than indicated by the SCDAP/RELAP5/MOD3 calculation.[b] The accumulator, intact hot leg, and cold leg flows also compare well.

The largest deviation between results occurs after the accumulators empty and discharge nitrogen into the system. In the SCDAP/RELAP5/MOD3 calculation,

---

b. An additional delay of 2.0 s to account for instrument response is assumed for the analysis.

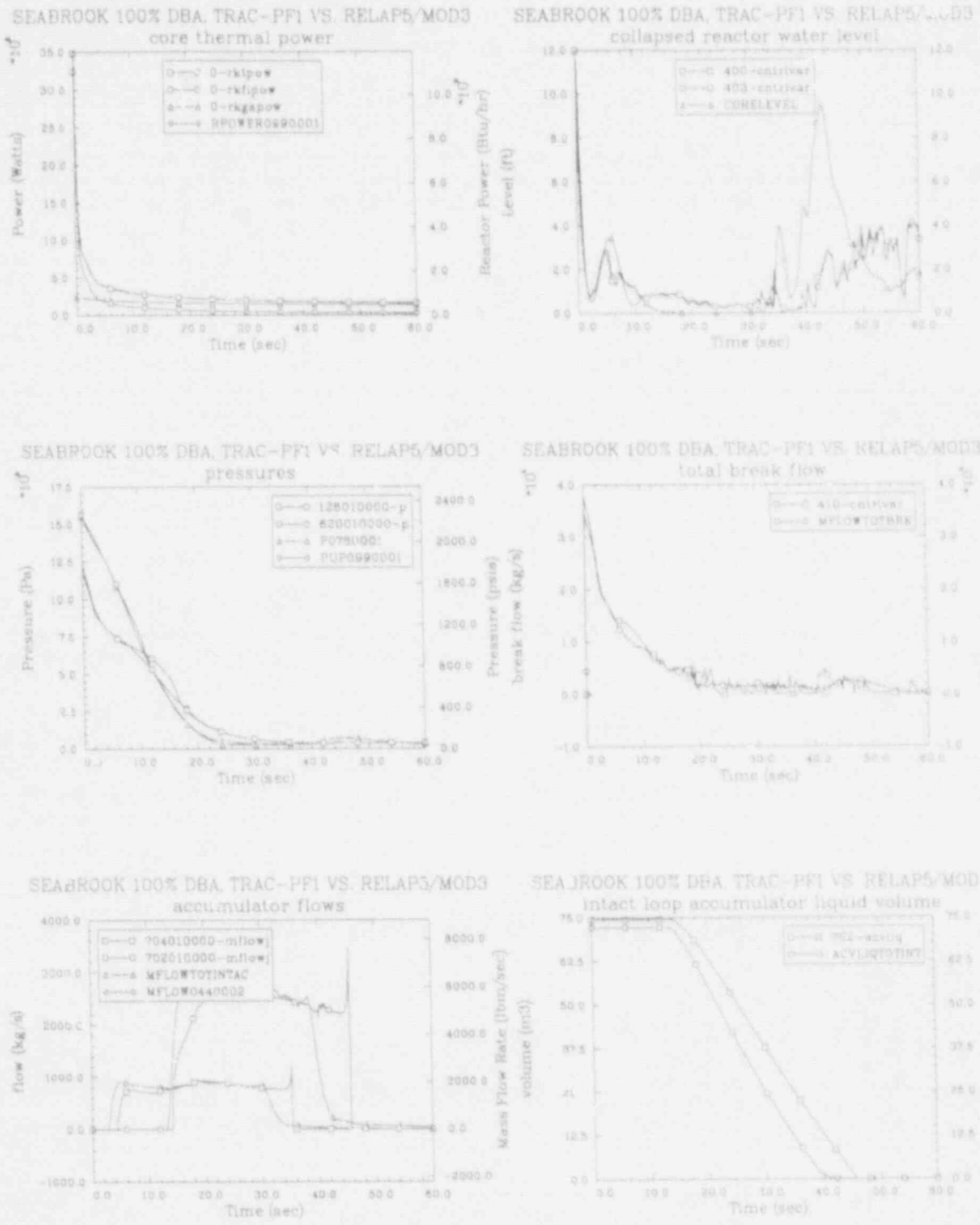

Figure 6. Plots of the transient results generated by SCDAP/RELAP5/MOD3 and TRAC-PF1/MOD1.

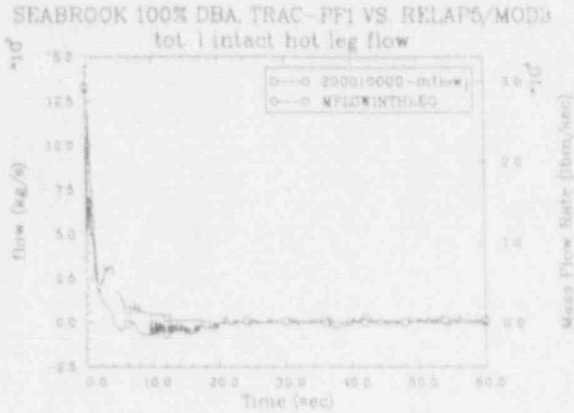

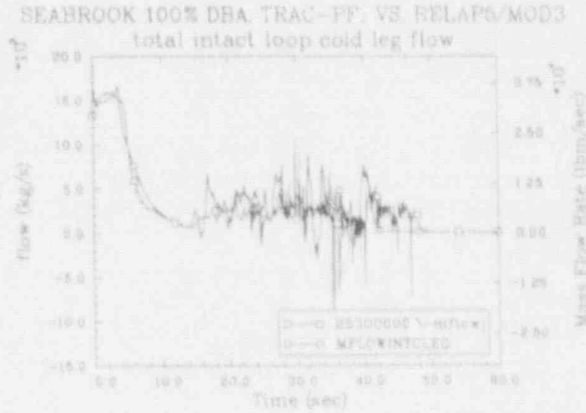

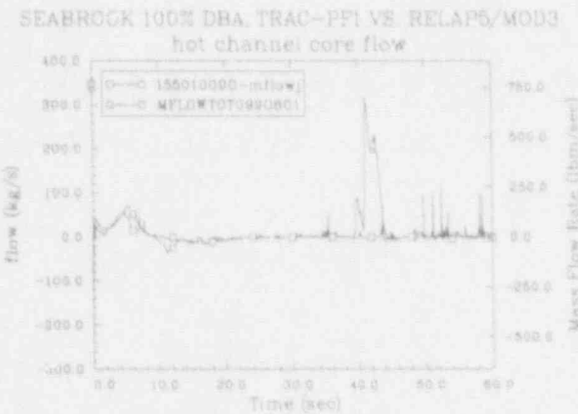

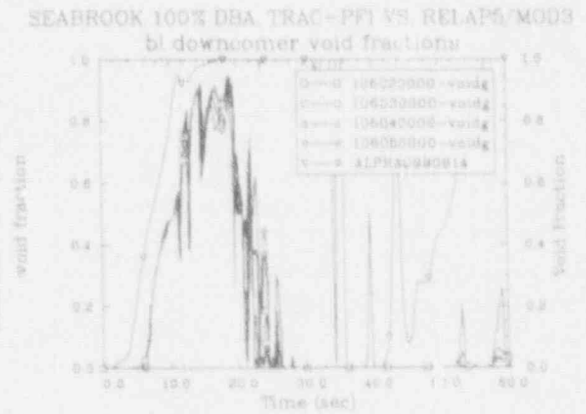

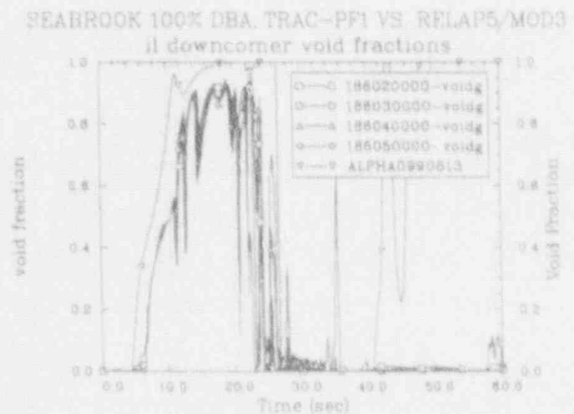

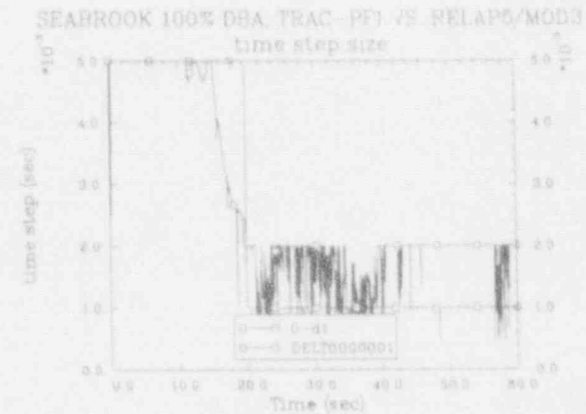

Figure 6. (continued)

Variable	Description
SCDAP/RELAP5/MOD3 Variables:	
0-rktpow	Total core thermal power (W)
0-rkfipow	Total core fission power (W)
0-rkgapow	Total core decay heat (W)
400-cntrlvar	Hot channel collapsed reactor water level (m)
403-cntrlvar	Core-average collapsed reactor water level (m)
128010000-p	Reactor upper head pressure (Pa)
620010000-p	Pressurizer dome pressure (Pa)
410-cntrlvar	Total break flow (kg/s)
704010000-mflowj	Accumulator flow for the broken loop (kg/s)
702010000-mflowj	Total accumulator flow for the intact loop (kg/s)
702-acvlig	Accumulator liquid volume for the intact loop (m^3)
200010000-mflowj	Total hot leg flow for the intact loop (kg/s)
253010000-mflowj	Total cold leg flow for the intact loop (kg/s)
155010000-mflowj	Hot channel flows at the core midplane (kg/s)
1060n0000-voidg	Broken loop downcomer void fraction for node n at the core midplane elevation
1860n0000-voidg	Intact loop downcomer void fraction for node n at the core midplane elevation
0-dt	Time step size (s)
TRAC-PF1/MOD1 Variables:	
RPOWER0990001	Total core thermal power (W)
CORELEVEL	Core-average collapsed reactor water level (m)
PUP0990001	Reactor upper head pressure (Pa)
P078001	Pressurizer dome pressure (Pa)
MFLOWTOTBRK	Total break flow (kg/s)
MFLOW0440002	Accumulator flow for the broken loop (kg/s)
MFLOWTOTINTAC	Total accumulator flow for the intact loop (kg/s)
ACQLIQTOTINT	Accumulator liquid volume for the intact loop (m^3)
MFLOWINTHLEG	Total hot leg flow for the intact loop (kg/s)
MFLOWINTCLEG	Total cold leg flow for the intact loop (kg/s)
MFLOWTOT990801	Hot channel flows at the core midplane (kg/s)
ALPHA0990814	Broken loop downcomer void fraction for node n at the core midplane elevation
ALPHA0990813	Intact loop downcomer void fraction for node n at the core midplane elevation
DELT0000001	Time step size (s)

Figure 6. (continued)

the accumulators were isolated as they approached an empty condition, in order to prevent code failure. In the TRAC-PF1/MOD1 calculation, however, as the accumulators empty, nitrogen gas is discharged into the cold leg and vessel. This surge of noncondensible gas pressurizes the upper downcomer, resulting in a surge of fluid into the core region. A surge can be seen as the broken loop accumulator empties at approximately 35 s and again as the intact accumulators empty at about 40 s. This surge of fluid is clearly seen in the hot channel mass flow at the midcore level. The downcomer void fraction plots indicate similar responses for voiding of the downcomer adjacent to the intact loops; however, the TRAC-PF1/MOD1 calculation indicates a quicker and more prolonged voiding of the downcomer quadrant adjacent to the broken cold leg.

The FRAP-T6 fuel pin failure times generated using TRAC-PF1/MOD1 are summarized in Table 4. The axial node in which failure occurred is given in parentheses. The corresponding transient fuel performance results calculated by FRAP-T6 for a fuel pin operating with a power peaking factor of 2.32 and a peak burnup of 50 GWD/MTU are shown in Figure 7.

Table 4. Fuel pin failure times (s) calculated by FRAP-T6 using thermal-hydraulic conditions generated by TRAC-PF1/MOD1.

Burnup/pf	5 GWd/MTU	20 GWd/MTU	35 GWd/MTU	50 GWd/MTU
2.32	> 60.0	41.4 (5)	41.3 (6)	34.9 (6)
2.2	> 60.0	> 60.0	41.4 (5)	41.2 (6)
2.0	> 60.0	> 60.0	> 60.0	> 60.0
1.8	> 60.0	> 60.0	> 60.0	> 60.0

Cladding surface temperatures calculated by FRAP-T6 using TRAC-PF1/MOD1 data are lower than those calculated using SCDAP/RELAP5/MOD3 data. As shown in Figure 7, this deviation becomes even more apparent after about 40 s, due to the

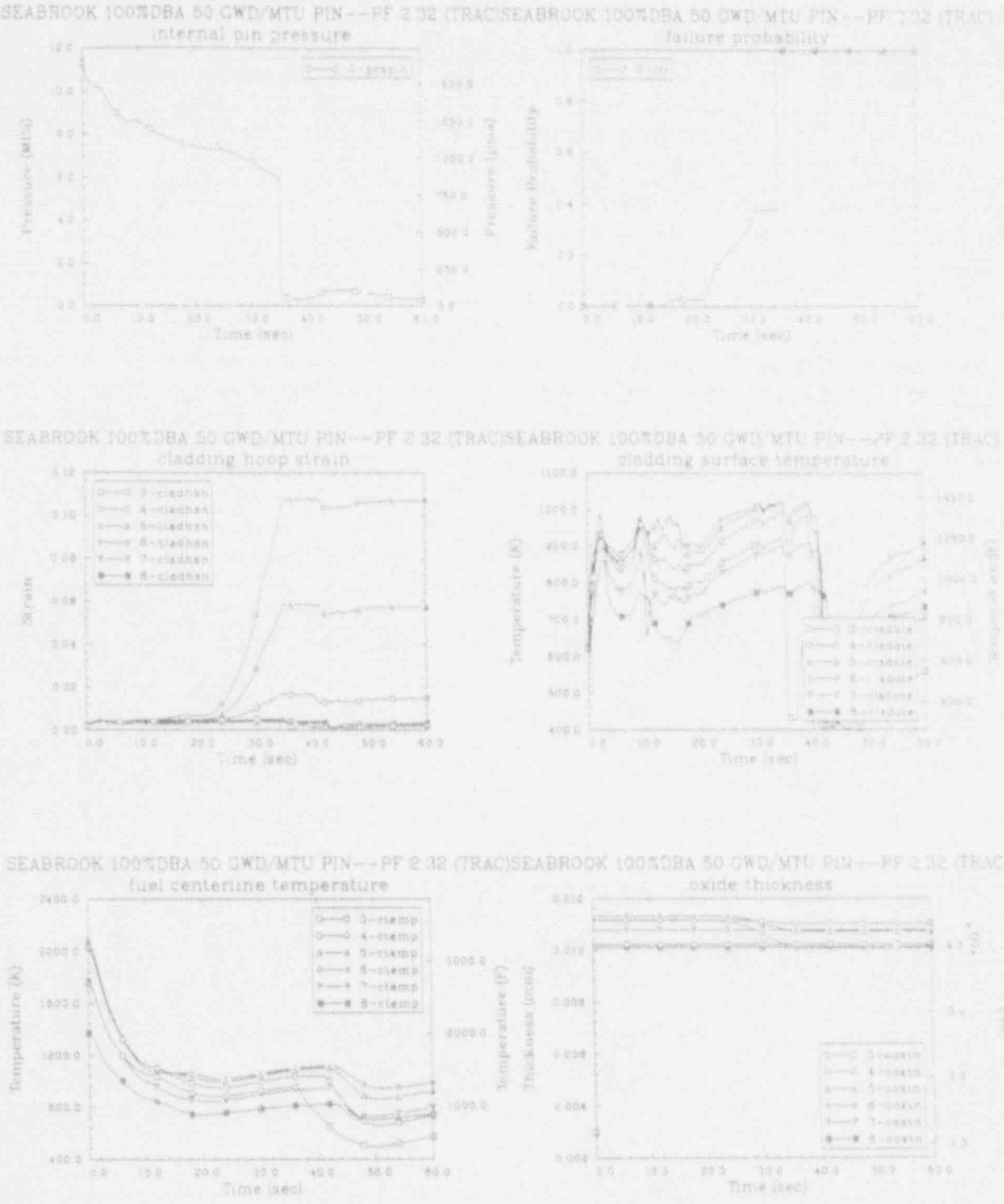

Figure 7. FRAP-T6 transient fuel performance results for the Seabrook hot channel hot pin, peaking factor 2.32, 50 GWd/MTU burnup, using TRAC-PF1/MOD1 thermal-hydraulic boundary condition data.

nitrogen-induced flow surge that results in a quenching of the cladding for the TRAC-PF1/MOD1 calculation. In the TRAC-PF1/MOD1 case, pin failure occurs during the initial coolant surge, prior to reaching the phase transition temperature range. Based on this single TRAC-PF1/MOD1 calculation, the methodology using SCDAP/RELAP5/MOD3 to provide thermal-hydraulic boundary conditions for FRAP-T6 appears to produce conservative results (earlier fuel pin failure).

6. CONCLUSIONS

The earliest fuel pin failure times calculated for a complete, double-ended offset-shear break of a cold leg, without pumped ECCS and assuming the main coolant pumps continued operating, are 13.0 s for Oconee using SCDAP/RELAP5/MOD3; 24.8 s for Seabrook using SCDAP/RELAP5/MOD3; and 34.9 s for Seabrook using TRAC-PF1/MOD1. The corresponding containment isolation signal times are 0.6, 3.73, and 3.84 s, respectively. A 2.0-s delay was assumed for instrument response. These values are summarized in Table 5, along with the minimum interval calculated between initiation of containment isolation and failure of the first fuel pin.

Table 5. Timing summary for worst-case LOCA runs using highest burnup and peaking factor results.

Plant	Thermal-hydraulic model	Containment isolation (s)	Earliest pin failure (s)	Interval (s)
Oconee	SCDAP/RELAP5/MOD3	2.6	13.0	11.4
Seabrook	SCDAP/RELAP5/MOD3	5.7	24.8	19.1
Seabrook	TRAC-PF1/MOD1	5.8	34.9	29.1

These values were obtained for fuel pins with the maximum discharge burnup, operating at the technical specification limits. This represents a conservative result, since fuel pins with such a high exposure would not be operating at such conditions. The fuel pin failure time can increase significantly for both lower burnup and lower peaking factor. An improved best-estimate approach would require detailed fuel-cycle-specific information on the core power and exposure distributions.

7. REFERENCES

1. *Code of Federal Regulations*, 10CFR Part 100, "Reactor Site Criteria," January 1, 1991.

2. G. A. Berna et al., *FRAPCON-2: A Computer Code for the Calculation of*

Steady State Thermal-Mechanical Behavior of Oxide Fuel Rods, NUREG/CR-1845, January 1981.

3. C. M. Allison et al. (Eds.), *SCDAP/RELAP5/MOD3 Code Manual*, NUREG/CR-5273, EGG-2555 (Draft), Revision 1, Volumes I-III, June 1990.

4. L. J. Siefken et al., *FRAP-T6: A Computer Code for the Transient Analysis of Oxide Fuel Rods*, NUREG/CR-2148, May 1981.

5. *TRAC-PF1/MOD1: An Advanced Best Estimate Computer Program for Pressurized Water Reactor Thermal-Hydraulic Analysis*, NUREG/CR-3858, April 1987.

6. G. A. Berna, D. D. Lanning, and W. N. Rausch, *FRAPCON-2 Developmental Assessment*, PNL-3849, NUREG/CR-1949, June 1981.

7. E. T. Laats, R. Chambers, and N. L. Hampton, *Independent Assessment of the Steady State Fuel Rod Analysis Code FRAPCON-2*, EGG-CAAP-5335, January 1981.

8. L. J. Siefken, *Developmental Assessment of FRAP-T6*, EGG-CDAP-5439, May 1981.

9. R. Chambers et al., *Independent Assessment of the Transient Fuel Rod Analysis Code FRAP-T6*, EGG-CAAD-5532, January 1981.

10. Technical Program Group, *Quantifying Reactor Safety Margins: Application of Code Scaling, Applicability, and Uncertainty Evaluation Methodology to a Large-Break, Loss-of-Coolant Accident*, EGG-2552, NUREG/CR-5249, December 1989.

11. D. M. Snider, K. L. Wagner, and W. Grush, *Nuclear Plant Analyzer (NPA) Reference Manual Mod-1*, EGG-EAST 9096, April 1990.

12. J. E. Streit et al., *GRAFITI User Manual*, EGG-CATT-9604, March 1991.

13. P. D. Bayless and R. Chambers, *Analysis of A Station Blackout Transient at the Seabrook Nuclear Power Plant*, EGG-NTP-6700, September 1984.

14. P. D. Wheatley et al., *Evaluation of Operational Safety at Babcock and Wilcox Plants; Volume 2 - Thermal-Hydraulic Results*, NUREG/CR-4966, November 1987.

15. Duke Power Co., *Final Safety Analysis Report, Oconee Nuclear Station Units 1, 2, and 3*, March 18, 1972.

16. *Updated Final Safety Analysis Report, Seabrook Station*, May 26, 1989.

17. D. A. Powers and R. O. Meyer, *Cladding Swelling and Rupture Models for LOCA Analysis*, NUREG-0630, April 1980.

18. *Code of Federal Regulations*, 10CFR Part 50, Appendix K, "ECCS Evaluation Models," January 1, 1991.

NOTICE

This report was prepared as an account of work sponsored by an agency of the United States Government. Neither the United States Government nor any agency thereof, or any of their employees, makes any warranty, expressed or implied, or assumes any legal liability or responsibility for any third party's use, or the results of such use, of any information, apparatus, product or process disclosed in this report, or represents that its use by such third party would not infringe privately owned rights. The views expressed in this report are not necessarily those of the U.S. Nuclear Regulatory Commission.

PWR Instrument Availability During Severe Accidents[a]

William C. Arcieri
Duane J. Hanson

Idaho National Engineering Laboratory
EG&G Idaho, Inc.
P.O. Box 1625
Idaho Falls, Idaho 83415

ABSTRACT

The ability of plant personnel to successfully manage severe accidents strongly depends on the availability of timely and accurate plant status information. The United States Nuclear Regulatory Commission (USNRC) recognizes the importance of reliable plant information by making instrumentation one of the five elements of its accident management framework. This paper describes the results of research sponsored by the NRC to evaluate the availability of plant instrumentation during a range of possible severe accidents at a PWR with a large dry containment.

The approach used to perform the instrument availability evaluation is based on the methodology developed during a previous NRC program which resulted in the publication of NUREG/CR-5513[1]. NUREG/CR-5513 discusses the instruments needed by plant personnel involved in accident management to determine the status of the plant. The availability of these instruments during a severe accident initiated by a small break LOCA was evaluated in NUREG/CR-5513.

This paper expands on the results presented in NUREG/CR-5513 by evaluating instrument availability based on the environmental conditions possible for a range of possible severe accidents that could occur at a pressurized water reactor (PWR) with a large dry containment. The expanded evaluation is presented in NUREG/CR-5691[2]. These results indicate that instrumentation in some plant locations will not be available during certain phases of severe accidents.

---

a. Work supported by the division of Systems Research, Office of Nuclear Reactor Research, U.S. Nuclear Regulatory Commission, Washington, D.C. 205555, under DOE Contract No. DE-AC07-76ID001570

INTRODUCTION

The capability currently exists to manage a broad range of accidents at nuclear power plants in the United States. Consequently, severe accidents at nuclear power plants will occur only if there are multiple failures of safety related equipment, serious human errors, or some combination of these two conditions. To manage this complex severe accident behavior, plant personnel must successfully diagnose the occurrence of an accident, determine the extent of challenge to plant safety, monitor the performance of automatic systems, select strategies to prevent or mitigate the safety challenge, implement the strategies, and monitor their effectiveness. One of the areas affecting the capability of personnel to effectively carry out these actions is the availability of timely and accurate plant status information. Plant instruments are relied upon to supply the information.

Safety-related instrumentation installed in a nuclear power plant is primarily designed and qualified for preventing and mitigating accidents that have a severity less than or equal to the severity of a design-basis accident. The ability of the instrumentation to supply the information needed for severe accident management has not been comprehensively investigated for conditions typical of a broad range of severe accidents.

In this paper, severe accident conditions that influence instrument availability and performance are identified and the availability of plant instrumentation for a wide range of severe accidents is assessed for a pressurized water reactor (PWR) with a large dry containment.

APPROACH

The following approach was used to evaluate instrument availability for various severe accident conditions. This approach is summarized in the following steps:

1. Identify severe accidents that influence risk for a PWR with a large, dry containment

2. Define expected thermal hydraulic, radiation and humidity conditions affecting instrumentation by location

3. Define envelopes that bound the range of parameters that impact instrument performance

4. Assess instrument availability based on location and conditions

Step 1: Identify Severe Accident Sequences

The probabilistic risk assessment results presented in NUREG-1150[3] for the Surry and Zion pressurized water reactors were used to identify the types of severe accident sequences having the potential to influence risk described in

Step 1 of the above approach. These results are from the most recent evaluation of all credible types of accidents that will dominate core damage frequency and risk to the public. Although the results are specific to the two plants, the sequence categories identified are sufficiently broad to apply to most PWRs.

The following five plant damage states from NUREG-1150 used in this assessment are:

1. Station blackout (SBO)

2. Large- and small-break loss-of-coolant accidents (LOCAs)

3. Anticipated transients without scram (ATWS)

4. All other transients except SBO and ATWS

5. Interfacing system LOCA (ISLOCA) steam generator tube rupture.

Each plant damage state is determined from the following seven plant damage state indicators: (1) status of the reactor coolant system at the onset of core damage, (2) status of the emergency core cooling system, (3) status of the containment heat removal capability, (4) status of the ac power, (5) refueling water storage tank injection capability, (6) steam generator heat removal capability, and (7) status of the reactor coolant pump (RCP) seal cooling. The NUREG-1150 analysis includes the full range of potential accident sequences, as represented by these plant damage states for a PWR with a large dry containment design.

Several accident progression bins are presented in NUREG-1150 to cover the range of outcomes for each plant damage state. Included in the accident progression bins is consideration of important events during a severe accident. These include core meltdown and lower head failure and the potential for hydrogen burns and direct containment heating. The accident progression bins from NUREG-1150 used in this assessment are:

- Vessel breach with an alpha mode failure and early containment failure
- Vessel breach at a pressure >200 psia with early containment failure
- Vessel breach at a pressure <200 psia with early containment failure
- Vessel breach with late containment failure
- Bypass

- o Vessel breach with no containment failure
- o No vessel breach.

An alpha mode failure results from a steam explosion. Early containment failure refers to containment failure at or before vessel breach (lower head failure).

Step 2: Define Expected Conditions

To accomplish Step 2, the conditions within the reactor coolant system and containment were defined based on a review of severe accident analyses available for PWR plants. From this review, the only analyses available that provide information on the thermal hydraulic conditions both in the reactor coolant system and containment for a range of important PWR accident sequences are found in BMI-2104[4,5] and NUREG/CR-4624[6,7] for the Surry and Zion plants. The Surry plant is a Westinghouse-designed, three-loop PWR in a subatmospheric containment building. The Zion plant is a Westinghouse-designed, four-loop PWR in a large dry containment building. The BMI-2104 and NUREG/CR-4624 analyses are also used because most of the important events expected during a severe accident, from core melt through lower head failure and beyond, are found in these reports, including possible containment failure modes. These analyses provide a baseline for gaining insight into challenges to instrument availability.

The accident sequence results from BMI-2104 and NUREG/CR-4624 are assigned to the NUREG-1150 plant damage states and accident progression bins as shown in Table 1. This assignment was made on the basis of the accident initiator, the RCS pressure at vessel failure, and the timing and mode of containment failure. In general, the accident initiator was used in the assignment of plant damage states, and the containment failure mode was used for assignment to accident progression bins. This categorization was performed to verify that the accident sequence results presented in BMI-2104 and NUREG/CR-4624 cover the range of accidents expected for the plant damage states and accident progression bins presented in NUREG-1150. It is judged that the range of conditions expected for any plant damage state and accident progression bin combination are generally reflected in the BMI-2104 and NUREG/CR-4624 analyses. Appendix B to NUREG/CR-5691 gives detailed information on this process.

It is recognized that hot leg natural circulation is not considered in BMI-2104 and NUREG/CR-4624, which can impact the performance of instruments in the reactor coolant system. Hot leg natural circulation will redistribute energy in the reactor coolant system and can result in the prediction of higher temperatures in reactor coolant system components outside the reactor vessel. Instruments that could be affected by higher temperatures would be

Table 1
Assignment of the BMI-2104 and NUREG/CR-4624 Results to the NUREG-1150 Plant Damage States/Accident Progression Bins

Accident Progression Bin	Plant Damage State: Station Blackout	ATWS	Transients	LOCA	Bypass
VB, alpha Early CF	-	-	-	-	-
VB > 200 psi Early CF	TMLB'-δ (Surry)	-	TMLB'-δ (Surry) TMLU-DCH (Zion)	S2D-γ (Surry)	-
VB < 200 psi Early CF	-	-	-	-	-
VB, BMT Late CL	TMLB'-ϵ (Surry)	-	-	AB-ϵ S2D-ϵ (Surry)	-
Bypass	-	-	-	-	V
VB, No CF	TMLB' (Zion)			S2D (Zion)	
No VB					

VB = vessel breach
CF = containment failure
BMT = basemat meltthrough
CL = containment leak

a. No analysis was found in BMI-2104 or NUREG/CR-4624 that corresponds to this plant damage state/accident progression bin.

located in the upper plenum, hot and cold legs, and the pressurizer. Estimates of conditions in the upper plenum, hot leg, and pressurizer were made using the results presented in NUREG/CR-5214[8]. Maximum hot leg temperatures of 1700°F (1200°K) are possible in the case of reactor coolant system depressurization by the operator when steam generator dryout occurs. The effect of natural circulation is factored into the instrument availability analysis.

The effect of radiation conditions was considered by comparing the integrated dose resulting from various radionuclide release scenarios based on release data presented in NUREG-0737 and radionuclide distribution data from BMI-2104. The data in NUREG-0737 assumes release of 100 percent of the noble gas, 50 percent of the halogen and 1 percent of the particulate (solid) radionuclides from the fuel for LOCA events that depressurize the reactor coolant system. This release is assumed to be to either the reactor coolant system or containment, depending on the limiting instrument location. The BMI-2104 report presents estimates of the releases of the fission products and other aerosols from the fuel during core melt and core concrete interaction. The magnitude of the iodine and particulate releases is the principal difference between the BMI-2104 and NUREG-0737 data.

Step 3: Define Envelopes

To account for changing conditions during the progression of the accident, the accident sequences were divided into five phases based on the timing of key events and the phenomena occurring in the reactor coolant system and the containment. These phases are described below:

- Phase 1. This phase begins with initiation of the sequence, including the blowdown/boiloff of water inventory in the reactor coolant system, and ends at the time of initial uncovery of the reactor core. Operator guidance for Phase 1 is included in the existing plant Emergency Operating Procedures.

- Phase 2. Core uncovery begins. Fuel heatup results from the lack of adequate cooling. This phase ends when fuel melting begins.

- Phase 3. Fuel melting occurs, including fuel and cladding relocation and the formation of debris beds. The phase ends with relocation of a significant amount of core material to the reactor vessel lower plenum. Hydrogen may burn during this phase, depending on the accident sequence

- Phase 4. Molten core debris accumulates in the lower head of the reactor vessel. The phase ends with failure of the lower head. Hydrogen may burn during this phase, depending on the accident sequence.

- Phase 5. The core debris directly interacts with the containment after lower head failure. During this phase, containment failure could occur because of overpressure, hydrogen burns, or basemat meltthrough resulting from core-concrete interaction. Containment failure resulting

from direct containment heating is also possible, depending on the reactor coolant system pressure when lower head failure occurred.

Plots of temperature and pressure typical of conditions at the approximate location of the plant instrumentation were developed to assess the magnitude and times of harsh conditions during the accidents analyzed in BMI-2104 and NUREG/CR-4624. The maximum value of key thermal hydraulic parameters reached during each of the accident phases and the timing of each accident phase to help in accounting for event timing was tabulated from these plots. The tabulation of the key thermal hydraulic parameters is presented in Table 2 and the event timing tabulation is presented in Table 3.

Comparison of the thermal hydraulic data for the various sequences show that there is a high degree of similarity particularly in the temperature predictions among the Surry and Zion accident sequences from the perspective of instrument availability. Similarity in the thermal hydraulic results simplifies assessment of instrument availability.

The principal reason for the similarity in the thermal hydraulic results is that certain severe accidents phenomena and certain plant engineering design features govern the temperature and pressure reached during a severe accident for a wide range of sequences. Severe accident phenomena important to the availability of instruments located in the reactor coolant system or containment include the core melting temperature, the timing and magnitude of hydrogen burns, the impact of natural circulation in the reactor coolant system, and the impact of direct containment heating for sequences where lower head failure occurs near the normal operating pressure of the reactor coolant system. Engineering design features can affect the maximum pressure and temperature possible in the reactor coolant system and containment which is important to instrument availability. The setpoints for the PORV and reactor coolant system safety relief valves, and the containment failure pressure would be included. It is these severe accident phenomena and key engineering design features as opposed to any particular accident sequence that determines if the performance of a particular instrument will degrade due to pressure and temperature conditions for a PWR with a large dry containment.

Step 4: Assess Instrument Availability

Instrument availability is evaluated based on: the physical location; the range; and the qualification ranges for temperature, pressure, humidity, and radiation levels. The instrument evaluations presented are based on the Regulatory Guide 1.97[9] review for the Calvert Cliffs Nuclear Power Station[10]. This information provided the measurement ranges and the qualification level of each instrument required for DBA events. Based on this information, the instrument qualification temperature and pressure conditions used were as follows:

Table 2
Maximum Value of Key Parameters
During Each Phase for All Accident Sequences

Parameter	Phase 1 Initiation to Core Uncovery	Phase 2 Uncovery to Start of Melt	Phase 3 Meltdown to Core Slump	Phase 4 Core Slump to Head Failure	Phase 5 Long Term Phase
Within the Reactor Vessel					
Average Core Temperature (F)	1175 (Z-S2D)	2335 (Z-S2D)	4285 (Z-S2D)	4285 (Z-S2D)	N/A
Core Exit Gas Temperature (F)	N/A	2300 (Z-S2D)	3700 (Z-S2D)	3900 (Z-TMLU)	N/A
Upper Plenum Structure Temp (F)	N/A	1150 (Z-S2D)	1800 (Z-S2D)	3450 (Z-TMLU)	N/A
Max Reactor System Pressure (psia)	2550 (Z-TMLB')	2550 (Z-TMLB')	2550 (Z-TMLB')	2550 (Z-TMLB')	N/A
Min Reactor System Pressure (psia)	40 (S-AB-ϵ)	36 (S-AB-ϵ)	32 (S-AB-ϵ)	34 (S-AB-ϵ)	N/A
Outside the Reactor Vessel					
RPV Exit Gas Temperature (F)	N/A	1250 (Z-S2D)	1800 (Z-S2D)	1500 (Z-S2D)	N/A
Hot Leg Temperature (F)	N/A	800 (Z-S2D)	850 (Z-S2D)	900 (Z-S2D)	N/A
Containment (No H2 Burns)					
Pressure (psia)	40 (S-AB-ϵ)	40 (Z-TMLB')	37 (Z-TMLB')	58 (Z-TMLB')	114 (Z-TMLB')
Temperature (F)	240 (S-AB-ϵ)	238 (Z-TMLB')	230 (Z-TMLB')	266 (S-TMLB')	362 (Z-TMLB')
Containment (H2 Burns, DCH)					
Pressure (psia)	29 (S-TMLB'-γ)	26 (S-TMLB'-γ)	23 (S-TMLB'-γ)	149 (S-TMLU-DCH)	150 (S-TMLB'-γ)
Temperature (F)	220 (S-TMLB'-γ)	211 (S-TMLB'-γ)	200 (S-TMLB'-γ)	1264 (S-TMLU-DCH)	2400 (S-TMLB'-γ)

Table 2 (continued)
Maximum Value of Key Parameters
During Each Phase for All Accident Sequences

Parameter	Phase 1 Initiation To Core Uncovery	Phase 2 Uncovery to Start of Melt	Phase 3 Meltdown to Core Slump	Phase 4 Core Slump to Head Failure	Phase 5 Long Term Phase
Auxiliary Building (V Sequence)					
Pressure (psia)	16 (S-V Seq)	16 (S-V Seq)	15 (S-V Seq)	15 (S-V Seq)	N/A
Temperature (psia)	215 (S-V Seq)	215 (S-V Seq)	428 (S-V Seq)	739 (S-V Seq)	N/A

Note: The plant and accident sequences for each parameter is given in parenthesis.

Table 3
Time Range of Key Events for
BMI-2104 and NUREG/CR-4624 Accident Sequences
(Minutes)

Accident Sequence	Phase 1 Initiation to Core Uncovery	Phase 2 Core Uncovery to Start of Meltdown	Phase 3 Core Meltdown to Core Slump	Phase 4 Core Slump to Lower Head Failure	Phase 5 Long Term Phase	Containment Failure Time
Surry Sequences						
S2D-γ	0.0 - 91.5 (91.5)	91.5 - 134.0 (43.1)	134.0 - 146.6 (12.6)	146.6 - 163.6 (17.0)	163.6 - 1114.6	163.7
S2D-ϵ	0.0 - 91.5 (91.5)	91.5 - 134.6 (43.1)	134.6 - 147.3 (12.7)	147.3 - 227.5 (80.2)	227.5 - 2210.4	-
TMLB'-δ	0.0 - 95.5 (95.5)	95.5 - 118.3 (22.8)	118.3 - 146.3 (28.0)	146.3 - 152.8 (6.5)	152.8 - 1073.4	152.9
TMLB'-ϵ	0.0 - 95.5 (95.5)	95.5 - 118.3 (22.8)	118.3 - 146.3 (28.0)	146.3 - 157.3 (11.0)	157.3 - 1100.0	738.2
TMLB'-γ	0.0 - 97.2 (97.2)	97.2 - 118.5 (21.3)	118.5 - 143.5 (25.0)	143.5 - 155.3 (11.8)	155.3 - 1402.2	486.7
V	0.0 - 20.6 (20.6)	20.6 - 39.7 (19.1)	39.7 - 56.6 (16.9)	56.6 - 149.9 (93.3)	149.9 - 750.2	-
AB-ϵ	0.0 - 9.4 (9.4)	9.4 - 24.8 (15.4)	24.8 - 42.1 (17.3)	42.1 - 110.1 (68.0)	110.1 - 1639.6	1450.6
Zion Sequences						
S2D	0.0 - 112.5 (112.5)	112.5 - 150.6 (38.1)	150.6 - 163.8 (13.2)	163.8 - 187.7 (23.9)	187.7 - 788.2	-
TMLB'	0.0 - 109.8 (109.8)	109.8 - 130.5 (20.7)	130.5 - 158.5 (28.0)	158.5 - 169.5 (11.0)	169.5 - 1001.8	-
TMLU-DCH	0.0 - 124.6 (124.6)	124.6 - 148.4 (23.8)	148.4 - 178.2 (29.8)	178.2 - 189.6 (11.4)	189.6 - 861.0	189.6

Notes:

- Number in parentheses is the elapsed time for each phase.
- For Phase 5, the value of the upper limit of the range is the accident time at which the MARCH case was terminated.

Instrumentation within the reactor coolant system

- Maximum temperature = 2300°F
- Maximum pressure = 2500 psia

Instruments within the containment building

- Maximum temperature = 300°F
- Maximum pressure = 60 psia.

Typical instrument dose qualification limits are on the order of 10^8 rads.

Typical instrument systems consist of transducers, cabling, electronics, and other components. For instruments located in the reactor coolant system, the evaluation focused on the sensors because of the harsh temperature conditions sensors could be exposed to during a severe accident. For instruments located in the containment, the cabling, splices, and other components of the instrument systems in addition to the sensors were considered.

The assessment of instrument performance based on temperature and pressure conditions assumes degraded instrument performance if the pressure and temperature environments exceed instrumentation qualification limits or if the system is operated outside of its range. Degraded instrument performance means that instrument system output may be unreliable, that is, the magnitude or trend (or both) of the parameter being monitored by the instrument is in error. This degraded performance may cause the operator to take inappropriate action resulting from the errors in instrument output. The definition of degraded instrument performance includes the possibility of instrument failure. An instrument is considered to be available if its performance has not degraded.

It is recognized that the assumption of degraded instrument performance may be conservative, particularly if the environmental conditions exceed the qualification conditions only by small amounts or for short periods of time. However, basic instrument capabilities are not well known when qualification conditions are exceeded. An assessment of the relationship between the instrument uncertainties and the timing and degree to which the qualification conditions are exceeded would require a detailed study of basic instrument capabilities and failure modes.

INSTRUMENT AVAILABILITY EVALUATION AND RESULTS

Results from the evaluation of instrument availability for a pressurized water reactor with a large dry containment can be summarized as follows:

- All plant instruments will be available during Phase 1 of all accident sequences (prior to fuel damage).

- Instruments located in the reactor pressure vessel will experience temperature conditions beyond their qualification temperatures when the fuel is approaching the melt temperature (Phase 2) or as the fuel is melting (Phase 3). Exposure to these temperatures will degrade instrument performance and limit the availability of these instruments for further use in accident management.

- Instruments located outside the reactor vessel but within the reactor coolant system may experience temperature conditions beyond the qualification temperature, as a result of natural circulation during fuel heatup (Phase 2) or fuel melting (Phase 3). Even if the qualification limit is not exceeded, some of the instruments that monitor temperature may be exposed to temperature conditions above their measurement range. Exposure to these temperature conditions will degrade instrument performance and limit the availability of these instruments for further use in accident management.

- Instruments located in containment will be exposed to high temperatures in the event of multiple hydrogen burns or direct containment heating. Hydrogen burns will occur during or after fuel heatup (Phase 2). Direct containment heating might occur following the failure of the reactor vessel lower head (during Phase 5). Exposure to these temperature conditions may degrade instrument performance and limit the availability of these instruments for accident management.

- For an accident sequence involving an interfacing system LOCA, instrument failure near the break location is possible, resulting from high temperature conditions. Because the instrumentation in the auxiliary building is generally not qualified for high temperature conditions, degraded instrument performance is possible following the initiation of core heatup (during Phase 2). Access to sampling and analysis equipment located in the auxiliary building away from the break location may not be possible, as a result of high radiation fields that may begin as early as when the cladding ruptures (during Phase 2).

- Degraded instrument performance for instruments located in the turbine building is possible during an accident initiated by a steam generator tube rupture, particularly instruments used to monitor radioactivity levels in the secondary side coolant, because of radiation levels beyond the range of the instrument.

Radiation exposure may impact instrument availability in the longer term. Instruments located in containment away from localized sources could reach 10^8 rads after about 30 days. Instruments near localized sources such as the hot leg could reach 10^8 rads after about 1 day.

Because of differences in the electrical power source configuration at different plants, it is not possible to generally evaluate instrument availability for a station blackout. Note that many plants provide battery backup for all Regulatory Guide 1.97, Category 1 instrumentation, though this is not specifically called for in the document. If battery backup is available, then most of the information required to monitor the status of the reactor coolant system and containment will be available until temperature conditions challenge instrument availability. Systems used to obtain and monitor samples of reactor coolant, containment atmosphere, and containment sump or cavity water may not be available in the event of a station blackout. As a result, information needs requiring sampling information may not be met.

Note that operators may not recognize that instrument performance has degraded. One possibility is that an instrument reading appears to be normal or the trends may be plausible when, in actuality, the plant conditions and trends are different. As a result, operators are misled about plant conditions and pursue inappropriate operation strategies. A more detailed evaluation of the expected accuracy and reliability of the instruments is recommended for conditions where the qualification limits are exceeded. Also needed are ways that erroneous instrument readings can be recognized by operators. Such evaluation should consider the entire instrument system, including the transducer, cabling, electronics, and other instrument system components. In particular, instrument performance during hydrogen burns or direct containment heating should be evaluated. It is possible that some components of the instrument systems are sufficiently protected to withstand the temperature pulse expected during these events, but that other components may fail. Cabling is expected to be particularly vulnerable to the high-temperature conditions that develop during multiple hydrogen burns.

ACCIDENT MANAGEMENT INFORMATION ASSESSMENT

An accident management information assessment based on the instrument availability evaluation is presented in NUREG/CR 5691. Important findings from this review for accidents where core cooling is reestablished and for bypass sequences are presented below.

Accidents Where Core Cooling Is Reestablished

One possible outcome of the accident progression for any of the NUREG-1150 plant damage states is that core cooling will be reestablished before core meltdown progresses to a non-coolable state. Once core cooling is reestablished, the ability to monitor the core and reactor coolant system heat removal would enhance the ability of plant personnel to safely recover the plant in a timely manner. If performance of instruments such as the core exit thermocouples, hot leg resistance temperature devices (RTD), reactor vessel level monitoring system (RVLMS) and subcooling monitor has degraded, the reactor coolant temperature or reactor vessel level cannot be reliably determined and the core heat removal safety functions would be difficult to monitor.

If core cooling is reestablished before core melt begins (Phase 3), then all instruments should be available. If core melt begins, the performance of the core exit thermocouples and the RVLMS is expected to degrade due to high temperatures near the core region.

Temperature in the hot leg may be above the range of the respective RTD's before core cooling is established. This upper limit is generally about 700°F. When core cooling is reestablished, cooling in the hot leg will bring the temperature back into the range of the hot leg RTD. Degraded performance of the hot leg RTD's means that the reliability of their temperature readings would be uncertain at this point. In a core cooling recovery situation, unreliable readings from the hot leg RTD's will increase the difficulty of determining whether adequate core or reactor system heat removal is occurring.

Effect of Bypass (ISLOCA) Sequences

The ability to meet information needs which require sampling and analysis of reactor coolant, containment sump water, containment atmosphere, and other process fluids may be impeded during an accident initiated by an ISLOCA or a steam generator tube rupture. During any accident, sampling and analysis of process fluids is needed to aid in determining the extent of fuel damage, radionuclide inventory in the containment atmosphere, and other parameters related to accident management. This need is illustrated by reviewing the information needs in Appendix A of NUREG/CR-5513 for various safety functions and noting that monitoring safety functions involving reactor vessel and containment integrity and fission product release mitigation requires sampling and analysis of reactor coolant and the containment atmosphere.

In many plants, the equipment used for sampling and analysis of process fluids is located in the auxiliary building. In the event of an accident initiated by an interfacing LOCA resulting in core damage, the radionuclide release to the auxiliary building will produce high radiation fields and high airborne radionuclide concentrations. The ability to continue activities that requires auxiliary building access depends upon location of the needed instruments and equipment relative to the break, building arrangement, and HVAC system operation. It is likely that the ability to obtain and analyze reactor coolant and containment atmosphere samples will be impeded in the event of an ISLOCA for the plant.

In addition to possibly restricting sampling and analysis activities, the ability to obtain readings from instruments that would be used during an ISLOCA may be restricted since some instruments have their readout panels located in the auxiliary building. At Calvert Cliffs for example, the instrument panel for the primary coolant and sump dissolved hydrogen monitor is located in the auxiliary building.

REFERENCES

1. D. J. Hanson, et. al., Accident Management Information Needs, Volume 1 - Methodology Development and Application to a Pressurized Water Reactor (PWR) with a Large Dry Containment, NUREG/CR-5513, March, 1990

2. W. C. Arcieri, D. J. Hanson, Instrument Availability for a Pressurized Water Reactor With a Large Dry Containment During Severe Accidents, NUREG/CR-5691, EGG-2638, March 1991.

3. U.S. Nuclear Regulatory Commission, Severe Accident Risks: An Assessment for Five Nuclear Power Plants, NUREG-1150, Volumes 1 and 2 (second draft, published June, 1989).

4. J. A. Gieseke et al., Radionuclide Release Under Specific LWR Accident Conditions - PWR Large Dry Containment Design (Surry Plant Recalculations), BMI-2104, Volume V, July, 1984.

5. J. A. Gieseke et al., Radionuclide Release Under Specific LWR Accident Conditions - PWR Large Dry Containment Design (Zion Plant), BMI-2104, Volume VI, July, 1984.

6. R. S. Denning et al., Radionuclide Release Calculations for Selected Severe Accident Scenarios - PWR, Subatmospheric Containment Design, NUREG/CR-4624, Volume 3, July, 1986

7. R. S. Denning et al., Radionuclide Release Calculations for Selected Severe Accident Scenarios - PWR, Large Dry Containment Design NUREG/CR-4624, Volume 5, July, 1986

8. P. D. Bayless, Analysis of Natural Circulation During a Surry Station Blackout Using SCDAP/RELAP5, NUREG/CR-5214, October, 1988

9. U.S. Nuclear Regulatory Commission, Instrumentation for Light Water Cooled Nuclear Power Plants to Assess Plant and Environs Conditions During and Following an Accident, Regulatory Guide 1.97, Revision 3 May, 1983.

10. Letter from Joseph A. Tiernan of Baltimore Gas and Electric to A.C. Thadani of the U.S. Nuclear Regulatory Commission, Calvert Cliffs Nuclear Power Plant Units Nos. 50-317 & 50-318, Regulatory Guide 1.97 Review, February 21, 1986.

MANAGING WATER ADDITION TO A DEGRADED CORE[a]

P. Kuan and D. J. Hanson
Idaho National Engineering Laboratory
EG&G Idaho, Inc.

F. Odar
U.S. Nuclear Regulatory Commission

ABSTRACT

In this paper we present information that can be used in severe accident management by providing an improved understanding of the effects of water addition to a degraded core. This improved understanding is developed using a diagram showing a sequence of core damage states. Whenever possible, a temperature and a time after accident initiation are estimated for each damage state in the sequence diagram. This diagram can be used to anticipate the evolution of events during an accident. Possible responses of plant instruments are described to identify these damage states and the effects of water addition. The rate and amount of water addition needed (a) to remove energy from the core, (b) to stabilize the core or (c) to not adversely affect the damage progression, are estimated. Analysis of the capability to remove energy from large cohesive and particulate debris beds indicates that these beds may not be stabilized in the core region and they may partially relocate to the lower plenum of the reactor vessel.

1. INTRODUCTION

Preventing severe accidents or mitigating their consequences requires implementation of strategies to add water to cool the core. However, under certain degraded core conditions, adding water may lead to enhanced hydrogen production, changes in core geometry that complicate recovery, pressurization of the system resulting from steam generation, steam explosion, or recriticality of the reactor core if unborated water is used. Therefore, plans for managing water addition to a degraded core must ensure that undesirable effects of water addition are understood so that: (1) these effects can be minimized and an accident can be terminated at the earliest possible stage, and (2) plant personnel can be better prepared to deal with plant responses that appear contrary to desired outcomes when water is added during a core degradation transient. The approach presented here provides information to enhance this understanding.

---

[a] Work supported by the U.S. Nuclear Regulatory Commission, Office of Nuclear Regulatory Research under DOE Contract No. DE-AC07-76ID01570.

2. APPROACH

The approach used here to gain an improved understanding of the effects of water addition to a degraded core revolves around a sequence of core damage states. Simplified descriptions and results of rough estimates of parameters associated with degraded cores are used to illustrate the steps of the approach. These steps are summarized below.

First, a diagram showing a sequence of core damage states is developed for severe accidents. Core states in the sequence where the core would have distinct responses to water addition include: (1) pre-damage heatup of the core, (2) fuel rod ballooning and bursting, (3) rapid oxidation of zircaloy, (4) debris bed formation, and (5) core relocation to the lower plenum. Temperatures and times of occurrence are estimated for the events in the sequence.

Second, evaluations are performed to characterize the responses of plant instruments to degraded core conditions and to adding water to a degraded core. Innovative uses of instruments to diagnose core conditions are also explored. In this paper, discussion of instrument responses will be limited to instruments available in pressurized water reactors

Third, bounding estimates for energy removal from degraded cores by water addition are given. These estimates yield the minimum rate and amount of water addition to a degraded core that would not adversely affect subsequent evolution of an accident. In addition, the minimum rate and amount of water to successfully remove energy from or stabilize the core are also given. These rates and amounts of water addition are compared with plant capabilities.

Fourth, critical heat removal boundaries are determined for expected geometries of core degradation. The geometries include those of cohesive as well as particulate debris beds. These boundaries indicate that for certain bed parameters, adding water to the core cannot prevent their heatup and, consequently, relocation of molten core materials to the lower plenum of the vessel should be expected.

3. SEQUENCE OF CORE DAMAGE STATES

Although the details of core damage progression depend on plant design and specific accident scenarios, severe fuel damage experiments and the TMI-2 accident [1,2] show that unmitigated core damage follows a sequence of broadly defined, distinct core damage states.

Figure 1 shows a conceptual diagram of the sequence of core damage states for a small-break loss-of-coolant accident (SBLOCA). The damage sequence starts with core uncovery and ends with relocation of molten core materials to the lower plenum of the reactor vessel. The stages of core damage progression corresponds to a temperature scale from approximately 600 K

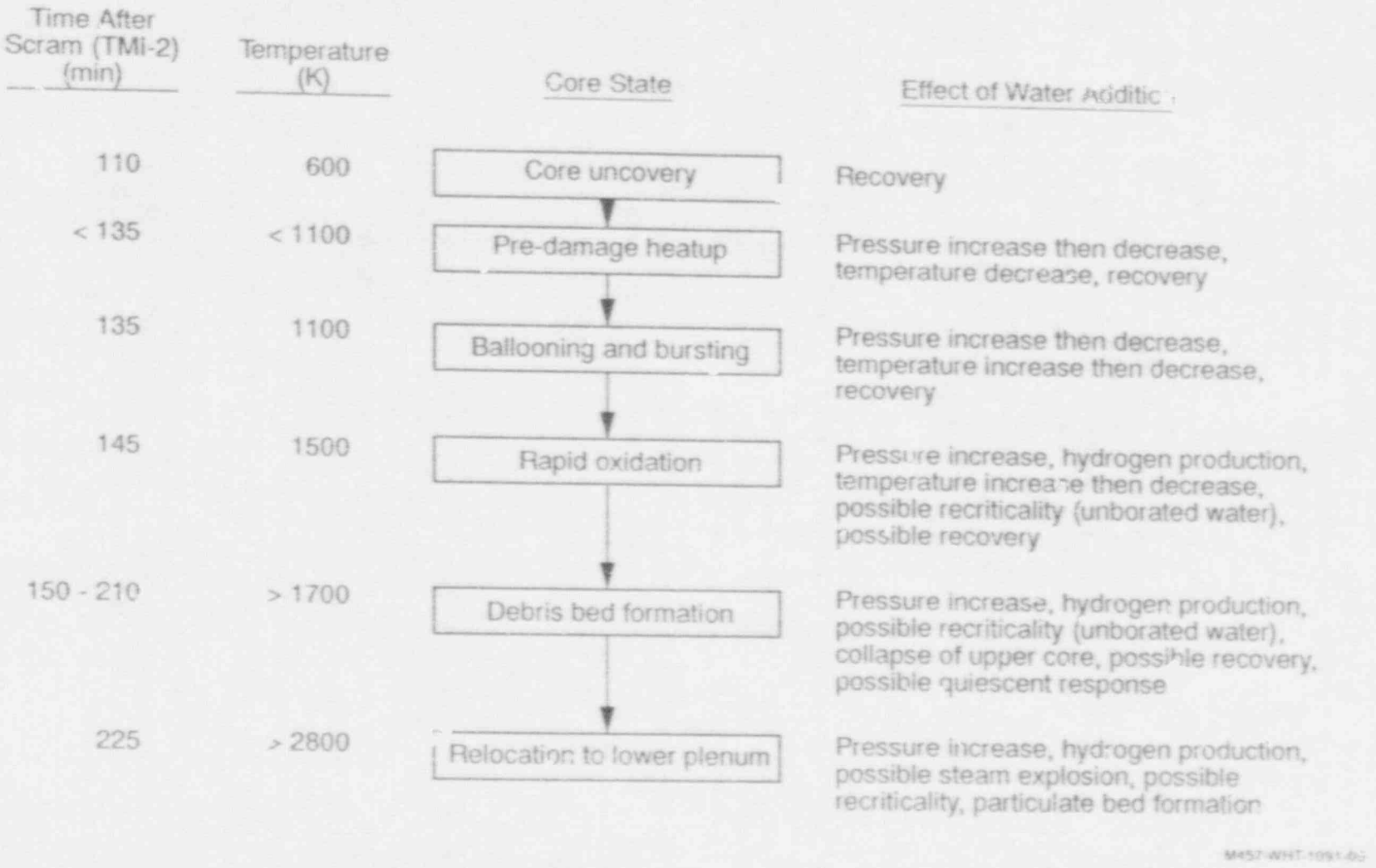

Figure 1. Sequence of core damage states.

(coolant saturation temperature) to over 3100 K (melting point of UO_2). The approximate times associated with the damage states in the TMI-2 accident and potential effects of water addition at each stage of core damage progression are also shown in the sequence diagram.

Pre-Damage Stage

In a small-break LOCA with no emergency core coolant injection, core uncovery generally begins approximately an hour after the initiation of the break. If the reactor coolant pumps are not running, the upper part of the core will be exposed to a steam environment and heatup of the core will begin. However, if the coolant pumps are running, the core will be cooled by a two-phase mixture of steam and water, and heatup of the fuel rods will be delayed until almost all of the water in the two-phase mixture is vaporized. The TMI-2 accident showed that operation of reactor coolant pumps may be sustained for up to approximately two hours to deliver a two-phase mixture that can prevent core heatup.

Ballooning and Bursting

In the absence of a two-phase mixture going through the core or of water addition to the core to compensate water boiloff, the fuel rods in a steam environment will heatup at a rate between 0.3 K/s and 1 K/s [3]. In less than half an hour, the peak core temperature would reach 1100 K. At this temperature, the zircaloy cladding of the fuel rods may balloon and burst. This is the first stage of core damage.

Cladding ballooning may block a substantial portion of the flow area of the core and restrict the flow of coolant. However, complete blockage of the core is unlikely because not all fuel rods balloon at the same axial location. In this case, sufficient water addition can cool the core and stop core damage progression.

Rapid Oxidation

The next stage of core damage, beginning at approximately 1500 K, is the rapid oxidation of the zircaloy by steam. In the oxidation process hydrogen is produced and a large amount of heat is released. Above 1500 K, the power from oxidation exceeds that from decay heat [4,5] unless the oxidation rate is limited by the supply of either zircaloy or steam.

If water is added to the core during this stage, steam generation will be rapid because of the high rate of heat transfer from the core materials to the incoming water. In the upper part of the core where the oxidation of zircaloy has been steam-starved before water is added, the addition of water to the core will provide steam for additional oxidation. If the sudden revival of oxidation in the upper part of the core releases energy at a rate that is higher than the rate of heat transfer to the water, the temperature there will escalate. This could happen when the temperature of

the rods is high or when the oxide layer on the surface of the cladding is thin; both conditions contribute to high rates of oxidation.

Rapid and sufficient amounts of water addition to the core will quench the core and stop core damage progression. However, if the addition of water is slow or intermittent, or if the core is not completely covered with water, the core will heat up to the next stage of degradation.

Debris Bed Formation

When the temperature in the core reaches about 1700 K, molten control materials [1,6] will flow to and solidify in the space between the lower parts of the fuel rods where the temperature is comparatively low. Above 1700 K, the core temperature may escalate in a few minutes to the melting point of zircaloy (2150 K) due to increased oxidation rate. When the oxidized cladding breaks, the molten zircaloy, along with dissolved UO_2 [1,7] would flow downward and freeze in the cooler, lower region of the core. Together with solidified control materials from earlier down-flows, the relocated zircaloy and UO_2 would form the lower crust of a developing cohesive debris bed.

If water is added to the core at this stage, steam and hydrogen invariably will be produced. It has been estimated that, in the TMI-2 accident, one-third of the hydrogen generation during the entire accident was produced within a few minutes after a coolant pump delivered water to the core at 174 min into the accident, at which time the peak core temperature is believed to have exceeded 1700 K [8]. As a result, the pressure of the primary system will rise. Because of loss of control materials in the upper part of the core, recriticality may also be a concern if the incoming water contains little or no boron to absorb neutrons.

If sufficient water is added to the core, the top surface of the molten pool will solidify to form a crust and the fuel rod remnants above the pool may be shattered to form a particulate bed, as happened during the TMI-2 coolant pump transient.

If a particulate bed formed in the upper part of the core is relatively deep or composed of relatively small particles, water may be prevented from penetrating the bed. After dryout, cooling of the particulate bed by steam inside the bed is inefficient and the particles comprising the bed will eventually melt. Melting of the particles will add to the growth of the cohesive debris bed.

If the cohesive bed is thin and small in radial extent, water addition may gradually cool the bed and the progression of core damage may be terminated. Water addition to a large cohesive bed will generally have little effect upon its subsequent evolution. The interior of a large cohesive bed will continue to heat up and melt until only a thin crust remains. Failure of the crust, either mechanically or by meltthrough,

would lead to the relocation of the enclosed molten core materials to the lower plenum.

Relocation to the Lower Plenum

In scenarios of small-break LOCAs, there is generally a pool of water in the lower plenum of the vessel at the time of core relocation. Release of molten core materials into water always generates large amounts of steam. If the molten stream of core materials breaks up rapidly in water, there is also a possibility of a steam explosion. During relocation, any unoxidized zirconium in the molten material may also be oxidized by steam, and in the process hydrogen is produced. Recriticality also may be a concern if the control materials are left behind in the core and the relocated material breaks up in unborated water in the lower plenum.

In the TMI-2 accident, progression of core damage was terminated with the relocation of approximately 20 metric tons of core material into the lower plenum of the vessel. The material partially broke up to form a particulate bed and was quenched by water in the lower plenum. If the relocated material is much in excess of 20 metric tons, it may not be quenched by water in the lower plenum. The unquenched, relocated core materials may eventually cause failure of the vessel. The possible failure modes of the vessel are not discussed in this paper.

4. INSTRUMENTATION SIGNATURES ASSOCIATED WITH WATER ADDITION

The sequence of core damage states provides a framework for understanding the evolution of core damage. However, judicious decision-making during an accident requires exploiting to the maximum extent possible the capabilities of existing plant instruments, possibly including innovative applications beyond their design purposes, to diagnose core conditions that may be evaluated relative to the damage states in the damage sequence. Potential instrumentation signatures, methods for verifying these signatures, and differentiation of outcomes with varying amounts of water addition are discussed in this section.

Pre-Damage Stage

During this stage, the reactor coolant system instruments most useful to operators are the core water level inference system (differential pressure sensors or heated-junction thermocouples), core exit thermocouples, hot leg resistance temperature devices (RTDs), system pressure transducers, source range power monitors, and self-powered neutron detectors (SPNDs).

The water level inference system gives direct measurement of core water inventory. Deviations of the source range monitor signals and the SPND signals from their normal decay curves may be used to substantiate the direct measurement. If water is added to the core during this stage, the operator should see an increase in inferred water level, and an initial

drop in system pressure as vapor is condensed by the incoming cold water. System pressure should eventually increase when vapor condensation stops and when the water compresses the vapor volume.

If water is not added at this stage, or is added but is not enough to compensate for the loss through the break, the inferred water level from the differential pressure readings and the source range monitor or SPND signals would continue to decrease. If water is added to the core when the temperature in the upper part of the core has risen sufficiently above the saturation temperature of the water, the temperatures recorded by the core exit thermocouples and the hot leg RTDs may increase as high temperature steam is produced, although the measured temperatures may be somewhat lower than the peak core temperatures due to the mixing of superheated steam and saturated water. In addition to the core exit thermocouples and hot leg RTDs, anomalous currents of SPNDs may indicate heatup of the core. Certain types of SPNDs are known to produce negative currents when their temperature reaches 850 K and then revert to large positive currents at higher temperatures. This initial increase in temperature would be followed by a drop in temperature if the core is recovered.

Ballooning and Bursting

During the cladding ballooning and bursting stage (1100 K), water addition will have a pronounced effect on core exit thermocouple readings. The time-dependent behavior of the interassembly temperature profile may be used as one indicator of the amount of water reaching the core.

If water is added to the core at a rate sufficient to cool the outer parts of the core but not the inner regions, or at a rate that results in an unfavorable flow split due to partial blockage of the core by ballooned rods, readings of thermocouples above regions where cooling is insufficient would stay high, but radial progression in increased thermocouple readings should reverse at some radial position.

If there is sufficient energy exchange between adjacent assemblies during water addition to the core, the whole core will be cooled before the rapid oxidation of zircaloy occurs. All core exit thermocouples should show a pronounced drop in temperature. This temperature drop would indicate that water is cooling the core. Coincident with the drop in temperature, the system pressure should increase (from steam generation), followed by a gradual decrease (from steam condensation) as water fills the core. The SPNDs should also return to normal shutdown readings.

Rapid Oxidation

After reaching this stage, because the temperatures will be outside their operating range, the core exit thermocouples can no longer provide reliable readings. Subsequent diagnosis of core damage states must rely on other instrumentation, such as the pressure monitors and the SPNDs. However, the

[illegible] core exit thermocouples may give indication that core damage has progressed beyond the ballooning and bursting stage. Another indication that the core may have reached this stage is the presence of excess radiation in the containment from fission gas released during the cladding bursting stage. It may take five to ten minutes for the released fission gas to migrate from the reactor core to the radiation monitors in the containment. During this time the core may have heated to a temperature that zircaloy can be rapidly oxidized.

If water addition is modest, resulting in the delivery of high quality steam to the upper core for oxidation of initially steam-starved zircaloy that releases energy and hydrogen, a significant, sustained pressure jump would be observed. In general, rapid oxidation of 20% of the cladding will release enough energy to melt the cladding and liquify a substantial amount of fuel. If this happens in the upper half of the core, the total hydrogen production would be approximately 100 kg. If the average temperature of the produced hydrogen is at 1500 K, the hydrogen would pressurize the primary system (volume at 350 m^3) by 1.8 MPa (260 psi).

If water is added at a sufficiently high rate, a pressure surge would occur initially after water addition, but, because of only limited energy and hydrogen release before quench, the pressure jump would be lower than in the case with modest water addition and would not be as sustained.

During this stage, control rods (PWRs) or blades (BWRs) are expected to fail, leading to the relocation of liquified control materials. The SPNDs are potentially of use in determining when control materials have slumped to the lower portions of the core. Abnormal readings of the SPNDs could indicate redistribution of control materials, but analysis is needed to distinguish between the effect of movement of control materials and that of water inventory changes. Toward the end of this stage, it would be advisable for the operator to withdraw the movable SPNDs (Westinghouse plants) from the core region to preserve their integrity so they may be used during later stages of degradation.

Debris Bed Formation

If an accident has progressed through the stage where the peak core temperature has exceeded 2000 K, it is likely that a debris bed would have formed in the core from the relocation of liquified materials. This stage may be indicated by the failure of core exit thermocouples, which would show sudden jumps in temperature as new junctions are formed in the core.

During this stage of core degradation, the operator may want to attempt to map the axial location of the debris bed using the movable SPNDs if the pressure conditions and the state of the system would allow. (If the thimbles guiding the SPNDs are breached and their interior is exposed to primary system pressure, the SPNDs cannot be moved toward the core against the system pressure. However, the SPNDs may be inserted along unbreached

thimbles or along breached thimbles that are later resealed by relocated core materials.) As the SPNDs are inserted into the core, positions where they encounter resistance may indicate the location of the bottom crust of the debris bed. Once the geometry of the high resistance area has been mapped out by the SPNDs, the SPNDs could be withdrawn from the pressure vessel for later use as a diagnostic tool to provide information on core relocation.

For modest water addition at this stage, superheated steam at temperatures comparable to peak cladding temperatures would reach the uppermost regions of the core, resulting in additional zircaloy oxidation and hydrogen generation. The pressure transducers in the primary system should transmit a sharp rise in pressure under these circumstances. The pressure rise would also be sustained for a relatively long period due to the noncondensible nature of hydrogen.

With a high rate of water addition that allows water to reach the top of the core without being completely vaporized, shattering of the oxidized cladding in the upper regions of the core may cause a particulate debris bed to form on top of an existing cohesive debris bed, as indeed happened in the TMI-2 accident when a reactor coolant pump was restarted at 174 minutes into the accident. Even if sufficient water is added to completely cover the cohesive and particulate debris beds, there is no assurance that the beds will not continue to heat up. Once a cohesive bed has reached a characteristic size, the surface area-to-volume ratio will not permit heat removal at a rate sufficient to arrest continued heatup of the bed. Similarly, a particulate bed consisting of sufficiently fine particles, or of sufficient depth, will prevent water from penetrating its interior. Under such conditions, water addition to the core may result in deceptively little response from the instruments.

Relocation to the Lower Plenum

The relocation of core materials to the lower plenum may be indicated by signals from several instruments. First, the source range monitors, located outside of the vessel, may register a sharp increase in signal from neutrons leaking out of the vessel and scattered by concrete around the vessel. Second, back-flow of steam generated by the relocated hot materials into the cold legs may increase the temperature readings of the cold leg RTDs. Third, system pressure may increase sharply due to rapid steam and, possibly, hydrogen production. Fourth, anomalous currents may appear from the lower levels of fixed SPNDs (B&W plants) not damaged earlier in the accident.

For Westinghouse plants, the amount of relocated core mass may be estimated from responses of the movable SPNDs if this system is still capable of functioning. Assuming that the operator has withdrawn the SPNDs from the reactor vessel following mapping of the cohesive debris bed, he may now be able to move the detectors axially outside the vessel. The ability to move

the detectors axially could help identify the size of the relocated mass. If a small amount of mass has relocated, for instance, the attenuation of SPND signals as the detectors are moved further away from the lower head should resemble the attenuation characteristics of a point source. If a large amount of mass has relocated, attenuation of signals from axial withdrawal should resemble the characteristics of a planar source.

5. ANALYSIS OF ENERGY REMOVAL FROM DEGRADED CORES BY WATER ADDITION

Another element that is crucial to the understanding of the system response during water addition to degraded cores is an analysis of the amount of water that is needed to remove energy from the core and the minimum rate of water addition that would arrest core degradation and bring the reactor to a safe shutdown condition. Again, the sequence of core damage states is useful as a guide in performing such an analysis. Instead of analyzing specific accident scenarios, the core damage states could be used as reference points in determining the required amount and rate of water addition. Results of simplified analysis are discussed in this section. This involves consideration of energy sources, stored heat of degraded cores as a function of damage state, and geometry of degraded cores.

Energy Sources

The predominant energy source in a reactor after scram is the decay of radioactive materials. Another important energy source in the core is the oxidation of zircaloy by steam when the core temperature exceeds 1500 K. The energy release rate from oxidation can be considerably higher than the energy release rate from decay heat, because oxidation may take place in only few minutes and the energy release during that time interval is approximately equivalent to the energy generated by decay heat in an hour (at 1% full power). Fission heat from recriticality could also be an energy source. However, it will be assumed that administrative controls will preclude the possibility of adding unborated water to the core, so that recriticality will not be a concern.

In a small-break LOCA with no emergency core coolant injection, the reactor core generally would not be damaged until after an hour after scram. Without much loss in accuracy, the decay heat level during core damage progression could be assumed to be at 1% of full operating power [9]. For full power operations at 3000 MW_t, the decay power is enough to vaporize 20 kg/s of water at saturation. Or, in terms of decay heat removal from the core, a 20 kg/s addition of water to the core would remove the decay heat when the temperature of the core is still near or slightly above the saturation temperature of the water. This is within the injection capacity (650 gpm, or approximately 40 kg/s) of one high pressure injection (HPI) pump, assuming that most of the injected water would go through the core. If the full-capacity operation of the HPI fails to stop the core temperature from rising, either the core has progressed beyond the pre-damage stage, or most of the injected water has failed to reach the core.

The energy release from the oxidation of 1 kg of zircaloy is 6.5 MJ. At 1800 K, oxidation of 20% of the original thickness of the cladding starting from an unoxidized state would take 150 s; at 2000 K, 30 s [4,5]. (For 20% oxidation of the cladding, the remaining zircaloy would have melted and liquified substantial amounts of fuel. The parabolic oxidation rates would no longer apply.) If the cladding in the upper half of the core is oxidized uniformly at such rates, the energy release rates from oxidation are approximately 100 MW and 500 MW, respectively. At such high powers, the minimum rates of water addition that would result in having not all the water vaporized would be approximately 70 kg/s and 350 kg/s, respectively, assuming that heat transfer to the water is limited to vaporizing the water at saturation. These rates of water addition are close to, or higher than the capacity of the high pressure injection pumps (two pumps at 650 gpm each, or a total of approximately 80 kg/s). Although these water addition rates to remove energy from oxidation are conservative estimates (it has been assumed that water addition will not diminish the oxidation rate), it may be advisable to consider starting the reactor coolant pumps to deliver additional water to the core from the cold legs, or to depressurize the system to allow accumulator discharge, or low pressure injection.

Stored Heat

The amount of stored heat depends on the core damage states. The stored heat of a core at different stages of degradation, as characterized by a temperature scale, is shown in Table 1. The amount of stored heat is defined to be zero at 600 K, and the temperature in the core is assumed to be uniform. Changes in specific heats due to changes in core composition (zirconium to zirconium dioxide) and heats of fusion are included in the calculation of the stored heat.

Table 1. Stored heat of a degraded core as a function of core temperature

Temperature (K)	600	1200	1700	2400	2800	3000
Stored heat (GJ)	0	24	53	99	149	161

If the core dries out at the end of the first hour after scram, adiabatic heatup of the core from decay heat alone will drive its temperature to approximately 2800 K at the end of the second hour. At temperatures above 1500 K, oxidation of the zircaloy cladding will also add to the stored heat in the core. Incidentally, the amount of heat stored in a core at 2800 K is equivalent to the energy release from the complete oxidation of the zircaloy in the core.

The required rate of water addition to remove stored energy in the core depends on the desired rate of energy removal. Assuming that the top half of the core is at 2800 K and the bottom half at the saturation temperature

of the water, the stored energy in the core is approximately 75 GJ. (See Table 1.) This amount of energy is sufficient to vaporize 50,000 kg of water at saturation. If the stored energy is to be removed in an hour, the required rate of water addition to the core is, on the average, approximately 14 kg/s, plus the 20 kg/s that is required to remove the continuing decay heat. (It may be assumed that most of the zircaloy is oxidized, or is alloyed with the fuel, and hence unavailable for rapid oxidation, after the core temperature has reached 2800 K for some time.) Of course, the actual rate of energy transfer from the core materials to the water depends on the temperature and the geometry of the core, and any entrainment of water droplets in the steam produced.

The Effect of Geometry

As discussed in Section 3, several major changes in core geometry occur during core degradation. The core geometry first changes when the cladding of fuel rods balloons at a temperature of approximately 1100 K. The flow resistance in the blocked region of the core will be larger than that in the unblocked region of the core. Consequently, in order to prevent the blocked region from continual heatup, the total rate of flow of water through the core must be above the rate that would prevent core heatup when the rods have not ballooned. Detailed calculations are planned to determine this required enhanced flow. The results of such calculations may also be used as a guide in evaluating core exit thermocouple responses as functions of their radial positions as water is added to the core during the ballooning stage.

A second major change in core geometry is the formation of a cohesive debris bed from the solidification of relocated materials. Because water is prevented from penetrating a cohesive bed, heat is conducted from the interior of the debris bed to its surface if it remains solid, or is convected to its surface if its interior re-melts. Heat loss by a cohesive debris bed occurs only on its surface. Such a mode of heat transfer considerably limits the energy removal rate from the interior of the bed even if the debris bed is immersed in water.

A third major change in core geometry is the formation of a particulate debris bed. A particulate debris bed may form in the core from the collapse of rod remnants in the upper part of the core, often as a result of water addition to the core. A particulate debris bed may also form in the lower plenum of the vessel when molten material in the core drops into a pool of water in the lower plenum. The coolability of a particulate debris bed depends on the ability of water to penetrate the bed. The heat transfer characteristics of cohesive and particulate beds are discussed below in further detail.

6. DEBRIS BED CHARACTERISTICS

When core damage has progressed to the stage of the formation of cohesive and particulate debris beds, because the heat transfer rate from the hot debris to water may be quite limited, the rate of water addition to the core may be less important than the total amount of water added to and retained in the core. The following sections describe the results of some analyses that define critical limits of heat removal for both cohesive and particulate debris beds. These limits indicate that, during a severe core damage accident, for certain parameters of the debris beds, the interior of the beds will continue to heat up regardless of water addition. Such heatups may eventually lead to failure of the beds and result in the relocation of core materials to the lower plenum of the vessel.

Energy Removal from Cohesive Debris Beds

Critical heat removal limits (or stability limits) for cohesive debris beds are defined in this study by the thickness of the crusts around the beds. It will be assumed that crusts having thicknesses less than the critical thicknesses are unstable and will fail open to allow the enclosed molten materials to relocate. Steady-state conditions are assumed in the calculations. At the limit, the material enclosed by the crust is assumed to be molten and to comprise 3/4 of the mass of the cohesive debris bed. (In TMI-2, molten interior of the cohesive bed comprised of over 90% of the mass of the bed.) If the decay heat generated exceeds that conducted through the crust, the excess heat will melt part of the crust so that the crust will become thinner and will be assumed to fail.

The critical heat removal limits for cohesive debris beds in Figure 2 are defined by the radii and the thermal conductivities of the debris beds. Two limit curves are shown in the figure, one labeled by a power density of 3.0 MW/m^3, which is a typical power density for a bed formed approximately two hours after scram, and another labeled by a power density of 1.5 MW/m^3, which is a typical power density for a bed formed approximately 8 hours after scram. These curves delineate the stability limits of cohesive beds having those power densities. For example, if a cohesive bed having a power density of 1.5 MW/m^3 is positioned by its radius and thermal conductivity in the figure to the right of the curve characterized by the power density of 1.5 MW/m^3, it is unstable; if it is positioned to the left, it is stable.

By probing the core with the movable SPNDs as discussed in Section 4, the operator may be able to estimate the size of a cohesive debris bed. The thermal conductivity of the bed depends on the core oxidation history, but, in general, it falls between the limits of 4 W/m-K and 8 W/m-K. If the core is heavily oxidized, the conductivity will be closer to the lower limit than to the upper limit; if the core is lightly oxidized, the situation is reversed. When a size and a thermal conductivity are assigned to a debris bed, the position of the cohesive debris bed in the stability

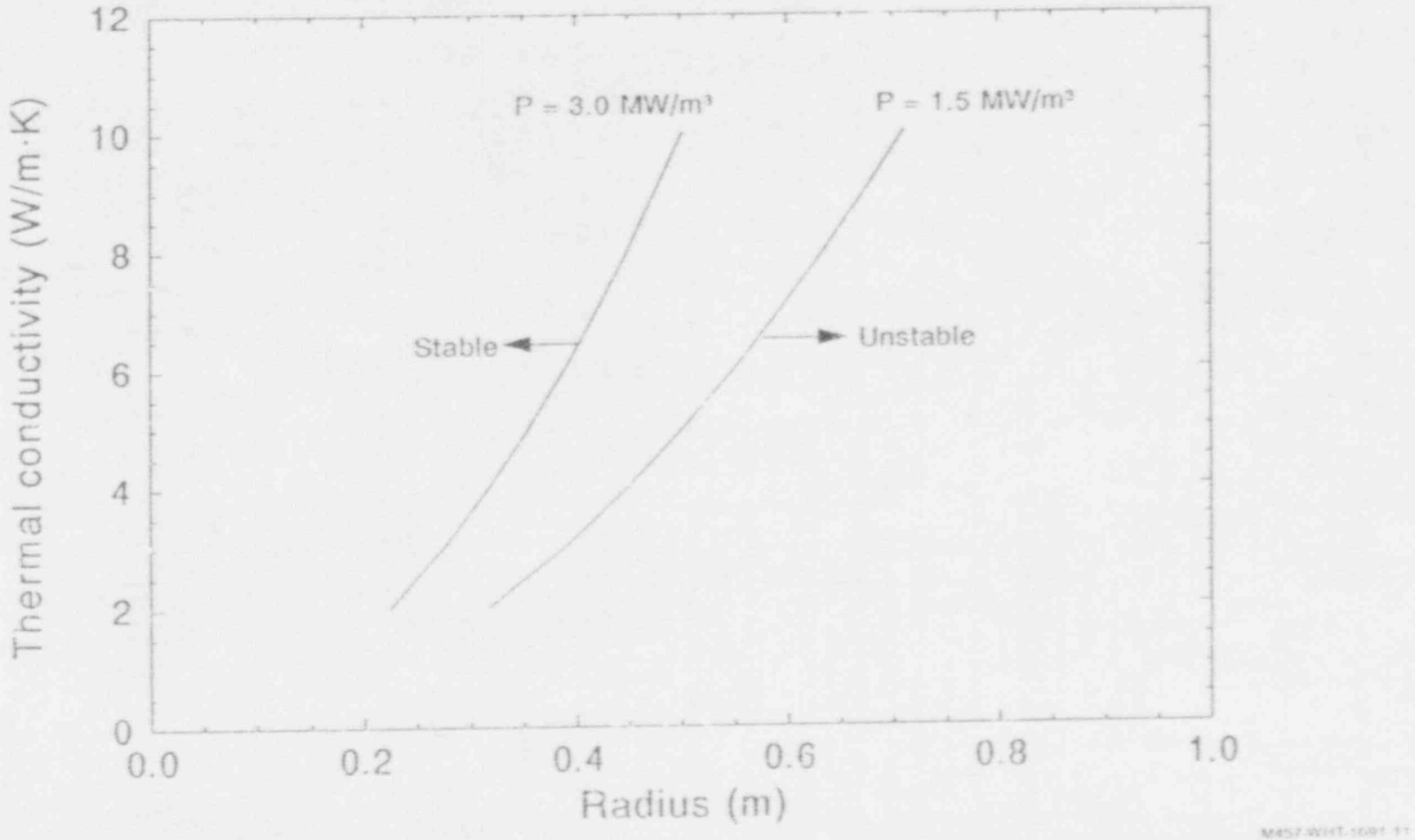

Figure 2. Power density (P) contours separating stable region from unstable region for spherical cohesive debris beds.

diagram is determined. By examining the position of the cohesive debris bed in the stability diagram in relation to the stability limit contour characterized by its power density (related to time after scram), the stability of the cohesive debris bed may be inferred.

Energy Removal from Particulate Debris Beds

The heat removal rate from a homogeneous particulate debris bed on top of an impermeable plate (e.g., the top crust of a cohesive debris bed) is determined by its porosity, the size of the particles comprising the bed, and the power density in the bed. The Lipinski model [10] is used to calculate the dryout heat flux for particulate beds in one dimension along the vertical direction. Figure 3 shows the dryout limits of particulate debris beds characterized by porosity and particle size at a system pressure of 6.9 MPa. The energy removal diagram for particulate beds is divided into regions of dryout and regions where energy can be removed from the interior of the debris bed by curves labeled by the dryout heat flux.

In the energy removal diagram for particulate debris beds, the dryout heat flux associated with each contour of dryout corresponds to the potential heat flux that can emerge from a particulate debris bed immersed in water. The heat flux could come from several sources. One source is the heat stored in the particles at elevated temperatures. Another source is the decay heat being generated in the debris bed. A third source is the heat liberated from the oxidation of zirconium in the bed when water penetrates the bed. During an accident, the size and characteristics of a particulate debris bed formed in the reactor core cannot be ascertained with existing instruments. However, if a particulate debris bed exists in the core and the interior of the bed can be cooled, steam will be generated when the water added to the core quenches the bed. There will also be a temporary increase in system pressure during the early stage of water addition when there is not yet enough water to condense the steam coming out of the particulate debris bed. If water is prevented from entering the bed, water added to the core cannot quench the bed and there will not be much of an increase in pressure because there will be little steam production.

7. SUMMARY AND CONCLUSION

The unmitigated core damage sequence presented in this study consists of: (1) Ballooning and rupture of fuel rod cladding, (2) rapid oxidation of zircaloy by steam, (3) formation of debris beds in the core, and (4) the relocation of core materials to the lower plenum of the reactor vessel. The above sequence of core damage is essentially a temperature sequence, ranging from ballooning of the fuel rod cladding at approximately 1100 K to melting of the UO_2 fuel at 3100 K. This sequence of core damage has been used as a guide in discussing the effects of water addition to degraded cores.

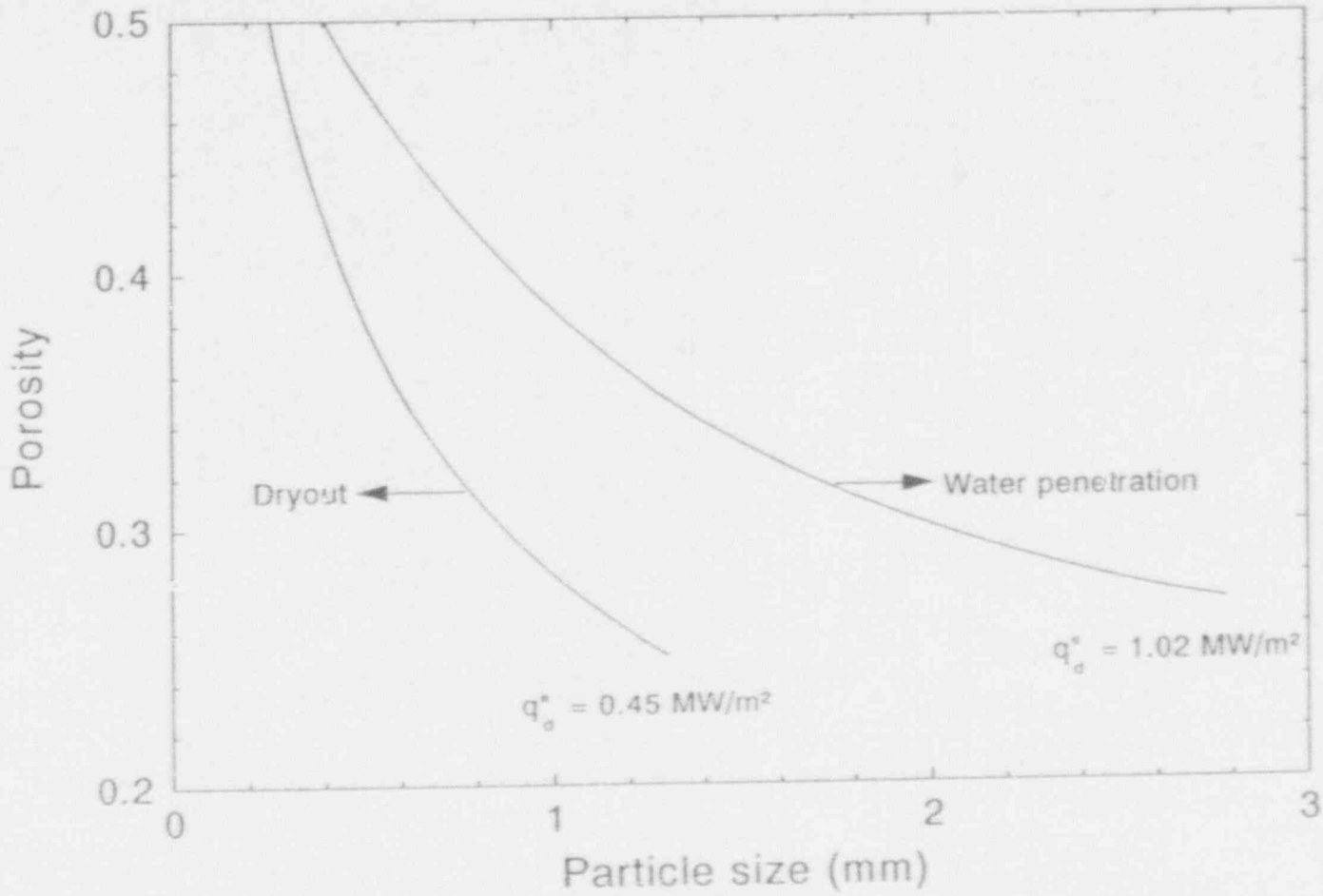

Figure 3. Dryout heat flux contours (q''_d) delineating dryout boundaries in the particle size-porosity plane for a one-dimensional particulate debris bed.

At the ballooning stage, core recovery can be assured if enough water is added, and this can be ascertained by a decrease to saturation temperature indicated by the core exit thermocouples.

If enough water is added to the core during the rapid oxidation stage, the subsequent recovery of the core, although also almost assured, will be accompanied by additional hydrogen production. Because temperature measurements would have become unreliable at this stage, confirmation of recovery of the core has to rely on measurements of system pressure and responses of the SPNDs .

Movement of significant amounts of core materials first occur when control rods, or blades, fail. Care must then be exercised that no unborated water is added to the core after the relocation of the control materials lest a re-criticality of the core occur.

If a cohesive debris bed is formed in the vessel from the relocation of core materials, complete energy removal from the interior of the bed cannot be assured even if unlimited amounts of water is added to the vessel. The energy removal from a cohesive debris bed depends on its size, the power density in the bed, and the thermal conductivity of the materials comprising the bed. During an accident, only the size the debris bed may be obtained by probing the core with the use of the movable SPNDs if these instruments are still functioning; information on the other parameters will have to rely on estimates based on accident scenarios. If remnants of fuel rods and unoxidized zircaloy remain above the cohesive bed, flooding the core will lead to rapid generation of steam and hydrogen, and also collapse of the materials to form a particulate bed.

The interpretation of the response of system pressure to water addition after the formation of a cohesive debris bed could be quite counterintuitive. Core materials may be partitioned into a cohesive bed, a particulate bed, and parts that are more permeable to water than the debris beds (intact and partially damaged assemblies). The larger the cohesive and particulate beds, the smaller would be the amount of materials that are more permeable to water. If water addition to the core produces rapid pressure rises, it is more likely the cohesive and the particulate beds are small and energy removal from their interiors can be accomplished. If there is hardly any appreciable rise in system pressure when water is added to the core, the debris beds are more likely to be large and energy removal from them will be minimal. The particulate bed may continue to heat up and melt and the crust of the cohesive debris bed may be thinned to a point that it may fail open to allow the enclosed molten materials to relocate.

Although a broad outline of core damage progression and possible instrumentation signatures at each stage of core degradation have been presented in this paper, much needs to be done to better understand the possible system responses when water is added to degraded cores. First, the effects of water addition at each stage of core degradation must be

better quantified as functions of the amount of water added to the core than what has been presented here. These include the temperature distributions at the exit of the core during the rod ballooning stage, the pressure responses during later stages, and SPND responses when core geometry changes. Second, for various accident scenarios, the stages of core degradation should be t.·J to times after core uncovery. As mentioned in Section 3, core damage could begin in less than an hour after core uncovery when emergency core cooling is unavailable. Oxidation of the zircaloy in the core can rapidly increase the core temperature to over 2000 K in a few minutes. After the rapid oxidation of zircaloy, there is a time interval of tens of minutes to an hour when the core geometry slowly changes from a rod-like geometry to one of cohesive and particulate beds. These estimates of the time intervals need to be refined by code calculations that include heat transfer between the core materials and the coolant in the core. Finally, the consequences of relocation of molten materials to the lower plenum must be considered.

ACKNOWLEDGMENT

The authors would like to thank Dr. R. R. Hobbins for reviewing a draft of the paper and for making very helpful suggestions to improve the paper. The authors are also indebted to Dr. R. J. Witt for some original ideas on instrumentation signatures.

REFERENCES

1. R. R. Hobbins, D. A. Petti, D. J. Osetek, and D. L. Hagrman, "Review of Experimental Results on Light Water Reactor Core Melt Progression," Nuclear Technology, Vol. 95, pp. 287-307, September 1991.

2. J. M. Broughton, P. Kuan, D. A. Petti, and E. L. Tolman, "A Scenario of the Three Mile Island Unit 2 Accident," Nuclear Technology, Vol. 87, pp. 34-53, August 1989.

3. C. M. Allison and S. T. Polkinghorne, "SCDAP/MOD1 Analysis of the Progress'on of Core Damage during the TMI-2 Accident," EGG-SAR-7104, November 1985.

4. R. E. Pawel, J. V. Cathcart, and R. A. McKee, "The Kinetics of Oxidation of Zircaloy-4 in Steam at High Temperatures," Electrical Chemical Science and Technology, Vol. 126, No. 7, July 1979.

5. V. F. Urbanic and T. R. Heidrick, "High-Temperature Oxidation of Zircaloy-2 and Zircaloy-4 in Steam," Journal of Nuclear Materials, Vol. 75, pp. 251-261, 1978.

6. R. O. Gauntt, R. D. Gasser, and L. J. Ott, "The DF-4 BWR Control Blade/Channel Box Fuel Damage Experiment," Draft, NUREG/CR-4671, SAND86-1443, March 1988.

7. P. Hofmann, S. J. L. Hagen, G. Schanz, and A. Skokan, "Reactor Core Materials Interactions at Very High Temperatures," Nuclear Technology, Vol. 87, pp. 146-186, August 1989.

8. P. Kuan, J. L. Anderson, and E. L. Tolman, "Thermal Interactions during the TMI-2 2-B Coolant Pump Transient," Nuclear Technology, Vol. 87, no. 1, August 1989.

9. ANSI/ANS-5.1, 1979 Decay Heat Standard for Light Water Reactors.

10. R. J. Lipinski, "A Coolability Model for Post-Accident Nuclear Reactor Debris," Nuclear Technology, Vol. 65, pp. 53-56, April 1984.

U.S. NUCLEAR INDUSTRY APPROACH TO SEVERE ACCIDENT MANAGEMENT GUIDANCE DEVELOPMENT AND IMPLEMENTATION

David Modeen
Nuclear Management & Resources Council

Larry Walsh
New Hampshire Yankee

Richard Oehlberg
Electric Power Research Institute

SUMMARY

The purpose of this paper is to discuss the United States nuclear industry activities occurring under the auspices of NUMARC, to define, develop and implement enhancements to utility accident management capabilities. This effort consists of three major parts:

1. Development of a practical framework for evaluation of plant-specific accident management capabilities and the subsequent implementation of selected enhancements.

2. Development of specific technical guidance that addresses arresting core damage assuming it occurs, either in-vessel or ex-vessel, and maintaining containment integrity. Preventing inadequate core cooling or minimizing the public exposure from offsite releases, while considered to be candidate areas for accident management enhancements, have been the subject of intense previous study and development.

3. Plant-specific implementation of accident management enhancements in three areas: (1) personnel resources (organization, training, communications); (2) systems and equipment (restoration and repair, instrumentation, use of alternatives); and (3) information resources (procedures and guidance, technical information, process information).

The integrated evaluation and application of insights from prior probabilistic risk assessments, plant-specific analysis, such as the Individual Plant Examination, and other industry and government programs, provide a means of improving a plant's integrated capability to respond to rather unlikely, yet potentially severe, events.

At the same time, a very important question yet to be answered in the industry activities is what constitutes an appropriate allocation of utility resources to this effort relative to other plant priorities, and how one judges "success" in implementation of these enhancements.

To assure a common understanding of the key terms used in this paper, a list of definitions is provided at the end of this paper in Table I.

INTRODUCTION AND OVERVIEW

In its Policy Statement on Severe Reactor Accidents [1], the U.S. Nuclear Regulatory Commission (NRC) stated that "operating [U.S.] nuclear power plants require[s] no further regulatory action to deal with severe accident issues unless significant new safety information arises to question whether there is adequate assurance of no undue risk to the public health and safety." The value of each licensee conducting a "limited-scope, accident safety analysis to discover instances (i.e., outliers) of particular vulnerability to core melt or to unusually poor containment performance, given core melt accidents," was also recognized.

In November 1988, NRC staff issued Generic Letter 88-20, "Individual Plant Examination for Severe Accident Vulnerabilities - 10 CFR § 50.54f." [2] In that document, besides requesting each plant perform a systematic examination to identify any plant-specific vulnerabilities to severe accidents, the NRC staff stated its intent to request at a later date that licensees apply the insights gained from these analyses to enhance their existing capabilities, collectively referred to as accident management capabilities, to prevent or mitigate severe accidents.

Consistent with the Commission finding in 1985, an important, initial precept of the industry effort is that **the existing utility organizational and emergency planning structure is adequate and accident management plans, to varying degrees, are already integrated into daily plant operations.** The question that remains to be answered is to what extent the accident management capabilities may be effectively and efficiently enhanced?

Many of the existing capabilities for assessing and responding to accident situations in place today are a direct result of the lessons learned by the industry and NRC staff from the Three Mile Island accident which occurred over twelve years ago. In the pursuit of excellence, and encouraged by a high level of management commitment, emergency planning has continued to evolve into a highly visible, high priority part of U.S. plant operations. For example, the following list of facilities, equipment or programs pertinent to the execution of an emergency plan exist today:

(1) Emergency response facilities and systems designed for the prevention, assessment and mitigation of transients and accidents.

(2) Sophisticated data collection systems, such as Safety Parameter Display Systems (SPDS), to serve as tools for plant staff identification, assessment and mitigation of transients and accidents.

(3) Detailed, extensive Emergency Operating Procedures (EOPs), including entry points based upon symptoms rather than necessitating correct event classification, have been developed based on operating experience and the collective knowledge of U.S.

industry groups involved in their composition, review and improvement.

(4) Improved communications technology for enhanced response of off-duty personnel and the sharing of plant and site status among physically separated facilities.

(5) Accredited training programs for plant operators and shift technical advisors, that include an integrated approach toward the EOPs, use of the SPDS and emergency plan implementing procedures, and related training for emergency response personnel.

(6) Quality assurance audit programs to assess major elements of the emergency preparedness program.

(7) Performance assessments, such as drills and exercises, to test and improve the plant staff response capability.

As discussed in the following sections, the U.S. nuclear industry has undertaken the development of generic accident management guidance that, along with plant-specific information, will support utility efforts to enhance their accident management (AM) capabilities. Achieving NRC staff acceptance, by reference in a generic letter, of the industry approach toward enhancement of utility accident management capabilities, is expected. Periodic meetings with NRC staff are being held to permit discussion of draft materials as they are developed by industry and allow NRC staff to provide feedback on industry's products as well as their own research.

U.S. INDUSTRY ORGANIZATIONS AND ROLES

In July 1988, NUMARC established a Severe Accident Working Group (SAWG) to coordinate industry activities and serve as the focal point for industry-NRC interactions in attaining resolution and closure of the severe accident issue. Individuals from selected utilities, as well as industry organizations, such as the Electric Power Research Institute (EPRI), the Institute of Nuclear Power Operations (INPO), and the four NSSS Owners Groups and their contractors, are actively involved. NUMARC coordinates these efforts with other related industry activities in order to avoid duplication and to attain a unified industry approach.

The industry concurs with the NRC staff view that enhancements to existing accident management programs to address prevention and mitigation of severe accidents at plants could be beneficial. Recognizing the close link between the clearer perspective regarding severe accidents that many utilities will achieve through performance of an IPE and the capabilities of plant staff to respond to a severe accident, the SAWG established the following objective:

> Provide for systematic and efficient implementation of certain insights and results from an IPE and other relevant information regarding severe accidents for the purpose of preplanning and enhancing a utility's capabilities during an accident to take preventive and mitigative actions.

In August 1989, the first product of the industry effort, the EPRI-developed draft "Guidelines for Evaluating Accident Management Capabilities" (now titled "A Process for Evaluating Accident Management Capabilities"), was issued. It provides a flexible framework for assessing the overall AM program for an individual site [3], to the NRC staff and utilities. Recognizing the need for specific technical guidance in order to complete an evaluation process and the economic benefits of a more coordinated effort, a second phase to develop explicit technical accident management guidance, relying heavily upon several EPRI projects underway, was initiated. As a result, in January 1990, the NUMARC Joint Owners Group Accident Management Advisory Committee (JOG AMAC) was established to effectively utilize the industry's knowledge and expertise in developing generic technical AM guidance while minimizing the financial and manpower burden on individual utilities. The scope of what they were to develop was the following:

(1) EPRI developing a generic "Severe Accident Management Guidance Technical Basis Report" (SAMG TBR),

(2) Each owners group developing owners group-specific severe accident management guidance by taking advantage of the EPRI SAMG TBR, and

(3) Individual utilities developing and implementing an appropriately enhanced plant-specific accident management capability, taking into account the IPE results, self-evaluation results (using for example the self assessment guidelines), and the owners group-specific accident management guidance.

While assessing the opportunity for enhancement to existing accident management capabilities is considered a beneficial activity, it is also one with provisions that can easily extend beyond what is warranted. Therefore, the JOG AMAC program not only guides development of the applicable technical basis, but is intended to: (i) ensure continued support by the industry at large, (ii) define a level of consistency desired by the individual owners groups, and (iii) provide a level of emphasis in balance with other plant staff priorities.

DEVELOPMENT OF GENERIC ACCIDENT MANAGEMENT GUIDANCE

To accomplish the objective of providing constructive, yet practical and balanced recommendations for enhancing plant accident management capabilities, issues such as level of verification and validation, operator responsibility for AM information on requalification exams, level of detail, etc., are addressed in order to bound the scope of the AM guidance consistent with the intent of the Commission's Severe Accident Policy Statement. The JOG AMAC suggested scope and minimum recommended level of implementation in the areas encompassed by SAMG are provided in a separate paper [4]. These positions have been reviewed and accepted by the NUMARC SAWG.

The "Severe Accident Management Guidance Technical Basis Report" is being developed for the NUMARC Joint Owners Group Accident Management Advisory Committee. It is intended to provide an industry-wide consistent technical basis addressing issues from the onset of core damage and beyond, consistent with the current state of technical knowledge. It is to be used for

development of owners group accident management guidance, from which individual utilities can develop plant-specific accident management guidance.

The EPRI SAMG TBR consists of two volumes. The first contains the technical basis for severe accident management guidance. The second volume consists of appendices supplying supporting information and technical detail. The first volume begins with an introduction, delineates three Reactor Coolant Systems (RCS) and four containment conditions descriptors. These descriptors and associated symptoms are designed to allow the plant staff to determine the plant status relative to the evolution of a particular accident without reference to pre-determined sequences. RCS/containment descriptor pairs are used to describe the system once a severe accident is underway. The next section of Volume I addresses fourteen "Candidate High Level Actions." It is anticipated that the owners groups will use these Candidate High Level Actions to devise strategies for their plants. These High Level Actions are generic operational actions which the plant staff could take (if equipment is available) under varying circumstances. The effects of these actions are documented under varying plant conditions described by RCS/containment condition pairs. Finally, special considerations are discussed, where appropriate, for converting action(s) into strategies.

Volume II consists of about 30 appendices. These appendices have a consistent format documenting the purpose of the appendix, relevant analytical information, relevant experimental information, details relevant to the technical basis, a summary, and References. Areas covered by these appendices include Core Integrity (Core Overheating), Primary System Integrity, Containment Integrity, and Mitigation of Release.

The effects of uncertainties are reflected in the "effects" tables of Volume I for the Candidate High Level Actions and as needed in the backup material of Volume II. References [5] and [6] discuss some example technical considerations.

To assure quality and completeness of the information in a form conducive to further development by the owners group, the work is being thoroughly reviewed by an engineering design review group consisting of members from academia, consulting companies, and each of the four owners groups. The most recent review of the main body of the report was completed on September 5. It was subsequently provided to NRC staff for comment on September 17, 1991.

The vendor owners groups are responsible for assessing and/or developing owners group-specific guidance in two discrete areas:

(1) Enhancement of the existing owners group-specific Emergency Procedure Guidelines (for BWROG and CEOG), Emergency Reference Guidelines (for WOG), or Generic Emergency Operating Guidelines (for B&WOG), up to the point of core damage, as appropriate (from hereon referred to collectively as EPGs); and

(2) From core damage through achievement, if possible within existing resources, of a stable condition.

The first area covers the actions of plant staff up to the onset of core damage, which are generally associated with the procedural tasks developed from the EPG and identified in plant-specific EOPs. Although there are differences in structure and nomenclature among the owners group-specific guidelines, the major objectives of each remain the same: control of reactivity and prevention of inadequate core cooling. Nonetheless, variations do exist in vendor designs and the development process. Consequently, although we will strive toward consistency in function, we anticipate differences in structure and implementation.

Each owners group has assessed the treatment by their particular EPGs of the accident management strategies outlined in NRC Generic Letter 88-20, Supplement 2, "Accident Management Strategies for Consideration in the Individual Plant Examination Process." It is expected that any further work will draw heavily from IPE insights and NSSS-specific designs and analyses. Owners groups will consider changes to the EPGs and their associated technical basis documents as a result of issues identified through the owners group-specific EPG Maintenance Feedback programs (IPE insights) or as a result of the assessment of interfaces between the EPGs and proposed SAMGs.

For the second area, onset of core damage and beyond, development of owners group-specific SAMG will be based principally upon the EPRI SAMG TBR and within the guidance of the accident management administrative scope and content positions. The understanding of severe accident phenomena relative to plant damage conditions and candidate accident management actions to be provided in the EPRI SAMG TBR should allow the owners groups to develop specific strategies that encompass the dominant severe accident challenges for each class of plants. Although a level of consistency among owners groups is a likely byproduct of the industry approach to resolution of the accident management issue, there will be no forced consistency or uniformity. As noted above, each owners group is embarking in the severe accident management area with preexisting constraints, such as vendor specific EOPs and accredited plant staff training programs.

UTILITY IMPLEMENTATION - Items for Consideration

The culmination of the industry development effort is the efficient utility integration and application of the generic industry accident management guidance documents with plant-specific information in order to identify and implement appropriate enhancements to existing plant capabilities. The objective of the U.S. industry's accident management guidance development effort is to provide for the efficient augmentation of these existing emergency preparedness entities, especially as they relate to stabilizing and recovering the reactor plant. It is anticipated that a utility interdisciplinary team, with representation from engineering, probabilistic safety assessment, training, operations, and emergency planning entities could adequately evaluate their plant's current severe accident management capabilities and the need for any enhancements.

Central to a utility's approach to accident management implementation is the plant-specific assessment of the existing capabilities within the context of severe accident response. The draft EPRI/NUMARC "A Process for Evaluating Accident Management Capabilities," may serve as an acceptable method for

integrating this information. The evaluation process assists the utility in integrating the wide variety of resource materials, including the owners group accident management guidance, results of NRC research projects, plant specific information, and any other technical information that is developed in support of this effort. This process is not unique, and we believe there are other approaches that would lead to implementation of an appropriate severe accident management program.

At the OECD/CSNI Specialists Meeting on Severe Accident Management Program Development in September 1991, Dr. Brian Sheron of the USNRC noted, and we agree, the responsibility to respond to a severe accident challenge, although highly unlikely, is solely that of the licensee. Actions by plant staff will have to be taken, regardless of the status of the USNRC's severe accident research program elements and the remaining areas of uncertainty. He also made several other observations very relevant to the issue of utility implementation of specific accident management guidance. They are:

1. Accident management is not a guarantee for mitigation.

2. If a severe accident occurs, it is highly unlikely that it will follow a well-prescribed, previously analyzed scenario. Hence, AM programs must be robust and flexible to allow plant staff to deal with unanalyzed or unevaluated scenarios.

3. We should not disillusion ourselves by going beyond our current level of technical understanding. Analysis should not focus on highly stylized scenarios and levels of accuracy inconsistent with existing phenomena uncertainties.

4. A major element of accident management is developing technically sound high level actions and strategies for managing beyond design basis accidents, and procedures and guidance for implementation. However, one should recognize that analysis of AM strategies must be approached in the opposite manner from conventional accident analysis:

   - First, identify the functionally desirable action,

   - Second, the range of conditions that could exist when the functionally desirable action could be taken must be established, and

   - Lastly, consequences of the action over the range of conditions must be evaluated.

5. While a key element is an effective method of transfer from symptom-based EOPs to an AM program, an equally important element is the integration with emergency preparedness programs.

6. AM is only as effective as the ability to carry it out. Practice drills that employ the AM program are a necessary part of success.

In general, we agree with the perspective offered by Dr. Sheron. That said, one asks how should those remarks be specifically interpreted and acted upon? Within the context of the industry effort to date, the charge to each utility is clear: (1) it is responsible for responding to any transient or accident that challenges plant safety, including degraded core events; (2) it must act in the face of uncertainties surrounding severe accident knowledge, because the scientific community will not have all the answers in the foreseeable future; and, (3) it is time to take significant steps toward implementation. With this in mind, let us assess each of Dr. Sheron's points as it relates to the industry (and utility) accident management programs.

Regarding the first three points, one must keep in mind the genesis of the severe accident management concept. From the industry's perspective, the last eleven years of research and current performance of IPEs provide the opportunity to further reduce the risks of nuclear power plant operation. This will occur in two steps: (1) changes to plant hardware and procedures to either eliminate/reduce the likelihood of event initiators or provide for their mitigation; and (2) development of guidance to address severe accident challenges that are currently not part of a typical licensee's emergency preparedness scope. In both instances, we are pushing the concept of defense in-depth beyond the traditional plant design basis. This is acceptable, as long as one is vigilant that this is a mutual effort, being pursued as diligently by the industry as it is by the NRC staff. Correspondingly, severe accident management is not an area in need of, nor conducive to, prescriptive regulatory criteria. Rather, flexibility and adaptability are necessary. Incremental enhancements to the existing plant infrastructure (e.g., personnel training, available guidance, calculational aids, minor hardware modifications) is all that is appropriate to address what are admittedly extremely low likelihood events.

Regarding the 4th point, we believe another way to state this is to say accident management requires a focus on success. This is logical, because a plant's staff will steadfastly attempt to terminate an accident (success), and will not rest until that is achieved. The structure of the SAMG is such that the decision to apply a strategy is for the most part independent of the need for a detailed understanding of the event. Rather, based on the RCS and containment descriptors, a prioritized list of actions can be considered for implementation. To some extent there will be uncertainty with respect to the effectiveness of those actions, especially for a few phenomenological issues. As much as possible, the generic EPRI guidance attempts to take an operational view, and where uncertainties would not make a difference in the action recommended, limits the consideration of those uncertainties. One must make the distinction between wanting to understand analytically, time-step by time-step, a melt progression sequence versus responding to an actual severe accident event. The information and level of precision necessary to achieve success noted above is all that is required. Anything more is superfluous. In other words, if by considering the credible range of views or uncertainties on a particular phenomena one would not be expected to appreciably alter the decisions and actions that one should take in responding to a given set of plant conditions, there is limited value in pursuing these differences.

Points #5 and #6 provide clear evidence as to why the industry is approaching the elements of training and decision-making very deliberately.

Utility resources are finite. Conducting more training in the severe accident area places pressure on utility staffs to perform less training in other areas. The relative worth of each training session must be carefully evaluated. Practicing response to extremely low likelihood events is not likely to be nearly as beneficial to overall plant safety and operation as practicing to handle the more likely plant challenges.

Decision-making relates executing the proper and unambiguous command and control authority during an emergency. As noted in the introductory section, emergency preparedness has received a great deal of scrutiny and enhancement since the TMI-2 accident in 1979. The industry believes the existing utility organizational and emergency planning structure is adequate and accident management plans exist. At this time, it is appropriate to identify the specific aspects of severe accidents that may challenge effective implementation of the emergency plan. Yet, we do not envision the severe accident issue justifying change to the existing emergency preparedness structures. We do agree with Dr. Sheron that practicing the application of the features of a severe accident management program is necessary in order to have confidence that it can be carried out in a time of crisis.

Since training and decision-making relative to severe accident considerations and emergency preparedness can involve so many more plant personnel beyond the Operations Department, what is feasible and practical to do requires careful consideration. In early 1992, we anticipate forming an ad hoc advisory committee to address specific aspects of each of these elements, especially in light of the owners group guidance being developed. The ad hoc advisory committee will assess what should be done in this area as it specifically relates to the accident management issue.

SUMMARY

The status of onsite accident management preparedness and the ability to manage complex transients or potential severe accidents is better now than at any time in the past. Plans and resources have evolved through years of plant and industry operating experience, lessons learned from drills and exercises, and advancements in technology. Established utility programs ensure such capabilities are maintained.

Nevertheless, the U.S. nuclear industry is now on the threshold of advancing that state-of-preparedness by systematically applying the insights gained from over a decade of probabilistic safety assessment and severe accident phenomenology studies. It should be left to each utility to determine what to implement from the generic accident management guidance documents. The NUMARC effort, although intended to provide an effective and efficient accident management implementation process, does not obligate the U.S. utilities to any particular course of action or level of detail. Other approaches are available and given our level of understanding of the severe accidents and the level of public safety currently provided by the existing plants, are believed to be adequate.

TABLE I - SEVERE ACCIDENT DEFINITIONS

Severe Accidents are those that result in catastrophic fuel rod failure, core degradation and fission product release into the reactor vessel, containment or the environment.

Accident Management refers to actions taken during the course of an event by the plant operating and technical staff to: (1) prevent the event from progressing to core damage; (2) terminate core damage if it begins; (3) maintain containment integrity for as long as possible; and (4) minimize offsite releases. Severe accident management is a subset of the above, addressing the latter three phases.

The EPRI/NUMARC A Process for Evaluating Accident Management Capabilities provides utilities a candidate approach for identifying plant-specific enhancements to a particular plant's existing accident management capabilities.

Utility Accident Management Plan outlines the actions to be pursued by the utility to enhance its existing accident management capabilities and is comprised of:

- A schedule for the development and implementation of the AM enhancements.
- A delineation of responsibilities within the utility organization for developing and implementing the AM enhancements.

The EPRI Severe Accident Management Guidance Technical Basis Report (SAMG TBR) will be developed by EPRI to generically define the technical bases of AM guidance. This will serve as a consistent technical basis from which each NSSS owners' group can develop **Severe Accident Management Guidance** for use by individual utilities.

Owners group-specific Severe Accident Management Guidance (SAMG) is to be developed by each NSSS owners group to facilitate diagnosing and arriving at a safe stable state following a severe accident including the mitigation of possible radioactivity releases. These guidelines may be used by individual utilities to develop plant specific **Utility SAMG**.

Utility Severe Accident Management Guidance (USAMG) is the plant-specific guidance developed to assist the plant operating and technical staff in implementing strategies for the best use of the existing plant capabilities to diagnose, respond to, and recover from a severe accident.

TABLE II - REFERENCES

1. "Policy Statement on Severe Reactor Accident Regarding Future Designs and Existing Plants," U. S. Nuclear Regulatory Commission, Federal Register 50FR32138, August 8, 1985.

2. D. M. Crutchfield, "Individual Plant Examination for Severe Accident Vulnerabilities," U.S. Nuclear Regulatory Commission Generic Letter 88-20, November 23, 1988.

3. G. Boyd and S. Lewis (SAROS), R. Oehlberg (EPRI), and D. Modeen (NUMARC), "A Process For Evaluating Accident Management Capabilities," American Nuclear Society (ANS) Nuclear Reactor Safety Division, International Topical Meeting on Safety of Thermal Reactors, Portland, Oregon, July 1991.

4. "Draft Severe Accident Management Issue Resolution Paper," Nuclear Management and Resources Council (NUMARC), April 1991.

5. R. Oehlberg (EPRI), R. Henry (FAI), and D. True (ERIN), "Practical Considerations in Accident Management," ANS Nuclear Reactor Safety Division, International Topical Meeting on Safety of Thermal Reactors, Portland, Oregon, July 1991.

6. J. Chao, E. Fuller, A. Machiels, and R. Oehlberg (EPRI), "Technical Issues in Developing Severe Accident Management Guidance," CSNI/OECD Specialist Meeting on Severe Accident Management, Rome, Italy, September 1991.

A STRUCTURED APPROACH TO INDIVIDUAL PLANT EVALUATION AND ACCIDENT MANAGEMENT

G. T. Klopp — Commonwealth Edison Company

ABSTRACT

The need for long term development of accident management programs is acknowledged and the key tool for that development is identified as the IPE Program. The Edison commitment to build an integrated program is cited and the effect on the IPE effort is considered. Edison's integrated program is discussed in detail. The key benefits, realism and long term savings, are discussed. Some of the highly visible products such as neural network artificial intelligence systems are cited.

INTRODUCTION:

The NRC's generic letter 88-20 and its various supplements provide the industry with clear requirements for performing Individual Plant Evaluations (IPE's) in support of severe accident issue resolution. The IPE's are part of a well thought out effort for achieving such resolution which includes programs for severe accident research, containment performance improvement assessments, consideration of external events, and, ultimately, the development of accident management programs. Indeed, we note that the NRC requirements for the conduct of the IPE's have the industry identifying those obvious accident management insights which surface during the performance of the IPE's. Subsequent dispositioning of those insights is expected to take place in the context of the IPE process rather than waiting for later accident management program development.

That development is ongoing and involves a cooperative effort between the NRC and the industry's Nuclear Utility Resources Management Council (NUMARC). Much work has already been done by NUMARC to explore the issues associated with accident management program development. The NRC and its contractors have also done a great deal of very useful work in developing the framework for program development.

Edison, however, noted early that their was no consensus on the definition of the term "accident management." Naturally, there was no consensus on the required scope and depth of the associated programs to be developed. Indeed, significant disagreement existed within the overall community on all key aspects of the issue.

Edison had the benefit of many years of exposure to the severe accident question starting with the Zion Probabilistic Safety Study and continuing through the course of the Industry Degraded Core Program (IDCOR). This depth of experience allowed Edison to take a critical look at the issue of accident management program development. In particular, Edison was able to evaluate the issue in the context of its own, existing emergency measures at each station. These ranged from the emergency operating procedures (EOP's) through the emergency plan (GSEP) itself. At the same time, Edison was looking at the expanded NRC requirements for IPE's which grew dramatically from the simple IDCOR IPE Methodology. These considerations led Edison to conclude that a major resource investment was being mandated by the IPE and probable, future accident management requirements. Edison had to consider means to gain the most from the required IPE program and to gain the most efficient use of the resources expended.

EDISON PROGRAM DEVELOPMENT HISTORY:

Edison recognized that the first, crucial step in treating the development of any accident management program involved obtaining a clear definition of what the term itself meant. Fortunately, past work with IDCOR, the experiences of key personnel with emergency plan exercises, and overall company philosophy led to a comprehensive definition without any need for extensive internal discussions. For Edison, accident management is defined as: "those activities and measures undertaken and in place to prevent an off-normal event; prevent such an event from becoming a core damage accident should it occur; prevent a core damage accident from rupturing the reactor vessel if it occurs; prevent a core damage accident with failed reactor vessel from failing the containment; and if containment should fail, minimize the radioactive releases to the environment. (Figure 1) This, we recognize, is a broad definition of accident management. The deliberate choice of such an approach was based on a perceived need to insure that all aspects of the issue were addressed with no

FIGURE 1

WHAT IS ACCIDENT MANGEMENT?

*ACTIVITIES TO PREVENT A CORE DAMAGE EVENT

*ACTIVITIES TO PRESERVE THE RX VESSEL GIVEN A CORE DAMAGE EVENT

*ACTIVITIES TO PREVENT CONTAINMENT FAILURE GIVEN A RX VESSEL FAILURE

*ACTIVITIES TO MINIMIZE RADIOACTIVE RELEASES GIVEN CONTAINMENT FAILURE

"gaps" which might decrease the effectiveness of our efforts.

Given the definition of accident management, the next task was the reconciliation of the IPE mission with the task of developing the **program definition** for accident management. In this case, Edison recognized that major building blocks were already existent in the EOP's and the GSEP. What was needed was an evaluation of these two program elements in the context of the growing body of knowledge regarding severe accident behavior; a search for "gaps" between these two; and an incorporation of the pertinent insights from the IPE Program. (Figure 2) Further thought yielded the conclusion that the IPE's themselves would provide an assessment of the EOP's if adequate human interaction modelling were performed.

At this same time, there developed a growing recognition of the need for evaluations which were based on realism to a previously unparalleled degree. The results of the IPE and the accident management program definition are intended to be used operationally. Indeed, they are projected to be used in the most critical and least practised operational area of all, severe accidents. Lastly, there was clear recognition of the fact that Edison could not begin to afford two, largely duplicative programs requiring the resource commitment of the IPE Program.

Edison therefore decided, early in the IPE process, to integrate the development of the accident management program definition with the conduct of the IPE Program. In addition to addressing the issues noted above, this process makes maximum use of the IPE analyst's abilities to develop ideas and helps insure that ideas may be captured while they are fresh and in a well understood context.

The importance of this last aspect cannot be overstressed. The individuals working with the IPE materials on a daily basis will develop a real and intimate understanding of what the IPE is revealing about a given plant. If they are carefully charged with the task of **really** thinking about what they are developing, a wide spectrum of insights and ideas will present themselves. These can be captured and utilized for both the development of IPE insights and for the development of accident management insights given an appropriately structured program. Conversely, it will be very difficult to re-visit the IPE, re-interview the analysts, and recapture these insights 6 months or a year after the IPE is completed. Many of the better thoughts will

FIGURE 2

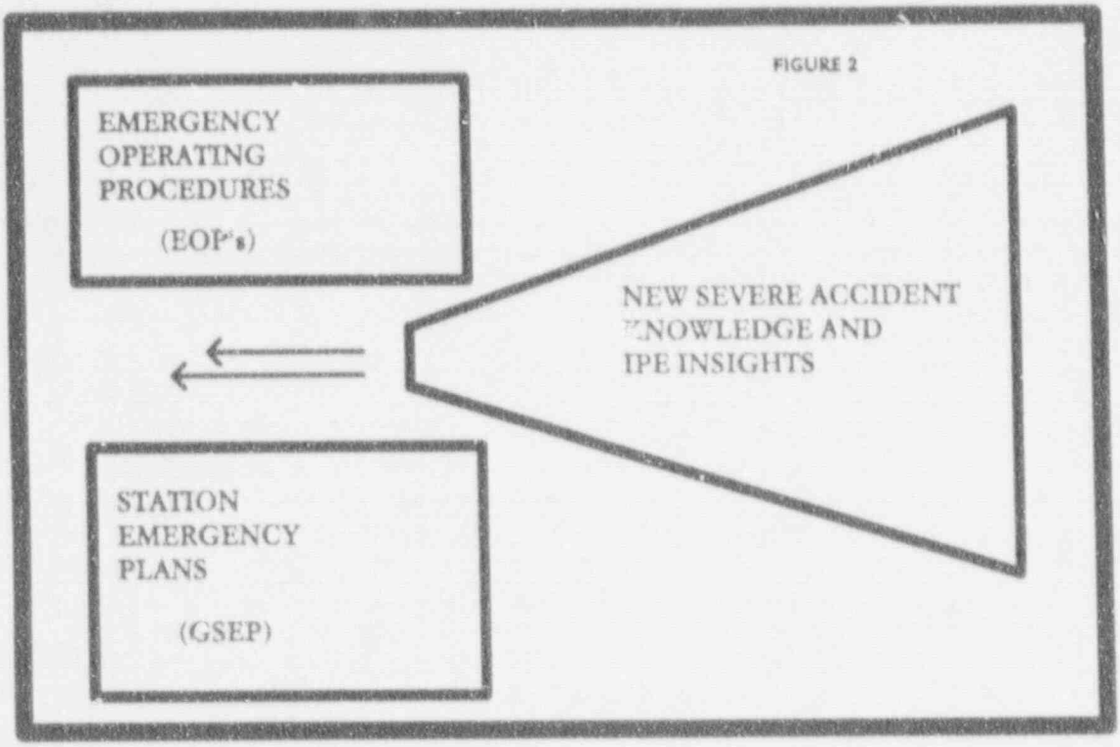
EMERGENCY
OPERATING
PROCEDURES
(EOP's)
NEW SEVERE ACCIDENT
KNOWLEDGE AND
IPE INSIGHTS
STATION
EMERGENCY
PLANS
(GSEP)

have been forgotten. In addition, unless the IPE process is appropriately structured, many important accident management insights will never be developed at all since the focus of people's thinking will be narrow, aimed just at the desired IPE product. In such cases, re-visiting the issue later will reveal even less.

So, Edison recognized the need to integrate the two program efforts and the need to structure the IPE so as to facilitate the development of a rich field of insights in both areas. That decision is both profound in its implications and challenging in its implementation. Edison is "jumping the gun" on the rest of the nuclear community in the development of an accident management program definition. This means that our efforts have to be good enough and comprehensive enough to encompass any of the good ideas which may surface from the NUMARC and owners groups efforts. Edison plans to, at worst, perform some simple comparisons to show the NRC that we have covered all the key points others may bring up in the future. Naturally, we will be following the NUMARC work as it evolves and we will be trying to insure that our efforts do not miss anything fundamental.

Part of the challenge stems from the current state of development of accident management material available to the industry in general. Much of this resembles a shotgun blast of ideas involving infant strategies, lists of questions for the review of existing tools (such as EOP's), and a veritable host of definitions for accident management itself. The most cogent, useful material initially available came from the NRC and its contractors. The identification of the 5 elements of accident management by the NRC appears ingenuously simple (Figure 3) but, is, in reality, very profound and far reaching. It permits the examination of the accident management issue from a number of different angles and helps to insure consistency and completeness within any well thought out program development effort. Edison has found that this identification, coupled with the basic definition of accident management noted earlier, provides a solid foundation for program definition and development.

How, then, has the Edison program developed? First of all, the process of development has, itself, evolved as time went on and work was accomplished. Today, we look at the Edison process as one which centers around detailed level 2 PRA's for each plant. These PRA's emphasize realism in their depiction of plant responses to various events. As a result, literally hundreds of transient analyses are run for each

FIGURE 3

ACCIDENT MANAGEMENT ELEMENTS

* ORGANIZATION
* STRATEGIES
* TRAINING
* COMPUTATIONAL TOOLS
* INFORMATION

plant using the Modular Accident Analysis Program (MAAP. In addition, the systemic interactions between the systems designed to protect the core, the core, the systems designed to protect the containment and the containment are explicitly depicted in plant response trees (PRT's), a form of integrated event tree. The actions of plant personnel, as set forth in the EOP's, are explicitly modelled in these PRT's. Naturally, we are identifying and addressing the relevant phenomena and associated uncertainties. Where these uncertainties have been of particular interest to us, we have conducted specific experiments for Edison plants to reduce the levels of uncertainty. The result is a set of solid IPE's for each station.

Next, we have considered how to extract accident management program definition from the IPE's and other, relevant information. (Figure 4) Edison has concluded that the way to extract insights, be they IPE insights or accident management insights, from the IPE is to "pause" the IPE at key choke points and survey the key analysts for concerns, ideas, thoughts, etc. A structured set of survey questions has been developed to guide this effort for each type of insight. A process has been put in place to collect, sort and aggregate these insights.

Secondly, Edison wanted to insure that the larger picture was not lost in the detail coming from the IPE's. Also, a means was needed to identify, early, those long lead time items which might appear as a natural part of the accident management program definition. A process was developed and employed for a "logical-intuitive" top down look by experienced people using the 5 elements of accident management as a base.

Thirdly, Edison was somewhat concerned at the thought of all these experienced plant engineers developing all these ideas for use by a wide variety of other people. Some non-engineering "sanity check" was clearly in order given the wide departure from the norms of power plant considerations involved in these deliberations. Edison employed a behavioral scientist to provide a "task analysis" of the key emergency plan tasks related to accident management under current program plans. That same person also, then, evaluated the tasks to be performed under the requirements imposed by proposed or likely accident management plan adjustments resulting from the increased state of knowledge associated with IPE's and from the proposed long lead time items derived from the top down look at accident management.

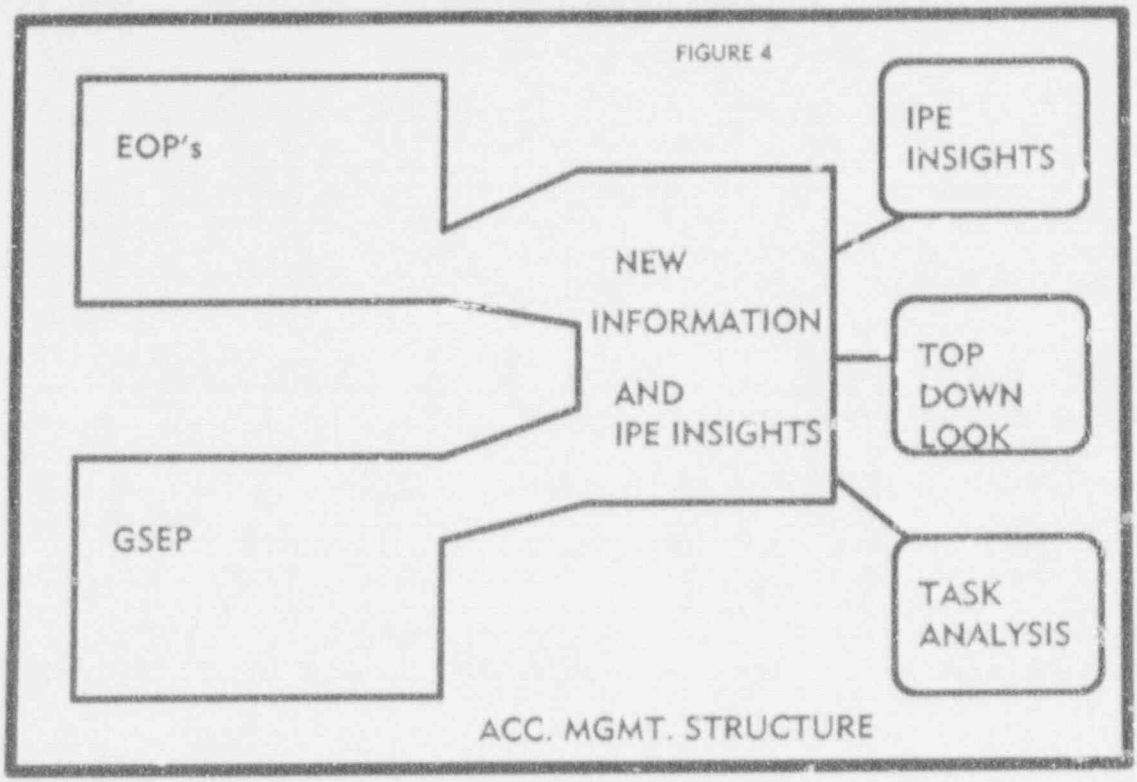
FIGURE 4
EOP's
GSEP
NEW
INFORMATION
AND
IPE INSIGHTS
IPE
INSIGHTS
TOP
DOWN
LOOK
TASK
ANALYSIS
ACC. MGMT. STRUCTURE

The fundamental concerns were self consistency; adequate task definition; adequate staffing and communication; adequate decision making; adequate skills, knowledge and training; and adequate tools, both calculational and informational.

The Edison accident management program definition will stem from the careful consideration of what we are being told by all three of these approaches.

FINE STRUCTURE OF THE DEVELOPMENT:

This section will provide some selected details on the vehicles employed by Edison to perform the IPE's, extract IPE insights, and to extract accident management insights from the IPE's. It will also discuss the top down accident management review and the behavioral scientist's work in a similar manner.

The Edison IPE's are, in a broad sense, classical level 2 PRA's. (Figure 5) The human reliability analyses are performed using "THERP" technology. The common cause failure analyses are performed using "MGL" techniques with plant specific data used wherever possible. The fault tree techniques are not unique. Support states are modelled using a matrix approach which feeds the basic event tree (plant response tree) models. Plant specific data is developed wherever possible and is employed in the initiating event catagorization and quantification. Similarly, component reliability is developed from plant specific data wherever possible. In the level two area, extensive consideration is given to the various relevant phenomena and to crucial uncertainties.

What then is different? As noted earlier, there has been much increased emphasis on realism. The structure of the plant response trees, for example, is based on the extensive use of two key tools. The first of these is the MAAP code which is used to model the realistic response of the plant to initiating events and system failures. Secondly, the plant response trees are structured to take into strict account the operator's responses to the various scenarios as set forth in the EOP's. These two tools are extremely powerful in forcing realism into the structures. As an aside, we believe that the Edison IPE's may be the first studies to ever model, in detail, the effect of the post-TMI, symptom based EOP's. In addition, the MAAP code provides the IPE's with realistic systems success criteria for use in clearly identifying the top events in the plant response trees and, consequently, for

FIGURE 5

EDISON IPE's

* CLASSICAL LEVEL 2 PRA's
* "THERP" TECHNOLOGY
* COMMON CAUSE VIA "MGL" TECHNIQUES
* IMPROVED FEATURES
  ** REALISTIC APPROACH USING "MAAP" CODE
  ** EXPLICIT TREATMENT OF NEW EOP's
  ** "PLANT RESPONSE TREES"

identifying the top events in system fault tree development. Both typical (number of pumps) values and crucial timing issues are resolved in this way.
This technique led, early to a decision to confine the PRT's to systemic and operator action top event questions. No phenomenological questions are included in these trees. The overall phenomenological questions and issues are addressed in separate discussions elsewhere in the IPE. The challenge to containment posed by such phenomena and the relevant uncertainties are covered in these discussions. Edison has participated in the performance of a number of experiments designed to reduce our uncertainties relative to specific phenomena. The results of these experiments are or will be reported in the open literature and in our IPE submittal.

The dominant accident sequences, or groups of sequences from the PRT's will be covered by explicit MAAP runs which will address containment failure or success, timing of failure, and related radioactive releases. As may be expected, many severe accidents take a great deal of time to progress through core melt all the way to containment failure if left unchecked. In some cases, for PWR plants, this can run out to 40 or 50 hours. In an effort to obtain some common frame of reference with the rest of the PRA industry, Edison has set a 24 hour "limit" on sequences. If core melt or containment failure has not occurred in 24 hours and is not imminent, the sequence is classified as "success with accident management" for the issue in question. This is a realistic appraisal of corporate mobilization effects and, at the same time, calls attention to those sequences of interest for accident management development as needed.

How, then, do we extract insights from the IPE? Both IPE insights and accident management insights are of interest and both derive, in part from the IPE. Edison evolved a matrix or array of questions for each purpose. One array addresses the insights classified as IPE insights. The second covers accident management. The distinction between the two becomes somewhat blurred at times but the demarcation is less important than the ideas generated. In each array, one axis consists of a series of natural "choke points" in the IPE. These are points where a major activity is complete, such as the development of PRT structure or the completion of phenomenological discussion papers. The second axis of the arrays changes with intent. The IPE array uses design and operational issues such as EOP's or system design questions. The accident management array uses the 5 elements of accident management discussed earlier. At each junction, specific

questions are asked of the analysts performing the IPE. The questions are used as thought provoking guides in both cases as opposed to rigid prescriptions. Examples of questions from an area of the array and a copy of the array itself are shown in figures 6 through 9. As can be seen, the questions induce consideration of IPE output in the context of the key, 5 elements cited earlier. The analyst is guided in evolving insights at each key stage of the IPE.

The results from this process are subjected to multiple levels of review. Initially, the review is conducted by a team of senior, plant and PRA experienced personnel who consolidate, categorize and screen insights. The results of this review are fed to a Senior Management Support Team consisting of individuals at or near the Program Manager level in Edison and its consultant organizations. Lastly, the insights, along with other study results are fed to a team of very senior Edison managers for final consideration and disposition. Clearly, in this latter case, the very many minor procedural changes which have no major impact but which are more in the line of "clean up" items will not go the final team unless requested. A copy of the data field for collecting and assessing insights is shown in figure 10.

The results of this process will include an aggregation of insights which are specifically and closely related to accident management. They will include insights addressing strategies, suggestions on training, possible hardware augmentation, etc., etc. All such insights will be considered in terms of the existing Edison accident management framework which consists of the current plant and emergency plan organizations and associated procedures, guidance training, etc. They will constitute useful additions to that existing framework. In some cases, they may actually adjust that framework by suggesting changes to an organization, etc.

We noted earlier that Edison has used three approaches to reviewing the issue of accident management program development. Extracting insights from the IPE Program was the first approach and the most significant in terms of resource commitment. Edison also took a top-down look at the issue and, in order to provide a human perspective, reviewed the actual management process, as typified by an emergency plan drill, with a behavioral scientist. These latter two approaches each provided a unique perspective.

The top-down review started with the 5 accident management

	Elements				
Choke Points	A Strategies	B Training	C Comp. Tools	D Organization	E Info.
1. Initiating Events	1A	1B	1C	1D	1E
2. Event Tree Structure	2A	2B	2C	2D	2E
3. Fault Tree Structure & Quantification	3A	3B	3C	3D	3E
4. Success Criteria	4A	4B	4C	4D	4E
5. Event Tree Quantification	5A	5B	5C	5D	5E
6. Pre-Melt Analysis	6A	6B	6C	6D	6E
7. Post Melt, Pre-RV Failure Analysis	7A	7B	7C	7D	7E
8. Post Melt, Post RV Failure Analysis	8A	8B	8C	8D	8E
9. Sequence Selection	9A	9B	9C	9D	9E

Figure 6 Accident Management Development Matrix

Accident Management Matrix Element 1C: Computational Tools

1. Do any of the identified initiating events progress in such unusual ways as to require special calculational tools to be developed to trace the course of the event or predict outcomes for AM purposes, e.g., MAAP auxiliary building model for "V" sequence?

Accident Management Matrix Element 1D: Organization

1. Are any of the initiating events so unusual as to point to possible changes in plant or GSEP organizations or assigned responsibilities of existing organization structure?

Accident Management Matrix Element 1E: Information

1. Do any of the initiating events point directly to a possible need for new instrumentation and/or informational systems? Do any of the strategies evolved from element 1A require such new systems?

2. EVENT TREE STRUCTURE

Accident Management Matrix Element 2A: Strategies

1. Does the event tree structure suggest any AM strategies or the need for the development of any such strategies?

2. Are there plant or utility resources not currently credited in the event tree structure which might ameliorate or terminate specific sequences or groups of sequences in the event tree?

3. Are there actions currently being projected as being taken which worsen or cause a sequence or group of sequences as represented in the event tree?

4. Are there actions which should or should not be taken which would ensure or prevent, respectively, the future use of resources and/or equipment needed to cope with the accident?

5. Are there actions not currently projected to be taken which might terminate or ameliorate a sequence or group of sequences as represented in the event tree?

6. Are there actions for which existing plant procedures might be clarified or enhanced to provide a greater level of assurance of success for implementation?

FIGURE 7

Accident Management Matrix Element 2B: Training

1. If the element 2A questions led to strategies, which positions should be afforded what type of level of training in the strategies in:

   - Normal plant staff?
   - GSEP staff?

2. If the element 2D questions led to new organizational slots, what type and level of training should be afforded to those new slots?

3. If the level 2C and 2E questions led to new computational tools or information systems, who should receive what type and level of training in these areas in:

   - Normal plant staff?
   - GSEP staff?

Accident Management Matrix Element 2C: Computational Tools

1. Do any of the sequences evolved in the event tree structure require new computational tools for full and realistic event representation to AM personnel? If so, identify them.

2. Do any of the suggested AM strategies for specific sequences or groups of sequences require new computational tools for full and realistic event representation to AM personnel? If so, identify them.

3. Does the use of resources or the implementation of actions not currently in the event tree structure require new computational tools for use by AM personnel in controlling an accident? If so, identify them.

Accident Management Matrix Element 2D: Organization

1. Does the event tree structure or any AM strategies evolved therefrom point to a need for any changes in the GSEP organization or assigned responsibilities within the existing organization structure? If so, identify them.

Accident Management Matrix Element 2E: Information

1. Does the event tree structure or any of the sequences derived therefrom point to a need for new instrumentation and/or informational systems or point to new uses for existing systems? If so, identify them.

FIGURE 8

2. Do any of the strategies evolved from element 2A point to a need for new informational systems or point to new uses for existing instrumentation and/or informational systems? If so, identify them.

3. Do any of the computational systems evolved from element 2C point to a need for new informational systems? If so, identify them.

3. FAULT TREE STRUCTURE & QUANTIFICATION

Accident Management Matrix Element 3A: Strategies

1. Does the structure of the system fault tree or the quantification of the fault tree suggest AM strategies or the need for the development of such strategies? If so, identify them.

2. Are there plant or company resources available to prevent system failure or restore an unavailable or failed system which are not credited in the fault tree analysis? If so, identify them.

3. Are there plant-specific failure data which are unusual enough to impact the development of AM strategies? If so, identify them.

4. Are there plant-specific maintenance data (duration of maintenance, etc.) which are unusual enough to impact the development of AM strategies? If so, identify them.

5. Are there plant-specific human failure rate data which are unusual enough to impact the development of AM strategies? If so, identify them.

6. Are there actions for which existing plant procedures might be clarified or enhanced to provide a greater level of assurance of successful implementation? If so, identify them.

Accident Management Matrix Element 3B: Training

1. If the element 3A questions led to strategies, what training should be afforded to what level, to which positions in:

   - Normal plant staff?
   - GSEP staff?

2. If the element 3D questions led to the identification of new organizational slots, what training should be afforded to personnel identified for those slots?

FIGURE 9

THROTTLE RCFC SERVICE WATER FLOWS LOG No. ZI - 218 / AM

ANALYST:

ANALYST: Lutz
SOURCE: Cint Spray Eval.
SYST/COMP/FUNCT: RC. W
EOP/AOP: None
ACC. PHASE: After Core Damage
EXPECTED RESULT: Accident Mitigation

OBSERVATION:

Following core damage, significant quantities of hydrogen may exist in the containment. Under these conditions, one of the accident management strategies is to maintain the containment in a steam inserted state (e.g., maintain containment pressure at 15 to 25 psig). With the present Zion Service Water alignment to the RCFCs, this would require starting and stopping RCFC units on a continual basis (e.g., "on" for 15 minutes; "off" for 30 minutes; "on for 15 minutes; etc.). However, starting of motors is a dominant failure mode for motor driven equipment. A modification to the RCFCs to permit throttling of the SW flow would be advantageous for long term implementation of this accident management activity. Each RCFC presently has two SW valves: one motor operated isolatin valve and one manual valve. Consideration should be given to modifying one of the valves in the SW line to each RCFC to permit throttling of the SW flow.

SEQUENCE / CONDITIONS:

This insight is applicable to all core damage sequences.

INSIGHT / STRATEGY:

An AM strategy to throttle the SW flow to each RCFC unit, should be considered to aid in the implmentation of the accident management strategy to maintain the containment in a steam inerted state. Analyses would likely be required to establish the degree of throttling required to maintain an inerted containment condition. The AM strategy should specify how the emergency response staff can detemine the margin to an de-inerted state during an event (e.g. containment pressure and temperature indications).

CONSTRAINTS:

This recommendation requires no change to the Zion EOPs, AOPs, licensing documents or FSAR analyses.

TIGER TEAM:

IMPLEMENTATION CATEGORY:

__ Hardware __ Test & Maint. __ Procedures __ Training __ Information
X A.M. Strategy __ A.M. Tools __ A.M. Organization __ A.M. Information __ A.M. Training

NATURE OF BENEFIT: __ Major X Minor __ None

__ Clarification X Utiliz. of Capab. __ Improve Efficiency X Risk Reduction __ Accident Prevention
X Accid. Mitigation __ Tech Spec Relax. __ Lic. Basis Simplif. __ Reduce Maint. __ Operation Simplif.
X Other (Specify) CONTAINMENT FAILURE

NATURE OF IMPACT: __ Major X Minor __ None

__ Licensing Basis __ Lic. Agreements __ Tech Specs __ Plant Hardware __ Operat. Complex.
__ Admin. Controls X Staff Knowledge __ Staffing Req'mnts __ Plant Procedures __ Gen. Procedures
__ Other (Specify) _____

RECOMMENDATION: __ No Further Action X Candidate for Distillation

20 August 91 / 13 September 91

FIGURE 10

elements and evaluated Edison's current framework against each element in an anticipatory manner. In other words, experienced people with severe accident backgrounds were asked to provide their estimates of where the existing framework was strong and where it might be strengthened in terms of each of the five elements. This process was intended to aid in flagging long lead time development items and in insuring that an overview of the entire process was available to all participants as the IPE's matured. It also provided a check on the degree to which IPE insights covered the entire accident management spectrum. The nature of the top down review is exemplified in figures 11 and 12 which show part of the structure of that process.

The behavioral sciences review, the last of the three approaches taken, was aimed at insuring that human engineering principles were not being ignored in either the current accident management framework or in the development of an augmented structure. In this review, behavioral scientists and senior Edison personnel reviewed the existing framework to identify those positions in the existing organization which are key to effective management of the accident and to making recovery decisions. Other tasks such as public information control, regulatory liaison, and environs monitoring, important as they are, were not central to this evaluation. Edison arranged for video taping of emergency plan exercises and furnished these tapes to the behavioral scientist after that person had become sufficiently familiar with the key personnel positions and their functions during an accident. The tapes were reviewed by the behavioral scientist in order to perform a task analysis for the key positions. Focus was initially maintained on the current framework and adequacy of organization, training, strategies, tools, and information was assessed for each position given the current framework. Then, the top down look and IPE preliminary insights were reviewed to make some judgements about the nature of future tasking for those same key positions. Key in this was gaining an appreciation of the volume of new, severe accident information flowing from the IPE process. Given that new understanding, revised tasking was proposed and agreed on for evaluation purposes. The task analysis was then repeated to ascertain the impact of the new material on the existing framework from a human engineering standpoint.

CONCLUSIONS:

The results of all of this effort will be presented to

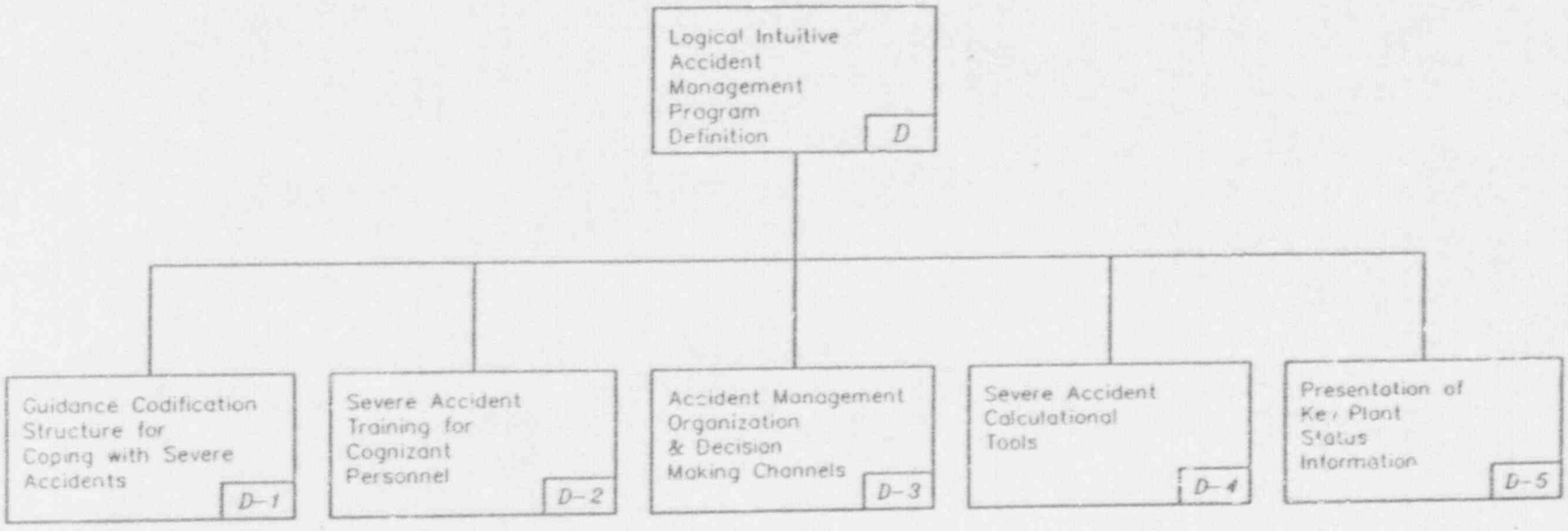

FIGURE 11

S726300AL

Development of Integrated IPE and Accident Management Effort

Process Overview

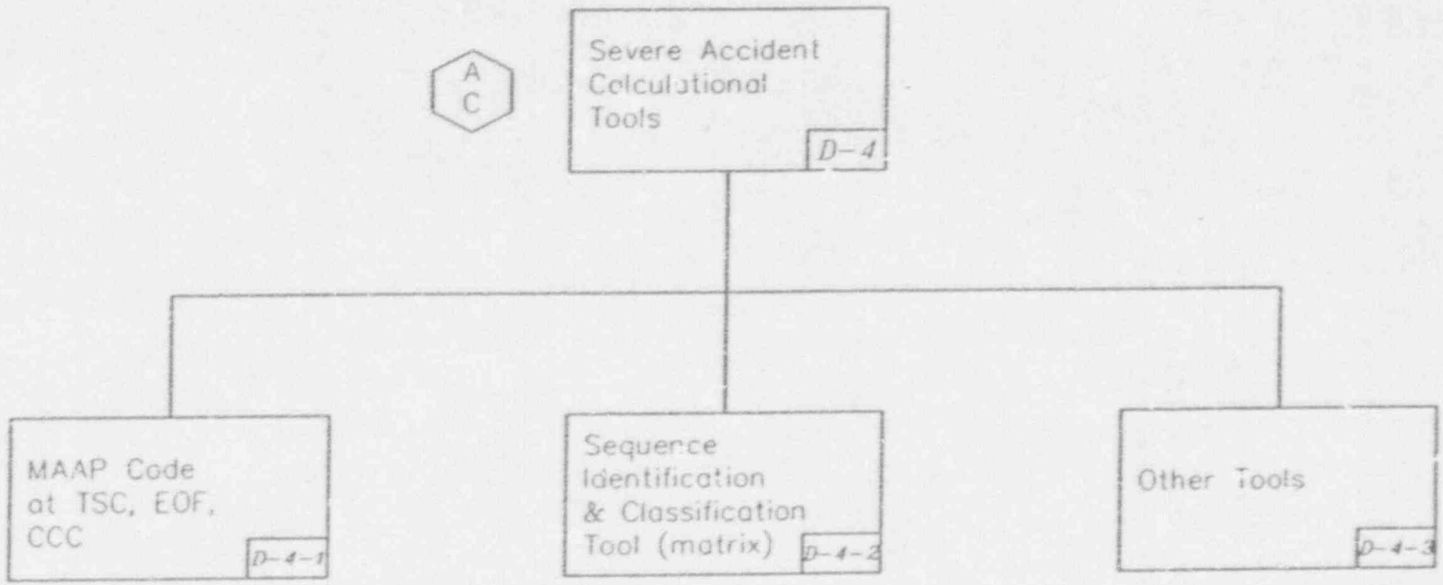

S726300AX

FIGURE 12

Edison's senior management for their review and consideration and for the formulation of those decisions which will set the new accident management framework in place in the near future. Edison believes that this structured process, involving IPE output, top down evaluations and behavioral sciences review will lead to a well developed accident management program which takes full advantage of new information and which is fully responsive to industry and NRC needs. We also believe that the results of this approach are likely to constitute the most significant risk reductions possible under joint NRC/industry program to close severe accident issues.

A FRAMEWORK FOR THE ASSESSMENT OF SEVERE ACCIDENT MANAGEMENT STRATEGIES

W.E. Kastenberg, G. Apostolakis, V.K. Dhir
D. Okrent, M. Jae, H. Lim, T. Milici
H. Park, J. Swider, L. Xing, D. Yu

Mechanical, Aerospace, Nuclear
Engineering Department
University of California
Los Angeles, CA 90024-1597

ABSTRACT

Accident management can be defined as the innovative use of existing and or alternative resources, systems and actions to prevent or mitigate a severe accident. A significant number of probabilistic safety assessments (PSA) have been completed which yield the principal plant vulnerabilities in terms of initiators and accident sequences. For each strategy there may be several options available to the operator and each involves phenomenological and operational considerations regarding uncertainty. The objective of this paper is to develop a framework for assessing severe accident management strategies given the key uncertainties. Based on Decision Trees and Influence Diagrams, the framework is applied to two case studies: Cavity flooding in a PWR to prevent vessel penetration or failure, and drywell flooding in a BWR to prevent or delay vessel and/or containment failure.

1. INTRODUCTION

Severe accident management can be defined as the innovative use of existing and or alternative resources, systems and actions to prevent or mitigate a core melt accident. Together with risk management (changes in plant operation and/or addition of equipment) and emergency planning (off-site actions), severe accident management provides an extension of the defense-in-depth safety philosophy for core melt accidents.

A significant number of probabilistic safety assessments (PSA) have been completed which yield the principal plant vulnerabilities. These vulnerabilities can be categorized as, a) dominant sequences with respect to core melt frequency, b) dominant sequences with respect to various risk measures, c) dominant threats which challenge safety functions, and d) dominant threats with respect to failure of safety systems

Severe accident management strategies can be generically classified as:

* the use of alternative resources (i.e., air, water, power),
* the use of alternative equipment (i.e., pumps, generators), and
* the use of alternative actions (i.e., manual depressurization, manual injection).

For each sequence/threat and each combination of strategy there may be several options available to the operator. Each strategy/option involves phenomenological and operational considerations regarding uncertainty. These considerations include uncertainty in key phenomena, uncertainty in operator behavior, uncertainty in system availability and behavior, and uncertainty in available information (i.e., instrumentation).

In order to better scope the uncertainty associated with these strategies, two workshops were held at UCLA, one each on PWRs and BWRs. As a result of these two workshops, a number of key uncertainties were delineated, and several new accident management strategies were developed. The proceedings of these workshops were summarized in two white papers [1,2].

The objective of this paper is to present a methodology for assessing severe accident management strategies given the key uncertainties delineated at the workshops. Based on Decision Trees and Influence Diagrams, the methodology is applied to two case studies:

* Cavity flooding in a PWR to prevent vessel penetration or vessel failure,

* Drywell flooding in a BWR to prevent vessel and/or containment failure.

Key Uncertainties

In general, the key uncertainties involve issues related to phenomena, operator actions, instrumentation and systems availability. The uncertainty in phenomena occur because operator actions change the progression of a severe accident, and introduce new physical regimes such as temperature or pressure, and new conditions such as the presence or absence of water. As a core melt accident progresses, the geometry change will also contribute to uncertainty. Uncertainties in phenomena exist with respect to the occurrence of steam explosions (both in-vessel and ex-vessel), hydrogen generation and combustion, and heat transfer in these new

regimes and under these new conditions).

In addition to the traditional uncertainties in operator and system behavior regarding severe accidents, there is additional uncertainty in attempting to manage a severe accident. This occurs because of the uncertain nature of the phenomena mentioned previously, a lack of knowledge regarding the state of the accident progression, and because the operators may not know whether or not their actions have been successful. Moreover, a lack of sufficient information due to damaged instrumentation may lead the operators to the wrong diagnosis and/or action. In order to include the various uncertainties mentioned above in assessing the viability of a potential severe accident management strategy, a framework has been developed using Decision Trees and Influence Diagrams. The framework is described in the next section.

2. DEVELOPMENT OF A FRAMEWORK

Introduction

Consider a simple example in which a consumer is confronted with the option of whether or not to purchase an extended warranty for an electronic component. Suppose the extended warranty costs $100; on the other-hand should failure occur, the cost of repair is $500. The key uncertainty is whether or not the electronic component will fail during it's lifetime. The decision can be graphically structured as shown in Figure 1. Suppose further that the consumer wishes to minimize his/her expected loss. The upper branch of the Decision Tree represents the purchase of insurance i.e., the extended warranty; the lower branch represents "self insurance". The square is a "Decision Node", and the circle is a "Chance Node" representing the uncertainty. If the chance of failure is estimated to be 10% (0.10), then the expected losses would be (EV = Expected Value):

$$EV_1 \text{ (Loss)} = - \$100 \qquad (1)$$

$$EV_2 \text{ (Loss)} = 0.9 \ (- \$0) + 0.1 \ (- \$500) = - \$50$$

If the consumer used this simple "Expected Value Rule", he/she would opt to self insure because EV in this case is -$50. If the consumer were more sophisticated, he/she could use an "Expected Utility Rule" in which a degree of risk aversion could be factored in. An Influence Diagram for this decision is also shown in Figure 1. In this paper used primarily to show what influences the value of the decision (given by the diamond), and it can be used to help structure the decision tree.

Accident Management

The Decision Tree and Influence Diagram shown in Figure 2 are simple examples of how severe accident management strategy can be represented. The upper branch, "Do Nothing", means follow the normal emergency procedures contained in the Emergency Operating Procedures which are incorporated in a risk assessment such as NUREG-1150. The circle indicates a chance node with two outcomes. In the first outcome, the accident progression is stopped, and ends with risk R_1. This risk (R_1) might be zero (if there is no core damage or release) or may be economic (if there is core-damage). In the second outcome, the normal emergency procedures fail, and there is a risk, R_2 such as that calculated in NUREG-1150.

The lower branch describes a severe accident management option for preventing vessel failure (e.g., Flooding the Cavity). This option can lead to success, but with risk R_3. The risk (R_3) might be economic with no radioactive release if the melt progression is stopped, as above. Failure of the strategy may lead to risk R_4 which may be greater or less than R_2, depending upon the physical and operational state of the system. For example, even though the vessel fails, the presence of water might scrub fission products, thereby reducing risk. Or it may lead to a steam explosion thereby increasing risk. This risk, R_4 represents an adverse effect.

The expected value EV for the two options, as depicted in Figure 2 are:

$$\begin{aligned} EV\ (\text{Do Nothing}) &= P_1R_1 + (1-P_1)R_2 \\ EV\ (\text{Flooding}) &= P_2R_3 + (1-P_2)R_4 \end{aligned} \qquad (2)$$

The Influence Diagram for this example is also shown in Figure 2. In this case, the diagram is simple because the chance node represents simple failure or success.

Evaluation Criteria

When assessing a severe accident management strategy five criteria should be considered:

* the feasibility of the strategy,
* the effectiveness of the strategy,
* the possibility of adverse effects,
* information needs, and
* compatibility with existing procedures.

For the strategy considered in the example above, the

feasibility is essentially a question whether or not the operators will be able to fill the cavity up to the required level in sufficient time. The **effectiveness** has to do with whether or not the heat transfer is sufficient to keep the molten core in the vessel, given that the water is there on time. A possible **adverse effect** is a steam explosion, should the strategy be feasible but not effective, i.e., the core penetrates the vessel, and finds water in the cavity, which otherwise would not be there. Information needs refers to instrumentation availability, and compatibility considers the impact on existing rules and procedures.

Figure 3 shows a case with adverse effects. The lower branch, "Do Nothing" is as before, the risk associated with employment of standard emergency operating procedures. (The two branches have been collapsed.) The upper branch, flood cavity, has three chance nodes. The first chance node C_1 represents the question of **feasibility**; whether or not the operators can fill the cavity up to the required level on time. The second chance node C_2 represents **effectiveness**; whether or not the water will keep the vessel cool enough. The third chance node C_3 represents **adverse effects**; whether or not there will be a steam explosion if the strategy is not effective. Note that this last question can also apply to the feasibility issue as well. The branch "flooding not successful" may also lead to the potential adverse effect (regarding a steam explosion) if the cavity is partially filled with water.

The expected value for each case is as follows:

$$EV\ (\text{Do Nothing}) = R_5$$

$$EV\ (\text{Flood Cavity}) = P_1R_4+(1-P_1)[(1-P_2)R_1+P_2(1-P_3)R_2+P_2P_3R_3] \quad (3)$$

The evaluation of such a tree would proceed as follows. The risks associated with each endpoint would be determined using PRA methodology. This risk might be in terms of early or latent fatalities, population dose, conditional probability of early containment failure, etc. The chance node probabilities would be evaluated using both deterministic and probabilistic methods. For example, the question of feasibility would require the use of Human Reliability Analysis (HRA) and a knowledge of system behavior (e.g., pump capacities, flow rates, etc.). The question of effectiveness would require mechanistic calculations regarding heat transfer, materials behavior etc. The same is true for questions regarding adverse effects.

An Example

As an example of the use of Decision Trees, we consider a decision regarding PWR cavity flooding as a means to prevent vessel

failure. The measure of success can be a reduction in the risk of early or latent fatalities, of core-melt frequency or of early containment failure. For this simple example we consider the measure of success the potential reduction in the Conditional Probability of Early Containment Failure, denoted P_{ecf}. Furthermore we wish to determine whether or not flooding the cavity to prevent vessel failure will reduce P_{ecf} given a potential adverse effect (in this simple example, an ex-vessel steam explosion).

The Simplified Decision Tree shown in Figure 3 can be used, with Equation (3), to evaluate this severe accident management strategy. Figure 7.3 in NUREG-1150 [3] gives a value of 0.25 for P_{ecf} , given a Station Blackout (SBO) sequence in Surry.

Early containment failure can be attributed to two phenomena: direct containment heating and ex-vessel steam explosions. In Section 3 of this paper we derive the following values for the risks (R_i) and the probabilities (P_i) as follows:

$R_1 = 0$	If there is no vessel failure, the Conditional Probability of Early Containment Failure, $P_{ecf} = 0$.
$R_2 = 0$	If the vessel fails and the melt is quenched, $P_{ecf} = 0$
$R_3 = 0.01$	If the vessel fails and there is an ex-vessel steam explosion, but no direct containment heating, P_{ecf} is reduced.
$R_4 = 0.025$	If flooding is not successful; same as "do nothing".
$R_5 = 0.025$	Given in NUREG-1150; "do nothing".
$P_1 = 0.41$	The probability that the option is not feasible; that the arrival of water is not timely.
$P_2 = 0.098$	The probability that the option is not effective, given the that water is there on time.
$P_3 = 0.5$	The probability of an adverse effect; i.e. of an ex-vessel steam explosion, given water in the cavity.

Before evaluating this strategy; we should note that if the flooding is not successful, there is the chance of an ex-vessel steam explosion when the cavity is partially full. This is treated in Section 3 along with other important phenomena.

Using Equations (3), the Expected values are as follows:

EV (Do Nothing) = 0.025

EV (Flood Cavity) = 0.011

In this example, and on an expected value basis, one would choose to flood the cavity, in spite of the potential for adverse effects.

3. PWR CAVITY FLOODING

Introduction

One of the candidate accident management strategies discussed during the PWR accident management workshop held at UCLA [1] is the idea of flooding the reactor cavity up to the level of the vessel lower head, with aim of cooling the vessel from the outside and possibly preventing vessel failure. This strategy could be especially useful for station blackout sequences, in which all emergency core cooling systems (ECCS) are unavailable. The operators could inject an alternative source of water, such as fire water, into the reactor cavity if they are unable to inject it directly into the vessel.

The evaluation of severe accident risks at Surry Unit 1 [3] has shown that the short term station blackout sequence is one of the most important contributors to risk. This sequence consists of the loss of off-site power as the initiating event followed by failure of the emergency diesel generators to provide back up AC power. In addition, the auxiliary feedwater system fails to provide emergency feedwater to the steam generators. Since the heat removal capability of the steam generators is lost, the RCS will heat up and pressurize leading to coolant loss through the power operated relief valves (PORVs). The loss of AC power results in the availability of all ECCS, and if power is not recovered, continued coolant loss will lead to core uncovery and damage.

The Surry plant was chosen for this evaluation because of the extensive information available on severe accidents at Surry, including the phenomena associated with their initiation and progression, and their consequent risks. The short term station blackout sequence was chosen because it is a significant contributor to risk and because many thermal-hydraulic analyses have been performed relating to it [5,6].

Since all emergency core cooling systems are rendered

unavailable by the loss of AC power, and heat removal by the steam generators is also unavailable, the operators have no options available to them with respect to preventing or arresting core damage (unless AC power is recovered). However, if they can cool the vessel from the outside they may be able to accomplish the second goal of accident management, prevention of vessel failure.

This strategy would also have the additional benefits (called secondary mitigative effects) of preventing high pressure melt ejection and associated direct containment heating because the vessel wouldn't be breached by a penetration failure if it does fail with water present in the cavity. Similarily, the presence of water would possibly prevent a core-concrete interaction if the vessel fails anyway. However, there may be adverse effects associated with the strategy. One concern is that should the strategy be successful in keeping the molten core inside the vessel, continued exposure of the steam generator tubes to hot gases circulating from the molten pool could result in their failure, if the hot leg surge line does not fail first. Another concern is that should the vessel fail with the cavity full of water, an ex-vessel steam explosion could result in early containment failure.

In assessing this strategy the potential benefits must be measured against the potential for adverse effects, in an integrated fashion. The feasibilty of this strategy, which is concerned with whether or not the operators will be able to fill the cavity up to the required level in time using the proposed equipment, must also be considered. These considerations involve determining what information would be needed by the operators to diagnose the situation and implement the strategy on time. The instruments that would supply this information have to be identified and their performance under the accident conditions must be assessed. The sequence of operator actions necessary to successfully implement the strategy must be identified in order to formulate a suitable human reliability model to evaluate the likelihood of success. Also, the reliability of the systems and equipment involved must be evaluated.

The Decision Tree

Figure 4 contains a simplified Decision Tree for this case. The first chance node on the left represents success/failure of cavity flooding, i.e. feasibility. This node represents the question of whether or not the reactor cavity is flooded up to the level of the vessel lower head, given that the operators were instructed to do so. The probability that this strategy is successfully implemented is composed of two parts: the probability that the operators successfully initiate the strategy in time and the probability that

the fire pump system functions correctly.

Based on the facts that the station would be blacked out and the instrumentation used to detect core uncovery would be available, the failure of the plant operators to correctly initiate the strategy would be governed by two uncertain variables: the critical time, T_c, which is the time available for the operators to diagnose the situation and decide to initiate the stratgey, and the action time, T_a, which is the time required for the operators to initiate flooding. The auxiliary operators outside the control room are assumed to be available to operate the fire pump system.

Flooding the reactor cavity might involve the following steps:

(1) The control room operators detect core uncovery and dispatch an auxiliary operator to the emergency fire pumps.
(2) The auxiliary operator goes to the emergency fire pumps.
(3) The auxiliary operator starts the fire pumps.

The major uncertainty is associated with the critical time. The critical time, $T_c = T_{cs}-T_{cu}$, is the time from core uncovery to core slump. The time to core slump is used because a film boiling situation will exist and the heat transfer will not be sufficient to cool the vessel enough to prevent melting and failure if the water reaches the vessel lower head after a significant amount of debris has relocated there [7]. Because the phenomena associated with melt progression and relocation are very complicated, the time to core slump is highly uncertain. Table 1 shows estimates of T_{cs} obtained by three different computer simulations [8].

Another relevant parameter is the time required to fill the reactor cavity up to the required level, T_f. This parameter is known [9] and is a function of the Surry reactor cavity volume (92,452 gal) and the fire pump capacity (2000 gpm) [10], and is calculated to be 46.2 min.

The human error probability (HEP), is the probability that $T_a + T_f$ exceeds T_{cs}, i.e.,

$$HEP = P(T_a + T_f > T_{cs}) = P(T_a > T_{cs} - T_f) = P(T_a > T_c)$$

$$= \int_0^\infty [1 - F_{T_a}(t)] f_{T_c}(t)\,dt, \qquad (4)$$

where

$f_{T_c}(t)$ = probability density function (pdf) of the critical time, and
$F_{T_a}(t)$ = cumulative distribution function (cdf) of the

time required to initiate the strategy.

Since the distributions in Equation (4) are not available, the probability that the operators successfully initiate the strategy on time can be obtained from the "Human Error Handbook" [11] using the times shown in Table 1. Since natural circulation in the reactor coolant system was not considered in the MARCH calculation in Table 1, the time calculated by SCDAP/RELAP is used for this study. Based on this time, a value of 0.62 for the success probability was obtained. The value of 0.95 is assumed for the availability of the fire system. Therefore, the probability that there is water in the cavity up to the level of the vessel lower head before the core slumps, P(WC), is the product of successful operator actions, (1-HEP), and the availability of the fire system. Hence the success probability is 0.59.

The next chance node represents vessel breach, with and without successful cavity filling. Without success, the accident progression is the same as NUREG-1150. With water in the cavity, (the success path), the chance node represents effectiveness. Based on the calculations of Park and Dhir [7], it is assessed at 0.9. The two adverse effects, late steam generator tube rupture and an ex-vessel steam explosion are as indicated in Figure 4.

Results

Figure 4 shows the risk associated with each branch of the Decision Tree in terms of Early and Latent Fatalities conditional on sequence frequency. Table 2 shows the effect of flooding on five risk measures. Flooding the cavity reduces the conditional probabilities of early and late containment failure by 53% and 95% respectively. The conditional probability of steam generator tube reputure increases however by 35%. There is however, a net decrease in early and late fatalities of 41% and 5% respectively.

4. BWR DRYWELL FLOODING

Introduction

One of the candidate accident management strategies for BWRs is flooding the drywell up to the level of the vessel lower head. The strategy to be assessed is whether to flood the containment in a long term station blackout sequence or do nothing different than is analyzed in NUREG-1150 [3]. Primary containment flooding is already included in the BWR Owners' Group Emergency Procedure Guidelines [12], but the concept is intended for LOCA situations

where the water within the drywell could enter the reactor vessel through the break. For severe accident sequences not involving a LOCA, flooding of the primary containment and the presence of water surrounding the reactor vessel might provide sufficient cooling of the bottom head to maintain the core and structural debris within the vessel [13]. Futhermore, given the proposals [14] for preventing failure of the Mark 1 drywell shell by flooding the drywell floor with water, primary containment flooding is a strategy worthy of consideration. Existing studies [15] indicate that a long time is required to raise the water level within the wetwell and drywell to surround the reactor vessel lower head, if existing systems are used. The long term station balckout sequence is chosen to examine the drywell flooding strategy because it is a dominant accident sequence and it has a relatively long time to core slump.

There are two concerns related to the feasibility of the strategy. The first concern is drywell venting in order to assure effective flooding. If the drywell is not vented during the flooding operation, the resulting high back-pressure would decrease the rate of low pressure injection from a system such as the fire pumps. The small drywell and wetwell volumes will result in pressures that may fail the drywell if there is insufficient venting. In Mark I containment, the wetwell volume would not completely fill because of a trapped airspace in the top of the torus above the wetwell-to-drywell vacuum breaker. The volume taken up by the trapped air is significant in reducing the total free volume that must be filled when these valves can still be opened with a handwheel or wrench on the stub protruding at the top of the motor operator. With a loss of instrument air, all air-operated valves fail closed. Backup air bottles are installed to facilitate opening air-operated valves locally. Due to drywell water elevation considerations, the 18-in lines to the SGTS might be opened instead of the 6-in ILRT line.

NUREG 1150 analysis assigned a probability of successful wetwell venting for SBO sequences as 0.1 because opening the venting system valves needs AC power and is difficult to do in the harsh environment in the reactor building (i.e., radiation from fission products). Reference [17] gives a fault tree for containment venting. Four failure mechanisms were considered: local equipment failure, operator fails to vent, failure of instrument air system to provide pressure, and loss of power to vent valves. In case of loss of all AC power, local and manual venting is necessary. In this case, only two factors are important for calculating venting failure probability, i.e., local equipment failure and operator fails to vent. Local equipment failure probability is 1.0×10^{-4} (1/demand)[17], and operator fails to vent probability is 0.5. Using the above , the containment venting failure probability is 0.50.

It is evident that operator error probability dominates the venting failure probability. As discussed previously, the operator error probability (0.5) as given in [17] is too large for the case of drywell flooding. The operator has at least 2 hours to perform venting, if the operator starts to prepare venting right after loss of all AC power. With AC power available, defeating the interlock is unnecessary, but the operator has to find the vent path and open the valve locally. In this case, 1 hour is a conservative upper bound and the time available is much larger than the time needed. There is still human error when the time available is greater than the critical time of about 80 minutes (non-response probability). The simulator exercises provide non-response probabilities that are moderately high; in particular, it has been indicated that they are larger than 2×10^{-2}. In this analysis operator failure probability is chosen as 2×10^{-2}, the containment venting failure probability is then 0.02.

The Decision Tree

Figures 5 and 6 are reduced decision trees for the BWR Drywell Flooding Strategy. The first node represents whether or not the operators are successful at venting. Drywell venting at Peach Bottom uses the following paths for the drywell [17]:

1) 2-in pipe from the drywell to the Standby Gas Treatment System (SGTS),
2) 6-in Integrated Leak Rate Test (ILRT) pipe from drywell,
3) 18-in drywell vent via ductwork to the SGTS,
4) 18-in drywell supply path, and
5) two 3-in drywell sump drain pipes.

In accident conditions, the 2-in lines will not be sufficient to prevent containment pressure from increasing so the 6-in ILRT line or other lines must be used. Also, if core damage has not occurred and the 6-in line is used, steam will be released directly to the environment and no adverse environments will be created in the reactor building. To open the 6-in ILRT path, a flange must be removed from the line. Also, two motor-operated valves and two air-operated valves must be open locally. With a loss of power, motor-operated valves fail in an "as is" position.

The second node represents the filling of the drywell upto the lower head. The probability of water presence up to the bottom head of the vessel before core slumping is dependent upon whether or not the drywell can be vented, and the capacity of the fire pumps. This analysis assumes that the injection system is a diesel driven fire pump that is already aligned and fitted to the containment spray system. This also assumes that water has to reach the lower head

before relocation of core debris begins (core slump), i e., 737 minutes after loss of AC power. The fire water system at Peach Bottom consists of two 2,500 gpm capacity, vertical turbine pumps (one electric-motor-driven and the other diesel-engine-driven).

It is estimated that 208,000 ft^3 (1,550,000 gals.) of water would have to be added to containment so that the water within the drywell can reach a level (about 35 ft above the drywell floor) sufficient to cover the reactor vessel bottom head. If only the fire pump is used, the timing for achieving this level is 620 min. The latest time that an operator could start flooding using the fire pump is 117 min (1.95 hr.) after loss of off-site power, if water has to surround the lower vessel before core slump. At this time the DC has not been depleted and HPCI/RCIC is still available. The operator would then be reluctant to start flooding. The only possible situation in which fire pump flooding is likely to be employed is that it is hopeless to recover off-site power in 10 hours (e.g. large power grid damage due to severe weather) and it is also hopeless to run the on-site diesel generators within 10 hours (e.g. due to unrecoverable severe damage). For this analysis, we determined that the probability of successful flooding is 0.93.

The vessel bottom head failure mechanism (node) is dependent upon factors such as temperature and composition of the corium, and the timing of its release from the degraded core region. For example, a sudden release of hot molten corium directly into the plug area such as a guide tube or a control rod drive mechanism tube will most likely result in a penetration failure. On the other hand, if low-temperature (i.e. containing metallic constituents) corium is gradually released into the lower plenum, a slow heatup of the entire vessel lower head can be anticipated, eventually leading to its gross failure. For this analysis, it was determined that the probability of no vessel failure is 0.8.

Results

Tables 3 and 4 summarize the results of this analysis. Flooding introduces two new, failure nodes, early containment failure at low vessel pressure and isolation failure (intentional venting).

The drywell flooding strategy seems to be beneficial for saving the reactor vessel and the containment for both liner melt-through and late overpressurization failure. However, this strategy has an adverse effect on early containment failure due to steam explosions. Also, it has an adverse effect on isolation containment failure due to drywell venting.

The most dominant containment failure mechanism (except liner melt-through at high reactor pressure), given vessel breach, is isolation failure in the flooded case. More importantly, the contribution due to liner melt-through could be reduced by half for the flooded case compared to the case of no flooding. The reduction in probability of late overpressurization containment failure is due to the drywell vent, which results in isolation failure before late containment failure. While flooding is expected to increase the possibility of an ex-vessel steam explosion, early containment failure due to an ex-vessel steam explosion or HPME is not a significant contributor compared to liner melt-through. Whether or not to flood, does not change the conditional probability of containment failure, given vessel failure. However, the most important result is that the risk reduction comes from the change of source terms. Drywell flooding can reduce liner melt-through which has a greater source term than that of the drywell vent.

To evaluate the strategy with respect to beneficial and adverse effects, both early and late fatalities should be calculated. Table 4 shows the results obtaines. From the table, it appears that containment flooding is beneficial, resulting in a risk reduction of 75.4% in early fatalities and 75.0% in late fatalities per long-term station blackout accident.

5. CONCLUSIONS AND RECOMENDATIONS

Some potential accident management strategies are inherently complex, involving both benefits and adverse aspects and subject to large uncertainties. Influence Diagrams represent a valuable tool for examining and illuminating the various interrelationships among the many factors involved. Decision Trees, equivalent to the Influence Diagram, both represent a second way of illustrating complex relationships and provide an automated tool for solving for the various outcomes of the potential strategy.

The use of Influence Diagrams/Decision Trees has a second valuable benefit. It requires a systematic examination of the various potential factors which could affect the outcome of a particular strategy. As a result of this requirement, a more complete examination and evaluation of candidate accident management strategies may result, and factors sometimes overlooked, such as spurious information and errors of commission, may be identified and factored into the assessment.

In this study, Influence Diagrams and Decision Trees have been used to examine two severe accident management strategies, PWR cavity flooding to prevent vessel failure, and BWR drywell flooding to prevent vessel failure and/or containment failure. A commercially available computer code called SUPERTREE was used to

quantify the Decision Tree, and a method for direct quantification of the Influence Diagrams was developed in this study. Data and models relied heavily on NUREG-1150 and on independent analyses by UCLA.

6. REFERENCES

[1]. W.E. Kastenberg, editor, "Proceedings of a Workshop on Severe Accident Management for PWRs," UCLA, (July 1991).

[2]. W.E. Kastenberg, editor, "Proceedings of a Workshop on Severe Accident Management for BWRs," UCLA, (July 1991).

[3]. USNRC, "Severe Accident Risks: An Assessment for Five Nuclear Power Plants," NUREG-1150, vols. 1 and 2, (June 1989).

[4]. SUPERTREE Decision Analysis Software, Version 5, Copyright 1987 SDG Decision Systems.

[5]. J.E. Kelly, R.J. Henninger and J.F. Dearing, "MELPROG?MODI Analysis of a TMLB' Accident Sequence," NUREG/CR-5214, (1988).

[6]. P.D. Bayless, "Analysis of Natural Circulation During a Surry Station Blackout Using SCDAP/RELAP5," NUREG/CR-5214, (1988).

[7]. H. Park and V. Dhir, "Steady-State Thermal Analysis of External Cooling of a PWR Vessel Lower Head," Proceedings of 27th ASME/AIChE/ANS National Heat Transfer Conference, Minneapolis, MN, (July 1991).

[8]. R.J. Breeding, J.C. Helton, W.B. Murfin, et.al., "Evaluation of Severe Accident Risks: Surry Unit 1 Appendices," NUREG/CR-4551, Vol. 3, Part 2, (Oct. 1990).

[9]. R.J. Breeding, J.C. Helton, W.B. Murfin, et.al., "Evaluation of Severe Accident Risks: Surry Unit 1 Main Report," NUREG/CR-4551, Vol. 3, Part 1, (Oct. 1990).

[10]. "Zion Final Safety Analysis Report," Vol. 4 (9.9), Commonwealth Edison Company, Chicago, (1982).

[11]. A.D. Swain and H.E. Guttman, "Handbook of Human Reliability Analysis with Emphasis on Nuclear Power Applications," NUREG/CR-1278, (1987).

[12]. "BWR Owners Group Emergency Procedure Guidelines," Revision

4, General Electric Topical Report NEDO-31331, (March 1987).

[13]. S.A. Hodge, "Recommendations for Further Assessment of Certain BWR (IN-VESSEL) Late Accident Mitigation Strategies," Letter Report, Sept. 25, 1990, ORNL/NRC/LTR-90/19.

[14]. T.G. Theofanuos, et.al., "The Probability of Liner Failure in a Mark I Containment," NUREG/CR-5423, to be published.

[15]. W.A. Condon, S.R. Greene, R.M. Harrington and S.A. Hodge, "SBLOCA Outside Containment at Browns Ferry Unit One-Accident Sequence Analysis," NUREG/CR-2672, vol. 1, ORNL/TM-8119/V1, (Nov. 1982).

[16]. S.A. Hodge et. al., "External Flooding of a BWR Reactor Vessel as a Late Accident Mitigation Strategy; Detailed Assessment of Boiling Water Reactor In-Vessel strategies Program," Letter Report, ORNL/NRC/LTR-91/9, (August 27, 1991).

[17]. A.M. Kolaczkowski, et.al., "Analysis of Core Damage Frequency: Peach Bottom, Unit 2, Internal Events," NUREG/CR-4550, Vol. 4, Part 1, (August 1989).

[18]. K.C. Wagner et. al., "An Overview of BWR Mark I Containment Venting Risk Implications, "NUREG/CR-5225, EGG-2548 Addemdum I, (June 1989).

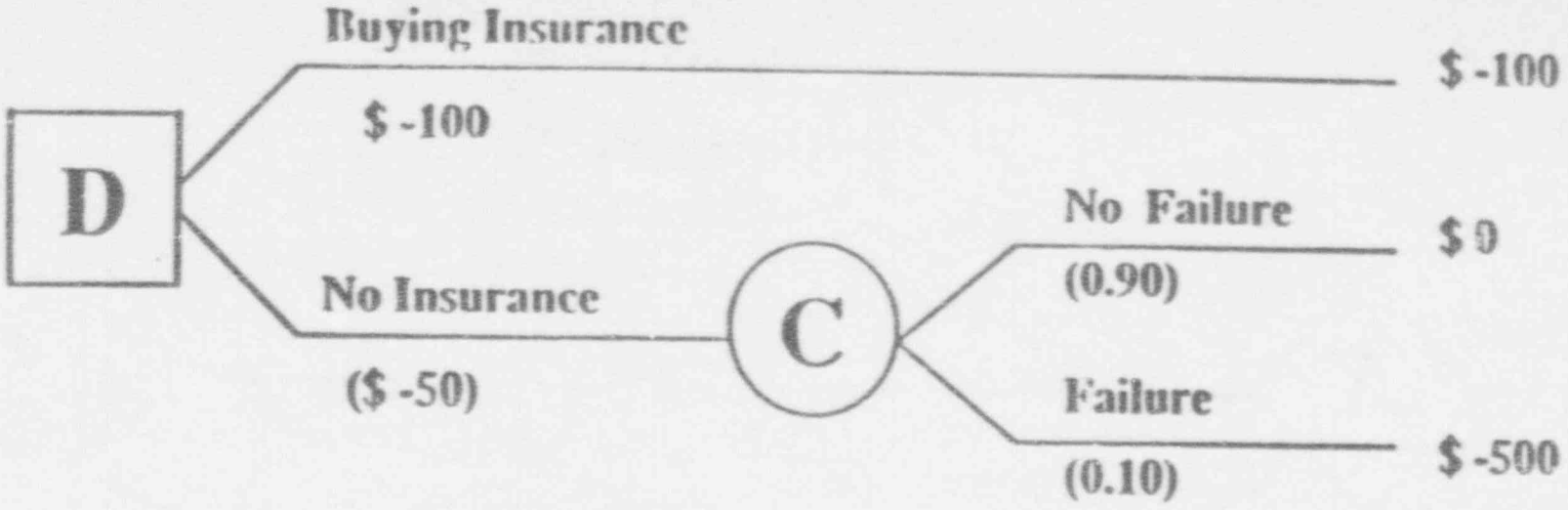

Decision Tree

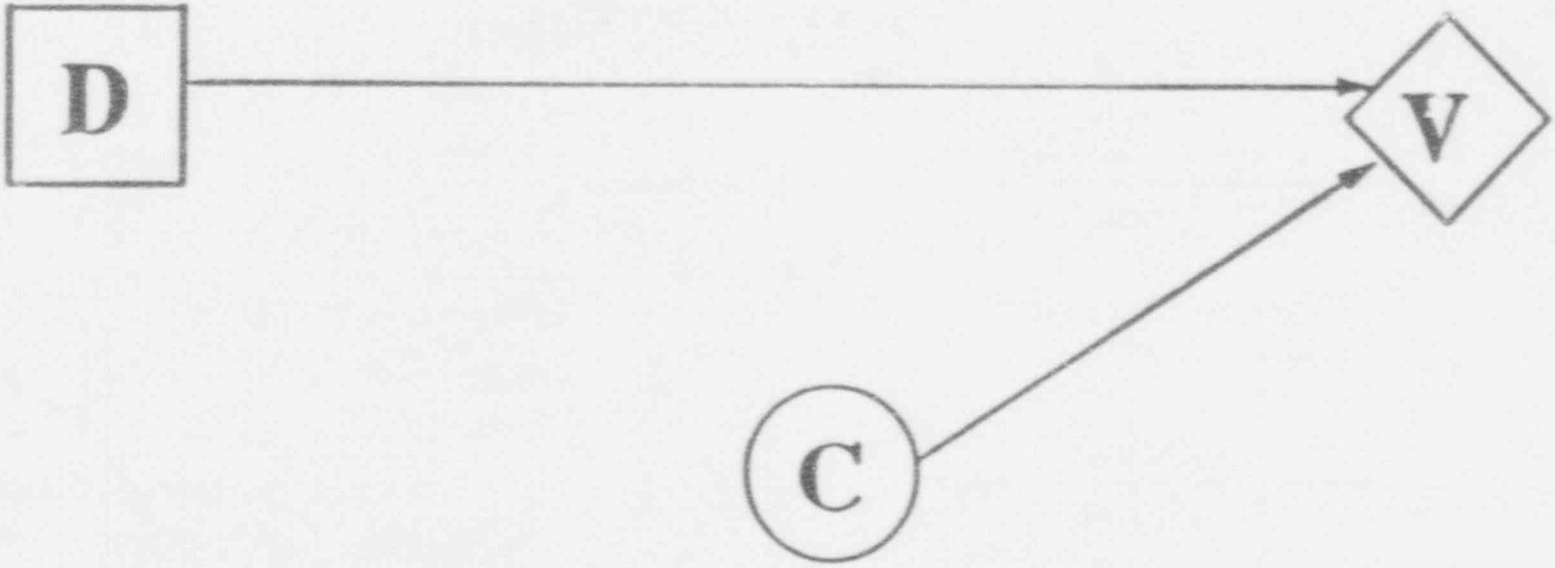

Influence Diagram

Figure 1

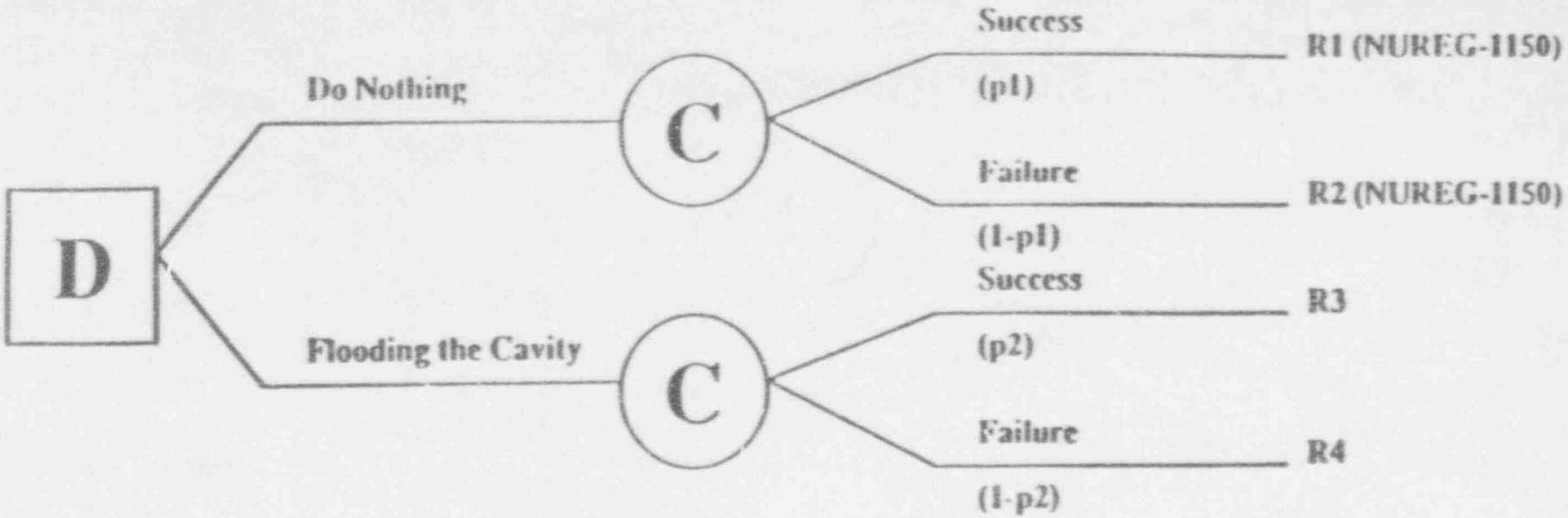

Decision Tree

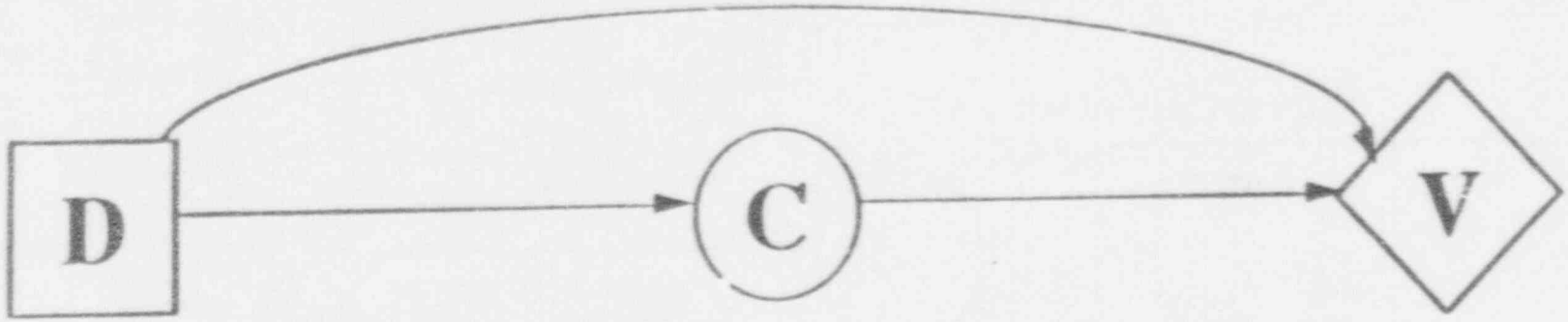

Influence Diagram

Figure 2

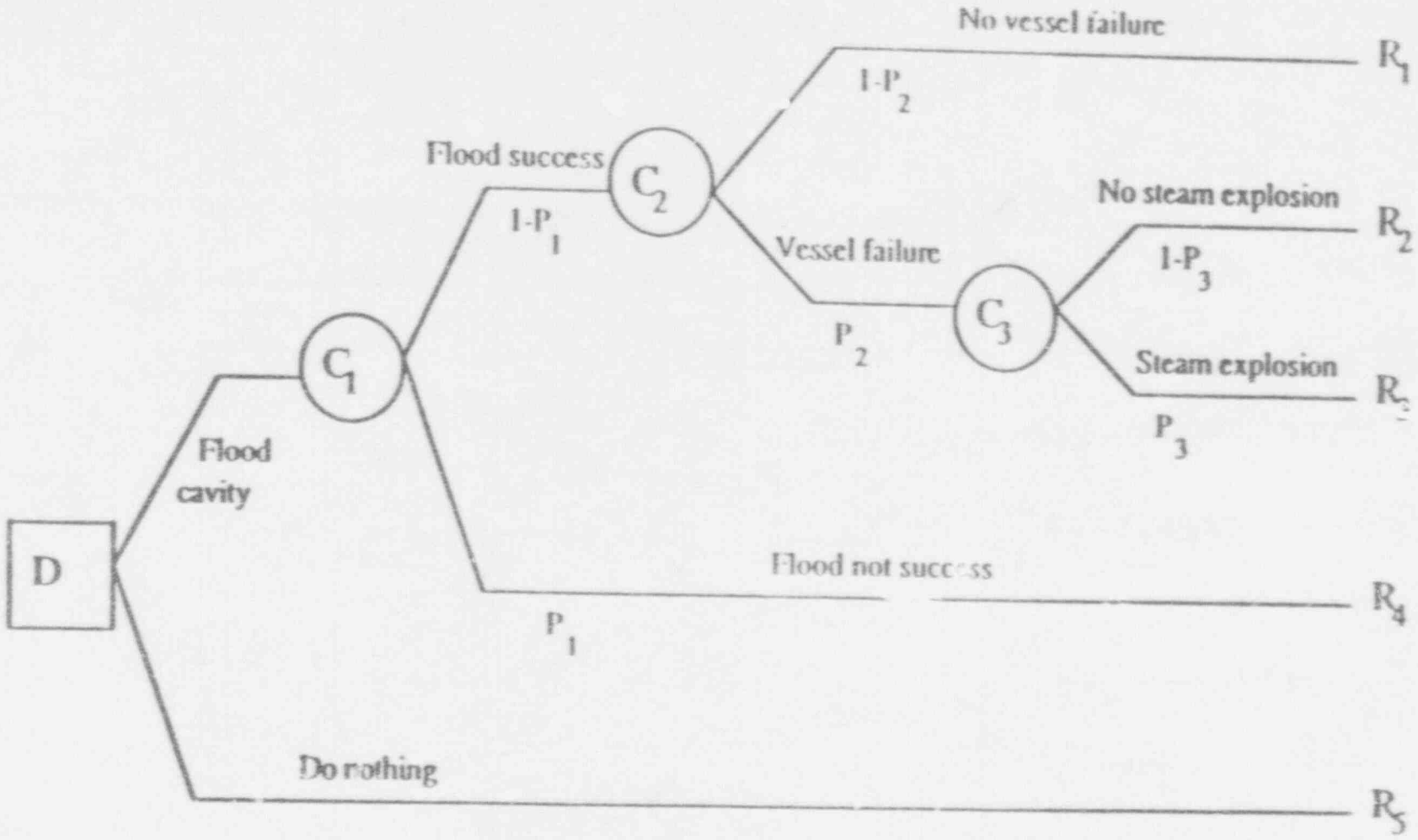

Competing Risks

Figure 3

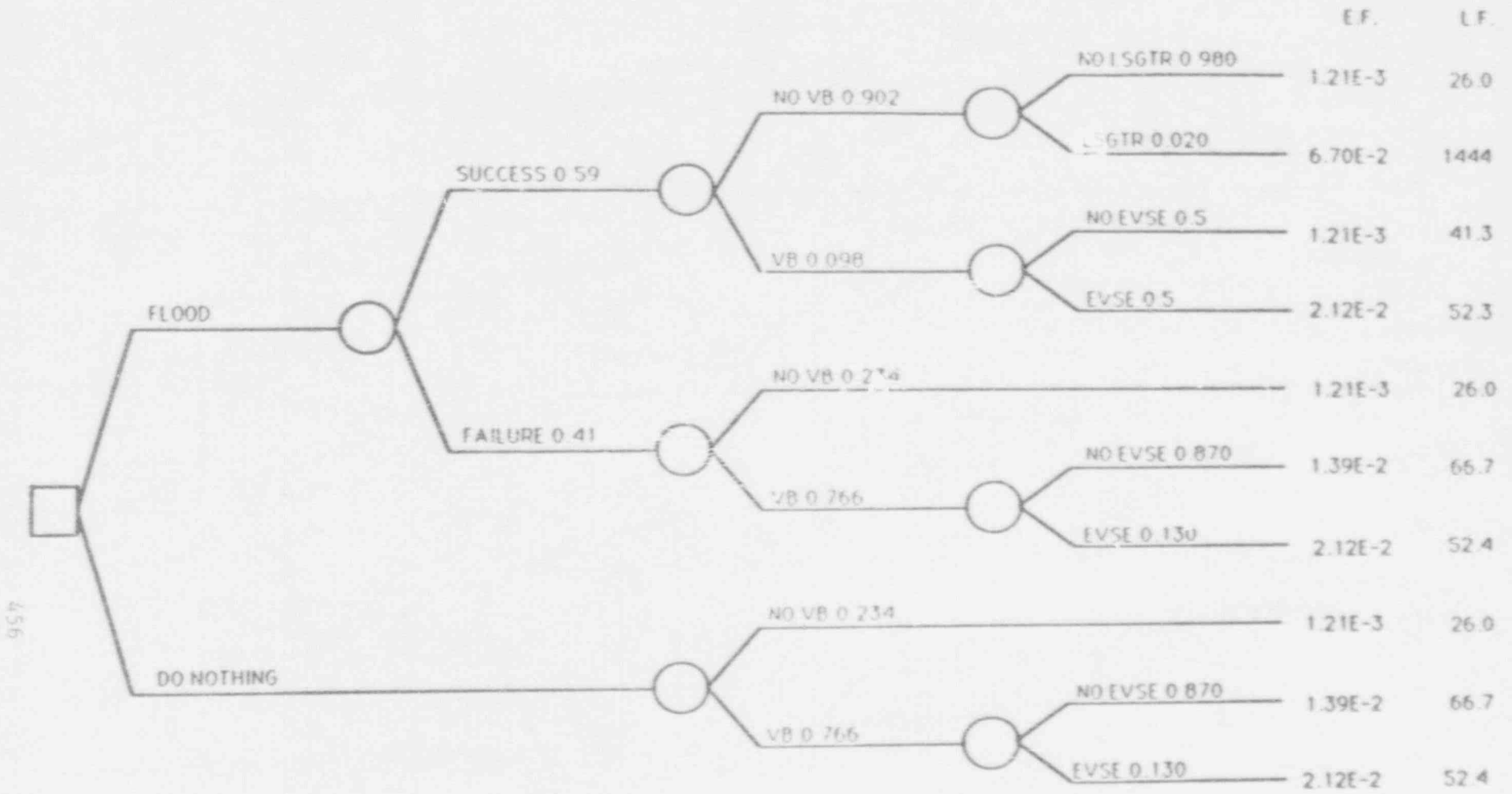

Figure 4. Simplified Decision Tree

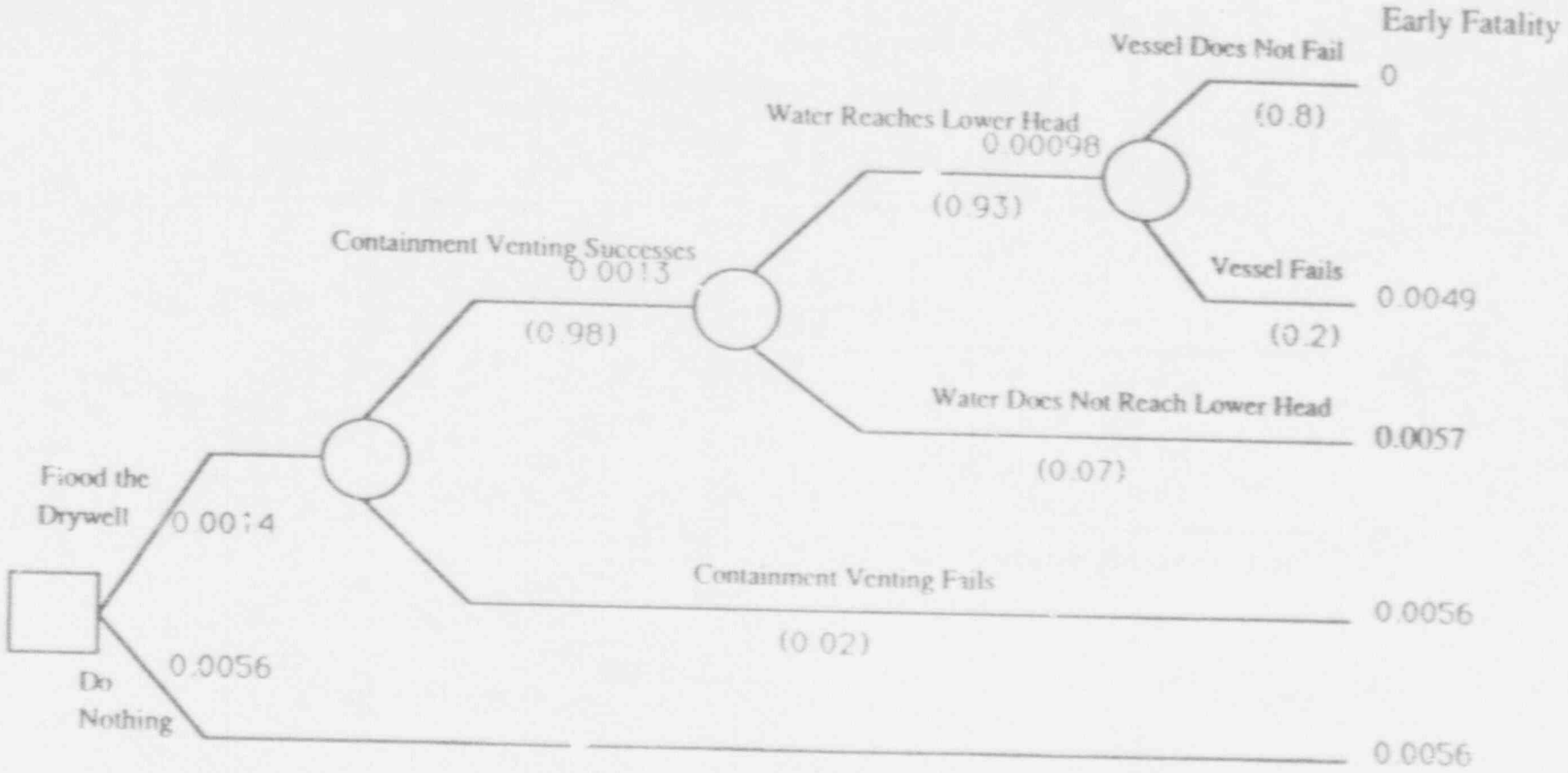

Figure 5. Simplified Decision Tree for BWR (Early Fatality)

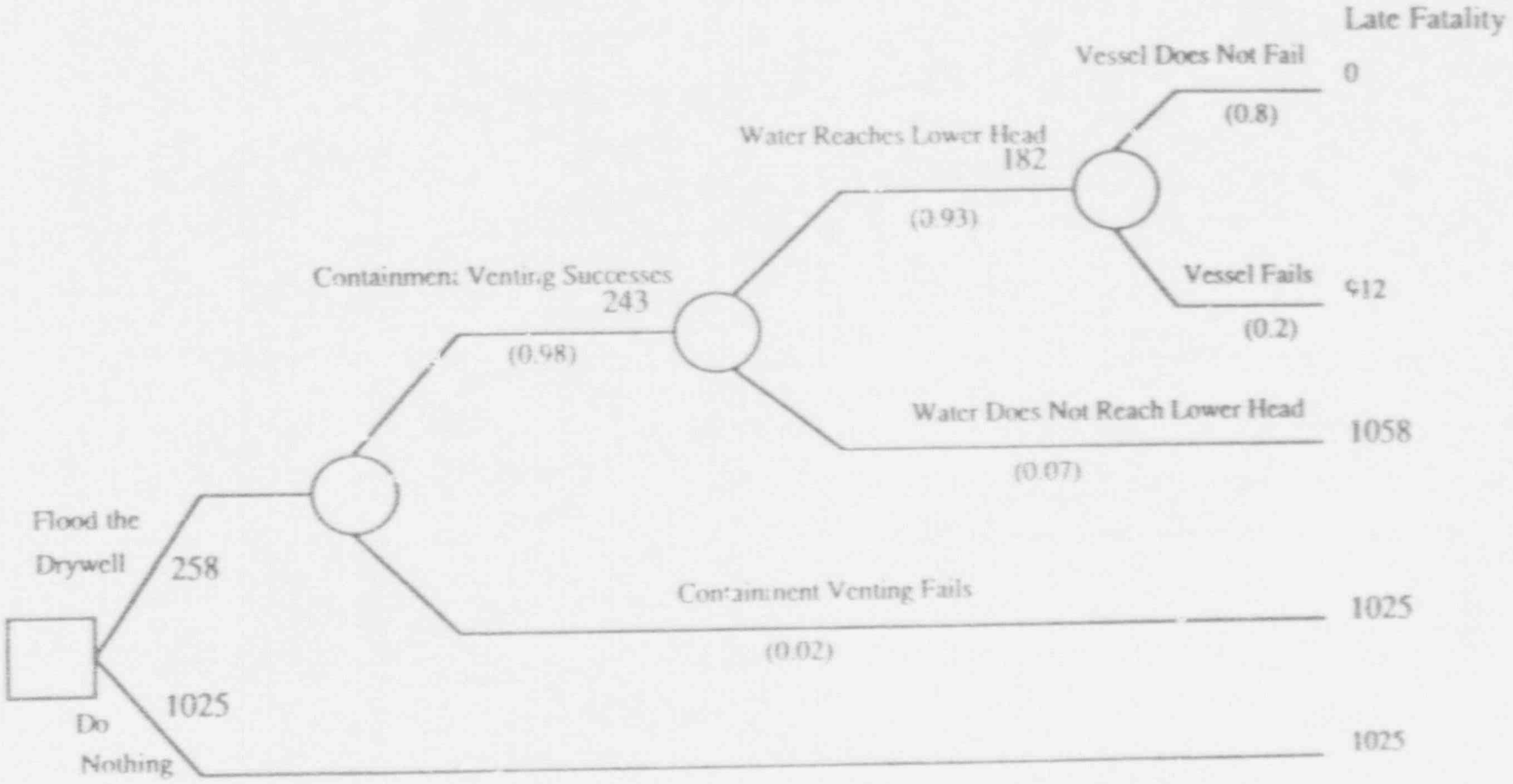

Figure 6. Simplified Decision Tree for BWR (Latent Cancer Fatality)

Table 1
The accident progress timing (min) for the Surry TMLB' sequence determined by three codes

	MARCH	SCDAP/RELAP5	MELPROG
Core Uncovery	97	129	117
Core Slumping	143	> 180	248
Vessel Breach	155	> 180	265
Time Interval between core uncovery and core slumping	46	> 50	130

Table 2
Results of base case calculation

Flood	No flood	ΔR	%
ECF 2.3 E-3	ECF 4.9 E-3	2.6 E-3	53
LCF 7.2 E-2	LCF 1.6 E-1	1.58 E-1	95
SGTR 2.8 E-2	SGTR 1.8 E-2	-1.0xE-2	-35
EF 6.4 E-3	EF 1.1 E-2	4.5E-3	
LF 5.4 E+1	LF 5.7 E+1	3.0E+0	5

ECF = Conditional Probability of Early Containment Failure
LCF = Conditional Probability of Late Containment Failure
SGTR = Conditional Probability of Steam Generator Tube Rupture
EF = Early Fatalities
LF = Late Fatalities

Table 3. Conditional probabilities of containment failure given vessel breach

Description	Flood	No Flood
Early Containment failure at high vessel pressure	2.46×10^{-1}	5.95×10^{-4}
Early Containment failure at low vessel pressure	1.85×10^{-2}	0.0
Liner Meltthrough at high vessel pressure	3.81×10^{-1}	7.34×10^{-1}
Liner Meltthrough at low vessel pressure	2.05×10^{-2}	3.50×10^{-2}
Isolation Failure	3.17×10^{-1}	0.0
Late Overpressurization Containment Failure	1.56×10^{-2}	2.30×10^{-1}
Total	1.00	1.00

Table 4. Expected Consequence Measures
for flood and no flood cases

Decision	Expected Early Fatalities	Expected Late Fatalities
Flood	1.396×10^{-3}	2.574×10^{2}
No Flood	5.675×10^{-3}	1.030×10^{3}

ASSESSMENT OF TWO BWR ACCIDENT MANAGEMENT STRATEGIES*

S. A. Hodge, M. Petek

Oak Ridge National Laboratory
Oak Ridge, Tennessee 37831

ABSTRACT

Candidate mitigative strategies for management of in-vessel events during the late phase (after core degradation has occurred) of postulated BWR severe accidents were considered at Oak Ridge National Laboratory (ORNL) during 1990. The identification of new strategies was subject to the constraint that they should, to the maximum extent possible, make use of the existing equipment and water resources of the BWR facilities and not require major equipment modifications or additions. As a result of this effort, two of these candidate strategies were recommended for additional assessment. The first is a strategy for containment flooding to maintain the core and structural debris within the reactor vessel in the event that vessel injection cannot be restored to terminate a severe accident sequence. The second strategy pertains to the opposite case, for which vessel injection would be restored after control blade melting had begun; its purpose is to provide an injection source of borated water at the concentration necessary to preclude criticality upon recovering a damaged BWR core.

Assessments of these two strategies have been performed during 1991 under the auspices of the Detailed Assessment of BWR In-Vessel Strategies Program. This paper provides a discussion of the motivation for and purpose of these strategies and the potential for their success.

1. INTRODUCTION

Boiling Water Reactors (BWRs) have unique features that would cause their behavior under severe accident conditions to differ significantly from that expected for the pressurized water reactor design[1-5]. Consequently, it has been necessary to analyze BWR accident sequences separately, and the NRC has sponsored programs at ORNL for this purpose since 1980[6]. The objective of these BWR severe accident programs has been to perform analyses of a spectrum of accident sequences beyond the design basis for typical specific U.S. BWR reactor designs. The accident sequences selected for analysis have been in general those identified as dominant in leading to core melt for BWRs by the methods of probabilistic risk assessment (PRA) as carried out by other programs. The specific plants modeled and the accident sequences considered were selected by the process of nomination by the ORNL program manager and approval by the NRC technical monitors.

The detailed analyses of the dominant severe accident sequences identified by PRA have been performed in recognition that PRA, by the basic nature of its requirements to consider every possible accident sequence, cannot enter into matters of detail. The purpose of the detailed analyses has been either to confirm the adequacy of or to challenge the simplifying assumptions necessarily applied to each accident sequence in the PRA and to provide a realistic appraisal of the sequence of events and the aftermath. Further preventive measures that might be taken to decrease the probability of each severe accident sequence studied and accident management procedures that might be implemented to reduce the consequences have been addressed. Feedback of the results of the detailed analyses has always been provided to the other facilities performing the PRA; most recently, this has involved close cooperation with the NUREG-1150 effort[7] at Sandia National Laboratories (SNL).

With the comprehensive information provided by NUREG-1150 concerning the relative probabilities of BWR severe accident sequences and with the knowledge and experience gained from the series of detailed accident analyses[8-22], the next logical step was to consider the facets of BWR severe accident management in a structured process, with the goal of identifying potential new strategies and enhancements. This was accomplished by means of an assessment of the current status of accident management procedures with respect to effective mitigation of the dominant BWR severe accident sequences. The accident sequences considered were Station Blackout and Anticipated Transient Without Scram (ATWS), which have been consistently identified by PRA to be the predominant contributors to the overall calculated core damage frequency for BWR internally-initiated accidents. There are two primary categories of Station Blackout, each leading to severe core damage if unmitigated, but at widely separated times. For the short-term case, reactor vessel injection capability is lost at the inception of the accident and core damage begins during the second hour after scram. For the long-term case, vessel injection is lost only after battery failure and core damage occur more than ten hours after scram. For ATWS as in Station Blackout, core damage would occur as a result of loss of vessel injection capability; this, however, is not expected to occur unless the ATWS involves reactor vessel isolation [closure of the main steam isolation valves (MSIVs)] and is compounded by failure of the plant boron injection system (or systems). The timing of core damage for an ATWS accident sequence that progressed this far would be determined by the effectiveness of the delaying actions taken by the plant operators.

The BWR Owners' Group Emergency Procedure Guidelines (EPGs)[23] were examined from the standpoint of their application to Station Blackout and ATWS. This was done for two reasons. The first objective was to determine the extent to which the EPGs currently implement the intent of the BWR accident management strategies that have been suggested in the report[24] *Assessment of Candidate Accident Management Strategies* (NUREG/CR-5474), published in March 1990. The second objective was to determine the extent to which the current operator actions specified by the EPGs would be effective in unmitigated severe accident situations. It was found that many of the recommended strategies are included in the current version (Revision 4) of the EPGs and that with one exception, the remaining involve plant-specific considerations to the extent that they may be more appropriate for inclusion within local plant emergency procedures than within the generic symptom-oriented EPGs. The exception is a strategy for injection of boron following core damage and control blade relocation, which clearly would be appropriate for the EPGs.

With respect to the second objective, the EPGs do not include guidelines for the late phase in-vessel events that would occur only after the onset of significant core damage. Instead, the guidance terminates with the specification of alternate methods for injecting water into the reactor vessel. The conclusions of this examination of the EPGs are documented in Reference 25; the

primary conclusions are that more can be done to provide guidance for late-phase operator actions and that the greatest potential for improvement of the existing BWR emergency procedure strategies lies in the area of severe accident management, both for determining the extent of ongoing damage to the in-vessel structures and for attempting to terminate the accident.

Based upon the results of these analyses, a second in-vessel severe accident management study[26] was undertaken to propose new strategies for mitigation of the late-phase events and to provide a discussion of the motivation for these strategies and a general description of the methods by which they might be carried out. Four candidate late accident mitigation strategies were proposed. These are:

1. Keep the Reactor Vessel Depressurized. Reactor vessel depressurization is important should an accident sequence progress to the point of vessel bottom head penetration failure because it would preclude direct containment heating (DCH) and reduce the initial threat to containment integrity. This candidate strategy would provide an alternate means of reactor vessel venting should the safety/relief valves (SRVs) become inoperable because of loss of control air or DC power. PRAs based upon the existing BWR facilities consistently include accident sequences involving loss of DC power and control air among the dominant sequences leading to core melt for BWRs.

2. Restore Injection in a Controlled Manner. Late accident mitigation implies actions to be taken after core melting, which requires at least partial uncovering of the core, which occurs because of loss of reactor vessel injection capability. BWRs have so many electric motor-driven injection systems that loss of injection capability implies loss of electrical power. (This is why Station Blackout is consistently identified by PRAs to be the dominant core melt precursor for BWRs.) If electric power were restored while core damage is in progress, then the automatic injection by the low-pressure, high-capacity pumping systems could be more than two hundred times greater than that necessary to remove the decay heat. This strategy would provide for controlled restoration of injection and would be particularly important if the control blades had melted and relocated from the core.

3. Inject Boron if Control Blade Damage Has Occurred. This strategy would provide that the water used to fill the reactor vessel after vessel injection capability was restored would contain a concentration of the boron-10 isotope sufficient to preclude criticality, even if none of the control blade neutron poison remained in the core region. This candidate strategy is closely related to Item 2, above.

4. Containment Flooding to Maintain Core and Structural Debris In-Vessel. This candidate strategy was proposed as a means to maintain the core residue within the reactor vessel in the event that vessel injection cannot be restored as necessary to terminate the severe accident sequence. Containment flooding to above the level of the core is currently incorporated within the EPGs as an alternative method of providing a water source to the vessel in the event of design-basis LOCA (the water would flow into the vessel from the drywell through the break). Here it is recognized that containment flooding might also be effective in preventing the release of molten materials from the reactor vessel for the risk-dominant non-LOCA accident sequences such as Station Blackout.

Finally, these four candidate strategies were evaluated for the purpose of selecting those that require and have sufficient potential to justify detailed quantitative assessment.[27]

The candidate strategy to keep the reactor vessel depressurized was not recommended for further assessment because it is believed far more practical to improve the reliability of the control air and DC power supplies for the SRVs than to invent alternative methods for venting the reactor vessel under severe accident conditions. Nevertheless, consideration of the reliability of control air and DC power should be an important part of the individual plant examination (IPE) process[28,29] since loss of these systems is inherent in the risk-dominant sequences leading to core melt consistently identified for BWRs by the PRA process.

The candidate strategy for containment flooding was recommended for further assessment. This proposed strategy has the potential of serving not only as a first-line defense in preventing the release of core and structural debris from the reactor vessel, but also as a second-line defense in preventing failure of the Mark I drywell shell if debris release from the reactor vessel did occur. All current considerations of the Mark I shell melt-through issue are based upon an assumption that the depth of water over the drywell floor would be limited to about 0.6 m (2 feet), the height at which overflow to the pressure suppression pool would occur. However, drywell flooding to surround the lower portion of the reactor vessel with water would provide more than 9 m (30 ft) of water over the floor. This would preclude direct shell failure considerations and, therefore, has the potential to be an excellent late mitigation strategy.

The candidate strategies for restoration of injection in a controlled manner and injection of boron if control blade damage has occurred were recommended to be combined into a single strategy for "Controlled Injection of Boron for Reactor Vessel Refill." This would provide for the addition of boron together with the injected flow being used to recover the core, in sufficient quantity to preclude criticality as the water level rises within the reactor vessel. A recent assessment by Pacific Northwest Laboratories[30] (PNL) indicates that criticality is probable should the BWR reactor vessel be reflooded after debris bed relocation has occurred, but suggests that the direct consequences might be controlled. On the other hand, criticality after core degradation and a shifting of the nature of the accident sequence is clearly undesirable.

It is the purpose of this paper to discuss the results of the detailed analyses of the two candidate strategies recommended for further assessment. The strategy for containment flooding is discussed in Section 2, while the strategy for controlled boron injection during vessel refill is described in Section 3.

2. DRYWELL FLOODING AS A LATE ACCIDENT MITIGATION STRATEGY

As described in the Introduction, candidate mitigative strategies for management of in-vessel events during the late phase (after core degradation has occurred) of postulated BWR severe accidents have been considered at Oak Ridge National Laboratory (ORNL). This identification of strategies was subject to the constraint that they should, to the maximum extent possible, make use of the existing equipment and water resources of the BWR facilities and not require major equipment modifications or additions. One of the recommendations developed by this Program for Detailed Assessment of BWR In-Vessel Strategies calls for additional assessment of a strategy for containment flooding to maintain the core and structural debris within

the reactor vessel in the unlikely event that vessel injection could not be restored as necessary to terminate a severe accident sequence.

Geometric effects of reactor vessel size dictate that the effectiveness of external cooling of the vessel bottom head as a means to remove decay heat from an internal debris pool would be least for the largest vessels. Considering also that the motivation for maintaining any core and structural debris within the reactor vessel is greatest for the Mark I drywells, the primary focus of this assessment was upon the largest BWR Mark I containment facilities such as Peach Bottom or Browns Ferry.

The immediate goal of the considered strategy for containment flooding would be to surround the lower portion of the reactor vessel with water, thereby protecting both the instrument guide tube penetration assemblies and the vessel bottom head itself from failure by overtemperature. The threat would be provided by the increasing temperature of the lower plenum debris bed after dryout. First, molten liquids forming within the bed would relocate downward into the instrument guide tubes challenging their continued integrity. Subsequently, heating of the vessel bottom head by conduction from the debris would threaten global failure of the wall by creep rupture.

Nevertheless, it seems beyond question that all portions of the reactor vessel pressure boundary (including the instrument guide tubes) that are contacted by water on their outer surfaces would survive any challenge imposed by a lower plenum debris bed or its relocated liquids. There is a problem, however, in that most of the upper portion of the reactor vessel could not be covered by water and, more significant in the short term, much of the outer surface of the vessel bottom head would be dry as well.

That the upper portion of the reactor vessel could not be covered is due to the location within the containment of the drywell vents. Since low-pressure pumping systems would be used for flooding, the drywell would have to be vented during filling and the water level could not rise above the elevation of the vents, at about two-thirds vessel height. That much of the outer surface of the reactor vessel bottom head would be dry is due to the gas pocket that would be trapped within the vessel support skirt during the process of raising the water level within the drywell. Figure 1 indicates the approximate size of this gas pocket for the Browns Ferry reactor vessel, with the assumption that gas leakage through the manhole access cover does not occur.

The results of this assessment demonstrate that the existence of a trapped gas pocket beneath the vessel skirt attachment would ultimately prove fatal to the integrity of the bottom head wall. Nevertheless, the most important attribute of drywell flooding, that of preventing early failure of the instrument guide tube penetration assemblies, would be realized. These results are among those listed in Table 1 where it is shown (first entry) that in the absence of water, penetration assembly failures would be expected at about 250 minutes after scram. If penetration failures did not occur, then creep rupture of the bottom head would be expected after 10 hours if the bottom head is dry and after 13 hours if the drywell is flooded. However, since penetration failures are expected to occur in the absence of water, the important contribution of drywell flooding is to shift the expected failure mode from penetration failures (Table 1 first entry) to bottom head creep rupture (Table 1 third entry).

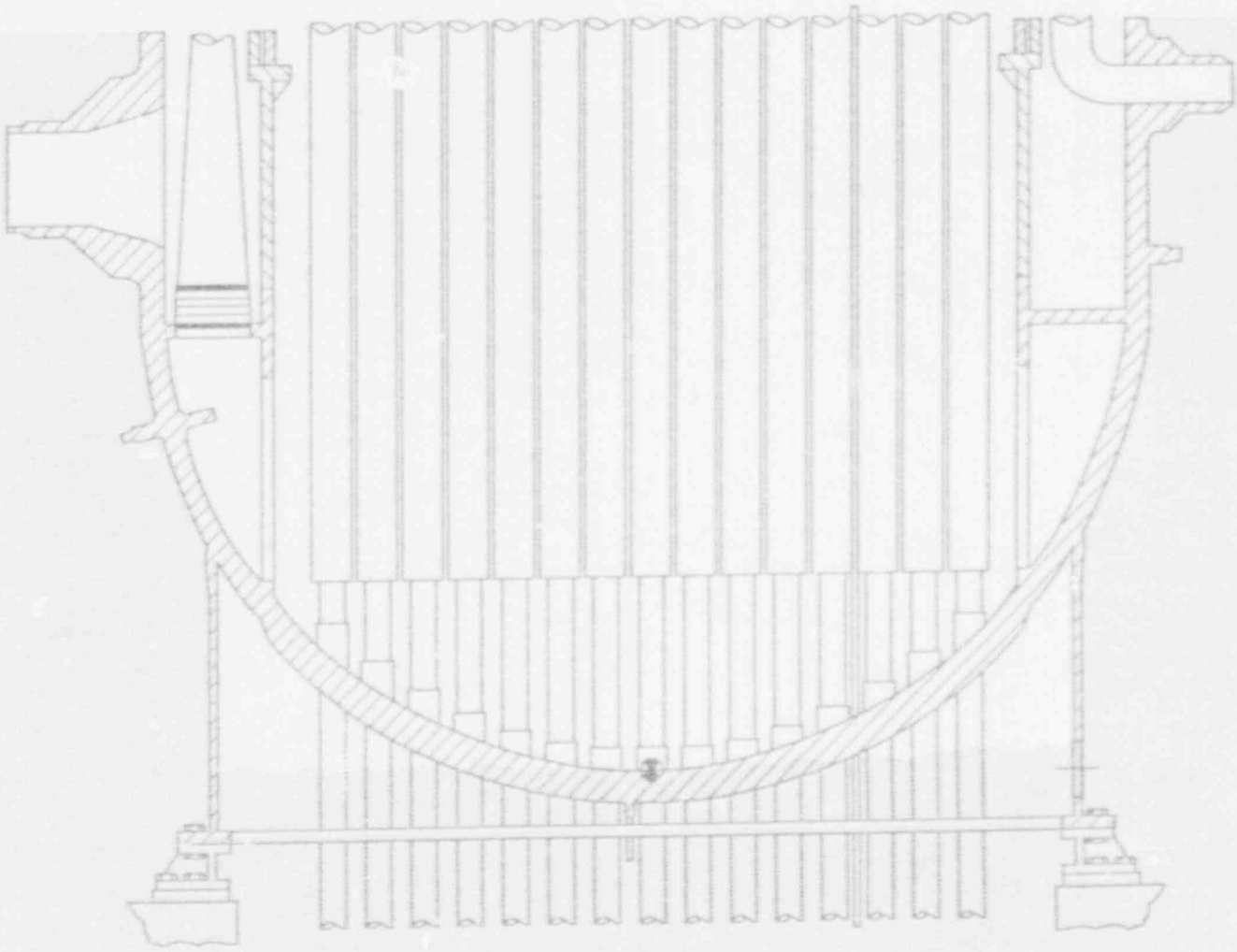

Fig. 1. The water level within the vessel skirt would be limited by the trapping of a portion of the drywell atmosphere.

Table 1. Estimated failure times for the reactor vessel bottom head pressure boundary for Peach Bottom/Browns Ferry short-term station blackout

Drywell Flooded	Failure Mechanism	Time to Failure	
		Minutes	Hours
No	Penetration Assemblies	250	4.2
No	Bottom Head Creep Rupture	600 – 640	10.0 – 10.7
Yes	Bottom Head Creep Rupture	780 – 840	13.0 – 14.0

The effectiveness of drywell flooding could be improved if the reactor vessel support skirt were vented in order to reduce the trapped gas volume and increase the fraction of bottom head surface area contacted by water. Partial venting could be achieved by loosening the cover on the support skirt manhole access. This would increase the covered portion of the bottom head from 55% to 73% of the total outer surface area, which delays the predicted time of bottom head creep rupture by about one hour. (The reduced gas pocket for this case is illustrated in Figure 2.) The predicted failure times for the basic case without skirt venting and for the case of partial venting at the manhole access are indicated in the first two entries of Table 2.

Table 2. Effect of skirt venting upon time to failure of the bottom head pressure boundary for Peach Bottom/Browns Ferry short-term station blackout with drywell flooding

Skirt Vented	Failure Mechanism	Time to Failure	
		Minutes	Hours
No	Bottom Head Creep Rupture	780 – 840	13.0 – 14.0
Partial	Bottom Head Creep Rupture	840 – 900	14.0 – 15.0
Complete	Melting of Upper Vessel Wall	>1200	>20.0

Complete venting of the reactor vessel support skirt would provide 100% water coverage of the vessel bottom head but would require special measures such as the drilling of small holes at the upper end of the skirt, just below the attachment weld. This is not considered to be a practical suggestion for the existing BWR facilities, but complete venting might be attainable for the advanced BWR designs. As indicated by the last entry in Table 2, 100% water coverage of the vessel bottom head would convert the failure mechanism from bottom head creep rupture to melting of the upper vessel wall and would delay the predicted time of failure to more than 20 hours after scram.

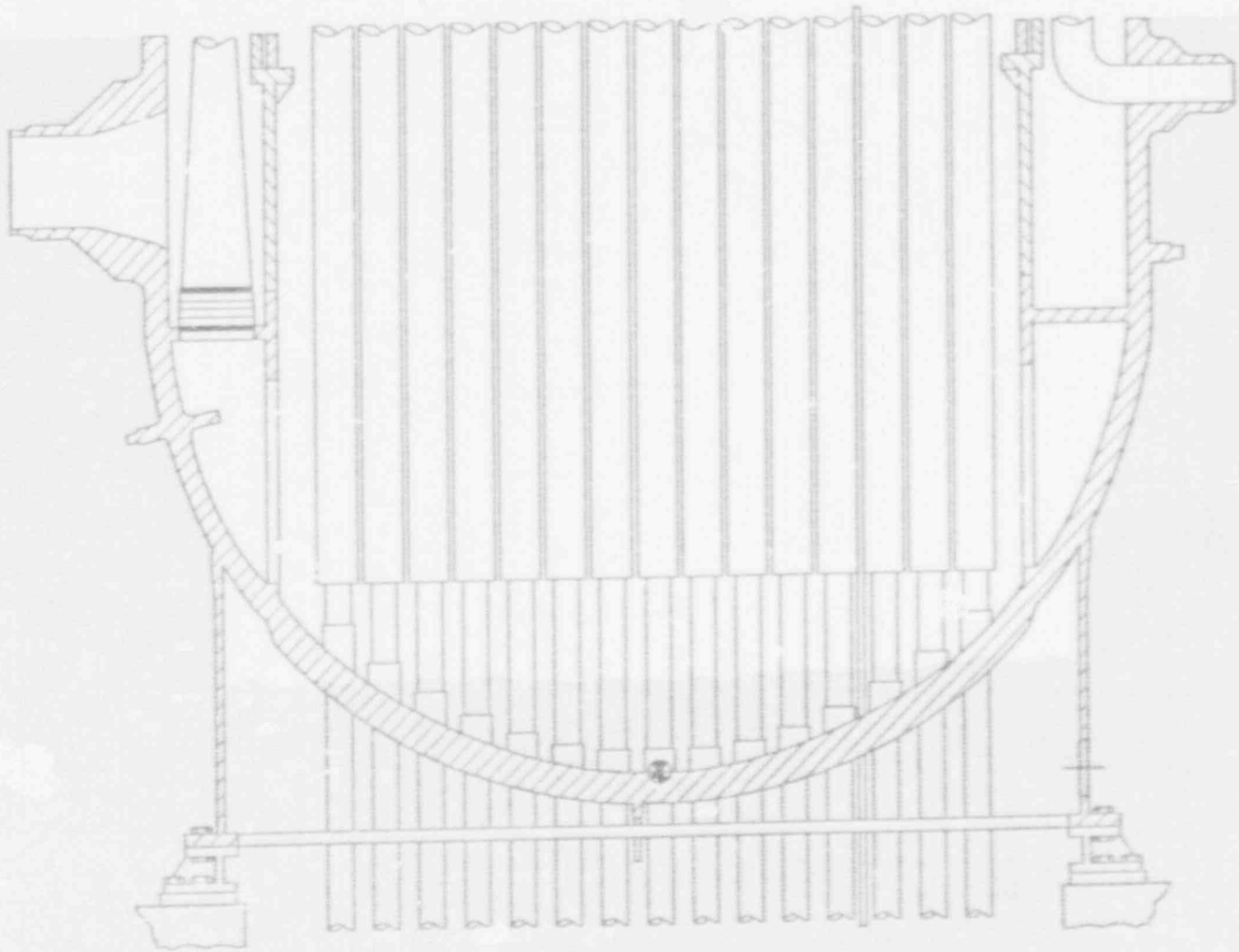

Fig. 2. The volume of gas trapped beneath the reactor vessel support skirt can be reduced by providing a vent path from the manhole access cover.

In summary, all portions of the reactor vessel wall that are covered by water would be adequately protected against failure by melting or creep rupture. For the cases with no venting or partial venting of the support skirt, the creep rupture failure is predicted to occur in the portion of the vessel wall adjacent to the trapped gas pocket beneath the skirt. Partial venting would reduce the size of the gas pocket and delay the predicted time of failure, but the failure mechanism would still be creep rupture beneath the skirt attachment weld. With complete venting, however, there would be no gas pocket and this failure mechanism would be eliminated.

What cannot be eliminated, however, is the radiative heat transfer upward within the reactor vessel from the surface of the lower plenum debris bed. About one-half to two-thirds of all energy release within the bed would be radiated upward after bottom head dryout. Initially, the primary heat sink for this radiation would be the water trapped in the downcomer region between the core shroud and the vessel wall above the debris bed. It is the heating of this water that creates the only steam source within the reactor vessel after lower plenum dryout.

After the water in the downcomer region became exhausted, the upward radiative heat transfer from the debris surface would serve to increase the temperature of the upper reactor vessel internal structures. For calculations with the existence of a gas pocket beneath the skirt, bottom head creep rupture is predicted to occur while the temperature of these internal stainless steel heat sinks remains below the melting point. If bottom head creep rupture did not occur, however, the debris would remain within the vessel, the upward radiation would continue, and the upper internal structures would melt.

The mass of the BWR internal structures (core shroud, steam separators, dryers) is large. Melting of these stainless steel structures under the impetus of the upward debris pool radiation (more than 14 hours after scram) would occur over a long period of time. Nevertheless, decay heating of the debris pool and the associated upward radiation would be relentless and, after exhaustion of the stainless steel, the only remaining internal heat sink above the pool surface would be the carbon steel of the upper vessel wall. All portions of the wall cooled by water on their outer surfaces would remain intact, but those upper portions of the vessel exposed to the well atmosphere would ultimately reach failure temperatures.

It should be obvious from this discussion of the effect of water upon cooling of the vessel wall that it would be desirable to have a drywell flooding strategy that would completely submerge the reactor vessel. This could not be achieved in existing facilities because of the limitation that the height of water within the drywell cannot exceed the elevation of the drywell vents. Future designs, however, might provide for complete coverage of the reactor vessel as a severe accident mitigation technique.

Table 3 provides a summary of the calculated failure times and release mechanisms for all of the cases considered in this study. These include the cases previously discussed in connection with Tables 1 and 2, plus one additional case (third entry) in which it is assumed that reactor vessel pressure control is lost at the time of drywell flooding, because of the submergence of the safety/relief valves. [The location of these valves (SRVs) within the Browns Ferry drywell is shown in Figures 3 and 4.] The increased wall tensile stress associated with this case would cause the wall creep rupture to occur at a lower temperature, advancing the time of failure by about two hours over the depressurized case (compare the third and fourth entries in Table 3).

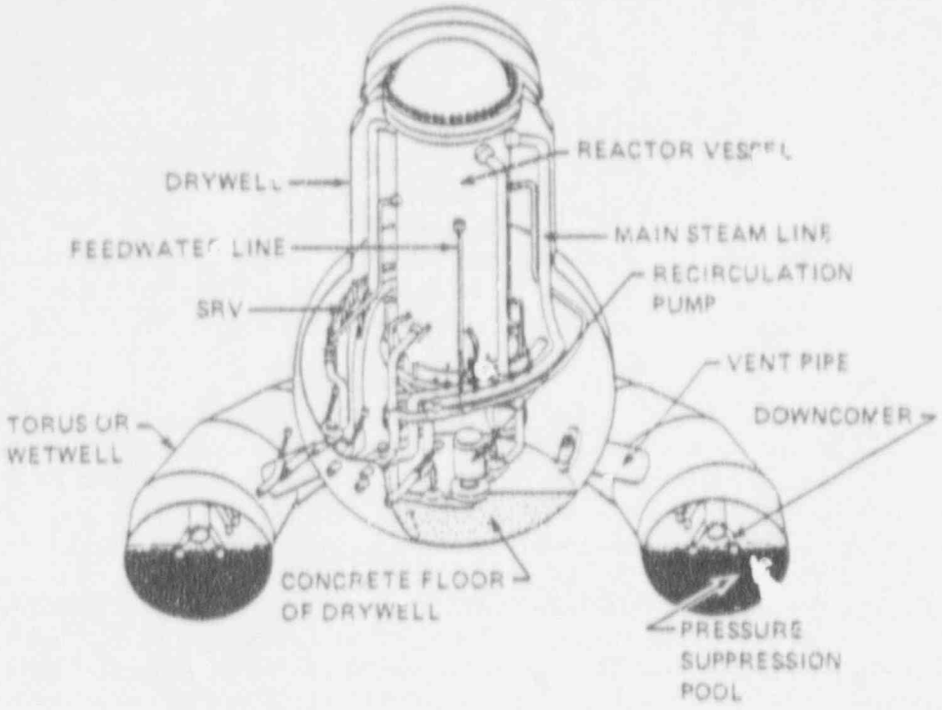

Fig. 3. The reactor vessel safety/relief valves are located on the horizontal runs of the main steam lines, near the bottom of the vessel.

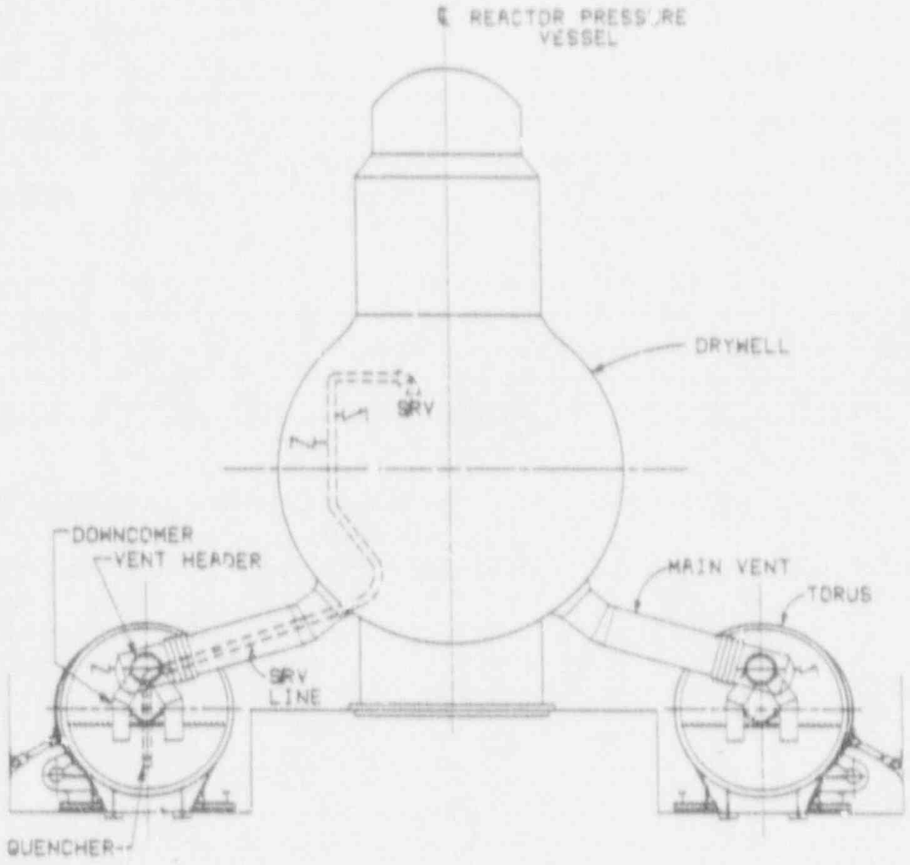

Fig. 4. Location of a typical safety/relief valve and its tailpipe within the BWR Mark I containment.

Table 3. Effect of drywell flooding upon time of debris release from the reactor vessel for the short-term station blackout accident sequence based upon Peach Bottom/Browns Ferry

Drywell Flooded	Skirt Vented	Reactor Vessel Depressurized	Release Mechanism	Time to Failure	
				Minutes	Hours
No	—	Yes	Penetration Failures	250	4.2
No	—	Yes	Bottom Head Creep Rupture	600 – 640	10.0 – 10.7
Yes	No	No	Bottom Head Creep Rupture	660 – 700	11.0 – 11.7
Yes	No	Yes	Bottom Head Creep Rupture	780 – 840	13.0 – 14.0
Yes	Partial	Yes	Bottom Head Creep Rupture	840 – 900	14.0 – 15.0
Yes	Complete	Yes	Melting of Upper Vessel Wall	>1200	>20.0

The most important disadvantage of a drywell flooding strategy for existing plants is the requirement for venting to the external atmosphere while the containment is being filled by the low-pressure pumping systems and during the subsequent steaming from the water surrounding the reactor vessel bottom head. Because of this, implementation of the drywell flooding strategy would initiate a noble gas release to the surrounding atmosphere as well as a limited escape of fission product particulates. All particulate matter released from the reactor vessel prior to failure of the vessel wall would enter the pressure suppression pool via the safety/relief valve T-quenchers and would be scrubbed by passage through the water in both the wetwell and drywell. Therefore, the concentration of particulates in the drywell atmosphere and any release through the drywell vents would remain small as long as the reactor vessel wall remained intact.

Creep rupture of the vessel bottom head beneath the support skirt attachment would release debris into the water-filled pedestal region to fall downward onto the drywell floor. Since containment flooding would provide a water depth of more than 9 m (30 ft) over the drywell floor, the particulate matter released from the debris mass should be adequately scrubbed provided,

of course, that violent steam explosions do not occur. Furthermore, the large volume of water in the drywell would protect the drywell shell from failure in Mark I containment facilities.

The advantages and disadvantages of a drywell flooding strategy for existing BWR facilities are summarized in Table 4. The listed advantages involve significant contributions to accident mitigation, which have previously been discussed. The listed disadvantages, however, are also important and will be discussed in the following paragraphs.

Table 4. Advantages and disadvantages of a drywell flooding strategy for severe accident mitigation in existing BWR facilities

Advantages	1. Prevent failure of the bottom head penetrations and vessel drain 2. Increased scrubbing of fission product particulate matter 3. Delay creep rupture of the reactor vessel bottom head 4. Prevent failure of the Mark I drywell shell when core debris does leave the vessel
Disadvantages	1. Requires availability of power source and pump capable of filling the drywell to the level of the vessel bottom head within 150 minutes under station blackout conditions. 2 Requires that the drywell be vented.

First, implementation of the proposed strategy would require equipment modifications and additions. Although there may be plant-specific exceptions, containment flooding with the existing pumping systems would require too much time; furthermore, the existing systems would not be available for the dominant station blackout accident sequences. What is needed is a reliable ability to sufficiently flood the drywell within a short period of time, since it would be unrealistic to expect that emergency procedures would call for containment flooding (and the associated undesirable effects upon installed drywell equipment) until after core degradation had begun. If the water did not reach the vessel bottom head until after lower plenum debris bed dryout and the initial heating of the vessel wall, it would be too late to prevent penetration assembly failures.

The second disadvantage, that the drywell vents would have to be opened to permit flooding of the containment, is particularly undesirable since it would involve early release of the fission product noble gases, beginning soon after the onset of core degradation. After the water had contacted the vessel bottom head, a continuous steam generation would begin within the

drywell that would be released to the outside atmosphere by means of the open vents. This would tend to sweep any particulate matter from the drywell atmosphere through the vents. The amount of particulate matter reaching the drywell atmosphere would, however, be limited by water scrubbing as long as the reactor vessel wall remained intact above the water level in the drywell. This is expected to be the case for the existing BWR facilities where the ultimate failure of the wall would occur by creep rupture beneath the skirt attachment weld.

It is interesting, however, to briefly consider the potential benefits of application of a drywell flooding strategy to future BWR facilities, where the disadvantages listed in Table 4 might be avoided by appropriate plant design. Much less water would be required since the reactor vessel would be located in a cavity instead of suspended high above a flat drywell floor. Provision could be made for complete venting of the reactor vessel support skirt so that all of the bottom head would be in contact with water. This would preclude creep rupture of the vessel bottom head, shifting the potential failure mode to melting of the upper vessel wall, above the water level in the drywell.

For the existing BWR facilities, failure of the upper reactor vessel wall would provide a direct path from the upper surface of the debris pool to the open drywell vents without the benefit of water scrubbing. This corresponds to the last entry in Table 3, which is based upon complete venting of the vessel support skirt (not considered practical for the existing facilities). For future plant designs, the potential for a direct release pathway could be avoided in two ways. First, complete vessel submergence would preclude failure of the upper vessel wall. Second, the requirement for containment venting could be eliminated by provision of an adequate water source within the containment and provision for condensation of the generated steam. Both of these approaches are within the scope of design features currently under consideration for the advanced passive design.

This study of the effectiveness of drywell flooding is currently documented by letter report (ORNL/NRC/LTR-91/9). However, it is anticipated that these results will be incorporated into a NUREG/CR report during 1992.

3. POISONING THE INJECTION SOURCE

The second recommendation developed as a result of the consideration of candidate mitigative strategies for in-vessel events during the late phase (after core degradation has occurred) of postulated BWR severe accidents addresses the prevention of undesired criticality.

If significant control blade melting and relocation were to occur during a period of temporary core uncovering, then criticality would follow restoration of reactor vessel injection capability if the core were rapidly recovered with unborated water using the high-capacity low-pressure injection systems. If the relatively slow Standby Liquid Control System (SLCS) were simultaneously initiated to inject sodium pentaborate solution, then the core would remain critical until sufficient boron for shutdown reached the core region. It would be preferable, if control blade melting and relocation has occurred, to inject only a boron solution provided that this can be done at a rate sufficient to provide core cooling and terminate core damage.

The specific goal of the proposed strategy is to provide for the addition of the boron-10 isotope together with the injected flow being used to recover the core, in sufficient quantity to preclude criticality as the water level rises within the reactor vessel. It is expected that this could be accomplished using only existing plant equipment. One way to do this would be to mix the boron directly with the water in the condensate storage tank and then take suction on the condensate storage tank with the low-pressure system pump to be used for vessel injection. It is, however, not a simple matter to invoke this strategy and preplanning and training would be required.

With respect to the rationale for incorporation of this strategy, a recent Pacific Northwest Laboratory (PNL) report[30] establishes that criticality upon reflooding with unborated water is likely for either standing fuel rods or for a debris bed subsequently formed in the core region. It is not unreasonable that this prediction alone should provide sufficient motivation for incorporation of a boration strategy since there is a strong potential for operator surprise and confusion should, for example, a station blackout accident sequence be converted into an ATWS-type sequence upon restoration of reactor vessel injection capability. However, the PNL report makes the conclusion that:

> "— it appears that a super prompt-critical excursion (in which some fuel vaporization, dispersal of molten fuel debris, rapid molten fuel-coolant interaction, and the production of a large pressure pulse capable of directly failing the vessel and/or containment occurs) is not credible under conditions of reflooding a hot, degraded core; even under conditions of maximum reflood rate. Doppler feedback, in itself, appears to be adequate to limit the energetics of reflood recriticality to a level below which the vessel would be threatened by a pressure pulse. It is more likely that the reactor would either achieve a quasi-steady power level or enter an oscillatory mode in which water periodically enters and is expelled from the core debris. In either case, the average power level achieved is determined by the balance between reactivity added and the feedback mechanisms. Criticality in debris beds will probably produce power levels no larger than 10 to 20 percent of normal power. At these levels, the coolant makeup systems could provide adequate coolant to remove the heat generated within the debris bed."

Thus, one might conclude that the criticality attendant to reflooding could be controlled in the same manner as an ATWS, that it could be terminated by normal means [use of the SLCS], and that no dedicated strategy for preventing the criticality is required.

Nevertheless, criticality produced by reflooding after core damage has characteristics very different from those associated with ATWS, including not being addressed by current procedures, the probable lack of nuclear instrumentation, and the factor of operator surprise. The configuration of the critical masses in the core region might be standing fuel rods alone, a combination of standing fuel rods (outer core) and debris beds (central core), or a core-wide debris bed. Consultation with Dr. Jose March-Leuba of ORNL, who has recently performed a series of BWR stability calculations[31], reveals that there is a potential for much more serious consequences of criticality by rapid reflooding than those indicated by the PNL report. While he does not recommend any further attempts at this time to calculate a power-vs-time profile for reflooding without control blades (the state of the art would not permit a definitive result), he does believe that the current state of knowledge, based upon available information from previous calculations, supports a conclusion that preventative measures are desirable.

The PNL report provides the estimate that a boron-10 concentration of between 700 and 1000 ppm would be required within the reactor vessel to preclude criticality once control blade melting had occurred. The next Section describes the concentration achievable with the SLCS.

3.1 INJECTION WITH THE STANDBY LIQUID CONTROL SYSTEM

The normal means of adding boron to the reactor vessel is by dedicated injection by the Standby Liquid Control System (SLCS). While this system is designed to inject sufficient neutron-absorbing sodium pentaborate solution into the reactor vessel to shut down the reactor from full power (independent of any control rod motion) and to maintain the reactor subcritical during cooldown to ambient conditions, the SLCS is not intended to provide a backup for the rapid shutdown normally achieved by scram.

As indicated in Figure 5, the basic system comprises a heated storage tank, two 100% capacity positive displacement pumps, and, as the only barrier to injection to the reactor vessel, two explosive squib valves. In most of the current BWR facilities, the sodium pentaborate solution enters the reactor vessel via a single vertical sparger located at one side of the lower plenum just below the core plate as indicated in Figures 6 and 7. An effort to improve the mixing and diffusion of the injected solution (which has a specific gravity of about 1.3) throughout the core region has lead some BWR facilities to provide a third positive displacement pump and to cause the injected solution to enter the reactor vessel via the core spray line and sparger.

For the purpose of reducing the time required for reactor shutdown for the ATWS accident sequence, the NRC has recently required that the SLCS injection be at a rate *equivalent* to 86 gpm of 13-weight percent sodium pentaborate solution, the boron being in its natural state with 19.8 atom percent of the boron-10 isotope.* This requirement is established by the "ATWS rule," which states, in part:

> "Each boiling water reactor must have a standby liquid control system (SLCS) with a minimum flow capacity and boron content equivalent in control capacity to 86 gallons per minute of 13-weight percent sodium pentaborate solution."[32]

Since the original SLCS standard design provided for single-pump operation at a rate of 43 gpm, the ATWS rule permits the requirement for the increased equivalent control capacity to be satisfied by simultaneous operation of both of the installed pumps, by increasing the concentration of sodium pentaborate solution, or by enriching the boron within the sodium pentaborate solution in the isotope boron-10. Different BWR facilities have taken different approaches.

The sodium pentaborate solution is normally prepared by dissolving stoichiometric quantities of borax and boric acid within hot demineralized water according to the reaction**

$$Na_2B_4O_7 \cdot 10H_2O + 6H_3BO_3 \rightarrow Na_2B_{10}O_{16} \cdot 10H_2O + 9H_2O.$$

As an illustrative example based upon a representative volume of the standby liquid control solution tank, 4076 lbs of borax and 3963 lbs of boric acid crystals dissolved within

---

* It is the ${}_5B^{10}$ isotope that has the large absorption cross section (3840 barns). The reaction is ${}_5B^{10} + {}_0n^1 \rightarrow {}_3Li^7 + {}_2He^4$.

** As written, the reaction shows equivalent sodium pentaborate as a product.

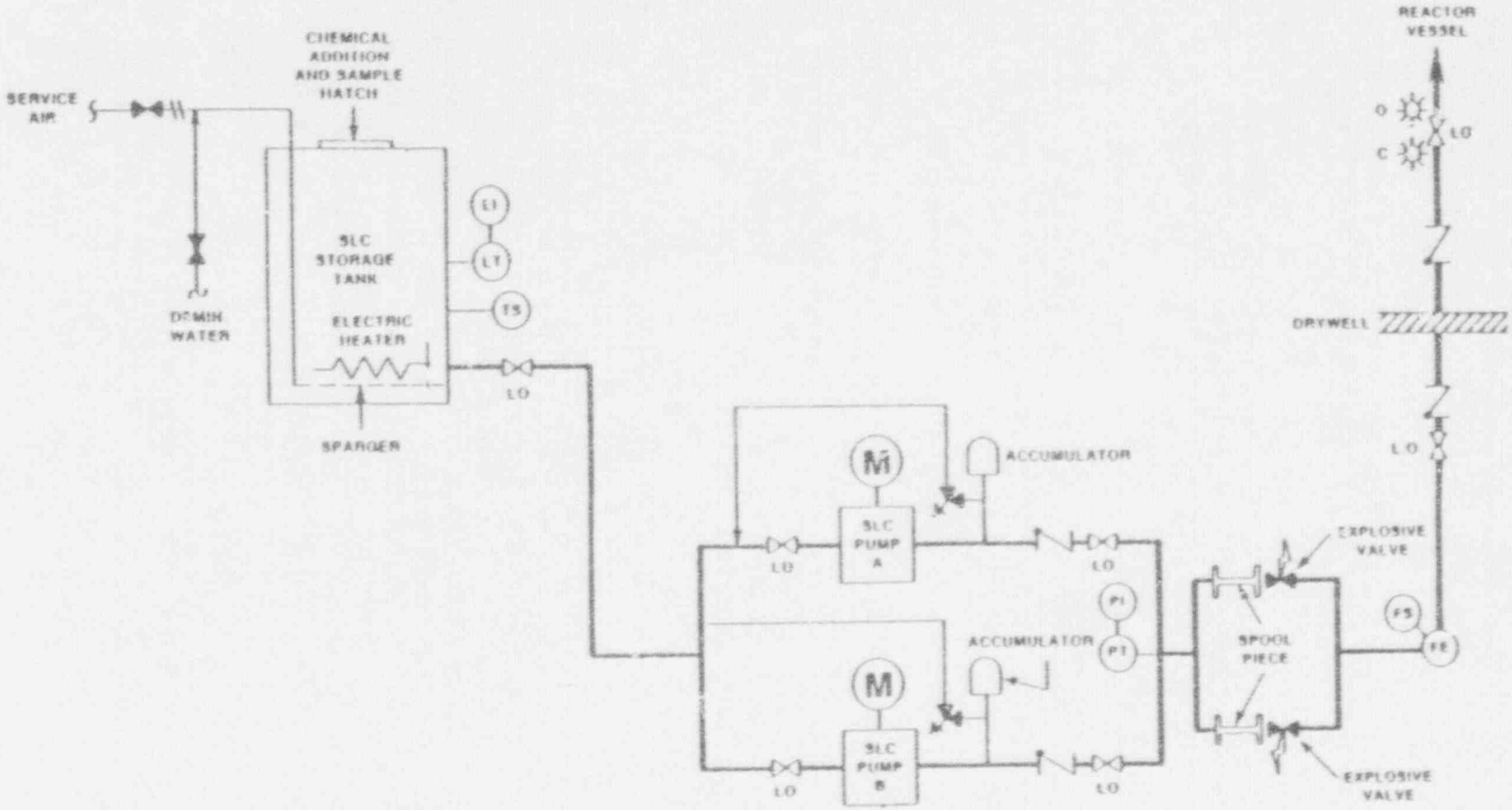

Fig. 5. Abbreviated schematic of the typical BWR standby liquid control system (SLCS). For clarity, all piping exclusively dedicated to system testing has been deleted from this drawing.

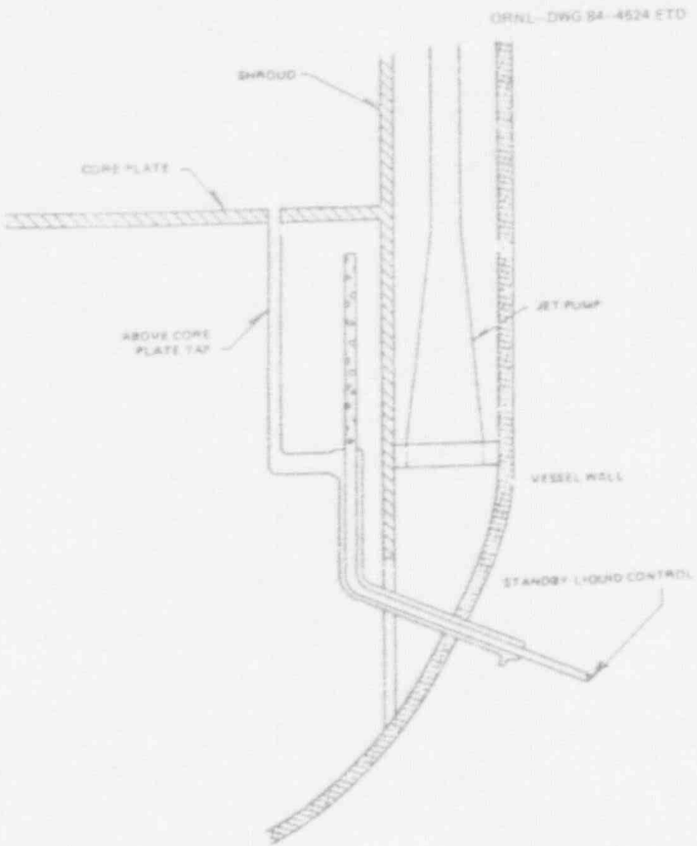

Fig. 6. Location of standby liquid control system injection sparger within the BWR-4 reactor vessel.

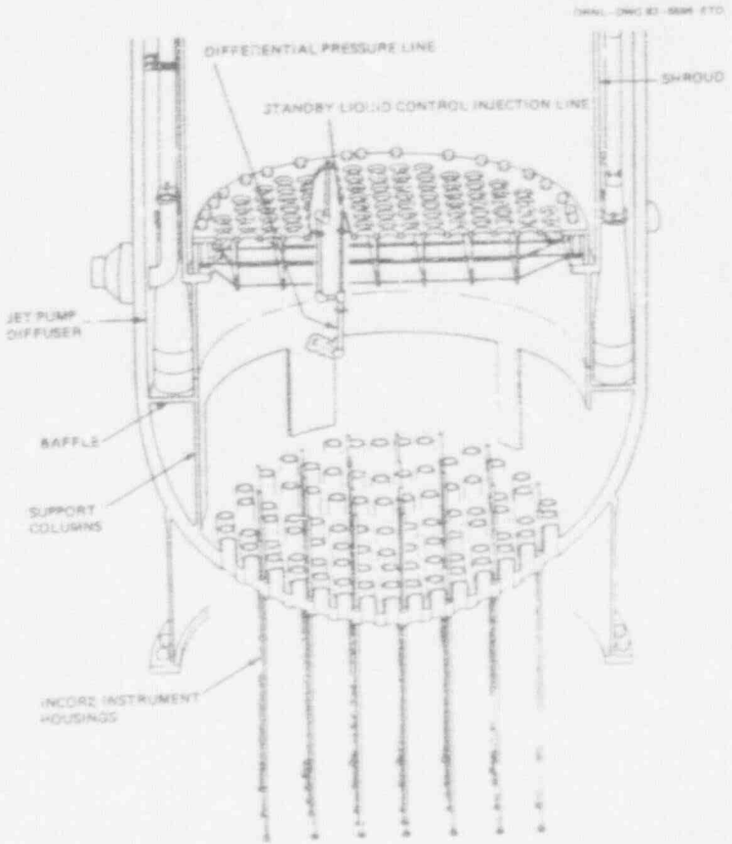

Fig. 7. The differential pressure and standby liquid control system injection line enters the reactor vessel as two concentric pipes, which separate in the lower plenum. The inner pipe, which terminates with a perforated length below the core plate is used during normal operation to sense the below-plate pressure and is used for sodium pentaborate injection when required. The outer pipe terminates immediately above the core plate and senses the pressure in the interstitial region of the core.

4608 gallons of water will produce an aqueous solution containing 6305 lbs of sodium pentaborate. This is 13.6% sodium pentaborate by weight. The tank contains 1155 lbs of boron and, assuming that the boron is in its natural state (not enriched), 228.5 lbs of the boron-10 isotope.

Continuing the example, the SLC tank contains 46,360 lbs of solution so the concentration of natural boron within the tank would be 24,900 ppm. Since the mass of water within the reactor vessel (at normal water level and operating temperature) is 628,300 lbs,** the concentration of natural boron within the reactor vessel after the contents of the SLC tank had been added would be approximately 1840 ppm (the concentration of the boron-10 isotope would be about 360 ppm).

After the reactor had been brought subcritical, the next steps toward complete shutdown would involve cooldown and vessel filling. The reactor vessel water mass with normal water level at 70°F would be 850,000 lbs so that water addition during cooldown would reduce the concentration of natural boron to 1360 ppm. Finally, with the vessel completely filled after cooldown, the water mass would be 1,400,000 lbs and the natural boron concentration would be 825 ppm. With the boron in its natural state, the concentration of the boron-10 isotope would be 163 ppm, which is sufficient to maintain the core shutdown in the cold, xenon-free condition.

Thus, the basic operational concept of the SLCS for ATWS control is that the very high concentration of boron in the relatively small SLC tank is diluted to the desired value when pumped into the much larger reactor vessel and mixed with the vessel water inventory.

Where BWR facilities have chosen to enrich the sodium pentaborate solution in the boron-10 isotope rather than to increase the pumping rate, it is the boric acid constituent that is enriched, typically to 92 atom percent. This approach maintains the SLCS redundancy of having two pumps capable of independent operation.

Under severe accident conditions, injection of neutron poison may be required for a situation very different than that normally associated with ATWS. If significant control blade melting and relocation from the core region were to occur during a period of temporary core uncovering, then criticality should be expected if reactor vessel injection capability is restored and the core is then covered with cold unborated water.[30] This situation is most likely to occur with restoration of electrical power after a period of station blackout. If the SLCS were used to inject the sodium pentaborate solution at a relatively slow rate while the core was rapidly covered using the high-capacity low-pressure injection systems, then criticality would occur and the core would remain critical until sufficient boron for shutdown reached the core region.

It would be preferable, if control blade melting and relocation has occurred, to reflood the vessel from an injection source such as the condensate storage tank containing a premixed solution of neutron poison so that there would be no threat of criticality as the core was recovered. This must be achievable, however, at a rate sufficient to provide immediate core cooling and, thereby, terminate core damage. The major diagnostic concern with respect to this strategy is that the operators would have no direct means of knowing whether or not significant control blade melting and relocation had occurred. Therefore, either the injection source would have to be poisoned after any non-trivial period of core uncovering or reliance would have to be made on precalculated values of time to control blade melting for the various accident situations.

** Water mass for a 251-inch ID BWR 3/4 reactor vessel, including the recirculation loops at the hot rated condition.

3.2 AN ALTERNATIVE METHOD OF FORMING THE POISON SOURCE

On two counts, operation of the SLCS would not prevent criticality upon vessel reflood following a period of temporary core uncovering with control blade melting. First, the injection of poison by this system would be too slow. Second, the amount of poison injected would be insufficient. Based upon the recent PNL analysis,[30] a concentration of 700-1000 ppm of the boron-10 isotope would be required to ensure that criticality would not occur as the damaged core was covered. As discussed in Section 3.1, the concentration provided by operation of the SLCS is less than 200 ppm.

In addition, formation of sodium pentaborate by the normal method of separately adding borax and boric acid crystals would not be feasible at low temperatures and without mechanical mixing. Information concerning an alternative boron form was obtained by contacting the U.S. Borax Company at Montvale, NJ. The Company produces disodium octaborate tetrahydrate ($Na_2B_8O_{13} \cdot 4H_2O$) in readily soluble powder form, under the tradename Polybor. Boron constitutes 20.97% of the total weight of Polybor, as opposed to 18.32% of the weight of sodium pentaborate. Using Polybor, the total amount of material needed to form a given concentration of natural boron is significantly (about one-third) less than for borax and boric acid. For example, preparation of a concentration of 24,900 ppm within 4,608 gallons of water (as in the example of Section 3.1, would require the addition of 8,039 lbs of borax and boric acid, but only 5,171 lbs of Polybor. Much of the difference lies in the excess water added with the borax ($Na_2B_4O_7 \cdot 10H_2O$).

The chief industrial use of Polybor is for fire retardant treatment of lumber by heavy spray application or by immersion of decorative and other cellulosic materials. It readily dissolves in water, forming supersaturated solutions. The following Table, supplied by the U.S. Borax Company, indicates its superior solubility (under equilibrium conditions) in water.

Table 5. Solubility of Polybor in water and corresponding concentrations of B_2O_3 compared with Borax at the same temperature

Temperature K	Temperature °F	weight % Polybor	% Concentration of B_2O_3 in saturated solutions of: Polybor	Borax
273	32	2.4	1.6	0.73
283	50	4.5	3.0	1.13
293	68	9.5	6.3	1.72
303	86	21.9	14.5	2.63
313	104	27.8	18.4	4.10
323	122	32.0	21.2	6.54
333	140	35.0	23.2	11.07
348	167	39.3	26.0	14.67
367	201	45.3	30.0	21.00

Polybor dissolves even in cool water to give supersaturated solutions of considerably higher concentration than indicated in Table 5. Simple table-top experiments at Oak Ridge have demonstrated that Polybor dissolves much more readily in water than does the normally used mixture of borax and boric acid crystals. (There is no need for two separate powders to interact in the case of Polybor.) This is of interest because the accident management strategy under consideration must be capable of use under station blackout conditions, when the water in the condensate storage tank may have cooled significantly at the time the borated solution was to be prepared and mechanical mixing of the tank contents would not be available.

3.3 PREPARING THE INJECTION SOURCE

The condensate storage tank is an important source of water to the reactor vessel injection systems. As indicated in Figure 8 (based upon the Browns Ferry arrangement), it is the normal suction source for the steam turbine-driven high pressure coolant injection (HPCI) and reactor core isolation cooling (RCIC) systems and the alternate source for the electric motor-driven residual heat removal (RHR) and core spray (CS) pumps. Other BWR facilities also have at least one motor-driven reactor vessel injection system capable of taking suction upon the condensate storage tank (CST). At least one BWR facility currently has in place a procedure for adding borax and boric acid crystals directly to the (partially drained) CST, for use as backup to the SLCS if needed in the event of ATWS.[33]

As discussed previously, a much higher concentration of boron would be required for the prevention of criticality for the case of a degraded core than would be required for the control of ATWS. The requirement stated in Reference 30 is for a concentration of 700–1000 ppm of the boron-10 isotope, which is 4 to 6 times greater than the reactor vessel concentration (163 ppm) obtained by operation of the SLCS.

During normal reactor operation, the CST provides makeup flow to the main condenser hotwells via an internal tank standpipe, as indicated on Figure 9. Any practical strategy for direct poisoning of the CST must provide for partial draining of this tank, particularly if boron-10 concentrations greater than 700 ppm are to be achieved. The CST could be gravity-drained through the standpipe under station blackout conditions. The residual water volume would be plant-specific, but a representative value for a 1060 MWe BWR-4 facility such as Browns Ferry is 135,000 gal (511 m^3).

Even with partial CST draining, however, the amount of powder required to obtain a boron-10 concentration of 1000 ppm is large. Assuming the use of Polybor to take advantage of its greater solubility, 27,775 lbs (12,600 kg) would have to be added to the partially drained tank. [If borax/boric acid were used, the requirement would be 41,000 lbs (18,600 kg).] Clearly, this is too much to be manhandled [50-lb (23-kg) bags] to the top of the tank and poured in. The practical way to poison the CST would be to prepare a slurry of extremely high concentration in a smaller tank at ground level; then to pump the contents of this small tank into the upper opening of the CST. (As indicated in Table 5, extremely high concentrations can be achieved with Polybor.) To avoid any requirement for procurement of additional plant equipment, a fire engine with its portable suction tank might be employed to perform the pumping function.

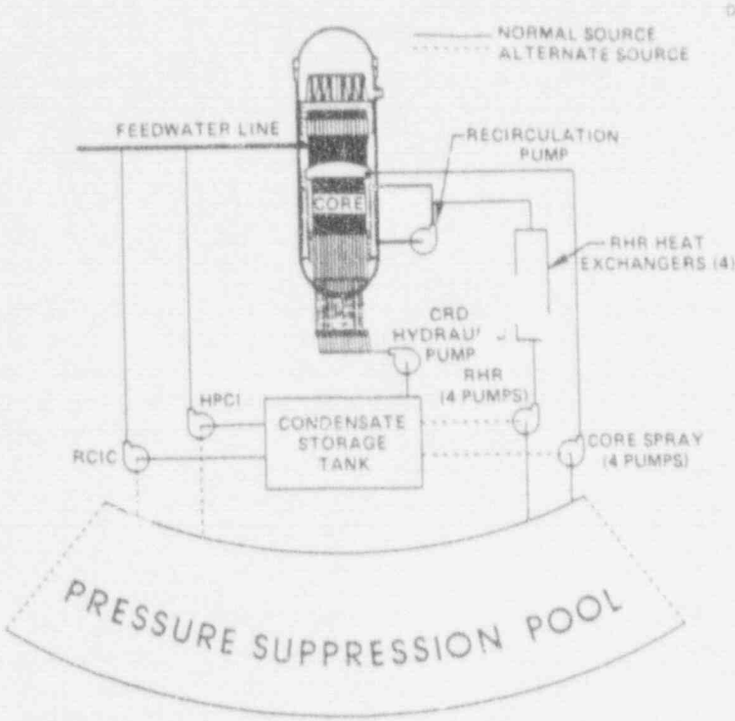

Fig. 8. The condensate storage tank is an important source of water for use in accident sequences other than large-break LOCA.

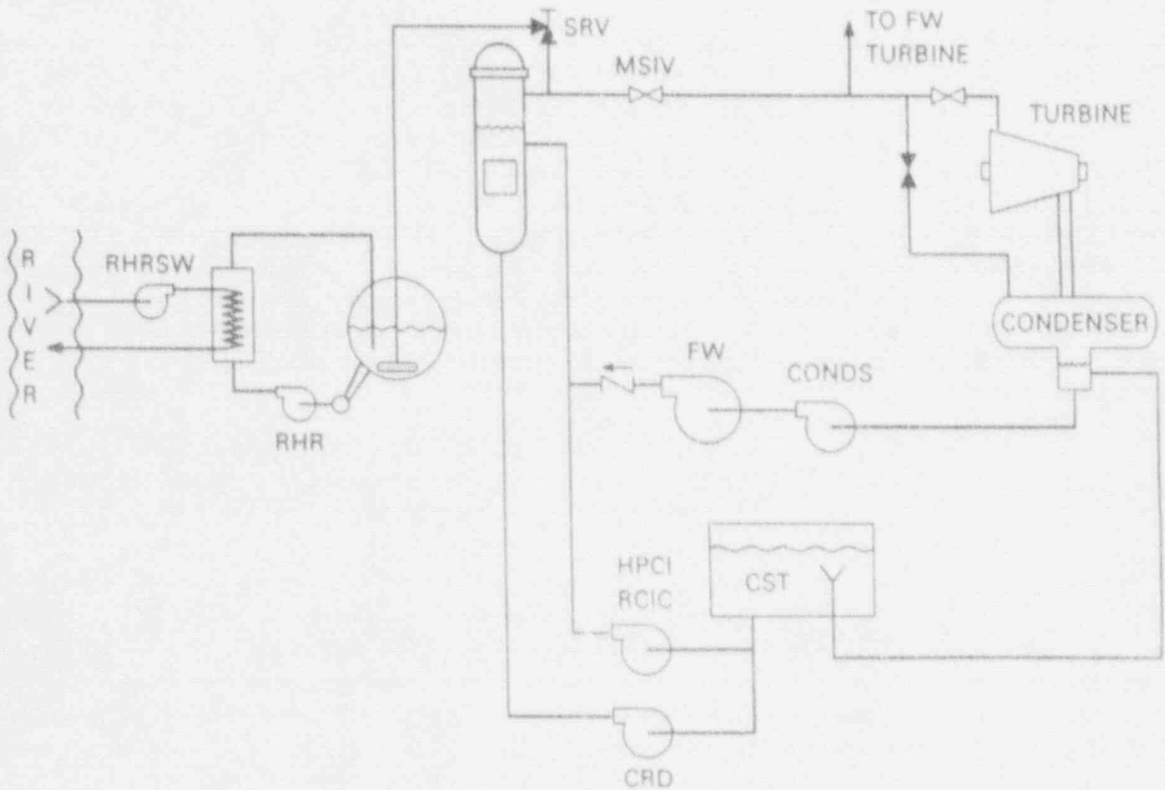

Fig. 9. The condensate storage tank can be drained to the main condenser hotwells via the internal standpipe, leaving a sufficient volume for reactor vessel injection.

4. SUMMARY

A recently completed Oak Ridge effort proposes two management strategies for mitigation of the events that might occur in-vessel after the onset of significant core damage in a BWR severe accident. While the probability of such an accident is extremely low, there may be effective yet inexpensive mitigation measures that could be implemented employing the existing plant equipment and requiring only additions to the plant emergency procedures. In this spirit, accident management strategies have been proposed for use of a borated solution for reactor vessel refill should control blade damage occur during a period of temporary core dryout and for containment flooding to maintain the core debris within the reactor vessel if the injection systems cannot be restored.

The proposed severe accident management strategy for poisoning of the water used for vessel reflood should injection systems be restored after control blade damage has occurred has great promise for practical implementation. It could be accomplished using only the existing plant equipment but employing a different chemical form for the boron poison. Available information concerning the poison concentration required indicates that much more boron would have to be injected than is available in the Standby Liquid Control System. Furthermore, the dominant BWR severe accident sequence is Station Blackout and without means for mechanical stirring or heating of the injection source, the question of being able to form the poisoned solution under accident conditions becomes of supreme importance. Hence the need for the alternate chemical form.

On the other hand, the proposed strategy for drywell flooding to cool the reactor vessel bottom head and prevent the core and structure debris from escaping to the drywell holds less promise. Although drywell flooding would preclude bottom head penetration failures and thereby greatly delay the release of debris, the bottom head would eventually fail by creep rupture. This is a consequence of not being able to completely surround the bottom head with water because of the gas pocket that would be trapped beneath the vessel support skirt. Since the drywell vents would have to remain open during and after the floodir.g process, the ultimate failure of the vessel wall would open a direct pathway for escape of fission products to the atmosphere. This strategy does, however, have potential for future plant designs for which gas release pathways might be provided for the vessel skirt and passive methods might be employed to completely submerge the reactor vessel under severe accident conditions without the need for containment venting.

5. REFERENCES

1. Greene, S. R., *Realistic Simulation of Severe Accidents in BWRs - Computer Modeling Requirements*, NUREG/CR-2940, ORNL/TM-8517, Oak Ridge National Laboratory, April 1984.

2. Ott, L. J., "Advanced Severe Accident Response Models for BWR Application," *Nuclear Engineering and Design*, No. 115, 1989, p. 289-303.

3. Hodge, S. A., "Thermalhydraulic Processes in the Reactor Coolant System of a BWR Under Severe Accident Conditions," Proceedings, ICHMT International Seminar on Heat and Mass Transfer Aspects of Fission Product Releases, Dubrovnik, Yugoslavia, May 1989.

4. Hodge, S. A., "BWR Reactor Vessel Bottom Head Failure Modes," Proceedings, ICHMT International Seminar on Heat and Mass Transfer Aspects of Fission Product Releases, Dubrovnik, Yugoslavia, May 1989.

5. Hodge, S. A. and Harrington, R. M. *Considerations Regarding Certain Aspects of Severe Accident Mitigation Afforded by Operation of Shoreham at Reduced Power*, letter report (ORNL/M-1011) to Mr. S. Singh Bajwa, Risk Applications Branch, NRR, USNRC, dated June 12, 1987.

6. Hodge, S. A., Hyman, C. R., and Ott, L. J., *Boiling Water Reactor Severe Accident Technology at Oak Ridge - Purpose and Goals -*, letter report (ORNL/M-1017) to Dr. Thomas J. Walker, Accident Evaluation Branch, Division of Systems Research, RES, USNRC, dated December 6, 1988.

7. *Severe Accident Risks: An Assessment for Five U.S. Nuclear Power Plants*, NUREG-1150, December 19[illegible].

8. Cook, D. H. et al., *Station Blackout at Browns Ferry Unit One - Accident Sequence Analysis*, Vol. 1, NUREG/CR-2182, ORNL/NUREG/TM-455/V1, November 1981.

9. Wichner, R. P. et al., *Station Blackout at Browns Ferry Unit One - Iodine and Noble Gas Distribution and Release*, Vol. 2, NUREG/CR-2182, ORNL/NUREG/TM-455/V2, August 1982.

10. Condon, W. A. et al., *SBLOCA Outside Containment at Browns Ferry Unit One - Accident Sequence Analysis*, Vol. 1, NUREG/CR-2672, ORNL/TM-8119/V1, October 1982.

11. Wichner, R. P. et al., *SBLOCA Outside Containment at Browns Ferry Unit One - Iodine, Cesium, and Noble Gas Distribution and Release*, Vol. 2, NUREG/CR-2672, ORNL/TM-8119/V2, September 1983.

12. Cook, D. H. et al., *Loss of DHR Sequences at Browns Ferry Unit One - Accident Sequence Analysis*, Vol. 1, NUREG/CR-2973, ORNL/TM-8532, May 1983.

13. Harrington, R. M. and Ott, L. J., *The Effect of Small-Capacity, High-Pressure Injection Systems on TQUV Sequences at Browns Ferry Unit One*, NUREG/CR-3179, ORNL/TM-8635, September 1983.

14. Harrington, R. M. and Hodge, S. A., *ATWS at Browns Ferry Unit One - Accident Sequence Analysis*, NUREG/CR-3470, ORNL/TM-8902, July 1984.

15. Wichner, R. P. et al., *Noble Gas Iodine, and Cesium Transport in a Postulated Loss of Decay Heat Removal Accident at Browns Ferry*, NUREG/CR-3617, ORNL/TM-9028, August 1984.

16. Harrington, R. M., *Evaluation of Operator Action Strategies for Mitigation of MSIV-Closure Initiated ATWS*, letter report to Dr. Thomas J. Walker, Accident Evaluation Branch, Division of Systems Research, RES, USNRC, dated November 11, 1985.

17. Harrington, R. M., *The Effect of Reactor Vessel Pressure and Water Level on Equilibrium BWR Core Thermal Power During MSIV-Closure-Initiated ATWS*, letter report to Dr. Thomas J. Walker, Accident Evaluation Branch, Division of Systems Research, RES, USNRC, dated January 10, 1986.

18. Harrington, R. M. and Hodge, S. A., *Loss of Control Air at Browns Ferry Unit One - Accident Sequence Analysis*, NUREG/CR-4413, ORNL/TM-9826, January 10, 1986.

19. Harrington, R. M. and Hodge, S. A., *Containment Venting as a Severe Accident Mitigation Technique for BWR Plants with Mark I Containment*, letter report to Dr. Thomas J. Walker, Accident Evaluation Branch, Division of Systems Research, RES, USNRC, dated June 26, 1986.

20. Ott, L. J. and Hodge, S. A., *Modeling of Time-Dependent Emergence of Core Debris from a Boiling Water Reactor Under Severe Accident Conditions*, letter report (ORNL/M-

1015), to Dr. Thomas J. Walker, Accident Evaluation Branch, Division of Systems Research, RES, USNRC, dated April 22, 1988.

21. Hodge, S. A., *Failure Modes of the EWR Reactor Vessel Bottom Head*, letter report (ORNL/M-1019), to Dr. Thomas J. Walker, Accident Evaluation Branch, Division of Systems Research, RES, USNRC, dated May 10, 1989.

22. Hodge, S. A. and Ott, L. J., "BWRSAR Calculations of Reactor Vessel Debris Pours for Peach Bottom Short-Term Station Blackout," *Nuclear Engineering and Design*, No. 121, 1990, p. 327-339.

23. *BWR Owners' Group Emergency Procedure Guidelines*, Revision 4, General Electric Topical Report NEDO-31331, March 1987.

24. Lucas, W. J., Vandenkieboom, J. J., and Lehner, J. R., *Assessment of Candidate Accident Management Strategies*, NUREG/CR-5474, BNL-NUREG-52221, March 1990.

25. Hodge, S. A., *Accident Management for Critical BWR Severe Accident Sequences–Assessment of Current Status*, letter report ORNL/NRC/LTR-90/12 to Dr. James T. Han, Reactor and Plant Systems Branch, Division of Systems Research, RES, USNRC, May 31, 1990.

26. Hodge, S. A., *BWR (In-Vessel) Late Accident Mitigation Strategies*, letter report ORNL/NRC/LTR-90/18 to Dr. James T. Han, Reactor and Plant Systems Branch, Division of Systems Research, RES, USNRC, September 15, 1990.

27. Hodge, S. A., *Recommendations for Further Assessment of Certain BWR (In-Vessel) Late Accident Mitigation Strategies*, letter report ORNL/NRC/LTR-90/19 to Dr. James T. Han, Reactor and Plant Systems Branch, Division of Systems Research, RES, USNRC, September 25, 1990.

28. *Individual Plant Examination for Severe Accident Vulnerabilities - 10CFR50.54(f)*, USNRC Generic Letter No. 88-20, November 23, 1988.

29. *Individual Plant Examination: Submittal Guidance, NUREG-1335*, USNRC, Final Report, August 1989.

30. Scott, W. B., et al., *Recriticality in a BWR Following a Core Damage Event*, NUREG/CR-5653, PNL-7476, December 1990.

31. March-Leuba, J., *Stability Calculations for the Grand Gulf-1 and Susquehanna-2 Boiling Water Reactors*, letter report (ORNL/NRC/LTR-87/08) to Mr. T. L. Huang, Office of Nuclear Reactor Regulation, USNRC, September 1987.

32. 10 CFR 50.62, *Requirements for Reduction of Risk from Anticipated Transients Without Scram (ATWS) Events for Light-Water-Cooled Nuclear Power Plants*, Paragraph (c) (4).

33. *NRC Inspection Report No. 50-416/91-02*, enclosure to letter from Thomas A. Peebles, Chief Operations Branch, Division of Reactor Safety to Mr. W. T. Cottle, Vice President Operations-Grand Gulf, Entergy Operations, Inc., Subject: NRC Inspection Report No. 50-416/91-02, dated February 14, 1991.

NRC FORM 335 (2-89) NRCM 1102, 3201, 3202

U.S. NUCLEAR REGULATORY COMMISSION

BIBLIOGRAPHIC DATA SHEET

(See instructions on the reverse)

1. REPORT NUMBER (Assigned by NRC, Add Vol., Supp., Rev., and Addendum Numbers, if any.)

NUREG/CP-0119
Vol. 2

2. TITLE AND SUBTITLE

Proceedings of the Nineteenth Water Reactor Safety Information Meeting

3. DATE REPORT PUBLISHED

MONTH: April — YEAR: 1992

4. FIN OR GRANT NUMBER

A-3988

5. AUTHOR(S)

Compiled by Allen J. Weiss, BNL

6. TYPE OF REPORT

Proceedings of conference on safety research

7. PERIOD COVERED (Inclusive Dates)

October 28-30, 1991

8. PERFORMING ORGANIZATION – NAME AND ADDRESS (If NRC, provide Division, Office or Region, U.S. Nuclear Regulatory Commission, and mailing address; if contractor, provide name and mailing address.)

Office of Nuclear Regulatory Research
U.S. Nuclear Regulatory Commission
Washington, D.C. 20555

9. SPONSORING ORGANIZATION – NAME AND ADDRESS (If NRC, type "Same as above"; if contractor, provide NRC Division, Office or Region, U.S. Nuclear Regulatory Commission, and mailing address.)

Same as Item 8 above

10. SUPPLEMENTARY NOTES

Proceedings prepared by Brookhaven National Laboratory

11. ABSTRACT (200 words or less)

This three-volume report contains 83 papers out of the 108 that were presented at the Nineteenth Water Reactor Safety Information Meeting held at the Bethesda Marriott Hotel, Bethesda, Maryland, during the week of October 28-30, 1991. The papers are printed in the order of their presentation in each session and describe progress and results of programs in nuclear safety research conducted in this country and abroad. Foreign participation in the meeting included 14 different papers presented by researchers from Canada, Germany, France, Japan, Sweden, Taiwan, and USSR. The titles of the papers and names of the authors have been updated and may differ from those that appeared in the final program of the meeting.

12. KEY WORDS/DESCRIPTORS (List words or phrases that will assist researchers in locating the report.)

reactor safety - meetings, research programs - reviews, reactor accidents, reactor components, nuclear power plants - reliability, nuclear power plants - risk assessment, probabilistic estimation, loss of coolant, reactor accidents - management, human factors, systems analysis, leading abstract - proceedings, seismic effects, hydraulics - heat transfer, environmental engineering

13. AVAILABILITY STATEMENT

Unlimited

14. SECURITY CLASSIFICATION

(This Page) Unclassified

(This Report) Unclassified

15. NUMBER OF PAGES

16. PRICE

UNITED STATES
NUCLEAR REGULATORY COMMISSION
WASHINGTON, D.C. 20555

OFFICIAL BUSINESS
PENALTY FOR PRIVATE USE, $300

SPECIAL FOURTH-CLASS RATE
POSTAGE AND FEES PAID
USNRC
PERMIT NO. G-67